METABOLIC REGULATION IN CARDIOVASCULAR HOMEOSTASIS AND DISEASE

EDITED BY: Kunhua Song, Kedryn K. Baskin and Zhong Wang
PUBLISHED IN: Frontiers in Cardiovascular Medicine

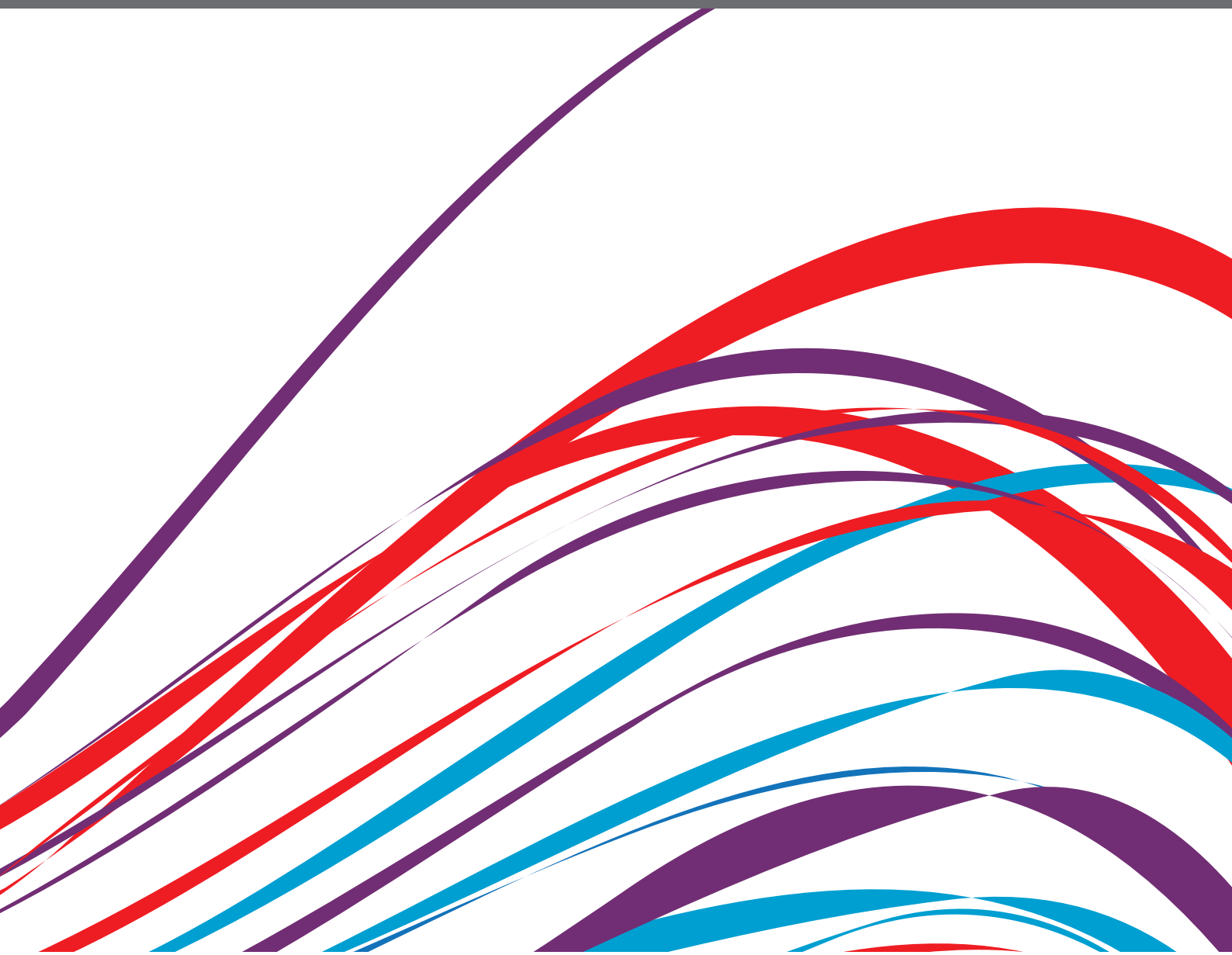

frontiers Research Topics

frontiers

ISSN 1664-8714
ISBN 978-2-88976-556-0
DOI 10.3389/978-2-88976-556-0

About Frontiers

Frontiers is more than just an open-access publisher of scholarly articles: it is a pioneering approach to the world of academia, radically improving the way scholarly research is managed. The grand vision of Frontiers is a world where all people have an equal opportunity to seek, share and generate knowledge. Frontiers provides immediate and permanent online open access to all its publications, but this alone is not enough to realize our grand goals.

Frontiers Journal Series

The Frontiers Journal Series is a multi-tier and interdisciplinary set of open-access, online journals, promising a paradigm shift from the current review, selection and dissemination processes in academic publishing. All Frontiers journals are driven by researchers for researchers; therefore, they constitute a service to the scholarly community. At the same time, the Frontiers Journal Series operates on a revolutionary invention, the tiered publishing system, initially addressing specific communities of scholars, and gradually climbing up to broader public understanding, thus serving the interests of the lay society, too.

Dedication to Quality

Each Frontiers article is a landmark of the highest quality, thanks to genuinely collaborative interactions between authors and review editors, who include some of the world's best academicians. Research must be certified by peers before entering a stream of knowledge that may eventually reach the public - and shape society; therefore, Frontiers only applies the most rigorous and unbiased reviews.
Frontiers revolutionizes research publishing by freely delivering the most outstanding research, evaluated with no bias from both the academic and social point of view. By applying the most advanced information technologies, Frontiers is catapulting scholarly publishing into a new generation.

What are Frontiers Research Topics?

Frontiers Research Topics are very popular trademarks of the Frontiers Journals Series: they are collections of at least ten articles, all centered on a particular subject. With their unique mix of varied contributions from Original Research to Review Articles, Frontiers Research Topics unify the most influential researchers, the latest key findings and historical advances in a hot research area! Find out more on how to host your own Frontiers Research Topic or contribute to one as an author by contacting the Frontiers Editorial Office: frontiersin.org/about/contact

METABOLIC REGULATION IN CARDIOVASCULAR HOMEOSTASIS AND DISEASE

Topic Editors:
Kunhua Song, University of Colorado Anschutz Medical Campus, United States
Kedryn K. Baskin, The Ohio State University, United States
Zhong Wang, University of Michigan, United States

Citation: Song, K., Baskin, K. K., Wang, Z., eds. (2022). Metabolic Regulation in Cardiovascular Homeostasis and Disease. Lausanne: Frontiers Media SA.
doi: 10.3389/978-2-88976-556-0

Table of Contents

05 ***Editorial: Metabolic regulation in cardiovascular homeostasis and disease***
Kunhua Song, Zhong Wang and Kedryn K. Baskin

08 ***Non-HDL-C Is More Stable Than LDL-C in Assessing the Percent Attainment of Non-fasting Lipid for Coronary Heart Disease Patients***
Li-Ling Guo, Yan-qiao Chen, Qiu-zhen Lin, Feng Tian, Qun-Yan Xiang, Li-yuan Zhu, Jin Xu, Tie Wen and Ling Liu

16 ***Plasma Metabolites Alert Patients With Chest Pain to Occurrence of Myocardial Infarction***
Nan Aa, Ying Lu, Mengjie Yu, Heng Tang, Zhenyao Lu, Runbing Sun, Liansheng Wang, Chunjian Li, Zhijian Yang, Jiye Aa, Xiangqing Kong and Guangji Wang

32 ***Impact of Acute Insulin Resistance on Myocardial Blush in Non-Diabetic Patients Undergoing Primary Percutaneous Coronary Intervention***
Soheir M. Kasem, Ghada Mohamed Saied, Abdel Nasser MA Hegazy and Mahmoud Abdelsabour

41 ***High-Energy Phosphates and Ischemic Heart Disease: From Bench to Bedside***
Hao Yi-Dan, Zhao Ying-Xin, Yang Shi-Wei and Zhou Yu-Jie

53 ***Post-translational Acetylation Control of Cardiac Energy Metabolism***
Ezra B. Ketema and Gary D. Lopaschuk

73 ***Homeostasis Disrupted and Restored—A Fresh Look at the Mechanism and Treatment of Obesity During COVID-19***
Jacqueline Dickey, Camelia Davtyan, David Davtyan and Heinrich Taegtmeyer

80 ***Mitochondrial Respiration Defects in Single-Ventricle Congenital Heart Disease***
Xinxiu Xu, Jiuann-Huey Ivy Lin, Abha S. Bais, Michael John Reynolds, Tuantuan Tan, George C. Gabriel, Zoie Kondos, Xiaoqin Liu, Sruti S. Shiva and Cecilia W. Lo

89 ***Glycolysis Inhibition Alleviates Cardiac Fibrosis After Myocardial Infarction by Suppressing Cardiac Fibroblast Activation***
Zhi-Teng Chen, Qing-Yuan Gao, Mao-Xiong Wu, Meng Wang, Run-Lu Sun, Yuan Jiang, Qi Guo, Da-Chuan Guo, Chi-Yu Liu, Si-Xu Chen, Xiao Liu, Jing-Feng Wang, Hai-Feng Zhang and Yang-Xin Chen

100 ***Stable Isotopes for Tracing Cardiac Metabolism in Diseases***
Anja Karlstaedt

117 ***Longevity Factor FOXO3: A Key Regulator in Aging-Related Vascular Diseases***
Yan Zhao and You-Shuo Liu

130 ***Association of Metabolic Syndrome With Long-Term Cardiovascular Risks and All-Cause Mortality in Elderly Patients With Obstructive Sleep Apnea***
Lin Liu, Xiaofeng Su, Zhe Zhao, Jiming Han, Jianhua Li, Weihao Xu, Zijun He, Yinghui Gao, Kaibing Chen, Libo Zhao, Yan Gao, Huanhuan Wang, JingJing Guo, Junling Lin, Tianzhi Li and Xiangqun Fang

141 ***MCC950, a Selective NLRP3 Inhibitor, Attenuates Adverse Cardiac Remodeling Following Heart Failure Through Improving the Cardiometabolic Dysfunction in Obese Mice***
Menglong Wang, Mengmeng Zhao, Junping Yu, Yao Xu, Jishou Zhang, Jianfang Liu, Zihui Zheng, Jing Ye, Zhen Wang, Di Ye, Yongqi Feng, Shuwan Xu, Wei Pan, Cheng Wei and Jun Wan

frontiers | Frontiers in Cardiovascular Medicine

TYPE Editorial
PUBLISHED 03 August 2022
DOI 10.3389/fcvm.2022.995207

OPEN ACCESS

EDITED AND REVIEWED BY
Ichiro Manabe,
Chiba University, Japan

*CORRESPONDENCE
Kunhua Song
kunhua.song@cuanschutz.edu
Zhong Wang
zhongw@med.umich.edu
Kedryn K. Baskin
Kedryn.Baskin@osumc.edu

SPECIALTY SECTION
This article was submitted to Cardiovascular Metabolism, a section of the journal Frontiers in Cardiovascular Medicine

RECEIVED 15 July 2022
ACCEPTED 20 July 2022
PUBLISHED 03 August 2022

CITATION
Song K, Wang Z and Baskin KK (2022) Editorial: Metabolic regulation in cardiovascular homeostasis and disease.
Front. Cardiovasc. Med. 9:995207.
doi: 10.3389/fcvm.2022.995207

Editorial: Metabolic regulation in cardiovascular homeostasis and disease

Kunhua Song[1,2]*, Zhong Wang[3]* and Kedryn K. Baskin[4]*

[1]Division of Cardiology, Department of Medicine, University of Colorado Anschutz Medical Campus, Aurora, CO, United States, [2]Gates Center for Regenerative Medicine and Stem Cell Biology, University of Colorado Anschutz Medical Campus, Aurora, CO, United States, [3]Department of Cardiac Surgery, University of Michigan-Ann Arbor, Ann Arbor, MI, United States, [4]Department of Physiology and Cell Biology, College of Medicine, the Ohio State University, Columbus, OH, United States

KEYWORDS

metabolism, cardiac disease, biomarkers, metabolic remodeling, metabolic therapeutics

Editorial on the Research Topic
Metabolic regulation in cardiovascular homeostasis and disease

Metabolic dysregulation is a common feature in cardiovascular disease from congenital heart defects to heart failure. The Research Topic, metabolic regulation in cardiovascular homeostasis and disease, focuses on recent advances and challenges in understanding of metabolic regulation in cardiac physiology and pathogenesis. Here, a collection of 12 review and original research articles in this topic highlights recent findings and innovative approaches in the field of cardiovascular metabolism.

Metabolic risks for cardiovascular disease

Many risk factors contribute to cardiovascular disease and mortality, such as obesity, aging, diabetes, metabolic syndrome, and obstructive sleep apnea (OSA). After following about one thousand participants, Liu et al. demonstrate that patients with metabolic syndrome and OSA have a higher risk of adverse cardiac events. These results may lead to the design of additional clinical studies to understand effects of multiple risk factors on cardiovascular disease. In a review article, Zhao and Liu summarize regulatory mechanisms of FOXO3, a critical regulator in aging-related vascular disease. Regarding roles of FOXO3 activation in vascular remodeling, FOXO3 has a potential for therapeutic targeting. Insulin resistance, a marker for metabolic syndrome also increases risk of heart disease. After investigating 240 non-diabetic patients with ST-segment elevation myocardial infarction (STEMI), Kasem et al. demonstrate that acute insulin resistance is associated with microvascular injury and poor hospital outcome in these patients. This study suggests that molecules related to insulin resistance may serve as predictors

of microvasculature injury in myocardium of patients post-coronary angiography and angioplasty. Abnormal cholesterol levels are also a marker of metabolic syndrome. Increased level of cholesterol is a risk factor for coronary heart disease (CHD). Treatment with statin and its derivative drugs is used to lower cholesterol levels, indicated by fasting level of low-density lipoprotein cholesterol (LDL-C) < 1.4 mmol/L and non-high-density lipoprotein cholesterol (non-HDL-C) level < 2.2 mmol/L. Measuring non-fasting levels of LDL-C and non-HDL-C has been recommended to prevent ischemic events. Guo et al. have measured fasting and non-fasting levels of LDL-C and non-HDL-C in 397 patients with CHD. This study shows that much lower level of LDL-C in non-fasting phase shall be considered as a healthy threshold.

Many factors contribute to alterations of metabolism in the pathogenesis of cardiovascular disease. Ketema and Lopaschuk provide a comprehensive review of one specific-regulatory mechanism mediated by post-translational acetylation of non-histone proteins, such as mitochondrial proteins. This review article highlights the importance of unraveling interconnections among metabolic protein acetylation, fatty acid β-oxidation, and glucose oxidation in the heart under physiological and pathological conditions.

Quantification of metabolites and measurement of metabolic dynamics in the heart could facilitate identification of biomarkers for cardiovascular disease and understanding disease pathogenesis. Using gas and liquid chromatography-mass spectrometry, Aa et al. have made efforts to identify metabolites that predict risk of myocardial infarction (MI) by profiling plasma metabolites in 85 patients with MI chest pain, 61 patients with non-MI chest pain, and 84 control subjects. This study demonstrates that higher plasma levels of deoxyuridine, homoserine, and methionine increase the risk for MI. Verification of these findings in large samples would benefit prognosis and prevention of MI. Patients who suffer from congenital heart disease with single-ventricle (SV-CHD) are susceptible to heart failure (HF). Identification of biomarkers to predict HF risk in patients with SV-CHD would benefit timely care management. Xu et al. have measured oxygen consumption rates (OCR) in peripheral blood mononuclear cells (PBMCs) isolated from human subjects with SV-CHD ($n = 20$), biventricular CHD (BV-CHD, $n = 16$), and healthy control ($n = 22$). SV-CHD patients with HF show higher maximal respiratory capacity and respiratory reserve in PBMCs, while SV-CHD patients without HF show less maximal respiratory capacity. Because the authors collected PBMCs from relatively small sample sizes, more studies are needed to verify whether alterations of mitochondrial respiration in PBMCs could serve as a biomarker for HF risk in patients with SV-CHD. Powerful approaches and mathematical tools are critical to accurately measuring metabolic dynamics in heart tissue. Karlstaedt summarizes techniques and concepts for *in vivo* or *ex vivo* stable isotope labeling in measuring metabolic flux in cardiovascular research and advancements in analytical methods at the tissue and single-cell levels. Consideration of challenges in accurate measurement of metabolic flux in clinics studies would assist with timely management of disease, estimation of treatment efficacy, and decision on therapeutic strategies.

Therapeutics targets of metabolic pathways

Dysregulation of metabolism is common in cardiovascular disease. Restoration of metabolic homeostasis has been regarded as a potential therapy for the disease. Obesity has been identified as a major risk factor of hospitalization, severe illness, and mortality of COVID-19 patients. Treatment of obesity plays an important role in ending the COVID-19 pandemic. Dickey et al. discuss metabolic impact of various treatments for obesity, including diet and calorie restriction and bariatric surgeries and highlight future studies needed to understand mechanisms of restoring metabolic homeostasis in obese patients by these treatments. Heart failure is accompanied by increased inflammation and glycolysis in myocardium. Wang et al. demonstrate that treatment with MCC950, a selective inhibitor of the inflammasome component NLRP3, ameliorated cardiac function and remodeling in obese mice with heart failure. This study indicates interactions between inflammation and metabolic alterations during cardiac pathogenesis in obese subjects. In another report, Chen et al. demonstrate that post-MI mice treated with 2-Deoxy-D-glucose (2-DG) show significantly decreased activation of cardiac fibroblasts and cardiac fibrosis. Although treatment with 2-DG 4 days post-MI significantly decreases cardiac fibrosis in mice, the treatment is not enough to ameliorate cardiac function and mortality. It is likely that cardiac fibrosis post-MI is activated by more than one pathway. Therefore, inhibition of only one pathway (e.g., glycolysis) appears insufficient to produce meaningful clinical outcomes. Reduction in ATP generation usually occurs in failing myocardium. Exogenous creatine phosphate (CrP), a high-energy phosphate provides cardiac protection by re-fueling ATP, attenuation of intracellular Ca^{2+} overload and oxidative stress, and anti-arrhythmias and platelet aggression in animal models. However, CrP does not improve long-term survival of patients with heart disease in various clinical trials. Yi-Dan et al. provide an overview of CrP physiology and pharmacological effects of exogenous CrP on ischemic myocardium. Yi-Dan et al. also summarize potential reasons why clinical benefits have not been observed in clinical trials, e.g., administration routs/dosage and lack of multicenter studies. Ultimately, treatment of cardiovascular disease by targeting metabolic

dysregulation holds promising, but needs extensive and collaborative studies.

Summary

Articles presented in this Research Topic provide in-depth insights into the relationship between metabolic homeostasis and cardiovascular pathogenesis. This editorial briefly summarizes each article in the collection. We are enthusiastic that this work will lead to the development of new approaches and discovery of novel mechanisms in the field of cardiovascular metabolism, which eventually results in designing of effective therapeutics for cardiovascular disease.

Author contributions

KS, ZW, and KB contributed to the writing of the manuscript. All authors contributed to the article and approved the submitted version.

Funding

This work was supported by the NIH R01HL133230, R01HL139735, R01HL163672, and K01DK116916.

Conflict of interest

The authors declare that the research was conducted in the absence of any commercial or financial relationships that could be construed as a potential conflict of interest.

Publisher's note

frontiers in Cardiovascular Medicine

ORIGINAL RESEARCH
published: 01 April 2021
doi: 10.3389/fcvm.2021.649181

Non-HDL-C Is More Stable Than LDL-C in Assessing the Percent Attainment of Non-fasting Lipid for Coronary Heart Disease Patients

Li-Ling Guo[1,2,3,4], *Yan-qiao Chen*[1,2,3,4], *Qiu-zhen Lin*[1,2,3,4], *Feng Tian*[1,2,3,4], *Qun-Yan Xiang*[1,2,3,4], *Li-yuan Zhu*[1,2,3,4], *Jin Xu*[1,2,3,4], *Tie Wen*[5] *and Ling Liu*[1,2,3,4]*

[1] Department of Cardiovascular Medicine, The Second Xiangya Hospital, Central South University, Changsha, China, [2] Research Institute of Blood Lipid and Atherosclerosis, Center South University, Changsha, China, [3] Modern Cardiovascular Disease Clinical Technology Research Center of Hunan Province, Changsha, China, [4] Cardiovascular Disease Research Center of Hunan Province, Changsha, China, [5] Department of Emergency, The Second Xiangya Hospital, Central South University, Changsha, China

This study aimed to compare the percentage attainment of fasting and non-fasting LDL-C and non-HDL-C target levels in coronary heart disease (CHD) patients receiving short-term statin therapy. This study enrolled 397 inpatients with CHD. Of these, 197 patients took statins for <1 month (m) or did not take any statin before admission (CHD1 group), while 204 patients took statins for ≥1 m before admission (CHD2 group). Blood lipid levels were measured at 0, 2, and 4 h after a daily breakfast. Non-fasting LDL-C and non-HDL-C levels significantly decreased after a daily meal ($P < 0.05$). Both fasting and non-fasting LDL-C or non-HDL-C levels were significantly lower in the CHD2 group. The percentage attainment of LDL-C <1.4 mmol/L at 2 and 4 h after a daily breakfast was significantly higher than that during fasting ($P < 0.05$), but the percent attainment of non-fasting non-HDL-C <2.2 mmol/L was close to its fasting value ($P > 0.05$). Analysis of c-statistic showed that non-fasting cut-off points for LDL-C and non-HDL-C were 1.19 and 2.11 mmol/L, corresponding to their fasting goal levels of 1.4 and 2.2 mmol/L, respectively. When post-prandial LDL-C and non-HDL-C goal attainments were re-evaluated using non-fasting cut-off points, there were no significant differences in percentage attainment between fasting and non-fasting states. Non-HDL-C is more stable than LDL-C in assessing the percent attainment of non-fasting lipid for coronary heart disease patients. If we want to use LDL-C to assess the percent attainment of post-prandial blood lipids, we may need to determine a lower non-fasting cut-off point.

Keywords: coronary heart disease, non-fasting, low-density lipoprotein cholesterol, non-high-density lipoprotein cholesterol, cut-off points

OPEN ACCESS

Edited by:
Zhong Wang,
University of Michigan, United States

Reviewed by:
Tetsuro Miyazaki,
Juntendo University Urayasu Hospital, Japan
Alon Schaffer,
Azienda Ospedaliero Universitaria Maggiore della Carità, Italy

***Correspondence:**
Ling Liu
feliuling@csu.edu.cn

Specialty section:
This article was submitted to Cardiovascular Metabolism, a section of the journal Frontiers in Cardiovascular Medicine

Received: *04 January 2021*
Accepted: *08 March 2021*
Published: *01 April 2021*

Citation:
Guo L-L, Chen Y-q, Lin Q-z, Tian F, Xiang Q-Y, Zhu L-y, Xu J, Wen T and Liu L (2021) Non-HDL-C Is More Stable Than LDL-C in Assessing the Percent Attainment of Non-fasting Lipid for Coronary Heart Disease Patients. Front. Cardiovasc. Med. 8:649181. doi: 10.3389/fcvm.2021.649181

INTRODUCTION

Elevated cholesterol level is an independent risk factor for coronary heart disease (CHD). To reduce the risk of ischemic events for CHD patients, fasting level of low-density lipoprotein cholesterol (LDL-C) should be controlled to <1.4 mmol/L as the primary target, then that of non-high-density lipoprotein cholesterol (non-HDL-C) should be <2.2 mmol/L as the secondary target of cholesterol control according to the 2019 European guidelines (1).

It is increasingly believed that atherosclerosis is a post-prandial phenomenon because, at least with respect to lipids, we are in the post-prandial phase for the most part of the day (2). Considering that either fasting or non-fasting (i.e., post-prandial) LDL-C level has a similar predictive value for all-cause death and cardiovascular death (3, 4), non-fasting lipids detection at a random time-point within at least 8 h after a daily meal has been recommended in the primary and secondary prevention against CHD (5–8). However, both LDL-C and non-HDL-C levels show a tendency of decrease in the non-fasting state (9–11). Moreover, there are only fasting cholesterol-lowering targets but not non-fasting ones in the published guidelines (1, 12–15). It is uncertain whether these fasting targets are applicable to assessing cholesterol control as well as how to evaluate it in the non-fasting stage.

Recently, we observed more substantial reductions in LDL-C and non-HDL-C levels in Chinese subjects with CHD at 2 and 4 h after a daily breakfast (9, 16), appearing to be greater than those reported in large-scale clinical studies conducted in other countries (10, 11, 17, 18), although the potential cause remains uncertain. Additionally, it was proposed that non-HDL-C level may be a better prognostic factor than LDL-C level to evaluate the risk of future cardiovascular events (19–24). Furthermore, non-fasting fluctuation of non-HDL-C level seem to be smaller than that of LDL-C (24). Nevertheless, there have been no studies comparing the goal attainment of LDL-C with that of non-HDL-C in the non-fasting state.

Therefore, this study aimed to compare the percent attainments of fasting and non-fasting LDL-C and non-HDL-C reaching their fasting targets in CHD patients receiving short-term statins therapy. Furthermore, analysis of c-statistic or receiver operating characteristic curve (ROC) analysis was used to determine the non-fasting cut-off points corresponding to their fasting targets, and the percent attainments of non-fasting LDL-C and non-HDL-C were re-evaluated according to the non-fasting cut-off points.

MATERIALS AND METHODS

Study Population

From March 2017 to July 2019, 397 inpatients with CHD were enrolled from the Department of Cardiovascular Medicine of the Second Xiangya Hospital, Central South University. A total of 84 patients did not take any statins and 109 patients took statins for <1 month (m) before admission (CHD1 group), and 204 patients took statins for ≥1 m before admission (CHD2 group). The definition of CHD was coronary atherosclerosis confirmed by coronary angiography and/or a history of myocardial infarction in patients with angina pectoris (AP). We asked all patients about their medical history and use of medication before enrollment. Patients with autoimmune disease, hepatic disorders, renal disease, cancer, or other serious diseases were excluded. The study was approved by the Ethics Committee of the Second Xiangya Hospital of Central South University. Informed consent was obtained from all patients.

Specimen Collection

All enrolled participants ate breakfast between 7 a.m. and 8 a.m. according to their regular diets after overnight fast for at least 8 h. The patients in this study are all Han nationality, and their daily breakfast were rich in carbohydrate, including steamed bread, noodles, rice porridge, and so on, which were purchased from the cafeteria in our hospital or brought from home according to their dietary habits. During 4-h test, subjects were allowed only to drink a little water and walk slowly. Drinking wine or eating any food were not recommended.

Determination of Blood Lipids Levels

Serum total cholesterol (TC) and triglyceride (TG) levels were measured using automated enzymatic assays. Serum high-density lipoprotein cholesterol (HDL-C) and LDL-C levels were measured using a chemical masking method (25). All measurements, including that of albumin, were carried out on a fully automatic biochemical analyser (Hitachi 7170A, Hitachi Inc., Tokyo, Japan) and performed by the expert who didn't know the details of the research (26). Non-HDL-C equals to TC minus HDL-C.

Statistical Analysis

Data were analyzed using SPSS version 19.0. (IBM Corp., Armonk, NY, USA) and Prism 6.0 (GraphPad Inc., San Diego, CA, USA). Continuous variable values data were shown as mean ± standard deviation (SD), and categorical data were shown as numbers and percentages. The *t*-test and chi-square test were used to analyse continuous variables and categorical variables, respectively. The optimal cut-off points for fasting LDL-C (1.4 mmol/L) and non-HDL-C (2.2 mmol/L) were determined using receiver operating characteristic (ROC curve) analysis. Based on the ROC curve, values determined using Youden analysis were used as cut-off points. All tests were two-tailed, and $P < 0.05$ was considered statistically significant.

RESULTS

Clinical Characteristics and Fasting Blood Lipids in Two CHD Groups

The baseline characteristics of the CHD patients are shown in **Table 1**. Both groups were similar in terms of age, sex, body mass index, percentages of hypertension, current smoking, and diabetes mellitus. There were 56.5% patients taking statins <1 m and 43.5% patients without statins treatment before admission in CHD1 group. Fasting serum levels of TC, LDL-C and non-HDL-C in CHD2 group were significantly lower than those in CHD1 group ($P < 0.05$). The differences in fasting serum TG and HDL-C levels between the groups did not differ significantly (**Table 1**). The proportion of STEMI and NSTEMI patients in CHD2 group was less than that in CHD1 group ($P < 0.05$). However, the proportion of schemic cardiomyopathy in CHD2 group was more than that in CHD1 group ($P < 0.05$). The differences in vascular disease (single or multiple vessel disease) did not differ significantly (**Table 1**).

TABLE 1 | Baseline characteristics of the study population.

	CHD1 ($n = 193$)	CHD2 ($n = 204$)
Age (y, SD)	60.3 ± 9.3	62.0 ± 8.7
Men, *n* (%)	156 (80.8)	157 (77.0)
BMI (kg/m^2, SD)	24.5 ± 3.5	24.9 ± 3.0
Hypertension, *n* (%)	141 (73.1)	152 (74.5)
Current smoking, *n* (%)	110 (57.0)	103 (50.5)
DM, *n* (%)	51 (26.4)	67 (32.8)
Taking statins, *n* (%)		
Statins ≥1 m	0	204 (100)*
Statins <1 m	109 (56.5)	0*
No statins	84 (43.5)	0*
Vascular disease, *n* (%)		
Single vessel disease	43 (22.3)	36 (17.6)
Multiple vessel disease	132 (68.4)	146 (71.6)
Without CAG	18 (9.3)	22 (10.8)
CHD subtype, *n* (%)		
STEMI	14 (7.3)	4 (2.0)*
NSTEMI	32 (16.6)	13 (6.4)*
UA	102 (52.8)	114 (55.9)
SAP	31 (16.1)	42 (20.6)
Schemic cardiomyopathy	4 (2.1)	16 (7.8)*
Others	10 (5.2)	15 (7.4)
TC (mmol/L, SD)	4.32 ± 0.91	3.93 ± 1.03*
LDL-C (mmol/L, SD)	2.72 ± 0.79	2.43 ± 0.90*
Non-HDL-C (mmol/L, SD)	3.20 ± 0.96	2.92 ± 0.98*
HDL-C (mmol/L, SD)	1.12 ± 0.27	1.01 ± 0.25
TG (mmol/L, SD)	1.74 ± 1.11	1.84 ± 1.29

*CHD1 group: CHD patients taking statins <1 m and without statins treatment before admission. CHD2 group: CHD patients taking statins ≥1 m before admission. BMI, body mass index; DM, diabetes mellitus; SAP, stable angina pectoris; Others in CHD subtype: Including coronary microangiopathy, etc. TG, triglyceride; TC, total cholesterol; HDL-C, high-density lipoprotein cholesterol; LDL-C, low-density lipoprotein. Continuous variable values were reported as mean ± SD, and categorical data were reported as numbers and percentages. *$P < 0.05$ when compared with CHD1 group.*

According to the time of statin using before admission, all patients were divided into three groups: CHD1 group (non-statin taking, $n = 93$), CHD2 group [short-term statin taking (<1 m), $n = 109$] and CHD3 group [long-term statin taking (≥1 m), $n = 204$], which were added as the supplement data in the new manuscript due to the small sample size in this study (**Supplementary Table 1**).

Comparison of Changes in Non-fasting Blood Lipids in the Two Groups

Levels of LDL-C and non-HDL-C decreased significantly at 2 and 4 h after a daily breakfast ($P < 0.05$). Non-fasting LDL-C and non-HDL-C in CHD2 group were significantly lower than those in CHD1 group ($P < 0.05$; **Figures 1A,B**). When the data at 2 and 4 h after a daily meal as a whole were used as non-fasting data for further analysis, non-fasting reductions in LDL-C were 0.47 and 0.46 mmol/L, and non-HDL-C were 0.26 and 0.24 mmol/L in CHD1 and CHD2 groups, respectively (**Figure 1C**). The percentages of reduction in LDL-C were 17.1 and 18.5%, and 7.2 and 7.7% in non-HDL-C in CHD1 and CHD2 groups, respectively (**Figure 1D**). There were no significant differences in the absolute reduction or percentage of reduction in LDL-C or non-HDL-C level between the groups. However, non-fasting reductions in LDL-C were greater than those of non-HDL-C (**Figure 1B**).

Non-fasting albumin levels were measured in 89 patients among all CHD patients. There was no significant change in the albumin level after a daily breakfast (**Table 2**), whereas the post-prandial TC, HDL-C, LDL-C, and non-HDL-C level dropped significantly ($P < 0.05$; **Table 2**).

Evaluating Goal Attainments of LDL-C and Non-HDL-C According to Various Targets in CHD2 Group

According to the 2019 European guidelines (1), the percent attainment of LDL-C <1.4 mmol/L in the fasting state was significantly lower than that of non-HDL-C <2.2 mmol/L (10.8 vs. 32.8%, $P < 0.001$). After a daily breakfast, the percent attainment of non-HDL-C and LDL-C gradually tightened, and there was statistical difference only at 2 h. The percent attainment of LDL-C at 2 or 4 h was significantly higher than its fasting value ($P < 0.05$), but there is no difference in non-HDL-C between fasting and post-prandial values ($P > 0.05$; **Figure 2A**).

ROC curve analysis showed that non-fasting cut-off points for LDL-C and non-HDL-C at 4 h were 1.19 mmol/L (sensitivity 90.1%, specificity 77.3%, and AUC 0.904) and 2.11 mmol/L (sensitivity 87.6%, specificity 80.6%, and AUC 0.913), corresponding to their fasting goal levels of 1.4 and 2.2 mmol/L, respectively (**Figures 2B,C**).

According to the non-fasting cut-off points, the percent attainment of LDL-C <1.19 mmol/L at 2 or 4 h was 14.7 or 17.2%, which was close to the percent attainment of LDL-C <1.4 mmol/L in the fasting state. The percent attainment of non-HDL-C <2.11 mmol/L at 2 or 4 h was close to the percent attainment of non-HDL-C <2.2 mmol/L in the fasting state. Moreover, the percent attainment of LDL-C <1.19 mmol/L was significantly lower than that of non-HDL-C <2.11 mmol/L at 2 or 4 h (**Figure 2D**).

DISCUSSION

In this study, we found that when LDL-C goal <1.4 mmol/L was used for evaluating cholesterol control in Chinese CHD patients after short-term statins treatment, the target percentage attainment in the non-fasting state was significantly higher than that of the fasting state. However, the percent attainment of non-fasting non-HDL-C was close to its fasting state, suggesting that non-HDL-C is more stable than LDL-C in assessing the percent attainment of non-fasting lipid for coronary heart disease patients. Notably, according to the new non-fasting cut-off points, 1.19 mmol/L, the non-fasting goal attainment of LDL-C was close to its fasting value.

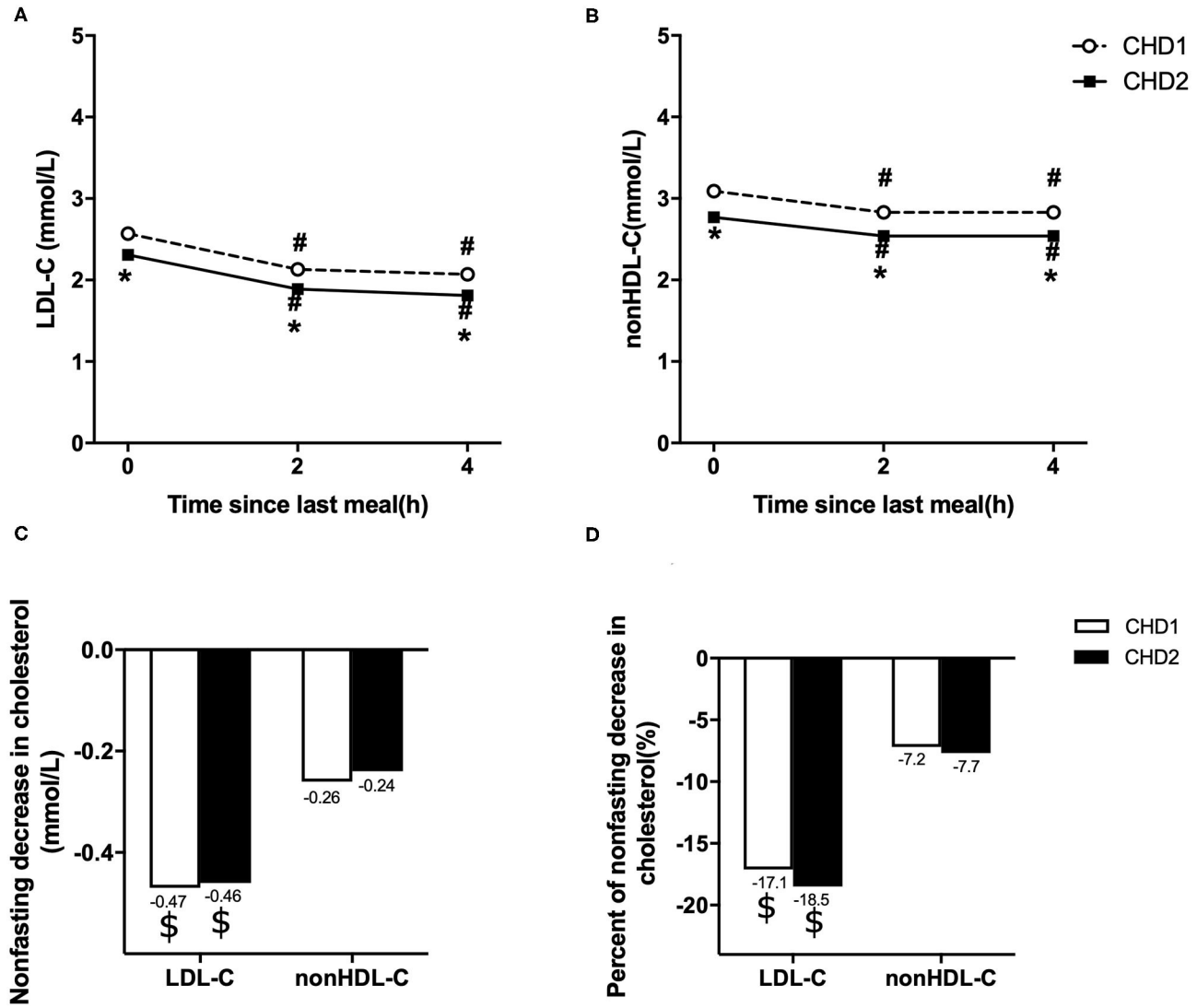

FIGURE 1 | Comparison of changes in non-fasting blood lipids in two groups. Non-fasting changes in serum levels of LDL-C **(A)** and non-HDL-C **(B)**. Values are mean ± Standard Error (SE). Comparison of non-fasting absolute reductions in LDL-C and non-HDL-C levels **(C)**. Comparison of non-fasting percentages of reductions in LDL-C and non-HDL-C levels **(D)**. CHD1 group: CHD patients taking statins <1 m and without statins treatment before admission. CHD2 group: CHD patients taking statins ≥1 m before admission. $^{\#}P < 0.05$ when compared with the fasting level in the same group. $^{*}P < 0.05$ when compared with CHD1 group at the same time point. $^{\$}P < 0.05$ when compared with the absolute reduction or percentage of reduction in non-HDL-C level.

This suggests that lower non-fasting targets could be needed to evaluate the efficacy of cholesterol-lowing therapy in the non-fasting state, particularly when fasting blood lipids are unavailable and the percentage reduction of LDL-C cannot be determined due to a lack of baseline non-fasting levels before treatment.

There are two targets to evaluate the efficacy of cholesterol-lowering treatment in CHD patients. First, LDL-C should achieve a ≥50% reduction from baseline or a goal <1.4 mmol/L according to the 2019 European guidelines (1). However, this recommendation refers only to cholesterol control in the fasting state. In this study, the goal attainment of LDL-C reduction ≥50% could not be evaluated because the baseline fasting or non-fasting LDL-C levels before treatment could not be obtained in most patients in the CHD2 group. Under these circumstances, a physician can only make clinical judgments based on LDL-C goal levels. A considerable number of CHD patients from other locations visit physicians but forget to remain in a fasting state. This is a common situation in the outpatient department of our hospital. As a result, physicians have to assess cholesterol control using non-fasting measurement of blood lipids. According to the joint consensus statement of European Atherosclerosis Society and European Federation of Clinical Chemistry and Laboratory Medicine (5), the non-fasting detection of blood lipids can

TABLE 2 | Changes in levels of blood lipids and albumin after a daily breakfast in 89 CHD patients.

	Fasting	2 h after meal	4 h after meal
TG (mmol/L, SD)	2.09 ± 1.93	2.34 ± 1.88	2.63 ± 2.19
TC (mmol/L, SD)	4.02 ± 1.07	3.72 ± 0.96*	3.71 ± 0.96*
HDL-C (mmol/L, SD)	1.03 ± 0.22	1.01 ± 0.21*	1.03 ± 0.28*
LDL-C (mmol/L, SD)	2.51 ± 0.95	2.11 ± 0.71*	2.07 ± 0.74*
Non-HDL-C (mmol/L, SD)	2.99 ± 1.10	2.71 ± 0.89*	2.69 ± 0.97*
Albumin (g/L, SD)	38.3 ± 2.85	38.3 ± 3.07	38.5 ± 3.00

*TG, triglyceride; TC, total cholesterol; HDL-C, high-density lipoprotein cholesterol; LDL-C, low-density lipoprotein. CHD patients including patients in CHD1 group and CHD2 group. Data are mean ± SD. *$P < 0.05$ when compared with fasting state.*

be routinely applied in CHD patients as long as they are willing to undergo non-fasting measurement. This suggests that measurement of LDL-C level in the non-fasting state is quite important.

Compared with some studies with large population in other countries (10, 11, 17, 18), the reduction in LDL-C level in CHD patients after a daily meal was more significant in the present study. The maximum mean reduction in LDL-C or non-HDL-C was ∼0.1–0.2 mmol/L in the European and North American subjects (10, 11, 17, 18); however, Chinese CHD patients in this study showed a greater decrease in either directly detected LDL-C (i.e., 0.4–0.5 mmol/L) or calculated non-HDL-C (i.e., 0.2–0.3 mmol/L) after a daily breakfast. Although our recent study showed that the post-prandial decline (i.e., 0.3–0.4 mmol/L) in calculated LDL-C was less than that of the directly detected LDL at 2–4 h after a daily breakfast in Chinese CHD patients (9), it was still more than the reduction of above the European and North American studies (10, 11, 17, 18). The underling mechanisms of non-fasting reduction in LDL-C may be complicated in the present study. First, in the Copenhagen General Population Study, they compared blood lipids levels of individuals at random time points after the last meal in the large-scale population. By contrast, our measurements were acquired from the same individuals at various times since the last meal, which was different from the Copenhagen General Population Study in terms of the observation time-points and monitoring method. Second, post-prandial reduction in LDL-C concentration is most likely haemodilution resulting from fluid intake in relation to the meal and thus adjusting the data for albumin concentration was recommended (7, 10). Langsted et al. (10) observed that the non-fasting LDL-C concentration no longer changed after adjustment for albumin concentration. However, a very slight change in the post-prandial albumin level was observed in our study; therefore, haemodilution may not be the only cause of post-prandial decline in the LDL-C level in the Chinese. Third, the diet structures of Chinese and western people are very different. For example, the Chinese people prefer carbohydrates (16). It is not clear whether the high-carbohydrate diet will cause a more significant decline in cholesterol. At any rate, the obvious decrease in non-fasting LDL-C might affect the evaluation of goal attainment when the LDL-C level was detected after a meal.

Indeed, non-HDL-C was more stable than LDL-C in assessing the percent attainment of non-fasting lipid for coronary heart disease patients. Non-fasting reduction in non-HDL-C was less than that in LDL-C and the difference between fasting and non-fasting percentage attainments of non-HDL-C <2.2 mmol/L was less than that of LDL-C <1.4 mmol/L. Non-HDL-C represents the cholesterol content of all atherosclerotic lipoproteins in the circulation, including chylomicrons, very-low-density-lipid and their remnants, intermediate-density lipoproteins, LDL, and lipoprotein (a) particles. Takahiro found that non-HDL cholesterol levels were clearly associated with future mortality and were less affected by fasting status or serum triglyceride levels (27). Meta-analyses and prospective studies with large populations supported the opinion that on-treatment levels of non-HDL-C were stronger than that of LDL-C for future CVD risk estimation (20, 21). Furthermore, non-HDL-C is a cheaper equivalent predictor of risk on and off statins, without the requirement for a fasting sample (28). Therefore, some scholars proposed that the clinical benefit obtained from controlling non-HDL-C would be greater than the one obtained from controlling LDL-C (19–21, 23).

Nevertheless, the percent attainment of non-HDL-C was higher than that of LDL-C in both fasting and non-fasting states according to the goals of LDL-C <1.4 mmol/L and non-HDL-C <2.2 mmol/L, respectively, in this study. The difference between non-HDL-C and LDL-C will increase with TG elevation, which could exert a substantial influence on evaluation of cholesterol-lowering treatment (29, 30). The fixed difference between fasting non-HDL-C and LDL-C goals was 30 mg/dl (i.e., 0.8 mmol/L) when fasting TG level was 1.7 mmol/L, reflecting the fact that cholesterol content within TG-rich lipoproteins was about 1.7/2.2 ≈ 0.8 mmol/L. Some scholars found that the goal attainment of non-HDL-C was higher than that of LDL-C when fasting TG was <1.7 mmol/L, while it was less than that of LDL-C when fasting TG >2.3 mmol/L (29). Su et al. reported that the specific and fixed goals as non-HDL-C 0.8 mmol/L (30 mg/dL) higher than the corresponding LDL-C goals were not sufficient for Chinese patients with CHD and proposed that flexible goals basing on TG level were more appropriate (30). This is consistent with our findings that the percent attainment of LDL-C <1.4 mmol/L was significantly lower than that of non-HDL-C <2.2 mmol/L in the fasting state; however, the difference in percent attainment between LDL-C and non-HDL-C after a daily breakfast became smaller with the increase in non-fasting TG level.

It was found that the percent attainment of post-prandial LDL-C was significantly higher than that of fasting values in the present study, suggesting that the fasting goals of LDL-C <1.4 mmol/L was indeed unsuitable for the evaluation of post-prandial cholesterol control. ROC analysis has been used to identify the optimal cut-off point for the diagnosis of post-prandial hypertriglyceridemia (16, 31, 32) but not for determining goals of LDL-C and non-HDL-C in the non-fasting state corresponding to the fasting goals. Because the non-fasting cut-off points acquired by ROC analysis corresponded to the fasting goals of LDL-C <1.4 mmol/L and non-HDL-C <2.2 mmol/L, the post-prandial percent attainments were very similar to their respective fasting values. This suggested that lower post-prandial cut-off

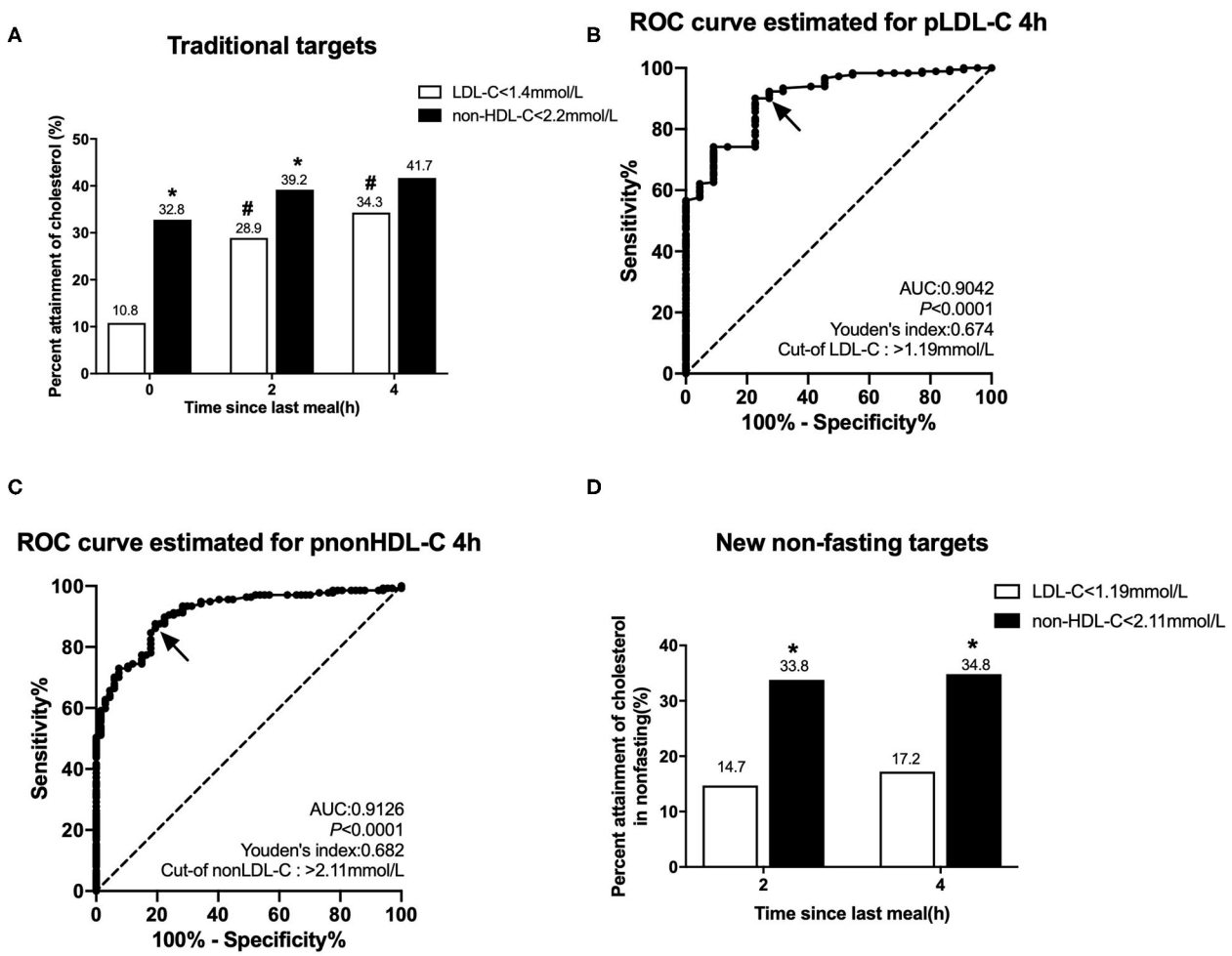

FIGURE 2 | Comparison of the percent attainments of LDL-C and non-HDL-C levels according to different targets in fasting and non-fasting states in Group CHD2. CHD2 group: CHD patients taking statins ≥1 m before admission. **(A)** Comparison of the percent attainments in both fasting and non-fasting states according to the recommended targets of LDL-C level <1.4 mmol/L and non-HDL-C level <2.2 mmol/L. **(B,C)** Non-fasting cut-off points in relation to fasting LDL-C level 1.4 mmol/L **(B)** and non-HDL-C level 2.2 mmol/L **(C)** determined by ROC analysis and Youden's index (marked by the solid arrows). **(D)** Comparison of the percent attainments according to non-fasting cut-off points of LDL-C <1.19 mmol/L and non-HDL-C <2.11 mmol/L. $^{\#}P < 0.05$ when compared with the percent attainment of the same target(s) in the fasting state. $^{*}P < 0.05$ when compared with the percent attainment of different LDL-C target at the same time point.

points, different from their fasting goals, should be adopted in the evaluation of post-prandial goal attainment, unless it is possible to assess the percentage reduction in the non-fasting LDL-C level. In this study, the difference (1.19 vs. 2.11 mmol/L) between non-fasting cut-off points of LDL-C and non-HDL-C was 0.92 mmol/L corresponding to non-fasting TG level of ∼2.0 mmol/L (i.e., $0.92 \times 2.2 = 2.024 \approx 2.0$). This suggests that a larger difference between LDL-C and non-HDL-C should be considered in the evaluation of non-fasting goal attainment even after a daily meal without high fat.

This study had some limitations. First, it was a single center study with a small sample size of inpatients. In the future, the suitability of non-fasting cut-off points in a large sample of arteriosclerotic cardiovascular disease patients, including patients with ischemic stroke and peripheral vascular disease, is worth exploring. Second, only the percent attainment of the goal, but not percentage reduction of LDL-C, was evaluated because of the lack of baseline levels of blood lipids. Third, it can only reflect the situation of patients admitted to the hospital. There are also a large number of outpatients with relatively stable conditions and their medication situation may be different from that of hospitalized patients. Therefore, the changes of post-prandial blood lipid may be different from our study. This needs further study in the future.

CONCLUSIONS

Non-HDL-C is more stable than LDL-C in assessing the percent attainment of non-fasting lipid for coronary heart disease patients. If we want to use LDL-C to assess the percent attainment of post-prandial blood lipids, we may need to determine a lower non-fasting cut-off point.

DATA AVAILABILITY STATEMENT

The original contributions generated for the study are included in the article/**Supplementary Material**, further inquiries can be directed to the corresponding author/s.

ETHICS STATEMENT

Written informed consent was obtained from the individual(s) for the publication of any potentially identifiable images or data included in this article.

AUTHOR CONTRIBUTIONS

L-LG, Y-qC, and LL designed and conducted of this study. Q-zL, FT, Q-YX, and L-yZ participated in the collection, analysis, and interpretation of the data. L-LG and TW contributed to the preparation of the manuscript. LL carried out the approval of the study. All authors read the study and approved the manuscript for publication.

FUNDING

This study has received support from the National Natural Science Foundation of China (grant numbers 81270956 and 81470577).

SUPPLEMENTARY MATERIAL

The Supplementary Material for this article can be found online at: https://www.frontiersin.org/articles/10.3389/fcvm.2021.649181/full#supplementary-material

REFERENCES

1. Mach F, Baigent C, Catapano AL, Koskinas KC, Casula M, Badimon L, et al. 2019 ESC/EAS Guidelines for the management of dyslipidaemias: lipid modification to reduce cardiovascular risk. *Eur Heart J.* (2019) 41:111–8. doi: 10.15829/1560-4071-2020-3826
2. Pastromas S, Terzi AB, Tousoulis D, Koulouris S. Postprandial lipemia: an under-recognized atherogenic factor in patients with diabetes mellitus. *Int J Cardiol.* (2008) 126:3–12. doi: 10.1016/j.ijcard.2007.04.172
3. Doran B, Guo Y, Xu J, Weintraub H, Mora S, Maron DJ, et al. Prognostic value of fasting versus nonfasting low-density lipoprotein cholesterol levels on long-term mortality: insight from the National Health and Nutrition Examination Survey III (NHANES-III). *Circulation.* (2014) 130:546–53. doi: 10.1161/CIRCULATIONAHA.114.010001
4. Langsted A, Nordestgaard BG. Nonfasting versus fasting lipid profile for cardiovascular risk prediction. *Pathology.* (2019) 51:131–41. doi: 10.1016/j.pathol.2018.09.062
5. Nordestgaard BG, Langsted A, Mora S, Kolovou G, Baum H, Bruckert E, et al. Fasting is not routinely required for determination of a lipid profile: clinical and laboratory implications including flagging at desirable concentration cut-points-a joint consensus statement from the European Atherosclerosis Society and European Federation of Clinical Chemistry and Laboratory Medicine. *Eur Heart J.* (2016) 37:1944–58. doi: 10.1093/eurheartj/ehw152
6. Steen DL, Khan I, Ansell D, Sanchez RJ, Ray KK. Retrospective examination of lipid-lowing treatment patterns in a real-world high-risk cohort in the UK in 2014: comparison with the National Institute for Health and Care Excellence (NICE) 2014 lipid modification guidelines. *BMJ Open.* (2017) 7:e013255. doi: 10.1136/bmjopen-2016-013255
7. Langsted A, Nordestgaard BG. Nonfasting lipids, lipoproteins, and apolipoproteins in individuals with and without diabetes: 58 434 individuals from the Copenhagen General Population Study. *Clin Chem.* (2011) 57:482–9. doi: 10.1373/clinchem.2010.157164
8. Downs JR, O'Malley PG. Management of dyslipidemia for cardiovascular disease risk reduction: synopsis of the 2014. U.S. Department of Veterans Affairs and U.S. Department of Defense clinical practice guideline. *Ann Intern Med.* (2015) 163:291–7. doi: 10.7326/M15-0840
9. Lin QZ, Chen YQ, Guo LL, Xiang QY, Tian F, Wen T, et al. Comparison of non-fasting LDL-C levels calculated by Friedewald formula with those directly measured in Chinese patients with coronary heart disease after a daily breakfast. *Clin Chim Acta.* (2019) 495:399–405. doi: 10.1016/j.cca.2019.05.010
10. Langsted A, Freiberg JJ, Nordestgaard BG. Fasting and nonfasting lipid levels: influence of normal food intake on lipids, lipoproteins, apolipoproteins, and cardiovascular risk prediction. *Circulation.* (2008) 118:2047–56. doi: 10.1161/CIRCULATIONAHA.108.804146
11. Mora S, Rifai N, Buring JE, Ridker PM. Fasting compared with nonfasting lipids and apolipoproteins for predicting incident cardiovascular events. *Circulation.* (2008) 118:993–1001. doi: 10.1161/CIRCULATIONAHA.108.777334
12. Stone NJ, Robinson JG, Lichtenstein AH, Bairey Merz CN, Blum CB, Eckel RH, et al. 2013 ACC/AHA guideline on the treatment of blood cholesterol to reduce atherosclerotic cardiovascular risk in adults: a report of the American College of Cardiology/American Heart Association Task Force on Practice Guidelines. *J Am Coll Cardiol.* (2014). 63:2889–934. doi: 10.1161/01.cir.0000437738.63853.7a
13. Joint committee for guideline revision National Expert Committee on Cardiovascular Diseases, National Center for Cardiovascular Diseases Chinese Society of Cardiology, Chinese Medical Association Chinese Diabetes Society, Chinese Medical Association Chinese Society of Endocrinology, Chinese Medical Association Chinese Society of laboratory Medicine, Chinese Medical Association Writing Group Members Group Leader, et al. 2016 Chinese guidelines for the management of dyslipidemia in adults. *J Geriatr Cardiol.* (2018). 15:1–29. doi: 10.11909/j.issn.1671-5411.2018.01.011
14. Catapano AL, Graham I, De Backer G, Wiklund O, Chapman MJ, Drexel H, et al. 2016 ESC/EAS guidelines for the management of dyslipidaemias. *Eur Heart J.* (2016) 37:2999–3058. doi: 10.1093/eurheartj/ehw272
15. Grundy SM, Stone NJ, Bailey AL, Beam C, Birtcher KK, Blumenthal RS, et al. 2018 AHA/ACC/AACVPR/AAPA/ABC/ACPM/ADA/AGS/APhA/ASPC/NLA/PCNA Guideline on the Management of Blood Cholesterol: A Report of the American College of Cardiology/American Heart Association Task Force on Clinical Practice Guidelines. *J Am Coll Cardiol.* (2019). 73:e285–350. doi: 10.1016/j.jacc.2018.11.004
16. Tian F, Xiang QY, Zhang MY, Chen YQ, Lin QZ, Wen T, et al. Changes in non-fasting concentrations of blood lipids after a daily Chinese breakfast in overweight subjects without fasting hypertriglyceridemia. *Clin Chim Acta.* (2019) 490:147–53. doi: 10.1016/j.cca.2019.01.004
17. Sidhu D, Naugler C. Fasting time and lipid levels in a community-based population: a cross-sectional study. *Arch Intern Med.* (2012) 172:1707–10. doi: 10.1001/archinternmed.2012.3708
18. Bansal S, Buring JE, Rifai N, Mora S, Sacks FM, Ridker PM. Fasting compared with nonfasting triglycerides and risk of cardiovascular events in women. *JAMA.* (2007) 298:309–16. doi: 10.1001/jama.298.3.309
19. Benn M. Apolipoprotein B levels, APOB alleles, and risk of ischemic cardiovascular disease in the general population, a review. *Atherosclerosis.* (2009) 206:17–30. doi: 10.1016/j.atherosclerosis.2009.01.004
20. Toth PP. Association of LDL cholesterol, non–HDL cholesterol, and apolipoprotein B levels with risk of cardiovascular events among patients treated with statins: a meta-analysis. *Yearbook Endocrinol.* (2012) 2012:65–8. doi: 10.1016/j.yend.2012.05.028

21. Ridker PM, Rifai N, Cook NR, Bradwin G, Buring JE. Non-HDL cholesterol, apolipoproteins A-I and B100, standard lipid measures, lipid ratios, and CRP as risk factors for cardiovascular disease in women. *JAMA*. (2005) 294:326–33. doi: 10.1001/jama.294.3.326
22. Di Angelantonio E, Gao P, Pennells L, Kaptoge S, Caslake M, Thompson A, et al. Lipid-related markers and cardiovascular disease prediction. *JAMA*. (2012) 307:2499–506. doi: 10.1001/jama.2012.6571
23. Carbayo Herencia JA, Simarro Rueda M, Palazon Bru A, Molina Escribano F, Ponce Garcia I, Artigao Rodenas LM, et al. Evaluation of non-HDL cholesterol as a predictor of non-fatal cardiovascular events in a prospective population cohort. *Clin Investig Arterioscler*. (2018) 30:64–71. doi: 10.1016/j.artere.2017.10.003
24. de Vries M, Klop B, Castro Cabezas M. The use of the non-fasting lipid profile for lipid-lowering therapy in clinical practice - point of view. *Atherosclerosis*. (2014) 234:473–5. doi: 10.1016/j.atherosclerosis.2014.03.024
25. Zhao Y, Peng R, Zhao W, Liu Q, Guo Y, Zhao S, et al. Zhibitai and low-dose atorvastatin reduce blood lipids and inflammation in patients with coronary artery disease. *Medicine*. (2017) 96:e6104. doi: 10.1097/MD.0000000000006104
26. Tian F, Wu CL, Yu BL, Liu L, Hu JR. Apolipoprotein O expression in mouse liver enhances hepatic lipid accumulation by impairing mitochondrial function. *Biochem Biophys Res Commun*. (2017) 491:8–14. doi: 10.1016/j.bbrc.2017.06.128
27. Ito T, Arima H, Fujiyoshi A, Miura K, Takashima N, Ohkubo T, et al. Relationship between non-high-density lipoprotein cholesterol and the long-term mortality of cardiovascular diseases: NIPPON DATA 90. *Int J Cardiol*. (2016) 220:262–7. doi: 10.1016/j.ijcard.2016.06.021
28. Welsh C, Celis-Morales CA, Brown R, Mackay DF, Lewsey J, Mark PB, et al. Comparison of conventional lipoprotein tests and apolipoproteins in the prediction of cardiovascular disease. *Circulation*. (2019) 140:542–52. doi: 10.1161/CIRCULATIONAHA.119.041149
29. Al-Hashmi K, Al-Zakwani I, Al Mahmeed W, Arafah M, Al-Hinai AT, Shehab A, et al. Non-high-density lipoprotein cholesterol target achievement in patients on lipid-lowering drugs and stratified by triglyceride levels in the Arabian Gulf. *J Clin Lipidol*. (2016) 10:368–77. doi: 10.1016/j.jacl.2015.12.021
30. Su X, Luo M, Tang X, Luo Y, Zheng X, Peng D, et al. Goals of non-high density lipoprotein cholesterol need to be adjusted in Chinese acute coronary syndrome patients: findings from the CCC-ACS project. *Clin Chim Acta*. (2019) 496:48–54. doi: 10.1016/j.cca.2019.06.022
31. White KT, Moorthy MV, Akinkuolie AO, Demler O, Ridker PM, Cook NR, et al. Identifying an optimal cutpoint for the diagnosis of hypertriglyceridemia in the nonfasting state. *Clin Chem*. (2015) 61:1156–63. doi: 10.1373/clinchem.2015.241752
32. Sevilla-Gonzalez MDR, Aguilar-Salinas CA, Munoz-Hernandez L, Almeda-Valdes P, Mehta R, Zubiran R, et al. Identification of a threshold to discriminate fasting hypertriglyceridemia with postprandial values. *Lipids Health Dis*. (2018) 17:156. doi: 10.1186/s12944-018-0803-8

Conflict of Interest: The authors declare that the research was conducted in the absence of any commercial or financial relationships that could be construed as a potential conflict of interest.

frontiers in Cardiovascular Medicine

ORIGINAL RESEARCH
published: 23 April 2021
doi: 10.3389/fcvm.2021.652746

Plasma Metabolites Alert Patients With Chest Pain to Occurrence of Myocardial Infarction

Nan Aa[1†], Ying Lu[2†], Mengjie Yu[3†], Heng Tang[1], Zhenyao Lu[3], Runbing Sun[3], Liansheng Wang[1], Chunjian Li[1], Zhijian Yang[1], Jiye Aa[3], Xiangqing Kong[1*] and Guangji Wang[3]*

[1] Department of Cardiology, The First Affiliated Hospital of Nanjing Medical University, Nanjing, China, [2] Department of Laboratory, The First Affiliated Hospital of Nanjing Medical University, Nanjing, China, [3] Laboratory of Metabolomics, Jiangsu Key Laboratory of Drug Metabolism and Pharmacokinetics, China Pharmaceutical University, Nanjing, China

OPEN ACCESS

Edited by:
Kunhua Song, University of Colorado Anschutz Medical Campus, United States

Reviewed by:
Jan F. C. Glatz, Maastricht University, Netherlands
Tetsuro Miyazaki, Juntendo University Urayasu Hospital, Japan

***Correspondence:**
Jiye Aa
jiyea@cpu.edu.cn
Xiangqing Kong
kongxq@njmu.edu.cn

[†]These authors have contributed equally to this work

Specialty section:
This article was submitted to Cardiovascular Metabolism, a section of the journal Frontiers in Cardiovascular Medicine

Received: *13 January 2021*
Accepted: *18 March 2021*
Published: *23 April 2021*

Citation:
Aa N, Lu Y, Yu M, Tang H, Lu Z, Sun R, Wang L, Li C, Yang Z, Aa J, Kong X and Wang G (2021) Plasma Metabolites Alert Patients With Chest Pain to Occurrence of Myocardial Infarction. Front. Cardiovasc. Med. 8:652746. doi: 10.3389/fcvm.2021.652746

Myocardial infarction (MI) is one of the leading causes of death worldwide, and knowing the early warning signs of MI is lifesaving. To expand our knowledge of MI, we analyzed plasma metabolites in MI and non-MI chest pain cases to identify markers for alerting about MI occurrence based on metabolomics. A total of 230 volunteers were recruited, consisting of 146 chest pain patients admitted with suspected MI (85 MIs and 61 non-MI chest pain cases) and 84 control individuals. Non-MI cardiac chest pain cases include unstable angina (UA), myocarditis, valvular heart diseases, etc. The blood samples of all suspected MI cases were collected not longer than 6 h since the onset of chest pain. Gas chromatography–mass spectrometry and liquid chromatography–mass spectrometry were applied to identify and quantify the plasma metabolites. Multivariate statistical analysis was utilized to analyze the data, and principal component analysis showed MI could be clearly distinguished from non-MI chest pain cases (including UA and other cases) in the scores plot of metabolomic data, better than that based on the data constructed with medical history and clinical biochemical parameters. Pathway analysis highlighted an upregulated methionine metabolism and downregulated arginine biosynthesis in MI cases. Receiver operating characteristic curve (ROC) and adjusted odds ratio (OR) were calculated to evaluate potential markers for the diagnosis and prediction ability of MI (MI vs. non-MI cases). Finally, gene expression profiles from the Gene Expression Omnibus (GEO) database were briefly discussed to study differential metabolites' connection with plasma transcriptomics. Deoxyuridine (dU), homoserine, and methionine scored highly in ROC analysis (AUC $>$ 0.91), sensitivity ($>$80%), and specificity ($>$94%), and they were correlated to LDH and AST ($p < 0.05$). OR values suggested, after adjusting for gender, age, lipid levels, smoking, type II diabetes, and hypertension history, that high levels of dU of positive logOR = 3.01, methionine of logOR = 3.48, and homoserine of logOR = 1.61 and low levels of isopentenyl diphosphate (IDP) of negative logOR = −5.15, uracil of logOR = −2.38, and arginine of logOR = −0.82 were independent risk factors of MI. Our study highlighted that metabolites belonging to pyrimidine, methionine, and arginine metabolism are deeply influenced in MI plasma

samples. dU, homoserine, and methionine are potential markers to recognize MI cases from other cardiac chest pain cases after the onset of chest pains. Individuals with high plasma abundance of dU, homoserine, or methionine have increased risk of MI, too.

Keywords: myocardial infarction, risk factors, biomarker, metabolomics, arginine, deoxyuridine

INTRODUCTION

A strangling feeling in the chest is a typical manifestation of coronary artery disease (CAD). In most cases, CAD develops as plaque builds up on the artery walls. When it progresses to myocardial infarction (MI), coronary heart disease will be life-threatening and extremely dangerous in the ensuing days or weeks due to its various fatal complications. Thus, its diagnosis and treatment is urgent. However, chest pain can be caused by other cardiovascular events or heart diseases (e.g., unstable angina, myocarditis) (1). Although there are cardiac damage biomarkers, such as creatine kinase-MB (CK-MB), aspartate aminotransferase (AST), and cardiac troponins (cTnT, cTnI), they are usually related to tissue damage only and not specific to MI. For example, cTnT elevation can also be observed in myocarditis, hypertrophic cardiomyopathy, sometimes unstable angina, etc. Sometimes, unexpected elevation of the markers can also be observed without obvious connection to cardiac injury (2–4).

With the development of metabolomics, more and more small molecule metabolic markers will be identified, analyzed, and studied. The newly found differential metabolites between MI cases and non-MI chest pain cases will expand our knowledge of myocardial infarction development. Since ischemic heart diseases are characterized by profound metabolic shifts at both the circulatory and local levels (5), metabolomics has been applied to study the metabolic pattern changes detected in the blood of CAD patients. Early in 2002, a pioneering work was published showing that NMR-based metabolomics had the potential to rapidly and non-invasively diagnose the presence and severity of coronary heart disease (6). In 2005, Marc Sabatine and his colleagues identified metabolic biomarkers of myocardial ischemia associated with physical exercise (7). Later studies focused on identifying biomarkers and metabolic pathways and exploring the underlying mechanisms associated with cardiovascular diseases (8–14). A panel of potential markers has been suggested for coronary heart diseases, such as arginine and homocysteine, and the underlying mechanisms of their action have been explored (15–17). However, candidate metabolites to recognize MI cases from other cardiac chest pain cases remain to be further studied and improved.

In this study, we mainly focus on detecting and assessing metabolites' ability to discriminate MI cases from non-MI chest pain cases. A metabolomic platform with GC/MS and LC/MS instrumentation was employed to profile plasma metabolites of hospitalized patients with chest pain (including MI and non-MI chest pain cases) and their controls. We first applied multivariate statistical analysis to address our question about how good these identified metabolites detect MI cases. Then, medical history and laboratory test variables (e.g., sex, age, smoking history, function of the primary organs, and biochemical assays) were introduced as variables in a new model and analyzed in the same way. Their performance can be demonstrated in PCA and OPLS-DA plots. Next, metabolic patterns were evaluated, and metabolic markers were screened and described based on semiquantitative data, ROC analysis, odds ratios (OR) (18), and their relations to well-recognized cardiovascular disease risk factors. Considering that plasma cells affect plasma metabolites most directly, the connection between plasma cells and metabolites is briefly explained in the discussion.

MATERIALS AND METHODS

Human Plasma Collection

A total of 84 individual controls (social recruitment) and 146 chest pain cases highly suspected of MI were recruited from October 2017 to March 2018. (Exclusions include coma, fever, NYHA IV heart failure, hepatic decompensation, renal failure, cancers, and uncontrolled endocrine and hematological diseases.) After routine diagnostic procedures, including ECGs, infarction biomarkers, and coronary angiography (or coronary CT angiography, CCTA), 85 were later confirmed to be non-ST-elevation myocardial infarction (NSTEMI) or ST-elevation myocardial infarction (STEMI) as the MI cases (MIs), and the remaining 61 were confirmed to be non-MI chest pain cases (non-MIs). All the non-MIs include 34 unstable angina (UA) cases and 27 other non-MI cardiac cases (non-MICs), including myocarditis, valvular heart diseases, atrial fibrillation, etc (**Figure 3A**). The blood samples of the patients were collected not longer than 6 h since the onset of chest pain symptoms, before reperfusion therapy.

The study followed the principles outlined in the Declaration of Helsinki, and informed written consent was given prior to the inclusion of subjects in the study. The study was also under the guidance and supervision of the Ethics Committee of the First Affiliated Hospital of Nanjing Medical University (*Lot number: 2018-SR-028*). The venous blood samples were collected from fasting state volunteers in EDTA-Na anticoagulated tubes in the morning. Within 2 h, blood samples were centrifuged at 1,000 g for 5 min, and each of the supernatant plasma was transferred to another tube, frozen at −80°C in a refrigerator. Before using the plasma samples, they were thawed by incubation at 37°C bath for 15 min, vortexed, and centrifuged at 650 g for 5 min.

Abbreviations: MI, myocardial infarction; CAD, coronary artery disease; UA, unstable angina; AUC, area under the ROC curve; QC, quality control; IS, internal standard; VIP, variable importance; OR, odds ratio; dU, deoxyuridine; TAC, transverse aortic constriction; GEO, Gene Expression Omnibus; IDP, isopentenyl diphosphate; CDA, cytidine deaminase; UPP1, uridine phosphorylase 1.

Equipment for Blood Examinations

The instrument blood count, SYSMEX model xn-10, is made in Hyogo, Japan. Both NT-proBNP and serum infarction markers (cTns) are analyzed in Roche Cobas 6000 (produced in Mannheim, Germany). The blood biochemical instrument is AU5800 from Beckman Coulter of the United States, produced in Shizuoka, Japan.

Chemicals and Reagents

Stable isotope internal standard 5-^{13}C-glutamine was purchased from Cambridge Isotope Laboratories (Andover, MA, USA). Myristic-1,2-^{13}C2 acid, methoxamine hydrochloride (purity 98%), and pyridine (≥99.8% GC) were purchased from Sigma-Aldrich (St. Louis, MO, USA). N-methyl-trimethylsilyl-trifluoroacetamide (MSTFA) and 1% trimethylchlorosilane (TMCS) were provided by Pierce Chemical (Rockford, IL, USA). Methanol, acetonitrile, and *n*-heptane were of HPLC grade and obtained from Merck (Darmstadt, Germany). Purified water was produced by a Milli-Q system (Millipore, Bedford, MA, USA). Ammonium acetate (purity 98.0%) and ammonia solution (25%, w/w) were purchased from Aladdin (Shanghai, China) and Nanjing Chemical Reagent (Nanjing, China), respectively.

Method S1 GC/MS Analysis, Instrumental Setting, and Parameters

The plasma samples were pretreated, extracted, and derivatized in a similar way to that reported previously (19). Briefly, an aliquot of plasma (50 μl) was added to 200 μl methanol (containing internal standard [^{13}C2]-myristic acid, 2.5 μg, 12.5 μg/ml) for GC/MS analysis and vigorously vortex-extracted for 5 min, and then placed in a fridge at 4°C for 1 h. After centrifuging at 20,000 g for 10 min in the SORVALL Biofuge Stratos centrifuge (Sollentum, Germany), a 200-μl aliquot of the supernatant was transferred into a GC vial and evaporated to dryness in a SpeedVac concentrator (Thermo Fisher Scientific, Savant™ SC250EXP, Holbrook, USA).

For GC/MS analysis, the dried plasma samples were then methoxymated, where 30 μl of 1% methoxyamine pyridine solution was added to the residue and incubated for 16 h at room temperature. Then, the analytes were trimethylsilylated using 30 μl of MSTFA containing 1% v/v trimethylchlorosilane (TMCS) as a catalyst. After trimethylsilylation for 1 h, 30 μl of *n*-heptane containing methyl myristate (30 μg/ml) was added into each GC vial as external standard to monitor the stability of GC/S instruments. The final mixture (90 μl in total) was vortexed for 1 min and was then ready for GC/MS analysis.

The derivatized samples were analyzed using gas chromatography coupled to a mass spectrometer (Shimadzu GCMS-QP2010 Ultra, Kyoto, Japan) equipped with an automatic sampler (Shimadzu AOC-20i, Kyoto, Japan). A 0.5-μl sample aliquot was injected into a liner connected with the Rtx-5MS capillary column (0.25 mm × 30 m × 0.25 μm, Restek, PA, USA) in split mode (split ratio 8:1). The injector temperature was set at 250°C. The septum purge was turned on with a flow rate of 6.0 ml/min. Helium was used as the carrier gas at a flow rate of 1.5 ml/min. The column temperature was initially maintained at 80°C for 5 min, then raised to 300°C at a rate of 20°C/min, and held for 5 min. The mass spectrometer ion source temperature was 220°C, and ionization was achieved with a 70-eV electron beam. Mass spectra were detected at −1,570 V, obtained from *m*/*z* 50 to 700 in a full scan mode, with each run of 19 min and a solvent cutting acquisition at 4.5 min. The quality control (QC) samples were prepared for the pool of plasma, with the same preparation procedure as mentioned above. To minimize systematic variations, all samples were analyzed at random order, with QC samples inserted.

LC/MS Analysis, Instrumental Setting, and Parameters

The plasma samples were pretreated and extracted in the same way as in GC/MS analysis with a few modifications, which used the other internal standard of 5-^{13}C-glutamine dissolved in methanol at 15 μg/ml. After vortexing and centrifugation, the final supernatant was transferred into an LC vial.

After evaporation, the residue was redissolved with 100 μl distilled water and centrifuged at 18,000 g for 5 min. Finally, 80 μl supernatant was transferred to an LC vial, and 10 μl was injected for UPLC-QTOF/MS analysis. Similarly, the QC samples were inserted and analyzed to check the stability of the system.

The HPLC-QTOF/MS analysis was carried out as previously reported (20). The chromatographic separation of the analyses was achieved with an Amide XBridge HPLC column (3.5 μm; 4.6 mm × 100 mm; Waters, USA). The column temperature was set to 40°C. The HPLC system consisting of a LC-30A binary pump, a SIL-30AC autosampler, and a CTO-30AC column oven (Shimadzu, Japan) was coupled with a hybrid quadrupole time-of-flight tandem mass spectrometer (AB SCIEX TripleTOF® 5600, Foster City, CA). The mobile phase was composed of 5 mM ammonium acetate in ultrapure water (pH = 9.0 ± 0.1 with ammonia) plus 5% acetonitrile (solvent A) and acetonitrile (solvent B). The mobile phase was delivered at 0.4 ml/min using a solvent gradient as follows: 0–3 min, 85% B; 3–6 min, 85–30% B; 6–15 min, 30–2% B; 15–18 min, 2% B; 18–19 min, 2–85% B; and 19–26 min, 85% B. A Turbo V electrospray ionization (ESI) was used in MS detection with negative ion modes. In the ESI source, parameters were set as follows: gas 1 pressure at 50 psi, gas 2 at 30 psi, and curtain gas at 30 psi; ion spray voltage was set at −4,500 V; turbo spray temperature was set at 500°C. Metabolic features were scanned in time-of-flight mass spectrometry over *m*/*z* 50–1,000, and the product ions were scanned over *m*/*z* 50–900, with declustering potential at −100 V and a collision energy at −35 V. The detected ions were all calibrated with the accurate masses of the reference standards containing amino-dPEG®4-acid (MW265.30, CAS: 663921-15-1), amino-dPEG®6-acid (MW353.41, CAS: 905954-28-1), amino-dPEG®8-acid (MW441.51, CAS: 756526-04-2), amino-dPEG®12-acid (MW617.72, CAS: 756526-07-4), and sulfinpyrazone (MW404.48, CAS: 57-96-5), for every eight samples.

Multivariate Statistical Analysis

Missing data were excluded before the analysis. After normalization against the IS, the data were evaluated using SIMCA-P 14.1 software (Umetrics, Umeå, Sweden) (21).

Principal component analysis (PCA), partial least square to latent structure discriminant analysis (PLS-DA), and orthogonal PLS-DA (OPLS-DA) models were built and plotted to show the clustering or separation of samples from different groups. For PLS-DA modeling, samples from the different groups were classified such that all samples were divided into different groups (e.g., MIs, non-MIs, controls, etc.) as the qualitative "dummy" variables, *Y*. The goodness of fit for the models was evaluated using three quantitative parameters: R^2X and R^2Y are the explained variation in *X* and *Y*, respectively, and Q^2Y is the predicted variation in *Y*. Permutation test was assessed for model validation, where a higher level of R^2Y and Q^2Y and a lower value of the intercept of R^2 (lower than 0.2) and Q^2 (lower than 0.0) suggested good model and prediction ability.

Discriminant Metabolites and Statistical Analysis

After normalization against the IS, all the semiquantitative data from both GC/MS and UPLC-QTOF/MS were logarized so that the state probabilities of the data queue tended to a normal distribution. The discriminant metabolites between groups were screened and chosen based on variable importance (VIP) using SIMCA-P 14.1 and the independent sample *t*-test of the logarized data using SPSS (version 23.0, SPSS Inc., Chicago, IL, USA). Fold change is calculated using raw but normalized data.

Metabolic pathway enrichment and topology analysis was performed online, using MetaboAnalyst 3.0 (https://www.metaboanalyst.ca/). The KEGG ID of discriminatory compounds was uploaded and embedded in human pathway library for pathway analysis and hypergeometric tests, with the pathway analysis algorithms of Fisher's exact test, topology algorithms of relative betweenness centrality, and KEGG pathway library version of *Homo sapiens*.

For data inconformity with normal distribution from clinical assaying, a non-parametric test (Mann–Whitney *U*-test, two-sided) was employed to evaluate statistical significance. ROC analysis and (adjusted) OR calculations were performed using SPSS as well. Before computing the OR value, the logarized data of a metabolite (*i*) for each subject of OR*i* were normalized by subtracting the mean value of ORmean within this group, and then divided by the standard deviation (SD) within the group, shown as the normalized ORs = (OR*i* – ORmean)/SD.

Transcriptomics Database

We studied transcriptomics data from the GEO database. The human myocardial infarction plasma data are from GSE48060 (https://www.ncbi.nlm.nih.gov/geo/query/acc.cgi?acc=GSE48060) and GSE103182 (https://www.ncbi.nlm.nih.gov/geo/query/acc.cgi?acc=GSE103182). Mice myocardial data are from GSE775 (https://www.ncbi.nlm.nih.gov/geo/query/acc.cgi?acc=GSE775). The data matrix was directly extracted by GEOquery in R 4.0.3. Limma package was used to produce false discovery rate (FDR), fold change (FC), and *p*-value.

RESULTS

Clinical Descriptions of Control, MI, and Non-MI Cases

Tables 1, **2** show the medical records and basic laboratory tests of the volunteers. Generally, higher glucose, AST, lactate dehydrogenase (LDH), hydroxybutyrate dehydrogenase (HBDH), and CK levels and lower albumin (ALB) and Ca^{2+} concentrations were detected in patients with chest pain. Among the 146 patients with cardiac chest pain, ∼65% had taken aspirin and statin treatments before blood collection. As a result, total cholesterol (TC), triglycerides (TG), low-density lipoprotein cholesterol (LDL-C), and high-density lipoprotein cholesterol (HDL-C) levels were all lower in chest pain inpatients than the controls.

Based on clinical parameters (listed in **Table 1** "variables"), including "biochemical items," "demographics," and "cardiac risk factors," an unsupervised PCA score plot was created. The model indicated a few outliers when the samples were either divided into three (controls, MIs, non-MIs) or four groups (controls, UA, MIs, and other non-MICs), and each of the groups generally overlapped with the others (**Figures 1A1,A2**). However, a supervised PLS-DA revealed a visible separation of the groups with only a little overlap when the samples were divided into three groups, i.e., MIs, non-MIs, and controls. When the samples were divided into four groups (MIs, UAs, other non-MICs, and controls), the controls, UAs, and MIs were fairly well-separated, but the other non-MICs primarily showed overlaps with UAs and MIs (**Figures 1A3,A4**). These findings suggest that the model was not powerful at differentiating non-MICs from MIs and UAs based on basic laboratory tests and history examinations.

Plasma Metabolomic Description of Chest Pain Individuals by PCA and OPLS-DA Plots

GC/MS and LC/MS analysis of the plasma samples aligned the metabolites in typical chromatograms (**Supplementary Figures 1, 2**). Deconvolution of the GC/MS chromatograms produced 135 independent peaks from the plasma samples, 83 of which were authentically identified as metabolites; LC/MS produced 279 peaks, and 76 metabolites were identified (**Supplementary Tables 1, 2**). Quantitative data were acquired for each metabolite in the plasma samples of the control, MI, UA, and other non-MI cardiac cases.

Based on the metabolomic data derived from GC/MS and LC/MS analysis, the PCA score plot again showed a few outliers when the samples were divided into three or four groups, as indicated above (**Figure 3A**). Unlike with the clinical data, unsupervised PCA analysis of metabolomic data showed that the majority of MIs deviated from the others, regardless of whether the three or four groups were defined, although the control, non-MICs, and UAs overlapped with each other to some extent (**Figures 1B1,B2**). This suggests that the identified plasma substances can naturally detect the difference between MI and

TABLE 1 | Sample characteristics: controls vs. all the chest pain cases.

Clinical concerns	Variables	Controls $n = 84$	Chest pain cases $n = 146$	Statistics p-values
Demographics	Male	56	99	0.26
	Age (years)	50.25 ± 1.76	59.28 ± 1.83	0.00
Cardiac risk factors	Hypertension	32	83	0.00
	Diabetes	8	36	0.00
	TC (mmol/L)	4.93 ± 0.15	4.08 ± 0.11	0.00
	TG (mmol/L)	1.43 ± 0.12	1.51 ± 0.08	0.17
	LDL-C (mmol/L)	3.15 ± 0.11	2.70 ± 0.08	0.00
	HDL-C (mmol/L)	**1.31 ± 0.04**	**0.95 ± 0.02**	0.00
	LPa (mg/L)	**349.35 ± 51.45**	**339.39 ± 27.47**	0.65
	Tobacco use	8	43	0.00
	Drinking history	0	16	0.00
Cardiovascular medications	Aspirin	1	88	0.00
	Statin therapy	6	94	0.00
	β-Blockers	0	7	0.00
Prior cardiovascular disease	2	22	0.01	
Biochemical items	ALT (U/L)	27.15 ± 2.48	39.33 ± 2.90	0.00
	AST (U/L)	26.31 ± 1.45	**77.35 ± 9.78**	0.00
	ALP (U/L)	78.20 ± 2.19	86.16 ± 2.26	0.03
	GGT (U/L)	30.69 ± 2.75	45.18 ± 3.80	0.02
	LDH (U/L)	169.30 ± 3.85	**398.72 ± 32.22**	0.00
	CK (U/L)	119.30 ± 11.27	**480.97 ± 78.58**	0.94
	HBDH (U/L)	107.80 ± 3.87	**297.38 ± 28.85**	0.00
	TBIL (μmol/L)	14.36 ± 0.56	13.74 ± 0.71	0.03
	DBIL (μmol/L)	4.51 ± 0.28	4.96 ± 0.26	0.83
	IBIL (μmol/L)	9.16 ± 0.42	8.77 ± 0.48	0.05
	TP (g/L)	70.80 ± 0.47	61.12 ± 0.48	0.00
	ALB (g/L)	44.68 ± 0.54	**35.80 ± 0.36**	0.00
	GLB (g/L)	25.78 ± 0.48	25.33 ± 0.39	0.14
	ALB/GLB	1.79 ± 0.05	1.45 ± 0.03	0.00
	GLU (mmol/L)	5.77 ± 0.13	6.01 ± 0.22	0.23
	Urea (mmol/L)	5.13 ± 0.18	7.37 ± 0.52	0.00
	Cr (μmol/L)	71.14 ± 2.00	102.13 ± 11.16	0.00
	UA (μmol/L)	325.57 ± 9.61	378.91 ± 13.24	0.04
	Ca (mmol/L)	2.36 ± 0.02	**2.17 ± 0.01**	0.00

Values are presented as mean ± SE. The Mann–Whitney U-test was applied to produce p-value. Bold values are abnormal findings of the test results.

other samples (including healthy controls, UA) and there are MI marker metabolites in the metabolite profile.

The supervised PLS-DA model revealed that samples from each group clustered closely and anchored away from the other groups when the samples were divided into three groups (**Figure 1B3**). When the samples were divided into four groups, the majority of MIs and controls clustered separately, while the UAs and non-MICs primarily overlapped with each other, with a minority overlapping with MIs and controls (**Figure 1B4**). The distant separation of MIs from the other groups suggested distinctly different metabolic patterns between MIs and the groups of UA and non-MICs, while the overlapping of the groups suggested similar plasma metabolic patterns between UA and the other non-MICs. In general, metabolomic data better characterized MIs than history examinations and laboratory tests, and the score plot of non-MI chest pain cases (including UA and non-MI cardiac cases) indicated that they had moderate metabolic perturbation relative to the MI cases because they anchored between MI and the controls (**Figure 1B3**). The above data suggest that subgroups of MI can be recognized by multivariate analysis of identified plasma metabolites more effectively than by routine clinical parameters.

Pathway Analysis of Differential Metabolites

OPLS-DA analysis showed a different metabolomic pattern of the non-MIs from the controls (**Figure 2A1**). Statistical analysis suggested 50 discriminant metabolites ($p < 0.05$) that differentiated non-MI chest pain inpatients from the

TABLE 2 | Sample characteristics: MI vs. non-MI chest pain cases.

Clinical concerns	Variables	Controls	Chest pain cases		Statistics
		(*n* = 84)	Non-MI (*n* = 61)	MI (*n* = 85)	*p*-values
Demographics	Male	56	32	67	0.00
	Age (years)	50.25 ± 1.76	60.18 ± 2.42	65.08 ± 1.60	0.12
Cardiac risk factors	Hypertension	32	32	51	0.28
	Diabetes	8	8	28	0.01
	Tobacco use	8	8	35	0.00
	TC (mmol/L)	4.93 ± 0.15	3.69 ± 0.12	4.28 ± 0.15	0.01
	TG (mmol/L)	1.43 ± 0.12	1.26 ± 0.09	1.65 ± 0.11	0.02
	LDL-C (mmol/L)	3.15 ± 0.11	2.40 ± 0.09	2.86 ± 0.11	0.01
	HDL-C (mmol/L)	1.31 ± 0.04	**0.96 ± 0.03**	**0.94 ± 0.03**	0.70
	LPa (mg/L)	**349.35 ± 51.45**	**334.55 ± 47.64**	**341.96 ± 33.82**	0.56
Prior cardiovascular disease	2	12	10	0.24	
Serum biomarkers	cTnT (ng/ml)	–	**756.13 ± 242.59**	**1,559.30 ± 276.64**	0.56
	CK-MB (U/L)	–	24.98 ± 6.08	**32.10 ± 5.89**	0.68
	Mb (ng/ml)	–	59.30 ± 23.79	66.99 ± 15.32	0.46
Biochemical items	ALT (U/L)	27.15 ± 2.48	32.17 ± 4.59	43.14 ± 3.65	0.04
	AST (U/L)	26.31 ± 1.45	29.12 ± 2.91	**102.99 ± 14.10**	0.00
	LDH (U/L)	169.30 ± 3.85	213.05 ± 10.22	**497.43 ± 45.36**	0.00
	CK (U/L)	119.30 ± 11.27	86.83 ± 12.99	**690.51 ± 113.49**	0.00
	HBDH (U/L)	107.80 ± 3.87	132.79 ± 6.71	**384.89 ± 40.81**	0.00
	TP (g/L)	70.80 ± 0.47	**61.95 ± 0.71**	**60.68 ± 0.62**	0.18
	GLU (mmol/L)	5.77 ± 0.13	5.49 ± 0.22	**6.28 ± 0.32**	0.06
	Ca (mmol/L)	2.36 ± 0.02	2.20 ± 0.02	**2.16 ± 0.02**	0.11

Values are presented as mean ± SE. The Mann–Whitney U-test was applied to produce p-value between MI and non-MI chest pain cases. Bold values are abnormal findings of the test results.

controls (**Table 3**, S-plot: **Figure 2A2**). Similarly, MI cases primarily showed different metabolomic patterns from non-MIs (**Figure 2B1**). According to the statistical analysis and the VIP values, 54 discriminant metabolites were identified between MIs and non-MIs (**Table 3**, S-plot: **Figure 2B2**).

Of the 50 metabolites differentiating non-MIs from the controls, the levels of gluconic acid and isoleucine were higher in non-MIs, while succinate, inosine, and arginine were lower, and all the above metabolites deviated further in MIs (**Figures 3C,D**). These findings indicate that the above metabolites are involved in the development of cardiac damage (from averagely very small damage to severe infarction).

Although glycerol, salicylic acid, and deoxyadenosine showed significant differences between the non-MI and control groups, they had no significant difference between the MI and non-MI cardiac groups. These are, thus, suggested as markers of non-MI chest pain. In addition to endogenous metabolites, we found that salicylic acid, an exogenous metabolite, also characterized the group of chest pain cases. Salicylic acid is the primary metabolite of aspirin, and a review of inpatient information and clinical data revealed that a large portion of chest pain patients had taken aspirin for the management of CAD.

Moreover, deviated levels of dU, methionine, homoserine, etc. were only observed in MI cases (vs. non-MI chest pains), and no significant difference was observed between the controls and non-MIs, indicating their association with the development of MI (**Figure 3B**).

The differential metabolites between acute coronary syndrome (ACS, including UA and MI) and healthy individuals (ACS vs. control) can play roles in lipid plaque rupture; thus, they have the potential in alerting the occurrence of ACS. We found 127 identified differential metabolites. **Supplementary Table 3** lists the top 20 metabolites (sort by *p*), and most of them are amino acids. KEGG analysis highlighted ACS's upregulated cysteine and methionine metabolism, phenylalanine metabolism, and synthesis and degradation of ketone bodies pathway and downregulated arginine biosynthesis, purine metabolism, and pyrimidine metabolism (FDR < 0.05). The metabolites with large FCs are salicylic acid, dU, guanosine diphosphate, gluconic acid, homocysteine, NADPH, methionine, tryptophan, mannopyranose, and isoleucine (top 10, FC > 1, $p < 0.05$). The metabolites with the smallest FCs ($p < 0.05$, FC < 1) are succinate, isopentenyl diphosphate (IDP), glutamine, inosine, uracil, citrate, lysine, N-acetylornithine, indole-3-propanate, and alanine.

A Venn diagram was created to show the discriminant metabolites between MI and non-MIs and those between non-MIs and controls. The overlapping region (B) in the Venn diagram (**Figure 3E**) lists the metabolites screened out in both of the two comparison groups, suggesting that they were

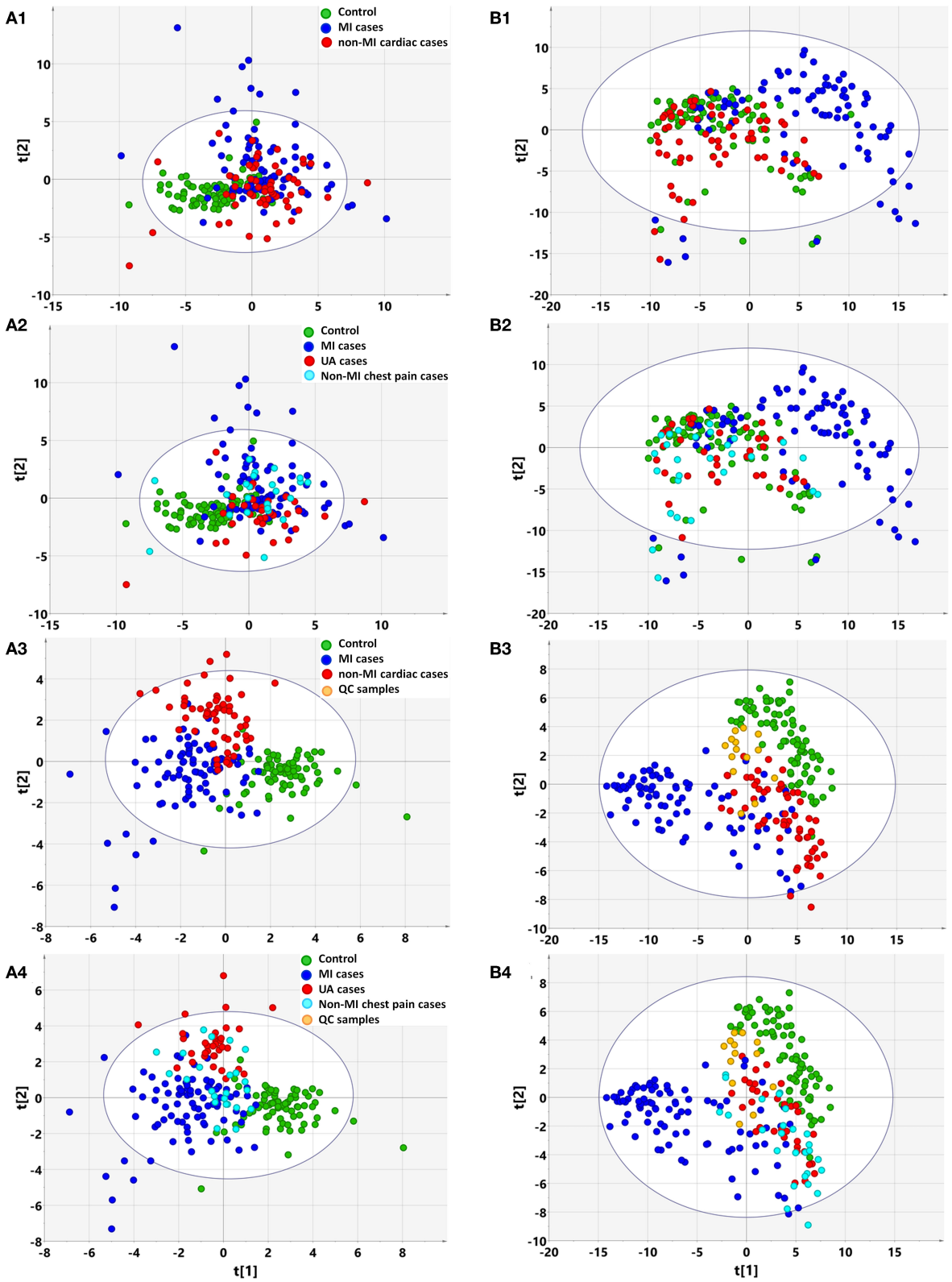

FIGURE 1 | Multivariate statistical analysis differentiates the groups of myocardial infarction (MI) cases, non-MI chest pain cases, and controls based on clinical information **(A)** and metabolomic data **(B)**, respectively. (1) Non-supervised PCA modeling displays the original similarity of the three groups: MI cases ($n = 85$), non-MI chest pain cases ($n = 61$), and controls ($n = 84$), without arbitrary grouping. (2) Non-supervised PCA modeling displays the original similarity of the four groups: MI

(Continued)

FIGURE 1 | cases, unstable angina (UA), other non-MI cardiac cases, and controls, without arbitrary grouping. **(A1,A2)** PC1: $R^2X(\text{cum}) = 0.0895$, $Q^2(\text{cum}) = 0.0106$; PC2: $R^2X(\text{cum}) = 0.167$, $Q^2(\text{cum}) = 0.0356$. **(B1,B2)** PC1: $R^2X(\text{cum}) = 0.205$, $Q^2(\text{cum}) = 0.189$; PC2: $R^2X(\text{cum}) = 0.310$, $Q^2(\text{cum}) = 0.274$; PC3: $R^2X(\text{cum}) = 0.386$, $Q^2(\text{cum}) = 0.338$. (3) Supervised PLS-DA modeling with the three groups: MI cases, non-MI chest pain cases, and controls. **(A3)** PC1: $R^2X(\text{cum}) = 0.073$, $R^2Y(\text{cum}) = 0.339$, $Q^2(\text{cum}) = 0.270$; PC2: $R^2X(\text{cum}) = 0.128$, $R^2Y(\text{cum}) = 0.544$, $Q^2(\text{cum}) = 0.362$; PC3: $R^2X(\text{cum}) = 0.174$, $R^2Y(\text{cum}) = 0.635$, $Q^2(\text{cum}) = 0.394$. Permutation tests with the intercepts of $R^2 < 0.23$, $Q^2 < -0.20$. **(B3)** PC1: $R^2X(\text{cum}) = 0.184$, $R^2Y(\text{cum}) = 0.215$, $Q^2(\text{cum}) = 0.207$; PC2: $R^2X(\text{cum}) = 0.249$, $R^2Y(\text{cum}) = 0.400$, $Q^2(\text{cum}) = 0.377$; PC3: $R^2X(\text{cum}) = 0.315$, $R^2Y(\text{cum}) = 0.547$, $Q^2(\text{cum}) = 0.512$. Permutation tests with the intercepts of $R^2 < 0.10$, $Q^2 < -0.05$. (4) Supervised PLS-DA modeling with the four groups: MI cases ($n = 85$), UA ($n = 34$), other non-MI cardiac cases ($n = 27$), and controls ($n = 84$). **(A4)** PC1: $R^2X(\text{cum}) = 0.073$, $R^2Y(\text{cum}) = 0.259$, $Q^2(\text{cum}) = 0.198$; PC2: $R^2X(\text{cum}) = 0.132$, $R^2Y(\text{cum}) = 0.397$, $Q^2(\text{cum}) = 0.269$; PC3: $R^2X(\text{cum}) = 0.173$, $R^2Y(\text{cum}) = 0.492$, $Q^2(\text{cum}) = 0.289$. Permutation test with the intercepts of $R^2 < 0.180$, $Q^2 < -0.15$. **(B4)** PC1: $R^2X(\text{cum}) = 0.183$, $R^2Y(\text{cum}) = 0.169$, $Q^2(\text{cum}) = 0.163$; PC2: $R^2X(\text{cum}) = 0.254$, $R^2Y(\text{cum}) = 0.300$, $Q^2(\text{cum}) = 0.277$; PC3: $R^2X(\text{cum}) = 0.317$, $R^2Y(\text{cum}) = 0.422$, $Q^2(\text{cum}) = 0.387$. Permutation test with the intercept of $R^2 < 0.11$, $Q^2 < -0.05$.

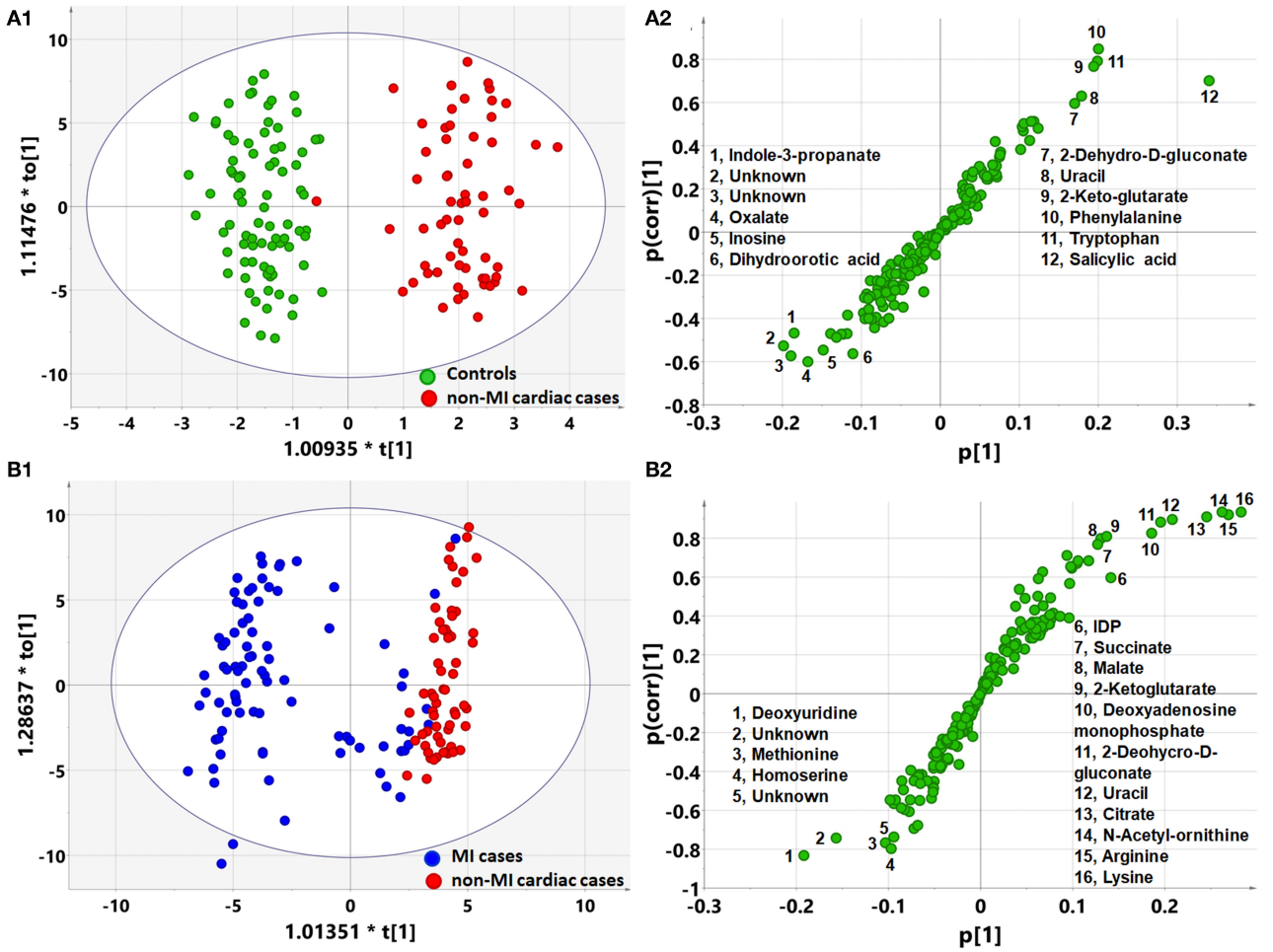

FIGURE 2 | Orthogonal partial least square to latent structure discriminant analysis (OPLS-DA) modeling and S-plots delineate different metabolic phenotypes and potential markers of MI and non-MI cardiac cases. **(A1)** OPLS-DA model differentiating non-MI cardiac cases ($n = 61$) from the controls ($n = 84$). **(A2)** S-plot highlights the potential markers of the non-MI cardiac cases. **(B1)** OPLS-DA model differentiating MI cases ($n = 85$) from non-MI cardiac cases ($n = 61$). **(B2)** S-plot highlights the potential markers of the MI cases.

most likely the risk factors or markers of the occurrence and development of MI, reflecting homeostatic disturbance induced by myocardia hypoxia. **Figure 3F** shows the pathway analysis of the metabolites in the Venn A+B region (control vs. non-MI), and **Figure 3G** shows the pathway analysis of discriminant metabolites in the Venn B+C region (MI vs. non-MI). Generally, arginine biosynthesis and pyrimidine metabolism were the most significantly altered metabolic pathways in non-MI chest pain patients' plasma compared with that in healthy individuals. Enrichment and pathway analysis for the metabolites of the Venn C area by MetaboAnalyst showed that arginine biosynthesis ($p < 0.01$, FDR < 1%) was the most altered metabolic pathway

TABLE 3 | List of discriminant metabolites: non-MIs vs. controls and MIs vs. non-MIs.

Differential metabolites	Controls ($n = 84$)		MI cases ($n = 85$)		Non-MI cases ($n = 61$)	MI vs. non-MI		Non-MI vs. Con		
	Mean	SE	Mean	SE	Mean	SE	FC	*t*-test	FC	*t*-test
Deoxyuridine	26,212	9,533	1,025,278	150,576	16,840	555	60.885	***	0.642	/
Adenosine phosphosulfate	51,723	4,141	99,104	8,542	42,213	3,793	2.348	***	0.816	/
Deoxyadenosine monophosphate	310,296	7,783	102,462	13,401	311,056	7,624	0.329	***	1.002	/
Guanosine diphosphate	7,379	469	27,614	4,153	6,648	530	4.154	***	0.901	/
Inosine 2′-phosphate	14,875	683	37,785	4,687	14,988	809	2.521	***	1.008	/
Adenosine monophosphate	20,124	1,044	25,648	1,689	19,902	1,016	1.289	***	0.989	/
Hypoxanthine	705,034	24,192	373,454	29,693	734,901	52,065	0.508	***	1.042	/
Glycolate	8,319	247	9,121	331	7,620	306	1.197	**	0.916	/
Methionine	113,239	2,830	335,994	27,792	109,192	2,631	3.077	***	0.964	/
Arginine	810,028	22,688	169,566	34,842	731,551	31,282	0.232	***	0.903	/
Valine	2,334,562	53,682	3,710,196	209,295	2,425,637	63,465	1.530	***	1.039	/
Citrulline	422,244	11,079	296,302	13,267	469,763	20,870	0.631	***	1.113	/
Shikimate	14,871	796	8,837	491	15,072	782	0.586	***	1.014	/
Ornithine	747,344	19,685	522,218	23,919	805,398	34,957	0.648	***	1.078	/
Alanine	402,892	10,006	663,687	37,026	446,350	16,079	1.487	***	1.108	/
Glycine	145,111	2,764	256,201	15,108	150,041	3,152	1.708	***	1.034	/
Homocysteine	7,517	382	20,169	2,293	7,693	504	2.622	***	1.023	/
Aspartate	155,030	10,889	194,713	12,674	123,523	10,287	1.576	***	0.797	/
Ribose	223,498	12,602	340,299	15,678	254,617	23,072	1.337	**	1.139	/
1-Monopalmitin	30,533	1,705	33,208	1,616	25,699	1,904	1.292	**	0.842	/
Glycerate	125,449	4,077	54,424	3,823	127,894	10,153	0.426	***	1.019	/
Citrate	6,687,162	203,004	1,395,841	280,056	6,186,805	304,233	0.226	***	0.925	/
NAD+	11,766	301	25,536	3,262	11,479	330	2.225	***	0.976	/
NADPH	5,344	269	35,996	7,862	4,157	192	8.659	***	0.778	###
Uracil	146,594	7,319	60,619	9,826	319,956	18,480	0.189	***	2.183	###
Xanthine	161,018	5,234	99,621	11,423	234,923	11,566	0.424	***	1.459	###
Adenosine	33,452	2,133	31,326	3,112	18,676	1,948	1.677	***	0.558	###
IDP	3,112,579	73,422	1,512,965	153,666	3,597,655	92,953	0.421	***	1.156	###
Adenine	15,026	2,519	13,092	2,292	5,543	393	2.362	**	0.369	###
Succinate	88,550	1,816	36,686	3,233	79,439	2,388	0.462	***	0.897	##
Malate	61,898	2,263	35,918	4,299	78,778	4,163	0.456	***	1.273	###
2-Ketoglutarate	33,628	1,314	21,806	2,264	78,634	4,864	0.277	***	2.338	###
Acetoacetate	132,245	2,671	235,115	13,087	160,911	7,415	1.461	***	1.217	###
Carbamoylphosphate	29,690	1,819	23,063	2,179	36,316	1,532	0.635	***	1.223	##
Dihydroorotate	33,819	1,003	31,876	2,619	22,310	579	1.429	***	0.660	###
Pantothenate	54,720	3,022	38,266	4,405	83,814	4,827	0.457	***	1.532	###
Phenylpyruvate	51,177	955	63,363	2,279	56,537	1,514	1.121	*	1.105	##
Cysteine	106,041	3,333	68,660	3,639	150,632	7,856	0.456	***	1.421	###
Isoleucine	1,694,252	47,827	4,794,207	400,231	2,264,556	105,757	2.117	***	1.337	###
Serine	187,997	4,449	345,414	14,192	211,966	5,374	1.630	***	1.127	###
Proline	805,696	27,760	1,281,948	56,175	912,165	3,390	1.405	***	1.132	#
Threonine	661,526	23,707	1,415,808	70,560	574,241	19,440	2.466	***	0.868	##
Phenylalanine	1,051,097	31,497	1,757,945	133,629	2,349,797	58,409	0.748	***	2.236	###
Glutamine	6,299,813	30,803	6,265,669	37,518	6,115,270	38,706	1.025	**	0.971	###
Histidine	3,756,407	54,216	2,876,183	73,183	3,370,631	66,123	0.853	***	0.897	###
Taurine	851,621	35,791	1,382,464	89,177	727,822	36,862	1.899	***	0.855	#
Lysine	1,733,874	38,073	505,537	102,029	2,002,743	55,294	0.252	***	1.155	###
N-acetylornithine	329,453	18,159	68,946	14,885	265,119	11,352	0.260	***	0.805	##
Cytosine	7,058	102	5,624	153	6,609	135	0.851	***	0.936	##
3-Phospho-serine	11,045	654	17,870	1,469	8,893	284	2.009	***	0.805	##

(Continued)

TABLE 3 | Continued

Differential metabolites	Controls ($n = 84$)		MI cases ($n = 85$)		Non-MI cases ($n = 61$)	MI vs. non-MI		Non-MI vs. Con		
	Mean	SE	Mean	SE	Mean	SE	FC	*t*-test	FC	*t*-test
Homoserine	661,526	23,707	1,415,808	70,560	574,241	19,440	2.466	***	0.868	##
1-Monostearin	17,548	911	19,128	896	13,626	841	1.404	***	0.777	##
2-Dehydro-D-gluconate	47,777	2,930	21,494	3,999	90,849	4,764	0.237	***	1.902	###
Oxalate	44,511	2,459	48,639	3,025	27,020	2,378	1.800	***	0.607	###
Tryptophan	647,430	23,608	1,366,119	100,129	1,584,205	58,633	0.862	/	2.447	###
Glutamate	253,094	9,911	384,958	35,729	384,612	16,588	1.001	/	1.520	###
Hydroxyproline	26,782	1,974	17,148	1,951	17,583	2,030	0.975	/	0.657	##
Salicylic acid	4,870	1,788	72,167	12,248	57,320	7,503	1.259	/	11.771	###
Pyruvate	121,954	5,245	183,553	22,838	184,240	7,253	0.996	/	1.511	###
Homocysterate	11,932	344	14,822	1,109	13,267	310	1.117	/	1.112	##
Cystathionine	10,857	625	13,618	1,322	17,869	1,568	0.762	/	1.646	###
2-Hydroxybutyrate	279,219	12,481	421,962	23,064	405,608	28,986	1.040	/	1.453	###
3-Hydroxybutyrate	52,649	3,298	79,377	10,282	85,759	13,390	0.926	/	1.629	#
Gluconic acid	105,169	4,261	289,949	39,667	203,681	34,215	1.424	/	1.937	##
Indole-3-propanate	55,659	16,898	8,531	1,748	5,464	801	1.561	/	0.098	##
Glycerol	400,975	13,803	290,401	11,659	303,966	15,733	0.955	/	0.758	###
Cholesterol	822,261	17,789	690,461	14,851	684,060	16,272	1.009	/	0.832	###
Alpha-tocopherol	116,918	2,949	93,627	2,218	94,284	2,954	0.993	/	0.806	###
Deoxyadenosine	23,123	1,541	17,568	2,255	13,041	1,288	1.347	/	0.564	###
Thymine	544,496	17,903	518,803	20,345	457,002	25,215	1.135	/	0.839	##
Inosine	65,657	2,868	28,268	3,939	35,665	2,829	0.793	/	0.543	###
NADP+	24,365	1,068	23,264	1,803	19,968	712	1.165	/	0.820	###

*The data were not logarized and expressed as mean ± SE. Fold change (FC) was calculated by the original, non-logarized data directly. Statistical significance was evaluated by using two-tailed t-test with equal variance, after ANOVA assessment of the variance. ***, **, *: $p < 0.001, 0.01, 0.05$, respectively, between MI and non-MI chest pain cases; ###, ##, #: $p < 0.001, 0.01, 0.05$, respectively, between non-MI chest pain cases and controls. "/" represents the statistical significance of p-values more than 0.05.*

(**Figure 3H**). Alanine, aspartate, and glutamate metabolism ($p < 0.01$, FDR < 1%) deserve attention in MI as well.

The pathway of pyrimidine metabolism was deranged in the MI cases, as shown by the dramatic changes in dU and uracil. **Figure 4D** shows metabolites and metabolic enzymes in the dU-related pathway.

Methionine, dU (Deoxyuridine), and Homoserine Are the Main Markers for MI Occurrence

A combined biosignature of homoserine, IDP, and 2-ketoglutarate discriminated MI from non-MI chest pain inpatients with high accuracy [**Supplementary Figure 3I**, area under the ROC curve (AUC) = 0.98, sensitivity = 94.1%, specificity = 100%].

The potential capacity of each discriminant metabolite to diagnose MI (MI vs. non-MI chest pain cases) was assessed by ROC analysis. Notably, although pathway analysis did not draw our attention to the methionine-related metabolic module, methionine and homoserine showed their potential in distinguishing MI from non-MI cardiac cases. Homoserine (AUC = 0.94, specificity = 100%, sensitivity = 81%) was more specific for MI diagnosis but less sensitive than methionine (AUC = 0.96, specificity = 94.6%, sensitivity = 89.4%) (**Figures 3J,K**). dU also scored highly, with an AUC over 90% (**Figure 3L**). dU level is also significantly higher in the proBNP-positive group than in the proBNP-negative chest pain group (**Figure 4H**). Some other metabolites that showed MI diagnostic potential were 2-ketoglutarate, arginine, 2-dehydro-D-gluconate, uracil, etc (**Table 4**).

cTnT, CK-MB, AST, LDH, and HBDH are well-recognized indicators involved in myocardial damage and infarction. As candidate markers of MI, methionine, dU, and homoserine were significantly and positively correlated with LDH, HBDH, and AST (**Supplementary Figure 3B**), but not with cTnT or CK-MB. Six metabolites, 2-hydroxybutyrate, 3-hydroxybutyrate, homocysteine, palmitic acid, stearic acid, and 1-monooleoylglycerol, were positively and significantly correlated with both cTnT and CK-MB (**Supplementary Figure 3C**).

Some other metabolites that showed good diagnostic potential were cysteine, 2-ketoglutarate, IDP, and uracil (**Table 4**).

Traditional CAD Risk Factors and Cardiac Function Influence the Metabolic Pattern

Correlation analysis showed that methionine, homoserine, homocysteine, and dU were all affected by smoking history, but none was obviously perturbed by hypertension (**Supplementary Table 4**). Moreover, to assess the role of

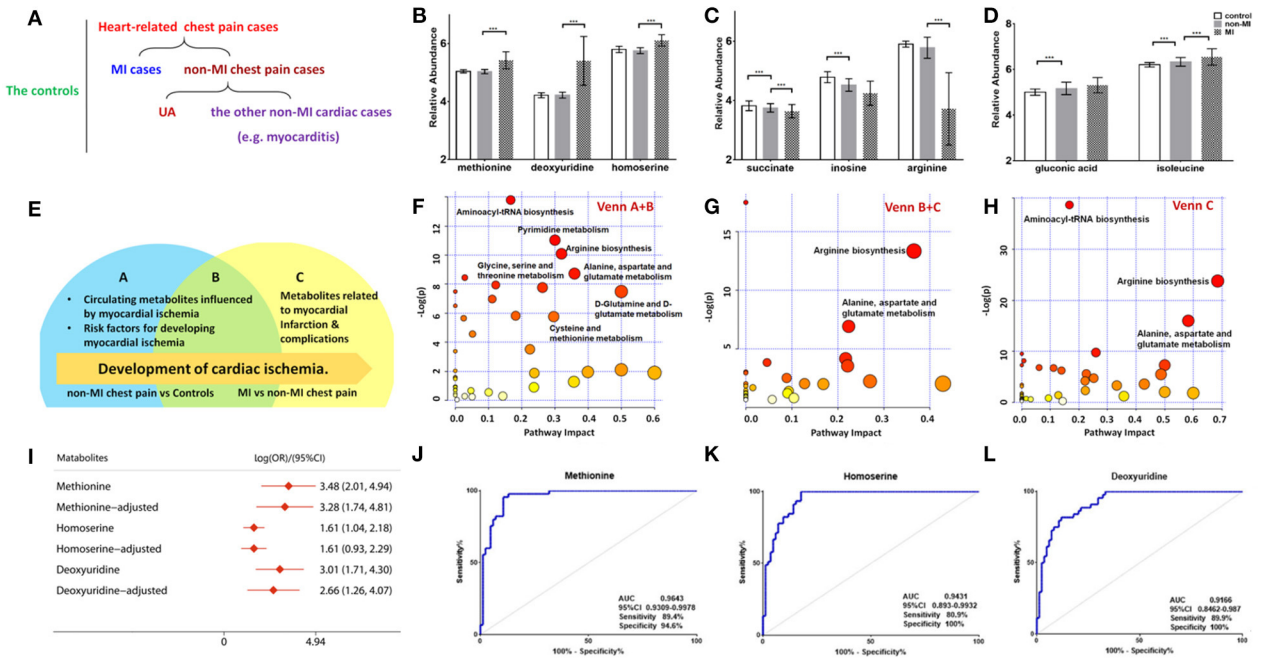

FIGURE 3 | Differential metabolites and pathways involved in the MI group. **(A)** Samples are divided into three groups: control ($n = 84$), MI ($n = 85$) cases, and non-MI chest pain cases ($n = 61$); or four groups: control ($n = 84$), MI cases ($n = 85$), UA ($n = 34$), and the other non-MI cardiac cases ($n = 27$) when OPLS-DA analysis is applied. **(B)** Plasma methionine, deoxyuridine, and homoserine levels spike in the MI group. **(C)** Succinate, inosine, and arginine levels drop as CAD progresses to MI. **(D)** Gluconic acid and isoleucine levels increase as CAD progresses to MI (relative abundance is shown in logarized form: mean with SD, $^{***}p < 0.05$). **(E)** Venn diagram shows discriminant metabolites can be classified into regions A, B, and C. **(F)** Pathway analysis of differential metabolites in Venn A and B regions (control vs. non-MI chest pain cases). **(G)** Pathway analysis of differential metabolites in Venn C and B (MI vs. non-MI cases). There is a remarkable change of arginine biosynthesis and alanine, aspartate, and glutamate metabolism. **(H)** Pathway analysis of differential metabolites in Venn C. There is a remarkable change of arginine biosynthesis and alanine, aspartate, and glutamate metabolism. **(I)** Unadjusted and adjusted (adjusted for age, gender, LDL-C, HDL-C, smoking/diabetic/hypertensive history) odds ratio of methionine, deoxyuridine, and homoserine. **(J)** Receiver operating characteristic curve (ROC) analysis of methionine [area under the ROC curve (AUC) 96.43%, sensitivity 89.4%, specificity 94.59%]. **(K)** ROC analysis of homoserine (AUC 94.31%, sensitivity 80.9%, specificity 100%). **(L)** ROC analysis of deoxyuridine (AUC 91.66%, sensitivity 80.9%, specificity 100%) ($^{***}p < 0.001$).

these metabolites as risk factors for the prediction of MI occurrence, OR values were calculated between the MI and non-MI groups. Homoserine, dU, and methionine had high scores (**Table 4**). After adjusting for age, sex, LDL-C, HDL-C, smoking/diabetes/hypertension history, and $\log OR^{(MI/non-MI)}$ of methionine, homoserine, and dU, all had ORs > 1 (MIs vs. non-MIs) (**Figure 3I**). In the subgroup analyses of smoking/non-smoking, hypertensive/normotensive, diabetic/non-diabetic, aged 45–54/55–65, and male/female, the means of homoserine, methionine, and dU were all higher in the MI cases (**Table 5**). It shows that higher methionine, homoserine, or dU plasma level increases the risk of chest pains being diagnosed as MI.

As a clinical indicator of cardiac function in MI, positive NT-proBNP represents cardiac dysfunction. Methionine, homoserine, and deoxyuridine were further elevated in NT-proBNP-positive cases. Pathway analysis of the discriminant metabolites (**Supplementary Table 5**) between the NT-proBNP-positive and NT-proBNP-negative groups suggested that only arginine biosynthesis was severely impaired ($p < 0.001$, FDR < 1%), indicating that arginine biosynthesis is closely associated with cardiac function (**Supplementary Figure 3A**).

DISCUSSION

Potential Markers of MI

This study identified a panel of discriminant metabolites that were also suggested as potential markers of MI in previous reports, such as taurine, methionine, leucine, isoleucine, valine, ornithine, tryptophan, citrate, and 2-ketoglutarate. Arginine biosynthesis and purine and pyrimidine metabolism pathways were also found to be seriously influenced in MI plasma samples. Among the differential metabolites between MI cases and non-MI cases, 10 of them in the MI group had more than twice the abundance as in the non-MI group (MIs/non-MIs, FC > 2); 17 metabolites had less than half the abundance as in the non-MI cases (MIs/non-MIs, FC < 0.5).

Elevated Markers in MI Cases

The pyrimidine metabolism pathway was also reprogrammed in MI cases. However, as an intermediate metabolite in

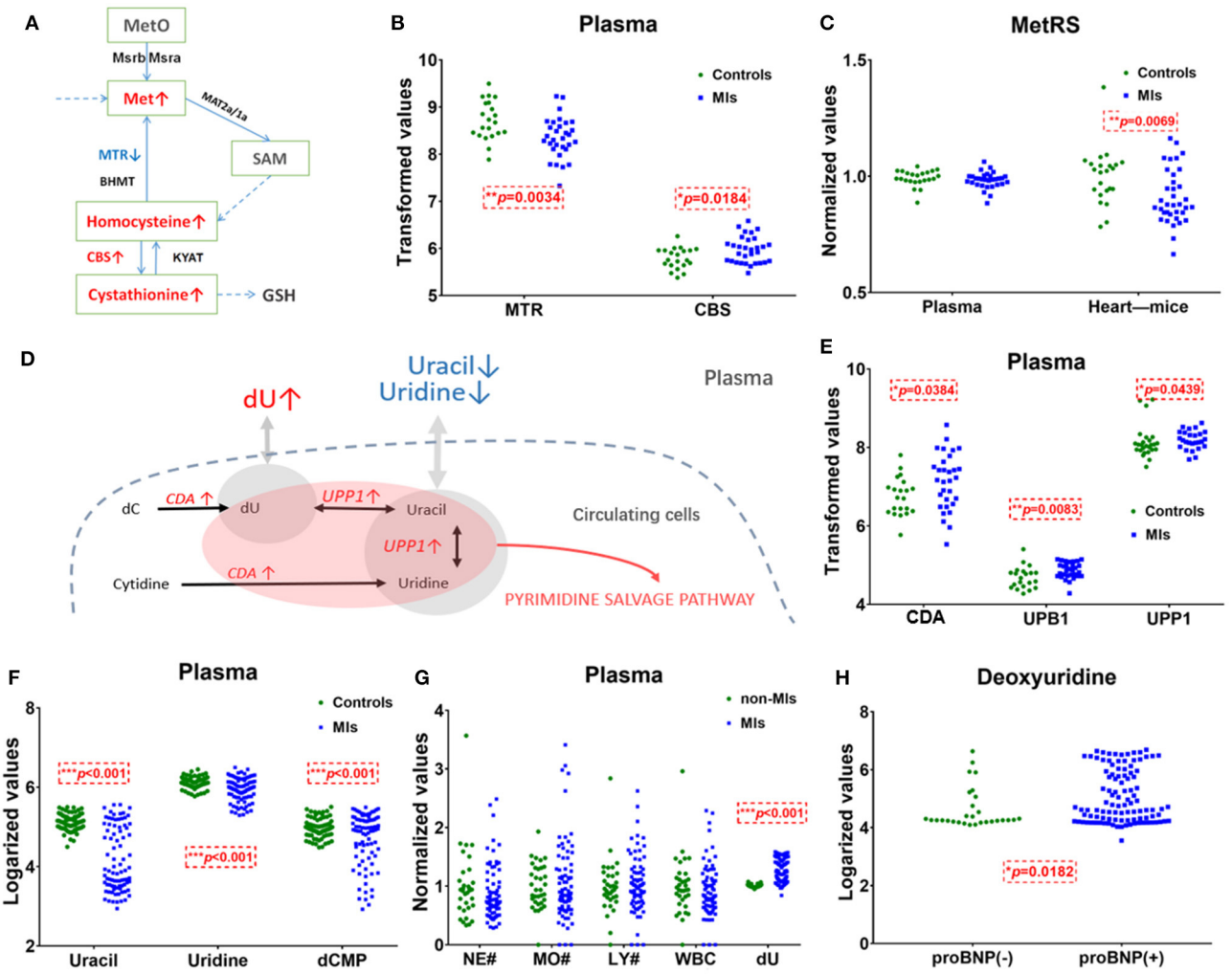

FIGURE 4 | Methionine and deoxyuridine (dU)-related pathways in plasma. **(A)** Methionine (Met) abundance-related pathway in plasma. **(B)** The Met-related enzyme *MTR* is significantly* decreased and *CBS* is significantly higher in MI cases ($n = 31$) compared with healthy individuals ($n = 21$). **(C)** The Met-related enzyme *MetRS*(*MARS2*) abundance in the myocardium of murine MI models ($n = 36$) is downregulated* compared with control ($n = 23$), while human plasma *MetRS* remains unchanged. **(D)** dU-centered metabolism in plasma cells. **(E)** dU-related enzymes *CDA*, *UPB1*, and *UPP1* are significantly* higher in the MI group ($n = 31$) plasma compared with those in healthy individuals ($n = 21$). **(F)** dU-related intermediates uracil, uridine, and dCMP significantly* dropped in MI cases ($n = 85$) compared with those in healthy individuals ($n = 84$). **(G)** Neutrophils, monocytes, lymphocytes, and white cell counts of non-MI cases ($n = 34$) and MI cases ($n = 74$). **(H)** dU is significantly* higher in the NT-proBNP(+) group ($n = 104$) than in the NT-proBNP(–) group ($n = 29$). **(A,D)**: *red* indicates upregulated metabolites or enzymes, *blue* indicates the downregulated, *black* indicates the unchanged, and *gray* indicates undetected metabolites. *Student's *t*-test, $p < 0.05$.

pyrimidine metabolism, dU has never been suggested to play a role in cardiovascular diseases before. Previously, reports demonstrated how exogenous dU largely abolished the uptake of thymidine in bone marrow cells and how dU can also slow down the incorporation of deoxyguanidine and deoxyadenosine into DNA (22, 23). Moreover, elevation of dU has been identified as a potential adverse factor for nucleotide pool balance and mitochondrial function in the case of mitochondrial neurogastrointestinal encephalomyopathy (24, 25). Some studies reported the relations between dU accumulation and cancer progression (26). It is speculated that a high dU level may be a risk for MI patients because it may lead to problems about DNA incorporation. Consistent with a previous report suggesting the relationship of dU with insulin resistance (27), our correlation analysis also suggested that dU is partially affected by diabetes (correlation analysis vs. diabetes, $p < 0.05$, Pearson's $r = 0.23$), in addition to tobacco use and HDL-C level.

Accumulated metabolites in the MI plasma sample demonstrate abnormal methionine and cysteine metabolism. In this metabolic module, methionine is a precursor of homocysteine and homoserine is utilized in the biosynthesis of methionine. Homoserine was reported as a serum marker for cardiac disease in atherosclerosis patients with stent restenosis (28). A high level of methionine has been identified as atherogenic (29) and metabo-toxic (30). As a precursor of homocysteine, methionine elevation is supposed to be a negative signal for the development of CAD. A previous study showed that methionine in CAD cases is significantly higher than in

TABLE 4 | Differential metabolites and the diagnostic potential between MI and non-MI chest pain cases.

Differential metabolites	AUROC	95% CI	Sensitivity (%)	Specificity (%)	LogOR	95% CI
Homoserine, IDP, and α-ketoglutarate	0.9810	0.9614–1.0000	94.10	100	3.02	2.12 to 3.93
Methionine	0.9643	0.9309–0.9978	89.40	94.60	3.48	2.01 to 4.94
Homoserine	0.9431	0.893–0.9932	80.90	100	1.61	1.04 to 2.18
α-Ketoglutarate	0.9390	0.8876–0.9905	100	0.00	−0.11	−0.28 to −0.03
Uracil	0.9166	0.8585–0.9747	100	0.00	−2.38	−3.45 to −1.32
Deoxyuridine	0.9166	0.8462–0.987	80.90	100	3.01	1.71 to 4.30
2-Dehydro-D-gluconate	0.9040	0.8362–0.9717	2.10	100	−1.69	−2.53 to −0.84
Cysteine	0.8976	0.8302–0.9651	100	0.00	−0.41	−0.61 to −0.20
Deoxyadenosine monophosphate	0.8976	0.8335–0.9618	100	0.00	−5.57	−8.61 to −2.53
IDP	0.8838	0.8124–0.9553	100	0.00	−5.15	−7.86 to −2.44
Glyceric acid	0.8758	0.8022–0.9493	100	0.00	−1.53	−2.08 to −0.98
Citrate	0.8568	0.7774–0.9362	100	0.00	−1.69	−2.50 to −0.88
Succinate	0.8562	0.7768–0.9357	100	0.00	−1.48	−2.14 to −0.83
Pantothenate	0.8332	0.7452–0.9213	100	0.00	−0.98	−1.36 to −0.59
Xanthine	0.8240	0.7312–0.9168	2.10	100	−1.06	−1.46 to −0.65
Arginine	0.8235	0.7319–0.9151	2.10	100	−0.82	−1.10 to −0.53

Logarization transformation of the data was applied to the data before the calculation.

TABLE 5 | Mean of deoxyuridine, methionine, and homoserine in certain subgroups of the controls, non-MIs, and MI cases.

Risk factors	Subgroups	Deoxyuridine	Methionine	Homoserine	Non-risk factors	Subgroups	Deoxyuridine	Methionine	Homoserine
Smokers	Controls	4.22	5.04	5.82	Non-smokers	Controls	4.24	5.05	5.8
	Non-MI cases	4.22	5.03	5.76		Non-MI cases	4.22	5.03	5.75
	MI cases	5.48*,#	5.44*,#	6.13*,#		MI cases	5.45*,#	5.43*,#	6.11*,#
Diabetic	Controls	4.22	5.04	5.8	Nondiabetic or insulin resistance	Controls	4.24	5.05	5.8
	Non-MI cases	4.2	5.03	5.75		Non-MI cases	4.21	5.04	5.73
	MI cases	5.44*,#	5.43*,#	6.12*,#		MI cases	5.34*,#	5.40*,#	6.09*,#
Hypertensive	Controls	4.24	5.05	5.8	Normotensive	Controls	4.22	5.04	5.8
	Non-MI cases	4.22	5.03	5.75		Non-MI cases	4.22	5.04	5.73
	MI cases	5.40*,#	5.42*,#	6.11*,#		MI cases	5.37*,#	5.42*,#	6.10*,#
Age 45–54	Controls	4.29	5.07	5.83	Age 55–65	Controls	4.23	5.03	5.83
	Non-MI cases	4.21	5.05	5.72		Non-MI cases	4.18	5.04	5.75
	MI cases	5.30*,#	5.37*,#	6.13*,#		MI cases	5.60*,#	5.45*,#	6.11*,#
Male	Controls	4.22	5.05	5.8	Female	Controls	4.28	5.05	5.82
	Non-MI cases	4.22	5.05	5.77		Non-MI cases	4.23	5	5.72
	MI cases	5.43*,#	5.44*,#	6.11*		MI cases	5.32*,#	5.35*,#	6.10*,#

*****MI *vs. controls,* $p < 0.05$; #MI *vs. non-MI,* $p < 0.05$.
All data were logarized before calculating, and the result showed the means of each subgroup.

controls and is a risk factor for CAD occurrence in unadjusted OR analysis (31). Our data further showed that methionine has the potential to be an independent biomarker for MI. Notably, we found that the diagnostic performance of biomarker candidates for MI varied with individual characteristics. When we studied individuals with a history of diabetes, methionine achieved an AUC score as high as 100% (sensitivity = 100.00%, specificity = 100.00%). For non-diabetic inpatients, the AUC score of methionine was only 73%, which is much lower than that of diabetic inpatients.

Our study suggests that a higher methionine, homoserine, or dU level has the potential in confirming MI diagnosis among chest pains and in contributing to the occurrence of MI. They could also be candidate predictors of future MI, but they still need to be further studied.

Moreover, methionine, homoserine, and dU also have the potential of being independent predictors of lipid plaque rupture. This is supported by the finding that logistic regression showed that the $\log OR^{(ACS/Control)}$ of dU is 40.767, methionine 10,596.739, and homoserine 434.394. After being adjusted for age, gender, diabetes/hypertension/smoking history, and lipid levels, the $\log OR^{(ACS/Control)}$ of methionine is 158,368.17, the $\log OR^{(ACS/Control)}$ of dU is 37.185, and that of homoserine is 628.728. The above data suggest that homoserine, dU, and methionine also have the potential to be indicators of ACS occurrence, which also has the potential to indicate coronary lipid

plaque rupture. However, their ability to predict future MI or ACS occurrence needs further cohort studies.

Decreased Metabolites in MI Cases

Both high level and low level of risk markers in plasma were detected in the MI. Among all the discriminant metabolites that declined in MI cases, arginine was the most noteworthy (**Figure 3C**). Arginine ROC analysis showed an AUC = 0.8865 (MIs vs. non-MIs). Our study showed that as cardiac damage and function worsened (further elevation of cTnT, AST, CK-MB, and NT-proBNP levels), these plasma arginine biosynthesis-related metabolites dropped more (**Table 3**). Arginine is the primary source of a vasodilator—nitric oxide. The lack of plasma arginine hints a deficiency of vasodilator in MI patients. Some reported that diminished global arginine bioavailability is predictive of increased CAD risk (17).

Uracil, a pyrimidine found in RNA, was also significantly decreased in MI plasma. **Figures 4D,F** show the relationship of uracil and dU in a brief dU-centered pathway. The panel implies the demand for damage repair after a heart attack. This suggests that after MI occurs, the body continues to repair itself by producing more RNA or even DNA (32).

Elevation of the ATP by-product inosine has been detected in human plasma samples as early as 15 min after exercise-induced myocardial damage (7). However, the level of inosine dropped in MI cases in this study. It is possible that circulating inosine change after myocardial infarction is very time-sensitive: it rises immediately after the myocardial damage but dropped within 1–2 days.

The Association Between Plasma Cells and Circulatory Metabolites

Although the causes of metabolite alterations could be many (e.g., gut microbial metabolites), we studied plasma transcriptomics data because circulating substances can cross the cell membranes and influence plasma metabolites most directly. We studied transcriptomics of circulating cells of MI patients and healthy controls from the GEO database (GSE48060). Differential genes between MI and controls were determined as those FDR < 0.05, FC > 1.2/FC < 0.8 (**Supplementary Table 6**). The metabolite–gene–disease interaction network analysis from MetaboAnalyst 3.0 (https://www.metaboanalyst.ca/MetaboAnalyst/Secure/network/MnetParamView.xhtml) showed the interaction network between differential metabolites from our study and differential genes from GSE48060 (**Supplementary Figure 4A**). Glucose, uric acid, cholesterol, glycine, and arginine are all important hubs with high-degree centrality.

Metabolite–gene interaction analysis showed that abnormal plasma level of purine metabolism intermediates ADP, ATP, GDP, and beta-alanine may relate to the expressions of plasma cells' *ADCY7*, *YES1*, *PTGDR*, etc. in mRNA level (**Supplementary Figure 4B**).

Plasma Cells Cannot Explain the Elevation of Plasma Methionine

Figure 4A shows methionine, homocysteine, and cystathionine in a panel. Inconsistent with the observed elevation of methionine, circulating transcriptomics of MI patients (GSE48060) showed that among the methionine abundance-related genes, methionine synthase *5-Methyltetrahydrofolate-Homocysteine Methyltransferase* (*MTR*) expression decreased and *Cystathionine β-synthase* (*CBS*, converting homocysteine to cystathionine) increased ($p < 0.05$, **Figure 4B**). The other genes involved in methionine turnover, including methionine-tRNA ligase (*MetRS*), *MrsB*/*MrsA* [*MARS*, reduced methionine-(S)-S-oxide), and *Mat2a*/*Mat1a* (methionine adenosyltransferase), remained statistically unchanged in plasma cells. The above data showed that plasma cells tend to utilize methionine and homocysteine to produce more cystathionine in MI blood samples. Considering that plasma cells cannot explain the elevation of plasma methionine, it is more likely that damaged cardiac tissues (or other tissues/germs) are responsible for that. A transcriptomics study of MI mouse model (induced by left anterior descending ligation, GEO accession: GSE775) revealed that in ischemic cardiac tissue, *MetRS* decreased significantly (p 0.05) in MI mouse cardiac samples, and the utilization of methionine is handicapped (**Figure 4C**).

dU Abundance Is Likely to Be Related to Blood Cells

Unlike methionine, the elevation of dU is likely to be related to injured cardiomyocytes or blood cells. Normally, little dU and purines can be detected in the plasma of a healthy volunteer. When there is pathological change of the tissue or the cells, intracellular substances are released and enter into the circulation system. According to the human metabolome database (HMDB0000012), dU is detected in the blood. However, we only identified dU peak in plasma, not in serum. According to GSE48060, cytidine deaminase (*CDA*) and uridine phosphorylase 1 (*UPP1*) are upregulated in MI-circulating cells ($p < 0.05$). *CDA* catalyzes the formation of deoxyuridine from deoxycytidine and *UPP1* catalyzes the reversible transformation of dU to uracil, and the above two upregulated enzymes can lead to dU elevation. **Figure 4D** shows the metabolites and metabolic enzymes in the dU-related pathway.

CDA and *UPP1* are both highly enriched in immune cells (mainly in neutrophils and monocytes). Immune cells increased in MI plasma samples. **Figure 4G** shows white blood cell (WBC) counts, neutrophil (NE) counts, monocyte (MO) and lymphocyte (LY) counts, and dU abundance in MI and non-MI cases. A previous study (GSE103182) showed that STEMI patients feature more neutrophils and *CDA* mRNA in plasma than NSTEMI patients. Consistent with this finding, our data showed that in the STEMI group, both dU and neutrophil counts were higher than those in the NSTEMI group (**Supplementary Figure 3G**).

On the one hand, dU originates from plasma neutrophils, and it could also originate from damaged and remodeling hearts. Our study on transverse aortic constriction (TAC) mouse models showed that cardiac *CDA* mRNA expression increased as *BNP* and *ANF* mRNA levels increased (**Supplementary Figures 3D–F,H**). It is possible that damaged human heart could also expressed more *CAD* and produce more dU. Hopefully, more plasma single-cell information (33, 34) and omics data (e.g., cfDNA methylome (35)) will reveal the mechanism behind the changes very soon.

Limitations

As indicated by adjusted and unadjusted OR values, traditional risk factors, such as diabetes, hypertension, and smoking, had confounding effects on the candidate MI metabolite markers (36). In this study, diabetes and smoking also ranked as the marked risk factors for MI occurrence, but the history of hypertension was not (OR < 1, $p > 0.05$). As for the key substances in lipid metabolism, higher levels of TC and TG are risk factors for MI groups.

However, the OR of LDL-C scored 0.58 between cardiac chest pains and control, indicating that LDL-C is not a risk for healthy controls to develop into cardiac chest pains (**Supplementary Table 6**). Similarly, hypertension has been recognized as a risk for developing CAD, but it is not indicated as a risk factor in this study on MI. Considering that around 65% of inpatients had received medical treatment either with antilipidemic or antihypertensive drugs, or both, before blood collection, their HDL-C, LDL-C, and blood pressure levels may had been normalized or improved, so as to bring deviation of the data.

DATA AVAILABILITY STATEMENT

Metabolome data is freely available upon request via email (jiyea@cpu.edu.cn). Publicly available datasets were analyzed in this study. This data can be found online at the following links: https://www.ncbi.nlm.nih.gov/geo/query/acc.cgi?acc=GSE48060, https://www.ncbi.nlm.nih.gov/geo/query/acc.cgi?acc=GSE103182, https://www.ncbi.nlm.nih.gov/geo/query/acc.cgi?acc=GSE775, https://www.ncbi.nlm.nih.gov/geo/query/acc.cgi?acc=GSE59867.

ETHICS STATEMENT

The studies involving human participants were reviewed and approved by Ethics Committee of the First Affiliated Hospital of Nanjing Medical University. The patients/participants provided their written informed consent to participate in this study.

AUTHOR CONTRIBUTIONS

XK and JA was responsible for the concept of the study. GW and JA provided the LC/MS and GC/MS platform. ZY, LW, and CL confirmed the diagnosis of MI and non-MI chest pain cases. NA, YL, and HT collected the blood samples, recorded the medical history of the volunteers, and prepared the plasma samples. NA, ZL, and RS performed the untargeted metabolomics. NA and MY analyzed the data. NA, MY, and JA produced the figures and tables. XK, NA, and YL wrote the manuscript. All authors contributed to the article and approved the submitted version.

FUNDING

This work was supported by the National Key Special Project of Science and Technology for Innovation Drugs of China (2017ZX09301013), the leading technology foundation research project of Jiangsu Province (BK20192005).

ACKNOWLEDGMENTS

We thank Mrs. Dongmei Shi and all the nursing staff of the Department of Cardiology, Nanjing Medical University, for the guidance and assistance in the collection of the blood samples. We thank Prof. Yongyue Wei, School of Public Health, Nanjing Medical University, for his valuable suggestion on the statistics.

SUPPLEMENTARY MATERIAL

The Supplementary Material for this article can be found online at: https://www.frontiersin.org/articles/10.3389/fcvm.2021.652746/full#supplementary-material

REFERENCES

1. Douglas PS, Hoffmann U, Patel MR, Mark DB, Al-Khalidi HR, Cavanaugh B, et al. Outcomes of anatomical versus functional testing for coronary artery disease. *N Engl J Med.* (2015) 372:1291–300. doi: 10.1056/NEJMoa1415516
2. Hammarsten O, Mair J, Mockel M, Lindahl B, Jaffe AS. Possible mechanisms behind cardiac troponin elevations. *Biomarkers.* (2018) 23:725–34. doi: 10.1080/1354750X.2018.1490969
3. Nowak R, Mueller C, Giannitsis E, Christ M, Ordonez-Llanos J, DeFilippi C, et al. High sensitivity cardiac troponin T in patients not having an acute coronary syndrome: results from the TRAPID-AMI study. *Biomarkers.* (2017) 22:709–14. doi: 10.1080/1354750X.2017.1334154
4. Riedlinger D, Mockel M, Muller C, Holert F, Searle J, von Recum J, et al. High-sensitivity cardiac troponin T for diagnosis of NSTEMI in the elderly emergency department patient: a clinical cohort study. *Biomarkers.* (2018) 23:551–7. doi: 10.1080/1354750X.2018.1460763
5. Lopaschuk GD. Metabolic modulators in heart disease: Past, present, and future. *Can J Cardiol.* (2017) 33:838–49. doi: 10.1016/j.cjca.2016.12.013
6. Brindle JT, Antti H, Holmes E, Tranter G, Nicholson JK, Bethell HW, et al. Rapid and noninvasive diagnosis of the presence and severity of coronary heart disease using 1H-NMR-based metabonomics. *Nat Med.* (2002) 8:1439–44. doi: 10.1038/nm1202-802
7. Sabatine MS, Liu E, Morrow DA, Heller E, McCarroll R, Wiegand R, et al. Metabolomic identification of novel biomarkers of myocardial ischemia. *Circulation.* (2005) 112:3868–75. doi: 10.1161/CIRCULATIONAHA.105.569137
8. Shah SH, Kraus WE, Newgard CB. Metabolomic profiling for the identification of novel biomarkers and mechanisms related to common cardiovascular diseases: form and function. *Circulation.* (2012) 126:1110–20. doi: 10.1161/CIRCULATIONAHA.111.060368
9. Lewis GD, Asnani A, Gerszten RE. Application of metabolomics to cardiovascular biomarker and pathway discovery. *J Am Coll Cardiol.* (2008) 52:117–23. doi: 10.1016/j.jacc.2008.03.043
10. Fan Y, Li Y, Chen Y, Zhao YJ, Liu LW, Li J, et al. Comprehensive metabolomic characterization of coronary artery diseases. *J Am Coll Cardiol.* (2016) 68:1281–93. doi: 10.1016/j.jacc.2016.06.044
11. Cheng ML, Wang CH, Shiao MS, Liu MH, Huang YY, Huang CY, et al. Metabolic disturbances identified in plasma are associated with outcomes in patients with heart failure: diagnostic and prognostic value of metabolomics. *J Am Coll Cardiol.* (2015) 65:1509–20. doi: 10.1016/j.jacc.2015.02.018

12. Stegemann C, Pechlaner R, Willeit P, Langley SR, Mangino M, Mayr U, et al. Lipidomics profiling and risk of cardiovascular disease in the prospective population-based Bruneck stu*dy*. *Circulation.* (2014) 129:1821–31. doi: 10.1161/CIRCULATIONAHA.113.002500
13. Zhang L, Wei TT, Li Y, Li J, Fan Y, Huang FQ, et al. Functional metabolomics characterizes a key role for N-Acetylneuraminic acid in coronary artery diseases. *Circulation.* (2018) 137:1374–90. doi: 10.1161/CIRCULATIONAHA.117.031139
14. Song JP, Chen L, Chen X, Ren J, Zhang NN, Tirasawasdichai T, et al. Elevated plasma beta-hydroxybutyrate predicts adverse outcomes and disease progression in patients with arrhythmogenic cardiomyopathy. *Sci Transl Med.* (2020) 12:eaay8329. doi: 10.1126/scitranslmed.aay8329
15. Wald DS, Law M, Morris JK. Homocysteine and cardiovascular disease: evidence on causality from a meta-analysis. *BMJ.* (2002) 325:1202. doi: 10.1136/bmj.325.7374.1202
16. Floegel A, Kuhn T, Sookthai D, Johnson T, Prehn C, Rolle-Kampczyk U, et al. Serum metabolites and risk of myocardial infarction and ischemic stroke: a targeted metabolomic approach in two German prospective cohorts. *Eur J Epidemiol.* (2018) 33:55–66. doi: 10.1007/s10654-017-0333-0
17. Tang WH, Wang Z, Cho L, Brennan DM, Hazen SL. Diminished global arginine bioavailability and increased arginine catabolism as metabolic profile of increased cardiovascular risk. *J Am Coll Cardiol.* (2009) 53:2061–7. doi: 10.1016/j.jacc.2009.02.036
18. Grund B, Sabin C. Analysis of biomarker data: logs, odds ratios, and receiver operating characteristic curves. *Curr Opin HIV AIDS.* (2010) 5:473–9. doi: 10.1097/COH.0b013e32833ed742
19. A J, Trygg J, Gullberg J, Johansson AI, Jonsson P, Antti H, et al. Extraction and GC/MS analysis of the human blood plasma metabolome. *Anal Chem.* (2005) 77:8086–94. doi: 10.1021/ac051211v
20. Zhang Y, Lu W, Wang Z, Zhang R, Xie Y, Guo S, et al. Reduced neuronal cAMP in the nucleus accumbens damages blood-brain barrier integrity and promotes stress vulnerability. *Biol Psychiatry.* (2020) 87:526–37. doi: 10.1016/j.biopsych.2019.09.027
21. Aa N, Guo JH, Cao B, Sun RB, Ma XH, Chu Y, et al. Compound danshen dripping pills normalize a reprogrammed metabolism of myocardial ischemia rats to interpret its time-dependent efficacy in clinic trials: a metabolomic study. *Metabolomics.* (2019) 15:128. doi: 10.1007/s11306-019-1577-3
22. Das KC, Herbert V. The lymphocyte as a marker of past nutritional status: persistence of abnormal lymphocyte deoxyuridine (dU) suppression test and chromosomes in patients with past deficiency of folate and vitamin B12. *Br J Haematol.* (1978) 38:219–33. doi: 10.1111/j.1365-2141.1978.tb01038.x
23. Wickramasinghe SN, Matthews JH. Deoxyuridine suppression: biochemical basis and diagnostic applications. *Blood Rev.* (1988) 2:168–77. doi: 10.1016/0268-960X(88)90022-7
24. Bax BE, Levene M, Bain MD, Fairbanks LD, Filosto M, Kalkan Ucar S, et al. Erythrocyte encapsulated thymidine phosphorylase for the treatment of patients with mitochondrial neurogastrointestinal encephalomyopathy: study protocol for a multi-centre, multiple dose, open label trial. *J Clin Med.* (2019) 8:1096. doi: 10.3390/jcm8081096
25. Marti R, Nishigaki Y, Hirano M. Elevated plasma deoxyuridine in patients with thymidine phosphorylase deficiency. *Biochem Biophys Res Commun.* (2003) 303:14–8. doi: 10.1016/S0006-291X(03)00294-8
26. Huang J, Mondul AM, Weinstein SJ, Derkach A, Moore SC, Sampson JN, et al. Prospective serum metabolomic profiling of lethal prostate cancer. *Int J Cancer.* (2019) 145:3231–43. doi: 10.1002/ijc.32218
27. Li LO, Hu YF, Wang L, Mitchell M, Berger A, Coleman RA. Early hepatic insulin resistance in mice: a metabolomics analysis. *Mol Endocrinol.* (2010) 24:657–6. doi: 10.1210/me.2009-0152
28. Hasokawa M, Shinohara M, Tsugawa H, Bamba T, Fukusaki E, Nishiumi S, et al. Identification of biomarkers of stent restenosis with serum metabolomic profiling using gas chromatography/mass spectrometry. *Circ J.* (2012) 76:1864–73. doi: 10.1253/circj.CJ-11-0622
29. Troen AM, Lutgens E, Smith DE, Rosenberg IH, Selhub J. The atherogenic effect of excess methionine intake. *Proc Natl Acad Sci USA.* (2003) 100:15089–94. doi: 10.1073/pnas.2436385100
30. Murphy-Chutorian DR, Wexman MP, Grieco AJ, Heininger JA, Glassman E, Gaull GE, et al. Methionine intolerance: a possible risk factor for coronary artery disease. *J Am Coll Cardiol.* (1985) 6:725–30. doi: 10.1016/S0735-1097(85)80473-3
31. Shah SH, Bain JR, Muehlbauer MJ, Stevens RD, Crosslin DR, Haynes C, et al. Association of a peripheral blood metabolic profile with coronary artery disease and risk of subsequent cardiovascular events. *Circ Cardiovasc Genet.* (2010) 3:207–14. doi: 10.1161/CIRCGENETICS.109.852814
32. Krokan HE, Drablos F, Slupphaug G. Uracil in DNA–occurrence, consequences and repair. *Oncogene.* (2002) 21:8935–48. doi: 10.1038/sj.onc.1205996
33. Abplanalp WT, John D, Cremer S, Assmus B, Dorsheimer L, Hoffmann J, et al. Single cell RNA sequencing reveals profound changes in circulating immune cells in patients with heart failure. *Cardiovasc Res.* (2020) 117:484–94. doi: 10.1093/cvr/cvaa101
34. Ren H, Liu X, Wang L, Gao Y. Lymphocyte-to-monocyte ratio: a novel predictor of the prognosis of acute ischemic stroke. *J Stroke Cerebrovasc Dis.* (2017) 26:2595–602. doi: 10.1016/j.jstrokecerebrovasdis.2017.06.019
35. Zemmour H, Planer D, Magenheim J, Moss J, Neiman D, Gilon D, et al. Non-invasive detection of human cardiomyocyte death using methylation patterns of circulating DNA. *Nat Commun.* (2018) 9:1443. doi: 10.1038/s41467-018-03961-y
36. Foody J, Huo Y, Ji L, Zhao D, Boyd D, Meng HJ, et al. Unique and varied contributions of traditional CVD risk factors: a systematic literature review of CAD risk factors in China. *Clin Med Insights Cardiol.* (2013) 7:59–86. doi: 10.4137/CMC.S10225

Conflict of Interest: The authors declare that the research was conducted in the absence of any commercial or financial relationships that could be construed as a potential conflict of interest.

frontiers in Cardiovascular Medicine

ORIGINAL RESEARCH
published: 10 May 2021
doi: 10.3389/fcvm.2021.647366

Impact of Acute Insulin Resistance on Myocardial Blush in Non-Diabetic Patients Undergoing Primary Percutaneous Coronary Intervention

Soheir M. Kasem[1], Ghada Mohamed Saied[2], Abdel Nasser MA Hegazy[3] and Mahmoud Abdelsabour[3]*

[1] Department of Internal Medicine, Faculty of Medicine, Assiut University, Assiut, Egypt, [2] Department of Clinical Pathology, Faculty of Medicine, Assiut University, Assiut, Egypt, [3] Department of Cardiology, Assiut University, Assiut, Egypt

OPEN ACCESS

Edited by:
Kunhua Song, University of Colorado Anschutz Medical Campus, United States

Reviewed by:
Hongyan Xu, Augusta University, United States
Di Ren, University of South Florida, United States

***Correspondence:**
Soheir M. Kasem
soheir@aun.edu.eg

Specialty section:
This article was submitted to Cardiovascular Metabolism, a section of the journal Frontiers in Cardiovascular Medicine

Received: *29 December 2020*
Accepted: *02 March 2021*
Published: *10 May 2021*

Citation:
Kasem SM, Saied GM, Hegazy ANM and Abdelsabour M (2021) Impact of Acute Insulin Resistance on Myocardial Blush in Non-Diabetic Patients Undergoing Primary Percutaneous Coronary Intervention. Front. Cardiovasc. Med. 8:647366. doi: 10.3389/fcvm.2021.647366

Background: Myocardial blush grading is considered to be a novel tool for assessment of coronary microvasculature and myocardial perfusion in patients undergoing coronary angiography and angioplasty, and its reduction identifies patients at high risk. Our study aimed to evaluate the association between acute insulin resistance and myocardial blush in non-diabetic patients with ST-segment elevation myocardial infarction (STEMI).

Methods: Two hundred forty non-diabetic patients with STEMI who underwent primary percutaneous coronary intervention were consecutively recruited. The relationship of homeostasis model assessment—estimated insulin resistance (HOMA-IR) to myocardial blush and in-hospital outcome was investigated.

Results: Higher HOMA-IR tertile was observed in obese patients, with hyperinsulinemia, had Killip class >1, with higher CPK-MB level and was correlated to impaired myocardial blush after adjusting for the other confounding risk factors. It was also concluded that higher HOMA-IR was independently associated with no/minimal myocardial blush after STEMI. Moreover, it was founded to be an independent predictor of pulmonary edema and impaired left ventricular systolic function.

Conclusion: This study revealed that acute insulin resistance was prevalent in non-diabetic patients with STEMI and was an independent predictor for post-infarction myocardial and microvascular injury and poor in-hospital outcome.

Trial Registration: The trial was registered at the registry of Clinicaltrials.gov, ClinicalTrials.gov Identifier: NCT04651842, Date of registration: 2nd December 2020 Registry URL, https://clinicaltrials.gov/ct2/show/NCT04385589?cond=Dapagliflozin+in+diabetic+patients&cntry=EG&draw=2&rank=1.

Keywords: acute insulin resistance, myocardial blush, non–diabetics, Primary PCI, Acute coronary syndromes

BACKGROUND

Complete myocardial reperfusion and restoration of coronary microcirculatory function (CMF) is a therapeutic goal in ST-segment elevation myocardial infarction (STEMI) (1). However, the success of primary percutaneous coronary intervention (pPCI) is not achieved in 30% to 50% of patients (2, 3).

It was found that insulin resistance (IR) plays substantial role in the development of cardiac-vascular infirmities and carries bad prognostic outcome for acute myocardial infarction (AMI) (4).

IR was found to be related to cardiac injuries on both muscular and microvascular levels after STEMI. Likewise, after adjusting for other integrals of metabolic syndrome, IR was associated with myocardial injury after elective PCI (5).

Now, IR was assessed by the homeostatic model assessment (HOMA) index in the early phase of acute coronary syndrome in non-diabetic patients. This "acute IR," considered a part of the acute glycol-metabolic response to stress, may be transient and also can occur even in patients without chronic glycol-metabolic derangements (6).

Acute IR includes acute hyperglycemia and/or acute hyperinsulinemia. Hyperglycemia has the importance of prognostic relevance of hyperinsulinemia in STEMI patients, but its relationship with coronary flow is still unclear (7, 8). However, the direct acute negative cardiovascular effects of hyperinsulinemia is acknowledged as it is contributing to incomplete myocardial reperfusion and CMF impairment (8).

Myocardial blush is a qualitative visual assessment of the amount of contrast medium filling a territory supplied by a pericardial coronary artery (9) (was first defined by Arnoud van't Hof et al.). Myocardial blush grade (MBG) is considered a reliable and valid tool for assessing coronary microvasculature and myocardial perfusion in patients undergoing coronary angiography and angioplasty (10). Decreased blush grade was used to identify those at increased risk who require intensive management both during the procedure to improve myocardial perfusion and later for secondary prevention (10).

The current study hypothesis was that acute IR can occur in the early post pPCI period even in non-diabetic patients as a dynamic phenomenon, and it could be related to the development of microvascular injury. Myocardial blush is defined as a marker of coronary microvascular function; accordingly, IR was evaluated in relation to myocardial blush in nondiabetic STEMI patients treated by pPCI as a primary endpoint. The residual ST-segment elevation, post-TFC% and major adverse cardiovascular events (MACE) were secondary endpoints. The HOMA index is a simple and inexpensive marker of IR, primary used in chronic states. It was recently validated in STEMI patients as feasible for assessing IR during myocardial infarction and therefore used in the current study (11).

Abbreviations: CMF, coronary microcirculatory function; STEMI, ST-segment elevation myocardial infarction; pPCI, primary percutaneous coronary intervention; STR, ST segment resolution; HOMA-IR, homeostatic modeling assessment—insulin resistance; AMI, acute myocardial infarction; MBG, myocardial blush grade; MACE, major adverse cardiovascular events.

METHODS

Study Participants

This cross-sectional comparative study included 240 non-diabetic patients with acute STEMI selected from the Cardiology Department, Assiut University Hospital, who underwent primary percutaneous coronary intervention (PCI) between May 1, 2018 and May 1, 2019. Sample size was calculated using the G*Power 3 software. With a power of 95% and type I error of 5% ($\alpha = 0.05$ and $\beta = 95\%$), the minimum required sample was 210 patients (further divided into three equal groups according to HOMA-IR tertiles) for an effect size of 10% in rate of myocardial blush grade.

Exclusion criteria were diabetic patients, renal insufficiency, advanced hepatic dysfunction, had malignancy, chronic heart failure/cardiomyopathy, prior myocardial infarction, and diseases requiring steroid therapy; patients on antioxidant supplement/therapy within 4 weeks before enrolment in the study, pregnant females, alcoholic, patients allergic to radiographic contrast, and uncooperative/refusal.

Ethical approval was obtained from the Medical Faculty, Assiut University (IRB No. 17300510) and was adherent to the guidelines of the declaration of Helsinki.

Clinical and Laboratory Assessment

After obtaining informed consent, the included patients were subjected to:

(1) Proper history taking including history for the presence of cardiovascular risk factors: hypertension, diabetes mellitus, dyslipidemia; smoking and family history of premature coronary artery disease, history of ischemia, previous CCU admission, and previous PCI.

(2) Complete physical examination including body mass index (BMI) was calculated using the formula of weight/height^2 (kilograms per square meter).
Blood pressure was measured in a seated position after a 10-min rest, using an electronic blood pressure monitor (Microlife AG, 9443 Widnau, Switzerland).

(3) Diagnosis of diabetes was made according to the criteria of the American Diabetes Association, and prediabetes was defined by fasting blood glucose of 100 mg to <126 mg/dl, 2-h plasma glucose of 140 to <200 mg/dl, or HbA1C of 5.7 to <6.5% (12).

(4) Hypertension was diagnosed according to the 8th Report of the Joint National Committee on Prevention, Detection, Evaluation, and Treatment of High Blood Pressure (JNC_8), and hyperlipidemia was diagnosed according to the guidelines of the National Cholesterol Education Program (ATP III) (13, 14).

(5) Blood samples were collected in an air-conditioned and quiet room. Serum glucose, blood urea, creatinine, total cholesterol, low-density lipoprotein—cholesterol (LDL-C), high-density lipoprotein—cholesterol (HDLC), and triglycerides were assessed using a HITACHI 912 Analyzer (Roche Diagnostics, Germany). Insulin and creatine kinase MB isoform level were assessed by AIA 900, fluorescence enzyme immunoassay (FEIA) method (Japanese).

HOMA-IR was calculated according to the formula (fasting insulin in mIU/L × fasting glucose in mg/dl)/405[15]. Normal reference levels for HOMA-IR range between 0.7 and 2.0. HOMA-IR is a preferred estimate for insulin resistance as glucose clamp methods, the current gold standard, are resource intensive and time consuming. Several studies use 2.0 as cutoff for increased insulin resistance (15).

Angiographic Assessment

After the angioplasty procedure immediately, epicardial and myocardial reperfusion was assessed and graded on the angiograms. In each patient, the best projection was chosen to assess the myocardial region of the infarct-related coronary artery, preferably without super positioning of non-infarcted myocardium. Angiographic runs must be long enough to allow some filling of the venous coronary system, and backflow of the contrast agent into the aorta have to be present to be sure of adequate contrast filling of the epicardial coronary artery.

All angiograms will be made after 400 μg of nitroglycerin intracoronary has been given immediately after the primary angioplasty procedures, and this procedure allows quantitative coronary artery analysis (16): First, epicardial reperfusion is assessed by thrombolysis in myocardial infarction (TIMI) flow grades (TFGs) as the following: Grade 0 means no perfusion, Grade 1 means penetration without perfusion, Grade 2 means partial perfusion, Grade 3 means complete perfusion (17). Epicardial reperfusion was also assessed by thrombolysis in myocardial infarction (TIMI) frame count (TFC), which is defined as the number of frames required for dye to first opacify a standard distal landmark (18). Second, myocardial reperfusion is assessed by TIMI myocardial perfusion grade (TMP) as the following: TMP Grade 0 denotes failure of dye to enter the microvasculature, TMP Grade 1 denotes dye slowly enters but fails to exit the microvasculature, TMP Grade 2 denotes delayed entry and exit of dye from the microvasculature, TMP Grade 3 denotes normal entry and exit of dye from the microvasculature (19).

Myocardial reperfusion had been also determined by measuring ST-segment resolution (STR) analysis so ECGs had been done on admission (first ECG) and 90 min after the primary PCI in the coronary care unit (second ECG). The second ECGs had been classified with regard to the ST segment resolution

TABLE 1 | Baseline demographic and clinical correlates of HOMA_IR.

Parameter	Low ($n = 80$)	Intermediate ($n = 80$)	High ($n = 80$)	*P*-value
Age/years	51.98 ± 10.2	52.95 ± 12.5	52.76 ± 12.3	= 0.855*
Sex (Male)	70 (87.5%)	63 (78.8%)	63 (78.8%)	= 0.256**
Smoker	51 (63.8%)	48 (60%)	52 (65%)	= 0.793**
Obesity	36 (45%)	40 (50%)	45 (56.3%)	**= 0.039****
Hypertensive	12 (15%)	23 (28.8%)	20 (25%)	= 0.093**
Killip class > 1	9 (11.3%)	7 (8.8%)	14 (17.5%)	**= 0.044****
GP IIb/IIIa Inhibitor	29 (36.3%)	32 (40%)	33 (41.3%)	= 0.518**
Pain-Balloon Time	4.24 ± 0.3	5.79 ± 0.6	4.19 ± 0.4	**= 0.035***
FBG	98.51 ± 6.6	99.33 ± 8.5	101.19 ± 11.3	**= 0.028***
Insulin Level	12.38 ± 0.5	23.03 ± 3.1	34.47 ± 7.5	**< 0.001***
LDL	105.14 ± 23.2	108.11 ± 22.1	104.47 ± 18.9	= 0.642*
HDL	46.85 ± 7.2	49.53 ± 7.5	49.16 ± 9.1	= 0.087*
TGD	122.46 ± 19.1	133.11 ± 21.3	134.76 ± 23.9	= 0.129*
Total Cholesterol	168.74 ± 18.5	170.55 ± 25.1	168.39 ± 21.6	= 0.898*
ALT	52.63 ± 4.9	53.71 ± 4.7	49.56 ± 2.4	= 0.468*
AST	129.35 ± 15.2	140.60 ± 15.5	128.10 ± 13.5	= 0.803*
S. Creatinine	0.85 ± 0.03	0.86 ± 0.03	0.87 ± 0.04	= 0.901*
CK-MB	213.09 ± 17.9	247.23 ± 19.5	270.73 ± 23.1	**= 0.031***

**ANOVA test was used to compare the mean difference between groups.*
***Chi-square test was used to compare proportions between groups.*
FBG, fasting blood glucose; LDL, low density lipoprotein; HDL, high density lipoprotein; TGD, triglycerides; ALT, alanine transaminase; AST, aspartate transaminase, Creatinine serum creatinine; CK-MB, Creatine kinase. Bold values mean statistically significant.

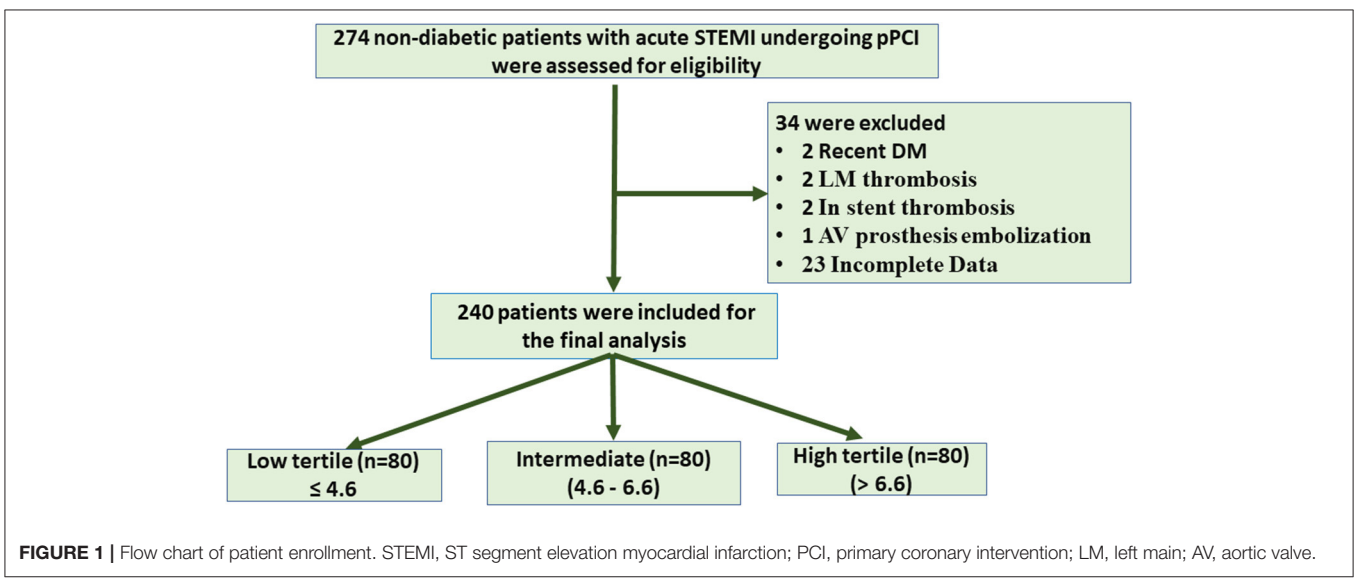

FIGURE 1 | Flow chart of patient enrollment. STEMI, ST segment elevation myocardial infarction; PCI, primary coronary intervention; LM, left main; AV, aortic valve.

into the following grades: Normalized, defined as no residual ST segment elevation; Improved, defined as a residual ST segment elevation <70% of that on the first ECG; Unchanged, defined as a residual ST segment elevation > 70% of that on the first ECG (20).

For all patients, postprocedural transthoracic echocardiography left ventricular ejection fraction was measured by biplane Simpson method using the end diastolic and end systolic apical four- and two-chamber views for estimation of left ventricular volume and calculation of ejection fraction. In hospital primary angioplasty procedures, major adverse cardiovascular events (MACEs) were determined and defined as the composite of death, stent thrombosis, re-infarction, cardiogenic shock, and stroke (20).

Data entry, verification, and validation were carried out by the researcher, and analyses were performed via IBM-SPSS software (Statistical Package for the Social Sciences, version 24, SSPS Inc, Chicago, IL, USA). Numerical data were expressed

TABLE 2 | Angiographic data correlates of HOMA_IR.

Parameter	Low ($n = 80$)	Intermediate ($n = 80$)	High ($n = 80$)	*P*-value
AWI	44 (55%)	40 (50%)	52 (65%)	= 0.150*
Baseline TIMI				**= 0.031****
• 0	66 (82.5%)	67 (83.8%)	70 (87.4%)	
• 1	3 (3.8%)	5 (6.3%)	8 (10%)	
• 2	9 (11.3%)	3 (3.8%)	1 (1.3%)	
• 3	2 (2.5%)	5 (6.3%)	1 (1.3%)	
Multi-vessel Dis.	27 (33.8%)	31 (38.8%)	28 (35%)	= 0.790*
Use of Stent	75 (93.8%)	74 (92.5%)	72 (90%)	= 0.670*
Type of Stent				= 0.858*
• BMS	58 (77.3%)	58 (78.4%)	54 (76.1%)	
• DES	17 (22.7%)	16 (21.6%)	17 (23.9%)	
Stent Length	26.75 ± 8.1	29.55 ± 9.3	29.93 ± 9.4	**= 0.045*****
Stent Diameter	3.28 ± 0.3	3.21 ± 0.3	3.29 ± 0.3	= 0.393***

**Chi-square test was used to compare proportions between groups.*
***Monte-Carlo Exact test was used to compare proportions between groups.*
****ANOVA test was used to compare the mean difference between groups.*
AWI, anterior wall infarction; TIMI, thrombolysis in myocardial infarction score; BMS, bare metal stent; DES, drug eluted stent Dis disease.
Bold values mean statistically significant.

TABLE 3 | Perfusion parameters data correlates of HOMA_IR.

Parameter	Low ($n = 80$)	Intermediate ($n = 80$)	High ($n = 80$)	*P*-value*
MBG				**< 0.001****
• 0	4 (4.9%)	2 (2.5%)	22 (27.4%)	
• 1	29 (36.3%)	37 (46.3%)	48 (60%)	
• 2	45 (56.3%)	30 (37.5%)	20 (25%)	
• 3	2 (2.5%)	1 (1.3%)	0 (0%)	
Post-TIMI				**= 0.010****
• 0	1 (1.3%)	0 (0%)	2 (2.5%)	
• 1	1 (1.3%)	1 (1.3%)	3 (3.8%)	
• 2	5 (6.3%)	2 (2.5%)	14 (17.5%)	
• 3	73 (91.3%)	61 (67.2%)	77 (96.3%)	
S-T Resolution				**= 0.035***
• Improved	63 (78.7%)	50 (62.5%)	46 (57.5%)	
• Normalized	5 (6.3%)	6 (7.5%)	6 (7.5%)	
• Unchanged	12 (15%)	24 (30%)	28 (35%)	
Post- TFC%	24.48 ± 6.4	26.64 ± 7.1	31.79 ± 8.4	**< 0.001*****

**Chi-square test was used to compare proportions between groups.*
***Monte-Carlo Exact test used to compare between groups.*
****ANOVA test was used to compare the mean difference between groups.*
MBG, myocardial blush grade; post-TIMI, post interventional TIMI; S-T ST, segment; Post-TFC, post interventional TIMI frame count.
Bold values mean statistically significant.

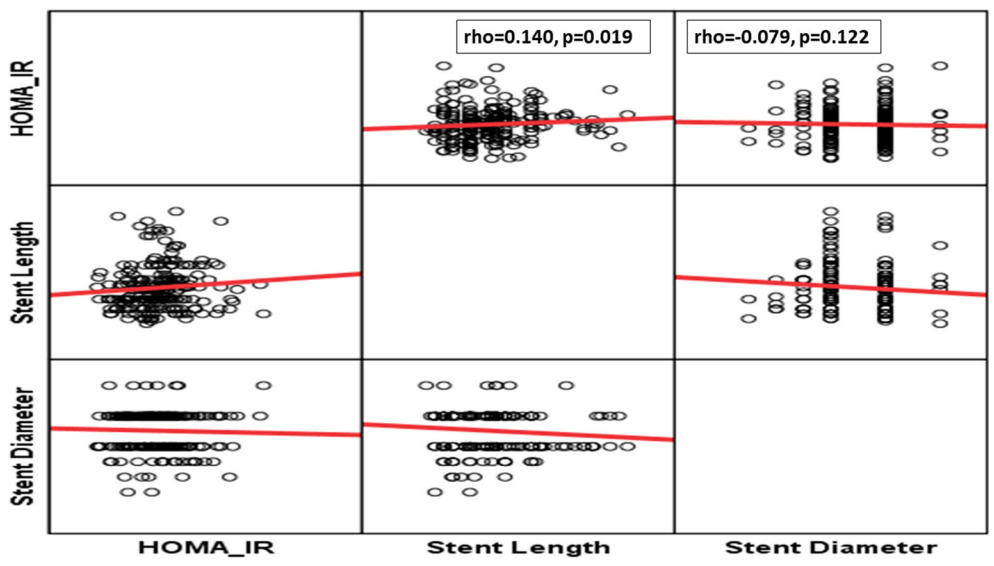

FIGURE 2 | Correlation between estimated insulin resistance (HOMA-IR) and stent parameters.

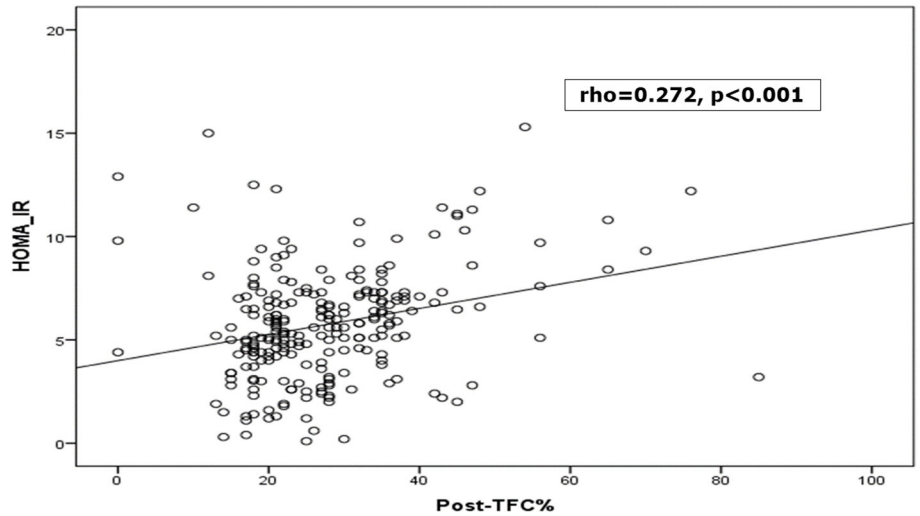

FIGURE 3 | Correlation between HOMA-IR and thrombolysis in myocardial infarction (TIMI) frame count (TFC) %.

TABLE 4 | HOMA_IR in relation with short and long disease outcomes.

Parameter	Low (n=80)	Intermediate (n = 80)	High (n = 80)	P-value
Hospital Stay/day	2.59 ± 0.2	2.33 ± 0.1	2.64 ± 0.1	= 0.200*
Arrhythmia	12 (15%)	17 (21.3%)	10 (12.5%)	= 0.303**
LVF	9 (11.3%)	6 (7.5%)	14 (17.5%)	= 0.146**
Pulmonary Edema	0 (0%)	0 (0%)	3 (3.8%)	**= 0.013*** **
Cardiogenic Shock	3 (3.8%)	0 (0%)	1 (1.3%)	= 0.094***
Re-Infarction	0 (0%)	2 (2.5%)	2 (2.5%)	= 0.208***
Stent Thrombosis	1 (1.3%)	3 (3.8%)	2 (2.5%)	= 0.623***
Post pPCI EF%	53.12 ± 8.6	50.91 ± 8.7	49.33 ± 9.6	**= 0.031***

**ANOVA test was used to compare the mean difference between groups.*
***Chi-square test was used to compare proportions between groups.*
****Monte-Carlo Exact test to compare proportions between groups.*
LVF, left ventricular failure; EF, ejection fraction; pPCI, primary percutaneous coronary intervention.
Bold values mean statistically significant.

as mean ± SD, and frequency tables with percentages were used for categorical variables. χ^2 and Monte Carlo exact test was used to compare the difference in the distribution of frequencies among different groups. One-way ANOVA was used to determine the mean difference between groups. Binary logistic forward regression analysis was used to define the independent predictors of MBG variables that showed significant differences among the studied groups. A value of $p < 0.05$ was considered statistically significant.

RESULTS

This study aimed to evaluate the impact of insulin resistance in non-diabetic (IR) on myocardial blush and in hospital MACE in the setting of STEMI patients treated with PCI. Non-diabetic patients (274), with anterior and non-anterior STEMI, who were admitted to the ICU during the study period, were recruited. Thirty-four patients were excluded for recently discovered diabetes mellitus, left main thrombosis, aortic valve prostheses with embolization, stent thrombosis, and defect of data counting. Hence, 240 patients (classified based on equal tertile of HOMA IR level into three equal groups (low ≤ 4.6, intermediate 4.6–6.6, and high > 6.6) were available for analysis (**Figure 1**).

The majority of the studied patients were males aged >50 years with insignificant difference between groups in relation to HOMA-IR. Moreover, acute insulin resistance as estimated by HOMA-IR tertile was significantly higher in obese, those with heart failure (Killip class >1), and higher plasma insulin level, CPK-MB, and fasting blood glucose level (**Table 1**).

Angiographic Data Correlates of Homeostasis Model Assessment—Estimated Insulin Resistance

Although, patients with anterior wall infarction (AWI) had insignificantly higher HOMA-IR levels, those with higher HOMA-IR experienced significantly low-grade baseline TIMI as higher tertile was founded on grade 0 baseline TIMI (**Table 2**). Also, patients who need longer stents experienced significantly higher levels of HOMA-IR levels (**Table 2** and **Figure 2**). However, no differences could be detected regarding stent diameter, presence of multivessel disease, and use of DES (**Table 2** and **Figure 2**).

Perfusion Parameters Data Correlates of Homeostasis Model Assessment—Estimated Insulin Resistance

It was found that patients with MBG 0, 1, 2 had higher HOMA-IR level than those with grade 3, and those who had unchanged ST segment in their ECG after reperfusion had higher HOMA-IR level. Furthermore, postprocedural TIMI frame count (TFC) was

TABLE 5 | Predictors of myocardial blush (No/Minimal MB) among patients: logistic regression model.

Variable	Univariate		Multivariate	
	OR (95% CI)	*P*-value	HR (95% CI)	*P*-value
Age/years	**1.029 (1.005–1.053)**	**= 0.017**	1.033 (0.976–1.093)	= 0.261
Sex (Male)	**1.253 (1.036–3.683)**	**= 0.039**	1.164 (0.477–3.812)	= 0.153
Smoker	**1.309 (1.099–4.024)**	**= 0.020**		
BMI (Obese)	0.894 (0.629–1.270)	= 0.531		
Pain-Balloon Time/h	**1.086 (1.004–1.174)**	**= 0.040**		
Previous CAD	**3.119 (1.224–7.946)**	**= 0.017**	**2.813 (1.195–5.001)**	**= 0.031**
Hypertensive	**1.941 (1.013–3.718)**	**= 0.046**	**3.274 (1.043–10.274)**	**= 0.042**
AWI	1.114 (0.663–1.875)	= 0.685		
Killip > 1	**11.789 (2.738–50.766)**	**= 0.001**		
ALT	**1.012 (1.001–1.024)**	**= 0.038**		
AST	**1.004 (1.001–1.006)**	**= 0.011**		
S. Creatinine	**2.582 (1.104–7.102)**	**= 0.016**		
Hospital Stay/days	1.197 (0.903–1.585)	= 0.211		
LVF	**11.270 (2.613–48.606)**	**= 0.001**	**5.157 (1.957–51.134)**	**= 0.024**
GP IIb/IIIa Inhibitor	**5.644 (3.041–10.475)**	**< 0.001**	**4.905 (1.649–14.586)**	**= 0.004**
Multi-vessel Affection	**2.199 (1.253–3.860)**	**= 0.006**	**2.602 (1.001–6.770)**	**= 0.049**
Baseline TIMI	**0.666 (0.461–0.964)**	**= 0.031**		
Use of Stent	0.360 (0.116–1.121)	= 0.078		
Stent Length	**1.049 (1.015–1.085)**	**= 0.005**	**1.066 (1.009–1.127)**	**= 0.023**
Post PCI TFC %	**1.229 (1.162–1.300)**	**< 0.001**	**1.328 (1.216–1.451)**	**< 0.001**
Post PCI LVEF%	**0.931 (0.899–0.963)**	**< 0.001**	**0.946 (0.840–0.979)**	**= 0.002**
Unchanged ST Resolution	**2.143 (1.517–3.028)**	**< 0.001**		
CK-MB	**1.003 (1.001–1.005)**	**= 0.001**	**1.009 (1.002–1.084)**	**= 0.034**
One-month LVEF%	**0.885 (0.851–0.920)**	**< 0.001**		
HOMA_IR	**1.202 (1.079–1.339)**	**= 0.001**	**1.156 (1.009–2.039)**	**= 0.011**

zOR = odds ratio; CI, confidence interval.

BMI, body mass index; CAD, coronary artery disease; AWI, anterior wall infarction; ALT, alanine transaminase; AST, aspartate transaminase; LVF, left ventricular failure; TIMI, the thrombolysis in myocardial infarction; TFC TIMI, frame count; LVEF, left ventricle ejection fraction; ST, st segment; CK-MB, creatine kinase MB; HOMA-IR, homeostatic model assessment of insulin resistance.

Bold values mean statistically significant.

longer in those with higher HOMA-IR level. Patients with low, intermediate HOMA-IR levels showed higher postprocedural TIMI flow grade than Grade 3 (**Table 3** and **Figure 3**).

Homeostasis Model Assessment—Estimated Insulin Resistance in Relation With Disease Outcome

A higher level of HOMA-IR was detected in those with post MI pulmonary edema; however, prolonged hospital stays, arrhythmias, LVF, cardiogenic shock, re-infarction, and early stent thrombosis complicated higher HOMA-IR level but with insignificant difference (**Table 4**).

Predictors of Myocardial Blush (No/Minimal MB) Among Patients

For final multivariate regression analysis model and after adjusting for age and sex, there were 10 predictors of no/minimal myocardial blush in the studied cohort (previous CAD, hypertension, LVF, use of GPIIb/IIIa inhibitor, stent length, postprocedural TFC %, post MI LVEF %, and CKMB level). Importantly, HOMA-IR level is considered an independent risk for decreasing myocardial blush, i.e., with one unit increase in HOMA-IR level, there was decreasing myocardial blush by 20% in univariate analysis (OR:1.2, 95% CI: 1.08–1.34, $p = 0.001$) and by 10% in the multivariate analysis (OR:1.6, 95% CI: 1.01–2.04, $p = 0.011$) (**Table 5**).

DISCUSSION

The present study analyzed IR in the acute phase of STEMI in non-diabetic patients treated by pPCI. First, it confirmed that acute IR in the early post pPCI period is common even in non-diabetic patients; second, IR, as estimated by HOMA-IR, affects myocardial perfusion especially MBG; and third, IR was related to the in-hospital MACE.

IR in the early phase of STEMI is considered part of the acute glycol-metabolic response to stress (21) Generally, in critically ill patients, acute IR is related to more severe acute illness and leads to poor clinical outcome (22, 23). The mean HOMA-IR level in this study was beyond the normal range as defined by

a substantial number of epidemiological studies (24, 25). The majority of patients were obese and have significantly earlier post PCI hyperinsulinemia and, hence, higher HOMA-IR tertile. The same increment in insulin in the early post PCI period in non-diabetic patients was previously reported (26); Nishio et al. did serial HOMA index measurements among patients who underwent pPCI and identified those with transient IR, in whom HOMA index correlated with stress hormones (catecholamine and cortisol) and patients with persistent IR, in whom HOMA index during follow-up correlated with leptin and contributed to stent restenosis (27).

More cardiac necrosis was reported in those with higher IR. The relationship between acute IR in non-diabetic STEMI patients and myocardial damage in terms of peak enzymes was previously reported (28, 29). In this study, both HOMA indices were correlated well with the peak CKMB in the presence or absence of other confounders and insignificantly higher insulin resistance among those with anterior wall STEMI.

Acute hyperglycemia and IR *per se* predicted impaired epicardial flow before pPCI (30). This matched with our study findings, which speculated that IR was significantly higher in those with grade 0 TIMI either at baseline or post-interventional, and this may explain why those with higher HOMA index needed significantly longer stents. Also, there was significantly higher IR in those with more postprocedural TFC%. It may be related to the increased oxidative stress in STEMI, increased vascular cell apoptosis, and hence induced acute endothelial dysfunction.

The relationship between ST-R and acute IR was not conclusive. Acute hyperglycemia was related to limited ST-R in mixed diabetic and non-diabetic STEMI population after thrombolytic therapy (31) and after pPCI (32) and was identified as a predictor of ST resolution after pPCI. In the current study, in patients without diabetes, incomplete ST resolution was significantly more frequent among those with acute IR. Although the inverse relationship between HOMA IR level and myocardial perfusion was described in different states; to the best of our knowledge the current study is the first to link acute IR assessed by the HOMA index and myocardial blush in non-diabetic STEMI patients to assess microvascular perfusion.

Moreover, it was found that acute IR significantly affect myocardial blush; higher HOMA-IR level was associated with lower MBG and vice versa. Higher levels of HOMA-IR either alone or after adjusting for all other confounders (hypertension, previous CAD, LVF, multivessel CAD, reduced LVEF, and increased CPK_MB level) were considered important predictors of markedly reduced myocardial blush. This may be explained by IR in the setting of STIMI being associated with poor myocardial reperfusion, impaired coronary microcirculation (33) and collateralization (34) and reduced collagen deposition in the scar (35). These factors potentially lead to greater infarct size, post-infarction LV dilation, and finally a higher incidence of heart failure (36). Nevertheless, the implicated mechanisms await precise characterization in future studies. It was speculated in this research that acute IR was associated with poorer outcome, as higher HOMA-IR tertile was significantly observed in those with pulmonary edema and reduced LVEF. On the other hand, IR was insignificantly higher in those with LVF, prolonged hospital stays, arrhythmia, stent thrombosis, re-infarction, and cardiogenic shock.

CONCLUSION

The current study revealed that acute IR was prevalent in non-diabetic patients with STEMI and was identified as an independent predictor of post infarction myocardial and microvascular injury. Likewise, it was found to be associated with poor in-hospital outcome.

DATA AVAILABILITY STATEMENT

The raw data supporting the conclusions of this article will be made available by the authors, without undue reservation.

ETHICS STATEMENT

The studies involving human participants were reviewed and approved by prof/Mahmoud abdel-Aleem- Medical ethics committee IRB no.17300510. The patients/participants provided their written informed consent to participate in this study. Written informed consent was obtained from the individual(s) for the publication of any potentially identifiable images or data included in this article.

AUTHOR CONTRIBUTIONS

SK and MA conceptualized and designed the study, conducted a literature search, conducted the clinical studies, prepared the experimental study manuscript, and edited and reviewed the article. AH was in charge of the definition of intellectual content, literature search and manuscript review, clinical studies, experimental studies, and data acquisition. GS conducted the clinical studies, experimental studies, and acquired the data. All authors contributed to the article and approved the submitted version.

ACKNOWLEDGMENTS

The authors expressed their profound gratitude and thanks to the Faculty of Medicine, Assiut University, for facilitating the current work. We acknowledge the participants who accepted to take part in the current study. It would not have been possible without their help and support.

REFERENCES

1. Task force on the management of ST-segment elevation acute myocardial infarction of the European society of cardiology (ESC): guidelines for the management of acute myocardial infarction in patients presenting with ST-segment elevation. *Eur Heart J*. (2012) 33:2569–619. doi: 10.1093/eurheartj/ehs215
2. Lerman A, Holmes DR, Herrmann J, Gersh BJ. Microcirculatory dysfunction in ST-elevation myocardial infarction: cause, consequence, or both? *Eur Heart J*. (2007) 28:788–97. doi: 10.1093/eurheartj/ehl501
3. Niccoli G, Burzotta F, Galiuto L, Crea F. Myocardial no-reflow in humans. *J Am Coll Cardiol*. (2009) 54:281–92. doi: 10.1016/j.jacc.2009.03.054
4. Arnold SV, Lipska KJ, Li Y, Goyal A, Maddox TM, McGuire DK, et al. The reliability and prognosis of in-hospital diagnosis of metabolic syndrome in the setting of acute myocardial infarction. *J Am Coll Cardiol*. (2013) 62:704–8. doi: 10.1016/j.jacc.2013.02.062
5. Uetani T, Amano T, Harada K, Kitagawa K, Kunimura A, Shimbo Y, et al. Impact of insulin resistance on post-procedural myocardial injury and clinical outcomes in patients who underwent elective coronary interventions with drug-eluting stents. *JACC Cardiovasc Interv*. (2012) 5:1159–67 doi: 10.1016/j.jcin.2012.07.008
6. Sanjuan R, Blasco ML, Huerta R, Palacios L, Carratala A, Nunyez J, et al. Insulin resistance and short-term mortality in patients with acute myocardial infarction. *Int J Cardiol*. (2014) 172:e269–70. doi: 10.1016/j.ijcard.2013.12.207
7. Zarich WS, Nesto RW. Implications and treatment of acute hyperglycemia in the setting of acute myocardial infarction. *Circulation*. (2007) 115:e436–9. doi: 10.1161/CIRCULATIONAHA.105.535732
8. Cruz-Gonzalez I, Chia S, Raffel OC, Sanchez-Ledesma M, Senatore F, Wackers FJ, et al. Hyperglycemia on admission predicts larger infarct size in patients undergoing percutaneous coronary intervention for acute ST-elevation myocardial infarction. *Diabetes Res Clin Pract*. (2010) 88:97–102. doi: 10.1016/j.diabres.2010.01.001
9. Van 't Hof AWJ, Liem A, Suryapranata H, Hoorntje JCA, Jan de Boer M, Zijlstra F. Angiographic assessment of myocar-dial reperfusion in patients treated with primary angioplasty for acute myocardial infarction myocardial blush grade. *Circulation*. (1998) 97:2302–6. doi: 10.1161/01.CIR.97.23.2302
10. Hristo Tsvetkov MD1 and morris mosseri MD2 myocardial blush grade: an interventional method for assessing myocardial perfusion. *IMAJ*. (2008) 10:465–467.
11. Moura FA, Carvalho LS, Cintra RM, Martins NV, Figueiredo VN, Quinaglia E, et al. Validation of surrogate indexes of insulin sensitivity in acute phase of myocardial infarction based on euglycemic hyper-insulinemic clamp. *Am J Physiol Endocrinol*. 306:E399–403. doi: 10.1152/ajpendo.00566.2013
12. American Diabetes A. Standards of medical care in diabetes-−2012. *Diabetes Care*. (2012) 35(Suppl 1):S11–63. doi: 10.2337/dc12-s011
13. James PA, Oparil S, Carter BL, Cushman WC, Dennison-Himmelfarb C, Handler J, et al. 2014 evidence-based guideline for the management of high blood pressure in adults: report from the panel members appointed to the Eighth Joint National Committee (JNC 8). *JAMA*. (2014) 311:507–20. doi: 10.1001/jama.2013.284427
14. Grundy SM, Cleeman JI, Merz CN, Brewer HB Jr, Clark LT, Hunninghake DB, et al. Implications of recent clinical trials for the national cholesterol education program adult treatment panel III guidelines. *Circulation*. (2004) 110:227–39. doi: 10.1161/01.CIR.0000133317.49796.0E
15. Hanley AJ, Williams K, Stern MP, Haffner SM. Homeostasis model assessment of insulin resistance in relation to the incidence of cardiovascular disease: the san antonio heart study. *Diabetes Care*. (2002) 25:1177–84. doi: 10.2337/diacare.25.7.1177
16. De Boer MJ, Reiber JHC, Suryapranata H, Brand MV, Hoorntje JC, Zulstra F, et al. Angiographic findings and catheterization laboratory events in patients with primary coronary angioplasty or streptokinase therapy for acute myocardial infarction. *Eur Heart J*. (1995) 16:1347–56. doi: 10.1093/oxfordjournals.eurheartj.a060741
17. Chesebro JH, Knatterud G, Roberts R, Borer J, Cohen LS, Dalen J, et al. Thrombolysis in myocardial infarction (TIMI) trial. *N Eng J Med*. (1985) 312:932–6. doi: 10.1056/NEJM198504043121437
18. Gibson CM, Cannon CP, Daley WL, Dodge Jr JT, Alexander B, Marble SJ, et al. TIMI frame count: a quantitative method of assessing coronary artery flow. *Circulation*. (1996) 93:879–88. doi: 10.1161/01.CIR.93.5.879
19. Gibson CM, Cannon CP, Murphy SA, Ryan KA, Mesley R, Marble SJ, et al. Relationship of TIMI myocardial perfusion grade to mortality after administration of thrombolytic drugs. *Circulation*. (2000) 101:125–30. doi: 10.1161/01.CIR.101.2.125
20. van't Hof AW, Liem A, de Boer MJ, Zijlstra F, Zwolle Myocardial Infarction Study Group. For the zwolle myocardial infarction study group. Clinical value of 12-lead electrocardiogram after successful reperfusion therapy for acute myocardial infarction. *Lancet*. (1997) 350:615–9. doi: 10.1016/S0140-6736(96)07120-6
21. IBM_SPSS. *Statistical Package for Social Science. Ver.21. Standard version*. New York, NY: Copyright © SPSS Inc., 2011-2012 (2012).
22. Nishio K, Shigemitsu M, Kusuyama T, Fukui T, Kawamura K, Itoh S, et al. Insulin resistance in nondiabetic patients with acute myocardial infarction. *Cardiovasc Revasc Med*. (2006) 7:54–60. doi: 10.1016/j.carrev.2005.12.004
23. Li L, Messina JL. Acute insulin resistance following injury. *Trends Endocrinol Metab*. (2009) 20:429–35. doi: 10.1016/j.tem.2009.06.004
24. Pretty CG, Le Compte AJ, Chase JG, Shaw GM, Preiser JC, Penning S, Desaive T. Variability of insulin sensitivity during the first 4 days of critical illness: implications for tight glycemic control. *Ann Intensive Care*. (2012) 2:17. doi: 10.1186/2110-5820-2-17
25. Hedblad B, Nilsson P, Engström G, Berglund G, Janzon L. Insulin resistancein non-diabetic subjects is associated with increased incidence of myocardial infarction and death. *Diabet Med*. (2002) 19:470–5. doi: 10.1046/j.1464-5491.2002.00719.x
26. Shah RV, Abbasi SA, Heydari B, Rickers C, Jacobs DR, Wang L, et al. Insulin resistance, subclinical left ventricular remodeling, and the obesity paradox: MESA (Multi-Ethnic Study of Atherosclerosis). *J Am Coll Cardiol*. (2013) 61:1698–706. doi: 10.1016/j.jacc.2013.01.053
27. Gruzdeva O, Uchasova E, Dyleva Y, Belik E, Shurygina E, Barbarash O. Insulin resistance and inflammation markers in myocardial infarction. *J Inflamm Res*. (2013) 6:83–90. doi: 10.2147/JIR.S43081
28. Lazzeri C, Valente S, Chiostri M, Picariello C, Gensini GF. Correlates of acute insulin resistance in the early phase of non-diabetic ST-elevation myocardial infarction. *Diab Vasc Dis Res*. (2011) 8:35–42. doi: 10.1177/1479164110396744
29. Lazzeri C, Sori A, Chiostri M, Gensini GF, Valente S. Prognostic role of insulin resistance as assessed by homeostatic model assessment index in the acute phase of myocardial infarction in nondiabetic patients submitted to percutaneous coronary intervention. *Eur J Anaesthesiol*. (2009) 26:856–62. doi: 10.1097/EJA.0b013e32832a235c
30. Timmer J, Ottervanger J, de Boer M, Dambrink JE, Hoorntje JCA, Gosselink ATM, et al. Hyperglycemia is an important predictor of impaired coronary flow before reperfusion therapy in ST-segment elevation myocardial infarction. *J Am Coll Cardiol*. (2005) 45:999–1002. doi: 10.1016/j.jacc.2004.12.050
31. L'Huillier I, Zeller M, Mock L, Beer JC, Laurent Y, Sicard P, et al. Relation of hyperglycemia toST-segment resolution after reperfusion for acute myocardial infarction(from Observatoire des Infarctus de Côte-d'Or Survey [RICO]). *Am J Cardiol*. (2006) 98:167–171. doi: 10.1016/j.amjcard.2006.01.087
32. Chi HJ, Zhang DP, Xu Y, Yang ZS, Wang LF, Cui L, Yang XC. Relation of hyperglycemia to ST-segment resolution after primary percutaneous coronary intervention for acute myocardial infarction. *Chin Med J*. (2007) 120:1874–77. doi: 10.1097/00029330-200711010-00004
33. Trifunovic D, Stankovic S, Sobic-Saranovic D, Marinkovic J, Petrovic M, Orlic D, et al. Acute insulin resistance in ST-segment elevation myocardial infarction in nondiabetic patients is associated with incomplete myocardial re-perfusion and impaired coronary microcirculatory function. *Cardiovasc Diabetol*. (2014) 13:73 doi: 10.1186/1475-2840-13-73
34. Chou E, Suzuma I, Way KJ, Opland D, Clermont AC, Naruse K, et al. Decreased cardiac expression of vascular endothelial growth factor and its

receptors in insulin-resistant and diabetic states: a possible explanation for impaired collateral formation in cardiac tissue. *Circulation.* (2002) 105:373–9. doi: 10.1161/hc0302.102143

35. Thakker GD, Frangogiannis NG, Bujak M, Zymek P, Gaubatz JW, Reddy AK, et al. Effects of diet-induced obesity on inflammation and remodeling after myocardial infarction. *Am J Physiol Heart Circ Physiol.* (2006) 291:H2504–14. doi: 10.1152/ajpheart.00322.2006
36. Vardeny O, Gupta DK, Claggett B, Burke S, Shah A, Loehr L, et al. Insulin resistance and incident heart failure the ARIC study (atherosclerosis risk in communities). *JACC; Heart Fail.* (2013) 1:531–6. doi: 10.1016/j.jchf.2013.07.006

Conflict of Interest: The authors declare that the research was conducted in the absence of any commercial or financial relationships that could be construed as a potential conflict of interest.

frontiers in Cardiovascular Medicine

REVIEW
published: 28 July 2021
doi: 10.3389/fcvm.2021.675608

High-Energy Phosphates and Ischemic Heart Disease: From Bench to Bedside

Hao Yi-Dan, Zhao Ying-Xin, Yang Shi-Wei and Zhou Yu-Jie**

The Key Laboratory of Remodeling-Related Cardiovascular Disease, Ministry of Education, Beijing Institute of Heart, Lung and Blood Vessel Disease, Beijing Anzhen Hospital, Capital Medical University, Beijing, China

The purpose of this review is to bridge the gap between clinical and basic research through providing a comprehensive and concise description of the cellular and molecular aspects of cardioprotective mechanisms and a critical evaluation of the clinical evidence of high-energy phosphates (HEPs) in ischemic heart disease (IHD). According to the well-documented physiological, pathophysiological and pharmacological properties of HEPs, exogenous creatine phosphate (CrP) may be considered as an ideal metabolic regulator. It plays cardioprotection roles from upstream to downstream of myocardial ischemia through multiple complex mechanisms, including but not limited to replenishment of cellular energy. Although exogenous CrP administration has not been shown to improve long-term survival, the beneficial effects on multiple secondary but important outcomes and short-term survival are concordant with its pathophysiological and pharmacological effects. There is urgent need for high-quality multicentre RCTs to confirm long-term survival improvement in the future.

Keywords: high-energy phosphates, creatine phosphate, energy metabolism, ischemic heart disease, cardioprotection

OPEN ACCESS

Edited by:
Zhong Wang,
University of Michigan, United States

Reviewed by:
Xu Chen,
University of Mississippi Medical Center, United States
Zhihua Wang,
Chinese Academy of Medical Sciences and Peking Union Medical College, China

****Correspondence:***
Yang Shi-Wei
yang.shiwei@ccmu.edu.cn
Zhou Yu-Jie
azzyj_12@163.com

Specialty section:
This article was submitted to Cardiovascular Metabolism, a section of the journal Frontiers in Cardiovascular Medicine

Received: *03 March 2021*
Accepted: *17 June 2021*
Published: *28 July 2021*

Citation:
Yi-Dan H, Ying-Xin Z, Shi-Wei Y and Yu-Jie Z (2021) High-Energy Phosphates and Ischemic Heart Disease: From Bench to Bedside. Front. Cardiovasc. Med. 8:675608. doi: 10.3389/fcvm.2021.675608

INTRODUCTION

The heart is more than a hemodynamic pump. It is also an organ that needs energy from metabolism (1). In fact, altered cardiac metabolism is the primary and upstream pathophysiologic manifestation of myocardial ischemia in humans (2). After coronary blood flow blockage, energy metabolism disorder occurs within a few seconds, followed by mechanical, electrophysiological and structural abnormalities of the myocardium. To date, standard treatments for ischemic heart disease (IHD), including revascularization (thrombolysis, percutaneous coronary intervention, and coronary artery bypass grafting), antithrombotic therapy (antiplatelet and anticoagulant agents), stabilization/reversal of atherosclerosis progression (control of atherosclerotic risk factors), and inhibition of myocardial remodeling (sympathetic and renin-angiotensin-aldosterone system inhibitors), focus on coronary anatomy and on the results of changes in myocardial metabolism rather than on the metabolic changes themselves (2–8). In addition, almost all of the above treatments exert cardioprotection by directly or indirectly affecting heart rate, blood pressure or myocardial perfusion. In contrast, myocardial energy metabolic therapy (MEMT) plays a protective role by regulating the energy synthesis and utilization of myocardial cells without significant impacts on heart rate, blood pressure and perfusion (9, 10). Because of residual cardiovascular risk, MEMT is promisingly emerging as an upstream treatment for IHD (11).

Since the discovery of creatine phosphate (CrP) in 1927 (12) and adenosine triphosphate (ATP) in 1929 (13), the biochemical, physiological, and pharmacological properties of high-energy phosphates (HEPs) have been gradually uncovered. Unlike the single metabolic process of glucose, free fatty acids or amino acids, the pathways and regulations of HEPs biosynthesis and degradation are involved in all metabolic substrates. Moreover, due to the production and consumption of HEPs in different cells and subcellular organelles, the transmembrane transport of HEPs is also a complex process requiring the assistance of many special transporters and catalytic enzymes (14). Therefore, although HEPs have been known for nearly a 100 years, clinicians still have a lot to learn. In recent years, a series of basic and clinical studies have shown potent protection for IHD by exogenous HEPs (15–19). These results have been confirmed in our laboratories (16, 20, 21).

Previous reviews focused either on the cellular and molecular mechanisms of HEPs which is too complex for clinical application (14, 22), or on presenting the clinical evidence which in turn is too simple for clinicians to understand their pathophysiological and pharmacological effects (15, 16). The purpose of this article is to bridge the gap between clinical and basic research.

OVERVIEW OF HIGH-ENERGY PHOSPHATES AND THEIR TRANSFORMATION

It is believed that energy would be concentrated in the chemical bond containing phosphate groups, which yields energy upon hydrolysis (23). Low-energy phosphates are usually linked to phosphoester bonds, which will release 2 and 3 kcal/mol energy. HEPs include a variety of phosphate compounds with energies of hydrolysis higher than 7 kcal/mol (24). ATP and CrP are considered to be the primary HEPs in human body. ATP is the intracellular energy currency, majority of which is not synthesized *de novo* but generated from adenosine diphosphate (ADP) by oxidative phosphorylation (OP) of mitochondria and cytoplasmic substrate phosphorylation (SP) (**Figure 1**) (25, 26). Thus, at any given time, the total amount of ATP and ADP remains fairly constant and recycled continuously (27). While, CrP is the storage and transport carrier of energy, which serves to transfer the HEP-bond from the site of ATP production to the site of ATP utilization through "CrP shuttle" (**Figure 1**) (28–35). Normally the total quantity of ATP in human body is about 0.1 mole (∼50 g). However, the energy used by human cells requires the hydrolysis of 100–150 moles (around 50–75 kg) of ATP daily (36). This means that each ATP molecule is recycled 1,000–1,500 times during a single day. The ATP and CrP activity combined, also referred to as the phosphagen system, is the most rapidly available source of energy (37). Unfortunately, the energy available from the store of phosphagen system is limited and can provide energy for a few seconds of maximal activity.

CrP, also known as phosphocreatine or phosphorylated creatine, is a small molecular compound with the formula of $C_4H_{10}N_3O_5P$, having a molecular weight of 211 daltons. There is one high-energy phosphate bond (N∼P) in the chemical structure. As compared, ATP has a relatively more complex molecular structure ($C_{10}H_{16}N_5O_{13}P_3$), larger molecular weight (507 daltons), and two high-energy phosphate bonds (O∼P). However, the N∼P bond of CrP has more energy than either one O∼P bond of ATP, 10.3 kcal/mol in comparison with 7.3 kcal/mol (**Figure 2**) (38). Therefore, CrP can easily provide enough energy and serve as a HEP-bond donor for ATP reconstitution through "CrP shuttle" (28).

The contents of HEPs vary significantly in different tissues. The highest levels of HEPs are found in muscle, heart, brain, spermatozoa, and retina (14). The concentration and distribution of HEPs *in vivo* can be determined non-invasively by 31^P-magnetic resonance spectroscopy (MRS) (39, 40). The myocardial CrP/ATP ratio measured by 31^P-MRS reflects the viability and energy metabolic status of cardiomyocytes (41). Over a wide range of cardiac workloads, the CrP/ATP ratio is essentially invariant and consistent with a constant free ADP concentration (42, 43). The cutoff point for CrP/ATP ratio (>1.60 and <1.60), which was established retrospectively and need to be evaluated prospectively, is a stronger predictor of cardiovascular death (44). The ratio is decreased upon myocardial ischemia (45, 46).

THE BIOSYNTHESIS, DEGRADATION AND TURNOVER OF ENDOGENOUS CREATINE PHOSPHATE

The biosynthesis of CrP begins by formation of creatine from three essential amino acids: arginine, glycine, and methionine (**Figure 3**) (14). The entire glycine molecule is incorporated whereas arginine furnishes its amidino group to yield guanidinoacetic acid (GAA), which then methylated at the amidino group to give creatine. It is postulated, but largely accepted, that the main route of creatine synthesis involves formation of guanidinoacetate in kidney, and methylation in liver (47–49). These reactions are respectively catalyzed by two rate-limiting enzymes, i.e., L-arginine:glycine amidinotransferase (AGAT) and S-adenosyl-L-methionine:N-guanidinoacetate methyltransferase (GAMT) (47–50). To complete the phosphorylation process, creatine is then transported to tissues such as muscle, heart, and brain by a specific Na^+- and Cl^--dependent plasma membrane transporter (51). CrP production is catalyzed by creatine kinase (CK), which is a dimer of M and B (M = muscle, B = brain) subunits produced by different structural genes. Three isozymes are possible: BB, MB, and MM. Cardiac muscle contains significant amounts of CK-MB (25–46% of total CK activity, as opposed to

Abbreviations: ADP, adenosine diphosphate; AGAT, L-arginine:glycine amidinotransferase; AMP, adenosine monophosphate; APD, action potential duration; ATP, adenosine triphosphate; CK, creatine kinase; CrP, creatine phosphate; ERP, effective refractory period; GAA, guanidinoacetic acid; GAMT, S-adenosyl-L-methionine:N-guanidinoacetate methyltransferase; HEPs, high-energy phosphates; IHD, ischemic heart disease; KATP, ATP-sensitive K^+ channels; LPLs, lysophospholipids; MDA, malondialdehyde; MEMT, myocardial energy metabolic therapy; MRS, magnetic resonance spectroscopy; OP, oxidative phosphorylation; RCTs, randomized controlled trials; SP, substrate phosphorylation.

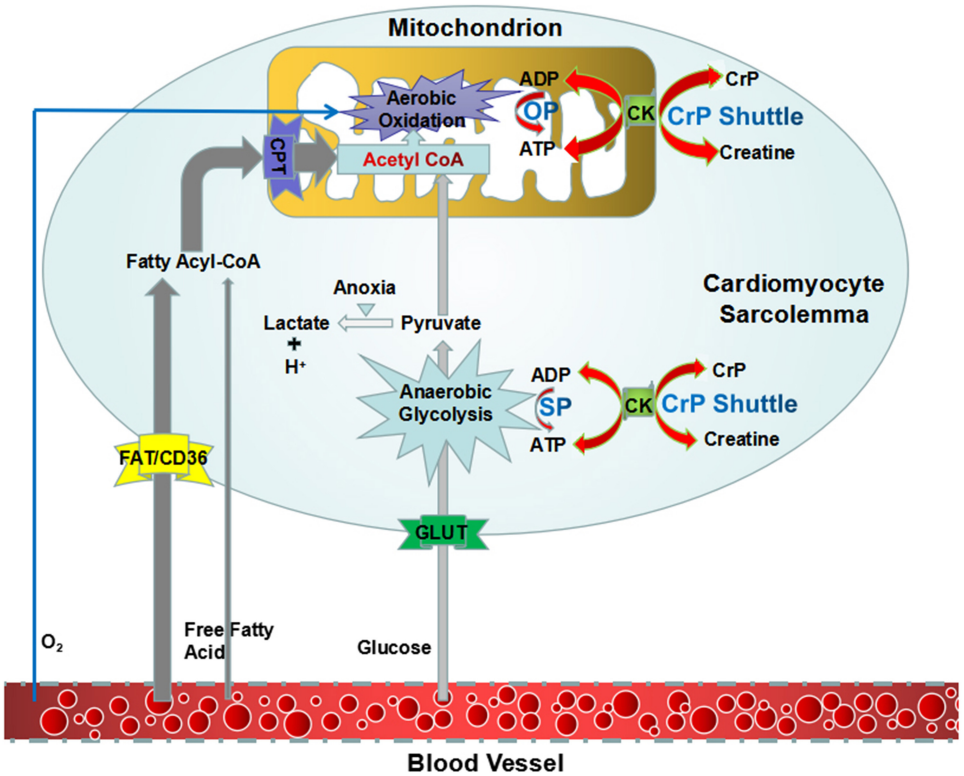

FIGURE 1 | An overview of synthesis of ATP and "CrP shuttle" in cardiomyocyte. ATP is the intracellular energy currency, majority of which is synthesized from ADP by oxidative phosphorylation of mitochondria (predominant) and cytoplasmic substrate phosphorylation (subordinate). CrP is the storage and transport carrier of energy, which serves to transfer the HEP-bond from the site of ATP production to the site of ATP utilization through "CrP shuttle." ADP, adenosine diphosphate; ATP, adenosine triphosphate; CK, creatine kinase; CrP, creatine phosphate; HEP, high-energy phosphate; OP, oxidative phosphorylation; SP, substrate phosphorylation.

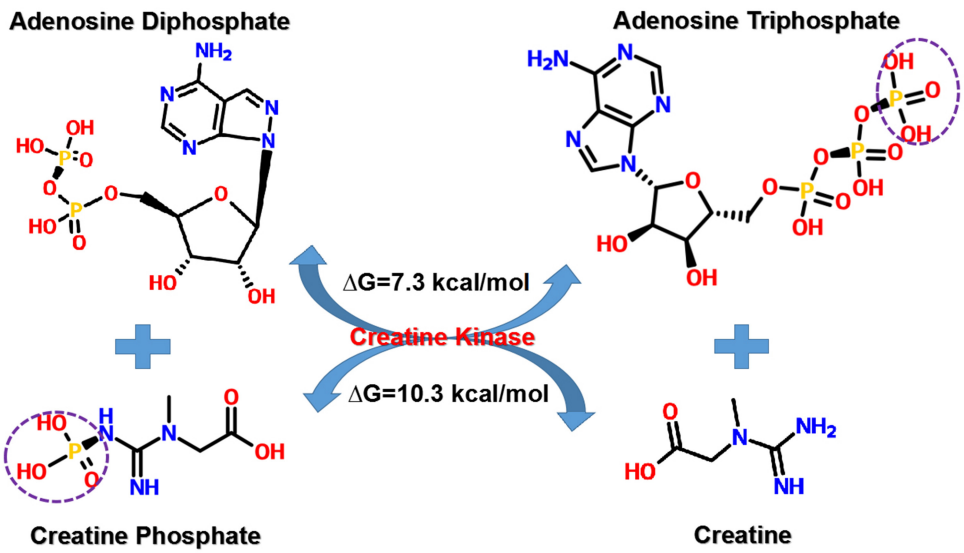

FIGURE 2 | Transfer of HEP-bond through "CrP shuttle." There is one HEP-bond (N~P) in the chemical structure of CrP. As compared, ATP has a relatively more complex molecular structure and two HEP-bonds (O~P). However, the N~P bond of CrP has more energy than either one O~P bond of ATP, 10.3 kcal/mol in comparison with 7.3 kcal/mol. ATP, adenosine triphosphate; CrP, creatine phosphate; HEP, high-energy phosphate; ΔG, Gibbs free energy change.

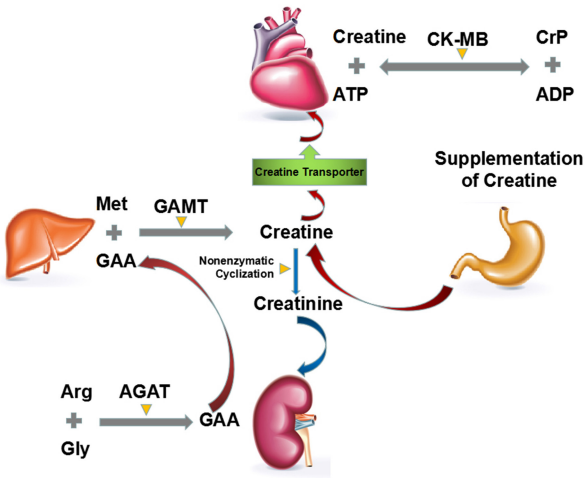

FIGURE 3 | Major routes of biosynthesis, degradation and turnover of endogenous CrP. The biosynthesis of CrP begins by formation of creatine from three essential amino acids: arginine, glycine, and methionine. The main route of creatine synthesis involves formation of GAA in kidney, and methylation in liver. These reactions are, respectively, catalyzed by AGAT and GAMT. Then creatine is transported to heart by a specific Na^+- and Cl^--dependent plasma membrane transporter. The degradation of creatine and CrP is an irreversible, non-enzymatic cyclization to creatinine, which should be supplemented by diet or *de novo* biosynthesis. ADP, adenosine diphosphate; AGAT, L-arginine:glycine amidinotransferase; ATP, adenosine triphosphate; CK, creatine kinase; CrP, creatine phosphate; GAA, guanidinoacetic acid; GAMT, S-adenosyl-L-methionine:N-guanidinoacetate methyltransferase.

<5% in skeletal muscle), so that in myocardial infarction the rise in serum total CK activity is accompanied by a parallel rise in that of CK-MB (14, 52, 53).

Unlike the biosynthesis, the degradation of creatine and CrP is an irreversible, non-enzymatic cyclization to creatinine (**Figure 3**) (54, 55). Almost constant fraction of the body creatine (1.1%/day) and CrP (2.6%/day) is converted into creatinine, giving an overall conversion rate for total creatine pool (creatine + CrP) of ∼1.7%/day (56).

For example, in a 70 kg man containing around 120 g of creatine pool, roughly 2 g/day are converted into creatinine and have to be replaced by creatine or CrP supplementation or from *de novo* biosynthesis (14).

MYOCARDIAL METABOLIC CHANGES DURING ISCHEMIA/REPERFUSION: SUBSTRATES, PATHWAYS, METABOLITES, AND PURINE NUCLEOTIDE CYCLE

Within a few seconds after coronary blood flow blockage, the oxygenated hemoglobin in ischemic zone rapidly depletes. The main pathway used to generate energy in myocardium changes from aerobic oxidation of mitochondria to cytoplasmic anaerobic glycolysis (**Table 1**) (57, 58). And the primary substrate of myocardial energy metabolism also changes from free fatty acids to glucose (**Table 1**) (57–61). However, the HEPs synthesized by glycolysis are far from meeting the energy requirements of heart. Under such condition, the ischemic myocardium preferentially utilizes the energy contained in endogenous CrP, followed by ATP, ADP, and adenosine monophosphate (AMP) (**Figure 4**) (62–67). AMP can also be decomposed into adenosine, hypoxanthine, etc. under the action of 5'-nucleotidase (**Figure 4**) (62, 68). The above reaction ultimately leads to a decrease in intracellular adenine nucleotide pool (ATP + ADP + AMP), resulting in a significant reduction in high-energy phosphate precursors. If the myocardium recover aerobic oxidation in a short period of time, AMP can be reoxidized to ADP and ATP to replenish energy. If not, it is no longer possible to reoxidize AMP to ADP or ATP. Furthermore, the lactic acid and other intermediate products produced by glycolysis accumulate in cardiomyocytes (**Figure 4**) (57, 58). After 10 min of ischemia, the intracellular pH will drop to 5.8–6.0 (69, 70). The rate of ADP rephosphorylation to ATP by anaerobic glycolysis is slowed down by acidosis (71).

Secondary to the metabolic changes, myocardial ischemia/reperfusion injuries occur as follows: intracellular Ca^{2+} overload, accumulation of arrhythmogenic intermediates and oxygen free radicals, myocardial membrane instability, electrophysiological changes in cardiomyocytes, mitochondrial damage, and platelet aggregation, etc (**Figure 4**).

PATHOPHYSIOLOGICAL AND PHARMACOLOGICAL EFFECTS OF EXOGENOUS CREATINE PHOSPHATE ON MYOCARDIAL ISCHEMIA

The clinical effects of ATP in patients with cardiovascular disorders have been evaluated in early studies (72–74). Intravenous administration of ATP can interrupt the reentry pathways through the atrial ventricular node and restore normal sinus rhythm accompanied by relatively high incidences of advanced atrioventricular block and other adverse reactions, which makes paroxysmal supraventricular tachycardia the primary cardiovascular indication (75). And it seems quite paradoxical that oral administration of ATP may lead to a progressive diminution of plasma ATP level (76). Furthermore, exogenous ATP is a charged molecule containing three negative charges that is not freely permeable through cell membranes (77–79). In addition, there are enzymes that decompose ATP on the surface of cell membrane, including ATPase, adenylate kinase and AMP deaminase, which can split ATP into ADP, AMP, adenosine, and inorganic phosphate (80, 81). Since the first publication by Parrat and Marshall (82), CrP has been substantially demonstrated to be effective in protection of ischemic myocardium. The following we will focus on the pathophysiological and pharmacological effects of exogenous CrP, including but not limited to supplementing cellular energy.

Replenishment of Intracelluar ATP

It has been observed that the exogenous CrP could be incorporated into intracellular ATP molecules and increase the

TABLE 1 | Myocardial energy metabolism: source, process and site of ATP production.

Source of ATP production	Pathway of ATP production	Oxygen consumption (per unit ATP)	Accumulation of acid metabolites	Rate of ATP production	Net ATP yield (per unit substrate)	Site of ATP production
CrP	CrP ⇆ ATP shuttle	None	–	Very fast	1	Cytoplasm
Glucose	Anaerobic glycosis	None	+ + +	Fast	2	Cytoplasm
Glucose	Aerobic oxidation	Less	–	Moderate	38	Mitochondria (predominant) and cytoplasm
Free fatty acids	Aerobic oxidation	More	–	Slow	Usually > 100 (depending on the number of carbon atoms in the molecule of free fatty acid)	Mitochondria (predominant) and cytoplasm

ATP, adenosine triphosphate; CrP, creatine phosphate/.

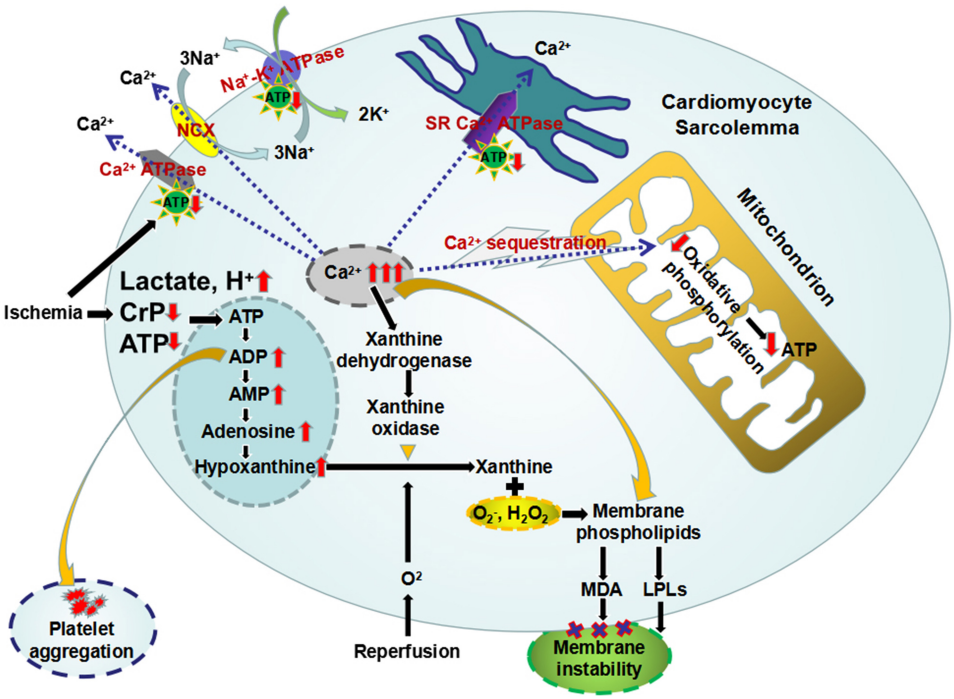

FIGURE 4 | The primary metabolic changes and the secondary celluar injuries during myocardial ischemia/reperfusion. Ischemic myocardium preferentially utilizes the energy contained in CrP, followed by ATP, ADP, and AMP. And AMP can be further decomposed into adenosine and hypoxanthine, which leads to a decrease in intracellular adenine nucleotide pool. Furthermore, the lactic acid produced by glycolysis accumulate in cardiomyocytes, resulting intracellular acidosis. The loss of HEPs eliminates three of the four mechanisms of cellular calcium homeostasis, leading intracellular Ca^{2+} overload. Mitochondrial sequestration, the remaining mechanism, causes overloading of the mitochondria with Ca^{2+} and diminished capacity for oxidative phosphorylation. And overloaded intracellular Ca^{2+} induces the conversion of xanthine dehydrogenase to xanthine oxidase. The latter can produce oxygen free radicals, which in turn oxidize the membrane phospholipids and produce MDA, causing the membrane instability. In addition, intracellular accumulation of metabolic intermediates, including AMP, lactic acid, Ca^{2+}, and H^+, etc, may activate membrane phospholipase to make cell membrane degrade to LPLs, which also contribute to myocardial membrane instability. Increased ADP can induce platelet adhesion and aggregation. ADP, adenosine diphosphate; AMP, adenosine monophosphate; ATP, adenosine triphosphate; CrP, creatine phosphate; HEPs, high-energy phosphates; LPLs, lysophospholipids; MDA, malondialdehyde.

tissue level of ATP (83). Although exogenous CrP uptake was 3–4 orders of magnitude lower than ATP conversion in the case of normal cardiac work, it may be important in maintaining subsarcolemmal pools of CrP or ATP (**Figure 4**) (35, 83). The exogenous CrP uptake rate can be markedly increased in hypokinetic segments of ischemic myocardium (35, 83–86).

Low-dose CrP may promote intracellular ATP synthesis mainly through substrate. After reaching a certain concentration of 10 mmol/L, it can significantly inhibit 5'-nucleotidase and AMP deaminase, thereby maintaining the nucleotide pool level, indicating that CrP does not only act as a energy substrate but also a regulator able to bind to the active sites of the enzymes and change their activity (62, 68, 87–90).

Attenuation of Intracellular Ca^{2+} Overload in Cardiomyocytes

Normally, extracellular fluid has a concentration of Ca^{2+} 10,000 times higher than intracellular fluid (91). Furthermore, there is an electrical force driving Ca^{2+} into the cell because of the negative resting membrane potential (91, 92). However, there is little leakage of Ca^{2+} into the cardiomyocyte except during the action potential. Even the Ca^{2+} that enters the cell during action potentials must be removed from the cell otherwise an accumulation of Ca^{2+} would lead to cellular dysfunction (92). Main mechanisms maintaining the intracellular to extracellular concentration and charge gradients include: (1) pumping Ca^{2+} out of the cytoplasm by the plasma membrane Ca^{2+} ATPase (93), (2) exchange of Ca^{2+} for Na^{+} driven by the intracellular to extracellular concentration gradient of Na^{+} as a result of the plasma membrane Na^{+}-K^{+} ATPase (94), (3) sequestration of cytoplasm Ca^{2+} in sarcoplasmic reticulum (SR) by the SR Ca^{2+} ATPase (95), and (4) accumulation of intracellular Ca^{2+} by oxidation-dependent calcium sequestration inside the mitochondria (96). The loss of HEPs during ischemia eliminates three of the four mechanisms of cellular calcium homeostasis (**Figure 4**). Mitochondrial sequestration, the remaining mechanism, causes overloading of the mitochondria with Ca^{2+} and diminished capacity for oxidative phosphorylation (**Figure 4**) (97). Furthermore, activation of phospholipases and protein kinases (98), production of arachidonic acid (99, 100), and oxygen free radicals (101) are all involved in the destruction of membrane integrity. This, in turn, causes a massive and rapid influx of Ca^{2+} into the cell.

Several studies have shown that intracellular Ca^{2+} overload is a major cause of myocardial cell damage and cardiac dysfunction in IHD. CrP can reduce Ca^{2+} influx by providing energy to ATP-dependent Ca^{2+} ATPase and Na^{+}-K^{+} ATPase on the plasma membrane (102, 103). At the same time, the Ca^{2+} ATPase activity on the sarcoplasmic reticulum is restored, and Ca^{2+} enter the sarcoplasmic reticulum to avoid the myocardial stiffness contracture (104). Furthermore, CrP binds to membrane phospholipids through zwitterionic interaction, which can enhance membrane stability (105, 106). In addition, CrP can also provide energy for the sliding of actin-myosin filaments, promoting the rapid recovery of myocardial contractility (107).

Protection of Heart From Oxidative Stress-Induced Myocardial Injury

And overloaded intracellular Ca^{2+} induces the conversion of xanthine dehydrogenase to xanthine oxidase (108–111). The latter can produce superoxide and xanthine from hypoxanthine upon reperfusion (**Figure 4**) (112). Furthermore, more damaging free radicals could be produced by the metal catalyzed Haber-Weiss reaction (113–115). The large amount of oxygen free radicals generated by the above reactions can in turn oxidize the membrane phospholipids and produce malondialdehyde (MDA), causing the membrane instability (**Figure 4**) (116). Zucchi et al. (117) found that supplementation of exogenous CrP could reduce the product of phospholipid peroxidation, MDA, by inhibiting ADP/AMP degradation and Ca^{2+} accumulation in cardiomyocytes. Myocardial peroxidation damage is alleviated through all of the above mechanisms.

Stabilization of Membrane Structure

Maintaining the integrity of the phospholipid bilayer membrane is a basic requirement for preserving overall cell viability. Myocardial membrane instability due to the decrease of ATP production and accumulation of acid metabolites plays a key role in the pathogenesis of ischemia-reperfusion injury, especially the electrophysiological manifestation of ischemia (118). The possibility that lysophospholipids (LPLs) contribute to myocardial membrane instability was first reported by Hajdu (119). Normally their concentration is maintained very low, but LPLs in sufficient quantities are potent detergents, which can alter general properties of the membrane such as fluidity and permeability (120). Furthermore, LPLs have been shown to affect the activities of plasma membrane Na^{+}-K^{+} ATPase (121). Upon myocardial ischemia, intracellular accumulation of metabolic intermediates, including AMP, lactic acid, Ca^{2+}, and H^{+}, etc, may activate membrane phospholipase to make cell membrane degrade to LPLs (**Figure 4**). At 8 min after ischemia, a 60% increase in LPLs levels occurred, which could either be reacylated or transacylated to form precursor phospholipids or further degraded, depending on the energy state of the cell (121–123). Supplementation of exogenous CrP can provide energy to ATP-dependent Ca^{2+} ATPase and Na^{+}-K^{+} ATPase on the plasma membrane and reduce the activation of anaerobic glycolysis, which blocks the process of phospholipids degradation and stabilizes the cell membrane. In addition, the integrity of the mitochondrial structure during ischemia is the basis for oxidative phosphorylation to synthesize ATP after reperfusion. CrP also has protective effects on the mitochondrial membrane and its oxidative phosphorylation function (124–126).

Broad Spectrum Antiarrhythmic Effects

Normally, the electrophysiological properties of cardiomyocytes require cell membrane integrity and maintaining of intracellular to extracellular concentration and charge gradients. Metabolic changes after myocardial ischemia, including the decrease of ATP production and accumulation of acid metabolites, lead to decreased activity of ATP-dependent transport systems. ATP-sensitive K^{+} channels (KATP), inactivated by normal cellular ATP levels, will open and permit K^{+} to leave the cell upon ischemia (127, 128). Furthermore, decreased activity of Na^{+}/K^{+}-ATPase leads to extracellular accumulation of K^{+} and inactivation of fast Na^{+} channels that are responsible for the rapid depolarization (129). These mechanisms lead to a series of electrophysiological changes in cardiomyocytes, including: (1) the resting membrane potential and the action potential

amplitude are significantly decreased; (2) the depolarization speed is slowed down; (3) the action potential duration (APD) is shortened; (4) the distance from the resting membrane potential to the K^+ equilibrium potential is increased; (5) the conduction velocity rate is slowed down (130). All of the above changes ultimately can contribute to arrhythmias.

Studies have shown that in myocardial ischemia and reperfusion, CrP can play a broad spectrum antiarrhythmic effects through several electrophysiological mechanisms, including but not limited to ATP replenishment (131). Firstly, by providing energy to ATP-dependent KATP channels and Na^+/K^+-ATPase, exogenous CrP can reduce extracellular accumulation of K^+ and reactivate the fast Na^+ channels, suggesting a Class I antiarrhythmic role (132). Secondly, by prolonging ventricular myocardium APD and effective refractory period (ERP) under normoxic but not ischemic conditions, exogenous CrP can prevent reentrant circuits forming between the ischemic and non-ischemic zone and play a class III antiarrhythmic role (132, 133). Thirdly, by attenuating intracellular Ca^{2+} overload, exogenous CrP can inhibit Ca^{2+}-mediated activation of inward current channels and triggered activity, exerting a class IV antiarrhythmic role (134, 135). Furthermore, exogenous CrP can also play an antiarrhythmic role by reducing the accumulation of arrhythmogenic lysophosphoglycerides and increasing the threshold of ventricular fibrillation (136–138).

Inhibiting Platelet Aggregation and Improving Microvascular Function

It is known that ADP can not only induce platelet adhesion and aggregation, but also amplify the aggregation effects of collagen, thrombin and other inducers (**Figure 4**) (139, 140). ADP may still affect the platelets when the arachidonate pathway is blocked (141). Exogenous CrP can inhibit platelet aggregation and then improve the microvascular function by rapid removal of ADP and formation of ATP, which is an inhibitor of ADP-induced platelet aggregation (19, 142).

CLINICAL APPLICATION OF EXOGENOUS CREATINE PHOSPHATE IN ISCHEMIC HEART DISEASE: EVIDENCE AND EVALUATION

As mentioned above, energy metabolic abnormalities are the upstream and primary pathophysiologic manifestation of myocardial ischemia. Whereas, hemodynamic, electrophysiological, morphological, clinical, biochemical and imaging changes are the downstream, and secondary consequence of myocardial energy metabolic abnormalities. The depletion of HEPs is involved in both upstream and downstream changes in myocardial ischemia. As demonstrated *in vitro* and animal experiments, CrP was suggested to be potentially beneficial in patients with acute and chronic myocardial ischaemic injury through multiple mechanisms, including but not limited to ATP replenishment. In fact, results from a large number of clinical studies substantially support that supplementation of exogenous CrP is associated with improved short-term survival (143, 144), enhancement of cardiac systolic and diastolic function (145–147), lower peak CK-MB/troponin release (20, 148–152), reduction in the incidence of major arrhythmias (144, 151, 153–156), etc. There is still uncertainty, however, whether the administration of exogenous CrP can improve long-term outcomes, rather than just the secondary endpoints or pathophysiological process of IHD.

LIMITATIONS AND PERSPECTIVES

According to a meta-analysis performed by Landoni et al. (16), although more than 4,000 articles were screened, only 12 studies comparing CrP with placebo or standard treatment in patients with IHD met the design requirements for controlled or case-matched clinical trials. Unfortunately, there is insufficient statistical power to obtain results on long-term survival due to the common limitations, including:

TABLE 2 | The indications, contraindications, side effects, and application instructions of CrP supplement for IHD.

Indications	Contraindications and relative contraindication	Side effects	Instructions of administration and dosage
• Cardiac metabolic abnormalities during myocardial ischemia. • Cardioprotection during heart surgery.	• Chronic renal failure (in high doses, for example, daily dose of 5–10 g). • Hypersensitivity to drug components. • Pregnancy.	• Allergic reactions. • Lowering of arterial pressure.	• Cardiac metabolic abnormalities during myocardial ischemia: 0–24 h—intravenous bystry infusion of 2–4 g of CrP divorced in water for injections of 50 ml with the subsequent intravenous infusion for 2 h 8–16 g in 250 ml of 5% of solution of glucose; during second day 2 times a day intravenously kapelno (infusion duration of 30 min) enter 2–4 g of the drug divorced in 50 ml of water for injections; during third day the drug is administered according to the same scheme in a dose 2 g (if necessary treatment is continued for 6 days). • Cardioprotection during heart surgery: intravenously kapelno (infusion duration of 30 min) 2 g of the drug divorced in 50 ml of water for injections with frequency rate of introduction 2 times a day. The course is begun in 3–5 days prior to surgical intervention and continued 1–2 more days after its carrying out. During operation it is necessary to add to composition of usual cardioplegic solution in concentration 10 mmol/l just before introduction.

CrP, creatine phosphate; IHD, ischemic heart disease.

(1) single center trial; (2) small sample size; (3) short-term follow-up; (4) secondary end-points; (5) choice of standard treatment rather than placebo as the comparator; (6) administration routes and doses of CrP varying significantly among the studies; (7) inadequate baseline information or baseline bias (20, 143, 144, 146, 150, 151, 153, 156). In addition, majority of the studies were published before the "era of revascularization" and patients were recruited from those undergoing non-revascularization therapy or mixed, significantly different from the current practice (143, 144, 146, 150, 153, 156).

At first glance, it is surprising that exogenous CrP has not been shown to improve long-term survival in clinical studies. In fact, there are two sides to the same issue. On one side, CrP may plays extensive roles in every physiological and pathophysiological process from upstream to downstream of myocardial ischemia. On the other side, the myocardial intracellular actions of CrP lack target and pathway specificity. Furthermore, the uptake and distribution of exogenous CrP *in vivo* lack of tissue and cell specificity. Such non-specificities lead to uncertainties in the dominant pharmacological mechanism, optimal administration route and dose, as well as treatment window of exogenous CrP in individualized patients with IHD. Moreover, the cardioprotection of exogenous CrP may be limited by endogenous CrP levels. However, owing to the physiological, pathophysiological, and pharmacological plausibility of its effects and to the concordance of the beneficial effects of exogenous CrP on multiple secondary but important outcomes and short-term survival, there is urgent need for high-quality multicentre randomized controlled trials (RCTs) to confirm long-term survival improvement. In addition, further studies are needed to investigate the causality between changes in endogenous/exogenous CrP levels and IHD progression and prognosis (157).

To better understand the pathophysiological and pharmacological effects, we specified the context for all cited researches as cell study (19, 23–27, 29–35, 48–54, 69, 70, 91–103, 118, 128), animal study (12, 41, 42, 45, 46, 65, 66, 68, 71–74, 76–78, 81–90, 99, 104, 111, 116–119, 129, 133–135) and human study (15–18, 20, 21, 37–40, 44, 58, 108–110, 143–156). Furthermore, we detailed the indications, contraindications, side effects, and application instructions of CrP supplement in **Table 2**.

CONCLUSIONS

The purpose of this article is to provide a comprehensive and concise description of the cellular and molecular aspects of cardioprotective mechanisms and a critical evaluation of the clinical evidence of HEPs in IHD. According to the well-documented physiological, pathophysiological and pharmacological properties of HEPs, exogenous CrP may be considered as an ideal metabolic regulator. It plays cardioprotection roles from upstream to downstream of myocardial ischemia through multiple complex mechanisms, including but not limited to replenishment of cellular energy. Although exogenous CrP administration has not been shown to improve long-term survival, the beneficial effects on multiple secondary but important outcomes and short-term survival are concordant with its pathophysiological and pharmacological effects. There is urgent need for high-quality multicentre RCTs to confirm long-term survival improvement in the future.

AUTHOR CONTRIBUTIONS

HY-D, ZY-X, and YS-W contributed toward drafting and critically reviewing the document and agree to be accountable for all aspects of the work. YS-W and ZY-J provided his views and comments on the manuscript, made the final decision about the journal selection as well as approved the submission of the manuscript to the journal. All authors contributed to the article and approved the submitted version.

REFERENCES

1. Opie LH. Proof that glucose-insulin-potassium provides metabolic protection of ischaemic myocardium. *Lancet.* (1999) 353:768–9. doi: 10.1016/S0140-6736(98)00385-7
2. Weiss RG, Bottomley PA, Hardy CJ, Gerstenblith G. Regional myocardial metabolism of high-energy phosphates during isometric exercise in patients with coronary artery disease. *N Engl J Med.* (1990) 323:1593–600. doi: 10.1056/NEJM199012063232304
3. Fihn SD, Blankenship JC, Alexander KP, Bittl JA, Byrne JG, Fletcher BJ, et al. 2014 ACC/AHA/AATS/PCNA/SCAI/STS focused update of the guideline for the diagnosis and management of patients with stable ischemic heart disease: a report of the American College of Cardiology/American Heart Association Task Force on Practice Guidelines, and the American Association for Thoracic Surgery, Preventive Cardiovascular Nurses Association, Society for Cardiovascular Angiography and Interventions, and Society of Thoracic Surgeons. *J Am Coll Cardiol.* (2014) 64:1929–49. doi: 10.1016/j.jacc.2014.07.017
4. Amsterdam EA, Wenger NK, Brindis RG, Casey DE, Ganiats TG, Holmes DR, et al. 2014 AHA/ACC Guideline for the Management of Patients with Non-ST-Elevation Acute Coronary Syndromes: a report of the American College of Cardiology/American Heart Association Task Force on Practice Guidelines. *J Am Coll Cardiol.* (2014) 64:e139–228. doi: 10.1016/j.jacc.2014.09.016
5. Levine GN, Bates ER, Blankenship JC, Bailey SR, Bittl JA, Cercek B, et al. 2015 ACC/AHA/SCAI Focused Update on Primary Percutaneous Coronary Intervention for Patients With ST-Elevation Myocardial Infarction: an Update of the 2011 ACCF/AHA/SCAI Guideline for Percutaneous Coronary Intervention and the 2013 ACCF/AHA Guideline for the Management of ST-Elevation Myocardial Infarction. *J Am Coll Cardiol.* (2016) 67:1235–50. doi: 10.1016/j.jacc.2015.10.005
6. Knuuti J, Wijns W, Saraste A, Capodanno D, Barbato E, Funck-Brentano C, et al. 2019 ESC Guidelines for the diagnosis and management of chronic coronary syndromes. *Eur Heart J.* (2020) 41:407–77. doi: 10.1093/eurheartj/ehz425
7. Ibanez B, James S, Agewall S, Antunes MJ, Bucciarelli-Ducci C, Bueno H, et al. 2017 ESC Guidelines for the management of acute myocardial infarction in patients presenting with ST-segment elevation: The Task Force for the management of acute myocardial infarction in patients presenting with ST-segment elevation of the European Society of Cardiology (ESC). *Eur Heart J.* (2018) 39:119–77. doi: 10.1093/eurheartj/ehx393

8. Roffi M, Patrono C, Collet JP, Mueller C, Valgimigli M, Andreotti F, et al. 2015 ESC Guidelines for the management of acute coronary syndromes in patients presenting without persistent ST-segment elevation: Task Force for the Management of Acute Coronary Syndromes in Patients Presenting without Persistent ST-Segment Elevation of the European Society of Cardiology (ESC). *Eur Heart J.* (2016) 37:267–315. doi: 10.1093/eurheartj/ehv320
9. Kolwicz SC, Tian R. Metabolic therapy at the crossroad: how to optimize myocardial substrate utilization. *Trends Cardiovasc Med.* (2009) 19:201–7. doi: 10.1016/j.tcm.2009.12.005
10. Stanley WC. Myocardial energy metabolism during ischemia and the mechanisms of metabolic therapies. *J Cardiovasc Pharmacol Ther.* (2004) 9(Suppl. 1):S31–45. doi: 10.1177/107424840400900104
11. Fruchart JC, Davignon J, Hermans MP, Al-Rubeaan K, Amarenco P, Assmann G, et al. Residual macrovascular risk in 2013: what have we learned. *Cardiovasc Diabetol.* (2014) 13:26. doi: 10.1186/1475-2840-13-26
12. Eggleton P, Eggleton GP. The inorganic phosphate and a labile form of organic phosphate in the gastrocnemius of the frog. *Biochem J.* (1927) 21:190–5. doi: 10.1042/bj0210190
13. Ennor AH, Morrison JF. Biochemistry of the phosphagens and related guanidines. *Physiol Rev.* (1958) 38:631–74. doi: 10.1152/physrev.1958.38.4.631
14. Wyss M, Kaddurah-Daouk R. Creatine and creatinine metabolism. *Physiol Rev.* (2000) 80:1107–213. doi: 10.1152/physrev.2000.80.3.1107
15. Mingxing F, Landoni G, Zangrillo A, Monaco F, Lomivorotov VV, Hui C, et al. Phosphocreatine in cardiac surgery patients: a meta-analysis of randomized controlled trials. *J Cardiothorac Vasc Anesth.* (2018) 32:762–70. doi: 10.1053/j.jvca.2017.07.024
16. Landoni G, Zangrillo A, Lomivorotov VV, Likhvantsev V, Ma J, De Simone F, et al. Cardiac protection with phosphocreatine: a meta-analysis. *Interact Cardiovasc Thorac Surg.* (2016) 23:637–46. doi: 10.1093/icvts/ivw171
17. Sharov VG, Saks VA, Kupriyanov VV, Lakomkin VL, Kapelko VI, AYa S, et al. Protection of ischemic myocardium by exogenous phosphocreatine. I. Morphologic and phosphorus 31-nuclear magnetic resonance studies. *J Thorac Cardiovasc Surg.* (1987) 94:749–61. doi: 10.1016/S0022-5223(19)36191-4
18. Semenovsky ML, Shumakov VI, Sharov VG, Mogilevsky GM, Asmolovsky AV, Makhotina LA, et al. Protection of ischemic myocardium by exogenous phosphocreatine. II. Clinical, ultrastructural, and biochemical evaluations. *J Thorac Cardiovasc Surg.* (1987) 94:762–9. doi: 10.1016/S0022-5223(19)36192-6
19. Sharov VG, Afonskaya NI, Ruda MY, Cherpachenko NM, EYa P, Markosyan RA, et al. Protection of ischemic myocardium by exogenous phosphocreatine (neoton): pharmacokinetics of phosphocreatine, reduction of infarct size, stabilization of sarcolemma of ischemic cardiomyocytes, and antithrombotic action. *Biochem Med Metab Biol.* (1986) 35:101–14. doi: 10.1016/0885-4505(86)90064-2
20. Ke-Wu D, Xu-Bo S, Ying-Xin Z, Shi-Wei Y, Yu-Jie Z, Dong-Mei S, et al. The effect of exogenous creatine phosphate on myocardial injury after percutaneous coronary intervention. *Angiology.* (2015) 66:163–8. doi: 10.1177/0003319713515996
21. Yang SW, Park KH, Zhou YJ. The impact of hypoglycemia on the cardiovascular system: physiology and pathophysiology. *Angiology.* (2016) 67:802–9. doi: 10.1177/0003319715623400
22. Strumia E, Pelliccia F, D'Ambrosio G. Creatine phosphate: pharmacological and clinical perspectives. *Adv Ther.* (2012) 29:99–123. doi: 10.1007/s12325-011-0091-4
23. Fiske CH, Subbarow Y. The nature of the "inorganic phosphate" in voluntary muscle. *Science.* (1927) 65:401–3. doi: 10.1126/science.65.1686.401
24. de Meis L. How enzymes handle the energy derived from the cleavage of high-energy phosphate compounds. *J Biol Chem.* (2012) 287:16987–7005. doi: 10.1074/jbc.X112.363200
25. Rosca MG, Hoppel CL. Mitochondria in heart failure. *Cardiovasc Res.* (2010) 88:40–50. doi: 10.1093/cvr/cvq240
26. Klingenberg M. The ADP and ATP transport in mitochondria and its carrier. *Biochim Biophys Acta.* (2008) 1778:1978–2021. doi: 10.1016/j.bbamem.2008.04.011
27. D'Alessandro M, Melandri BA. ATP hydrolysis in ATP synthases can be differently coupled to proton transport and modulated by ADP and phosphate: a structure based model of the mechanism. *Biochim Biophys Acta.* (2010) 1797:755–62. doi: 10.1016/j.bbabio.2010.03.007
28. Langen P, Hucho F. Karl Lohmann and the discovery of ATP. *Angew Chem Int Ed Engl.* (2008) 47:1824–7. doi: 10.1002/anie.200702929
29. Erickson-Viitanen S, Geiger P, Yang WC, Bessman SP. The creatine-creatine phosphate shuttle for energy transport-compartmentation of creatine phosphokinase in muscle. *Adv Exp Med Biol.* (1982) 151:115–25. doi: 10.1007/978-1-4684-4259-5_17
30. McClellan G, Weisberg A, Winegrad S. Energy transport from mitochondria to myofibril by a creatine phosphate shuttle in cardiac cells. *Am J Physiol.* (1983) 245:C423–7. doi: 10.1152/ajpcell.1983.245.5.C423
31. Savabi F, Geiger PJ, Bessman SP. Myofibrillar end of the creatine phosphate energy shuttle. *Am J Physiol.* (1984) 247:C424–32. doi: 10.1152/ajpcell.1984.247.5.C424
32. Bessman SP, Carpenter CL. The creatine-creatine phosphate energy shuttle. *Annu Rev Biochem.* (1985) 54:831–62. doi: 10.1146/annurev.bi.54.070185.004151
33. Bessman SP. The creatine phosphate energy shuttle–the molecular asymmetry of a "pool". *Anal Biochem.* (1987) 161:519–23. doi: 10.1016/0003-2697(87)90483-0
34. Saks VA, Rosenshtraukh LV, Smirnov VN, Chazov EI. Role of creatine phosphokinase in cellular function and metabolism. *Can J Physiol Pharmacol.* (1978) 56:691–706. doi: 10.1139/y78-113
35. Jacobus WE. Respiratory control and the integration of heart high-energy phosphate metabolism by mitochondrial creatine kinase. *Annu Rev Physiol.* (1985) 47:707–25. doi: 10.1146/annurev.ph.47.030185.003423
36. *StatPearls*. Treasure Island, FL: StatPearls Publishing (2020).
37. Kerksick CM, Roberts MD, Dalbo VJ, Sunderland KL. Intramuscular phosphagen status and the relationship to muscle performance across the age spectrum. *Eur J Appl Physiol.* (2016) 116:115–27. doi: 10.1007/s00421-015-3246-1
38. Stroud RM. Balancing ATP in the cell. *Nat Struct Biol.* (1996) 3:567–9. doi: 10.1038/nsb0796-567
39. Solaiyappan M, Weiss RG, Bottomley PA. Neural-network classification of cardiac disease from 31P cardiovascular magnetic resonance spectroscopy measures of creatine kinase energy metabolism. *J Cardiovasc Magn Reson.* (2019) 21:49. doi: 10.1186/s12968-019-0560-5
40. Melenovsky V, Hlavata K, Sedivy P, Dezortova M, Borlaug BA, Petrak J, et al. Skeletal muscle abnormalities and iron deficiency in chronic heart failurean exercise 31P magnetic resonance spectroscopy study of calf muscle. *Circ Heart Fail.* (2018) 11:e004800. doi: 10.1161/CIRCHEARTFAILURE.117.004800
41. Weiss RG, Chatham JC, Georgakopolous D, Charron MJ, Wallimann T, Kay L, et al. An increase in the myocardial PCr/ATP ratio in GLUT4 null mice. *FASEB J.* (2002) 16:613–5. doi: 10.1096/fj.01-0462fje
42. Balaban RS, Kantor HL, Katz LA, Briggs RW. Relation between work and phosphate metabolite in the in vivo paced mammalian heart. *Science.* (1986) 232:1121–3. doi: 10.1126/science.3704638
43. Zhang J, Duncker DJ, Xu Y, Zhang Y, Path G, Merkle H, et al. Transmural bioenergetic responses of normal myocardium to high workstates. *Am J Physiol.* (1995) 268:H1891–905. doi: 10.1152/ajpheart.1995.268.5.H1891
44. Neubauer S, Horn M, Cramer M, Harre K, Newell JB, Peters W, et al. Myocardial phosphocreatine-to-ATP ratio is a predictor of mortality in patients with dilated cardiomyopathy. *Circulation.* (1997) 96:2190–6. doi: 10.1161/01.CIR.96.7.2190
45. McDonald KM, Yoshiyama M, Francis GS, Ugurbil K, Cohn JN, Zhang J. Myocardial bioenergetic abnormalities in a canine model of left ventricular dysfunction. *J Am Coll Cardiol.* (1994) 23:786–93. doi: 10.1016/0735-1097(94)90769-2
46. Liao R, Nascimben L, Friedrich J, Gwathmey JK, Ingwall JS. Decreased energy reserve in an animal model of dilated cardiomyopathy. Relationship to contractile performance. *Circ Res.* (1996) 78:893–902. doi: 10.1161/01.RES.78.5.893
47. Kreider RB, Kalman DS, Antonio J, Ziegenfuss TN, Wildman R, Collins R, et al. International Society of Sports Nutrition position stand: safety and efficacy of creatine supplementation in exercise, sport, and medicine. *J Int Soc Sports Nutr.* (2017) 14:18. doi: 10.1186/s12970-017-0173-z

48. Popolo A, Adesso S, Pinto A, Autore G, Marzocco S. L-Arginine and its metabolites in kidney and cardiovascular disease. *Amino Acids.* (2014) 46:2271–86. doi: 10.1007/s00726-014-1825-9
49. Barcelos RP, Stefanello ST, Mauriz JL, Gonzalez-Gallego J, Soares FA. Creatine and the liver: metabolism and possible interactions. *Mini Rev Med Chem.* (2016) 16:12–8. doi: 10.2174/1389557515666150722102613
50. Iqbal F, Hoeger H, Lubec G, Bodamer O. Biochemical and behavioral phenotype of AGAT and GAMT deficient mice following long-term creatine monohydrate supplementation. *Metab Brain Dis.* (2017) 32:1951–61. doi: 10.1007/s11011-017-0092-3
51. Sora I, Richman J, Santoro G, Wei H, Wang Y, Vanderah T, et al. The cloning and expression of a human creatine transporter. *Biochem Biophys Res Commun.* (1994) 204:419–27. doi: 10.1006/bbrc.1994.2475
52. Wallimann T, Wyss M, Brdiczka D, Nicolay K, Eppenberger HM. Intracellular compartmentation, structure and function of creatine kinase isoenzymes in tissues with high and fluctuating energy demands: the 'phosphocreatine circuit' for cellular energy homeostasis. *Biochem J.* (1992) 281 (Pt 1):21–40. doi: 10.1042/bj2810021
53. Saks VA, Ventura-Clapier R, Aliev MK. Metabolic control and metabolic capacity: two aspects of creatine kinase functioning in the cells. *Biochim Biophys Acta.* (1996) 1274:81–8. doi: 10.1016/0005-2728(96)00011-4
54. Brosnan ME, Brosnan JT. Renal arginine metabolism. *J Nutr.* (2004) 134:2791S−5S; discussion 2796S−2797S. doi: 10.1093/jn/134.10.2791S
55. Kashani K, Rosner MH, Ostermann M. Creatinine: from physiology to clinical application. *Eur J Intern Med.* (2020) 72:9–14. doi: 10.1016/j.ejim.2019.10.025
56. Walker JB. Creatine: biosynthesis, regulation, and function. *Adv Enzymol Relat Areas Mol Biol.* (1979) 50:177–242. doi: 10.1002/9780470122952.ch4
57. Mallet RT, Manukhina EB, Ruelas SS, Caffrey JL, Downey HF. Cardioprotection by intermittent hypoxia conditioning: evidence, mechanisms, and therapeutic potential. *Am J Physiol Heart Circ Physiol.* (2018) 315:H216–32. doi: 10.1152/ajpheart.00060.2018
58. Ait-Aissa K, Blaszak SC, Beutner G, Tsaih SW, Morgan G, Santos JH, et al. Mitochondrial oxidative phosphorylation defect in the heart of subjects with coronary artery disease. *Sci Rep.* (2019) 9:7623. doi: 10.1038/s41598-019-43761-y
59. Lopaschuk GD, Ussher JR, Folmes CD, Jaswal JS, Stanley WC. Myocardial fatty acid metabolism in health and disease. *Physiol Rev.* (2010) 90:207–58. doi: 10.1152/physrev.00015.2009
60. Lopaschuk GD, Collins-Nakai RL, Itoi T. Developmental changes in energy substrate use by the heart. *Cardiovasc Res.* (1992) 26:1172–80. doi: 10.1093/cvr/26.12.1172
61. Kodde IF, van der Stok J, Smolenski RT, de Jong JW. Metabolic and genetic regulation of cardiac energy substrate preference. *Comp Biochem Physiol A Mol Integr Physiol.* (2007) 146:26–39. doi: 10.1016/j.cbpa.2006.09.014
62. Scolletta S, Biagioli B. Energetic myocardial metabolism and oxidative stress: let's make them our friends in the fight against heart failure. *Biomed Pharmacother.* (2010) 64:203–7. doi: 10.1016/j.biopha.2009.10.002
63. Heather LC, Clarke K. Metabolism, hypoxia and the diabetic heart. *J Mol Cell Cardiol.* (2011) 50:598–605. doi: 10.1016/j.yjmcc.2011.01.007
64. Sano M, Fukuda K. [Metabolic remodeling in the ischemic and non-ischemic failing heart]. *Nihon Rinsho.* (2011) 69(Suppl. 7):60–8.
65. Braasch W, Gudbjarnason S, Puri PS, Ravens KG, Bing RJ. Early changes in energy metabolism in the myocardium following acute coronary artery occlusion in anesthetized dogs. *Circ Res.* (1968) 23:429–38. doi: 10.1161/01.RES.23.3.429
66. Neely JR, Rovetto MJ, Whitmer JT, Morgan HE. Effects of ischemia on function and metabolism of the isolated working rat heart. *Am J Physiol.* (1973) 225:651–8. doi: 10.1152/ajplegacy.1973.225.3.651
67. Jennings RB, Murry CE, Steenbergen C, Reimer KA. Development of cell injury in sustained acute ischemia. *Circulation.* (1990) 82:II2.
68. Headrick JP, Willis RJ. 5'-Nucleotidase activity and adenosine formation in stimulated, hypoxic and underperfused rat heart. *Biochem J.* (1989) 261:541–50. doi: 10.1042/bj2610541
69. Vanheel B, Van de Voorde J. Differential influence of extracellular and intracellular pH on K^+ accumulation in ischaemic mammalian cardiac tissue. *J Mol Cell Cardiol.* (1995) 27:1443–55. doi: 10.1006/jmcc.1995.0136
70. Beauloye C, Bertrand L, Krause U, Marsin AS, Dresselaers T, Vanstapel F, et al. No-flow ischemia inhibits insulin signaling in heart by decreasing intracellular pH. *Circ Res.* (2001) 88:513–9. doi: 10.1161/01.RES.88.5.513
71. Lancaster MK, Harrison SM. Changes in contraction, cytosolic Ca^{2+} and pH during metabolic inhibition and upon restoration of mitochondrial respiration in rat ventricular myocytes. *Exp Physiol.* (1998) 83:349–60. doi: 10.1113/expphysiol.1998.sp004118
72. Kopf GS, Chaudry I, Condos S, Baue AE. Reperfusion with ATP-MgCl2 following prolonged ischemia improves myocardial performance. *J Surg Res.* (1987) 43:114–7. doi: 10.1016/0022-4804(87)90152-1
73. Thelin S, Hultman J, Ronquist G, Hansson HE. Myocardial high-energy phosphates, lactate and pyruvate during moderate or severe normothermic ischemia in rat hearts perfused with phosphoenolpyruvate and ATP in cardioplegic solution. *Scand J Thorac Cardiovasc Surg.* (1987) 21:245–9. doi: 10.3109/14017438709106033
74. Martinesi L, Belli C. [Experimental study on the effects of polarizing solutions with and without ATP on the electrocardiographic pattern of myocardial ischemia caused by pitressin]. *G Clin Med.* (1967) 48:720–46.
75. Camm AJ, Garratt CJ. Adenosine and supraventricular tachycardia. *N Engl J Med.* (1991) 325:1621–9. doi: 10.1056/NEJM199112053252306
76. Kichenin K, Seman M. Chronic oral administration of ATP modulates nucleoside transport and purine metabolism in rats. *J Pharmacol Exp Ther.* (2000) 294:126–33.
77. Glynn IM. Membrane adenosine triphosphatase and cation transport. *Br Med Bull.* (1968) 24:165–9. doi: 10.1093/oxfordjournals.bmb.a070620
78. Dieterle Y, Ody C, Ehrensberger A, Stalder H, Junod AF. Metabolism and uptake of adenosine triphosphate and adenosine by porcine aortic and pulmonary endothelial cells and fibroblasts in culture. *Circ Res.* (1978) 42:869–76. doi: 10.1161/01.RES.42.6.869
79. Chaudry IH. Does ATP cross the cell plasma membrane. *Yale J Biol Med.* (1982) 55:1–10.
80. Dunkley CR, Manery JF, Dryden EE. The conversion of ATP to IMP by muscle surface enzymes. *J Cell Physiol.* (1966) 68:241–7. doi: 10.1002/jcp.1040680305
81. Fedelesová M, Ziegelhöffer A, Krause EG, Wollenberger A. Effect of exogenous adenosine triphosphate on the metabolic state of the excised hypothermic dog heart. *Circ Res.* (1969) 24:617–27. doi: 10.1161/01.RES.24.5.617
82. Parratt JR, Marshall RJ. The response of isolated cardiac muscle to acute anoxia: protective effect of adenosine triphosphate and creatine phosphate. *J Pharm Pharmacol.* (1974) 26:427–33. doi: 10.1111/j.2042-7158.1974.tb09308.x
83. Down WH, Chasseaud LF, Ballard SA. The effect of intravenously administered phosphocreatine on ATP and phosphocreatine concentrations in the cardiac muscle of the rat. *Arzneimittelforschung.* (1983) 33:552–4.
84. Thelin S, Hultman J, Ronquist G, Juhlin C, Hansson HE, Lindgren PG. Improved myocardial protection by creatine phosphate in cardioplegic solution. An *in vivo* study in the pig during normothermic ischemia. *Thorac Cardiovasc Surg.* (1987) 35:137–42. doi: 10.1055/s-2007-1020217
85. Thelin S, Hultman J, Ronquist G, Hansson HE. Metabolic and functional effects of creatine phosphate in cardioplegic solution. Studies on rat hearts during and after normothermic ischemia. *Scand J Thorac Cardiovasc Surg.* (1987) 21:39–45. doi: 10.3109/14017438709116917
86. Rosenshtraukh LV, Saks VA, Yuriavichus IA, Nesterenko VV, Undrovinas AI, Smirnov VN, et al. Effect of creatine phosphate on the slow inward calcium current, action potential, and contractile force of frog atrium and bentricle. *Biochem Med.* (1979) 21:1–5. doi: 10.1016/0006-2944(79)90049-8
87. Schopf G, Rumpold H, Müller MM. Alterations of purine salvage pathways during differentiation of rat heart myoblasts towards myocytes. *Biochim Biophys Acta.* (1986) 884:319–25. doi: 10.1016/0304-4165(86)90180-7
88. Lewandowski ED, White LT. Pyruvate dehydrogenase influences postischemic heart function. *Circulation.* (1995) 91:2071–9. doi: 10.1161/01.CIR.91.7.2071
89. Snaith CD, Wright G, Lofkin M. The effects of aspartate and 2-oxoglutarate upon glycolytic energy metabolites and mechanical recovery following global ischaemia in isolated rat hearts. *J Mol Cell Cardiol.* (1992) 24:305–15. doi: 10.1016/0022-2828(92)93167-I

90. Ronca-Testoni S, Raggi A, Ronca G. Muscle AMP aminohydrolase. 3. A comparative study on the regulatory properties of skeletal muscle enzyme from various species. *Biochim Biophys Acta.* (1970) 198:101–12. doi: 10.1016/0005-2744(70)90038-0
91. Peters T. Basic mechanisms of cellular calcium homeostasis. *Acta Otolaryngol Suppl.* (1988) 460:7–12. doi: 10.3109/00016488809125129
92. Dawson AP. Regulation of intracellular Ca^{2+}. *Essays Biochem.* (1990) 25:1–37.
93. Carafoli E, Malmström K, Sigel E, Crompton M. The regulation of intracellular calcium. *Clin Endocrinol.* (1976) 5(Suppl.):49S−59S. doi: 10.1111/j.1365-2265.1976.tb03815.x
94. Carafoli E. The regulation of intracellular calcium. *Adv Exp Med Biol.* (1982) 151:461–72. doi: 10.1007/978-1-4684-4259-5_51
95. Blaustein MP, Ratzlaff RW, Kendrick NK. The regulation of intracellular calcium in presynaptic nerve terminals. *Ann N Y Acad Sci.* (1978) 307:195–212. doi: 10.1111/j.1749-6632.1978.tb41943.x
96. Mitchell P, Moyle J. Chemiosmotic hypothesis of oxidative phosphorylation. *Nature.* (1967) 213:137–9. doi: 10.1038/213137a0
97. Nayler WG. The role of calcium in the ischemic myocardium. *Am J Pathol.* (1981) 102:262–70.
98. Golfman LS, Haughey NJ, Wong JT, Jiang JY, Lee D, Geiger JD, et al. Lysophosphatidylcholine induces arachidonic acid release and calcium overload in cardiac myoblastic H9c2 cells. *J Lipid Res.* (1999) 40:1818–26. doi: 10.1016/S0022-2275(20)34898-7
99. Hoffmann P, Richards D, Heinroth-Hoffmann I, Mathias P, Wey H, Toraason M. Arachidonic acid disrupts calcium dynamics in neonatal rat cardiac myocytes. *Cardiovasc Res.* (1995) 30:889–98. doi: 10.1016/S0008-6363(95)00133-6
100. Oe H, Kuzuya T, Hoshida S, Nishida M, Hori M, Kamada T, et al. Calcium overload and cardiac myocyte cell damage induced by arachidonate lipoxygenation. *Am J Physiol.* (1994) 267:H1396–402. doi: 10.1152/ajpheart.1994.267.4.H1396
101. Chang JC, Lien CF, Lee WS, Chang HR, Hsu YC, Luo YP, et al. Intermittent hypoxia prevents myocardial mitochondrial Ca^{2+} overload and cell death during ischemia/reperfusion: the role of reactive oxygen species. *Cells.* (2019) 8:564. doi: 10.3390/cells8060564
102. Semb SO, Sejersted OM. Calcium induced contracture stimulates Na,K-pump rate in isolated sheep cardiac Purkinje fibers. *J Mol Cell Cardiol.* (1997) 29:2197–212. doi: 10.1006/jmcc.1997.0455
103. Dhalla NS, Singh JN, McNamara DB, Bernatsky A, Singh A, Harrow JA. Energy production and utilization in contractile failure due to intracellular calcium overload. *Adv Exp Med Biol.* (1983) 161:305–16. doi: 10.1007/978-1-4684-4472-8_16
104. Tani M, Hasegawa H, Suganuma Y, Shinmura K, Kayashi Y, Nakamura Y. Protection of ischemic myocardium by inhibition of contracture in isolated rat heart. *Am J Physiol.* (1996) 271:H2515–9. doi: 10.1152/ajpheart.1996.271.6.H2515
105. Tokarska-Schlattner M, Epand RF, Meiler F, Zandomeneghi G, Neumann D, Widmer HR, et al. Phosphocreatine interacts with phospholipids, affects membrane properties and exerts membrane-protective effects. *PLoS ONE.* (2012) 7:e43178. doi: 10.1371/journal.pone.0043178
106. Saks VA, Dzhaliashvili IV, Konorev EA, Strumia E. [Molecular and cellular aspects of the cardioprotective mechanism of phosphocreatine]. *Biokhimiia.* (1992) 57:1763–84.
107. Günther J, Oddoy A, Schubert E. [Mechanical characteristics of isotonic work and high-energy phosphates in frog ventricle after 1-fluoro-2,4-dinitrobenzene]. *Acta Biol Med Ger.* (1978) 37:613–21.
108. Srivastava SK, Ansari NH, Liu S, Izban A, Das B, Szabo G, et al. The effect of oxidants on biomembranes and cellular metabolism. *Mol Cell Biochem.* (1989) 91:149–57. doi: 10.1007/BF00228090
109. Malis CD, Bonventre JV. Mechanism of calcium potentiation of oxygen free radical injury to renal mitochondria. A model for post-ischemic and toxic mitochondrial damage. *J Biol Chem.* (1986) 261:14201–8. doi: 10.1016/S0021-9258(18)67004-8
110. Kock R, Delvoux B, Sigmund M, Greiling H. A comparative study of the concentrations of hypoxanthine, xanthine, uric acid and allantoin in the peripheral blood of normals and patients with acute myocardial infarction and other ischaemic diseases. *Eur J Clin Chem Clin Biochem.* (1994) 32:837–42. doi: 10.1515/cclm.1994.32.11.837
111. Gneushev ET, Naumova VV, Bogoslovskii VA. [Hypoxanthine content of peripheral venous blood in infarct and ischemia of the myocardium]. *Ter Arkh.* (1978) 50:20–4.
112. McCord JM. Oxygen-derived free radicals in postischemic tissue injury. *N Engl J Med.* (1985) 312:159–63. doi: 10.1056/NEJM198501173120305
113. Fridovich I. Superoxide radical: an endogenous toxicant. *Annu Rev Pharmacol Toxicol.* (1983) 23:239–57. doi: 10.1146/annurev.pa.23.040183.001323
114. McCord JM. The superoxide free radical: its biochemistry and pathophysiology. *Surgery.* (1983) 94:412–4.
115. Tien M, Svingen BA, Aust SD. An investigation into the role of hydroxyl radical in xanthine oxidase-dependent lipid peroxidation. *Arch Biochem Biophys.* (1982) 216:142–51. doi: 10.1016/0003-9861(82)90198-9
116. Ballagi-Pordány G, Richter J, Koltai M, Aranyi Z, Pogátsa G, Schaper W. Is malondialdehyde a marker of the effect of oxygen free radicals in rat heart tissue. *Basic Res Cardiol.* (1991) 86:266–72. doi: 10.1007/BF02190606
117. Zucchi R, Poddighe R, Limbruno U, Mariani M, Ronca-Testoni S, Ronca G. Protection of isolated rat heart from oxidative stress by exogenous creatine phosphate. *J Mol Cell Cardiol.* (1989) 21:67–73. doi: 10.1016/0022-2828(89)91494-6
118. Houang EM, Bartos J, Hackel BJ, Lodge TP, Yannopoulos D, Bates FS, et al. Cardiac muscle membrane stabilization in myocardial reperfusion injury. *JACC Basic Transl Sci.* (2019) 4:275–87. doi: 10.1016/j.jacbts.2019.01.009
119. Hajdu S, Weiss H, Titus E. The isolation of a cardiac active principle from mammalian tissue. *J Pharmacol Exp Ther.* (1957) 120:99–113.
120. Weltzien HU. Cytolytic and membrane-perturbing properties of lysophosphatidylcholine. *Biochim Biophys Acta.* (1979) 559:259–87. doi: 10.1016/0304-4157(79)90004-2
121. Shaikh NA, Downar E. Time course of changes in porcine myocardial phospholipid levels during ischemia. A reassessment of the lysolipid hypothesis. *Circ Res.* (1981) 49:316–25. doi: 10.1161/01.RES.49.2.316
122. van den Bosch H. Phosphoglyceride metabolism. *Annu Rev Biochem.* (1974) 43:243–77. doi: 10.1146/annurev.bi.43.070174.001331
123. Sobel BE, Corr PB. Biochemical mechanisms potentially responsible for lethal arrhythmias induced by ischemia: the lysolipid hypothesis. *Adv Cardiol.* (1979) 26:76–85. doi: 10.1159/000402391
124. Scott ID, Nicholls DG. Energy transduction in intact synaptosomes. Influence of plasma-membrane depolarization on the respiration and membrane potential of internal mitochondria determined *in situ*. *Biochem J.* (1980) 186:21–33. doi: 10.1042/bj1860021
125. Nakahara T, Takeo S. Irreversible changes in oxidative phosphorylation activity of the mitochondrial membrane from hearts subjected to hypoxia and reoxygenation. *Can J Cardiol.* (1986) 2:24–33.
126. Berkich DA, Salama G, LaNoue KF. Mitochondrial membrane potentials in ischemic hearts. *Arch Biochem Biophys.* (2003) 420:279–86. doi: 10.1016/j.abb.2003.09.021
127. Grant AO. Cardiac ion channels. *Circ Arrhythm Electrophysiol.* (2009) 2:185–94. doi: 10.1161/CIRCEP.108.789081
128. Shaw RM, Rudy Y. Electrophysiologic effects of acute myocardial ischemia: a theoretical study of altered cell excitability and action potential duration. *Cardiovasc Res.* (1997) 35:256–72. doi: 10.1016/S0008-6363(97)00093-X
129. Kléber AG. Resting membrane potential, extracellular potassium activity, and intracellular sodium activity during acute global ischemia in isolated perfused guinea pig hearts. *Circ Res.* (1983) 52:442–50. doi: 10.1161/01.RES.52.4.442
130. Klabunde RE. Cardiac electrophysiology: normal and ischemic ionic currents and the ECG. *Adv Physiol Educ.* (2017) 41:29–37. doi: 10.1152/advan.00105.2016
131. Hoffman BF, Rosen MR. Cellular mechanisms for cardiac arrhythmias. *Circ Res.* (1981) 49:1–15. doi: 10.1161/01.RES.49.1.1
132. Rosenshtraukh LV, Witt RC, Nance PN, Rozanski GJ. Electrophysiologic effects of exogenous phosphocreatine in cardiac tissue: potential antiarrhythmic actions. *Am Heart J.* (1990) 120:1111–9. doi: 10.1016/0002-8703(90)90124-G

133. Singh BN, Nademanee K. Control of cardiac arrhythmias by selective lengthening of repolarization: theoretic considerations and clinical observations. *Am Heart J.* (1985) 109:421–30. doi: 10.1016/0002-8703(85)90629-5
134. El-Sherif N, Gough WB, Zeiler RH, Mehra R. Triggered ventricular rhythms in 1-day-old myocardial infarction in the dog. *Circ Res.* (1983) 52:566–79. doi: 10.1161/01.RES.52.5.566
135. Ferrier GR, Moffat MP, Lukas A. Possible mechanisms of ventricular arrhythmias elicited by ischemia followed by reperfusion. Studies on isolated canine ventricular tissues. *Circ Res.* (1985) 56:184–94. doi: 10.1161/01.RES.56.2.184
136. Kryzhanovskii SA, Kacharava VG, Marko R, Kelemen K, Kaverina NV, Sakhs VA. [Electrophysiologic study of the anti-arrhythmic mechanism of action of phosphocreatine in acute myocardial ischemia and reperfusion]. *Kardiologiia.* (1991) 31:66–9.
137. Anyukhovsky EP, Javadov SA, Preobrazhensky AN, Beloshapko GG, Rosenshtraukh LV, Saks VA. Effect of phosphocreatine and related compounds on the phospholipid metabolism of ischemic heart. *Biochem Med Metab Biol.* (1986) 35:327–34. doi: 10.1016/0885-4505(86)90090-3
138. Robinson LA, Braimbridge MV, Hearse DJ. Creatine phosphate: an additive myocardial protective and antiarrhythmic agent in cardioplegia. *J Thorac Cardiovasc Surg.* (1984) 87:190–200. doi: 10.1016/S0022-5223(19)37413-6
139. Niewiarowski S, Thomas DP. Platelet aggregation by ADP and thrombin. *Nature.* (1966) 212:1544–7. doi: 10.1038/2121544a0
140. Packham MA, Guccione MA, Chang PL, Mustard JF. Platelet aggregation and release: effects of low concentrations of thrombin or collagen. *Am J Physiol.* (1973) 225:38–47. doi: 10.1152/ajplegacy.1973.225.1.38
141. Zucker MB, Peterson J. Effect of acetylsalicylic acid, other nonsteroidal anti-inflammatory agents, and dipyridamole on human blood platelets. *J Lab Clin Med.* (1970) 76:66–75.
142. Macfarlane DE, Mills DC. The effects of ATP on platelets: evidence against the central role of released ADP in primary aggregation. *Blood.* (1975) 46:309–20. doi: 10.1182/blood.V46.3.309.309
143. Golikov AP, Riabinin VA. [Neoton in the treatment of myocardial infarct and unstable stenocardia]. *Kardiologiia.* (1993) 33:15–7, 3–4.
144. Samarenko MB. [Effect of phosphocreatine on the incidence of ventricular heart rhythm disorders in the 1st 24 hours of myocardial infarct]. *Kardiologiia.* (1986) 26:47–50.
145. Du XH, Liang FY, Zhao XW. [Effects of phosphocreatine on plasma brain natriuretic peptide level in elderly patients with chronic congestive heart failure]. *Nan Fang Yi Ke Da Xue Xue Bao.* (2009) 29:154–55, 159.
146. Perepech NB, Nedoshivin AO, Nesterova IV. [Neoton and thrombolytic therapy of myocardial infarction]. *Ter Arkh.* (2001) 73:50–55.
147. Perepech NB, Nedoshivin AO, Kutuzova AE. [Exogenous phosphocreatine in the prevention and treatment of cardiac insufficiency in patients with myocardial infarction]. *Klin Med.* (1993) 71:19–22.
148. Chambers DJ, Braimbridge MV, Kosker S, Yamada M, Jupp RA, Crowther A. Creatine phosphate (Neoton) as an additive to St. Thomas' Hospital cardioplegic solution (Plegisol). Results of a clinical study. *Eur J Cardiothorac Surg.* (1991) 5:74–81. doi: 10.1016/1010-7940(91)90004-4
149. Cheng SX, Hu QH. [Cardioprotective effect of exogenous phosphocreatine in patients undergoing open heart surgery]. *Hunan Yi Ke Da Xue Xue Bao.* (2001) 26:353–5.
150. Cisowski M, Bochenek A, Kucewicz E, Wnuk-Wojnar AM, Morawski W, Skalski J, et al. The use of exogenous creatine phosphate for myocardial protection in patients undergoing coronary artery bypass surgery. *J Cardiovasc Surg.* (1996) 37:75–80.
151. Guo-han C, Jian-hua G, Xuan H, Jinyi W, Rong L, Zhong-min L. Role of creatine phosphate as a myoprotective agent during coronary artery bypass graft in elderly patients. *Coron Artery Dis.* (2013) 24:48–53. doi: 10.1097/MCA.0b013e32835aab95
152. Pagani L, Musiani A. [The use of systemic phosphocreatine in heart surgery]. *Minerva Anestesiol.* (1992) 58:199–205.
153. Cerný J, Nemec P, Bucek J, Cerný E, Papousek F, Lojek A. [The effect of creatine phosphate in patients after surgery in ischemic heart disease]. *Vnitr Lek.* (1993) 39:153–9.
154. Chambers DJ, Haire K, Morley N, Fairbanks L, Strumia E, Young CP, et al. St. Thomas' Hospital cardioplegia: enhanced protection with exogenous creatine phosphate. *Ann Thorac Surg.* (1996) 61:67–75. doi: 10.1016/0003-4975(95)00819-5
155. Zhidkov IL, Ivanov VA, Kozhevnikov VA, Charnaia MA, Mukhamedzianova AR, Trekova NA. [Intraoperative myocardial protection with extracellular cardioplegic solutions in patients with cardiac valve diseases]. *Anesteziol Reanimatol.* (2007) 2:38–42.
156. MYa R, Samarenko MB, Afonskaya NI, Saks VA. Reduction of ventricular arrhythmias by phosphocreatine (Neoton) in patients with acute myocardial infarction. *Am Heart J.* (1988) 116:393–7. doi: 10.1016/0002-8703(88)90611-4
157. Kitzenberg D CSP, Glover LE. Creatine kinase in ischemic and inflammatory disorders. *Clin Transl Med.* (2016) 5:31. doi: 10.1186/s40169-016-0114-5

Conflict of Interest: The authors declare that the research was conducted in the absence of any commercial or financial relationships that could be construed as a potential conflict of interest.

frontiers in Cardiovascular Medicine

REVIEW
published: 02 August 2021
doi: 10.3389/fcvm.2021.723996

Post-translational Acetylation Control of Cardiac Energy Metabolism

*Ezra B. Ketema and Gary D. Lopaschuk**

Department of Pediatrics, Cardiovascular Research Centre, University of Alberta, Edmonton, AB, Canada

Perturbations in myocardial energy substrate metabolism are key contributors to the pathogenesis of heart diseases. However, the underlying causes of these metabolic alterations remain poorly understood. Recently, post-translational acetylation-mediated modification of metabolic enzymes has emerged as one of the important regulatory mechanisms for these metabolic changes. Nevertheless, despite the growing reports of a large number of acetylated cardiac mitochondrial proteins involved in energy metabolism, the functional consequences of these acetylation changes and how they correlate to metabolic alterations and myocardial dysfunction are not clearly defined. This review summarizes the evidence for a role of cardiac mitochondrial protein acetylation in altering the function of major metabolic enzymes and myocardial energy metabolism in various cardiovascular disease conditions.

Keywords: mitochondria, fatty acid oxidation, succinylation, sirtuins, lysine acetylation, glucose oxidation

OPEN ACCESS

Edited by:
Kunhua Song,
University of Colorado Anschutz Medical Campus, United States

Reviewed by:
Bradley S. Ferguson,
University of Nevada, Reno, United States
Matt Stratton,
The Ohio State University, United States

***Correspondence:**
Gary D. Lopaschuk
gary.lopaschuk@ualberta.ca

Specialty section:
This article was submitted to Cardiovascular Metabolism, a section of the journal Frontiers in Cardiovascular Medicine

Received: *11 June 2021*
Accepted: *30 June 2021*
Published: *02 August 2021*

Citation:
Ketema EB and Lopaschuk GD (2021) Post-translational Acetylation Control of Cardiac Energy Metabolism. Front. Cardiovasc. Med. 8:723996. doi: 10.3389/fcvm.2021.723996

INTRODUCTION

Following the discovery of histone acetylation and its regulatory effect on RNA synthesis by Allfrey et al. (1), it has been established that alterations in the level of histone acetylation can modulate gene expressions via chromatin remodeling and epigenetic modifications (2, 3). Indeed, dysregulation of histone acetylation level has been strongly linked with the development and progression of cancer and other human diseases (4, 5). This was further reinforced by the identification of histone acetyltransferases (HAT) and histone deacetylases (HDACs), enzymes that mediate the addition or removal of an acetyl group to and from a lysine residue of histone proteins (6, 7), and the development of several HDAC inhibitors to treat cancer and heart diseases (8–10).

In addition to nuclear histone acetylation, the potential for non-histone protein acetylation of non-nuclear proteins has also recently generated considerable interest. The first acetylation of cytoplasmic proteins was described in microtubules (α-tubulin) in 1987 by Piperno et al. (11). The involvement of acetylation of non-nuclear proteins was further confirmed by the isolation of other acetylated proteins in both the cytosol and mitochondria, as well as the presence of deacetylase enzymes, such as SIRT2 and SIRT3 outside the nucleus (12–15). Since then, a number of acetylases and deacetylases have been identified outside the nucleus (**Figure 1**) (16). However, it is the advancements in protein acetylome quantitative methods, and the identification of several thousands of cytosolic and mitochondrial acetylated proteins using these techniques, that have recently helped advance our understanding of non-histone acetylation dynamics and its biological implications.

Kim et al. reported the first large acetyl proteomic data profile by identifying 388 acetylation sites in 195 proteins in HeLa cells and mouse liver using immunoprecipitation of lysine-acetylated

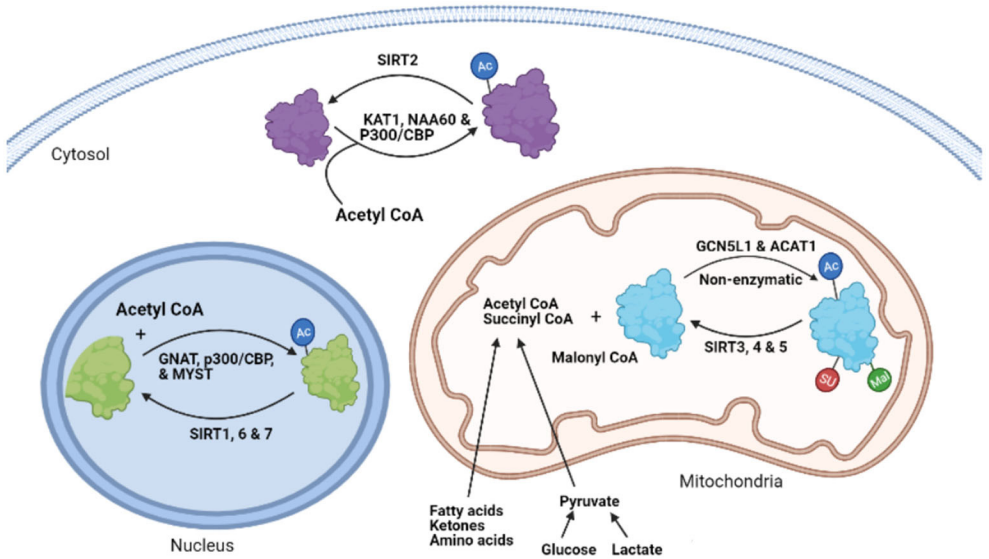

FIGURE 1 | The process of protein lysine acetylation/acylation and deacetylation/deacylation. KAT1, lysine acetyltransferase; NAA60, N-α-acetyltransferase 60; CBP, CREB-binding protein; SIRT, sirtuin, GNAT, GCN5-related N-acetyltransferases; MYST, MYST family acetyltransferase; GCN5L1, General control of amino acid synthesis 5 (GCN5) like-1; ACAT1, acetyl-CoA acetyltransferase; AC, lysine Acetylation; SU, succinylation; MU, malonylation.

peptides and mass spectrometry analysis (17). Of these, 133 proteins with 277 lysine acetylation sites were from mitochondria, showing for the first time the abundance of the acetylation process in mitochondria. Subsequently, several hundred acetylated proteins were also identified in other studies using either nutritional or acetylase/deacetylase enzymatic manipulations (18, 19). For example, in response to caloric restriction in mice, Schwer et al. reported acetylation of several proteins involved in metabolic pathways in the liver (19). Another study by Zhao et al. revealed the prevalence of acetylation of several metabolic enzymes and its possible regulatory role using both HDAC and non-histone acetylation inhibitors (20). Similarly, Lombard et al. demonstrated extensive mitochondrial protein acetylation in SIRT3 knockout (KO) mice (21), a finding confirmed by Hirschey et al. (22). Strikingly, these studies described the exceptional susceptibility of mitochondrial proteins to acetylation modification in response to various stressors, with up to 60% of mitochondrial proteins reported to being acetylated (23). Of importance, the majority of these acetylated proteins were enzymes catalyzing energy metabolic processes (19–21, 24). Similar to acetylation modifications, several studies have demonstrated increased succinylation and malonylation of a large number of cytosolic and mitochondrial proteins in response to SIRT5 deletion (25–27). For instance, in liver mitochondria isolated from SIRT5 KO mice, Rardin et al. identified 1190 succinylation sites, of which 386 sites on 140 proteins were seen in enzymes involved in energy metabolism, including fatty acid β-oxidation and ketogenesis (26). Despite these studies, that have revealed widespread acyl modifications on proteins in most of the metabolic pathways, its biological significance and regulation are still poorly understood. Understanding these post-translational modifications is particularly important in heart failure, where significant alterations in mitochondrial metabolism are seen, and disturbances in the metabolites used as a substrate for these post-translational modifications occur.

Impairments in myocardial energy substrate metabolism are a major contributor to the pathogenesis of heart failure (28–30). However, the underlying causes of these metabolic perturbations remain unclear. In the failing heart, changes in the transcription of genes encoding metabolic enzymes, particularly fatty acid metabolic enzymes, have been suggested as one of the mechanisms for altered energy substrate metabolism (31–34). Nevertheless, transcriptional regulation alone is not sufficient to explain all the metabolite and enzyme activity changes observed in the failing heart (35, 36). Several post-transcriptional and post-translational processes have been shown to modulate the original transcription products, and thus can significantly alter energy metabolism in the failing heart. Post-translational acetylation-mediated modification of metabolic proteins is thought to have a regulatory role in these energy metabolic changes (37–39).

In addition to acetylation, many other post-translational modifications including phosphorylation, malonylation, succinylation, glutarylation, ubiquitination, SUMOylation, O-GlcNAcylation, N-glycosylation, methylation, citrullination, and S-nitrosylation play important roles in cardiac disease pathogenesis, including metabolic perturbations (40–42). However, the focus of this review will be on the role of acetylation (and some acylation) modifications of energy metabolic enzymes and their contributions to altering cardiac energy metabolism. Although the relevance of protein acetylation changes have also been reported in other pathological processes, including

inflammation, oxidative stress, and apoptosis, this review will mainly discuss the connections between acetylation imbalances and cardiac energy metabolic changes.

THE PROCESS OF PROTEIN ACETYLATION

Lysine acetylation of proteins occurs through the covalent attachment of an acetyl group to the lysine residues of proteins. This acylation modification causes important changes to the protein at its lysine residue, which includes altering its charge status and adding an extra structural moiety (43, 44). These changes impact the proteins' native structure, its interactions with other proteins or regulatory molecules, its stability, and its function (45). Similar to acetylation, lysine succinylation, and malonylation have also emerged as functionally important acyl group modifications. These acyl modifications occur by the addition of malonyl and succinyl groups to the same or different lysine residues modified by acetylation (25, 26, 46). As discussed in the following section, cellular protein acetylation dynamics are regulated by various factors including pathological stressors, substrate availability, and the balances between acylation and deacylation enzymes (47).

While several acyltransferases have been characterized and shown to catalyze histone and other nuclear protein acetylation processes (48, 49), the involvement of these acyltransferases in the transfer of acetyl (acyl) group during cytosolic and mitochondrial protein acetylation (acylation) modifications remains to be clearly defined. A few studies suggest that some of the nuclear acetyltransferases, such as p300/CBP, may shuttle between the nucleus and cytoplasm and participate in the acetylation of cytosolic proteins (44, 50, 51). Type B lysine acetyltransferases (KATs), which include KAT1 and NAA60, are also cytoplasmic enzymes (48). The GNAT family, ATAT1 and general control of amino acid synthesis 5-like 1 (GCN5L1) acetyltransferase, also contribute to mitochondrial protein acetylation changes (**Figure 1**) (52, 53). However, it has also been suggested that mitochondrial protein acetylation can occur through non-enzymatic modifications (54, 55). Although widespread protein malonylation and succinylation have been described in the mitochondria (25, 56), no specific succinyltransferases or malonytransferases have been identified to date. As a result, some researchers have proposed that non-enzymatic mechanisms may be responsible for such acyl modifications (55), while others suggest that some nuclear acetyltransferases, such as histone acetyltransferase 1 (HAT1), may be involved in nuclear protein lysine succinylation (57).

Deacetylation of cytoplasmic and mitochondrial proteins mainly involves the actions of sirtuin enzymes. Sirtuins are class III NAD^+-dependent protein deacetylases, which are considered as orthologs of silent information regulator 2 (SIR2) in yeast (58, 59). SIR2 regulates the transcription of silencing of mating-type loci, telomeres, and ribosomal DNA, thereby prolonging the yeast's lifespan (60, 61). Sirtuins can also regulate mammalian lifespan (62–64). This effect of sirtuins has led to the suggestion that sirtuins are mediators of the favorable effects of calorie restriction on health and aging, including metabolic reprogramming and stress tolerance. In support of this, caloric restriction is also shown to increase the expression of sirtuins (21, 22, 65, 66).

There are seven mammalian sirtuin proteins (SIRT1–SIRT7) with variation in their tissue specificity, subcellular localization, enzymatic activity, and targets (16). SIRT1, 6, and 7 are mainly localized in the nucleus (16, 67, 68), while SIRT2 is predominantly localized in the cytoplasm (12). However, SIRT1 and SIRT2 can shuttle between the nucleus and the cytoplasm and acetylate proteins in both compartments (67, 69). SIRT1 can regulate the acetylation state of diverse cellular proteins in the nucleus (70). In contrast, SIRT 3, 4, and 5 are mainly localized in the mitochondria (13, 16, 71), although some studies have reported cytosolic localization of SIRT5 (25). In terms of their enzymatic activity, SIRT 1–3 possess potent deacetylase activity, regulating protein acetylation status in the respective organelles (21, 23, 72). The other sirtuins, SIRT 4–7, have weak or no detectable deacetylase activity or either have very protein specific deacetylation activity (73) or mediate other deacylation processes (21). Of importance, SIRT5 has potent lysine demalonylation and desuccinylation activity (25, 56, 74). Additionally, SIRT4 and 6 have been shown to possess ADP-ribosyltransferase activity in the mitochondria and nucleus, respectively (71, 75). Also, SIRT7 has been described to have desuccinylase activity on nuclear histones (76). Combined, deacylation by sirtuins regulates diverse processes including, metabolism, gene expression, cell survival, and several other processes in the heart (77). In addition to sirtuins, recent studies have also suggested the participation of non-sirtuin HDACs in the regulation of mitochondrial acetylation dynamics (78, 79). In support of this, HDAC1 and HDAC2 have been detected in the mitochondrial isolates from mouse hearts (79).

MYOCARDIAL CONTROL OF ACETYLATION/ACYLATION

Lysine acylation in the heart can be driven and affected by several factors including the altered level and function of acetyltransferases (such as GCN5L1) and deacylation enzymes (sirtuins), the levels of acetyl-CoA and short-chain acyl-CoAs, the levels of NAD^+, and the underlying disease state (39, 80, 81). However, it is not yet clear how these individual factors contribute to the degree of mitochondrial protein acetylation/acylation, and whether their contribution varies according to variable conditions. As a result, despite the increased recognition of excessive protein acetylation and acylation in various forms of heart failure, there is a need to better understand the actual mechanism that is responsible for these protein post-translational modifications (PTMs).

Altered Acyl-CoA Levels

Short-chain acyl-CoA species such as acetyl-CoA, malonyl-CoA, and succinyl-CoA are important metabolite intermediates generated during catabolism of various energy fuels. They are also donors of acetyl, malonyl, and succinyl groups for protein lysine

acetylation, malonylation, and succinylation, respectively. Thus, the levels and distribution of these short acyl-CoA species can significantly affect cellular PTMs patterns.

Previous studies have suggested that increased acetylation largely arises from the non-enzymatic reaction of high levels of acetyl-CoA generated during a high-fat diet (HFD), obesity, and diabetes (82–86). Myocardial fatty acid ß-oxidation increases with a HFD, diabetes, and obesity, leading to an increase in acetyl-CoA generation (84, 87, 88). Compromised mitochondrial tricarboxylic acid (TCA) cycle activity, such as during ischemia and severe heart failure, can also increase mitochondrial acetyl-CoA levels. The mitochondrial acetyl-CoA production in these conditions may exceed the oxidative capacity of the TCA cycle and therefore increase the mitochondrial acetyl-CoA pool size. As acetyl-CoA is a substrate for acetylation, this excess acetyl-CoA has the potential to drive acetylation of mitochondrial proteins. In agreement with this, Pougovkina et al., using radioactively labeled palmitate, showed that acetyl-CoA generated by fatty acid ß-oxidation in cultured liver cells is sufficient to drive global protein hyperacetylation (89). Similarly, in a recent study, Deng et al. observed a high incorporation of fatty acid-derived ^{13}C isotope onto acetylated peptides in failing mouse hearts. The authors also demonstrated a significant elevation in the levels of protein acetylation in H9c2 cells when incubated with palmitate, suggesting an association between fatty acid ß-oxidation and protein hyperacetylation (90). Wagner and Payne also demonstrated that widespread protein acetylation in the mitochondria may be facilitated by alkaline pH and high concentrations of reactive acyl-CoAs independent of any enzymatic action (55). Although these studies suggest that elevations in acetyl-CoA levels during increased fatty acid utilization enhances protein acetylation events, it has not yet been demonstrated whether an increased acetyl-CoA production from other fuels also contributes to protein acetylation modification in the mitochondria.

Unlike acetyl-CoA, the association between malonyl-CoA and succinyl-CoA levels and corresponding changes in lysine acylation in the heart has not been examined. However, in contrast to acetyl-CoA levels, malonyl-CoA levels are reduced under conditions of increased fatty acid ß-oxidation as a result of increased malonyl-CoA decarboxylase (MCD) enzymatic activity, the enzyme that degrades malonyl-CoA (91, 92). Others have also suggested that malonyl-CoA levels are unchanged during obesity or with a HFD (93, 94). High levels of fatty acids seen in these conditions also increase myocardial MCD expression, contributing to a decrease in malonyl-CoA levels (95). In contrast, increased malonyl-CoA levels in MCD deficient human fibroblast cells resulted in a two-fold increase in the levels malonylation, suggesting that malonyl-CoA levels may impact malonylation status (96). Although succinyl-CoA is one of the most abundant acyl-CoAs in the heart (46), it is not known if succinyl-CoA levels alter succinylation status in the heart. It is known that protein lysine succinylation is increased in mice hearts lacking SIRT5 (46), and that many of these proteins participate in metabolic pathways that include oxidative phosphorylation, fatty acid ß-oxidation, ketogenesis, branched-chain amino acid (BCAAs) catabolism, and the TCA cycle (97).

Altered Expression of Acyltransferases

In contrast to the well-characterized role of multiple acetyltransferases for histone or nuclear protein acetylation, less is known regarding the role of acetyltransferases in cytosolic and mitochondrial lysine acetylation. Enzymatic acetylation of mitochondrial or cytosolic proteins may involve the GNAT family of acetyltransferases, including acetyl-CoA acetyltransferase (ACAT1) (98) and GCN5L1 (52, 53). Studies by Thapa et al. demonstrated a correlation between an excess nutrient (i.e., a HFD), upregulation of GCN5L1 expression, and increased mitochondrial lysine acetylation (53), although we observed no changes in GCN5L1 expression under similar experimental conditions (39). Reduced mitochondrial protein acetylation in GCN5L1 cardiac-specific KO mice subjected to a HFD has also been reported (99). We have also shown an increased expression of GCN5L1 in association with increased lysine acetylation in the newborn heart (100).

As discussed, protein lysine malonylation and succinylation modifications are highly prevalent in enzymes of mitochondrial metabolism and the TCA cycle (25, 56, 74). However, it is still unknown whether these processes are catalyzed by succinyl or malonyl transferases or whether they occur passively. Therefore, it remains unclear how these protein acylation modifications are regulated during pathological conditions.

Altered Expression of Sirtuins

SIRT3 is a major mitochondrial deacetylase. Studies have shown an association between SIRT3 deletion and mitochondrial protein hyperacetylation, supporting its critical deacetylating role (21, 22). Many key enzymes in fatty acid and carbohydrate metabolism are substrates for SIRT3 deacetylation (72, 101, 102). Downregulation of SIRT3 occurs in response to stressors such as a HFD or various heart diseases (81, 103). Decreased SIRT3 has been also implicated in various cardiac pathologies in association with hyperacetylation of mitochondrial proteins (54, 104). For instance, a change in the expression of SIRT3 isoforms (long and short forms) is seen in mice hearts subjected to different hypertrophic stimuli (105). However, there is a lack of understanding as to how SIRT3 gene expression is affected by altered metabolic (nutrient) state or heart failure. Moreover, most previous studies have focused on the expression levels of SIRT3, as opposed to actual SIRT3 enzymatic activity.

Cardiac SIRT1, a deacetylase enzyme in the nucleus and cytosol, is also downregulated in advanced heart failure (106). Similar findings in other heart failure studies have also been observed, which demonstrated an association between decreased SIRT1 expression and increased oxidative stress (107). Paradoxically, other researchers have shown a correlation between constitutive overexpression of SIRT1 and impaired cardiac function, as well as disturbed cardiac energy metabolism in response to acute pressure overload (108). SIRT1 protein is also negatively regulated by HFD, which induces its cleavage by the inflammation-activated caspase-1 in adipose tissue (109).

Some studies have indicated a high level of SIRT5 expression in normal hearts (16). However, the pattern of changes in SIRT5 levels under stress conditions is not well-characterized. A previous study on mouse primary hepatocytes have suggested

upregulation of SIRT5 by peroxisome proliferator-activated receptor coactivator-1α (PGC-1α), and downregulation by AMP-activated protein kinase (AMPK) (110). Unlike SIRT1 and 3, the absence of SIRT5 does not affect the development of HFD-induced metabolic abnormalities and insulin resistance (111).

HDACs are known to modulate histone acetylation status and thus affect its interaction with DNA, which results in chromatin remodeling and transcriptional changes (2). However, recent studies have also implicated a role for HDAC in modifying the mitochondrial acetylome directly in a non-transcriptional manner using various HDAC inhibitors (78, 79, 112). Both hyperacetylation and hypoacetylation of mitochondrial proteins was observed in response to a pan-HDAC inhibitor in a feline model of heart failure (78). However, the effects of these acetylation modifications was not investigated in this study. Moreover, though a positive association has been made between HDAC inhibition and improved cardiac function in relation to acetylation changes, it has not yet been explored how HDAC inhibition affects sirtuin functions or whether the patterns of acetylation regulated by HDAC inhibition is different from those regulated by mitochondrial sirtuins.

Altered NAD^+ Levels

NAD^+ is an important cofactor for sirtuins, and as such fluctuation in NAD^+ levels may be one of the contributing factors for altered protein acetylation levels (58). Through NAD^+, sirtuin activity is directly linked to the energy status of the cell. NAD^+ is synthesized from different biosynthetic precursors. In the salvage pathway, the major NAD^+ generating pathway, nicotinamide riboside (NR) and nicotinamide (NAM) are converted into nicotinamide mononucleotide (NMN) by nicotinamide riboside kinase (NRK) and nicotinamide phosphoribosyltransferase (NAMPT) enzymes, respectively. Nicotinamide mononucleotide adenyltransferases (NMNAT) then converts NMN to NAD^+. In the *de novo* pathway, NAD^+ is generated from the amino acid tryptophan, which is ultimately converted into the biosynthetic intermediate, nicotinic acid mononucleotide (NaMN) through multiple enzymatic steps. Nicotinic acid mononucleotide is then converted to nicotinic acid dinucleotide ($NaAD^+$) by NMN/NaMN adenylyltransferases (NMNATs) and then converted to NAD^+ by NAD^+ synthetase through deamination (113). Intracellular NAD^+ levels can also be altered by rates of glycolytic and mitochondrial metabolic pathways using NAD^+ to produce NADH, rates of mitochondrial electron transport chain activity that produce NAD^+ from NADH, and by enzymes that consume or catabolize NAD^+, such as the poly ADP-ribosyltransferases (PARPs) and the NAD^+ cyclases (CD38) (113, 114).

Alterations in the NAD^+ biosynthetic or degradation pathways may directly affect the activity of sirtuins and thus protein acetylation status (115, 116). Kinetics studies on sirtuins and NAD^+ metabolites, have demonstrated the sensitivity of sirtuins to changes in nicotinamide and NAD^+ levels, which inhibits and activates its enzymatic activity, respectively (58, 117, 118). While both the NADH and NAD^+/NADH ratio have been previously suggested to impact lysine acetylation status (80, 119, 120), recent studies indicated that alterations in NADH have insignificant effect on sirtuin regulation (117, 121). Accordingly, NADH has a very poor binding affinity to sirtuins (117), and sirtuins are insensitive to NADH inhibition at the concentration of NADH found in the cell (121). As a result, changes in NAD^+, as opposed to commonly reported changes in the NAD^+/NADH ratio, should be used for assessing NAD^+ regulation of sirtuin activity (122). Both NADH & NAD^+, as well as NAD^+/NADH ratio, also significantly varies across cellular compartments and in response to various disease or metabolic states, making it difficult to interpret the implication of NAD^+/NADH ratio in controlling sirtuin activity (122). In addition, the NAD^+/NADH ratio alone does not also provide specific information on the direction of changes to the individual nucleotides. Thus, measurement of free NAD^+ levels is most relevant when it comes to the regulation of sirtuins and perturbations in protein acetylation.

Previous studies have demonstrated changes in the activity of sirtuins and protein acetylation levels by modulating both NAD^+ synthetic and catabolic pathways (41, 115, 123). Accordingly, Lee et al. observed a significant decrease in the mitochondrial proteins acetylome in response to NAMPT overexpression or NAD^+ supplementation (80). Similarly, other studies have also shown increased NAD^+ levels accompanied by enhanced SIRT1 and SIRT3 activities in responses to NR supplementation, which was accompanied by an increase in oxidative metabolism and protection against HFD-induced metabolic abnormalities (123). Supporting this, producing a CD38 deficiency (which is a NAD^+ degrading enzyme) protects the heart from HFD-induced oxidative stress by increasing NAD^+ availability and activating SIRT3 mediated protein deacetylation (115). NAD^+ depletion occurs in many cardiac pathologies, such as during ischemia-reperfusion (I/R) injury, and several therapeutic strategies to increase NAD^+ levels have been proposed (124, 125). However, the mechanisms which mediate the favorable effects of increasing NAD^+ levels are not completely understood, although emerging data suggests activation of sirtuins and decreasing protein acylation modifications as key effectors (126–129).

ACETYLATION/ACYLATION OF ENERGY METABOLIC ENZYMES AND MYOCARDIAL METABOLIC ALTERATIONS

Alterations in myocardial energy metabolism, both in terms of changes in energy substrate preference, and decreased mitochondrial oxidative metabolism and ATP production, are key contributors to heart failure development (28, 130–133). Various injury or stress signals, including ischemia, hypertrophy or neurohormonal changes, are thought to mediate these metabolic derangements (130). While these disturbances result in an unbalanced use of glucose and fatty acids and a decreased contractile efficiency during heart failure, it remains controversial whether the shifts occur toward increased glucose use or increased fatty acid use, and whether these shifts are adaptive or pathological (30, 33, 134–139). Our limited understanding of the underlying mechanisms regulating these metabolic changes is a major challenge to better characterizing these alterations for potential therapeutic interventions.

Changes in metabolic gene expressions, predominantly downregulation of fatty acid transporting and metabolizing proteins, have been described as one of the contributors to the metabolic changes seen in heart failure (31–34, 139). Recently, apart from transcription regulation, several post-transcriptional and post-translational processes have been shown to modulate transcriptional and protein products (41, 42). There is also an inconsistency in these transcriptional changes, within both the metabolic pathways and across species (31). For instance, while downregulation of fatty acid metabolic enzymes expression is observed in various animal models of heart failure, no significant alterations are observed in genes regulating glucose metabolism, or changes are largely inconsistent, in human heart failure samples (31, 35). Even within the fatty acid metabolic genes, transcriptional downregulation has been observed only in a few of them compared to the widespread post-translational modification seen in most of these enzymes (34, 35). In support to this, Sack et al. observed, a mismatch between mRNA levels and activities of some of the fatty acid metabolic enzymes in the failing heart (139), suggesting a role for post-transcriptional and post-translational changes.

Growing evidence suggests that post-translational acetylation modification may play a significant role in altering myocardial metabolism during heart failure by modifying the function and structure of major metabolic proteins (39, 104, 140). Hyperacylation of key metabolic enzymes involved in fatty acid and glucose metabolism has been shown in heart failure as well as response to excess nutrition or sirtuin deletions (81, 83, 97, 141, 142). However, despite the modification of many of these enzymes by acetylation or other acylations, the actual impact of these PTMs on individual pathways and enzymes remains poorly understood. In this section, we summarize recent evidence on the impact of hyperacetylation on selected metabolic enzyme activity in the heart as well as in other organs or cells (**Figure 2**).

Fatty Acid ß-Oxidation

The enzymes catalyzing the cyclic reactions of fatty acid β-oxidation (which converts fatty acid carbons into acetyl-CoA moeities) includes long-chain acyl CoA dehydrogenase (LCAD), enoyl-CoA hydratase, L-3-hydroxy acyl-CoA dehydrogenase (β-HAD), and 3-ketoacyl-CoA thiolase (KAT) (143, 144). Acetylation of these enzymes has been widely reported in various studies (**Table 1**) (20, 22, 83). The functional consequences of acetylation are relatively well-studied for LCAD and β-HAD. However, most of these studies were conducted in the liver and skeletal muscle, and only a few studies examined the direct impact of acetylation on fatty acid metabolism in the heart.

The exact effect of acetylation on fatty acid metabolizing enzymes' activity remains controversial, and there are two opposing views. Using both HFD and SIRT3 KO mice, we demonstrated a positive correlation between increased acetylation of myocardial LCAD and β-HAD and their enzymatic activities as well as increased fatty acid ß-oxidation rates in the heart (83). A similar relationship between acetylation and increased fatty acid ß-oxidation was also seen in newborn rabbits and human hearts. In the early newborn period, a dramatic maturational change in myocardial energy substrate metabolism occurs, accompanied by an increase in fatty acid ß-oxidation. In association with this, we have shown increased acetylation of LCAD and β-HAD, accompanied by an increase in their activities, during the maturation of fatty oxidation in neonatal rabbit hearts (100). The increased acetylation of these enzymes is accompanied by an up-regulation of the acetyltransferase, GCN5L1. In a separate study, we also found a decreased LCAD and βHAD activities and a decrease in fatty acid ß-oxidation rates in hypertrophied newborn human and rabbit hearts in association with decreased acetylation status of these enzymes (154). Similarly, Thapa et al. revealed a positive association between increased acetylation and activities of several cardiac fatty acid ß-oxidation enzymes, including LCAD, β-HAD, and short-chain acyl-CoA dehydrogenase in chronic HFD mice, along with GCN5L1 upregulation (53). Furthermore, decreasing acetylation by GCN5L1 knockdown leads to diminished fatty acid ß-oxidation in cultured H9C2 cells, supporting the idea that lysine acetylation promotes fatty acid ß-oxidation in the heart (53).

Additional evidence for a positive correlation between increased acetylation and increased activities of fatty acid ß-oxidation enzymes have been reported from studies in diabetic animals. In streptozotocin-induced type 2 diabetic rat hearts, Vazquez et al. found a significant increase in mitochondrial lysine acetylation compared to the controls (143). Increased activities of medium- and long-chain acyl-CoA dehydrogenases (MCAD, LCAD) and fatty acid ß-oxidation rates were observed in the hearts of diabetic animals. Analysis of substrate preference in these hearts also revealed an increase in state 3 respiration using palmitoylcarnitine as a substrate (146). Similarly, in type 1 diabetic mice, a 2.5-fold increase in total acetylation levels compared to age-matched controls was observed in the heart. In this study, the maximal rate of respiration remained unchanged only when palmitoylcarnitine or a fatty acid-based substrate was used (85). Furthermore, data from the two most recent studies also indicated that fatty acid utilization in the heart is either unaffected or proceed in harmony with increased acetylation state (90, 155).

Activation of fatty acid ß-oxidation by acetylation is also reported in other tissues/cells. A direct relationship between hyperacetylation and activity of enoyl-coenzyme A hydratase/3-hydroxy acyl-coenzyme A was demonstrated in the presence of high fat and deacetylase inhibitors in cultured Chang human liver cells (20). Other investigators have also found a link between HDAC3 mediated deacetylation of 3-hydroxy acyl-coenzyme A and its decreased activity in macrophages, while HDAC3 depletion reversed this effect (112). Moreover, in SIRT3 KO mice and SIRT3 deficient skeletal muscle cells, Jing et al. showed an increase in palmitate oxidation rates in the presence of excessive acetylation (155). In the presence of high palmitate, oxygen consumption rates are significantly higher in SIRT3 lacking myoblasts, which is lost in the presence of etomoxir, a fatty acid ß-oxidation inhibitor (156). Together, these studies demonstrate that increased acetylation of myocardial fatty acid ß-oxidation enzymes is associated with their enhanced activities. This is further supported by the fact that both myocardial fatty acid utilization and mitochondrial acetylation are enhanced during a

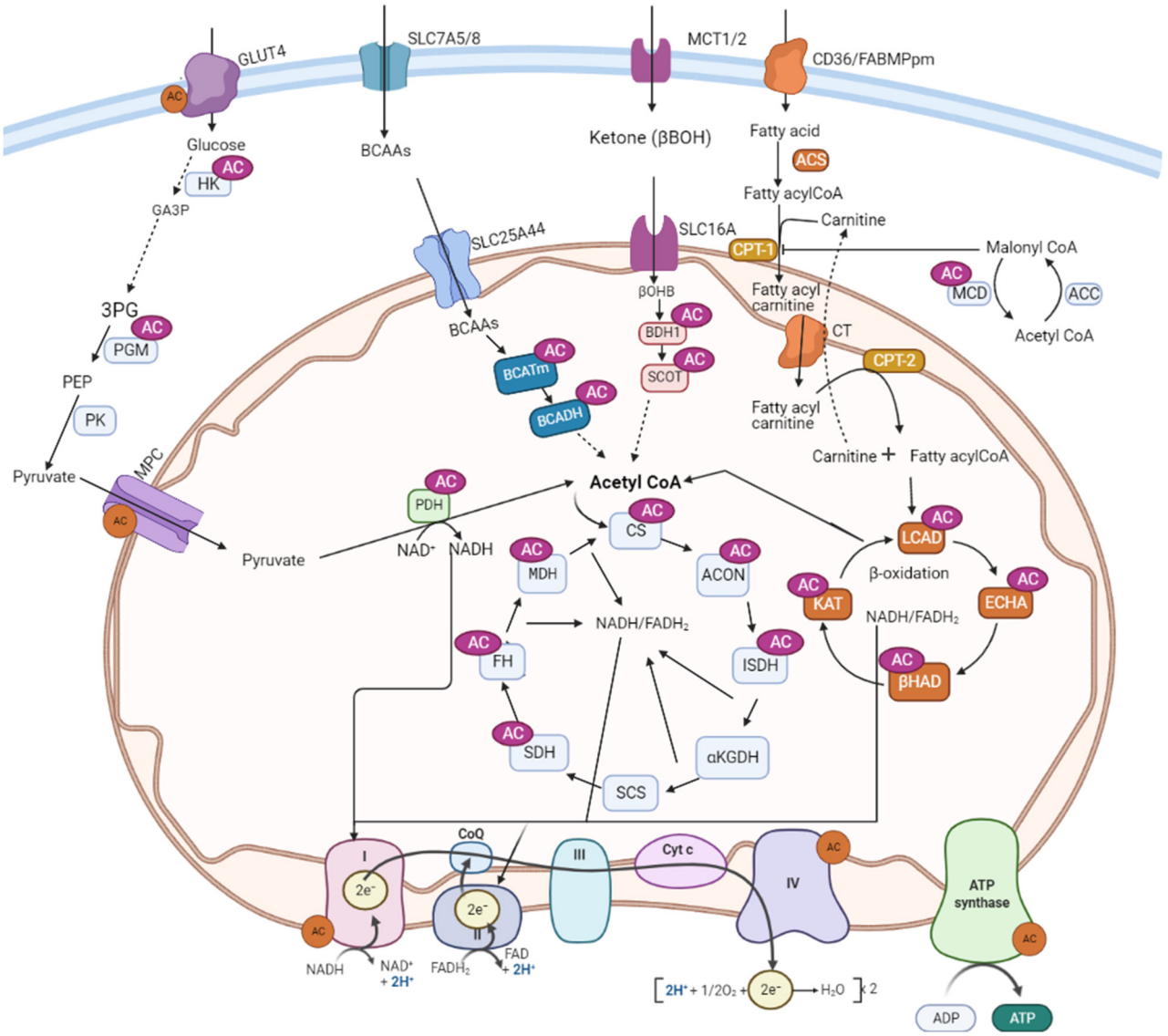

FIGURE 2 | Metabolic proteins subjected to acetylation control in the heart. AC, lysine acetylation; GLUT4, glucose transporter isoform 4; SLC7A5/8, solute carrier family-7; SLC25A44, solute carrier family-25; SLC16, solute carrier family-16; MCT, monocarboxylate transporter 1; CD36, cluster of differentiation 36; FABPpm, plasma membrane fatty acid-binding protein; MCD, malonyl CoA decarboxylase; ACC, acetyl CoA carboxylase; PDH, pyruvate dehydrogenase; LCAD, long-chain acyl CoA dehydrogenase; β-HAD, β-hydroxyacyl CoA dehydrogenase; KAT, 3-ketoacyl-coa thiolase; ECH, enoyl-CoA hydratase; FAS, fatty acyl CoA synthase; CPT-1, carnitine palmitoyltransferase 1; CPT-2, carnitine palmitoyltransferase-2; CT, carnitine acyl translocase; BCAA, branched-chain amino acids; BCATm, mitochondrial branched-chain aminotransferase; BCADH, branched-chain amino acid dehydrogenase; β-OHB, β-hydroxybutyrate; BDH-1, 3-hydroxybutyrate dehydrogenase 1; SCOT, 3-ketoacid CoA transferase; CS, citrate synthase; ISDH, iso-citrate dehydrogenase; α-KGDH, alpha-ketoglutarate dehydrogenase; SCS, succinate CoA synthetase; MDH, malate dehydrogenase; SDH, succinate dehydrogenase; FH, fumarate hydratase; OAA, oxaloacetate; MCD, malonyl CoA decarboxylase; ACON, aconitase; HK, hexose kinase; GA3P, glyceraldehyde 3-phosphate; 3PG: 3-phosphoglycerate; PGM, Phosphoglycerate mutase; PK, pyruvate kinase; CoQ, coenzyme Q; Cytc: cytochrome C; FAD/$FADH_2$, flavin adenine dinucleotide; NAD/NADH2, nicotinamide adenine dinucleotide.

HFD, obesity, and diabetes (157). The high fatty acid ß-oxidation rate seen in these conditions may also lead to the increased production of acetyl-CoA that can serve as a substrate for acetylation (82). Thus, it is reasonable to assume that increased acetylation of fatty acid oxidative enzymes can further trigger the enzyme activity and led to the continuation of fatty acid ß-oxidation in the heart in these circumstances.

In contrast to the scenarios discussed above, a study by Koentges et al., in isolated working hearts, found a negative correlation between hyperacetylation of LCAD and its activity along with reduced palmitate oxidation in SIRT3 deficient transverse aortic constriction (TAC) mice (158). However, these hearts were perfused with a buffer that contained an ultra-physiological high concentration of glucose (11 mM)

TABLE 1 | Effect of lysine acetylation on major metabolic enzymes in the heart.

Metabolic pathway	Enzymes	Effect on enzyme activity	References
Fatty acid oxidation	LCAD	↑, ↓	(53, 83, 145)
	β-HAD	↑	(53, 83)
	MCAD	↑	(146)
	MCD	↑	(73)
Glucose oxidation	PDH	↓	(53, 83, 147)
	MPC	↓	(148)
Glycolysis	HK	↓	(100)
	PGM	↓	(100)
	GLUT4	↓	(149)
Insulin signaling	Akt	↓	(147, 150)
TCA cycle	ICDH	↓,⇔	(151)
	SDH	↓	(81)
	ACON	↑	(152)
ETC	Complex I	↓	(24, 153)
	Complex III	↓	(24)
	Complex V	↓	(24, 153)

GLUT4, glucose transporter isoform 4; PDH, pyruvate dehydrogenase; LCAD, long-chain acyl CoA dehydrogenase; β-HAD, β-hydroxyacyl CoA dehydrogenase; ICDH, iso-citrate dehydrogenase; MCAD, medium-chain acyl CoA-dehydrogenase; MCD, malonyl CoA decarboxylase; MPC, mitochondrial pyruvate carrier; SDH, succinate dehydrogenase; ETC, electron transport chain; Akt, protein kinase B; PGM, phosphoglucomutase; ACON, aconitase; HK, hexokinase; TCA, tricarboxylic acid; ↑, increased activity; ↓, decreased activity; ⇔, no change in the activity of the enzyme.

and a lower fatty acid to albumin ratio (1.5%) where both conditions may contribute to decreased fatty acid ß-oxidation rates. Likewise, Chen et al. also reported an abnormal lipid accumulation and decreased palmitate ß-oxidation rates in TAC-induced hypertrophic hearts, with a further decline in SIRT3 KO mice hearts in association with hyperacetylation of LCAD (145). A recent study by Davidson et al. showed reduced expression of genes of fatty acid catabolism despite no overt abnormalities in mitochondrial respiration in mice deficient for cardiac carnitine acetyltransferase and SIRT3, despite the fact that the hearts exhibited extreme acetylation (159). In common, these three studies were done in mice with TAC-induced heart failure, while the last two did not assess directly the acetylation status of the enzymes. Overall, it is not clear if TAC alters the dynamics of acetylation on LCAD differently, such as through distinctive sites or multiple site modifications. However, several acyl modifications may likely coexist under these circumstances, which possibly compete with acetylation for the same lysine residue (104). However, experimental data are lacking regarding these interactions in heart failure.

Unlike the heart, studies conducted in the liver reported an inhibitory effect of acetylation on fatty acid metabolism. Hirschey et al. described a decreased activity of LCAD enzyme and reduced fatty acid ß-oxidation following hyperacetylation of these enzymes in SIRT3 KO mice. The authors further reported an accumulation of long-chain acylcarnitine species, fatty acid ß-oxidation intermediate products, and triacylglycerol in livers from SIRT3 KO mice that could suggest a decreased rate of fatty acid ß-oxidation. From the eight acetylated lysine residues detected on LCAD, lysine residue 42 was identified as a critical regulation site for acetylation (22). Furthermore, analysis of the rate of conversion of radiolabeled palmitate revealed lowered oxidizing capacity and ATP production in tissue homogenates from SIRT3–/– compared to wild-type tissue at a high substrate concentration. Reduced activities of fatty acid ß-oxidation enzymes in the liver by acetylation were also reported in other studies (160). In addition to LCAD and β-HAD, hyperacetylation of hydroxy acyl-CoA dehydrogenase, another important enzyme in fatty acid ß-oxidation, led to its decreased activity and decline in overall fatty acid oxidation rate in the mouse liver. Deletion of GCN5L1 acetylase enzyme or overexpression of SIRT3 reduced hydroxy acyl-CoA dehydrogenase acetylation and increased its activity as well as fatty acid ß-oxidation in the liver (161, 162). However, there is presently no agreement on the functionally significant acetylation sites or SIRT3 target sites in these studies. While Hirschey et al. noted lysine 42 residue on LCAD as an important regulation site (22), using chemically acetylated recombinant proteins, Bharathi et al. identified Lys-318 and Lys-322 residues as an important site for LCAD acetylation/sirt3 deacetylation (160). To date, a detailed analysis of lysine residue modification and functional acetylation/deacetylation target sites for LCAD and β-HAD is lacking in the heart. Not all lysine residues within LCAD that are acetylated are expected to impact LCAD activity in the same manner. Understanding the acetylation status of different acetylation sites, and their effect on the enzyme function in multiple tissues will help to characterize the tissues specific effects of acetylation dynamics.

Compared to acetylation, the effect of succinylation and malonylation modification on fatty acid ß-oxidation enzymes is not clear. Some studies have shown an impaired β-oxidation and accumulation of medium- and long-chain acylcarnitines in the liver and muscles of SIRT5 KO mice (26). Most of the acyl-CoA dehydrogenase enzymes, including very long-chain acyl-CoA dehydrogenase (VLCAD), LCAD, and MCAD, were found to be hypersuccinylated, suggesting a suppressive effect of excessive succinylation on fatty acid oxidizing enzymes (26). In contrast, cardiac ECH is desuccinylated and activated by SIRT5 (46, 97). But the effects of similar modifications on other enzymes in this pathway have yet to be determined.

Overall, from all these data it is possible to suggest that the effect of lysine acetylation on fatty acid ß-oxidative enzymes may not be similar between different tissues, at least between the liver and heart. Reasonably, these differences may account for the specialization of these tissues in regulating fatty acid ß-oxidation differently in line with their physiological functions. The liver has a high capacity for both synthesizing and oxidizing fatty acids and the two processes are regulated reciprocally during a fed or fasting state as well in disease conditions such as in obesity or diabetes. On the contrary, the heart continually uses fatty acids as a source of energy, which accounts for up 60–90% of the total energy requirements for its normal contractile function irrespective of the fed state or disease conditions. While acetylation may serve as a feedback regulation in the liver as suggested by Bharathi et al. (160), the same mechanism

would potentially compromise the heart's ability to produce energy if fatty acid ß-oxidation enzymes were down-regulated by acetylation induced by excess fatty acid ß-oxidation. Thus, future studies are needed to determine the differences in acetylome between the two tissues, and if acetylation-mediated regulation of fatty acid ß-oxidation is tissue- or site-specific.

Glucose Metabolism

Glucose Oxidation

In contrast to fatty acid metabolism, the effects of acetylation on glucose metabolism have received less attention, especially in the heart. However, recent studies reported the acetylation of several proteins involved in glucose transport, glycolysis, and glucose oxidation (83, 149, 156). The pyruvate dehydrogenase complex (PDH) is one of the most widely investigated glucose metabolizing enzymes in relation to acetylation. It is a key enzyme that catalyzes the irreversible and rate-limiting step in glucose oxidation that links glycolysis to the TCA cycle. PDH is regulated by several mechanisms, but the change in its phosphorylation status is critical to its activity. It is inhibited by phosphorylation on the E1 subunit by a specific PDH kinase (PDK), PDK4, and is activated when dephosphorylated by PDH phosphatase (163, 164).

Modification of PDH by acetylation has been demonstrated in several studies (53, 83, 156). In HFD induced obese mice subjected to a TAC, we showed a significant increase in PDH acetylation with a decrease in glucose oxidation rates (147). Similarly, Thapa et al. reported increased acetylation of the α-subunit of PDH in the heart after HFD feeding, and its hyperacetylation was shown to inhibit its activity (53). Reduced activity of PDH in association with its increased acetylation and decreased SIRT3 level has been also demonstrated in mice with angiotensin II-induced cardiac hypertrophy (165).

In addition, increased acetylation has also been implicated in a reduced transport of pyruvate into the mitochondria. Akita type 1 diabetic mice hearts exhibit a significant hyperacetylation state, along with a 70% decrease in the rate of mitochondrial pyruvate transport that occurs without any changes in the protein level of the mitochondrial pyruvate carriers 1 and 2 (MPC1 and MPC2). Mass spectrometry analysis revealed that acetylation of lysines 19 and 26 of MPC2 were increased in Akita mice heart mitochondria, and that acetylation at these sites is associated with impaired pyruvate metabolism in the heart (148).

The impact of acetylation on PDH has also been examined in skeletal muscle by Jing et al. Deletion of SIRT3, both *in vivo* in SIRT KO mice and *in vitro* in myoblasts, lead to a significant increase in acetylation associated with decreased PDH activity along with a reduced glucose oxidation rate and accumulation of pyruvate and lactate metabolites. Six acetylation sites have been identified on the PDH E1α subunit, with lysine 336 being significantly altered by SIRT3 deletion (156). Interestingly, it was also shown that hyperacetylation of the PDH E1α at lysine 336 enhances its phosphorylation leading to suppressed PDH enzymatic activity. Additionally, Ozden et al. and Fan et al. also demonstrated the inhibitory effect of acetylation at lysine 321 on PDH activity in cancer cells, which is completely reversed by SIRT3 activation (97, 164). In the latter study, it was also shown that lysine acetylation at lysine 202 inhibits PDP1 by dissociating it from PDHA1, thus promoting its phosphorylation (97).

Hypersuccinylation of PDH accompanied by a decrease in SIRT5 expression is also associated with a decrease in PDH activity as the heart maturates in postnatal rabbits (100). Unexpectedly, Park et al. observed the suppressive effect of SIRT5 catalyzed desuccinylation on PDH in *SIRT5* KO mouse embryonic fibroblasts (MEFs), while SIRT5 deletion led to an increase in PDH activity (25). In contrast, Zhang et al. found significantly reduced malate/pyruvate-driven respiration in SIRT5-deficient HEK293 cells, as well as in homogenates prepared from SIRT5 KO livers (166). While these discrepancies need further investigation, tissue/cell-specific variation in these modifications may contribute to these differences.

Glycolysis

Acetylation of glycolytic enzymes has been reported in hearts as well as various other cells. In newborn rabbit hearts, we showed a significant decline in glycolysis rates in line with hyperacetylation of its enzymes, including hexokinase (HK-1) and phosphoglycerate mutase (PGM) (100). In contrast, Hallows et al. have shown a negative regulation of PGM by SIRT1 (165). Acetylated PGM displayed enhanced activity, while Sirt1-mediated deacetylation reduced its activity in human embryonic kidney (HEK293) cells (167). Glyceraldehyde-3-phosphate dehydrogenase (GAPDH) is another glycolytic enzyme subjected to acetylation modification. Similar to PGM, acetylation of GAPDH at lysine 254 increases its enzymatic activity in response to glucose in HEK293T cells (168). In contrast, GAPDH acetylation enhances its translocation from the cytoplasm to the nucleus in NIH3T3 cells, thereby inhibiting downstream glycolysis and accumulation of glycolytic intermediates (169). In another study, Xiong et al. showed an inhibitory effect of acetylation of pyruvate kinase (PK), which catalyzes the last step of glycolysis (170). In addition to acetylation, other acyl modifications can regulate glycolysis. GAPDH, PGK, and enolase are hypermalonylated in livers of *db/db* mice (142), although the effects of this hypermalonylation on the activities of these enzymes has not been investigated. Another study in hepatocytes demonstrated SIRT5 mediated demalonylation of GAPDH and increased activity, suggesting that malonylation decreases glycolytic flux (27). Similarly, desuccinylation of PK by SIRT5 increases its kinase activity (171). In contrast, Xiangyun et al. reported that desuccinylation of PKM2 by SIRT5 inhibits its activity in tumor cells (172). Unfortunately, there is a lack of data on the effect of malonylation and succinylation modifications on glycolysis in the heart.

At the transcriptional level, glycolysis is regulated by the level of hypoxia-inducible factor-1α (HIF-1α), a master transcriptional regulator of glycolytic enzymes (173). Studies by Geng et al. have shown a positive correlation between increased acetylation of HIF-1α by p300 at lysine 709 and its stability, or decreased polyubiquitination, in HEK293 cells (174). Similarly, other studies also showed an inhibition of HIF-1α by SIRT1 mediated deacetylation at lysine 674, in HT1080 and HEK293 cells (175). These results were also found in SIRT6 deficient embryonic stem cells and MEFs cells (174). Interestingly, these cells exhibit

increased glucose uptake with up-regulation of glycolysis in association with increased HIF-1α activity.

The impact of acetylation on glucose uptake and its transporters has also been described. In both cultured cardiomyocytes and perfused hearts, Renguet et al. found that acetylation of GLUT 4 inhibits glucose uptake in adult cardiomyocytes, as well as in perfused hearts, by decreasing its translocation to the plasma membrane (173). Strikingly, treatment with inhibitors of acetyltransferases prevents the increase in protein acetylation and reverses the inhibition of glucose uptake and GLUT4 translocation (149). Unfortunately, the direct acetylation status of GLUT4 was not analyzed in this study. However, the inhibitory effect of acetylation on glucose uptake is supported by other studies. Using SIRT3 KO mice and hyperinsulinemic-euglycemic clamp experiments, Lantier et al. showed that increased acetylation leads to insulin resistance and reduced muscle glucose uptake that is associated with decreased hexokinase II (HKII) binding to the mitochondria in HFD-fed SIRT3 KO mice (176). This suggests a reduced HKII activity and translocation as a result of increased acetylation. Similar to the above study, unfortunately, there was no direct analysis of the acetylation status of the proteins involved in glucose uptake or glucose phosphorylation.

Insulin Signaling

Insulin resistance in type 2 diabetes and obesity as well as in other heart conditions contributes to a number of adverse changes in the heart that includes alterations in cardiac energy metabolism, lipotoxicity, and hypertrophy, and is associated with an increased risk of heart failure (84, 177, 178). Cardiac insulin signaling is impaired in heart failure, diabetes, and obesity (147, 178, 179). Recent studies have shown that several proteins in the insulin signaling pathway are targets for acetylation modification, which therefore may impact insulin signaling. Akt is an important component of the insulin signaling pathway. Akt activation requires binding with phosphatidylinositol 3,4,5-trisphosphate [PIP (3)], which promotes its membrane localization and phosphorylation by the upstream kinase, phosphoinositide-dependent protein kinase 1 (PDK1). Previously, we have shown a negative association between acetylation of insulin signaling mediators, such as Akt and PDK1, and their decreased activation as a result of changes in their phosphorylation status due to acetylation (147). In support of this, Sundaresan et al. showed that acetylation of Akt and PDK1 occurs in their pleckstrin homology (PH) domains, which blocks PIP (3) binding, and that this is reversed by SIRT1 deacetylation (150). SIRT2 also binds and activates Akt in insulin-responsive cells, through its interaction with the PH domain, whereas SIRT2 inhibition impairs AKT activation by insulin (180).

Acetylation and Metabolism of Other Fuel Substrates

Ketone body and BCAA oxidation can impact cardiac energy metabolism and heart failure progression (179, 181, 182). Both pathways may also contribute to mitochondrial acetylation changes. However, only a few studies have characterized the acetylation status and its impact on enzymes involved in ketone and BCCA metabolism.

In hepatic mitochondria of SIRT3 KO mice, hydroxymethyl-glutaryl (HMG)-CoA synthase (HMGCS2), the rate-limiting enzyme in ketogenesis, is hyperacetylated and its enzymatic activity reduced, leading to a decrease in β-hydroxybutyrate synthesis. Deacetylation of HMGCS2 by SIRT3 increases its enzymatic activity and β-hydroxybutyrate levels (183). Similar to the acetylation effect, loss of SIRT5 results in hypersuccinylation of HMGCS2 and reduces its activity both *in vivo* and *in vitro* in liver mitochondria, which leads to reduced β-hydroxybutyrate levels during fasting (26).

With regard to ketone oxidation, succinyl-CoA:3-ketoacid-CoA transferase (SCOT), a key enzyme of ketone oxidation, is hyperacetylated in the brain and heart at multiple sites in SIRT3 KO mice (184). *In vitro* biochemical analysis of recombinant SCOT demonstrates that acetylation at lysine 451 residues results in decreased enzyme activity that is reversed by SIRT3 activation. Moreover, in brain homogenates from WT and SIRT3 KO mice, acetoacetate-dependent acetyl-CoA production is decreased by three-fold in SIRT3 KO mice, suggesting decreased ketone oxidation rates upon increased acetylation (180). In contrast, a decrease in ketogenesis capacity was noted in the liver of mice lacking SIRT3 (184). However, similar studies are lacking in the heart.

Similarly, enzymes in BCAA (isoleucine, leucine, and valine) catabolic pathways are among the proteins regulated by acetylation and SIRT3 in the liver. Some acetylation sites were detected in branched-chain alpha-keto acid dehydrogenase (BCKDH), a key enzyme catalyzing the breakdown of BCAAs, in SIRT3 KO mice (181, 182). As BCAA levels were raised, the authors suggested that acetylation may have an inhibitory effect on branched-chain ketoacid dehydrogenase (BCKDH) activity (23, 185). Other investigators have also suggested that acetylation of BCAA aminotransferase (BCAT) promotes its degradation in the ubiquitin-proteasome pathway, thereby decreasing BCAA catabolism in the pancreas (186). cAMP-responsive element-binding (CREB)-binding protein (CBP) and SIRT4 were identified as the acetyltransferase and deacetylase for BCAT at lysine 44 (K44), respectively (186).

Acetylation and TCA Cycle Enzymes

Acetyl-CoA is the final common product in the oxidative metabolism of various fuels, and is a substrate for the TCA cycle. While acetylation of all TCA cycle enzymes have been reported in the liver (20), 6 of the 8 enzymes were found to be acetylated in the heart (151). However, examination of the effect of acetylation on the TCA cycle has produced mixed results. Increased acetylation of malate dehydrogenase (MDH) in Chang liver cells enhances its enzyme activity. When cells were treated with deacetylase inhibitors, trichostatin A (TSA) and NAM, MDH acetylation doubled the endogenous MDH activity, while *in vitro* deacetylation of purified MDH decreased its activity (20). Similarly, significant acetylation-dependent activation of aconitase was found in both isolated heart mitochondria subjected to *in vitro* chemical acetylation, and in hearts of HFD fed obese mice (152). Increased aconitase

acetylation at multiple sites were found, with acetylation at K144 identified as a responsible site for structural change at the active site that was reversed by increasing SIRT3 overexpression (152).

Although acetylation at multiple sites was detected on the TCA cycle enzyme isocitrate dehydrogenase (IDH), no significant effect of this acetylation on enzyme activity was found (151). In contrast, others have reported a significant loss of function of IDH when acetylated at lysine 413, which is fully restored by SIRT3 mediated deacetylation (187). Additionally, increased acetylation of succinate dehydrogenase (SDH), which functions both in the TCA cycle and electron transport chain, is associated with a decrease in activity in human and mice heart failure (81). Further investigation on its acetylation sites revealed that lysine 179 of SDH as an important site for acetylation that regulates enzyme activity by interfering in FAD^+ binding to the enzyme. However, despite widespread acetylation of its enzymes, the overall TCA cycle activity appears to be unaffected by excessive acetylation (83).

Succinylation and malonylation of TCA cycle enzymes have also been reported (25, 26, 142). However, the impact of this succinylation and malonylaton has been assessed on only a few enzymes. SIRT5 mediated desuccinylation activates IDH (188). Paradoxically, SDH desuccinylation has been suggested to inhibit its activity in MEFs, while SIRT5 deletion leads to an increase in SDH activity (25).

Acetylation of Proteins in Electron Transport Chain and Oxidative Phosphorylation

Lysine acetylation of mitochondrial respiratory complex enzymes, NADH dehydrogenase 1, ubiquinol cytochrome c reductase core protein 1, and ATP synthase mitochondrial F1 complex assembly factor 1 is increased in mice hearts that lack SIRT3. In these hearts, functional studies demonstrated inhibition of Complex I activity (24). In another study, a similar effect was observed in neonatal rat cardiomyocytes, as well as in H9c2 cells treated with high glucose, oleate, and palmitate (153). Treatment with HDACs and sirtuin inhibitors, TSA and NAM, respectively, further increase the levels of acetylated proteins in mitochondrial complexes I, III, and V, with a concomitant decrease in ATP production. However, treatment with exogenous H_2S elevates the NAD^+/NADH ratio and the activity of SIRT3, both of which are decreased in the presence of high glucose and fatty acid as well as in diabetes (153). Similarly, a decrease in the activity of complex V in association with increased acetylation was shown by Kerner et al. (151).

Nuclear Acetylation Control of Mitochondrial Metabolism

Acetylation can also affect transcription factors that regulate energy metabolism. Peroxisome proliferators-activated receptors (PPARs) are a family of nuclear receptors that have a critical role in regulating the expression of proteins involved in fatty acid metabolism. The PPAR transcription factors, comprised of PPARα, PPARδ, and PPARγ, form a complex with retinoid X receptor (RXR) and bind the peroxisome proliferator response element (PPRE) in the promoter region of target genes, thereby initiating their transcription (189, 190). Similarly, estrogen receptor-related receptors (ERRs) including ERR α, β, and γ affect the expression of enzymes in the glucose and fatty acid metabolic pathways after binding with ERR responsive elements (191). Peroxisome proliferator-activated receptor-gamma coactivator-1 alpha (PGC-1α) is an inducible cofactor of both PPARs and ERRs (192). Activation of PGC-1α together with PPAR and ERR promotes fatty acid utilization while suppressing glucose metabolism. All of these transcription factors have been shown to be subject to acetylation/acylation.

SIRT1 interaction with PPARα positively affects PPARα activity. While SIRT1 deficiency impairs PPARα signaling and decreases fatty acid ß-oxidation, while its overexpression upregulates PPARα targets (193). On the contrary, SIRT4 decreases PPARα activity and consequently the expression of PPARα target genes (194). Acetylation of PPARγ at different lysine residues has been shown in various tissues (195, 196). Repression of PPARγ by SIRT1 is seen in 3T3-L1 adipocytes (197). Activation of PPARγ has been seen with acetylation and its suppression by histone deacetylase 3 (HDAC3) (198). In contrast, PGC-1α is deacetylated and activated by SIRT1 (199–201). ERRα is another transcription regulator that is modified by acetylation with suppressed sensitivity after acetylation (202).

Altered energy metabolism may also influence the expression pattern of metabolic genes through chromatin modification by post-translational histone acetylation. Accordingly, increased glucose supply leads to increased histone acetylation with a corresponding activation of glucose metabolism genes *in vitro* (203). Similarly, upregulation of several lipid metabolism-related genes is observed in response to fatty acid-derived acetyl-CoA-induced histone hyperacetylation (204). While these data support substrate-dependent induction of specific metabolic genes, it unclear how cells respond differently to the acetyl-CoA derived from either glucose and fatty acid ß-oxidation. Additionally, the contribution of histone acetylation modifications as a result of metabolite imbalances has not been determined in the transcription dysregulation seen in pathological states.

PROTEIN ACETYLATION IN HEART FAILURE

Studies in both animal models and humans have shown increases in acetylation of mitochondrial proteins in the failing heart compared to healthy control hearts (**Figure 3**) (80, 81). Davidson et al. compared the acetyl proteomics profile between dual KO mice for SIRT3 and carnitine acetyltransferase (which causes extreme mitochondrial acetylation) and TAC induced heart failure mice (159). These authors found an approximately 86% overlap in acetylated peptides between the double KO mice and the experimental heart failure mice. Furthermore, in rat models of hypertensive heart failure, the Dahl salt-sensitive (SS) and spontaneously hypertensive heart failure-prone (SHHF) rats, a large number of proteins were found exclusively hyperacetylated in the failing hearts compared to control hearts (140). Increased acetylation was accompanied by a reduced level of SIRT3 in these pressure-overload-induced failing hearts (140). Similarly, in failing hearts of obese patients, Castillo et al. found a 46%

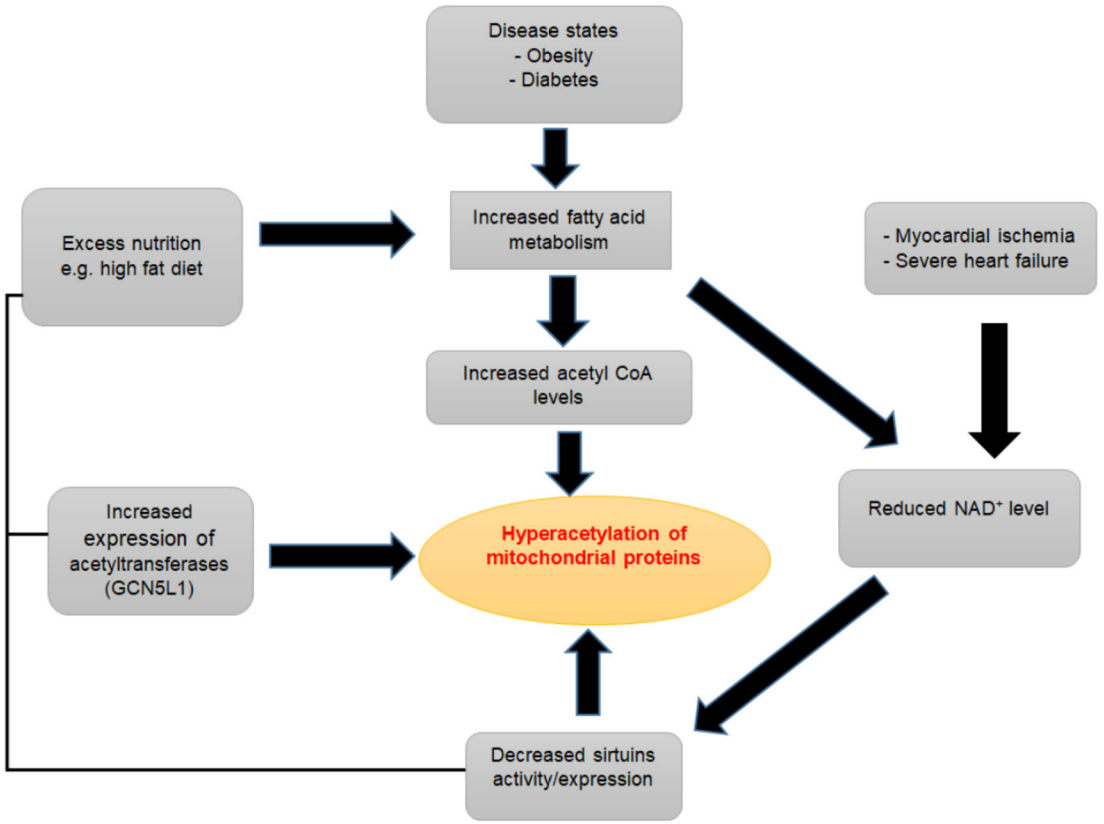

FIGURE 3 | Contributing factors to mitochondrial protein hyperacetylation.

decline in SIRT3 expression and increased acetylation profiles in heart failure patients with a BMI >30, as well as in obese rat hearts (205). Increased cardiac acetylation was also observed in obesity-related left ventricular remodeling and cardiac fibrosis (206). A dramatic increase in protein lysine acetylation was also seen in the heart and mitochondria from diabetic mice, along with decreased deacetylation reactions (146). Several other studies have also revealed the abundance of hyperacetylation of different proteins in various forms of heart failure (207–209). Although these data have consistently shown the increased protein acetylation in heart failure settings, the specific impact, regulations, and the mechanisms of how these changes are linked to heart failure remain incompletely understood. Moreover, the mass spectrometry-based acetylome proteomics used in these studies have inherent limitations to measure acetylation changes at the protein level and individual acetylation sites within each protein, which would be necessary to understand the biological significance of acetylation (210–213).

Acetylation and Shifts in Myocardial Energy Metabolism During Heart Failure

Numerous studies have demonstrated altered substrate preferences and metabolism in the failing heart [see (28) for review]. However, the actual direction of these shifts in energy substrate utilization remains controversial. While the shift toward increased oxidation of fatty acid is widely observed in ischemic and diabetic heart failure, other studies have suggested a shift in myocardial metabolism away from fatty ß-oxidation and its association with the progression to ventricular dysfunction in hypertrophic hearts (214). According to the principles outlined by Randle (215), glucose and fatty acid metabolism are regulated reciprocally. As highlighted in the preceding sections, lysine acetylation affects the main enzymes of both fatty acid and glucose oxidation inversely in the heart. In fact, various animal studies, as described below, have demonstrated that acetylation may be sufficient to cause shifts in myocardial substrate preference in the presence of pathological stressors.

In type 1 diabetic mice hearts, increased acetylation induces mitochondria metabolic inflexibility accompanied by decreased activities of PDH and complex II enzyme activities (85). A dramatic decrease in mitochondrial respiration in the presence of non-fatty acid substrates was observed in contrast to minimal inhibition in palmitoylcarnitine-supported respiration (85). Similarly, other studies have shown a switching in cardiac energy metabolic substrate preference toward fatty utilization by lysine hyperacetylation in type 2 diabetes mice (216). In *db/db*

mice, and in cardiomyocytes in culture, increased acetylation of enzymes involved in mitochondrial fatty acid ß-oxidation and glucose oxidation were found, with a concomitant decrease in the expression and activity of SIRT3. While LCAD acetylation is accompanied by a significant upregulation in its activity, the hyperacetylation of PDH is associated with a decrease in its activity. In support of this, decreasing acetylation by increasing the expression and activities of SIRT3 (through exogenous hydrogen sulfide administration) switches cardiac substrate utilization from fatty acid ß-oxidation to glucose oxidation in diabetic mice hearts (216).

Additionally, Romanick et al. observed marked changes in lysine acetylation in cardiac tissues with obesity (206). Of those significantly impacted by increased acetylation due to obesity were very long-chain specific acyl-CoA dehydrogenase, aconitate hydratase 2, and dihydrolipoyl dehydrogenase. Interestingly, increased transcriptional activation of KLF15 and PPARα, with increased expression of downstream target genes and their interaction with these significantly acetylated proteins, was observed in diet-induced obesity. In addition, the authors of this study found enhanced expression of PDK4 and MCD in the heart (206). PDK4 is known to inhibit glucose oxidation by inhibiting pyruvate dehydrogenase, while malonyl CoA decarboxylase promotes fatty acid ß-oxidation via activation of carnitine palmitoyltransferase 1 (CPT1). Together this suggests that shifting toward fatty acid ß-oxidation, at the expense of glucose oxidation, occurs in the presence of hyperacetylation (206). We and others have also observed that hyperacetylation on PDH, LCAD, and β-HAD, accompanied by a decrease in glucose oxidation and an increase in fatty acid oxidation, is seen in the heart in response to HFD feeding (28, 53). Likewise, as discussed in the preceding sections, in skeletal muscle a switch in substrate utilization from glucose oxidation toward fatty acid utilization is also induced by SIRT3 KO, as a result of PDH inhibition by hyperacetylation of its E1α subunit (156). Thus, acetylation could contribute to the metabolic inflexibility seen in heart failure by regulating metabolic enzyme activities differently.

Myocardial I/R is another pathology where shifts in energy substrate utilization are implicated in heart injury. Increased fatty acid ß-oxidation rates following ischemia result in suppression of glucose oxidation and a subsequent uncoupling of glucose oxidation from glycolysis, which contributes to ischemic damage (217, 218). As discussed in the preceding section, the increased acetylation of proteins following enhanced fatty acid ß-oxidation and increased acetyl-CoA generation may contribute to the metabolic phenotype observed in I/R. In addition, as NAD^+ availability is a critical determinant for Sirtuin activity, ischemia-induced decreases in the NAD^+/NADH redox couple during I/R may inactivate SIRT3 and lead to the hyperacetylation of mitochondrial proteins (80). Furthermore, the mRNA and protein levels of NAMPT, the rate-limiting enzyme that converts NAM to NMN in the NAD^+ salvage synthesis pathway is downregulated in the heart during I/R injury, further reducing NAD^+ levels and thus Sirtuin activity (219). Several studies have demonstrated the cardioprotective role of NAD^+ in I/R injury either by exogenous NAD^+ supplementation or enzymatic manipulation (80, 125, 219, 220). However, this mechanism has not yet been investigated in relation to changes in metabolic enzymes activity or metabolic alterations as a result of acetylation suppression by NAD^+ boosting. There is little data that support the idea that this effect may be related to increased glucose oxidation rates. Accordingly, in rats subjected to I/R after prolonged caloric restriction, Shinmura et al. showed a decreased level of acetylated mitochondrial proteins associated with enhanced Sirtuin activity and attenuated myocardial oxidative damage. Interestingly, caloric restriction increases respiratory control index and oxygen consumption in the presence of pyruvate/malate substrates in mitochondria isolated from I/R hearts (221). However, the hearts in this study were reperfused for only 3–5 min after ischemia and the proteomic analysis was not robust enough to analyze the acetylome changes in metabolic enzymes.

Contribution of Hyperacetylation to Cardiac Dysfunction

As discussed above, hyperacetylation of myocardial proteins is common in heart failure. In addition to its regulatory role in myocardial energy metabolism, several studies have also analyzed the impact of hyperacetylation of myocardial proteins on heart failure development and progression. While the majority of the studies suggested a link between hyperacetylation and worsening of heart failure (80, 81, 105, 146, 206, 222, 223), others found no association between myocardial dysfunction and hyperacetylation (159, 224). The cause for the discrepancies in these studies awaits further studies.

Hypertrophy is one of the pathological processes where increased acetylation is implicated in disease progression. In response to various hypertrophic stimuli, SIRT3-deficient mice appear to be more sensitive to injuries and manifested various abnormalities compared to their wild-type counterparts (105). On the other hand, SIRT3 transgenic mice are protected from hypertrophic injuries (105). Activation of forkhead box O3a-dependent (Foxo3a) and manganese superoxide dismutase and catalase are also seen in response to SIRT3 activation. Activation of SIRT3 has been also implicated in lessening the severity of cardiac hypertrophy by blocking interstitial fibrosis, as well as fibroblast proliferation and differentiation (222). Furthermore, in SIRT5 KO mice subjected to TAC, Herschberger et al. observed a reduced survival of SIRT5 KO mice compared with wild-type mice (225). The increased pathological hypertrophy and mortality in these mice is associated with several biochemical abnormalities including reduced fatty acid ß-oxidation and glucose oxidation, suggesting that SIRT5-mediated desuccinylation plays an important role in regulating cardiac metabolism during stress.

Changes in protein acetylation have been also shown in myocardial I/R injury in association with decreased SIRT3 protein levels (158, 223, 226). In support of this, increased mitochondrial protein acetylation in SIRT3 KO mice is associated with increased sensitivity to injury, as shown by larger infarct size, less functional recovery, and low O_2 consumption rates

(223). In contrast to these findings, the study by Koentges et al. found no additional susceptibility to I/R-specific injury in SIRT3 KO mice that underwent permanent ligation of the left anterior descending coronary artery (LAD) (125). On the other hand, Boylston et al. found an increase in infarct size and impaired recovery during I/R in SIRT5 KO hearts compared to WT littermates (97). This injury was decreased by pretreatment with dimethyl malonate, a competitive inhibitor of SDH, suggesting that the enhanced activity of SDH by hypersuccinylation is an important cause for increased ischemic injury (which inconsistent with other reports) (25). Similarly, using exogenous NAD administration, Liu et al. demonstrated that SIRT5-mediated SDH desuccinylation decreased the activity of SDH, which attenuated the succinate accumulation during I/R and alleviated reactive oxygen species generation (227). In a separate study, accumulation of succinate during ischemia and its rapid oxidation by SDH during reperfusion can drive extensive ROS generation in a murine I/R injury model (228).

Though complete data are unavailable on the acetylation status of metabolic enzymes and its impact specifically in I/R, several studies have investigated this modification in other proteins or pathways. The permeability transition pore (PTP) is an important inner membrane channel that has a role in I/R injury (229). Permeability transition pore opening is facilitated by the translocation of cyclophilin D (CyPD) from matrix protein to the inner mitochondrial membrane (230). The study by Bochaton et al. in SIRT3 KO mice demonstrated that increased acetylation of CyPD following myocardial I/R facilitates PTP opening and subsequent cell death, which was prevented by attenuation of CyPD acetylation at reperfusion (231). A similar result was found in mice subjected to renal I/R where dexmedetomidine induced SIRT3 overexpression and significantly reduced I/R related mitochondrial damage by decreasing cyclophilin D acetylation (232).

SUMMARY

Although excessive mitochondrial metabolic enzyme acetylation occurs in heart failure, its contribution to cardiac metabolic alterations remains incompletely defined. However, accumulating evidence supports the hypothesis that acetylation alters energy substrate utilization in heart failure by activating fatty acid ß-oxidation and inhibiting glucose oxidation. While the inhibitory effect of acetylation on glucose oxidation is widely accepted, there are still disagreements as to the relationship between acetylation and fatty acid ß-oxidation. While most of the studies done in the heart and skeletal muscle tissues illustrate a positive association between acetylation and fatty acid ß-oxidation, others studies suggest a suppressive effect of acetylation on fatty acid ß-oxidation in the liver. Tissue or site-specific variation in acetylation of these enzymes, as well differences in underlying pathologies, could contribute to such discrepant data. Available data also suggests that acetylation does not always has an inhibitory effect on metabolic enzymes.

AUTHOR CONTRIBUTIONS

All authors listed have made a substantial, direct and intellectual contribution to the work, and approved it for publication.

FUNDING

Funded by a Foundation Grant from the Canadian Institutes for Health Research to GL. EK is supported by an Alberta Diabetes Institute Graduate Studentship Award.

REFERENCES

1. Allfrey VG, Faulkner R, Mirsky AE. Acetylation and methylation of histones and their possible role in the regulation of RNA synthesis. *Proc Natl Acad Sci USA.* (1964) 51:786–94. doi: 10.1073/pnas.51.5.786
2. Verdone L, Caserta M, Mauro ED. Role of histone acetylation in the control of gene expression. *Biochem Cell Biol.* (2005) 83:344–53. doi: 10.1139/o05-041
3. Sabari BR, Zhang D, Allis CD, Zhao Y. Metabolic regulation of gene expression through histone acylations. *Nat Rev Mol Cell Biol.* (2017) 18:90–101. doi: 10.1038/nrm.2016.140
4. Audia JE, Campbell RM. Histone modifications and cancer. *Cold Spring Harb Perspect Biol.* (2016). 8:a019521. doi: 10.1101/cshperspect.a019521
5. Wang R, Xin M, Li Y, Zhang P, Zhang M. The functions of histone modification enzymes in cancer. *Curr Protein Pept Sci.* (2016) 17:438–45. doi: 10.2174/1389203717666160122120521
6. Brownell JE, Zhou J, Ranalli T, Kobayashi R, Edmondson DG, Roth SY, et al. Tetrahymena histone acetyltransferase a: a homolog to yeast GCN5P linking histone acetylation to gene activation. *Cell.* (1996) 84:843–51. doi: 10.1016/S0092-8674(00)81063-6
7. Taunton J, Hassig CA, Schreiber SL, A mammalian histone deacetylase related to the yeast transcriptional regulator RPD3P. *Science.* (1996) 272:408–11. doi: 10.1126/science.272.5260.408
8. Yoon S, Eom GH. HDAC and HDAC inhibitor: from cancer to cardiovascular diseases. *Chonnam Med J.* (2016) 52:1–11. doi: 10.4068/cmj.2016.52.1.1
9. Zhao L, Duan YT, Lu P, Zhang ZJ, Zheng XK, Wang JL, et al. Epigenetic targets and their inhibitors in cancer therapy. *Curr Top Med Chem.* (2018) 18:2395–419. doi: 10.2174/1568026619666181224095449
10. Bagchi RA, Weeks KL. Histone deacetylases in cardiovascular and metabolic diseases. *J Mol Cell Cardiol.* (2019) 130:151–9. doi: 10.1016/j.yjmcc.2019.04.003
11. Piperno G, LeDizet M, Chang XJ. Microtubules containing acetylated alpha-tubulin in mammalian cells in culture. *J Cell Biol.* (1987) 104:289–302. doi: 10.1083/jcb.104.2.289
12. North BJ, Marshall BL, Borra MT, Denu JM, Verdin E. The human Sir2 ortholog, SIRT2, is an NAD^+-dependent tubulin deacetylase. *Mol Cell.* (2003) 11:437–44. doi: 10.1016/S1097-2765(03)00038-8
13. Onyango P, Celic I, McCaffery JM, Boeke JD, Feinberg AP. SIRT3, a human SIR2 homologue, is an NAD-dependent deacetylase localized to mitochondria. *Proc Natl Acad Sci USA.* (2002) 99:13653–8. doi: 10.1073/pnas.222538099
14. Hallows WC, Lee S, Denu JM. Sirtuins deacetylate and activate mammalian acetyl-CoA synthetases. *Proc Natl Acad Sci USA.* (2006) 103:10230–5. doi: 10.1073/pnas.0604392103
15. Schwer B, Bunkenborg J, Verdin RO, Andersen JS, Verdin E. Reversible lysine acetylation controls the activity of the mitochondrial enzyme

acetyl-CoA synthetase 2. *Proc Natl Acad Sci USA*. (2006) 103:10224–9. doi: 10.1073/pnas.0603968103
16. Michishita E, Park JY, Burneskis JM, Barrett JC, Horikawa I. Evolutionarily conserved and nonconserved cellular localizations and functions of human sirt proteins. *Mol Biol Cell.* (2005) 16:4623–35. doi: 10.1091/mbc.e05-01-0033
17. Kim SC, Sprung R, Chen Y, Xu Y, Ball H, Pei J, et al. Substrate and functional diversity of lysine acetylation revealed by a proteomics survey. *Mol Cell.* (2006) 23:607–18. doi: 10.1016/j.molcel.2006.06.026
18. Choudhary C, Kumar C, Gnad F, Nielsen ML, Rehman M, Walther TC, et al. Lysine acetylation targets protein complexes and co-regulates major cellular functions. *Science.* (2009) 325:834–40. doi: 10.1126/science.1175371
19. Schwer B, Eckersdorff M, Li Y, Silva JC, Fermin D, Kurtev MV, et al. Calorie restriction alters mitochondrial protein acetylation. *Aging Cell.* (2009) 8:604–6. doi: 10.1111/j.1474-9726.2009.00503.x
20. Zhao S, Xu W, Jiang W, Yu W, Lin Y, Zhang T, et al. Regulation of cellular metabolism by protein lysine acetylation. *Science.* (2010) 327:1000–4. doi: 10.1126/science.1179689
21. Lombard DB, Alt FW, Cheng H-L, Bunkenborg J, Streeper RS, Mostoslavsky R, et al. Mammalian Sir2 homolog SIRT3 regulates global mitochondrial lysine acetylation. *Mol Cell Biol.* (2007) 27:8807–14. doi: 10.1128/MCB.01636-07
22. Hirschey MD, Shimazu T, Goetzman E, Jing E, Schwer B, Lombard DB, et al. SIRT3 regulates mitochondrial fatty-acid oxidation by reversible enzyme deacetylation. *Nature.* (2010) 464:121–5. doi: 10.1038/nature08778
23. Hebert AS, Dittenhafer-Reed KE, Yu W, Bailey DJ, Selen ES, Boersma MD, et al. Calorie restriction and SIRT3 trigger global reprogramming of the mitochondrial protein acetylome. *Mol Cell.* (2013) 49:186–99. doi: 10.1016/j.molcel.2012.10.024
24. Ahn B-H, Kim H-S, Song S, Lee IH, Liu J, Vassilopoulos A, et al. A role for the mitochondrial deacetylase Sirt3 in regulating energy homeostasis. *Proc Natl Acad Sci USA*. (2008) 105:14447–52. doi: 10.1073/pnas.0803790105
25. Park J, Chen Y, Tishkoff DX, Peng C, Tan M, Dai L, et al. SIRT5-mediated lysine desuccinylation impacts diverse metabolic pathways. *Mol Cell.* (2013) 50:919–30. doi: 10.1016/j.molcel.2013.06.001
26. Rardin MJ, He W, Nishida Y, Newman JC, Carrico C, Danielson SR, et al. SIRT5 regulates the mitochondrial lysine succinylome and metabolic networks. *Cell Metab.* (2013) 18:920–33. doi: 10.1016/j.cmet.2013.11.013
27. Nishida Y, Rardin MJ, Carrico C, He W, Sahu AK, Gut P, et al. SIRT5 regulates both cytosolic and mitochondrial protein malonylation with glycolysis as a major target. *Mol Cell.* (2015) 59:321–32. doi: 10.1016/j.molcel.2015.05.022
28. Karwi QG, Uddin GM, Ho KL, Lopaschuk GD. Loss of metabolic flexibility in the failing heart. *Front Cardiovasc Med.* (2018). 5:68. doi: 10.3389/fcvm.2018.00068
29. Fukushima A, Milner K, Gupta A, Lopaschuk GD. Myocardial energy substrate metabolism in heart failure : from pathways to therapeutic targets. *Curr Pharm Des.* (2015) 21:3654–64. doi: 10.2174/1381612821666150710150445
30. Bertero E, Maack C. Metabolic remodelling in heart failure. *Nat Rev Cardiol.* (2018) 15:457–70. doi: 10.1038/s41569-018-0044-6
31. Barth AS, Kumordzie A, Frangakis C, Margulies KB, Cappola TP, Tomaselli GF. Reciprocal transcriptional regulation of metabolic and signaling pathways correlates with disease severity in heart failure. *Circ Cardiovasc Genet.* (2011) 4:475–83. doi: 10.1161/CIRCGENETICS.110.957571
32. Osorio JC, Stanley WC, Linke A, Castellari M, Diep QN, Panchal AR, et al. Impaired myocardial fatty acid oxidation and reduced protein expression of retinoid x receptor-α in pacing-induced heart failure. *Circulation.* (2002) 106:606–12. doi: 10.1161/01.CIR.0000023531.22727.C1
33. Dávila-Román VG, Vedala G, Herrero P. de las Fuentes L, Rogers JG, Kelly DP, et al. Altered myocardial fatty acid and glucose metabolism in idiopathic dilated cardiomyopathy. *J Am Coll Cardiol.* (2002) 40:271–7. doi: 10.1016/S0735-1097(02)01967-8
34. Razeghi P, Young ME, Alcorn JL, Moravec CS, Frazier OH, Taegtmeyer H. Metabolic gene expression in fetal and failing human heart. *Circulation.* (2001) 104:2923–31. doi: 10.1161/hc4901.100526
35. Lai L, Leone TC, Keller MP, Martin OJ, Broman AT, Nigro J, et al. Energy metabolic reprogramming in the hypertrophied and early stage failing heart: a multisystems approach. *Circ Heart Fail.* (2014) 7:1022–31. doi: 10.1161/CIRCHEARTFAILURE.114.001469
36. van Bilsen M, van der Vusse GJ, Reneman RS. Transcriptional regulation of metabolic processes: implications for cardiac metabolism. *Pflugers Arch.* (1998) 437:2–14. doi: 10.1007/s004240050739
37. Lu Z, Scott I, Webster BR, Sack MN. The emerging characterization of lysine residue deacetylation on the modulation of mitochondrial function and cardiovascular biology. *Circ Res.* (2009) 105:830–41. doi: 10.1161/CIRCRESAHA.109.204974
38. Hirschey MD, Shimazu T, Huang JY, Schwer B, Verdin E. SIRT3 regulates mitochondrial protein acetylation and intermediary metabolism. *Cold Spring Harb Symp Quant Biol.* (2011) 76:267–77. doi: 10.1101/sqb.2011.76.010850
39. Fukushima A, Lopaschuk GD. Acetylation control of cardiac fatty acid β-oxidation and energy metabolism in obesity, diabetes, and heart failure. *Biochim Biophys Acta Mol Basis Dis.* (2016) 1862:2211–20. doi: 10.1016/j.bbadis.2016.07.020
40. Yan K, Wang K, Li P. The role of post-translational modifications in cardiac hypertrophy. *J Cell Mol Med.* (2019) 23:3795–807. doi: 10.1111/jcmm.14330
41. Lee A, Oh JG, Gorski PA, Hajjar RJ, Kho C. Post-translational modifications in heart failure: small changes, big impact. *Heart Lung Circ.* (2016) 25:319–24. doi: 10.1016/j.hlc.2015.11.008
42. Liddy KA, White MY, Cordwell SJ. Functional decorations: post-translational modifications and heart disease delineated by targeted proteomics. *Genome Med.* (2013) 5:20. doi: 10.1186/gm424
43. Zhang Z, Tan M, Xie Z, Dai L, Chen Y, Zhao Y. Identification of lysine succinylation as a new post-translational modification. *Nat Chem Biol.* (2011) 7:58–63. doi: 10.1038/nchembio.495
44. Drazic A, Myklebust LM, Ree R, Arnesen T. The world of protein acetylation. *Biochim Biophys Acta Proteins Proteom.* (2016) 1864:1372–401. doi: 10.1016/j.bbapap.2016.06.007
45. Narita T, Weinert BT, Choudhary C. Functions and mechanisms of non-histone protein acetylation. *Nat Rev Mol Cell Biol.* (2019) 20:156–74. doi: 10.1038/s41580-018-0081-3
46. Sadhukhan S, Liu X, Ryu D, Nelson OD, Stupinski JA Li Z, et al. Metabolomics-assisted proteomics identifies succinylation and SIRT5 as important regulators of cardiac function. *Proc Natl Acad Sci USA*. (2016) 113:4320–5. doi: 10.1073/pnas.1519858113
47. Hirschey MD, Zhao Y. Metabolic regulation by lysine malonylation, succinylation, and glutarylation. *Mol Cell Proteomics.* (2015) 14:2308–15. doi: 10.1074/mcp.R114.046664
48. Li P, Ge J, Li H. Lysine acetyltransferases and lysine deacetylases as targets for cardiovascular disease. *Nat Rev Cardiol.* (2020) 17:96–115. doi: 10.1038/s41569-019-0235-9
49. Berndsen CE, Denu JM. Catalysis and substrate selection by histone/protein lysine acetyltransferases. *Curr Opin Struct Biol.* (2008) 18:682–9. doi: 10.1016/j.sbi.2008.11.004
50. Hu A, Britton L, Garcia B, editors. Investigating the specificity of histone acetyltransferase activity for producing rare modifications on histones using mass spectrometry. In: *The 62nd Annual American Society for Mass Spectrometry Conference on Mass Spectrometry and Allied Topics*. Baltimore, MD (2014).
51. Tan M, Peng C, Anderson KA, Chhoy P, Xie Z, Dai L, et al. Lysine glutarylation is a protein posttranslational modification regulated by sirt5. *Cell Metab.* (2014) 19:605–17. doi: 10.1016/j.cmet.2014.03.014
52. Scott I, Webster BR Li JH, Sack MN. Identification of a molecular component of the mitochondrial acetyltransferase programme: a novel role for GCN5l1. *Biochem J.* (2012) 443:655–61. doi: 10.1042/BJ20120118
53. Thapa D, Zhang M, Manning JR, Guimarães DA, Stoner MW, O'Doherty RM, et al. Acetylation of mitochondrial proteins by GCN5l1 promotes enhanced fatty acid oxidation in the heart. *Am J Physiol Heart Circ Physiol.* (2017) 313:H265–74. doi: 10.1152/ajpheart.00752.2016
54. Baeza J, Smallegan MJ. Denu JM. Site-specific reactivity of nonenzymatic lysine acetylation. *ACS Chem Biol.* (2015) 10:122–8. doi: 10.1021/cb500848p
55. Wagner GR, Payne RM. Widespread and enzyme-independent nϵ-acetylation and nϵ-succinylation of proteins in the chemical conditions of the mitochondrial matrix. *J Biol Chem.* (2013) 288:29036–45. doi: 10.1074/jbc.M113.486753

56. Peng C, Lu Z, Xie Z, Cheng Z, Chen Y, Tan M, et al. The first identification of lysine malonylation substrates and its regulatory enzyme. *Mol Cell Proteomics.* (2011) 10:9. doi: 10.1074/mcp.M111.012658
57. Yang G, Yuan Y, Yuan H, Wang J, Yun H, Geng Y, et al. Histone acetyltransferase 1 is a succinyltransferase for histones and non-histones and promotes tumorigenesis. *EMBO Rep.* (2021) 22:29. doi: 10.15252/embr.202050967
58. Imai S-i, Armstrong CM, Kaeberlein M, Guarente L. Transcriptional silencing and longevity protein Sir2 is an NAD-dependent histone deacetylase. *Nature.* (2000) 403:795–800. doi: 10.1038/35001622
59. Greiss S, Gartner A. Sirtuin/Sir2 phylogeny, evolutionary considerations and structural conservation. *Mol Cells.* (2009) 28:407–15. doi: 10.1007/s10059-009-0169-x
60. Kaeberlein M, McVey M, Guarente L. The *SIR2/3/4* complex and *SIR2* alone promote longevity in *Saccharomyces cerevisiae* by two different mechanisms. *Genes Dev.* (1999) 13:2570–80. doi: 10.1101/gad.13.19.2570
61. Klar AJ, Fogel S, Macleod K. MAR1-a regulator of the HMA and HMα loci in *Saccharomyces cerevisiae*. *Genetics.* (1979) 93:37–50. doi: 10.1093/genetics/93.1.37
62. Satoh A, Brace CS, Rensing N, Cliften P, Wozniak DF, Herzog ED, et al. Sirt1 extends life span and delays aging in mice through the regulation of Nk2 homeobox 1 in the DMH and LH. *Cell Metab.* (2013) 18:416–30. doi: 10.1016/j.cmet.2013.07.013
63. Kanfi Y, Naiman S, Amir G, Peshti V, Zinman G, Nahum L, et al. The sirtuin SIRT6 regulates lifespan in male mice. *Nature.* (2012) 483:218–21. doi: 10.1038/nature10815
64. Albani D, Ateri E, Mazzuco S, Ghilardi A, Rodilossi S, Biella G, et al. Modulation of human longevity by SIRT3 single nucleotide polymorphisms in the prospective study "treviso longeva (trelong)". *Age.* (2014) 36:469–78. doi: 10.1007/s11357-013-9559-2
65. Cohen HY, Miller C, Bitterman KJ, Wall NR, Hekking B, Kessler B, et al. Calorie restriction promotes mammalian cell survival by inducing the SIRT1 deacetylase. *Science.* (2004) 305:390–2. doi: 10.1126/science.1099196
66. Someya S, Yu W, Hallows WC, Xu J, Vann JM, Leeuwenburgh C, et al. Sirt3 mediates reduction of oxidative damage and prevention of age-related hearing loss under caloric restriction. *Cell.* (2010) 143:802–12. doi: 10.1016/j.cell.2010.10.002
67. Tanno M, Sakamoto J, Miura T, Shimamoto K, Horio Y. Nucleocytoplasmic shuttling of the NAD^+-dependent histone deacetylase SIRT1. *J Biol Chem.* (2007) 282:6823–32. doi: 10.1074/jbc.M609554200
68. Ford E, Voit R, Liszt G, Magin C, Grummt I, Guarente L. Mammalian Sir2 homolog SIRT7 is an activator of RNA polymerase I transcription. *Genes Dev.* (2006) 20:1075–80. doi: 10.1101/gad.1399706
69. North BJ, Verdin E. Interphase nucleo-cytoplasmic shuttling and localization of SIRT2 during mitosis. *PLoS ONE.* (2007) 2:0000784. doi: 10.1371/journal.pone.0000784
70. Chen Y, Zhao W, Yang JS, Cheng Z, Luo H, Lu Z, et al. Quantitative acetylome analysis reveals the roles of SIRT1 in regulating diverse substrates and cellular pathways. *Mol Cell Proteomics.* (2012) 11:1048–62. doi: 10.1074/mcp.M112.019547
71. Ahuja N, Schwer B, Carobbio S, Waltregny D, North BJ, Castronovo V, et al. Regulation of insulin secretion by SIRT4, a mitochondrial ADP-ribosyltransferase. *J Biol Chem.* (2007) 282:33583–92. doi: 10.1074/jbc.M705488200
72. Sol EM, Wagner SA, Weinert BT, Kumar A, Kim H-S, Deng C-X, et al. Proteomic investigations of lysine acetylation identify diverse substrates of mitochondrial deacetylase Sirt3. *PLoS ONE.* (2012). 7:e50545. doi: 10.1371/journal.pone.0050545
73. Laurent G, German NJ, Saha AK, de Boer VC, Davies M, Koves TR, et al. SIRT4 coordinates the balance between lipid synthesis and catabolism by repressing malonyl CoA decarboxylase. *Mol Cell.* (2013) 50:686–98. doi: 10.1016/j.molcel.2013.05.012
74. Du J, Zhou Y, Su X, Yu JJ, Khan S, Jiang H, et al. Sirt5 is a NAD-dependent protein lysine demalonylase and desuccinylase. *Science.* (2011) 334:806–9. doi: 10.1126/science.1207861
75. Liszt G, Ford E, Kurtev M, Guarente L. Mouse Sir2 homolog SIRT6 is a nuclear adp-ribosyltransferase. *J Biol Chem.* (2005) 280:21313–20. doi: 10.1074/jbc.M413296200
76. Li L, Shi L, Yang S, Yan R, Zhang D, Yang J, et al. SIRT7 is a histone desuccinylase that functionally links to chromatin compaction and genome stability. *Nat Commun.* (2016). 7:12235. doi: 10.1038/ncomms12235
77. Matsushima S, Sadoshima J. The role of sirtuins in cardiac disease. *Am J Physiol Heart Circ Physiol.* (2015) 309:31. doi: 10.1152/ajpheart.00053.2015
78. Wallner M, Eaton DM, Berretta RM, Liesinger L, Schittmayer M, Gindlhuber J, et al. HDAC inhibition improves cardiopulmonary function in a feline model of diastolic dysfunction. *Sci Transl Med.* (2020). 12:eaay7205. doi: 10.1126/scitranslmed.aay7205
79. Herr DJ, Baarine M, Aune SE Li X, Ball LE, Lemasters JJ, et al. HDAC1 localizes to the mitochondria of cardiac myocytes and contributes to early cardiac reperfusion injury. *J Mol Cell Cardiol.* (2018) 114:309–19. doi: 10.1016/j.yjmcc.2017.12.004
80. Lee CF, Chavez JD, Garcia-Menendez L, Choi Y, Roe ND, Chiao YA, et al. Normalization of NAD^+ redox balance as a therapy for heart failure. *Circulation.* (2016) 134:883–94. doi: 10.1161/CIRCULATIONAHA.116.022495
81. Horton JL, Martin OJ, Lai L, Riley NM, Richards AL, Vega RB, et al. Mitochondrial protein hyperacetylation in the failing heart. *Jci Insight.* (2016) 2:25. doi: 10.1172/jci.insight.84897
82. Hansen BK, Gupta R, Baldus L, Lyon D, Narita T, Lammers M, et al. Analysis of human acetylation stoichiometry defines mechanistic constraints on protein regulation. *Nat Commun.* (2019) 10:1055. doi: 10.1038/s41467-019-09024-0
83. Alrob OA, Sankaralingam S, Ma C, Wagg CS, Fillmore N, Jaswal JS, et al. Obesity-induced lysine acetylation increases cardiac fatty acid oxidation and impairs insulin signalling. *Cardiovasc Res.* (2014) 103:485–97. doi: 10.1093/cvr/cvu156
84. Fukushima A, Lopaschuk GD. Cardiac fatty acid oxidation in heart failure associated with obesity and diabetes. *Biochim Biophys Acta.* (2016) 10:18. doi: 10.1016/j.bbalip.2016.03.020
85. Vadvalkar SS, Baily CN, Matsuzaki S, West M, Tesiram YA, Humphries KM. Metabolic inflexibility and protein lysine acetylation in heart mitochondria of a chronic model of type 1 diabetes. *Biochem J.* (2013) 449:253–61. doi: 10.1042/BJ20121038
86. Meyer JG, Softic S, Basisty N, Rardin MJ, Verdin E, Gibson BW, et al. Temporal dynamics of liver mitochondrial protein acetylation and succinylation and metabolites due to high fat diet and/or excess glucose or fructose. *PLoS ONE.* (2018) 13:e0208973. doi: 10.1371/journal.pone.0208973
87. Lopaschuk GD, Tsang H. Metabolism of palmitate in isolated working hearts from spontaneously diabetic "BB" wistar rats. *Circ Res.* (1987) 61:853–8. doi: 10.1161/01.RES.61.6.853
88. Herrero P, Peterson LR, McGill JB, Matthew S, Lesniak D, Dence C, et al. Increased myocardial fatty acid metabolism in patients with type 1 diabetes mellitus. *J Am Coll Cardiol.* (2006) 47:598–604. doi: 10.1016/j.jacc.2005.09.030
89. Pougovkina O. te Brinke H, Ofman R, van Cruchten AG, Kulik W, Wanders RJA, et al. Mitochondrial protein acetylation is driven by acetyl-CoA from fatty acid oxidation. *Hum Mol Genet.* (2014) 23:3513–22. doi: 10.1093/hmg/ddu059
90. Deng Y, Xie M, Li Q, Xu X, Ou W, Zhang Y, et al. Targeting mitochondria-inflammation circuit by β-hydroxybutyrate mitigates HFpEF. *Circ Res.* (2020) 12:317933. doi: 10.1161/CIRCRESAHA.120.317933
91. Kudo N, Barr AJ, Barr RL, Desai S, Lopaschuk GD. High rates of fatty acid oxidation during reperfusion of ischemic hearts are associated with a decrease in malonyl-CoA levels due to an increase in 5'-AMP-activated protein kinase inhibition of acetyl-CoA carboxylase. *J Biol Chem.* (1995) 270:17513–20. doi: 10.1074/jbc.270.29.17513
92. Sakamoto J, Barr RL, Kavanagh KM, Lopaschuk GD. Contribution of malonyl-CoA decarboxylase to the high fatty acid oxidation rates seen in the diabetic heart. *Am J Physiol Heart Circ Physiol.* (2000). 278:H1196–204. doi: 10.1152/ajpheart.2000.278.4.H1196
93. Zhang L, Ussher JR, Oka T, Cadete VJJ, Wagg C, Lopaschuk GD. Cardiac diacylglycerol accumulation in high fat-fed mice is associated with impaired insulin-stimulated glucose oxidation. *Cardiovasc Res.* (2010) 89:148–56. doi: 10.1093/cvr/cvq266
94. Keung W, Cadete VJJ, Palaniyappan A, Jablonski A, Fischer M, Lopaschuk GD. Intracerebroventricular leptin administration

differentially alters cardiac energy metabolism in mice fed a low-fat and high-fat diet. *J Cardiovasc Pharmacol.* (2011) 57:103–13. doi: 10.1097/FJC.0b013e31820014f9

95. Young ME, Goodwin GW, Ying J, Guthrie P, Wilson CR, Laws FA, et al. Regulation of cardiac and skeletal muscle malonyl-CoA decarboxylase by fatty acids. *Am J Physiol Endocrinol Metab*. (2001). 280:E471–9. doi: 10.1152/ajpendo.2001.280.3.E471
96. Colak G, Pougovkina O, Dai L, Tan M, Te Brinke H, Huang H, et al. Proteomic and biochemical studies of lysine malonylation suggest its malonic aciduria-associated regulatory role in mitochondrial function and fatty acid oxidation. *Mol Cell Proteomics.* (2015) 14:3056–71. doi: 10.1074/mcp.M115.048850
97. Boylston JA, Sun J, Chen Y, Gucek M, Sack MN, Murphy E. Characterization of the cardiac succinylome and its role in ischemia-reperfusion injury. *J Mol Cell Cardiol.* (2015) 88:73–81. doi: 10.1016/j.yjmcc.2015.09.005
98. Fan J, Shan C, Kang H-B, Elf S, Xie J, Tucker M, et al. Tyr phosphorylation of PDP1 toggles recruitment between ACAT1 and SIRT3 to regulate the pyruvate dehydrogenase complex. *Mol Cell.* (2014) 53:534–48. doi: 10.1016/j.molcel.2013.12.026
99. Thapa D, Manning JR, Stoner MW, Zhang M, Xie B, Scott I. Cardiomyocyte-specific deletion of GCN5L1 in mice restricts mitochondrial protein hyperacetylation in response to a high fat diet. *Sci Rep*. (2020). 10:10665. doi: 10.1038/s41598-020-67812-x
100. Fukushima A, Alrob OA, Zhang L, Wagg CS, Altamimi T, Rawat S, et al. Acetylation and succinylation contribute to maturational alterations in energy metabolism in the newborn heart. *Am J Physiol Heart Circ Physiol.* (2016) 311:3. doi: 10.1152/ajpheart.00900.2015
101. Weinert BT, Moustafa T, Iesmantavicius V, Zechner R, Choudhary C. Analysis of acetylation stoichiometry suggests that SIRT3 repairs nonenzymatic acetylation lesions. *EMBO J.* (2015) 34:2620–32. doi: 10.15252/embj.201591271
102. Wagner GR, Hirschey MD. Nonenzymatic protein acylation as a carbon stress regulated by sirtuin deacylases. *Mol Cell.* (2014) 54:5. doi: 10.1016/j.molcel.2014.03.027
103. Carrer A, Parris JL, Trefely S, Henry RA, Montgomery DC, Torres A, et al. Impact of a high-fat diet on tissue acyl-CoA and histone acetylation levels. *J Biol Chem.* (2017) 292:3312–22. doi: 10.1074/jbc.M116.750620
104. Parodi-Rullán RM, Chapa-Dubocq XR, Javadov S. Acetylation of mitochondrial proteins in the heart: the role of SIRT3. *Front Physiol*. (2018). 9:1094. doi: 10.3389/fphys.2018.01094
105. Sundaresan NR, Gupta M, Kim G, Rajamohan SB, Isbatan A, Gupta MP. Sirt3 blocks the cardiac hypertrophic response by augmenting Foxo3a-dependent antioxidant defense mechanisms in mice. *J Clin Invest.* (2009) 119:2758–71. doi: 10.1172/JCI39162
106. Lu T-M, Tsai J-Y, Chen Y-C, Huang C-Y, Hsu H-L, Weng C-F, et al. Downregulation of SIRT1 as aging change in advanced heart failure. *J Biomed Sci.* (2014) 21:57. doi: 10.1186/1423-0127-21-57
107. Akkafa F, Halil Altiparmak I, Erkus ME, Aksoy N, Kaya C, Ozer A, et al. Reduced SIRT1 expression correlates with enhanced oxidative stress in compensated and decompensated heart failure. *Redox Biol.* (2015) 6:169–73. doi: 10.1016/j.redox.2015.07.011
108. Kawashima T, Inuzuka Y, Okuda J, Kato T, Niizuma S, Tamaki Y, et al. Constitutive SIRT1 overexpression impairs mitochondria and reduces cardiac function in mice. *J Mol Cell Cardiol.* (2011) 51:1026–36. doi: 10.1016/j.yjmcc.2011.09.013
109. Chalkiadaki A, Guarente L. High-fat diet triggers inflammation-induced cleavage of SIRT1 in adipose tissue to promote metabolic dysfunction. *Cell Metab.* (2012) 16:180–8. doi: 10.1016/j.cmet.2012.07.003
110. Buler M, Aatsinki SM, Izzi V, Uusimaa J, Hakkola J. SIRT5 is under the control of PGC-1α and ampk and is involved in regulation of mitochondrial energy metabolism. *FASEB J.* (2014) 28:3225–37. doi: 10.1096/fj.13-245241
111. Yu J, Sadhukhan S, Noriega LG, Moullan N, He B, Weiss RS, et al. Metabolic characterization of a *Sirt5* deficient mouse model. *Sci Rep.* (2013). 3:2806. doi: 10.1038/srep02806
112. Chi Z, Chen S, Xu T, Zhen W, Yu W, Jiang D, et al. Histone deacetylase 3 couples mitochondria to drive IL-1β-dependent inflammation by configuring fatty acid oxidation. *Mol Cell.* (2020). 80:43.e7–58.e7. doi: 10.1016/j.molcel.2020.08.015
113. Hershberger KA, Martin AS, Hirschey MD. Role of NAD^+ and mitochondrial sirtuins in cardiac and renal diseases. *Nat Rev Nephrol.* (2017) 13:213–25. doi: 10.1038/nrneph.2017.5
114. Cantó C, Menzies KJ, Auwerx J. NAD(+) metabolism and the control of energy homeostasis: a balancing act between mitochondria and the nucleus. *Cell Metab.* (2015) 22:31–53. doi: 10.1016/j.cmet.2015.05.023
115. Wang LF, Huang CC, Xiao YF, Guan XH, Wang XN, Cao Q, et al. CD38 deficiency protects heart from high fat diet-induced oxidative stress via activating Sirt3/FOXO3 pathway. *Cell Physiol Biochem.* (2018) 48:2350–63. doi: 10.1159/000492651
116. Koltai E, Szabo Z, Atalay M, Boldogh I, Naito H, Goto S, et al. Exercise alters SIRT1, SIRT6, NAD and NAMPT levels in skeletal muscle of aged rats. *Mech Ageing Dev.* (2010) 131:21–8. doi: 10.1016/j.mad.2009.11.002
117. Schmidt MT, Smith BC, Jackson MD, Denu JM. Coenzyme specificity of Sir2 protein deacetylases: implications for physiological regulation*. *J Biol Chem.* (2004) 279:40122–9. doi: 10.1074/jbc.M407484200
118. Bitterman KJ, Anderson RM, Cohen HY, Latorre-Esteves M, Sinclair DA. Inhibition of silencing and accelerated aging by nicotinamide, a putative negative regulator of yeast Sir2 and human SIRT1. *J Biol Chem.* (2002) 277:45099–107. doi: 10.1074/jbc.M205670200
119. Lin SJ, Ford E, Haigis M, Liszt G, Guarente L. Calorie restriction extends yeast life span by lowering the level of NADH. *Genes Dev.* (2004) 18:12–6. doi: 10.1101/gad.1164804
120. Fulco M, Schiltz RL, Iezzi S, King MT, Zhao P, Kashiwaya Y, et al. Sir2 regulates skeletal muscle differentiation as a potential sensor of the redox state. *Mol Cell.* (2003) 12:51–62. doi: 10.1016/S1097-2765(03)00226-0
121. Madsen AS, Andersen C, Daoud M, Anderson KA, Laursen JS, Chakladar S, et al. Investigating the sensitivity of NAD^+-dependent sirtuin deacylation activities to NADH. *J Biol Chem.* (2016) 291:7128–41. doi: 10.1074/jbc.M115.668699
122. Anderson KA, Madsen AS, Olsen CA, Hirschey MD. Metabolic control by sirtuins and other enzymes that sense NAD(+), NADH, or their ratio. *Biochim Biophys Acta Bioenerg.* (2017) 1858:991–8. doi: 10.1016/j.bbabio.2017.09.005
123. Cantó C, Houtkooper RH, Pirinen E, Youn DY, Oosterveer MH, Cen Y, et al. The NAD(+) precursor nicotinamide riboside enhances oxidative metabolism and protects against high-fat diet-induced obesity. *Cell Metab.* (2012) 15:838–47. doi: 10.1016/j.cmet.2012.04.022
124. Diguet N, Trammell SAJ, Tannous C, Deloux R, Piquereau J, Mougenot N, et al. Nicotinamide riboside preserves cardiac function in a mouse model of dilated cardiomyopathy. *Circulation.* (2018) 137:2256–73. doi: 10.1161/CIRCULATIONAHA.116.026099
125. Yamamoto T, Byun J, Zhai P, Ikeda Y, Oka S, Sadoshima J. Nicotinamide mononucleotide, an intermediate of NAD^+ synthesis, protects the heart from ischemia and reperfusion. *PLoS ONE.* (2014) 9:e98972. doi: 10.1371/journal.pone.0098972
126. de Picciotto NE, Gano LB, Johnson LC, Martens CR, Sindler AL, Mills KF, et al. Nicotinamide mononucleotide supplementation reverses vascular dysfunction and oxidative stress with aging in mice. *Aging Cell.* (2016) 15:522–30. doi: 10.1111/acel.12461
127. Kane AE, Sinclair DA. Sirtuins and NAD^+ in the development and treatment of metabolic and cardiovascular diseases. *Circ Res.* (2018) 123:868–85. doi: 10.1161/CIRCRESAHA.118.312498
128. Nelson MM, Efird JT, Kew KA, Katunga LA, Monroe TB, Doorn JA, et al. Enhanced catecholamine flux and impaired carbonyl metabolism disrupt cardiac mitochondrial oxidative phosphorylation in diabetes patients. *Antioxid Redox Signal.* (2020) 25. doi: 10.1089/ars.2020.8122
129. Martin AS, Abraham DM, Hershberger KA, Bhatt DP, Mao L, Cui H, et al. Nicotinamide mononucleotide requires SIRT3 to improve cardiac function and bioenergetics in a friedreich's ataxia cardiomyopathy model. *JCI Insight.* (2017) 2:20. doi: 10.1172/jci.insight.93885
130. Ardehali H, Sabbah HN, Burke MA, Sarma S, Liu PP, Cleland JGF, et al. Targeting myocardial substrate metabolism in heart failure: potential for new therapies. *Eur J Heart Fail.* (2012) 14:120–9. doi: 10.1093/eurjhf/hfr173
131. Neubauer S. The failing heart — an engine out of fuel. *N Engl J Med.* (2007) 356:1140–51. doi: 10.1056/NEJMra063052
132. Fillmore N, Lopaschuk GD. Targeting mitochondrial oxidative metabolism as an approach to treat heart failure. *Biochim Biophys*

Acta Mol Cell Res. (2013) 1833:857–65. doi: 10.1016/j.bbamcr.2012.08.014
133. Glatz JFC, Nabben M, Young ME, Schulze PC, Taegtmeyer H, Luiken JJFP. Re-balancing cellular energy substrate metabolism to mend the failing heart. *Biochim Biophys Acta Mol Basis Dis.* (2020) 1866:165579. doi: 10.1016/j.bbadis.2019.165579
134. Lopaschuk GD, Ussher JR. Evolving concepts of myocardial energy metabolism. *Circ Res.* (2016) 119:1173–6. doi: 10.1161/CIRCRESAHA.116.310078
135. Stanley WC, Recchia FA, Lopaschuk GD. Myocardial substrate metabolism in the normal and failing heart. *Physiol Rev.* (2005) 85:1093–129. doi: 10.1152/physrev.00006.2004
136. Allard MF, Schönekess BO, Henning SL, English DR, Lopaschuk GD. Contribution of oxidative metabolism and glycolysis to atp production in hypertrophied hearts. *Am J Physiol.* (1994). 267(2 Pt 2):H742–50. doi: 10.1152/ajpheart.1994.267.2.H742
137. Degens H, de Brouwer KF, Gilde AJ, Lindhout M, Willemsen PH, Janssen BJ, et al. Cardiac fatty acid metabolism is preserved in the compensated hypertrophic rat heart. *Basic Res Cardiol.* (2006) 101:17–26. doi: 10.1007/s00395-005-0549-0
138. Kato T, Niizuma S, Inuzuka Y, Kawashima T, Okuda J, Tamaki Y, et al. Analysis of metabolic remodeling in compensated left ventricular hypertrophy and heart failure. *Circ Heart Fail.* (2010) 3:420–30. doi: 10.1161/CIRCHEARTFAILURE.109.888479
139. Sack MN, Rader TA, Park S, Bastin J, McCune SA, Kelly DP. Fatty acid oxidation enzyme gene expression is downregulated in the failing heart. *Circulation.* (1996) 94:2837–42. doi: 10.1161/01.CIR.94.11.2837
140. Grillon JM, Johnson KR, Kotlo K, Danziger RS. Non-histone lysine acetylated proteins in heart failure. *Biochim Biophys Acta.* (2012) 4:607–14. doi: 10.1016/j.bbadis.2011.11.016
141. Karamanlidis G, Lee CF, Garcia-Menendez L, Kolwicz SC Jr, Suthammarak W, Gong G, et al. Mitochondrial complex i deficiency increases protein acetylation and accelerates heart failure. *Cell Metab.* (2013) 18:239–50. doi: 10.1016/j.cmet.2013.07.002
142. Du Y, Cai T, Li T, Xue P, Zhou B, He X, et al. Lysine malonylation is elevated in type 2 diabetic mouse models and enriched in metabolic associated proteins. *Mol Cell Proteomics.* (2015) 14:227–36. doi: 10.1074/mcp.M114.041947
143. Lopaschuk GD, Ussher JR, Folmes CDL, Jaswal JS, Stanley WC. Myocardial fatty acid metabolism in health and disease. *Physiol Rev.* (2010) 90:207–58. doi: 10.1152/physrev.00015.2009
144. Houten SM, Wanders RJ. A general introduction to the biochemistry of mitochondrial fatty acid β-oxidation. *J Inherit Metab Dis.* (2010) 33:469–77. doi: 10.1007/s10545-010-9061-2
145. Chen T, Liu J, Li N, Wang S, Liu H, Li J, et al. Mouse SIRT3 attenuates hypertrophy-related lipid accumulation in the heart through the deacetylation of LCAD. *PLoS ONE.* (2015). 10:e0118909. doi: 10.1371/journal.pone.0118909
146. Vazquez EJ, Berthiaume JM, Kamath V, Achike O, Buchanan E, Montano MM, et al. Mitochondrial complex i defect and increased fatty acid oxidation enhance protein lysine acetylation in the diabetic heart. *Cardiovasc Res.* (2015) 107:453–65. doi: 10.1093/cvr/cvv183
147. Karwi QG, Zhang L, Altamimi TR, Wagg CS, Patel V, Uddin GM, et al. Weight loss enhances cardiac energy metabolism and function in heart failure associated with obesity. *Diabetes Obes Metab.* (2019) 21:1944–55. doi: 10.1111/dom.13762
148. Vadvalkar SS, Matsuzaki S, Eyster CA, Giorgione JR, Bockus LB, Kinter CS, et al. Decreased mitochondrial pyruvate transport activity in the diabetic heart: role of mitochondrial pyruvate carrier 2 (MPC2) acetylation. *J Biol Chem.* (2017) 292:4423–33. doi: 10.1074/jbc.M116.753509
149. Renguet E, Ginion A, Gélinas R, Bultot L, Auquier J, Frayne IR, et al. Metabolism and acetylation contribute to leucine-mediated inhibition of cardiac glucose uptake. *Am J Physiol Heart Circ Physiol.* (2017) 313:H432–45. doi: 10.1152/ajpheart.00738.2016
150. Sundaresan NR, Pillai VB, Wolfgeher D, Samant S, Vasudevan P, Parekh V, et al. The deacetylase SIRT1 promotes membrane localization and activation of Akt and PDK1 during tumorigenesis and cardiac hypertrophy. *Sci Signal.* (2011) 4:2001465. doi: 10.1126/scisignal.2001465
151. Kerner J, Yohannes E, Lee K, Virmani A, Koverech A, Cavazza C, et al. Acetyl-l-carnitine increases mitochondrial protein acetylation in the aged rat heart. *Mech Ageing Dev.* (2015) 145:39–50. doi: 10.1016/j.mad.2015.01.003
152. Fernandes J, Weddle A, Kinter CS, Humphries KM, Mather T, Szweda LI, et al. Lysine acetylation activates mitochondrial aconitase in the heart. *Biochemistry (Mosc).* (2015) 54:4008–18. doi: 10.1021/acs.biochem.5b00375
153. Sun Y, Teng Z, Sun X, Zhang L, Chen J, Wang B, et al. Exogenous H(2)S reduces the acetylation levels of mitochondrial respiratory enzymes via regulating the NAD(+)-SIRT3 pathway in cardiac tissues of *db/db* mice. *Am J Physiol Endocrinol Metab.* (2019) 317:E284–97. doi: 10.1152/ajpendo.00326.2018
154. Fukushima A, Zhang L, Huqi A, Lam VH, Rawat S, Altamimi T, et al. Acetylation contributes to hypertrophy-caused maturational delay of cardiac energy metabolism. *JCI Insight.* (2018) 3:e99239. doi: 10.1172/jci.insight.99239
155. Kerr M, Miller JJ, Thapa D, Stiewe S, Timm KN, Aparicio CNM, et al. Rescue of myocardial energetic dysfunction in diabetes through the correction of mitochondrial hyperacetylation by honokiol. *Jci Insight.* (2020) 5:140326. doi: 10.1172/jci.insight.140326
156. Jing E, O'Neill BT, Rardin MJ, Kleinridders A, Ilkeyeva OR, Ussar S, et al. Sirt3 regulates metabolic flexibility of skeletal muscle through reversible enzymatic deacetylation. *Diabetes.* (2013) 62:3404–17. doi: 10.2337/db12-1650
157. Lopaschuk GD, Folmes CDL, Stanley WC. Cardiac energy metabolism in obesity. *Circ Res.* (2007) 101:335–47. doi: 10.1161/CIRCRESAHA.107.150417
158. Koentges C, Pfeil K, Schnick T, Wiese S, Dahlbock R, Cimolai MC, et al. SIRT3 deficiency impairs mitochondrial and contractile function in the heart. *Basic Res Cardiol.* (2015) 110:015–0493. doi: 10.1007/s00395-015-0493-6
159. Davidson MT, Grimsrud PA, Lai L, Draper JA, Fisher-Wellman KH, Narowski TM, et al. Extreme acetylation of the cardiac mitochondrial proteome does not promote heart failure. *Circ Res.* (2020) 127:1094–108. doi: 10.1161/CIRCRESAHA.120.317293
160. Bharathi SS, Zhang Y, Mohsen A-W, Uppala R, Balasubramani M, Schreiber E, et al. Sirtuin 3 (SIRT3) protein regulates long-chain acyl-coa dehydrogenase by deacetylating conserved lysines near the active site. *J Biol Chem.* (2013) 288:33837–47. doi: 10.1074/jbc.M113.510354
161. Thapa D, Wu K, Stoner MW, Xie B, Zhang M, Manning JR, et al. The protein acetylase GCN5L1 modulates hepatic fatty acid oxidation activity via acetylation of the mitochondrial β-oxidation enzyme HADHA. *J Biol Chem.* (2018) 293:17676–84. doi: 10.1074/jbc.AC118.005462
162. Nassir F, Arndt JJ, Johnson SA, Ibdah JA. Regulation of mitochondrial trifunctional protein modulates nonalcoholic fatty liver disease in mice. *J Lipid Res.* (2018) 59:967–73. doi: 10.1194/jlr.M080952
163. Denton RM, Randle PJ, Bridges BJ, Cooper RH, Kerbey AL, Pask HT, et al. Regulation of mammalian pyruvate dehydrogenase. *Mol Cell Biochem.* (1975) 9:27–53. doi: 10.1007/BF01731731
164. Gray LR, Tompkins SC, Taylor EB. Regulation of pyruvate metabolism and human disease. *Cell Mol Life Sci.* (2014) 71:2577–604. doi: 10.1007/s00018-013-1539-2
165. Mori J, Alrob OA, Wagg CS, Harris RA, Lopaschuk GD, Oudit GY. Ang II causes insulin resistance and induces cardiac metabolic switch and inefficiency: a critical role of PDK4. *Am J Physiol Heart Circ Physiol.* (2013) 304:H1103–13. doi: 10.1152/ajpheart.00636.2012
166. Zhang Y, Bharathi SS, Rardin MJ, Lu J, Maringer KV, Sims-Lucas S, et al. Lysine desuccinylase SIRT5 binds to cardiolipin and regulates the electron transport chain. *J Biol Chem.* (2017) 292:10239–49. doi: 10.1074/jbc.M117.785022
167. Hallows WC Yu W, Denu JM. Regulation of glycolytic enzyme phosphoglycerate mutase-1 by SIRT1 protein-mediated deacetylation. *J Biol Chem.* (2012) 287:3850–8. doi: 10.1074/jbc.M111.317404
168. Li T, Liu M, Feng X, Wang Z, Das I, Xu Y, et al. Glyceraldehyde-3-phosphate dehydrogenase is activated by lysine 254 acetylation in response to glucose signal. *J Biol Chem.* (2014) 289:3775–85. doi: 10.1074/jbc.M113.531640
169. Ventura M, Mateo F, Serratosa J, Salaet I, Carujo S, Bachs O, et al. Nuclear translocation of glyceraldehyde-3-phosphate dehydrogenase is

regulated by acetylation. *Int J Biochem Cell Biol.* (2010) 42:1672–80. doi: 10.1016/j.biocel.2010.06.014
170. Xiong Y, Lei QY, Zhao S, Guan KL. Regulation of glycolysis and gluconeogenesis by acetylation of PKM and PEPCK. *Cold Spring Harb Symp Quant Biol.* (2011) 76:285–9. doi: 10.1101/sqb.2011.76.010942
171. Wang F, Wang K, Xu W, Zhao S, Ye D, Wang Y, et al. SIRT5 desuccinylates and activates pyruvate kinase M2 to block macrophage IL-1β production and to prevent dss-induced colitis in mice. *Cell Rep.* (2017) 19:2331–44. doi: 10.1016/j.celrep.2017.05.065
172. Xiangyun Y, Xiaomin N, Linping G, Yunhua X, Ziming L, Yongfeng Y, et al. Desuccinylation of pyruvate kinase M2 by SIRT5 contributes to antioxidant response and tumor growth. *Oncotarget.* (2017) 8:6984–93. doi: 10.18632/oncotarget.14346
173. Kierans SJ, Taylor CT. Regulation of glycolysis by the hypoxia-inducible factor (HIF): implications for cellular physiology. *J Physiol.* (2021) 599:23–37. doi: 10.1113/JP280572
174. Geng H, Liu Q, Xue C, David LL, Beer TM, Thomas GV, et al. HIF1α protein stability is increased by acetylation at lysine 709. *J Biol Chem.* (2012) 287:35496–505. doi: 10.1074/jbc.M112.400697
175. Lim JH, Lee YM, Chun YS, Chen J, Kim JE, Park JW. Sirtuin 1 modulates cellular responses to hypoxia by deacetylating hypoxia-inducible factor 1α. *Mol Cell.* (2010) 38:864–78. doi: 10.1016/j.molcel.2010.05.023
176. Lantier L, Williams AS, Williams IM, Yang KK, Bracy DP, Goelzer M, et al. Sirt3 is crucial for maintaining skeletal muscle insulin action and protects against severe insulin resistance in high-fat–fed mice. *Diabetes.* (2015) 64:3081–92. doi: 10.2337/db14-1810
177. Riehle C, Abel ED. Insulin signaling and heart failure. *Circ Res.* (2016) 118:1151–69. doi: 10.1161/CIRCRESAHA.116.306206
178. Zhang L, Jaswal JS, Ussher JR, Sankaralingam S, Wagg C, Zaugg M, et al. Cardiac insulin-resistance and decreased mitochondrial energy production precede the development of systolic heart failure after pressure-overload hypertrophy. *Circ Heart Fail.* (2013) 6:1039–48. doi: 10.1161/CIRCHEARTFAILURE.112.000228
179. Uddin GM, Zhang L, Shah S, Fukushima A, Wagg CS, Gopal K, et al. Impaired branched chain amino acid oxidation contributes to cardiac insulin resistance in heart failure. *Cardiovasc Diabetol.* (2019) 18:019–0892. doi: 10.1186/s12933-019-0892-3
180. Ramakrishnan G, Davaakhuu G, Kaplun L, Chung W-C, Rana A, Atfi A, et al. Sirt2 deacetylase is a novel AKT binding partner critical for AKT activation by insulin. *J Biol Chem.* (2014) 289:6054–66. doi: 10.1074/jbc.M113.537266
181. Fillmore N, Wagg CS, Zhang L, Fukushima A, Lopaschuk GD. Cardiac branched-chain amino acid oxidation is reduced during insulin resistance in the heart. *Am J Physiol Endocrinol Metab.* (2018) 315:E1046–52. doi: 10.1152/ajpendo.00097.2018
182. Lopaschuk GD, Karwi QG, Ho KL, Pherwani S, Ketema EB. Ketone metabolism in the failing heart. *Biochim Biophys Acta Mol Cell Biol Lipids.* (2020) 12:158813. doi: 10.1016/j.bbalip.2020.158813
183. Shimazu T, Hirschey MD, Hua L, Dittenhafer-Reed KE, Schwer B, Lombard DB, et al. Sirt3 deacetylates mitochondrial 3-hydroxy-3-methylglutaryl CoA synthase 2 and regulates ketone body production. *Cell Metab.* (2010) 12:654–61. doi: 10.1016/j.cmet.2010.11.003
184. Dittenhafer-Reed Kristin E, Richards Alicia L, Fan J, Smallegan Michael J, Fotuhi Siahpirani A, Kemmerer Zachary A, et al. Sirt3 mediates multi-tissue coupling for metabolic fuel switching. *Cell Metab.* (2015) 21:637–46. doi: 10.1016/j.cmet.2015.03.007
185. Rardin MJ, Newman JC, Held JM, Cusack MP, Sorensen DJ Li B, et al. Label-free quantitative proteomics of the lysine acetylome in mitochondria identifies substrates of Sirt3 in metabolic pathways. *Proc Natl Acad Sci USA.* (2013) 110:6601–6. doi: 10.1073/pnas.1302961110
186. Lei M-Z, Li X-X, Zhang Y, Li J-T, Zhang F, Wang Y-P, et al. Acetylation promotes BCAT2 degradation to suppress BCAA catabolism and pancreatic cancer growth. *Signal Transduct Target Ther.* (2020) 5:1–9. doi: 10.1038/s41392-020-0168-0
187. Yu W, Dittenhafer-Reed KE, Denu JM. Sirt3 protein deacetylates isocitrate dehydrogenase 2 (IDH2) and regulates mitochondrial redox status. *J Biol Chem.* (2012) 287:14078–86. doi: 10.1074/jbc.M112.355206
188. Zhou L, Wang F, Sun R, Chen X, Zhang M, Xu Q, et al. SIRT5 promotes IDH2 desuccinylation and G6PD deglutarylation to enhance cellular antioxidant defense. *EMBO Rep.* (2016) 17:811–22. doi: 10.15252/embr.201541643
189. Azhar S. Peroxisome proliferator-activated receptors, metabolic syndrome and cardiovascular disease. *Future Cardiol.* (2010) 6:657–91. doi: 10.2217/fca.10.86
190. Grygiel-Górniak B. Peroxisome proliferator-activated receptors and their ligands: nutritional and clinical implications - a review. *Nutr J.* (2014) 13:17. doi: 10.1186/1475-2891-13-17
191. Audet-walsh É, Giguére V. The multiple universes of estrogen-related receptor α and γ in metabolic control and related diseases. *Acta Pharmacol Sin.* (2015). 36:51–61. doi: 10.1038/aps.2014.121
192. Finck BN, Kelly DP. Peroxisome proliferator-activated receptor γ coactivator-1 (PGC-1) regulatory cascade in cardiac physiology and disease. *Circulation.* (2007) 115:2540–8. doi: 10.1161/CIRCULATIONAHA.107.670588
193. Purushotham A, Schug TT, Xu Q, Surapureddi S, Guo X, Li X. Hepatocyte-specific deletion of SIRT1 alters fatty acid metabolism and results in hepatic steatosis and inflammation. *Cell Metab.* (2009) 9:327–38. doi: 10.1016/j.cmet.2009.02.006
194. Laurent G, de Boer VCJ, Finley LWS, Sweeney M, Lu H, Schug TT, et al. Sirt4 represses peroxisome proliferator-activated receptor α activity to suppress hepatic fat oxidation. *Mol Cell Biol.* (2013) 33:4552–61. doi: 10.1128/MCB.00087-13
195. Qiang L, Wang L, Kon N, Zhao W, Lee S, Zhang Y, et al. Brown remodeling of white adipose tissue by SIRT1-dependent deacetylation of pparγ. *Cell.* (2012) 150:620–32. doi: 10.1016/j.cell.2012.06.027
196. Lin W, Zhang Q, Liu L, Yin S, Liu Z, Cao W. Klotho restoration via acetylation of peroxisome proliferation–activated receptor γ reduces the progression of chronic kidney disease. *Kidney Int.* (2017) 92:669–79. doi: 10.1016/j.kint.2017.02.023
197. Picard F, Kurtev M, Chung N, Topark-Ngarm A, Senawong T, Machado De Oliveira R, et al. SIRT1 promotes fat mobilization in white adipocytes by repressing ppar-gamma. *Nature.* (2004) 429:771–6. doi: 10.1038/nature02583
198. Jiang X, Ye X, Guo W, Lu H, Gao Z. Inhibition of HDAC3 promotes ligand-independent pparγ activation by protein acetylation. *J Mol Endocrinol.* (2014) 53:191–200. doi: 10.1530/JME-14-0066
199. Nemoto S, Fergusson MM, Finkel T. SIRT1 functionally interacts with the metabolic regulator and transcriptional coactivator PGC-1α. *J Biol Chem.* (2005) 280:16456–60. doi: 10.1074/jbc.M501485200
200. Gerhart-Hines Z, Rodgers JT, Bare O, Lerin C, Kim SH, Mostoslavsky R, et al. Metabolic control of muscle mitochondrial function and fatty acid oxidation through SIRT1/PGC-1α. *EMBO J.* (2007) 26:1913–23. doi: 10.1038/sj.emboj.7601633
201. Lerin C, Rodgers JT, Kalume DE. Kim S-h, Pandey A, Puigserver P. Gcn5 acetyltransferase complex controls glucose metabolism through transcriptional repression of PGC-1α. *Cell Metab.* (2006) 3:429–38. doi: 10.1016/j.cmet.2006.04.013
202. Wang C, Fu M, Angeletti RH, Siconolfi-Baez L, Reutens AT, Albanese C, et al. Direct acetylation of the estrogen receptor alpha hinge region by P300 regulates transactivation and hormone sensitivity. *J Biol Chem.* (2001) 276:18375–83. doi: 10.1074/jbc.M100800200
203. Wellen KE, Hatzivassiliou G, Sachdeva UM, Bui TV, Cross JR, Thompson CB. ATP-citrate lyase links cellular metabolism to histone acetylation. *Science.* (2009) 324:1076–80. doi: 10.1126/science.1164097
204. McDonnell E, Crown SB, Fox DB, Kitir B, Ilkayeva OR, Olsen CA, et al. Lipids reprogram metabolism to become a major carbon source for histone acetylation. *Cell Rep.* (2016) 17:1463–72. doi: 10.1016/j.celrep.2016.10.012
205. Castillo EC, Morales JA, Chapoy-Villanueva H, Silva-Platas C, Treviño-Saldaña N, Guerrero-Beltrán CE, et al. Mitochondrial hyperacetylation in the failing hearts of obese patients mediated partly by a reduction in SIRT3: the involvement of the mitochondrial permeability transition pore. *Cell Physiol Biochem.* (2019) 53:465–79. doi: 10.33594/000000151
206. Romanick SS, Ulrich C, Schlauch K, Hostler A, Payne J, Woolsey R, et al. Obesity-mediated regulation of cardiac protein acetylation: parallel analysis of total and acetylated proteins via TMT-tagged mass spectrometry. *Biosci Rep.* (2018) 38:31. doi: 10.1042/BSR20180721

207. Gorski PA, Jang SP, Jeong D, Lee A, Lee P, Oh JG, et al. Role of SIRT1 in modulating acetylation of the sarco-endoplasmic reticulum Ca^{2+}-atpase in heart failure. *Circ Res.* (2019) 124:e63–80. doi: 10.1161/RES.0000000000000277
208. Hu Q, Zhang H, Cortés NG, Wu D, Wang P, Zhang J, et al. Increased Drp1 acetylation by lipid overload induces cardiomyocyte death and heart dysfunction. *Circ Res.* (2020) 126:456–70. doi: 10.1161/CIRCRESAHA.119.315252
209. Stram AR, Wagner GR, Fogler BD, Pride PM, Hirschey MD, Payne RM. Progressive mitochondrial protein lysine acetylation and heart failure in a model of Friedreich's ataxia cardiomyopathy. *PLoS ONE.* (2017). 12:e0178354. doi: 10.1371/journal.pone.0178354
210. Olsen JV, Mann M. Status of large-scale analysis of post-translational modifications by mass spectrometry. *Mol Cell Proteomics.* (2013) 12:3444–52. doi: 10.1074/mcp.O113.034181
211. Xiong Y, Guan K-L. Mechanistic insights into the regulation of metabolic enzymes by acetylation. *J Cell Biol.* (2012) 198:155–64. doi: 10.1083/jcb.201202056
212. Baeza J, Dowell JA, Smallegan MJ, Fan J, Amador-Noguez D, Khan Z, et al. Stoichiometry of site-specific lysine acetylation in an entire proteome. *J Biol Chem.* (2014) 289:21326. doi: 10.1074/jbc.M114.581843
213. Weinert BT, Iesmantavicius V, Moustafa T, Schölz C, Wagner SA, Magnes C, et al. Acetylation dynamics and stoichiometry in *Saccharomyces cerevisiae*. *Mol Syst Biol.* (2014). 10:716. doi: 10.1002/msb.134766
214. Sambandam N, Lopaschuk GD, Brownsey RW, Allard MF. Energy metabolism in the hypertrophied heart. *Heart Fail Rev.* (2002) 7:161–73. doi: 10.1023/A:1015380609464
215. Randle PJ, Garland PB, Hales CN, Newsholme EA. The glucose fatty-acid cycle. Its role in insulin sensitivity and the metabolic disturbances of diabetes mellitus. *Lancet.* (1963) 1:785–9. doi: 10.1016/S0140-6736(63)91500-9
216. Sun Y, Tian Z, Liu N, Zhang L, Gao Z, Sun X, et al. Exogenous H(2)S switches cardiac energy substrate metabolism by regulating Sirt3 expression in *db/db* mice. *J Mol Med.* (2018) 96:281–99. doi: 10.1007/s00109-017-1616-3
217. Liu B, Clanachan AS, Schulz R, Lopaschuk GD. Cardiac efficiency is improved after ischemia by altering both the source and fate of protons. *Circ Res.* (1996) 79:940–8. doi: 10.1161/01.RES.79.5.940
218. Kantor PF, Dyck JRB, Lopaschuk GD. Fatty acid oxidation in the reperfused ischemic heart. *Am J Med Sci.* (1999) 318:3–14. doi: 10.1016/S0002-9629(15)40566-X
219. Hsu CP, Oka S, Shao D, Hariharan N, Sadoshima J. Nicotinamide phosphoribosyltransferase regulates cell survival through NAD^+ synthesis in cardiac myocytes. *Circ Res.* (2009) 105:481–91. doi: 10.1161/CIRCRESAHA.109.203703
220. Liu L, Wang P, Liu X, He D, Liang C, Yu Y. Exogenous NAD(+) supplementation protects H9C2 cardiac myoblasts against hypoxia/reoxygenation injury via SIRT1-p53 pathway. *Fundam Clin Pharmacol.* (2014) 28:180–9. doi: 10.1111/fcp.12016
221. Shinmura K, Tamaki K, Sano M, Nakashima-Kamimura N, Wolf AM, Amo T, et al. Caloric restriction primes mitochondria for ischemic stress by deacetylating specific mitochondrial proteins of the electron transport chain. *Circ Res.* (2011) 109:396–406. doi: 10.1161/CIRCRESAHA.111.243097
222. Pillai VB, Samant S, Sundaresan NR, Raghuraman H, Kim G, Bonner MY, et al. Honokiol blocks and reverses cardiac hypertrophy in mice by activating mitochondrial Sirt3. *Nat Commun.* (2015). 6:6656. doi: 10.1038/ncomms7656
223. Porter GA, Urciuoli WR, Brookes PS, Nadtochiy SM. Sirt3 deficiency exacerbates ischemia-reperfusion injury: implication for aged hearts. *Am J Physiol Heart Circ Physiol.* (2014) 306:18. doi: 10.1152/ajpheart.00027.2014
224. Koentges C, Pfeil K, Meyer-Steenbuck M, Lother A, Hoffmann MM, Odening KE, et al. Preserved recovery of cardiac function following ischemia-reperfusion in mice lacking Sirt3. *Can J Physiol Pharmacol.* (2016) 94:72–80. doi: 10.1139/cjpp-2015-0152
225. Hershberger KA, Abraham DM, Martin AS, Mao L, Liu J, Gu H, et al. Sirtuin 5 is required for mouse survival in response to cardiac pressure overload. *J Biol Chem.* (2017) 292:19767–81. doi: 10.1074/jbc.M117.809897
226. Klishadi MS, Zarei F, Hejazian SH, Moradi A, Hemati M, Safari F. Losartan protects the heart against ischemia reperfusion injury: Sirtuin3 involvement. *J Pharm Pharm Sci.* (2015) 18:112–23. doi: 10.18433/J3XG7T
227. Liu L, Wang Q, Zhao B, Wu Q, Wang P. Exogenous nicotinamide adenine dinucleotide administration alleviates ischemia/reperfusion-induced oxidative injury in isolated rat hearts via Sirt5-SDH-succinate pathway. *Eur J Pharmacol.* (2019) 858:3. doi: 10.1016/j.ejphar.2019.172520
228. Chouchani ET, Pell VR, Gaude E, Aksentijević D, Sundier SY, Robb EL, et al. Ischaemic accumulation of succinate controls reperfusion injury through mitochondrial ROS. *Nature.* (2014) 515:431–5. doi: 10.1038/nature13909
229. Griffiths EJ, Halestrap AP. Mitochondrial non-specific pores remain closed during cardiac ischaemia, but open upon reperfusion. *Biochem J.* (1995) 307:93–8. doi: 10.1042/bj3070093
230. Di Lisa F, Bernardi P. A capful of mechanisms regulating the mitochondrial permeability transition. *J Mol Cell Cardiol.* (2009) 46:775–80. doi: 10.1016/j.yjmcc.2009.03.006
231. Bochaton T, Crola-Da-Silva C, Pillot B, Villedieu C, Ferreras L, Alam MR, et al. Inhibition of myocardial reperfusion injury by ischemic postconditioning requires sirtuin 3-mediated deacetylation of cyclophilin D. *J Mol Cell Cardiol.* (2015) 84:61–9. doi: 10.1016/j.yjmcc.2015.03.017
232. Si Y, Bao H, Han L, Chen L, Zeng L, Jing L, et al. Dexmedetomidine attenuation of renal ischaemia-reperfusion injury requires sirtuin 3 activation. *Br J Anaesth.* (2018) 121:1260–71. doi: 10.1016/j.bja.2018.07.007

Conflict of Interest: The authors declare that the research was conducted in the absence of any commercial or financial relationships that could be construed as a potential conflict of interest.

frontiers in Cardiovascular Medicine

MINI REVIEW
published: 27 August 2021
doi: 10.3389/fcvm.2021.721956

Homeostasis Disrupted and Restored—A Fresh Look at the Mechanism and Treatment of Obesity During COVID-19

Jacqueline Dickey[1,2], *Camelia Davtyan*[3], *David Davtyan*[4] *and Heinrich Taegtmeyer*[1,5]*

[1] McGovern Medical School at The University of Texas Health Science Center at Houston, Houston, TX, United States, [2] The University of Texas Health Science Center at Houston School of Public Health, Houston, TX, United States, [3] Department of Internal Medicine, University of California Los Angeles, Los Angeles, CA, United States, [4] Department of General Surgery, Cedars-Sinai Medical Center, Glendale, CA, United States, [5] Department of Internal Medicine, Division of Cardiology, McGovern Medical School at The University of Texas Health Science Center at Houston, Houston, TX, United States

The prevalence of obesity in the United States approaches half of the adult population. The COVID-19 pandemic endangers the health of obese individuals. In addition, the metabolic syndrome poses a challenge to the health of obese adults. Bariatric surgery and diet restore metabolic homeostasis in obese individuals; however, it is still unclear which strategy is most effective. For example, intermittent fasting improves insulin sensitivity and diet alone decreases visceral adipose tissue at a disproportionately high rate compared to weight loss. Bariatric surgery causes rapid remission of type 2 diabetes and increases incretins for long-term remission of insulin resistance before meaningful weight loss has occurred. Malabsorptive surgeries have provided insight into the mechanism of altering metabolic parameters, but strong evidence to determine the duration of their effects is yet to be established. When determining the best method of weight loss, metabolic parameters, target weight loss, and risk-benefit analysis must be considered carefully. In this review, we address the pros and cons for the optimal way to restore metabolic homeostasis.

Keywords: obesity, weight reduction, bariatric surgery, metabolism, COVID-19

OPEN ACCESS

Edited by:
Kedryn K. Baskin,
The Ohio State University,
United States

Reviewed by:
Jan F. C. Glatz,
Maastricht University, Netherlands
Junichi Sadoshima,
University of Medicine and Dentistry of New Jersey, United States

***Correspondence:**
Heinrich Taegtmeyer
Heinrich.Taegtmeyer@uth.tmc.edu

Specialty section:
This article was submitted to Cardiovascular Metabolism, a section of the journal Frontiers in Cardiovascular Medicine

Received: *07 June 2021*
Accepted: *09 August 2021*
Published: *27 August 2021*

Citation:
Dickey J, Davtyan C, Davtyan D and Taegtmeyer H (2021) Homeostasis Disrupted and Restored—A Fresh Look at the Mechanism and Treatment of Obesity During COVID-19. Front. Cardiovasc. Med. 8:721956. doi: 10.3389/fcvm.2021.721956

KEY POINTS

- Obesity is a state of metabolic dysregulation, and affects susceptibility to COVID-19 infections.
- Bariatric surgery results in the most sustainable weight loss of known strategies for obesity treatment and causes rapid, persistent improvement in insulin resistance.
- Bariatric surgery has metabolic benefits independent of weight loss, but the exact mechanisms are still unclear.
- Malabsorptive bariatric surgery restores metabolic health to a greater extent than solely restrictive bariatric surgery.
- More knowledge is needed to account for the distinction between bariatric surgery's effect on visceral adipose tissue and subcutaneous adipose tissue.
- Intermittent fasting improves metabolic health by inducing adaptations that respond to periods of fasting and feeding, thereby increasing metabolic flexibility.

Obesity is a vexing problem. Despite an abundance of data on the serious health risks of obesity, its prevalence is increasing around the world. In the United States, the prevalence of obesity (defined by BMI of 30–39.9 kg/m^2) is currently 42.4%, and the prevalence of severe obesity (defined by BMI >40 kg/m^2) is 9.2% (1). In addition to adverse effects on people's well-being, the costs for the treatment of obesity and related comorbidities are formidable. More importantly, in the last year obesity has also been identified as a major risk factor for susceptibility to severe COVID-19 disease (**Figure 1**). Obesity may also decrease efficacy of the COVID-19 vaccine (2, 3) Here, we discuss obesity as a process of disrupted fuel homeostasis, and the treatment of obesity as an attempt to restore this homeostasis and possibly also lower susceptibility to severe COID-19 infections (**Figure 2**).

The long-term success rates of weight loss vary considerably depending on the treatment strategy (4). Historically, diet and exercise were the mainstay of obesity treatment. Pharmacotherapy was subsequently introduced without much success, while bariatric surgery was offered to patients with a BMI > 40 kg/m^2 or those with comorbidities and a BMI > 30–35 kg/m^2, depending on the surgical method.

Surgical procedures include Roux-en-Y gastric bypass surgery, sleeve gastrectomy, adjustable gastric banding, and the less commonly used biliopancreatic diversion (5). Many studies have already investigated metabolic outcomes of bariatric surgery, but study protocols in the existing literature are heterogeneous. Consequently, meta-analyses are difficult to perform due to the inconsistencies between different studies.

More work is needed to address this important public health issue, including a standardized comparison of the metabolic consequences of various bariatric surgery options, as well as diet and pharmacotherapy. As rigorously controlled comparative data begin to emerge, a fresh look at obesity and its treatment may offer a new perspective.

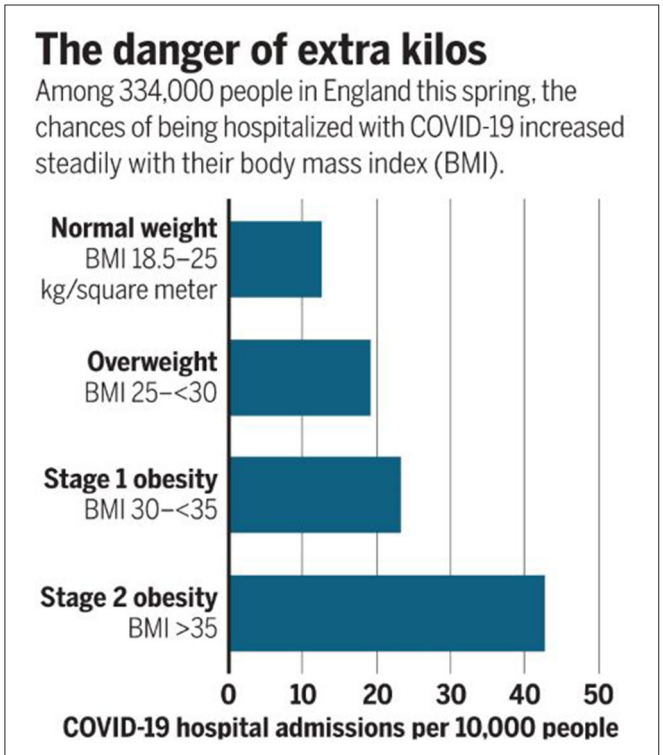

FIGURE 1 | Direct relationship between BMI and risk of severe COVID-19 illness. Data from Hamer et al. reveal an increase from <15 COVID-19 hospital admissions per 10,000 people in patients with normal weight compared to >40 admissions in those with Stage 2 obesity. Reproduced from Wadman with permission (2).

DISRUPTED FUEL HOMEOSTASIS

The Metabolic Syndrome and COVID-19

Metabolic syndrome is defined by an increase in any three of the following parameters: waist circumference, blood pressure, blood glucose level, or triglyceride level, or high-density lipoprotein cholesterol concentration (6). The interplay among these features is difficult to sort out, as some are seen in one patient but not the next. However, in all the leading theories, insulin resistance is a core component. Metabolic syndrome is particularly important in the context of COVID-19, as it causes a three times higher chance of death, and a four to five times higher probability of invasive mechanical ventilation, acute respiratory distress syndrome, and admission to the intensive care unit. Obesity may also impair an immune response to the COVID-19 vaccine (3, 7). In addition, compared to COVID-19 patients with normal glucose or with diabetes, those with hyperglycemia at hospital admission had higher mortality and lower PaO2/FiO2 (8).

To address the significance of insulin resistance, we discuss a recent study by Yoshino et al., in which the authors concluded that weight loss, whether induced by bariatric surgery, or by strict dieting alone, was key to restoring insulin sensitivity (9). In this matched prospective cohort study, obese individuals with type 2 diabetes underwent either Roux-en-Y gastric bypass or were placed on a diet to achieve 16–24% weight loss. Weight loss in both groups increased hepatic insulin sensitivity as indicated by increased suppression of glucose production and increased glucose disposal, with no significant difference between groups (9). The report by Yoshino et al. suggests, at first glance, that the mechanism of weight loss does not impact the outcomes concerning insulin sensitivity. However, this study has considerable limitations, and the results must be interpreted with caution. As the authors mentioned, the subjects were not randomized, and the sample size may have been inadequate. We also noted that two-thirds of the participants were women, whose metabolic profiles differ from men with respect to lipid metabolism, and to their predisposition for central obesity. Most importantly, both groups, the surgical and the non-surgical group, were placed on diets to achieve weight loss, suggesting that the lack of between-group differences may be due to diet and weight loss combined. Several studies also suggest that various metabolic improvements, such as decreased visceral adipose tissue, increased insulin sensitivity, and increased levels of high-density lipoprotein cholesterol occur in the absence of weight loss (10). Given these confounders, it is difficult to determine whether other, more important, factors are at play.

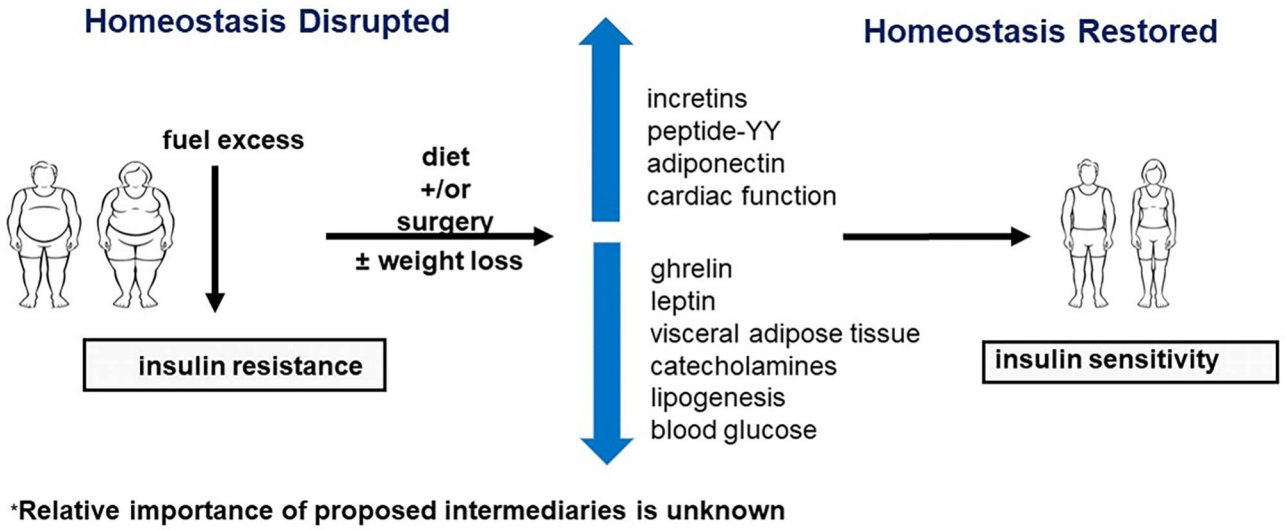

FIGURE 2 | Restoration of homeostasis by neuroendocrine regulation. Surgery and diet may improve insulin sensitivity by affecting various components of the neuroendocrine axis. Refer to text for further discussion.

Another confusing component of disrupted fuel homeostasis in metabolic syndrome is that there are two groups of outliers in the general population: "metabolically healthy" obese individuals and "metabolically obese" normal weight individuals. Metabolically obese normal weight individuals (24% of normal weight individuals) are primarily a result of genetics and lifestyle factors, whereas metabolically healthy obese individuals (32% of obese individuals) are impacted by a multitude of factors, such as inflammation of adipose tissue (11, 12). In both groups, poor metabolic "fitness" is strongly correlated with increased hepatic fat stores, which are likely a result of de novo lipid synthesis, increased uptake, and decreased disposal (13). These individuals with disrupted fuel homeostasis complicate the hypothesis that weight loss alone is the mechanism of restoring insulin sensitivity (14).

Additionally, considerable differences in metabolic risk factors in obese individuals (BMI 30–40 kg/m^2) exist, depending primarily on ectopic fat and lifestyle factors, such as diet and exercise (4, 13). In a landmark paper by Reaven et al., the authors noted an association between insulin resistance and upregulation of the sympathetic nervous system, even suggesting a potential causal relationship (6). An increased adrenergic response may be the mechanism behind other components of metabolic syndrome, such as increased non-estrified long-chain fatty acids (FAs) in the plasma and arterial hypertension. Indeed, recent data have demonstrated a bidirectional relationship of leptin with the sympathetic nervous system and thus, energy storage and mobilization (15). Furthermore, lifestyle changes which decrease insulin resistance and sympathetic nervous system activity, including exercise and caloric control, appear to protect against the metabolic syndrome. It is not proven, however, that these lifestyle modifications are exclusively responsible for the mechanism to restore metabolic normalcy, and the genetic profile likely plays a role as well (6, 12).

RESTORING FUEL HOMEOSTASIS

Metabolic Impacts of Diet and Calorie Restriction

Metabolic Impact: Insulin Resistance

To understand which metabolic improvements to attribute to weight loss, diet, or surgery, it is helpful to consider how diet impacts insulin resistance in the absence of significant weight loss. De Cabo et al. established that a 2.5% weight loss caused by 22 days of fasting every other day resulted in a disproportionately high (57%) decrease in fasting insulin levels (16). In another study, individuals not undergoing surgery showed improvements in insulin sensitivity and beta-cell function similar to operated individuals both following similar fasting protocols. These results suggest that fasting may be responsible for the acute metabolic improvements in the surgery group (4).

Metabolic Impact: Visceral and Ectopic Excess Body Fat

Another parameter followed by the research work in obesity is the assessment of visceral adipose tissue (VAT), estimated by waist circumference and BMI taken together. Increased VAT, regardless of BMI, is associated with increased cardiovascular and metabolic risk (4). Similarly, excess body fat is highly associated with poor metabolic health and is a far better predictor of metabolic health than BMI (13). The accumulation of visceral and ectopic fat represents disrupted lipid homeostasis due to excessive fuel intake, excessive fuel storage, or deficient fuel breakdown. The amount of visual adipose tissue is readily decreased and insulin sensitivity is readily restored at 3 months after bariatric surgery (17). In contrast there is no effect on liposuction on insulin action with evidence for fatty liver disease (18, 19).

Diet: Intermittent Fasting

Intermittent fasting is an increasingly popular strategy for obesity. Intriguingly, after 6 months, women who followed an intermittent fasting protocol of 5 days of regular diet and 2 days of significant calorie restriction per week had a greater decrease in waist circumference than women who just reduced caloric intake by 25% every day (16). Hence, it is reasonable to assume that intermittent fasting per se improves metabolic abnormalities, including insulin resistance.

Supportive evidence suggests improved insulin sensitivity with intermittent fasting in a randomized crossover study that supervised standardized meal consumption in prediabetic men over a five-week period (20). In this study, food intake was matched in both arms with the goal of maintaining current weight. Compared to the matched group that consumed meals over a 12-h period, subjects consuming the same amount of calories over 6-h period, mean postprandial insulin levels were significantly lower (26.9 mU/l) (20). This proof-of-concept study provided the first evidence for the effectiveness of early time-restricted feeding (eTRF) which stresses eating early in the day in alignment with circadian rhythms of metabolism (21). The improvements in insulin levels persisted during the 7-week washout period, indicating that a fasting protocol may be necessary in the diet-only group before one can draw firm conclusions in the Yoshino et al. study (9).

Another important factor is the duration of follow-up. In one 12-month study, insulin sensitivity and lipid levels failed to improve despite weight loss from bariatric surgery (22). Other studies have reported improved insulin and lipid levels after weight loss, indicating that results may differ when taken in an acute vs. long-term setting (9). Although it is tempting to deduce that weight loss accounted for improved insulin sensitivity, it seems that fasting protocol, diet, and time since surgery are potential confounders.

A Comparison of Bariatric Surgeries

The most common bariatric surgery procedures performed in the United States are currently sleeve gastrectomy (61%), and RYGB (17%), with LAGB and biliopancreatic diversion (2% together) falling out of favor (23). Novel gastrointestinal surgeries that target diabetes, such as duodenal-jejunal bypass and ileal interposition, provide helpful clues to the mechanism of restored insulin sensitivity following bariatric surgery (5). Briefly, RYGB excludes most of the stomach just distal to the gastroesophageal junction (GEJ). It bypasses the entire duodenum and part of the jejunum as the 30 cc stomach pouch attached to the esophagus is anastomosed to the distal jejunum. Sleeve gastrectomy removes a significant portion (60–80%) of the stomach along the greater curvature, and adjustable gastric banding is an inflatable/adjustable silicone band placed around the superior portion of the stomach, just distal to the GEJ. Biliopancreatic diversion removes the stomach just as in gastric sleeve, which is anastomosed to the distal portion of the ileum. The excluded duodenum, jejunum, and proximal ileum are anastomosed to the alimentary limb, allowing biliary and pancreatic secretions to mix with ingested nutrients (5).

The current standard of care in the United States is to allow the patient to choose among these procedures, and patients may find the following information helpful in the decision (**Table 1**) (23, 24). After 5 years, 35% of LAGB patients had failed to lose weight compared to 4% of RYGB patients, and metabolic parameters were inferior in LAGB patients after 2 years (25). In general, bypass surgeries have caused more durable weight loss and better insulin control than restrictive surgeries, or than lifestyle management (5, 23). Long-term improvements in dyslipidemia and hypertension have been less consistent across studies. Of note, RYGB has higher complication rates than sleeve gastrectomy, including a higher rate of reoperation, perioperative mortality, and readmission (23). However, overall perioperative mortality remains low with RYGB (around 0.2%), and adverse events occur in 1–9% of patients undergoing RYGB (23).

Metabolic Benefit of Bariatric Surgery Independent of Weight Loss

There are several findings that indicate that bariatric surgery has benefits independent of weight loss. There is a rapid resolution of type 2 diabetes within days following bariatric surgery that persists at one and five years (4, 5). Another important finding is a remarkably higher rate of type 2 diabetes remission at 2 years with malabsorptive RYGB (72%) compared to restrictive LAGB (17%) in patients who had lost approximately 30% of their body weight (26).

In addition to remission of diabetes, subjects in a non-randomized, prospective cohort study showed decreased glucose, insulin, and leptin levels within 3 months of surgery, and glucagon-like peptide 1 (GLP-1), glucose-sensitive insulinotropic peptide (GIP), peptide-YY, while pancreatic polypeptide concentrations increased within days (4, 5, 24), On the contrary, fasting did not affect high molecular weight adiponectin, ghrelin, leptin, or GLP-1, suggesting unique effects of surgery compared to diet (20). One explanation for the rapid change in disrupted fuel homeostasis may be that surgery excises or interrupts regions of the digestive system involved in some of the pathologic adaptations of fuel excess. Additional support for these unique benefits of surgery include the nearly identical skeletal muscle gene expression of diabetogenic hormones, such as stearoyl-CoA desaturase (SCD), pyruvate dehydrogenase kinase 4 (PDK-4), and peroxisome proliferator-activated receptor alpha (PPAR-α) among participants who

TABLE 1 | Malabsorptive surgeries cause more dramatic weight loss and metabolic impacts than purely restrictive surgeries.

Surgery type	Malabsorptive	Restrictive
Sleeve gastrectomy		X
RYGB	X	X
LAGB		X
Biliopancreatic diversion	X	X
Duodenal-jejunal bypass	X	
Ileal interposition	X	

underwent LAGB vs. RYGB despite significant variation in weight loss between the two groups (222% greater mean weight loss at 9 months in RYGB participants compared to LAGB participants) (24). However, lengthening of the intestinal bypass by RYGB does not affect GLP-1 secretion, which suggests that the GLP-1 response after RYGB may not require delivery of nutrients to more distal intestinal segments (27). It is not known whether the metabolic effects of RYGB persist long-term, but the duration of surgery's impact may provide clues as to the mechanism of restored fuel homeostasis. For example, return of a disruption in fuel homeostasis over time may suggest that surgery merely interrupts pathologic metabolic adaptations, whereas permanent improvement in metabolic health may indicate that surgery removes an element of the metabolic pathway essential to disrupted fuel homeostasis.

Intermediate Steps Between Disruption and Restoration of Metabolic Homeostasis From Diet and Surgery

Given these important mediators, we postulate that there are intermediate steps between diet and surgery and increased insulin sensitivity (**Figure 2**). These interposed steps may include incretins, appetite-suppressing hormones, known metabolic risk factors, such as VAT, catecholamines, and unknown upper gastrointestinal effects that impact the regulation of blood glucose and lipogenesis. A possible mechanism for these hormonal changes may be related to the impressive reduction of oil-red-O staining in skeletal muscle post-operatively, which may occur in other organs, dramatically impacting the neuroendocrine signaling between adipose tissue and other organs (24). These findings also support the observation that ectopic fat, such as in skeletal muscle, is a key component of global metabolic dysfunction throughout the body (13).

Additional mechanisms may include surgical removal of the gastric fundus with sleeve gastrectomy, which is the site of ghrelin secretion, or hyperstimulation of appetite-suppressing hormone production by increased nutrient delivery to distal portions of the gastrointestinal tract, such as with RYGB. Antidiabetic effects are also observed in patients with decreased nutrient delivery to the upper gastrointestinal tract, possibly due to anti-incretin factors released from the proximal bowel (4, 26, 28).

Return to Normalcy in the Cardiovascular System After Surgery-Induced Weight Loss

Obesity affects the cardiovascular system at many different levels. In one study, 42% of obese participants had left ventricular diastolic dysfunction on tissue Doppler imaging (14, 24). Compared to non-obese patients with heart failure with preserved ejection fraction (HFpEF), obese patients with HFpEF had greater volume overload and right ventricular dysfunction, and decreased levels of brain natriuretic peptide and cardiac efficiency (4, 29). Obese patients also have an approximately 50% higher prevalence of atrial fibrillation than normal-weight patients, but the reversibility of arrhythmias following bariatric surgery is still unknown (4). These obesity-related abnormalities may be related to cardiac fibrosis, hypertrophy, and impaired microvascular coronary perfusion (in hearts of diabetic patients), and the cardiovascular impact of COVID-19 has the potential to further compound these problems (5).

Given the detrimental cardiac effects of obesity, pharmacologic agents have been tested as treatment options without success. We have previously proposed that obesity related cardiac dysfunction is likely a result of fuel excess, which results in production of reactive oxygen species (ROS). The overwhelmed heart may protect itself from further damage with insulin resistance in response to ROS. As a result, abruptly inducing insulin sensitivity overrides this protective response, resulting in cytotoxic damage (30). Worsening cardiac dysfunction with thiazolidinedione (TZD) use in a diabetic heart supports this proposition, as TZDs contribute to fuel overload by increasing glucose uptake and oxidation. Alternatively, metformin has protective effects on the heart by enhancing peripheral glucose oxidation and decreasing FAs (31).

In this context, it is important to emphasize that bariatric surgery-induced weight loss is a feasible solution to improve metabolic abnormalities, as well as cardiac function. Surgery decreased the incidence of major adverse cardiovascular events by more than 40% among a matched cohort of 2,600 obese patients with cardiac disease and by more than 55% among those with heart failure (32, 33). Surgery also decreases the use of antihypertensive drugs (33%), and diet induces a 0.43 mmHg decrease in systolic blood pressure per 1% decrease in body mass index (10, 20, 24). Interestingly, blood pressure is one of the first parameters to change with exercise before any meaningful weight loss occurs (10). Tissue Doppler diastolic velocity also increased by 1.9 cm/sec (95% CI 0.52–3.4) and 1.2 cm/sec (95% CI 0.32–2.1) at 3 and 9 months, respectively, along with improved septal mitral annular velocity (24). Lastly, left ventricular mass decreased linearly for 2 years post-operatively even as weight loss plateaued (14). Correction of metabolism by non-pharmacologic means is the most beneficial way to restore cardiac function.

CONSIDERING WEIGHT LOSS: DIET VS. SURGERY

Bariatric surgery is significantly more efficacious and long-lasting for weight loss than lifestyle modifications or medical management, inducing up to 70% excess weight loss (5). Surgery also increases survival by three years compared to obese subjects on standard obesity treatment over a 24-year period (34). Patients with type 2 diabetes and excess VAT appear to selectively lose VAT with exercise irrespective of the amount of weight loss, and patients who enrolled in a lifestyle intervention program following bariatric surgery had increased weight loss (4). In addition, exercise and diet seem to disproportionately boost outcomes in overweight and obese COVID-19 patients and may

be beneficial to prevent hyperglycemia in the context of COVID-19 (2). Weight loss independent benefits of exercise, such as translocation of GLUT-4 receptors to the skeletal muscle surface, enhanced FAs oxidation by an exercise-induced increase in the number of mitochondria, and increased high density lipoprotein cholesterol may be accounted for when devising a patient-specific weight loss plan (10). Other considerations include bariatric surgery for medically refractory type 2 diabetes, and diet and exercise as a first line option for normal-weight patients with type 2 diabetes and other metabolic derangements. However, a combination of diet, exercise, and surgery will likely lead to the best outcomes.

CONCLUSIONS

Obesity treatment continues to confound healthcare professionals. More research is needed to establish a mechanism for the restoration of metabolic homeostasis, a process in for which multiple factors are likely to be responsible. Important concepts to consider include the role of neuroendocrine interactions between adipose tissue and the brain, the hypothesis that sympathetic nervous system upregulation is associated with insulin resistance and perhaps responsible for metabolic syndrome, and the change in skeletal muscle gene expression and reduced ectopic fat deposition following bariatric surgery (15). Intermittent fasting or eTRF appear to be an effective strategy to improve metabolic health by increasing metabolic flexibility, as if conditioning the body's metabolism to undergo periods of stress. The paradoxically damaging effects of abruptly correcting insulin resistance in a fuel-overloaded heart is also significant. Future studies may include a study cohort comprised of a diet and surgery group with matched waist-to-hip ratios and identical fasting protocols or an animal study (with a sham-operated control group) to assess the impact of weight loss on insulin resistance. Additional long-term research is also needed to understand obesity-induced cardiac dysfunction. Gradual weight loss in a time of COVID-19 may decrease morbidity and mortality at a relatively high rate in obese patients, and bariatric surgery should not be postponed (2). Determining long-term outcomes and solidifying our understanding of mechanisms will allow patients and physicians to choose rationally among available weight loss options to restore metabolic health in the patient with disrupted fuel homeostasis. It still remains unknown whether restoring fuel homeostasis also reduces susceptibility to COVID-19 infections. But it seems likely.

AUTHOR CONTRIBUTIONS

HT and JD: conceived, designed, and wrote the manuscript. CD and DD: provided critical comments, suggestions, and text. All authors contributed to the article and approved the submitted version.

ACKNOWLEDGMENTS

We thank Ms. Anna Menezes for expert editorial assistance. The corresponding author's lab is supported by grants from the United States Public Health Service: R01-HL-061483; R01-HL-073162.

REFERENCES

1. National Center for Health Statistics CfDCaP. Adult Obesity. *National Center for Health Statistics, and Centers for Disease Control and Prevention*. United states: National Center for Health Statistics (2020).
2. Wadman M. Why obesity worsens COVID-19. *Science.* (2020) 369:1280–1. doi: 10.1126/science.369.6509.1280
3. Ledford H. How obesity could create problems for a COVID vaccine. *Nature.* (2020) 586:488–9. doi: 10.1038/d41586-020-02946-6
4. Piche ME, Tchernof A, Despres JP. Obesity phenotypes, diabetes, and cardiovascular diseases. *Circ Res.* (2020) 126:1477–500. doi: 10.1161/CIRCRESAHA.120.316101
5. Rubino F, Schauer PR, Kaplan LM, Cummings DE. Metabolic surgery to treat type 2 diabetes: clinical outcomes and mechanisms of action. *Annu Rev Med.* (2010) 61:393–411. doi: 10.1146/annurev.med.051308.105148
6. Reaven GM, Lithell H, Landsberg L. Hypertension and associated metabolic abnormalities—the role of insulin resistance and the sympathoadrenal system. *N Engl J Med.* (1996) 334:374–81. doi: 10.1056/NEJM199602083340607
7. Xie J, Zu Y, Alkhatib A, Pham TT, Gill F, Jang A, et al. Metabolic syndrome and COVID-19 mortality among adult black patients in new orleans. *Diabetes Care.* (2020) 44:188–93. doi: 10.2337/dc20-1714
8. Coppelli A, Giannarelli R, Aragona M, Penno G, Falcone M, Tiseo G, et al. Hyperglycemia at hospital admission is associated with severity of the prognosis in patients hospitalized for COVID-19: the pisa COVID-19 study. *Diabetes Care.* (2020) 43:2345–8. doi: 10.2337/dc20-1380
9. Yoshino M, Kayser BD, Yoshino J, Stein RI, Reeds D, Eagon JC, et al. Effects of diet versus gastric bypass on metabolic function in diabetes. *N Engl J Med.* (2020) 383:721–32. doi: 10.1056/NEJMoa2003697
10. Heffron SP, Parham JS, Pendse J, Aleman JO. Treatment of obesity in mitigating metabolic risk. *Circ Res.* (2020) 126:1646–65. doi: 10.1161/CIRCRESAHA.119.315897
11. Gómez-Zorita S, Queralt M, Vicente MA, González M, Portillo MP. Metabolically healthy obesity and metabolically obese normal weight: a review. *J Physiol Biochem.* (2021) 77:175–89. doi: 10.1007/s13105-020-00781-x
12. Huang LO, Loos RJF, Kilpeläinen TO. Evidence of genetic predisposition for metabolically healthy obesity and metabolically obese normal weight. *Physiol Genomics.* (2018) 50:169–78. doi: 10.1152/physiolgenomics.00044.2017
13. Thomas EL, Frost G, Taylor-Robinson SD, Bell JD. Excess body fat in obese and normal-weight subjects. *Nutr Res Rev.* (2012) 25:150–61. doi: 10.1017/S0954422412000054
14. Khalaf KI, Taegtmeyer H. Clues from bariatric surgery: reversing insulin resistance to heal the heart. *Curr Diab Rep.* (2013) 13:245–51. doi: 10.1007/s11892-013-0364-1
15. Caron A, Lee S, Elmquist JK, Gautron L. Leptin and brain-adipose crosstalks. *Nat Rev Neurosci.* (2018) 19:153–65. doi: 10.1038/nrn.2018.7
16. de Cabo R, Mattson MP. Effects of intermittent fasting on health, aging, and disease. *N Engl J Med.* (2019) 381:2541–51. doi: 10.1056/NEJMra1905136
17. Leichman JG, Aguilar D, King TM, Mehta S, Majka C, Scarborough T, et al. Improvements in systemic metabolism, anthropometrics, and left ventricular geometry 3 months after bariatric surgery. *Surg Obes Relat Dis.* (2006) 2:592–9. doi: 10.1016/j.soard.2006.09.005
18. Klein S, Fontana L, Young VL, Coggan AR, Kilo C, Patterson BW, et al. Absence of an effect of liposuction on insulin action and risk factors for coronary heart disease. *N Engl J Med.* (2004) 350:2549–57. doi: 10.1056/NEJMoa033179
19. Friedman J. Fat in all the wrong places. *Nature.* (2002) 415:268–9. doi: 10.1038/415268a

20. Sutton EF, Beyl R, Early KS, Cefalu WT, Ravussin E, Peterson CM. Early time-restricted feeding improves insulin sensitivity, blood pressure, and oxidative stress even without weight loss in men with prediabetes. *Cell Metab.* (2018) 27:1212–21.e3. doi: 10.1016/j.cmet.2018.04.010
21. Brewer RA, Collins HE, Berry RD, Brahma MK, Tirado BA, Peliciari-Garcia RA, et al. Temporal partitioning of adaptive responses of the murine heart to fasting. *Life Sci.* (2018) 197:30–9. doi: 10.1016/j.lfs.2018.01.031
22. Swarbrick MM, Austrheim-Smith IT, Stanhope KL, Van Loan MD, Ali MR, Wolfe BM, et al. Circulating concentrations of high-molecular-weight adiponectin are increased following Roux-en-Y gastric bypass surgery. *Diabetologia.* (2006) 49:2552–8. doi: 10.1007/s00125-006-0452-8
23. Arterburn DE, Telem DA, Kushner RF, Courcoulas AP. Benefits and risks of bariatric surgery in adults: a review. *JAMA.* (2020) 324:879–87. doi: 10.1001/jama.2020.12567
24. Leichman JG, Wilson EB, Scarborough T, Aguilar D, Miller CC III, Yu S, et al. Dramatic reversal of derangements in muscle metabolism and left ventricular function after bariatric surgery. *Am J Med.* (2008) 121:966–73. doi: 10.1016/j.amjmed.2008.06.033
25. Trakhtenbroit MA, Leichman JG, Algahim MF, Miller CC III, Moody FG, Lux TR, et al. Body weight, insulin resistance, and serum adipokine levels 2 years after 2 types of bariatric surgery. *Am J Med.* (2009) 122:435–42. doi: 10.1016/j.amjmed.2008.10.035
26. Pok EH, Lee WJ. Gastrointestinal metabolic surgery for the treatment of type 2 diabetes mellitus. *World J Gastroenterol.* (2014) 20:14315–28. doi: 10.3748/wjg.v20.i39.14315
27. Miras AD, Kamocka A, Pérez-Pevida B, Purkayastha S, Moorthy K, Patel A, et al. The effect of standard versus longer intestinal bypass on GLP-1 regulation and glucose metabolism in patients with type 2 diabetes undergoing Roux-en-Y Gastric bypass: the long-limb study. *Diabetes Care.* (2021) 44:1082–90. doi: 10.2337/dc20-0762
28. Rubino F, R'Bibo SL, del Genio F, Mazumdar M, McGraw TE. Metabolic surgery: the role of the gastrointestinal tract in diabetes mellitus. *Nat Rev Endocrinol.* (2010) 6:102–9. doi: 10.1038/nrendo.2009.268
29. Taegtmeyer H, Algahim MF. Obesity and cardiac metabolism in women. *JACC Cardiovasc Imaging.* (2008) 1:434–5. doi: 10.1016/j.jcmg.2008.04.008
30. Taegtmeyer H, Beauloye C, Harmancey R, Hue L. Insulin resistance protects the heart from fuel overload in dysregulated metabolic states. *Am J Physiol Heart Circ Physiol.* (2013) 305:H1693–7. doi: 10.1152/ajpheart.00854.2012
31. Algahim MF, Sen S, Taegtmeyer H. Bariatric surgery to unload the stressed heart: a metabolic hypothesis. *Am J Physiol Heart Circ Physiol.* (2012) 302:H1539–45. doi: 10.1152/ajpheart.00626.2011
32. Doumouras AG, Wong JA, Paterson JM, Lee Y, Sivapathasundaram B, Tarride JE, et al. Bariatric surgery and cardiovascular outcomes in patients with obesity and cardiovascular disease: a population-based retrospective cohort study. *Circulation.* (2021) 143:1468–80. doi: 10.1161/CIRCULATIONAHA.120.052386
33. Schauer PR, Nissen SE. After 70 years, metabolic surgery has earned a cardiovascular outcome trial. *Circulation.* (2021) 143:1481–3. doi: 10.1161/CIRCULATIONAHA.120.051752
34. Carlsson LMS, Sjöholm K, Jacobson P, Andersson-Assarsson JC, Svensson PA, Taube M, et al. Life expectancy after bariatric surgery in the Swedish obese subjects study. *N Engl J Med.* (2020) 383:1535–43. doi: 10.1056/NEJMoa2002449

Conflict of Interest: The authors declare that the research was conducted in the absence of any commercial or financial relationships that could be construed as a potential conflict of interest.

frontiers in Cardiovascular Medicine

ORIGINAL RESEARCH
published: 23 September 2021
doi: 10.3389/fcvm.2021.734388

Mitochondrial Respiration Defects in Single-Ventricle Congenital Heart Disease

Xinxiu Xu[1†], Jiuann-Huey Ivy Lin[1,2†], Abha S. Bais[1], Michael John Reynolds[3], Tuantuan Tan[1], George C. Gabriel[1], Zoie Kondos[1], Xiaoqin Liu[1], Sruti S. Shiva[3,4] and Cecilia W. Lo[1]*

[1] Department of Developmental Biology, School of Medicine, University of Pittsburgh, Pittsburgh, PA, United States, [2] Department of Critical Care Medicine, School of Medicine, University of Pittsburgh, Pittsburgh, PA, United States, [3] School of Medicine, Pittsburgh Heart, Lung, Vascular Medicine Institute, University of Pittsburgh, Pittsburgh, PA, United States, [4] Department of Pharmacology and Chemical Biology, School of Medicine, University of Pittsburgh, Pittsburgh, PA, United States

OPEN ACCESS

Edited by:
Zhong Wang, University of Michigan, United States

Reviewed by:
Ming Sing Si, University of Michigan, United States
Jose Francisco Islas, Autonomous University of Nuevo León, Mexico

***Correspondence:**
Cecilia W. Lo
cel36@pitt.edu

[†]These authors have contributed equally to this work

Specialty section:
This article was submitted to Cardiovascular Metabolism, a section of the journal Frontiers in Cardiovascular Medicine

Received: *01 July 2021*
Accepted: *16 August 2021*
Published: *23 September 2021*

Citation:
Xu X, Lin J-HI, Bais AS, Reynolds MJ, Tan T, Gabriel GC, Kondos Z, Liu X, Shiva SS and Lo CW (2021) Mitochondrial Respiration Defects in Single-Ventricle Congenital Heart Disease. Front. Cardiovasc. Med. 8:734388. doi: 10.3389/fcvm.2021.734388

Background: Congenital heart disease (CHD) with single-ventricle (SV) physiology is now survivable with a three-stage surgical course ending with Fontan palliation. However, 10-year transplant-free survival remains at 39–50%, with ventricular dysfunction progressing to heart failure (HF) being a common sequela. For SV-CHD patients who develop HF, undergoing the surgical course would not be helpful and could even be detrimental. As HF risk cannot be predicted and metabolic defects have been observed in *Ohia* SV-CHD mice, we hypothesized that respiratory defects in peripheral blood mononuclear cells (PBMCs) may allow HF risk stratification in SV-CHD.

Methods: SV-CHD ($n = 20$), biventricular CHD (BV-CHD; $n = 16$), or healthy control subjects ($n = 22$) were recruited, and PBMC oxygen consumption rate (OCR) was measured using the Seahorse Analyzer. Respiration was similarly measured in *Ohia* mouse heart tissue.

Results: Post-Fontan SV-CHD patients with HF showed higher maximal respiratory capacity ($p = 0.004$) and respiratory reserve ($p < 0.0001$), parameters important for cell stress adaptation, while the opposite was found for those without HF (reserve $p = 0.037$; maximal $p = 0.05$). This was observed in comparison to BV-CHD or healthy controls. However, respiration did not differ between SV patients pre- and post-Fontan or between pre- or post-Fontan SV-CHD patients and BV-CHD. Reminiscent of these findings, heart tissue from *Ohia* mice with SV-CHD also showed higher OCR, while those without CHD showed lower OCR.

Conclusion: Elevated mitochondrial respiration in PBMCs is correlated with HF in post-Fontan SV-CHD, suggesting that PBMC respiration may have utility for prognosticating HF risk in SV-CHD. Whether elevated respiration may reflect maladaptation to altered hemodynamics in SV-CHD warrants further investigation.

Keywords: oxygen consumption rate (OCR), single ventricle congenital heart disease (SV-CHD), peripheral blood mononuclear cells (PBMC), heart failure, Fontan, reserve OCR, maximal respiratory capacity, hypoplastic left heart syndrome (HLHS)

INTRODUCTION

Hypoplastic left heart syndrome (HLHS) is a critical congenital heart disease (CHD) characterized by hypoplasia of left-sided structures of the heart, including the ascending aorta, left ventricle (LV), and aortic and mitral valves. As there is only a single pumping chamber in HLHS [the right ventricle (RV)], it is a type of single-ventricle (SV) CHD. While HLHS and other SV-CHDs were previously uniformly fatal, it is now survivable with a three-stage surgical palliation that includes the final Fontan surgery. Together, this creates an SV circulation with venous blood routed directly to the lungs by gravity, while the single pumping chamber (LV or RV) serves as the systemic chamber pumping blood to the rest of the body (1).

While such SV physiology (2) allows most SV-CHD patients to survive, 10-year transplant-free survival for HLHS patients stands at only 39–50%. This high morbidity/mortality is largely due to ventricular dysfunction and heart failure (HF) (3) for which heart transplantation remains the ultimate therapy. Therapies developed for adult HF have been ineffective for SV-CHD (3). As it is not possible to predict which SV-CHD patients will have HF, it has not been possible to prioritize SV-CHD patients for early heart transplantation. For SV-CHD patients who will develop HF, undergoing the palliative surgical course would not be helpful and could even be detrimental.

Our previous study of a mouse model of HLHS (4) uncovered mitochondrial abnormalities that suggested metabolic disturbance contributing to the pathogenesis of HLHS. Consistent with this, transcriptome profiling of the HLHS mouse heart tissue yielded metabolic pathways among the top pathways impacted (4). Supporting clinical evidence has come from a recent study showing that serum isolated from SV-CHD patients can induce pathological changes in neonatal rat cardiomyocytes (5). Transcriptome profiling of the treated cardiomyocytes showed that 23% of the genes impacted were related to metabolic processes (5). Another study of adults at early stages of HF showed that their peripheral blood mononuclear cells (PBMCs) had mitochondrial respiration defects in association with inflammation and oxidative stress (6).

Based on these previous findings, in the present pilot study, we investigated the hypothesis that respiratory parameters in PBMC may have prognostic value for assessing HF risk in SV-CHD. For this study, we recruited SV-CHD patients pre- vs. post-Fontan completion and also age-matched BV-CHD patients and control subjects.

METHODS

Patient Recruitment

CHD patients and healthy control subjects were recruited from the Children's Hospital of Pittsburgh of University of Pittsburgh Medical Center (UPMC) under a human study protocol approved by the University of Pittsburgh Institutional Review Board. Informed consent was obtained, and for infants and minors, informed consent was obtained from the parent or legal guardian. Recruitment criteria comprised subjects with complex SV-CHD or BV-CHD. For SV-CHD, this included HLHS, critical aortic stenosis, pulmonary atresia with intact ventricular septum, double outlet RV with mitral atresia, and unbalanced atrioventricular septal defect with total or partial anomalous pulmonary venous return, while BV-CHD included Tetralogy of Fallot, transposition of the great arteries, Ebstein's anomaly, aortic arch hypoplasia, aortic stenosis, ventricular septal defect, and pulmonary stenosis. Three pediatric dilated cardiomyopathy (DCM) patients with HF were recruited as BV-HF disease controls, two having received a heart transplant and the third listed for transplant and having received an interim ventricular assist device. Patient demographics are summarized in **Table 1**, **Supplementary Spreadsheet S1**.

Peripheral Blood Mononuclear Cell Isolation and Measurement of Oxygen Consumption Rate

Whole blood was used to recover fresh PBMCs using standard protocol with Ficoll-Paque PLUS from Pharmacia Biotech (or a similar separation medium). After centrifugation, PBMCs at the interphase were collected, washed twice, and resuspended in RPMI 1640 with 10% fetal bovine serum, and the cells were counted. For measurement of oxygen consumption rate (OCR) and extracellular acidification rate (ECAR), 20,000 PBMCs were seeded into each well of a Seahorse XFe96 plate. OCR and ECAR were determined using the Seahorse XF Cell Mito Stress Kit (Agilent). Basal respiration was measured in unstimulated cells. Afterward, oligomycin (1 μM) was added to quantify respiration coupled to ATP production and proton leak followed by carbonyl cyanide-4-(trifluoromethoxy)-phenylhydrazone (FCCP; 1 μM) injection to assess maximal cellular respiration (respiratory capacity). Finally, antimycin A (1 μM) and rotenone (1 μM) were used to assess non-mitochondrial respiration. For mouse heart tissue, OCR was obtained for the quantification of basal respiration. For this analysis, 2-mm^2 pieces of heart tissue were plated into individual wells of a Seahorse XF24 microplate, and OCR was measured using the same Seahorse XF Cell Mito Stress Kit without stimulation during two cycles of measurement.

RESULTS

CHD patients with BV-CHD ($n = 16$) or SV-CHD ($n = 20$) and 22 healthy controls without CHD were recruited with informed consent, and blood samples were obtained for PBMC isolation. Among the 20 SV-CHD patients, 16 had HLHS with dominant/systemic RV, and four had dominant/systemic LV (**Table 1**). Twelve of the SV patients were <1 year old, while eight were ≥10 years old, all having completed the Fontan surgery (**Table 1**). Of the BV patients, five were ≥10 years old, and 11 were <1 year old. All the control subjects were ≥10 years old (**Table 1**).

All of the BV-CHD ($n = 16$) patients and 15 of the 20 SV-CHD patients survived heart transplant-free and were classified as having a favorable clinical outcome without HF. Among the SV patients, five HLHS patients had an unfavorable cardiac outcome related to HF, one having died from acute HF, and four exhibiting cardiac death. The latter was indicated by having had a heart

TABLE 1 | Demographic and clinical outcome summary.

	≥10 years of age				≤1 year of age		
	Control	**BV**	**SV non-HF**	**SV HF**	**BV**	**SV non-HF**	**SV HF**
No. subjects	22	5	4	4	**11**	11	1
Male (%)	9 (59%)	2 (40%)	4 (100%)	3(75%)	8 (73%)	4 (36.3%)	1 (100%)
Mean age (years) [@]	29 ± 1.4	25.8 ± 8.79	23.75 ± 10.5	17.3 ± 4.92	0.28 ± 0.34	0.38 ± 0.31	0.096
Caucasian		4 (80%)	4 (100%)	2 (50%)	8 (72.7%)	8 (72.7%)	1 (100%)
African American		1 (20%)	0	2 (50%)	3 (27.3%)	3 (27.3%)	
Mean BMI (kg/m^2)		25.2 ± 6.06	25.7 ± 8.09	20.9 ± 2.56	13.9 ± 2.36	15.3 ± 3.82	12.5
Age of Fontan		NA	2.75 ± 0.5	5.5 ± 3.11	NA	NA	NA
Mean Fontan Years		NA	21 ± 10.1	11.8 ± 4.99	NA	NA	NA
$SpO_2^{\$}$		98.8 ± 0.84	91.5 ± 7.14	92 ± 4.6	98.2 ± 2.7	82.54 ± 6	83
NYHA Class[#*]		1.6 ± 0.55	1.25 ± 0.5	2.75 ± 0.5	1.63 ± 0.9	2.18 ± 0.87	3
Systemic ventricle							
Dominant RV			3 (75%)	4 (100%)		8 (72.7%)	1 (100%)
Dominant LV			1 (25%)	0		3 (27.3%)	

[@]*Mean age (years): ≥10 years old, Control vs. SV HF, p = 0.0003.*

[$]*$SpO_2$: BV vs. SV-HF ≥10 years old, p = 0.014; BV vs. SV non-HF ≤1-year old, p < 0.0001.*

[#]*NYHA (26) Functional Classification was used to classify patients' heart failure.*

**NYHA: BV vs. SV non-HF ≥10 years old, p = 0.36; BV vs. SV HF, ≥10 years old, p = 0.014; SV non-HF vs. SV HF, ≥10 years old, p = 0.005.*

BMI, body mass index; BV, biventricular; HF, heart failure; LV, left ventricle; NYHA, New York Heart Association; RV, right ventricle; SV, single ventricle.

transplant ($n = 3$) or having been listed for heart transplant for decompensated HF ($n = 1$). Using the New York Heart Association (NYHA) HF classification, the four HLHS patients ≥10 years old with HF had significantly higher or worse NYHA scores than either the BV-CHD patients ($p = 0.014$) or the SV-CHD patients with favorable outcome ($p = 0.005$) (**Table 1**).

Mitochondrial Respiration in Peripheral Blood Mononuclear Cells of SV-CHD and BV-CHD Patients

PBMCs isolated from the blood of patients and controls were analyzed for OCR using the Seahorse Analyzer. Measurements of the different mitochondrial respiratory parameters were obtained by assessing the changes in OCR with the addition of different inhibitors of respiration. No significant difference in OCR was observed among the control subjects stratified by age, although a trend for lower OCR was observed in patients >40 years old (**Supplementary Figure S1A**). This is consistent with a previous observation of lower mitochondrial respiration in platelets from older subjects (7). Hence, we excluded OCR measurements from subjects >40 years of age and used only the 22 control subjects between 10 and 40 years of age (**Supplementary Figure S1A**).

Comparisons between the SV-CHD and BV-CHD patients showed no difference in mitochondrial respiration (**Figure 1A**, **Supplementary Figure S1B**). A similar comparison of the SV-HLHS vs. BV-CHD patients also showed no difference (**Figure 1B**, **Supplementary Figure S1C**). We further examined the BV and SV patients grouped by age, either <1 year old or >10 years old (**Supplementary Table S1**). This also showed no difference for any mitochondrial respiratory parameter (**Figures 1C,D**). For individuals ≥10 years old, no difference was observed for any of the CHD groups when compared with healthy controls (**Figure 1D**). We further examined basal glycolysis with the measurement of the ECAR, and this also showed no difference between the SV-CHD and BV-CHD patients (**Supplementary Figure S1D**).

Respiration in Pre- and Post-fontan SV-CHD Patients

Comparison of the pre-Fontan (<1 year old) vs. post-Fontan (>10 years old) SV or HLHS patients showed no difference in mitochondrial respiration (**Figures 2A,B**). ECAR data also showed no difference (**Supplementary Figure S1E**). We further investigated the impact of HF on mitochondrial respiration in the pre- vs. post-Fontan patients. Among the 12 pre-Fontan SV patients, only one had an unfavorable outcome with sudden cardiac death. This subject showed higher respiratory maximum and reserve when compared to the SV or BV patients without HF (**Figure 2C**). As this patient had HLHS, comparison was also made to the eight non-failing pre-Fontan HLHS patients. This also showed higher maximal respiration and reserve capacity in the pre-Fontan HLHS patient with HF (**Figure 2D**). For one HLHS patient, we obtained PBMCs for OCR measurements before and after heart transplant. No change was observed in any respiratory parameter after heart transplantation, suggesting that patient intrinsic factors and not hemodynamic factors underlie the respiratory dysfunction in this HLHS patient (**Supplementary Figure S1F**).

Respiration and Clinical Outcome in Post-fontan HLHS Patients

Of the eight SV-CHD patients with Fontan completion, four had HF. These patients showed a significantly higher OCR

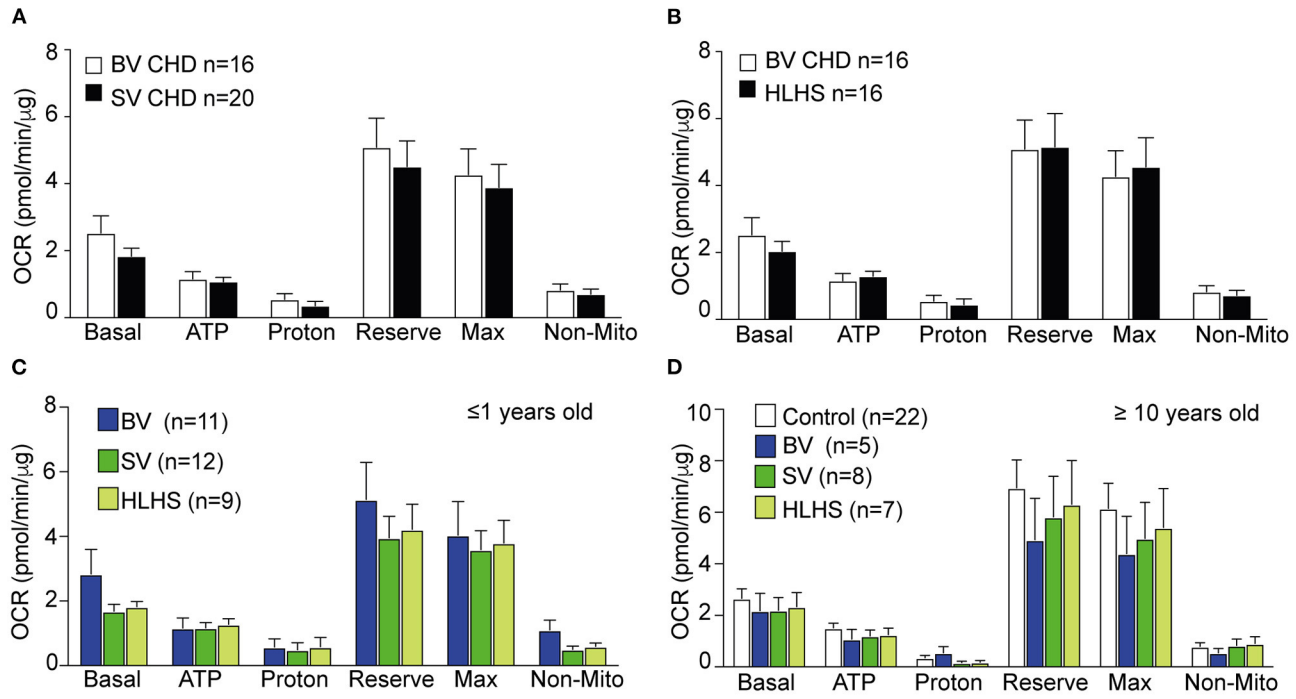

FIGURE 1 | Comparison of mitochondrial respiration in the PBMCs of CHD patients stratified by lesion type, age, and Fontan status. **(A,B)** There was no difference in any of the respiratory parameters in OCR of PBMCs of BV-CHD vs. SV-CHD and between BV-CHD and HLHS. **(C)** No significant difference was observed in the parameters of mitochondrial respiration among BV-CHD, SV-CHD, and HLHS patients ≤1 year old. **(D)** No significant difference in mitochondrial respiration was observed among control, BV-CHD, SV-CHD, and HLHS subjects ≥10 years old. Bar graphs show mean ± SEM with one-way ANOVA. Subjects' numbers were indicated in the graphs. BV, biventricular; CHD, congenital heart disease; HLHS, hypoplastic left heart syndrome; OCR, oxygen consumption rate; PBMC, peripheral blood mononuclear cell; SV, single ventricle.

when compared to those of SV-CHD patients without HF, BV-CHD patients, or healthy controls (**Figures 2E,F**). These changes were observed in two related respiratory parameters, respiratory maximum and respiratory reserve. In contrast, SV-CHD patients without HF showed a significantly lower OCR when compared to SV-CHD patients with HF, BV-CHD patients, or healthy controls (**Figures 2E,F**).

Given that SV-CHD with systemic RV is known to have worse clinical outcome than SV-CHD patients with systemic LV (8–10), we reanalyzed the data focusing on only SV patients with HLHS (systemic RV) either with or without HF. This analysis yielded similar findings with significantly higher respiratory maximum and reserve observed in the post-Fontan HLHS patients with HF, while the opposite was observed in HLHS patients without HF (**Figures 2G,H**). We also examined basal glycolysis with the measurement of ECAR, but no significant difference was found between post-Fontan SV and HLHS patients either with or without HF when compared to BV-CHD patients or control subjects (**Supplementary Figures S2E,F**).

To further investigate whether the increase in respiration in the SV-CHD patients with HF may be attributable to HF in general, we recruited three pediatric DCM patients with HF and obtained PBMCs for a similar analysis of mitochondrial respiration. However, no significant difference was observed in the mitochondrial respiration of the DCM patients with HF vs. the BV-CHD patients without HF (**Supplementary Figure S2G**). We also examined medication use among the SV patients with and without HF and observed no correlation between inotropic infusion, brain natriuretic peptide (BNP) levels, or other medication use and changes in mitochondrial respiration. Similarly, no hemodynamic parameters were correlated with changes in mitochondrial respiration in the SV-CHD patients (**Supplementary Spreadsheet S1**).

Mitochondrial Respiration in Heart Tissue of *Ohia* Mutant Mice

HLHS mutants from the *Ohia* mouse line were previously shown to suffer early HF with severe pericardial effusion (4) and prenatal/neonatal lethality. This was associated with mitochondria abnormalities that suggested metabolic dysfunction (4). Transcriptome profiling with RNA sequencing (RNA-seq) analysis of the HLHS heart tissue (4) recovered many metabolic pathways in the hypoplastic LV, and a few of the same metabolic pathways were also recovered in the RV but with lower fold change (**Figures 3A,B**, **Supplementary Figures S3A,B**).

Given that CHD showed incomplete penetrance in the *Ohia* mutant mice, this allowed us to further assess respiration in mice with the same HLHS-causing mutations but either with or without CHD/HLHS. Measurement of basal respiration in the heart tissue of the *Ohia* mutant mice using the Seahorse Analyzer

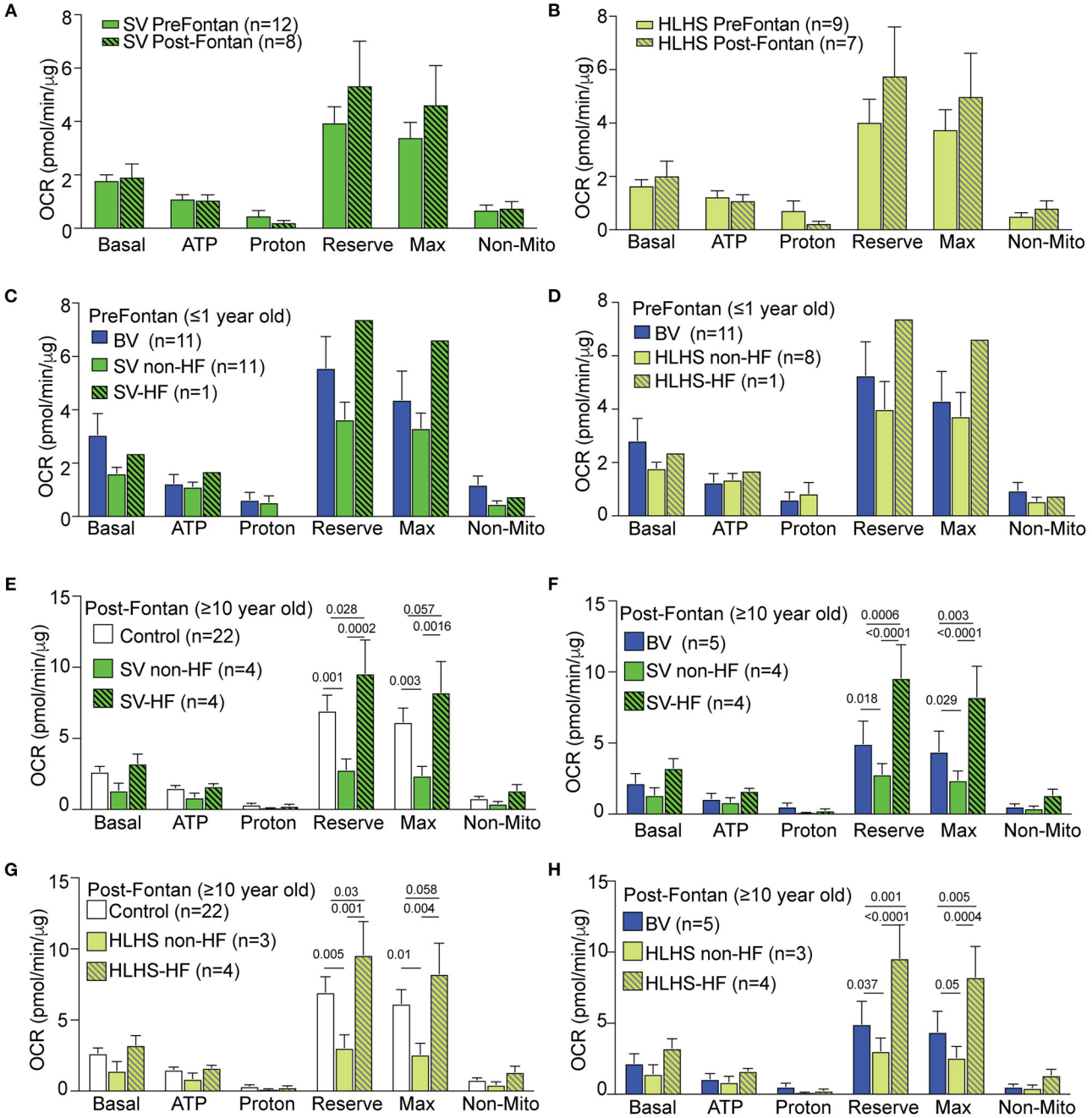

FIGURE 2 | Mitochondrial respiration in SV-CHD patients stratified by Fontan palliation and HF status. **(A,B)** No significant difference was observed for respiration in pre- vs. post-Fontan SV and HLHS patient groups. **(C,D)** Mitochondrial respiration in the PMBCs of pre-Fontan SV **(C)** or HLHS patients **(D)** ≤1 year old as compared to age-matched BV patients. **(E,F)** Mitochondrial respiration in the PBMCs of SV-CHD patients ≥10 years old with and without HF vs. age-matched controls **(E)** and BV-CHD patients **(F)**. **(G,H)** Mitochondrial respiration in the PBMCs of HLHS-CHD patients ≥10 years old with and without HF vs. age-matched controls **(G)** and BV-CHD patients **(H)**. Mean ± SEM with one-way ANOVA test. Subjects' numbers are indicated in the legend for the graphs. BV, biventricular; CHD, congenital heart disease; HF, heart failure; HLHS, hypoplastic left heart syndrome; OCR, oxygen consumption rate; PBMC, peripheral blood mononuclear cell; SV, single ventricle.

showed elevated basal OCR in the LV tissue of HLHS mutants (**Figure 3C**), a result reminiscent of the elevated OCR observed in the PBMCs of HLHS/SV patients with HF. In contrast, the LV tissue of *Ohia* mice without CHD showed markedly lower basal OCR, a result that seems to parallel the lower mitochondrial respiration in the post-Fontan HLHS patients without HF (**Figure 3E**). However, a similar analysis of the RV tissue from *Ohia* mutant mice, whether with HLHS or without CHD, showed

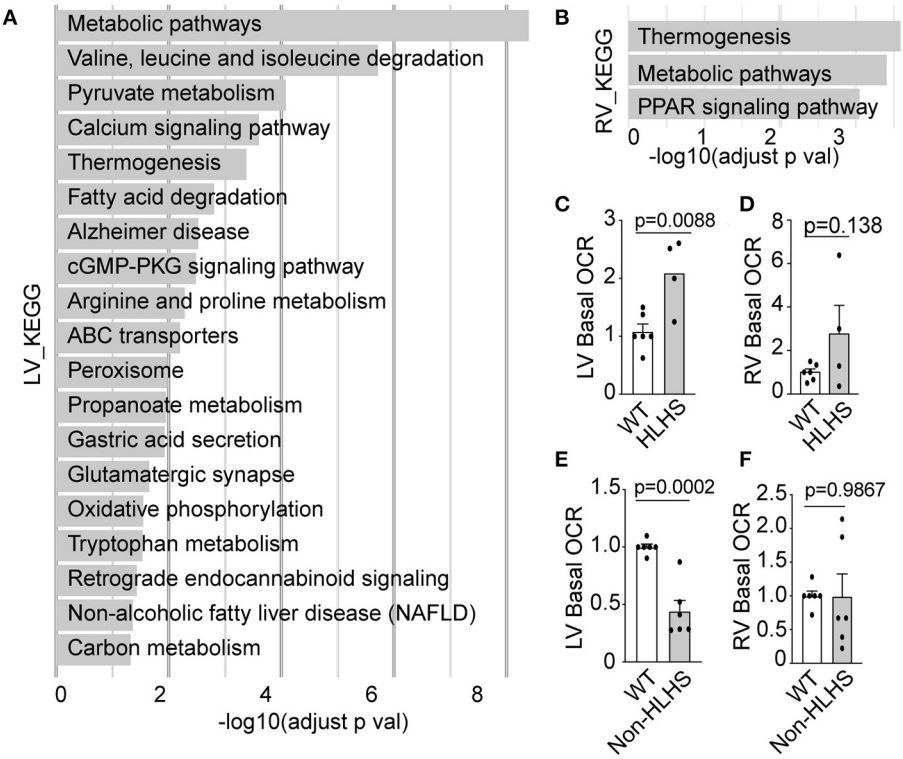

FIGURE 3 | Mitochondrial respiration in *Ohia* mutant mouse heart. **(A,B)** Pathways recovered among downregulated genes at FDR 0.05 from RNA-seq analysis of HLHS-LV **(A)** or RV **(B)** tissue compared to that of WT littermate control. Pathway enrichment analysis was performed using KEGG pathway analysis with g: Profiler and FDR < 0.05. **(C–F)** Basal OCR in LV and RV heart tissue from E14.5–16.5 *Ohia* line with *Sap130/Pcdha9* mutations known to cause HLHS. This analysis was obtained using the Seahorse Analyzer. **(C,D)** Data obtained from litters comprising WT ($n = 7$) and HLHS ($n = 4$). **(E,F)** Quantitative analysis of five Sap130/Pcdha9 mutants with normal cardiac anatomy without HLHS **(E,F)** and six WT controls. Bar graphs show mean ± SEM with Student's *t*-test. Each dot represents one mouse embryo heart tissue. FDR, false discovery rate; HLHS, hypoplastic left heart syndrome; KEGG, Kyoto Encyclopedia of Genes and Genomes; LV, left ventricle; OCR, oxygen consumption rate; PPAR, peroxisome proliferator-activated receptor; RNA-seq, RNA sequencing; RV, right ventricle; WT, wild-type.

no significant change in respiration (**Figures 3D,F**). These observations point to an intrinsic mitochondrial respiration defect arising from the genetic predisposition for HLHS. Western immunoblotting showed that the respiration perturbations were not associated with altered expression of the electron transport chain (ETC) components (**Supplementary Figures S3C,D**).

DISCUSSION

Our study showed that mitochondrial respiration in PBMCs is significantly elevated in post-Fontan SV-CHD patients with poor cardiac outcome associated with HF, operationally defined as death or cardiac death with heart transplant or listing for heart transplant. This operational definition is supported by the significantly higher NYHA classification score for HF observed for HLHS/SV-CHD patients ≥10 years old identified with HF. Thus, we found that post-Fontan HLHS patients with HF exhibited higher maximal OCR and respiratory reserve, respiratory parameters often elevated in response to cell stress. In contrast, post-Fontan HLHS patients without HF showed lower maximal and reserve respiratory capacity. These findings are consistent with observations in the *Ohia* mutant mice, which also showed opposing changes in basal respiration in mutant mice with or without CHD/HLHS.

Heart tissue from *Ohia* mutant mice with HLHS showed elevated basal respiration. This is also associated with HF, shown by *in utero* echocardiography observation of poor cardiac contractility, low cardiac output, and severe pericardial effusion in the *Ohia* HLHS fetal mice (4). In contrast, genetically identical *Ohia* mutants without CHD showed reduced basal respiration but with entirely normal cardiac function. Together, these findings suggest intrinsic metabolic defects in patients with HLHS with a shared genetic etiology with their structural heart defects, a possibility supported by other studies showing mitochondrial metabolism (11) playing an important role in heart development and the regulation of cardiomyocyte differentiation (12).

Many adverse sequelae in SV-CHD patients have been attributed to the Fontan circulation with its non-pulsatile flow in the venous system (13), such as in promoting venous hypertension and hepatic congestion. However, the Fontan circulation is unlikely to account for the metabolic perturbations, as post-Fontan patients can have either hyper-elevated or reduced mitochondrial respiration. In one HLHS

patient, a significant increase in mitochondrial respiration was observed before and after heart transplantation, indicating that the metabolic defects in this patient is likely intrinsic and could cause oxidative stress leading to apoptosis and HF. Supporting this possibility, induced pluripotent stem cell-derived cardiomyocytes from HLHS patients with early HF were found to have a failed antioxidant response that could exacerbate metabolic defects causing redox stress (14, 15).

While defects in mitochondrial respiration in PBMCs have been reported in patients with HF, such as in the setting of cardiomyopathies (16), this is typically associated with reduced respiratory capacity, not the hyper-elevated mitochondrial respiration observed in the post-Fontan HLHS patients with HF. Our analysis of DCM-HF patients showed no change in mitochondrial respiration when compared to that of the BV-CHD patients without HF. This would suggest that mechanistic differences may explain why existing therapies for BV-HF have been ineffective for SV-CHD. Thus, hyper-elevated mitochondrial respiration may cause increased production of reactive oxygen species (ROS) with oxidative stress ensuing and triggering apoptosis that can predispose to HF in post-Fontan patients. In contrast, reduced mitochondrial respiration in the post-Fontan SV patients without HF may keep ROS levels in check and provide cardioprotection.

The elevated maximal respiration and reserve respiratory capacity in HLHS patients with HF is not likely to be an adaptive response to the SV physiology or Fontan circulation, since only SV-CHD patients with HF showed elevated respiration. As cells usually function at only a fraction of their maximal respiratory capacity and with a correspondingly large reserve capacity (17), the elevation of these two parameters in the SV-CHD patients with HF might reflect an adaptive response to cell stress related to intrinsic mitochondrial defects. That this could be genetically encoded by the same mutations causing HLHS is suggested by observations in the *Ohia* mouse model.

While our patient assessments were conducted using PBMCs, the analysis of the *Ohia* mouse model entailed assaying OCR in heart tissue. The use of PBMCs assumes a systemic defect in mitochondrial respiration that may broadly impact a variety of different cells and tissues. This could include platelets that are cell fragments derived from megakaryocytes. Interestingly, an increase in mitochondrial reserve and maximal capacity has also been reported in the platelets of adults with pulmonary hypertension (18), a common comorbidity in CHD patients. We noted a previous study that showed that serum from SV-CHD patients (5) can cause pathological remodeling with the reactivation of fetal gene programs in neonatal rat cardiomyocytes. The expression of HF markers, such as BNP (19) and atrial natriuretic factor (20) were observed, with transcriptome profiling showing metabolic process as one of the top enriched pathways. Together, these findings suggest systemic effects impacting mitochondrial respiration in SV-CHD patients. Further studies are warranted to verify the potential utility of a simple blood test with measurement of respiration in PBMCs as a biomarker for HF risk assessment in SV-CHD patients. The possibility that platelets might also be employed for such assessments should be further investigated.

Limitations

There are various limitations to our study, one being the complicated clinical course of older SV-CHD patients that could confound the interpretation of metabolic defects in post-Fontan patients, such as morbidity/mortality associated with protein-losing enteropathy, plastic bronchitis, or liver cirrhosis (21–24). The relatively small number of SV-CHD patients included in this study is also a limitation, largely a reflection of SV-CHD being relatively rare, comprising only 1.25% of infants with CHD (25). Due to the small cohort size, we were unable to assess the differences in mitochondrial respiration between systemic RV and systemic LV SV-CHD. Thus, a multicenter study will be needed to verify and extend the findings from this pilot study with longitudinal assessments of PBMC respiration in SV-CHD patients with dominant RV vs. LV and before and after Fontan surgery. Yet another limitation is the fact that mitochondrial respiration was investigated only in the PBMCs but not in human heart tissue. Heart tissue from patients is difficult to procure, but this can be obtained from patients undergoing heart transplant. However, changes detected in explanted heart tissue could be secondary to the HF. The lack of control pediatric PBMC measurements precluded the analysis of the CHD subjects $\leq$1 year of age. This limitation is partially addressed by the inclusion of age-matched pediatric BV-CHD subjects as disease controls. Finally, while our data showed a significant association between alterations in mitochondrial respiration in the PBMCs and HF risk in SV-CHD patients, establishing a causal link will require further mechanistic studies in the future. Additional studies are also needed to investigate whether PBMC respiration may be altered in other types of HF not related to CHD.

DATA AVAILABILITY STATEMENT

The datasets presented in this study can be found in online repositories. The names of the repository/repositories and accession number(s) can be found at: NCBI [accession: GSE77799].

ETHICS STATEMENT

The studies involving human participants were reviewed and approved by University of Pittsburgh Institutional Review Board. Written informed consent to participate in this study was provided by the participants' legal guardian/next of kin. The animal study was reviewed and approved by University of Pittsburgh Institutional Animal Care and Use Committee. Written informed consent was obtained from the individual(s), and minor(s)' legal guardian/next of kin, for the publication of any potentially identifiable images or data included in this article.

AUTHOR CONTRIBUTIONS

CL, XX, and J-HL contributed to the study design. CL and J-HL contributed to the recruitment of subjects and human blood sample collection. XX contributed to the PBMC isolation. XX, MR, SS, and ZK contributed to the Seahorse measurement.

TT, XL, and XX contributed to the mouse fetal ultrasound imaging and mouse phenotyping. GG and XX contributed to the mouse embryo dissection. AB and XX contributed to the mouse RNA-seq and data analysis. XX contributed to the statistics. CL, XX, J-HL, and SS contributed to the manuscript preparation. All authors contributed to the article and approved the submitted version.

FUNDING

This work was supported by NIH grants HL132024 and HL142788 (CL), UPMC Fellows Grant (XX), and American Heart Association/ Children's Heart Foundation postdoctoral fellowship (XX) and support from Department of Critical Care Medicine (J-HL).

ACKNOWLEDGMENTS

We are truly indebted to all family members for their research participation and contribution to this project.

SUPPLEMENTARY MATERIAL

The Supplementary Material for this article can be found online at: https://www.frontiersin.org/articles/10.3389/fcvm.2021.734388/full#supplementary-material

REFERENCES

1. Delmo Walter EM, Hubler M, Alexi-Meskishvili V, Miera O, Weng Y, Loforte A, et al. Staged surgical palliation in hypoplastic left heart syndrome and its variants. *J Card Surg.* (2009) 24:383–91. doi: 10.1111/j.1540-8191.2008.00759.x
2. Ohye RG, Schranz D, D'Udekem Y. Current therapy for hypoplastic left heart syndrome and related single ventricle lesions. *Circulation.* (2016) 134:1265–79. doi: 10.1161/CIRCULATIONAHA.116.022816
3. Garcia AM, Beatty JT, Nakano SJ. Heart failure in single right ventricle congenital heart disease: physiological and molecular considerations. *Am J Physiol Heart Circ Physiol.* (2020) 318:H947–65. doi: 10.1152/ajpheart.00518.2019
4. Liu X, Yagi H, Saeed S, Bais AS, Gabriel GC, Chen Z, et al. The complex genetics of hypoplastic left heart syndrome. *Nat Genet.* (2017) 49:1152–9. doi: 10.1038/ng.3870
5. Garcia AM, Nakano SJ, Karimpour-Fard A, Nunley K, Blain-Nelson P, Stafford NM, et al. Phosphodiesterase-5 is elevated in failing single ventricle myocardium and affects cardiomyocyte remodeling *in vitro*. *Circ Heart Fail.* (2018) 11:e004571. doi: 10.1161/CIRCHEARTFAILURE.117.004571
6. Li P, Wang B, Sun F, Li Y, Li Q, Lang H, et al. Mitochondrial respiratory dysfunctions of blood mononuclear cells link with cardiac disturbance in patients with early-stage heart failure. *Sci Rep.* (2015) 5:10229. doi: 10.1038/srep10229
7. Braganza A, Corey CG, Santanasto AJ, Distefano G, Coen PM, Glynn NW, et al. Platelet bioenergetics correlate with muscle energetics and are altered in older adults. *JCI Insight.* (2019) 4:e128248. doi: 10.1172/jci.insight.128248
8. Hinton RB, Ware SM. Heart failure in pediatric patients with congenital heart disease. *Circ Res.* (2017) 120:978–94. doi: 10.1161/CIRCRESAHA.116.308996
9. Lamour JM, Kanter KR, Naftel DC, Chrisant MR, Morrow WR, Clemson BS, et al. Pediatric Heart Transplant, the effect of age, diagnosis, and previous surgery in children and adults undergoing heart transplantation for congenital heart disease. *J Am Coll Cardiol.* (2009) 54:160–5. doi: 10.1016/j.jacc.2009.04.020
10. Adams PS, Zahid M, Khalifa O, Feingold B, Lo CW. Low nasal NO in congenital heart disease with systemic right ventricle and postcardiac transplantation. *J Am Heart Assoc.* (2017) 6:e007447. doi: 10.1161/JAHA.117.007447
11. Nakano H, Minami I, Braas D, Pappoe H, Wu X, Sagadevan A, et al. Glucose inhibits cardiac muscle maturation through nucleotide biosynthesis. *Elife.* (2017) 6:e29330. doi: 10.7554/eLife.29330
12. Hom JR, Quintanilla RA, Hoffman DL, de Mesy Bentley KL, Molkentin JD, Sheu SS, et al. The permeability transition pore controls cardiac mitochondrial maturation and myocyte differentiation. *Dev Cell.* (2011) 21:469–78. doi: 10.1016/j.devcel.2011.08.008
13. Rychik J, Goldberg DJ. Late consequences of the Fontan operation. *Circulation.* (2014) 130:1525–8. doi: 10.1161/CIRCULATIONAHA.114.005341
14. Xu X, Jin K, Bais AS, Zhu W, Yagi H, Feinstein TN, et al. iPSC modeling shows uncompensated mitochondrial mediated oxidative stress underlies early heart failure in hypoplastic left heart syndrome. *bioRxiv [Preprint].* (2021). doi: 10.1101/2021.05.09.443165
15. Xu X, Tan T, Ivy Lin J-H, Adams P, Liu X, Feinstein Timothy N, et al. Intrinsic cardiomyocyte mitochondrial defects underlie cardiac dysfunction and heart failure risk associated with hypoplastic left heart syndrome. *Circulation.* (2018) 138A:15746.
16. Zhou B, Wang DD, Qiu Y, Airhart S, Liu Y, Stempien-Otero A, et al. Boosting NAD level suppresses inflammatory activation of PBMCs in heart failure. *J Clin Invest.* (2020) 130:6054–63. doi: 10.1172/JCI138538
17. Pfleger J, He M, Abdellatif M. Mitochondrial complex II is a source of the reserve respiratory capacity that is regulated by metabolic sensors and promotes cell survival. *Cell Death Dis.* (2015) 6:e1835. doi: 10.1038/cddis.2015.202
18. Nguyen QL, Corey C, White P, Watson A, Gladwin MT, Simon MA, et al. Platelets from pulmonary hypertension patients show increased mitochondrial reserve capacity. *JCI Insight.* (2017) 2:e91415. doi: 10.1172/jci.insight.91415
19. Shah A, Feraco AM, Harmon C, Tacy T, Fineman JR, Bernstein HS. Usefulness of various plasma biomarkers for diagnosis of heart failure in children with single ventricle physiology. *Am J Cardiol.* (2009) 104:1280–4. doi: 10.1016/j.amjcard.2009.06.046
20. Alkan T, Sarioglu A, Samanli UB, Sarioglu T, Akcevin A, Turkoglu H, et al. Atrial natriuretic peptide: could it be a marker for postoperative recurrent effusions after Fontan circulation in complex congenital heart defects? *ASAIO J.* (2006) 52:543–8. doi: 10.1097/01.mat.0000235275.65027.1d
21. Alsaied T, Bokma JP, Engel ME, Kuijpers JM, Hanke SP, Zuhlke L, et al. Factors associated with long-term mortality after Fontan procedures: a systematic review. *Heart.* (2017) 103:104–10. doi: 10.1136/heartjnl-2016-310108
22. Byrne RD, Weingarten AJ, Clark DE, Huang S, Perri RE, Scanga AE, et al. More than the heart: hepatic, renal, and cardiac dysfunction in adult Fontan patients. *Congenit Heart Dis.* (2019) 14:765–71. doi: 10.1111/chd.12820
23. Foulks MG, Meyer RML, Gold JI, Herrington CS, Kallin K, Menteer J. Postoperative heart failure after stage 1 palliative surgery for single ventricle cardiac disease. *Pediatr Cardiol.* (2019) 40:943–9. doi: 10.1007/s00246-019-02093-4
24. Pundi K, Pundi KN, Kamath PS, Cetta F, Li Z, Poterucha JT, et al. Liver disease in patients after the fontan operation.

Am J Cardiol. (2016) 117:456–60. doi: 10.1016/j.amjcard.2015.11.014

25. Steinberger EK, Ferencz C, Loffredo CA. Infants with single ventricle: a population-based epidemiological study. *Teratology.* (2002) 65:106–15. doi: 10.1002/tera.10017
26. Dolgin M, Criteria Committee of the New York Heart Association. *Nomenclature and Criteria for Diagnosis of Diseases of the Heart and Great Vessels, Little, Brown*. Boston, MA (1994).

Conflict of Interest: The authors declare that the research was conducted in the absence of any commercial or financial relationships that could be construed as a potential conflict of interest.

Publisher's Note: All claims expressed in this article are solely those of the authors and do not necessarily represent those of their affiliated organizations, or those of the publisher, the editors and the reviewers. Any product that may be evaluated in this article, or claim that may be made by its manufacturer, is not guaranteed or endorsed by the publisher.

frontiers in Cardiovascular Medicine

ORIGINAL RESEARCH
published: 29 September 2021
doi: 10.3389/fcvm.2021.701745

Glycolysis Inhibition Alleviates Cardiac Fibrosis After Myocardial Infarction by Suppressing Cardiac Fibroblast Activation

Zhi-Teng Chen[1,2,3†], Qing-Yuan Gao[1,2,3†], Mao-Xiong Wu[1,2,3†], Meng Wang[4], Run-Lu Sun[1,2,3], Yuan Jiang[1,2,3], Qi Guo[1,2,3], Da-Chuan Guo[1,2,3], Chi-Yu Liu[1,2,3], Si-Xu Chen[1,2,3], Xiao Liu[1,2,3], Jing-Feng Wang[1,2,3], Hai-Feng Zhang[1,2,3*] and Yang-Xin Chen[1,2,3*]*

[1] Department of Cardiology, Sun Yat-Sen Memorial Hospital, Sun Yat-Sen University, Guangzhou, China, [2] Guangzhou Key Laboratory of Molecular Mechanism and Translation in Major Cardiovascular Disease, Sun Yat-Sen Memorial Hospital, Sun Yat-Sen University, Guangzhou, China, [3] Laboratory of Cardiac Electrophysiology and Arrhythmia in Guangdong Province, Guangzhou, China, [4] Department of Cardiovascular Surgery, Sun Yat-Sen Memorial Hospital, Sun Yat-Sen University, Guangzhou, China

OPEN ACCESS

Edited by:
Kunhua Song,
University of Colorado Anschutz Medical Campus, United States

Reviewed by:
Fuyang Zhang,
Fourth Military Medical University, China
Walter Knight,
University of Colorado, United States

***Correspondence:**
Jing-Feng Wang
wjingf@mail.sysu.edu.cn
Hai-Feng Zhang
zhanghf9@mail.sysu.edu.cn
Yang-Xin Chen
chenyx39@mail.sysu.edu.cn

†These authors have contributed equally to this work and share first authorship

Specialty section:
This article was submitted to Cardiovascular Metabolism, a section of the journal Frontiers in Cardiovascular Medicine

Received: 28 April 2021
Accepted: 07 September 2021
Published: 29 September 2021

Citation:
Chen Z-T, Gao Q-Y, Wu M-X, Wang M, Sun R-L, Jiang Y, Guo Q, Guo D-C, Liu C-Y, Chen S-X, Liu X, Wang J-F, Zhang H-F and Chen Y-X (2021) Glycolysis Inhibition Alleviates Cardiac Fibrosis After Myocardial Infarction by Suppressing Cardiac Fibroblast Activation. Front. Cardiovasc. Med. 8:701745. doi: 10.3389/fcvm.2021.701745

Objective: To explore the role of glycolysis in cardiac fibroblast (CF) activation and cardiac fibrosis after myocardial infarction (MI).

Method: *In vivo*: 2-Deoxy-D-glucose (2-DG), a glycolysis inhibitor, was injected into the abdominal cavity of the MI or sham mice every day. On the 28th day, cardiac function was measured by ultrasonic cardiography, and the hearts were harvested. Masson staining and immunofluorescence (IF) were used to evaluate the fibrosis area, and western blot was used to identify the glycolytic level. *In vitro*, we isolated the CF from the sham, MI and MI with 2-DG treatment mice, and we also activated normal CF with transforming growth factor-β1 (TGF-β1) and block glycolysis with 2-DG. We then detected the glycolytic proteins, fibrotic proteins, and the concentrations of lactate and glucose in the culture medium. At last, we further detected the fibrotic and glycolytic markers in human fibrotic and non-fibrotic heart tissues with masson staining, IF and western blot.

Result: More collagen and glycolytic protein expressions were observed in the MI mice hearts. The mortality increased when mice were treated with 2-DG (100 mg/kg/d) after the MI surgery (Log-rank test, $P < 0.05$). When the dosage of 2-DG declined to 50 mg/kg/d, and the treatment was started on the 4th day after MI, no statistical difference of mortality between the two groups was observed (Log-rank test, $P = 0.98$). The collagen volume fraction was smaller and the fluorescence signal of α-smooth muscle actin (α-SMA) was weaker in mice treated with 2-DG than PBS. *In vitro*, 2-DG could significantly inhibit the increased expression of both the glycolytic and fibrotic proteins in the activated CF.

Conclusion: Cardiac fibrosis is along with the enhancement of CF activation and glycolysis. Glycolysis inhibition can alleviate cardiac fibroblast activation and cardiac fibrosis after myocardial infarction.

Keywords: heart failure, myocardial infarction, glycolysis, fibroblast activation, cardiac fibrosis

INTRODUCTION

Heart failure is a cardiovascular disease with high morbidity and mortality, which cause a great burden on society (1). Among the various etiologies, myocardial infarction (MI) is the most important one which is responsible for more than half of the cases (2). As cardiomyocyte is hard to regenerate after ischemia and hypoxia, fibrotic scar helps to maintain the integrity and function of the heart (3). However, excessive fibrosis reduces its compliance, thereby impairing its systolic and diastolic function (4). Consequently, it is a hotspot to find new strategies to restrict excessive fibrosis after MI (5).

As heart is the energy metabolism core in the body, alterations in cardiac energy metabolism contribute to several cardiovascular pathologies. Glycolysis is one of the major energy-yielding manners, which is enhanced when MI occurs (6). When the heart suffers ischemia, glycolysis can supply amounts of energy quickly, thus meeting the demands for heart contraction and blood transportation (7). Though glycolysis is well-investigated in heart failure (8, 9) and MI (10), few studies focus on the glycolysis in cardiac fibrosis after MI. Nevertheless, various fibrosis-related studies in other organs such as lung (11), liver (12), skin (13), and kidney (14) have reported that glycolysis contributes to the fibrotic process. Glycolysis contributes to fibroblast activation *via* several ways in fibrotic diseases. It not only produces several key metabolites responsible for CF activation, like glycine and triphosadenine, it also produced abundant lactate, which was important for the activity of proline hydroxylase, TGF-β1 and the hydroxylation of collagen (15, 16). Due to the specific hemodynamics of the heart, role of glycolysis in cardiac fibrosis after MI seems more complicated. It is well-acknowledged that cardiac fibroblast (CF) activation is the most important contributor to cardiac fibrosis after MI (17). Interestingly, our previous research demonstrates that enhanced glycolysis promotes cardiac fibroblast (CF) activation (18). Accordingly, it is of great significance to investigate the role of glycolysis in cardiac fibrosis after MI.

Thus, to explore the relationship between glycolysis and cardiac fibrosis after MI. We firstly detected the glycolysis-related proteins in the mouse MI model. Then, by delivering a glycolysis-specific inhibitor 2-Deoxy-D-glucose (2-DG), we demonstrated the role of glycolysis in the fibrotic process of the heart. At last, we also measured the glycolysis change in human fibrotic and non-fibrotic tissues, thus providing more clinical evidence.

MATERIALS AND METHODS

Animals

C57BL/6J mice were used to perform a MI or sham surgery. Then 2-DG (100 mg/kg/d or 50 mg/kg/d; Sigma-Aldrich, #D8375) was delivered by intraperitoneal injection immediately after the surgery or started at the 4th-day after the surgery. Trans-thoracic echocardiography was performed on the 28th day after the surgery to evaluate the cardiac function. The animal use protocol was approved by Institutional Animal Care and Use Committee, Sun Yat-sen University. Detailed information was provided in the **Supplementary Material**.

Human Heart Specimens

Human heart specimens were harvested during cardiac surgeries in Sun Yat-sen Memorial Hospital. Among them, the resected ventricular aneurysm tissues were used as fibrotic tissues while papillary muscle tissues from the diseased valve were served as non-fibrotic tissues. The study design was approved by the Ethics Committee of Sun Yat-sen Memorial Hospital.

Masson Staining

Heart tissues from the mice or patients were collected and fixed in 4% paraformaldehyde in phosphate-buffered saline (PBS; Servicebio, #G4202) overnight after being perfused with cold normal saline. Then the hearts were processed for paraffin embedding and subsequently cut into slices. Slices then undergo dewaxing, rehydration and stained for collagen fibers with Masson's Trichrome staining Kit (Servicebio, #G1006) following the manufacturer's instructions. Fibrotic tissues and muscle tissues were segmented using ImageJ (NIH) and fibrosis was expressed as the percentage of fibrotic tissue in each section.

Tissue Immunofluorescence

Slices from human or mice undergo dewaxing, rehydration, antigen retrieval and blocking. Then tissues were incubated with primary antibodies overnight, followed by fluorescigenic secondary antibodies incubation. At last, the nucleus was stained, and photos were taken with the fluorescence microscope. The fluorescence signal quantification was conducted with Image J.

Cell Culture

Neonatal mouse CFs (NMCFs) and human CFs were used for the *in vitro* experiments. The NMCFs were separated from the ventricle of the neonatal 1–3-day-old mice as described previously (19), and the human CFs were isolated from human juvenile ventricle. The detailed separation method of the NMCFs was described in the **Supplementary Material**. The human CFs were purchased from Sciencell (#6310, the detail separation method could be found with the following link: https://www.sciencellonline.com/human-cardiac-fibroblasts-juvenile-ventricular.html).

Human CFs at the passage between 6 and 8 and NMCFs at passage 2–3 were pre-treated with 2-DG (1 mmol/L) for 1 h. Then human/mouse transforming growth factor-β1 (TGF-β1; PeproTech, 100-21; 10 ng/mL; TGF-β1; Novus Biologicals, 7666-MB; 10ng/mL) was added to induce an activated phenotype. Cells were treated for 48 h and harvested. For HK2 knockdown tests, NMCFs were treated with small interfering RNA against HK2 (si-HK2: GGACAAGCUACAGAUCAAAdTdT) or scrambled siRNA (negative control, NC: UUCUCCGAACGUGUCACGUdTdT). Cell medium was refreshed after 12 h treatment and harvested after 48 h cultivation.

Adult mouse CFs (AMCFs) were separated from the ventricle of the MI or sham mice with or without 2-DG treatment on the 28th day after the sham or MI surgery as described previously (20, 21). As inadequate cells could be harvested from only one heart, two hearts were isolated together and mixed to produce one group of cardiac cells with an enzymolysis approach. After the

differential adherent method, primary AMCFs were harvested for the next experiments. The detailed separation method of the AMCFs was described in the **Supplementary Material**.

Lactate and Glucose Detections

Lactate in the cell medium were detected with Lactate Assay Kit II (Sigma, # MAK065), and the glucose in the cell medium were detected with Glucose Colorimetric/Fluorometric Assay Kit (Biovision, #K606–100) according to the manufacturer's instructions. All results were normalized to the total protein concentration.

Western Blot

Western blot was performed as previously described (18). Antibodies are listed in **Supplementary Table 1**. The western blot band density quantification was analyzed with Image J (National Institutes of Health, Maryland, USA).

Cell Immunofluorescence

Cells were fixed with 4% paraformaldehyde (Servicebio, #G1101). After being permeabilized with 0.5% Triton X-100 (Sigma-Aldrich, #X100) for 20 min, cells were blocked with 5% bovine serum albumin (Sigma-Aldrich, #A1933). Afterwards, cells were incubated with the indicated the primary antibodies overnight and then the fluorescigenic secondary antibodies for 1 h at room temperature. At last, fluorescence were captured with the fluorescence microscope. Antibodies are listed in **Supplementary Table 1**. The fluorescence signal quantification was conducted with Image J.

Statistical Analysis

Data were showed as mean ± SEM. Statistical analyses were performed with GraphPad Prism Software (version 8.0.1). Statistical comparison among multiple groups was carried out by one-way ANOVA followed by the *Bonferroni* test. Student's *t*-test was used to analyze differences between two groups. Kaplan-Meier method was used for the survival analysis, and the *log-rank* test was used for the statistical analyses. P-value < 0.05 indicated statistical significance.

RESULTS

Glycolysis Was Increased in the Fibrotic Heart After MI

To explore the role of glycolysis in cardiac fibrosis, we measured the glycolytic markers in the fibrotic heart after MI. As is shown in **Figure 1A**, compared with the sham group, cardiac function of mice in MI group obviously decreased (sham *vs.* MI: LVEF (%): 75.84 ± 0.96 vs. 21.46 ± 3.70, LVFS (%): 43.67 ± 0.80 vs. 9.87 ± 1.83, LVDd (mm): 3.44 ± 0.10 vs. 4.54 ± 0.38, LVSd (mm): 1.94 ± 0.07 vs. 5.04 ± 0.41; $P < 0.05$). Masson staining showed that plentiful collagen was deposited in the heart after MI (collagen volume fraction (%): sham *vs.* myocardial infarction: 1.93 ± 0.71% vs. 26.49 ± 4.87%; $P < 0.05$; **Figure 1B**), which indicated that cardiac fibrosis occurred after MI. To further explore the change of glycolysis during this process, we harvested the heart tissue protein and detected the glycolysis-related proteins and CF activation markers. As a result, we found the increased expressions of hexokinase 1 (HK1), 6-phosphofructo-2-kinase/fructose-2, 6-bisphosphatase 3 (PFKFB3), and pyruvate kinase isoform M2 (PKM2), along with the CF activation markers (periostin, POSTN; Alpha smooth muscle actin, α-SMA) (**Figure 1C**). Thus, we concluded that cardiac fibrosis after MI was accompanied by enhanced glycolysis.

Glycolysis Inhibition Alleviated Cardiac Fibrosis After MI

Next, we aimed to figure out whether cardiac fibrosis could be reversed when glycolysis was inhibited. We delivered a glycolysis inhibitor, 2-DG (100 mg/kg/d) or an equal volume of PBS into mice in the MI group by intraperitoneal injection immediately after the surgery and maintained the injection daily. We found that the mortality increased in MI mice with 2-DG injection than that with PBS injection (Log-rank test, $P < 0.05$, **Figure 2A**). The animal autopsy revealed that heart rupture was the leading cause of death. Considering the possibility that glycolysis was beneficial for the early repairment of the heart, we reduced the dosage of 2-DG to 50 mg/kg/d and delayed the start time to the 4th day after the surgery. In contrast, there was no difference in mortality between the two groups (Log-rank test, $P = 0.98$, **Figure 2B**). Echocardiography was taken and the hearts were harvested for further experiments on the 28th day after the surgery. As is shown in **Figure 2C**, there was no statistical difference of cardiac function between the two groups with or without 2-DG. To further explore the role of glycolysis in cardiac fibrosis after MI, we detected collagen deposition with masson staining. Results showed that collagen volume fraction was smaller in mice treated with 2-DG than PBS (2-DG vs. PBS: 26.68 ± 2.11% vs. 13.54 ± 1.14%, $P < 0.05$; **Figures 2D,E**). Thus, our findings demonstrated that glycolysis inhibition could alleviate cardiac fibrosis after MI.

Glycolysis Inhibition Could Reverse the Fibroblasts Activation *in vivo* and *in vitro*

CF activation was the main force for cardiac fibrosis after MI. Thus, we then detected the markers of CF activation (α-SMA) in the heart tissues of mice in sham, MI, and MI combined 2-DG groups. As is shown in **Figures 2F,G**, immunofluorescent staining showed a significant reduction of α-SMA in the 2-DG treated group (MI+PBS *vs.* MI+2-DG: 1.17 ± 0.09% vs. 0.26 ± 0.03%, $P < 0.01$). To further ensure that glycolysis inhibition could alleviate the CF activation *in vivo*, we isolated the AMCFs from the MI or sham mice with or without 2-DG treatments on the 28th day after the surgery. As is shown in **Figure 3A**, CF isolation was successful with abundant vimentin expressions and few troponin and CD31 expressions, which were markers of CF, cardiomyocyte and endothelial cells, respectively. We then measured the expressions of the key fibrotic and glycolytic proteins. As is shown in **Figure 3B**, fibrotic markers such as type I collagen (COLIA1), connective

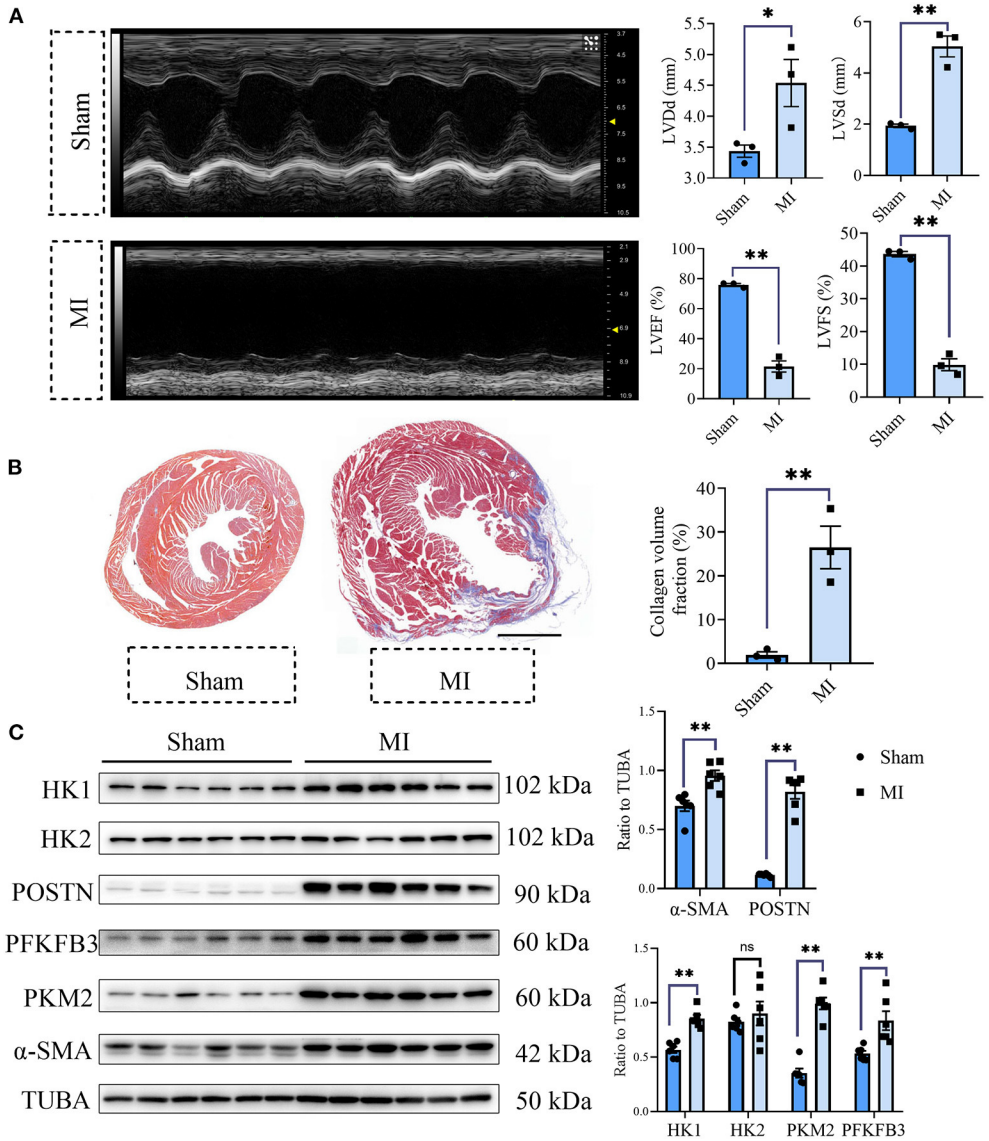

FIGURE 1 | Cardiac fibrosis was accompanied by enhanced glycolysis in MI mice. **(A)** The cardiac function measured by echocardiography was shown. Representative images of the M-mode of the echocardiography results, and the related parameters (LVEF, LVFS, LVDd, LVSd) measurement were displayed, respectively. **(B)** Masson staining of the heart harvested on the 28th day after the MI or sham surgery. Representative images (left) and the statistical analysis (right) were shown. **(C)** Western blot of the expressions of glycolytic and CF activation markers between the MI and sham mice. The representative image (left) and the statistical analysis (right) were shown. LVEF, left ventricular ejection fraction; LVFS, left ventricular fractional shortening; LVDd, left ventricular end diastolic dimension; LVSd, left ventricular end systolic diameter; MI, myocardial infarction; Sham, sham operation; HK1, hexokinase 1; PFKFB3, 6-phosphofructo-2-kinase/fructose-2, 6-bisphosphatase 3; PKM2, pyruvate kinase isoform M2; POSTN, periostin; α-SMA, Alpha smooth muscle actin; $n = 3$ in **(A,B)**; $n = 6$ in **(C)**; $^{*}P < 0.05$; $^{**}P < 0.01$; ns, no significance. Scale bar = 1000 μm.

tissue growth factor (CTGF) and α-SMA were significantly up-regulated in AMCFs with MI surgery. However, when the mice were treated with 2-DG after MI, the fibrotic effect exerted by MI was alleviated (**Figures 3B,C**). To confirm the role of glycolysis in this process, we measured the glycolytic proteins, as well as the lactate and glucose concentration in the culture medium, which were vital glycolytic indicators. Compared with the sham group, lactic dehydrogenase A (LDHA), but not PFKFB3, HK2 or PKM2, was significantly up-regulated in the MI group. Interestingly, 2-DG could reduce the expressions of both PFKFB3 and LDHA rather than HK2 and PKM2 (**Figures 3B,D**). More importantly, 2-DG could reverse the increase of lactate concentration and the decrease of glucose concentration in the culture medium in the MI plus 2-DG group, compared with the MI group (**Figures 3E,F**). Besides, we also performed an *in vitro* test to make sure whether 2-DG could inhibit CF

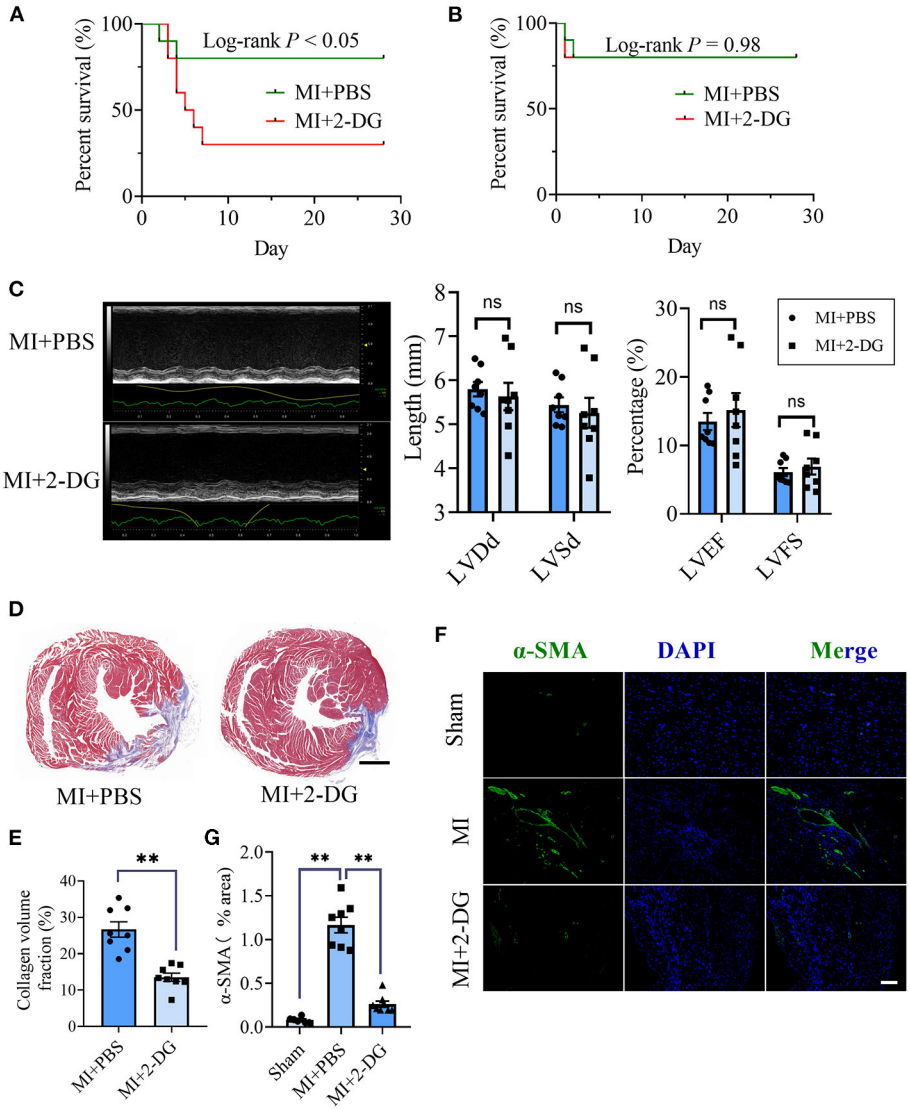

FIGURE 2 | Glycolysis inhibition alleviates cardiac fibrosis after MI. **(A)** Survival analysis of the mice undergoing MI or sham surgery when 2-DG was delivered immediately after the surgery at a dosage of 100 mg/kg/d. **(B)** Survival analysis of the mice undergoing MI or sham surgery when 2-DG treatment was started on the 4th day after the surgery at a dosage of 50 mg/kg/d. **(C)** The cardiac function of the MI mice with or without 2-DG treatment at a dosage of 50 mg/kg/d started on the 4th day after the surgery was measured by echocardiography. Representative images of the M-mode of the echocardiography results (left), and the related parameters (LVEF, LVFS, LVDd, LVSd) measurement (right) were displayed, respectively. **(D,E)** The hearts of the MI mice with or without 2-DG treatment at a dosage of 50 mg/kg/d started at the 4th day after the surgery were harvested on the 28th day after the surgery. Masson staining was performed. Representative image **(D)** and the statistical analysis **(E)** were shown, respectively. **(F)** Immunofluorescence of the hearts from the MI and sham mice with or without 2-DG treatment. The green fluorescence signal represented α-SMA, and the blue fluorescence signal represented DAPI. **(G)** Fluorescence signal statistics of the green α-SMA signals. LVEF, left ventricular ejection fraction; LVFS, left ventricular fractional shortening; LVDd, left ventricular end diastolic dimension; LVSd, left ventricular end systolic diameter; MI, myocardial infarction; Sham, sham operation; $n = 8$; ns, no significance; $^{**}P < 0.01$. The scale bar in **(D)** was 1000 μm. The scale bar in **(F)** was 100 μm.

activation directly. We used TGF-β1 to induce human cardiac fibroblast activation. In **Figure 4A**, 2-DG not only inhibited TGF-β1 induced CF activation, but also alleviated the CF spontaneous activation during the cultivation. We made the same conclusion with NMCFs (**Figure 4B**). To eliminate the off-target effects of 2-DG, we conducted the same experiments with siRNA against HK2 (si-HK2) in NMCFs. As a result, si-HK2 could also reverse the pro-fibrotic effect exerted by TGF-β1. Although si-HK2 did not influence the expression of α-SMA, it significantly decreased the expressions of COLIA1 and CTGF (**Figure 4B**). To better confirm the function of glycolysis in this process, we also detect the lactate and glucose concentration in the cell culture medium. As a result, the lactate concentration decreased, and the glucose concentration

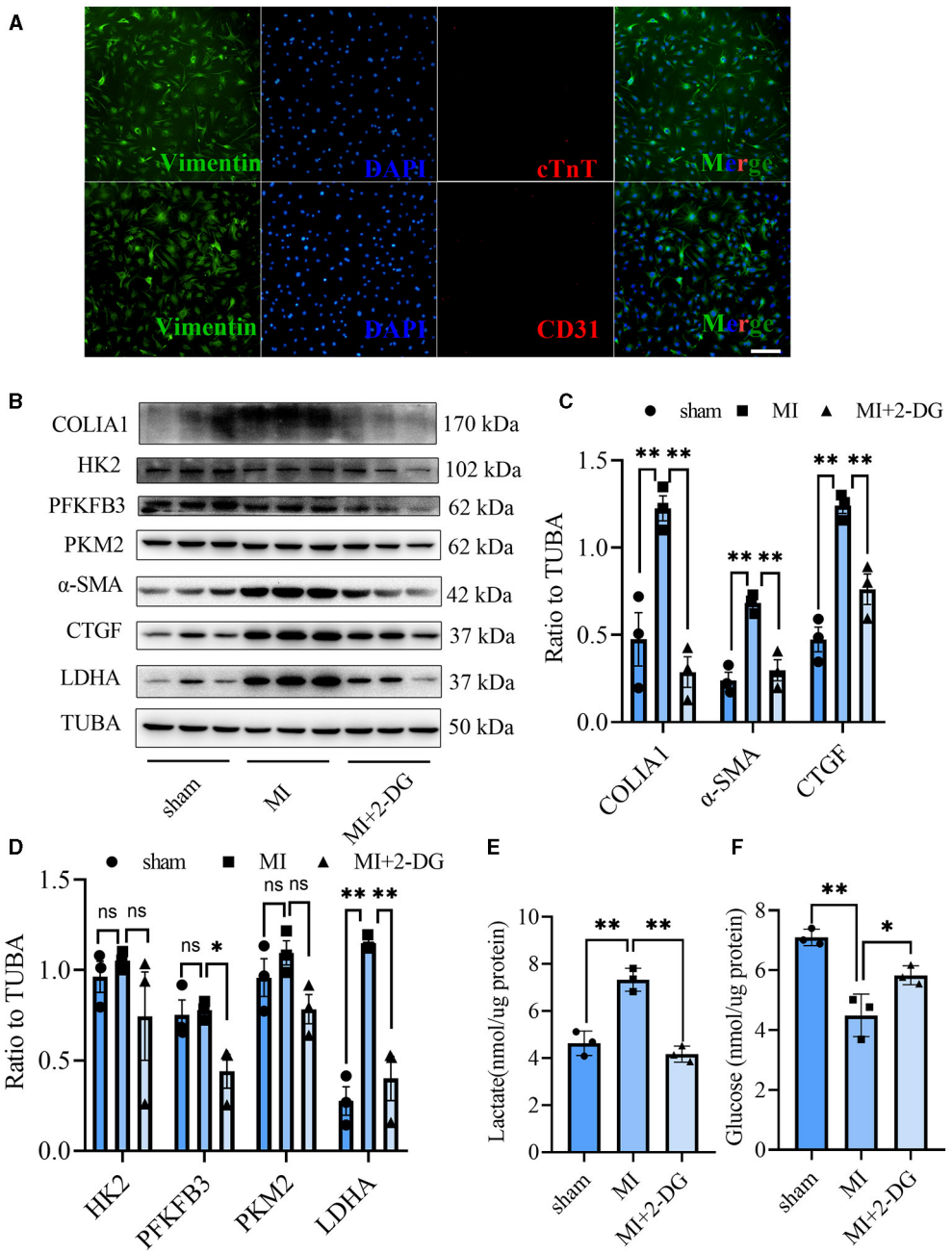

FIGURE 3 | Glycolysis inhibition could reverse the fibroblasts activation *in vivo*. **(A)** Cell identification of CF isolated from the adult mice. Green represented Vimentin. Red represented cTnT or CD31. Blue represented DAPI. **(B)** Western blot of the expressions of glycolytic and CF activation markers from cells isolated from the sham, MI and MI with 2-DG treatment mice. **(C,D)** Gray value statistics of the western blot of **(B)**. **(E,F)** Lactate **(E)** and glucose measurement **(F)** in the culture medium from cells isolated from the sham, MI and MI with 2-DG treatment mice. COLIA1, type I collagen; α-SMA, alpha smooth muscle actin; CTGF, connective tissue growth factor; PFKFB3, 6-phosphofructo-2-kinase/fructose-2, 6-bisphosphatase 3; PKM2, pyruvate kinase isoform M2; HK2, hexokinase 2; TUBA, α-tubulin; LDHA, lactic dehydrogenase A; cTnT, troponin T; $n = 3$, each sample was composed of CFs from two mice hearts; $^{*}P < 0.05$; $^{**}P < 0.01$; ns, no significance. Scale bar = 100 μm.

increased, which could be reversed with si-HK2 or 2-DG treatments (**Figure 4C**).

Consequently, our results demonstrated that glycolysis inhibition could reverse the fibroblast activation *in vivo* and *in vitro*.

Glycolysis Was Increased in Human Fibrotic Heart Tissues Compared With the Non-fibrotic Heart Tissues

To acquire the clinical evidence, we further detected the fibrotic and glycolytic markers in human fibrotic and non-fibrotic

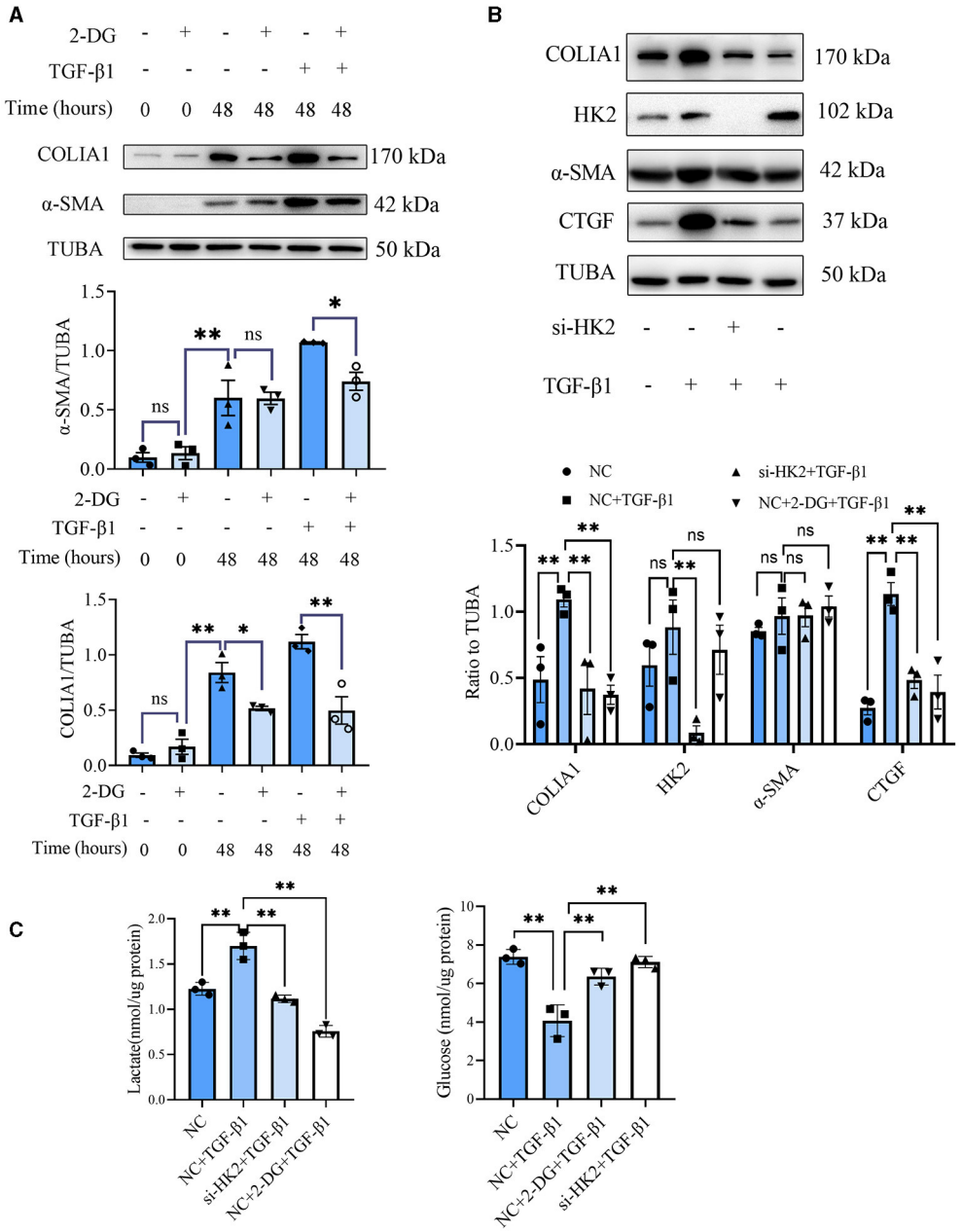

FIGURE 4 | Glycolysis inhibition could reverse the fibroblasts activation *in vitro*. **(A)** Western blot of 2-DG effect on TGF-β1-induced human CF activation. **(B)** Western blot of 2-DG effect on TGF-β1-induced mouse CF activation. **(C)** Lactate and glucose measurement in the culture medium from cells. The representative image and the statistical analysis were shown, respectively. COLIA1, type I collagen; α-SMA, alpha smooth muscle actin; CTGF, connective tissue growth factor; TUBA, α-tubulin; 2-DG, 2- deoxy-D-glucose; TGF-β1, transforming growth factor-β1; NC, negative control; si-HK2, siRNA against HK2; $n = 3$, $^{*}P < 0.05$; $^{**}P < 0.01$; ns, no significance. Scale bar = 100 μm.

heart tissues. The clinical information of enrolled patients was shown in **Supplementary Table 2**. Masson staining showed that obvious collagen deposited in the human fibrotic heart tissues (collagen volume fraction (%): non-fibrotic heart tissues *vs.* fibrotic heart tissues: 17.48 ± 1.84 vs. 82.45 ± 10.45, $P < 0.05$; **Figure 5A**). Immunofluorescence staining showed the increased expression of α-SMA in the fibrotic hearts than the non-fibrotic hearts (α-SMA fluorescence percentage (%): non-fibrotic heart tissues *vs.* fibrotic heart tissues: 0.38 ± 0.11 vs. 2.48 ± 0.74, $P < 0.05$; **Figure 5B**). Consistent with the aforementioned animal experiments, fibrotic markers were increased in the human fibrotic heart tissues, which is accompanied by the increase of glycolytic markers (**Figure 5C**).

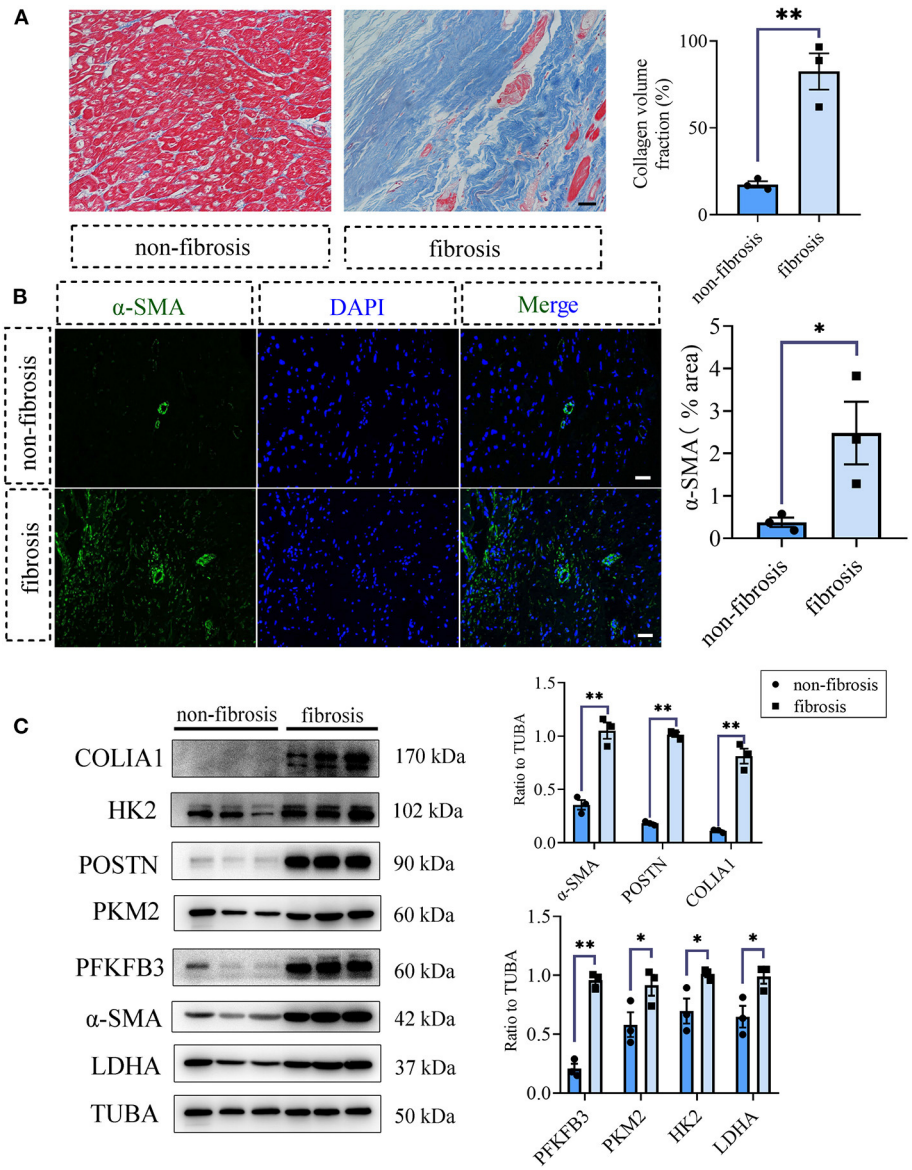

FIGURE 5 | Glycolysis increased in human fibrotic heart tissues compared with the non-fibrotic heart tissues. **(A)** Masson staining of the human fibrotic and non-fibrotic heart tissues. The representative image (left) and the statistical analysis (right) were shown. **(B)** Immunofluorescence of the human fibrotic and non-fibrotic heart tissues. The green fluorescence signal represented α-SMA, and the blue fluorescence signal represented DAPI. **(C)** Western blot of the expressions of glycolytic and CF activation markers of the human fibrotic and non-fibrotic heart tissues. The representative image (left) and the statistical analysis (right) were shown, respectively. $N = 3$; $^{*}P < 0.05$; $^{**}P < 0.01$; ns, no significance. Scale bar = 100 μm.

DISCUSSION

Although treatments for heart failure have made great progress, it is still a global refractory disease with high mortality and rehospitalization rate (22). Regardless of the various etiologies of heart failure, cardiac fibrosis is the common physiopathologic progress. New strategies targeting cardiac fibrosis may serve as an alternative way to improve the prognosis of heart failure.

In our study, glycolysis inhibition could alleviate the CF activation and cardiac fibrosis after MI, just as the previous reports in other fibrotic diseases (14, 23, 24). Nevertheless, in contrast to our results, Donthi et al. uncovered that the inhibition of cardiac glycolysis by overexpressing kinase-deficient PFK-2 exacerbated myocardial hypertrophy and cardiac fibrosis (25). However, when they overexpressed kinase-deficient PFK-2 with a cardiomyocyte-specific promotor, α-myosin heavy chain, glycolysis in cardiomyocyte was inhibited, which might contribute to changes in the fibrotic process indirectly (26). In another study, Hu et al. demonstrated that paroxysmal atrial fibrillation could induce glycolysis in the canine atrium,

and glycolysis inhibition could completely reverse myocardial fibrosis remodeling, the results of which were consistent with our present study (27). Our findings further supported the view that glycolysis contributed to cardiac fibrosis, and glycolysis inhibition at a proper time and extent could effectively alleviate the excessive fibrosis after MI.

In our study, 2-DG delivery from the day of MI surgery at a dosage of 100 mg/kg/day increased the mortality of mice. After we lowered the dosage of 2-DG to 50 mg/kg/day and delayed the time of initial drug administration to the 4th day after the surgery, the mortality of the mice decreased, and the fibrosis area of the heart lessened. To our knowledge, fibrosis is an important event and a dynamic process after MI (28). In the first 3 days, inflammation activates along with the apoptosis of cardiomyocytes while fibroblast presents as an inflammatory phenotype by secreting plentiful inflammatory factors during this stage. From the 4th day, fibroblast tends to trans-differentiate into myofibroblasts, which drives a vast production of the extracellular matrix. In this stage, inflammation fades, and the scar arises (28). During the process of fibrosis development after MI, modest fibrosis will help the heart to complete the repairment of the heart while inadequate fibrosis may result in the increased risk of heart rupture due to the insufficient repairment. On the contrary, excessive fibrosis contributes to the stiffness of the heart, with resultant impaired systolic and diastolic functions. In our experiments, sufficient 2-DG delivery might block both the cardiomyocyte survival and the fibroblast activation, which did harm to the heart repair, thus accelerating the rupture of the heart. When the dosage of 2-DG was decreased and the delivery time was delayed, the side effect alleviates, and 2-DG can effectively inhibit the cardiac fibroblast activation, thus contributing to the improvement of the cardiac fibrosis. Anyway, the side effect of 2-DG on the cardiomyocyte exist, which may explain the little improvement in the cardiac function. Thus, cell-specific reagent invention was in need in the future studies. Searching the downstream of the 2-DG might be another alternative way to reduce the side effect of 2-DG. More works need to be done in the future to promote the application of glycolysis inhibitors in the cardiac fibrosis treatment.

In our study, we did not explore the further mechanism of the anti-fibrotic effect of 2-DG. 2-DG might contribute to CF activation in several ways. As several critical metabolites in glycolysis were responsible for CF activation, like glycine and triphosadenine (15), 2-DG might inhibit CF activation by reducing the production of these pro-fibrotic intermediate metabolites. Besides, glycolysis also produced abundant lactate, which was essential for the activity of proline hydroxylase, TGF-β1, and the hydroxylation of collagen (16). Interestingly, 2-DG could cut down the secretion of lactate significantly. As proline, collagen and TGF-β1 were important molecular for CF activation, 2-DG might exert the anti-fibrotic effects by restricting the production of lactate. What's more, glycolysis could also enhance the expression of the fibrotic proteins by epigenetic modification, which could be another intervention target for the anti-fibrotic effect of 2-DG (29). Last but not the least, hypoxia was an important change after MI, and hypoxia was a key inducer of glycolysis. In the kidney fibrosis investigation, it was reported that TEPP-46-induced PKM2 tetramer formation and pyruvate kinase activity resulted in the suppression of HIF-1α and lactate accumulation, thus contributing to kidney fibrosis (30). In another study of diabetic kidney disease, sodium-glucose cotransporter 2 inhibition could suppress HIF-1α-mediated metabolic switch from lipid oxidation to glycolysis and exert a kidney protective effect (31). It was fascinating that hypoxic signaling post MI (such as HIF1α activation) might drive this presumed glycolytic shift. More works are needed in the future study to illustrate the inner mechanism.

Some other limitations should be acknowledged in our study. Firstly, we delivered 2-DG by intraperitoneal injection, which may exert a systemic effect. Though we have demonstrated the role of glycolysis on CF activation *in vivo* and *in vitro*, we cannot eliminate the possible confounding contribution by other cardiac cells. Secondly, we explored the role of glycolysis in cardiac fibrosis and CF activation after MI. We did not further explore the role of tricarboxylic acid cycle and oxidative phosphorylation. Thirdly, as human tissues were hard to acquire, especially normal heart tissues and tissues from remote sections of the human MI heart, we had to use papillary muscles tissues as candidates of non-fibrotic heart tissues.

In conclusion, our study demonstrates that glycolysis inhibition can alleviate CF activation and cardiac fibrosis after MI. Glycolysis may be a new target for the treatment of cardiac fibrosis.

DATA AVAILABILITY STATEMENT

The raw data supporting the conclusions of this article will be made available by the authors, without undue reservation.

ETHICS STATEMENT

The studies involving human participants were reviewed and approved by the Ethics Committee of Sun Yat-sen Memorial Hospital. The patients/participants provided their written informed consent to participate in this study. The animal study was reviewed and approved by Institutional Animal Care and Use Committee, Sun Yat-sen University.

AUTHOR CONTRIBUTIONS

Z-TC, Q-YG, and M-XW were responsible for most of the experiments. MW provided the human heart specimens. YJ, R-LS, and D-CG provided the experimental assistances. QG, C-YL, XL, and S-XC provided writing assistances. J-FW, H-FZ, and Y-XC designed and directed the study. All authors have read and approved the final submitted manuscript.

FUNDING

This work was supported by grants from the National Natural Science Foundation of China (No. 81870170,

81970200, and 82100369), Guangdong Basic and Applied Basic Research Foundation (2020A151501886, 2019A1515110129), the Yat-sen Start-up Foundation (No. YXQH202014), the Science and Technology Program of Guangzhou City of China (201803040010), the Guangzhou Regenerative Medicine and Health Guangdong Laboratory (No. 2019GZR110406004), and the Guangzhou Key Laboratory of Molecular Mechanism and Translation in Major Cardiovascular Disease (No. 202102010007).

SUPPLEMENTARY MATERIAL

The Supplementary Material for this article can be found online at: https://www.frontiersin.org/articles/10.3389/fcvm.2021.701745/full#supplementary-material

REFERENCES

1. Metra M, Teerlink JR. Heart failure. *Lancet.* (2017) 390:1981–95. doi: 10.1016/S0140-6736(17)31071-1
2. Bahit MC, Kochar A, Granger CB. Post-myocardial infarction heart failure. *JACC Heart Fail.* (2018) 6:179–86. doi: 10.1016/j.jchf.2017.09.015
3. González A, Schelbert EB, Díez J, Butler J. Myocardial interstitial fibrosis in heart failure: biological and translational perspectives. *J Am Coll Cardiol.* (2018) 71:1696–706. doi: 10.1016/j.jacc.2018.02.021
4. Frangogiannis NG. Cardiac fibrosis: Cell biological mechanisms, molecular pathways, and therapeutic opportunities. *Mol Aspects Med.* (2019) 65:70–99. doi: 10.1016/j.mam.2018.07.001
5. Fan Z, Guan J. Antifibrotic therapies to control cardiac fibrosis. *Biomater Res.* (2016) 20:13. doi: 10.1186/s40824-016-0060-8
6. Zuurbier CJ, Bertrand L, Beauloye CR, Andreadou I, Ruiz-Meana M, Jespersen NR, et al. Cardiac metabolism as a driver and therapeutic target of myocardial infarction. *J Cell Mol Med.* (2020) 24:5937–54. doi: 10.1111/jcmm.15180
7. Heywood SE, Richart AL, Henstridge DC, Alt K, Kiriazis H, Zammit C, et al. High-density lipoprotein delivered after myocardial infarction increases cardiac glucose uptake and function in mice. *Sci Transl Med.* (2017) 9:eaam6084. doi: 10.1126/scitranslmed.aam6084
8. Bertero E, Maack C. Metabolic remodelling in heart failure. *Nat Rev Cardiol.* (2018) 15:457–70. doi: 10.1038/s41569-018-0044-6
9. Birkenfeld AL, Jordan J, Dworak M, Merkel T, Burnstock G. Myocardial metabolism in heart failure: purinergic signalling and other metabolic concepts. *Pharmacol Ther.* (2019) 194:132–44. doi: 10.1016/j.pharmthera.2018.08.015
10. Wang X, Ha T, Liu L, Hu Y, Kao R, Kalbfleisch J, et al. TLR3 mediates repair and regeneration of damaged neonatal heart through glycolysis dependent YAP1 regulated miR-152 expression. *Cell Death Differ.* (2018) 25:966–82. doi: 10.1038/s41418-017-0036-9
11. Cho SJ, Moon JS, Nikahira K, Yun HS, Harris R, Hong KS, et al. GLUT1-dependent glycolysis regulates exacerbation of fibrosis via AIM2 inflammasome activation. *Thorax.* (2020) 75:227–36. doi: 10.1136/thoraxjnl-2019-213571
12. Mejias M, Gallego J, Naranjo-Suarez S, Ramirez M, Pell N, Manzano A, et al. CPEB4 increases expression of PFKFB3 to induce glycolysis and activate mouse and human hepatic stellate cells, promoting liver fibrosis. *Gastroenterology.* (2020) 159:273–88. doi: 10.1053/j.gastro.2020.03.008
13. Zhao X, Psarianos P, Ghoraie LS, Yip K, Goldstein D, Gilbert R, et al. Metabolic regulation of dermal fibroblasts contributes to skin extracellular matrix homeostasis and fibrosis. *Nat Metab.* (2019) 1:147–57. doi: 10.1038/s42255-018-0008-5
14. Srivastava SP, Li J, Kitada M, Fujita H, Yamada Y, Goodwin JE, et al. SIRT3 deficiency leads to induction of abnormal glycolysis in diabetic kidney with fibrosis. *Cell Death Dis.* (2018) 9:997. doi: 10.1038/s41419-018-1057-0
15. Zhao X, Kwan JYY, Yip K, Liu PP, Liu FF. Targeting metabolic dysregulation for fibrosis therapy. *Nat Rev Drug Discov.* (2020) 19:57–75. doi: 10.1038/s41573-019-0040-5
16. Comstock JP, Udenfriend S. Effect of lactate on collagen proline hydroxylase activity in cultured L-929 fibroblasts. *Proc Natl Acad Sci U S A.* (1970) 66:552–57. doi: 10.1073/pnas.66.2.552
17. Travers JG, Kamal FA, Robbins J, Yutzey KE, Blaxall BC. Cardiac fibrosis: the fibroblast awakens. *Circ Res.* (2016) 118:1021–40. doi: 10.1161/CIRCRESAHA.115.306565
18. Chen ZT, Zhang HF, Wang M, Wang SH, Wen ZZ, Gao QY, et al. Long non-coding RNA Linc00092 inhibits cardiac fibroblast activation by altering glycolysis in an ERK-dependent manner. *Cell Signal.* (2020) 74:109708. doi: 10.1016/j.cellsig.2020.109708
19. Wu MX, Wang SH, Xie Y, Chen ZT, Guo Q, Yuan WL, et al. Interleukin-33 alleviates diabetic cardiomyopathy through regulation of endoplasmic reticulum stress and autophagy via insulin-like growth factor-binding protein 3. *J Cell Physiol.* (2021) 236:4403–19. doi: 10.1002/jcp.30158
20. Melzer M, Beier D, Young PP, Saraswati S. Isolation and characterization of adult cardiac fibroblasts and myofibroblasts. *J Vis Exp.* (2020) 10.3791/60909. doi: 10.3791/60909
21. Zhao Y, Iyer S, Tavanaei M, Nguyen NT, Lin A, Nguyen TP. Proarrhythmic electrical remodeling by noncardiomyocytes at interfaces with cardiomyocytes under oxidative stress. *Front Physiol.* (2021) 11:622613. doi: 10.3389/fphys.2020.622613
22. Tamargo J, Caballero R, Delpón E. New drugs in preclinical and early stage clinical development in the treatment of heart failure. *Expert Opin Investig Drugs.* (2019) 28:51–71. doi: 10.1080/13543784.2019.1551357
23. Wei Q, Su J, Dong G, Zhang M, Huo Y, Dong Z. Glycolysis inhibitors suppress renal interstitial fibrosis via divergent effects on fibroblasts and tubular cells. *Am J Physiol Renal Physiol.* (2019) 316: F1162-72. doi: 10.1152/ajprenal.00422.2018
24. Hu X, Xu Q, Wan H, Hu Y, Xing S, Yang H, et al. PI3K-Akt-mTOR/PFKFB3 pathway mediated lung fibroblast aerobic glycolysis and collagen synthesis in lipopolysaccharide-induced pulmonary fibrosis. *Lab Invest.* (2020) 100:801–11. doi: 10.1038/s41374-020-0404-9
25. Donthi RV, Ye G, Wu C, McClain DA, Lange AJ, Epstein PN. Cardiac expression of kinase-deficient 6-phosphofructo-2-kinase/fructose-2, 6-bisphosphatase inhibits glycolysis, promotes hypertrophy, impairs myocyte function, and reduces insulin sensitivity. *J Biol Chem.* (2004) 279:48085–90. doi: 10.1074/jbc.M405510200
26. Alvarez R Jr., Wang BJ, Quijada PJ, Avitabile D, Ho T, Shaitrit M, et al. Cardiomyocyte cell cycle dynamics and proliferation revealed through cardiac-specific transgenesis of fluorescent ubiquitinated cell cycle indicator (FUCCI). *J Mol Cell Cardiol.* (2019) 127:154–64. doi: 10.1016/j.yjmcc.2018.12.007
27. Hu HJ, Zhang C, Tang ZH, Qu SL, Jiang ZS. Regulating the Warburg effect on metabolic stress and myocardial fibrosis remodeling and atrial intracardiac waveform activity induced by atrial fibrillation. *Biochem Biophys Res Commun.* (2019) 516:653–60. doi: 10.1016/j.bbrc.2019.06.055
28. Ma Y, Iyer RP, Jung M, Czubryt MP, Lindsey ML. Cardiac fibroblast activation post-myocardial infarction: current knowledge gaps. *Trends Pharmacol Sci.* (2017) 38:448–58 doi: 10.1016/j.tips.2017.03.001

29. Zhang W, Li Q, Li D, Li J, Aki D, Liu YC. The E3 ligase VHL controls alveolar macrophage function via metabolic-epigenetic regulation. *J Exp Med.* (2018) 215:3180–93. doi: 10.1084/jem.20181211
30. Liu H, Takagaki Y, Kumagai A, Kanasaki K, Koya D. The PKM2 activator TEPP-46 suppresses kidney fibrosis via inhibition of the EMT program and aberrant glycolysis associated with suppression of HIF-1α accumulation. *J Diabetes Investig.* (2021) 12:697–709. doi: 10.1111/jdi.13478
31. Cai T, Ke Q, Fang Y, Wen P, Chen H, Yuan Q, et al. Sodium-glucose cotransporter 2 inhibition suppresses HIF-1α-mediated metabolic switch from lipid oxidation to glycolysis in kidney tubule cells of diabetic mice. *Cell Death Dis.* (2020) 11:390. doi: 10.1038/s41419-020-2544-7

Conflict of Interest: The authors declare that the research was conducted in the absence of any commercial or financial relationships that could be construed as a potential conflict of interest.

Publisher's Note: All claims expressed in this article are solely those of the authors and do not necessarily represent those of their affiliated organizations, or those of the publisher, the editors and the reviewers. Any product that may be evaluated in this article, or claim that may be made by its manufacturer, is not guaranteed or endorsed by the publisher.

frontiers in Cardiovascular Medicine

REVIEW
published: 11 November 2021
doi: 10.3389/fcvm.2021.734364

Stable Isotopes for Tracing Cardiac Metabolism in Diseases

Anja Karlstaedt [1,2]*

[1] Department of Cardiology, Smidt Heart Institute, Cedars-Sinai Medical Center, Los Angeles, CA, United States,
[2] Department of Biomedical Sciences, Cedars-Sinai Medical Center, Los Angeles, CA, United States

Although metabolic remodeling during cardiovascular diseases has been well-recognized for decades, the recent development of analytical platforms and mathematical tools has driven the emergence of assessing cardiac metabolism using tracers. Metabolism is a critical component of cellular functions and adaptation to stress. The pathogenesis of cardiovascular disease involves metabolic adaptation to maintain cardiac contractile function even in advanced disease stages. Stable-isotope tracer measurements are a powerful tool for measuring flux distributions at the whole organism level and assessing metabolic changes at a systems level *in vivo*. The goal of this review is to summarize techniques and concepts for *in vivo* or *ex vivo* stable isotope labeling in cardiovascular research, to highlight mathematical concepts and their limitations, to describe analytical methods at the tissue and single-cell level, and to discuss opportunities to leverage metabolic models to address important mechanistic questions relevant to all patients with cardiovascular disease.

Keywords: metabolism, stable-isotope tracer, metabolic flux analysis, systems biology, cardiovascular disease

OPEN ACCESS

Edited by:
Kedryn K. Baskin,
The Ohio State University,
United States

Reviewed by:
Seitaro Nomura,
The University of Tokyo, Japan
Zhao Wang,
University of Texas Southwestern Medical Center, United States

***Correspondence:**
Anja Karlstaedt
anja.karlstaedt@csmc.edu

Specialty section:
This article was submitted to Cardiovascular Metabolism, a section of the journal Frontiers in Cardiovascular Medicine

Received: *01 July 2021*
Accepted: *18 October 2021*
Published: *11 November 2021*

Citation:
Karlstaedt A (2021) Stable Isotopes for Tracing Cardiac Metabolism in Diseases. Front. Cardiovasc. Med. 8:734364. doi: 10.3389/fcvm.2021.734364

INTRODUCTION

Measuring the dynamic range of cardiac metabolism has been a corner stone of cardiovascular research. Understanding how altered metabolism supports cardiac adaptation during stress and diseases requires a systems-wide approach. Translational models that recapitulate cardiac pathophysiology are critical to advance our understanding of cardiovascular diseases (CVDs) and to utilize metabolic vulnerabilities as biomarkers or for the development of therapeutics. Targeted or untargeted measurements of metabolites allow to assess the metabolic state in an organism *in vivo*. Measurements of metabolic changes in a variety of biological samples are feasible due to advances in chromatographic separation (e.g., hydrophilic interaction chromatography, HILIC; poroshell columns) and improved detection like nuclear magnetic resonance (NMR) and mass spectrometry (MS). However, the interpretation of complex disease models or patient derived samples can be challenging with large scale metabolomics and when a systems-wide understanding of specific pathways is required. Measuring changes in metabolite concentration do not allow to draw any conclusions on metabolic rates or the direction of a flux. Changes in metabolite levels can either result from differential production or utilization of a given intermediate due to increased flux from synthesizing reactions, decreased flux toward consuming reactions, or alterations in transporter activities. For example, during ischemia-reperfusion injury, glycolytic intermediates accumulate despite a reduction in glucose uptake (1–3). Therefore, accurate determination of metabolic flux is necessary for understanding cellular physiology and the pathophysiology of diseases. Steady states in cellular systems are defined by constant values of flux and metabolite concentrations (4). In experimental settings, steady states can be achieved in controlled cell cultures

or *ex vivo* perfusions. However, commonly experiments are performed at pseudo-steady state, where changes in flux or metabolite concentrations are minimal over the observed time frame.

What is metabolic flux? Generally, flux describes the movement of particles across a given area in a specified time. It is important to distinguish between reaction rates and metabolic fluxes. A reaction rate describes the velocity of a given biochemical reaction in response to a substrate and enzyme in isolation, while metabolic fluxes describe the same reaction in the context of a biological system and pathway. Measuring metabolic flux is challenging and cannot be done directly, thus metabolic fluxes are estimations from measurable quantities. Tracer-based approaches provide an apparent straight-forward way of quantitatively assessing dynamic changes in cardiac metabolism. Especially, stable-isotope tracers allow to administer probes to a biological system (e.g., animal cells) in cost-efficient and safe way. At the same time metabolic conversions of labeled nutrients or small molecules allow to track the incorporation of isotopic label (e.g., carbon, nitrogen, or hydrogen) into downstream products and pathways. The detection of specific metabolic products then allows to assess total metabolite changes alongside enzyme activities, flux rates, and overall contribution of specific pathways to the metabolic profile. Tracer studies in isolated perfused murine hearts are commonly used to evaluate metabolic changes in model systems that resemble *in vivo* conditions as closely as possible (5). *In vitro* models using cultured cardiomyocytes have also shown to provide valuable information albeit with a limited scope. The selection of a specific method largely depends on the biological question and inherent limitations of models. Radioactive probes are a stable of both clinical cardiology and basic cardiovascular research (e.g., ^{18}F, ^{3}H, ^{14}C) and are used to study *in vivo* or *ex vivo* metabolic changes in the heart. There are several clinically relevant radiopharmaceuticals such as 99mtechnetium-sestamibi (^{99m}TC-MIBI, or CardioLite) (6) or [^{18}F]-Fluorodeoxyglucose

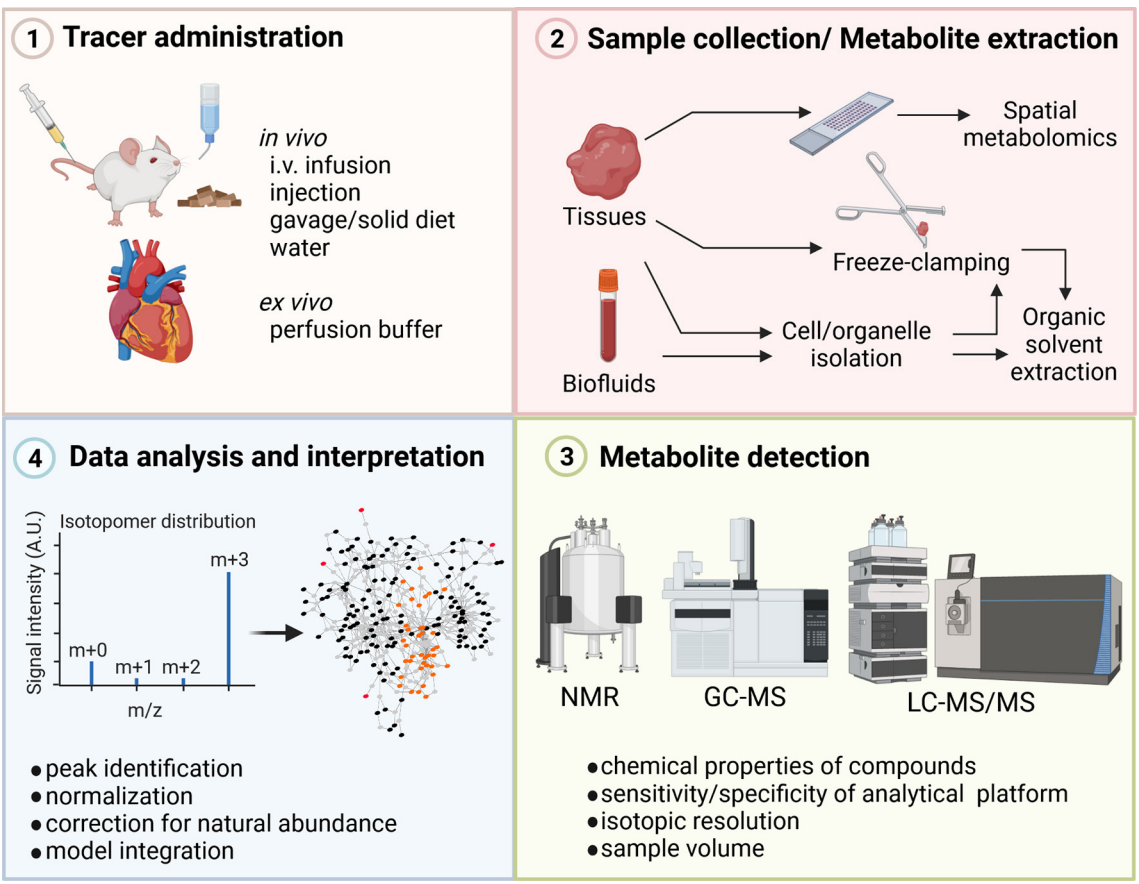

FIGURE 1 | Steps in stable-isotope metabolomics analysis. Stable-isotope tracers to study cardiac metabolism are administered to the model organism or patient using different delivery approaches including, infusion, injections, diet, or *ex vivo* perfusion. Heart tissue or biofluids are collected and metabolites are extracted based on downstream analytical methods. For examples, tissue sample for total metabolite extraction are freeze-clamped in liquid nitrogen and tissue is quenched during extraction using organic solvents. To assess spatial metabolite abundances, tissue slides need to be prepared. Incorporation of isotopic label into metabolites is determined using analytical techniques such as NMR or MS. The isotopic enrichment profile of different metabolites is assessed after normalization and correction for natural abundances. GC, gas chromatography; i.v., intravenous; LC, liquid chromatography, MS, mass spectrometry; NMR, Nuclear magnetic resonance. Figure was created with BioRender.com.

([^{18}F]-FDG) (7) for interrogating metabolic parameters such as nutrient uptake rates. These probes allow safe, non-invasive tracing of metabolic changes *in vivo*. However, readouts of these measurements are serving as surrogates for multiple metabolic pathways. The desire to measure more in-depth metabolic changes in the heart have led to increased application of stable-isotope tracers in clinical studies (8–10). Stable isotope probes (e.g., ^{2}H, ^{13}C, ^{15}N) are less sensitive than radioactive probes, but in a single experiments stable isotope labeling approaches allow to assess multiple pathways simultaneously over longer experimental time periods. Like radiopharmaceuticals, stable-isotope tracers allow flux assessments, but at the same time these probes provide more in-depth analysis of metabolism both using targeted and untargeted discovery oriented analytical approaches. Increased availability and advancements in analytical techniques for metabolomics have made stable isotope tracers increasingly popular in studying cardiac metabolism *in vivo* and *ex vivo*. In this review, we describe recent advances in applying stable isotope tracers in cardiovascular research and discuss important aspects to consider during data analysis allowing accurate assessments of metabolic changes (**Figure 1**).

STABLE-ISOTOPE TRACER METHODS FOR MEASURING CARDIAC METABOLISM *IN VIVO AND EX VIVO*

Multiple techniques are available for the *in vivo* or *ex vivo* delivery of stable-isotope tracers including oral administration *via* diets, gavage or drinking water, direct intravenous infusion, injection, or perfusion of the heart (**Figure 1**). Each experimental method has its limitation thus the choice for the specific delivery needs to be driven by the biological question. In *ex vivo* heart perfusions, tracers are delivered via the perfusion buffer. The perfusion technique itself determines how close to physiologic conditions flux rates and metabolic changes can be measured. Two *ex vivo* perfusion techniques for studying cardiac metabolism and muscle physiology are the method of choice: (1) the Langendorff method and (2) the working heart preparation. The aortic perfusion of Langendorff remains a standard preparation and is popular to this date due to its simpler technical requirements and perfusion apparatus (11–14). However, hearts in this preparation do little or no external work and may require external stimulation which can obfuscate metabolic measurements. The more advanced working heart preparation allows arterial perfusion of the heart. This preparation maintains the physiologic contractile function of the heart and prevents periods of anoxia that may occur during Langendorff preparations (15). Several recent studies applied perfusion techniques in a diverse range of disease models to assess cardiac metabolism (**Table 1**). Regardless of the perfusion technique, tracers are applied through the chemically defined perfusion buffer and allow collection of samples in small time intervals which facilitates dynamic measurements of cardiac metabolism (**Table 1**).

Infusion techniques are likely the most advanced method for the delivery of tracers. Stable isotope tracers are introduced intravenously into the systemic circulation of an animal (e.g., mouse, rat) or human participant. Blood or tissue samples are collected before and after tracer infusion, and isotopic enrichment is then analyzed. Another important factor during stable-tracer experiments is the dynamics of tracers and the determination of metabolite pool sizes (e.g., extracellular vs. intracellular), as well as turnover (or half-life) of metabolites (37). For example, the circulatory system or tubing in heart perfusions can be considered as a single pool. Tracers can be administered (1) continuously or (2) in a bolus. Constant infusion of tracer allows to start sample collections once an isotopic equilibrium is reached, while bolus injection results in an initial increase over time followed by an exponential decrease (37). In either case, pool sizes and compartmentalization of metabolites need to be considered for the estimation of intracellular fluxes (37). Recent studies have shown that pool sizes for metabolites need to be treated as parameters and measured as accurately as possible to improve quality of flux estimations from non-stationary fluxes (38). In metabolomics studies, control and monitoring of the nutrient environment is important. For *in vivo*, special attention needs to be paid to feeding, fasting, diet composition and number of animals per cage. For *ex vivo* studies, special care for the composition of perfusion buffers and reagent purities needs to be taken. For both *in vivo* and *ex vivo* studies it is important to assess if any anesthetic agents may obfuscate metabolic measurements through alterations of plasma metabolite concentrations. The duration of labeling depends on the pathway of interest and whether steady-state data needs to be achieved. In *ex vivo* heart perfusions, steady-state labeling can be reached within 10 to 20 min for key metabolic pathways (39), whereas *in vivo* labeling may require longer timeframes depending on the pathways of interest and tracer (10).

Selecting the right tracer depends on the scope of the study and ultimately which metabolic readout is required for a given biological question. The substrate class (e.g., carbohydrate, amino acid, fatty acid), type of atoms (e.g., ^{13}C, ^{15}N), number of labeled atoms (e.g., uniform vs. single) and position of labeled atoms will determine which products and pathways will incorporate the label. Any of these options increase the complexity of the experimental design and subsequent data analysis. Selecting the right combination of tracers allows delivering multiple probes and interrogation of multiple pathways simultaneously. Parallel tracing experiments are limited to few applications, but recent advances in high resolution mass spectrometry and development of new probes show promise. For a comprehensive overview of stable-isotope tracers and their readouts, readers are referred to **Table 2** in (78). In uniformly labeled tracers, all atoms of interest are substituted with a stable isotope, while single or select position labeled tracers only carry isotopes at specific atoms. The advantage of uniform labeling is better coverage of a variety of different pathways while select position labeling allows to target specific reaction.

Considering the diversity and versatility of stable isotope tracers, which criteria can we apply to select the optimal probe for a given experiment? The chemical properties, including kinetics, specificity, and turnover, are critical components of tracer selection. Tracer kinetics must be almost identical to

TABLE 1 | Overview of recent *in vivo* and *ex vivo* stable-isotope tracer studies in cardiovascular research, including administration methods, analytical platform, and chromatographic modes.

Disease/model	Organism	System	Tracer	Administration method	Analysis	Chromatographic Mode	Mathematical Model	Measurement	References
Glucose									
Type II Diabetes	Mouse	Cardiac progenitor cells	[U-^{13}C] glucose	Replacement of glucose in cell culture medium	FT-ICR MS	N/A		Incorporation of ^{13}C into different metabolites	(16)
Assessing pentose phosphate pathway flux	Mouse	Heart, Liver	[2,3-^{13}C]-glucose	Adminstration during *ex vivo* Langendorff perfusion	NMR	N/A		Incorporation of carbons into glutamine intermediates	(17, 18)
Hexosamine biosynthesis pathway	Mouse	Heart	[U-^{13}C]-glucosamine	Administration during *ex vivo* working heart and Langendorff perfusion	LC-MS	HILIC		Incorporation of carbons into different metabolites	(19)
			[U-^{13}C] glucose						
Mitochondrial pyruvate carrier	Mouse	Heart	[U-^{13}C]-glucose	Administration during *ex vivo* Lagendorff perfusion	LC-MS	HILIC		Incorporation of carbons into different metabolites	(20)
					GC-MS	GC			
Fatty acids									
Type II Diabetes	Mouse	Heart	[U-^{13}C] glucose	Administration during *ex vivo* Lagendorff perfusion	LC-MS	HILIC		Incorporation of 13C into different metabolites	(21)
			[U-^{13}C] palmitate						
Absorption of dietary lipids during infancy and adulthood	Mouse	Multiple internal organs	[U-^{13}C]-trolein	Intragastric administration of lipid bolus	GC-MS	GC		Incorporation of carbons and hydrogen into fatty acids	(22)
			[U-^{2}H]-oleate						
			[1,2,3,4-^{13}C]-stearate						
			[U-^{13}C]-palmitate						
Doxycyline mediated cardiac dysfunction	Rat	H9C2	[U-^{13}C] glucose	Replacement of glucose in cell culture medium	LC-MS	HILIC		Incorporation of carbons into different metabolites	(23)
Perinatal myocardial glucose metabolism	Sheep	Heart	[U-^{13}C] glucose	Infusion through fetal tibial artery/inferior vena cava and fetal brachial artery/coronary sinus	NMR	N/A		Determination of AV-differences in the incorporation of carbons into different metabolites	(24)
Nutrient utilization	Rat	neontal cardiomyocytes	[U-^{13}C] glucose	Replacement of glucose in cell culture medium	FT-ICR MS	N/A		Incorporation of carbons into different metabolites	(25)
Glucose/fatty acids									
Primary carnitine deficiency	Human	whole body assessment	[U-^{13}C]-palmitate	continuous intra venous infusion into cubital vein	GC-MS	GC		Measurement of $^{13}CO_2$ to determine total fatty acid and palmitate oxidation rates	(26)
			[2-^{2}H]-glucose	Bolus intra venous infusion into cubital vein					

(Continued)

TABLE 1 | Continued

Disease/model	Organism	System	Tracer	Administration method	Analysis	Chromatographic Mode	Mathematical Model	Measurement	References
Influence of dietary fats	Human	Plasma/breath	[2-^{2}H]-palmitate	Continuous intra venous infusion into antecubital vein	GC-MS	GC		Incorporation of hydrogen into NEFA, TAG and lipoprotein-TAG fractions	(27)
		Plasma	$^{2}H_2O$	Drinking water				Incorporation of hydrogen into VLDL-TAG palmitate	
		Plasma/breath	[U-^{13}C]palmitate					Measurement of ^{13}CO2 to determine palmitate oxidation rates; Incorporation of carbons into NEFA, TAG, and lipoprotein-TAG fraction	
Propionate-mediated pertubance of cardiac metabolism	Rat	Heart, Liver	[U-^{13}C] glucose	Administration during *ex vivo* Langendorff and liver perfusion	GC-MS	GC		Incorporation of carbons into different metabolites	(28)
			[1-^{13}C]-palmitate						
			[1-^{13}C]-octanoate						
			[U-^{13}C]-propionate						
Hexokinase II function	Mouse	Heart	[U-^{13}C] glucose	Administration during *ex vivo* Lagendorff perfusion	GC-MS	GC		Incorporation of carbons into lactate, pyruvate, and Krebs cycle intermediates	(2)
			[U-^{13}C] palmitate						
Amino acids									
Insulin-resistance	Mouse	Multiple internal organs	[U-^{13}C]-BCAA	^{13}C-BCAA infusion at ~20% of rate of appearance	LC-MS	Amide Column	Modeling of tissue and organ oxidation flux	Incorporation of carbons into tissues and proteins	(10)
Type II Diabetes	Rat	cardiomyocytes	[U-^{13}C]-leucine	Replacement of leucine in cell culture medium	GC-MS	GC		Incorporation of leucine derived carbons into different metabolites	(29)
Multiple tracer									
Hypertrophy	Rat	Adult Cardiomyocytes	[U-^{13}C]-FA mix	replacement of nutrients in cell culture medium	GC-MS	GC		Enrichment of different metabolites in cardiomyocytes or tissue sample and determination of pathway activities	(3)
	Mouse	Heart	[U-^{13}C] glucose	13C6-glucose injection after sham/TAC surgery, replacement of nutrients in cell culture medium	LC-MS	HILIC			
	Rat	Adult Cardiomyocytes	[U-^{15}N]-aspartate	replacement of nutrients in cell culture medium	LC-MS	Amide Column			

(Continued)

TABLE 1 | Continued

Disease/model	Organism	System	Tracer	Administration method	Analysis	Chromatographic Mode	Mathematical Model	Measurement	References
Ischemia reperfusion injury	Mouse	Heart	[U-^{13}C]-aspartate	Administration during *ex vivo* heart perfusion	LC-MS	reversed phase		Enrichment of different metabolites	(30)
			[U-^{13}C]-glucose						
			[U-^{13}C/^{15}N]glutamine						
Oxidative stress	Rat	Neontal cardiomyocytes	[U-^{13}C] glucose	Replacement of glucose and glutamine in cell culture medium	GC-MS	GC		Incorporation of ^{13}C into different metabolites	(31)
			[U-^{13}C]glutamine						
Nutrient utilization	Rat	Heart	[U-^{13}C]-glucose	Administration during *ex vivo* Langendorff perfusion	LC-MS	C18 reversed phase	Prediction model of isotopomer distribution and experimental validation	Incorporation of ^{13}C into different metabolites	(32)
			[U-^{13}C]-TAG mix						
Modeling of perfused working hearts	Mouse	Heart	[U-^{13}C]-lacate	Administration during working heart perfusion	GC-MS	GC	^{13}C-Metabolic flux analysis	Incorporation of carbons into different metabolites	(33, 34)
			[U-^{13}C]-pyruvate						
			[U-^{13}C]-glucose						
			[U-^{13}C]-oleate						
Absorption of dietary lipids during infancy and adulthood	Mouse	Multiple internal organs	[U-^{13}C]-trolein	Intragastric administration of lipid bolus	GC-MS	GC		Incorporation of carbons and hydrogen into fatty acids	(22)
			[U-^{2}H]-oleate						
			[1,2,3,4-^{13}C]-stearate						
			[U-^{13}C]-palmitate						
Myocardial Sodium elevation	Mouse	Heart	[U-^{13}C]glucose; [1-H]	Administration during ex vivo Langendorff perfusion	NMR	N/A	Flux balance analysis using CardioNet	Incorporation of carbons and hydrogen into metabolic intermediates	(38, 39)

TABLE 2 | Resources for network reconstruction, simulation and visualization of metabolic flux analysis using stable-isotope tracers.

	Details	Resource link	References
Metabolic networks of cardiac metabolism			
CardioNet	Genome-scale metabolic network of mammalian/human cardiac metabolism	https://karlstaedtlab.github.io/cardionet/cardionet	(35, 36)
CardioGlyco	Kinetic model of myocardial glycolysis and oxidative phosphorylation	https://karlstaedtlab.github.io/cardionet/resources; https://www.ebi.ac.uk/biomodels/MODEL1910170001	(39)
iCardio	Metabolic network of cardiac metabolism based on proteomics information from the human protein atlas and existing human metabolic network reconstructions	https://github.com/csbl/iCardio	(40)
Reactome	Comprehensive open-source pathway database that allows visualization, data integration and interpretation across different data types and organisms	https://reactome.org	(41)
Recon3D	Genome-scale network reconstruction of human metabolic functions; network captures information across organ systems	http://bigg.ucsd.edu/models/Recon3D; https://www.vmh.life/	(42)
TSEM	Tissue-Specific Encyclopedia of Metabolism (TSEM) using the metabolic Context-specificity Assessed by Deterministic Reaction Evaluation (mCADRE)	https://hood-price.isbscience.org/research/tsem/	(43)
Databases			
Uniprot	Database for protein sequence and functional information	https://www.uniprot.org/	(44)
Human metabolome	Comprehensive resource and coverage of the human metabolome with biofluid or tissue concentration data, annotation of compounds to reference spectra, chemical structure visualization, chemical taxonomy, and interactive pathway maps	https://hmdb.ca/	(45)
Brenda	Enzyme information database including classification, nomenclature, reaction and specificity, structures, and organism-related information	https://www.brenda-enzymes.org/	(46–48)
KEGG	Kyoto Encyclopedia of Genes and Genomes; database resource for understanding biological systems	https://www.genome.jp/kegg/	(49–52)
Tools for correction of naturally occurring isotopes			
MIDcor	Tool for the correction of raw MS spectra for naturally occurring isotopes and overlapping peaks; Requires R	https://github.com/seliv55/mid_correct	(53)
IsoCorrectoR	R-base tool comprising several correction functions	http://bioconductor.org/packages/release/bioc/html/ IsoCorrectoR.html	(54)
IsoCor	Open-source tool for the correction of MS data for naturally occurring isotopes	https://isocor.readthedocs.io/en/latest/#; https://github.com/MetaSys-LISBP/IsoCor/	(55, 56)
Software for metabolic flux analysis			
13CFLUX2	Simulation of ^{13}C-MFA; allows network modeling, isotope labeling states, parameter estimation and statistical analysis; implementation of cumomer and EMU simulation algorithms	https://www.13cflux.net/13cflux2/	(57, 58)
SumoFlux	Tool integrates modeling and machine learning algorithms to estimate flux ratios from measurable ^{13}C-data	https://gitlab.ethz.ch/z/sumoflux	(59)
OpenFLUX	MATLAB-base modeling software for ^{13}C-MFA; includes EMU simulation algorithm	https://github.com/lakeeeq/OpenFLUX	(60)
Influx_s	Open-source tool for metabolic flux estimation and metabolite concentrations from stationary and instationary labeling (MFA and INST-MFA)	https://metasys.insa-toulouse.fr/software/influx/	(61)
INCA-MFA	Isotopomer Network Compartmental Analysis (INCA) MFA suite is a MATLAB-based package for isotopomer network modeling and metabolic flux analysis; INCA-MFA allows INST-MFA and constrained based analysis of stable-isotope data	https://mfa.vueinnovations.com/	(62, 63)
SpaceM	SpaceM is an open-source method for *in situ* single-cell metabolomics that integrates microscopy with MALDI-imaging mass spectrometry.	https://github.com/alexandrovteam/SpaceM	(64)

(Continued)

TABLE 2 | Continued

	Details	Resource link	References
COBRA Toolbox	Constraint-based reconstruction analysis (COBRA) allows the reconstruction, modeling, topological analysis, strain and experimental design, network analysis, and network integration of chemoinformatic, metabolomic, proteomic, and thermochemical data; integration with MATLAB, Gurobi or python	https://github.com/opencobra/cobratoolbox/	(65)
MATLAB	Matlab is a commercial programming and numeric computing platform; Optimization Toolbox™ provides functions for optimization problems including solvers for linear programming, mixed-integrer linear programming, and constrained linear least squares	https://www.mathworks.com	(66)
Solvers			
Gurobi Optimizer	Commercial optimization solver for linear programming, quadratic programming, and mixed integer quadratic programming optimization problems	https://www.gurobi.com	(67)
IBM-ILOG CPLEX	Commercial optimization studio to solve complex optimization models	https://www.ibm.com/analytics/cplex-optimizer	(68)
Programming languages			
R	R is a programming language for statistical computing and graphics	https://www.r-project.org/	(69)
Perl 5	Perl is a family of high-level, general-purpose, interpreted, dynamic programming languages	https://www.perl.org/	(70)
Python	Python is a high-level, general-purpose, interpreted, dynamic programming languages		(71)
Network visualization and data integration			
Cytoscape	Open source platform for the visualization of complex networks and multi-omics data analysis	https://cytoscape.org/	(72)
Metaboverse	Interactive desktop tool for visualization and multi-omics data integration across different species; reactome database integration	https://github.com/Metaboverse/	
Other useful resources for data analysis and sharing of metabolomics data			
ChemRich	Tool to analyze metabolomics data based on chemical similarity. ChemRich utilizes chemical ontologies and structural similarity to group metabolites	https://chemrich.idsl.me/; https://chemrich.fiehnlab.ucdavis.edu/	(73)
Chemical Translation Service	Tool for single or batch conversion of metabolite; allows annotation between over 200 databases	http://cts.fiehnlab.ucdavis.edu/	(74)
PubChem Identifier Exchange Service	Tool for single or batch conversion of metabolite within the PubChem database	https://pubchem.ncbi.nlm.nih.gov/idexchange/idexchange.cgi	(75)
Metabolomics Workbench	International open-access curated repository for metabolomics metadata and experimental data across various species and experimental platforms, metabolite standards, metabolite structures, protocols, tutorials, and educational resources	http://www.metabolomicsworkbench.org/	(76)
MetaboLights repository	Open-access curated repository for metabolomics studies, their raw experimental data and associated metadata	http://www.ebi.ac.uk/metabolights	(77)

unlabeled compounds and probes should not accumulate in tissue. Non-specific binding to other proteins and lipids is generally a concern when using radionucleotides but similar demands need to be met by stable isotope tracers. Lastly, turnover time and tissue concentration of tracers should follow the range of non-labelled metabolites to avoid mass effects and optimal signal-to-noise ratios. Selection of tracers can also be based on metabolic read-outs and targeted toward a pathway of interest. Uniformly labeled tracers of common nutrients (e.g., glucose, fatty acids, or amino acids) can be used to determine how these nutrients are utilized in multiple pathways. Combination with single labeled tracers in parallel experiments then allows to detect specific metabolic fluxes. Different labeling strategies are best described using glucose because of its high abundance, commercial availability, and ease of use in experimental settings. For example, [1-^{13}C]glucose can be used to measure the decarboxylation of 6-phosphogluconate to ribulose 5-phosphate in the oxidative branch of the pentose phosphate pathway and the decarboxylation of pyruvate to acetyl-CoA by pyruvate dehydrogenase in the Krebs cycle (**Figure 2A**). Pentoses produced via the oxidative pentose phosphate pathway can reenter glycolysis via the non-oxidative pentose phosphate pathway branch. Resolution of both glycolysis and pentose phosphate pathway fluxes can be achieved using

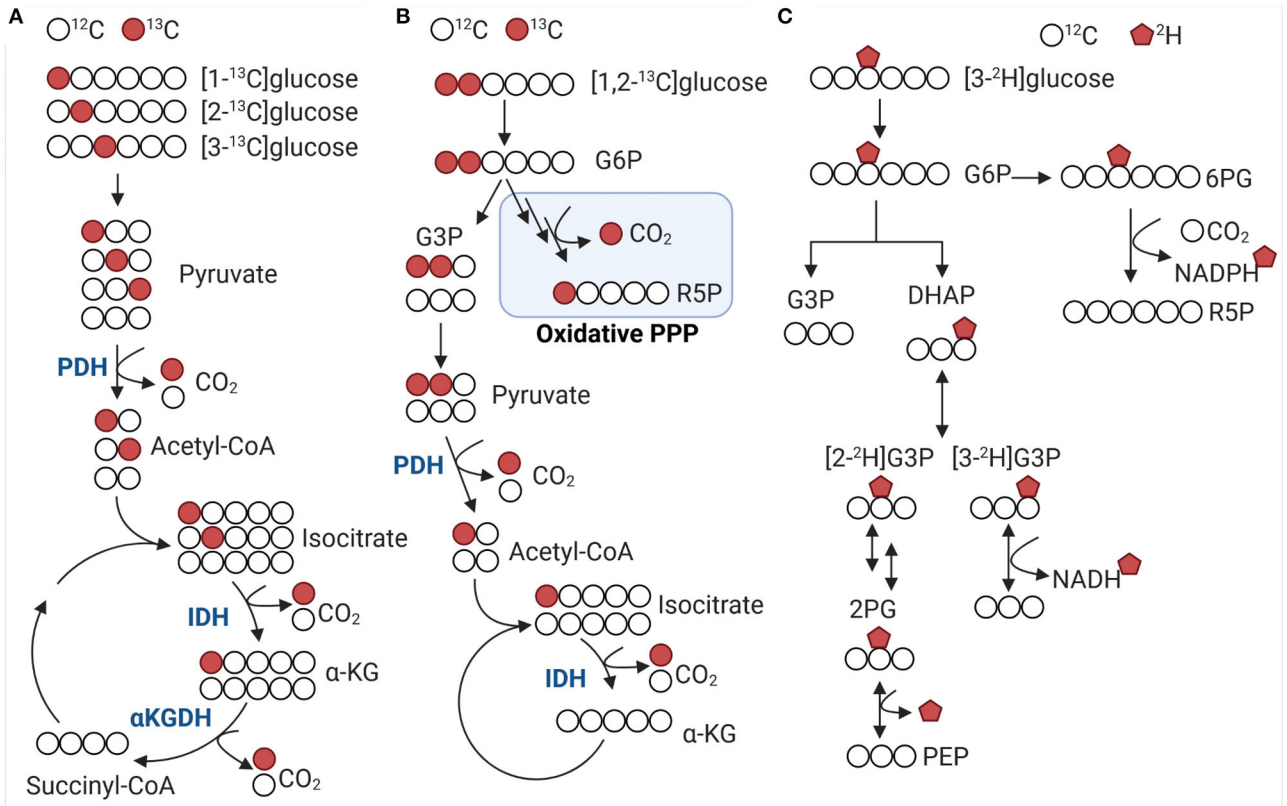

FIGURE 2 | ^{13}C and ^{2}H distribution from labeled glucose in glycolysis and Krebs cycle. **(A,B)** ^{13}C-glucose is decarboxylated at different steps in the Krebs cycle and oxidative pentose phosphate pathway. Colored circles indicate ^{13}C label for selected metabolic intermediates. [2-^{13}C]glucose and [3-^{13}C]glucose are associated with pyruvate dehydrogenase (PDH) activity producing m+2 and m+3 acetyl-CoA, respectively. Using [1,2-^{13}C]glucose allows to distinguish between glycolysis and oxidative pentose phosphate pathway (PPP) flux. **(C)** [3-^{2}H]glucose enters the PPP *via* glucose 6-phosphate (G6P) and decarboxylated to ribulose 5-phosphate (R5P), which generates ^{2}H-NADPH. DHAP, dihydroxyacetone phosphate; G6P, glucose 6-phosphate; G3P, glyceraldehyde 3-phosphate; IDH, isocitrate dehydrogenase; α-KG, α-ketoglutarate; α-KGDH, α-Ketoglutarate dehydrogenase; PDH, pyruvate dehydrogenase; PPP, pentose phosphate pathway; 6PG, 6-phosphogluconate; 2PG, 2-Phosphoglycerate; PEP, phosphoenolpyruvate; R5P, ribulose 5-phosphate.

[1,2-^{13}C]glucose tracer (**Figure 2B**). When glucose is converted through glycolysis, unlabeled (m + 0) and twice labeled (m + 2) pyruvate is produced. Conversion of glucose through glycolysis and the oxidative pentose phosphate pathway produces unlabeled (m + 0), single (m + 1) and twice labeled (m + 2) pyruvate. These flux alterations can occur in the background of increased pentose production via the non-oxidative pentose phosphate pathway which will make it difficult to detect changes in pyruvate labeling (79, 80). Parallel labeling using [1-^{13}C], [1,2-^{13}C], and [U-^{13}C]glucose can improve detection of subtle, aberrant changes in metabolic flux (**Figure 2B**) (81). Alternatively, [3-^{2}H]glucose can also be used to determine redox changes in central carbon metabolism by gaining insight into the *de novo* NADPH synthesis in the oxidative pentose phosphate pathway (**Figure 2C**) (82). Likewise [2-^{13}C] and [3-^{13}C]glucose can be used to evaluate the decarboxylation of isocitrate to α-ketoglutarate by isocitrate dehydrogenase and α-ketoglutarate to succinyl-CoA by α-ketoglutarate dehydrogenase (**Figure 2A**), respectively. Additionally, [2-^{13}C] and [3-^{13}C] glucose enable determining acetyl-CoA and fatty acid synthesis in the mitochondria and cytosol. The measurement of transporter activities can be achieved by using chemical analogs as tracers. Chemical analogs are compounds that have chemical structures like natural substrates, but with modifications at key positions. These modifications limit how these molecules can be metabolized and lead to accumulation of substrates in tissues. For example, the analog 2-deoxyglucose is transported across the cell membrane and phosphorylated by hexokinase in the same manner as glucose, but because the second carbon has been replaced by a hydrogen it cannot undergo further reactions. As such, 2-deoxyglucose competitively inhibits phosphoglucose isomerase and limits glycolysis. Using analogs 2-deoxyglucose or methyl-D-glucose allows determining uptake flux of glucose. In combination with other tracers it is possible to determine the overall utilization (uptake and metabolization) of glucose. To gain insight into the systems-wide response during disease development, it is also necessary to assess how metabolic alterations are linked to protein dynamics and posttranslation modifications (83, 84). Stable isotope tracers enable measuring posttranslational modifications of proteins. Protein methylation

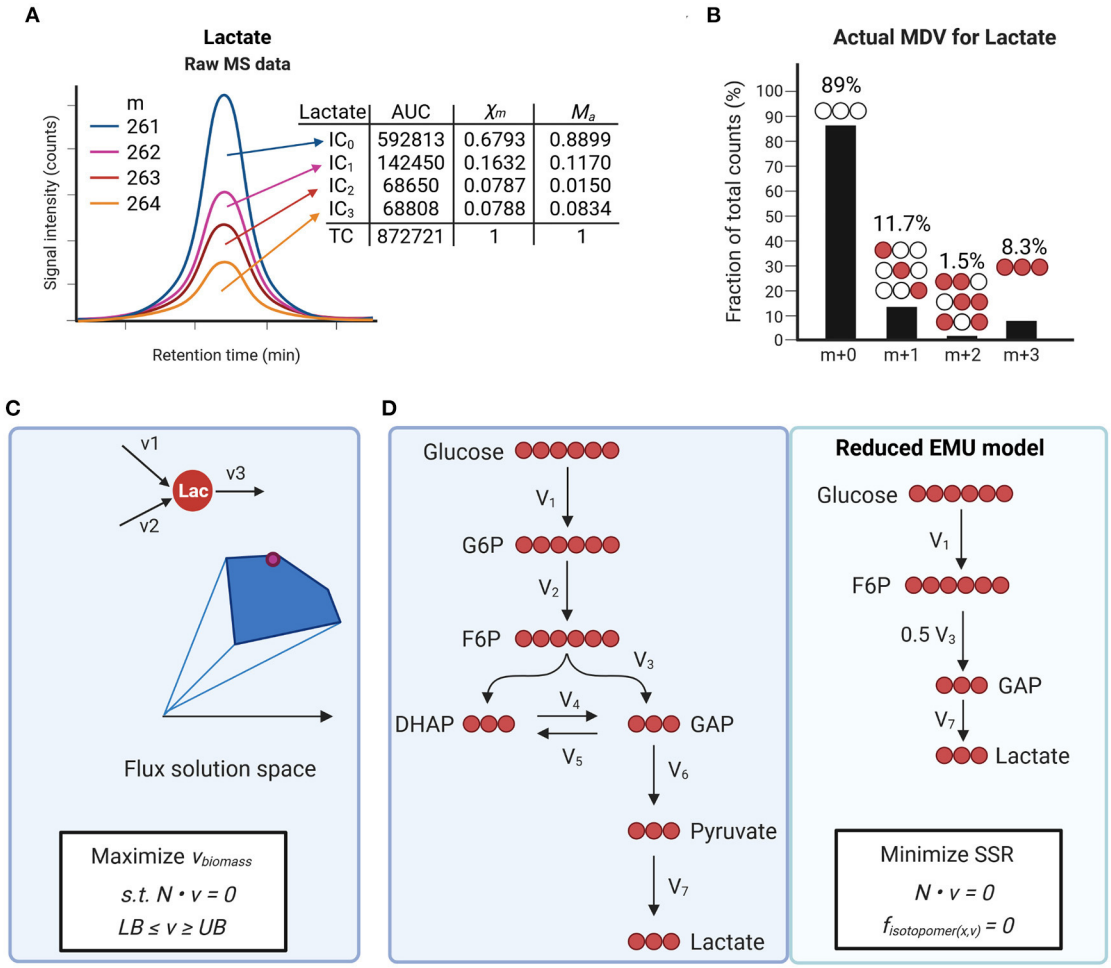

FIGURE 3 | Isotope tracing to measure metabolic fluxes. **(A,B)** Example of isotopomer distribution analysis using mass spectrometry (MS) for ^{13}C-lactate. Ion counts for different isotopologues (IC) are determined by measuring the area under the curve (AUC). Mass distribution vectors (MDVs) for lactate (X_m) are determined by dividing each IC by the total counts (TC). Measured MDVs are then corrected for naturally occurring isotopes **(B)**. Actual MDVs for lactate can now be used for further data analysis such as metabolic flux analysis. **(C)** Flux balance analysis allows estimating flux distributions at steady state. Optimization functions are defined based on biological questions and applied to a network. Constraints for each flux vector are defined as lower bonds (LB) and upper bonds (UB) which allow to define flux solution spaces. **(D)** Schematic of carbon atom distribution in a simplified model of glycolysis using [U-^{13}C]-glucose infusion. Network reactions can be further reduced to a define a final reduced EMU model. Flux distributions are estimated by minimizing the sum of least-squared residuals (SSR) between the measured rates and model predicted rates subject to stoichiometric constrain.

and acetylation can be determined by combining ^{13}C-glucose with ^{15}N or ^{13}C-alpha ketoacids and ^{11}C acetate, respectively. The methionine analog, azidohomoalanine, is enables labeling newly synthesized proteins during a short pulse-labeling period (85). The advantage of amino acid analogs compared to ^{13}C or ^{15}N-labeled amino acids is high sensitivity even at early time points when protein alterations are difficult to identify and often obscured by higher abundant proteins (e.g., structural proteins).

A prerequisite for accurate metabolic measurements is the sample collection and preparation. Metabolites have different turnover rates and differences in their abundance can easily lead to obfuscation of experimental data. For example, rapid degradation of NADPH and CoA derivatives during sample preparation have been well-documented (86, 87). Developing methods and additives to preserve metabolites remains an area of active research. For tissue specimens, freeze clamping using the Wollenberger technique allows rapid freezing of tissue in liquid-nitrogen (88–90). In contrast to flash freezing, this technique has been shown to be superior in homogenously freezing tissue sample and preserving metabolic data. Tissue specimen can then be stored at −80°C for further processing. Similar, metabolite extractions using organic solvents (e.g., methanol:water, 80:20 w/w) quench metabolic profiles and help to reduce enzymatic activities. Measuring more instable metabolites such as NADPH or AMP, a mixture of acetonitrile:methanol:water (40:40:20, w/w) with 0.1 M formic acid can effectively capture and preserve readouts (86, 91). Additionally, adding internal standards during sample extraction can help tracking sample loss and allows

correction between batches (87). Independent of the model system or delivery technique, special attention needs to be paid toward standardization of experimental conditions, and sample collection and preparation to ensure rigor and reproducibility of metabolic tracer experiments (76).

MATHEMATICAL MODELING OF METABOLIC FLUX DISTRIBUTIONS

Mathematical modeling and computer simulations can help to understand the complex dynamics and interactions of biological processes. A network of biochemical reactions within an organism can be represented by mathematical equations based on established knowledge or extrapolation from other systems. Metabolic models or networks can help to conceptualize and test biological hypothesis *in silico*. In the context of stable-isotope tracer analysis, models are required to estimate flux distributions and explain labeling states for specific metabolites. These modeling approaches can describe the metabolic state of a biological system, but they cannot predict or explain it by identifying regulatory enzymes or principles (e.g., feedback interactions) (4).

Tracer studies can be analyzed using different approaches and level of depth. Most studies determine the relative incorporation of tracer into metabolites and assess qualitative changes in pathway activities. Isotopomers are defined as isomers of a given metabolite that differ only in the mass shift of their individual atoms, for example, ^{13}C vs. ^{12}C and ^{2}H vs. ^{1}H in carbon- and hydrogen-labeling studies, respectively. Stable-isotopomer measurements are interpreted by defining mass-distribution vectors (MDVs) that reflect the incorporation of label from a tracer into downstream metabolites (**Figure 3A**) (57, 92). MDVs are defined as follows:

$$\vec{X} = \{X_0, X_1, \ldots, X_n\} \quad (1)$$

$$\sum_{j=0}^{n} X_j = 1 \quad (2)$$

Where each component X_j (with $j = 0, 1, \ldots, n$) represents the fraction of a metabolite's pool that corresponds to the jth labeled isotopolog and n is the maximum number of labeled atoms that a metabolite can incorporate. The fractional isotope enrichments, X_j, and their sum equal 1 or 100%. In stable isotope labeling, incorporation of j labeled atoms causes a mass shift of j atomic units nominal to the mass M of the unlabeled metabolite. Therefore, the MDV is often denoted as follows:

$$\vec{X}_m = \{X_{m0}, X_{m1}, \ldots, X_{mn}\} \quad (3)$$

$$X_{mj} = \frac{IC_j}{TC}$$

Where IC denotes the isotopolog count for a given metabolite j and TC denotes the sum of all isotopolog counts. For example, the MDV for ^{13}C-labeled glucose can be determined as:

$$\vec{X}_{glucose} = \left\{X_{m0}, X_{m1}, X_{m2}, X_{m3}, X_{m4}, X_{m5}, X_{m6}\right\} \quad (4)$$

with $n = 6$, because a glucose molecule has six carbon atoms where ^{13}C-label can be incorporated. X_{m0} represents the fraction of unlabeled glucose within the total metabolite pool, and $X_{m2} = 0.1$ would indicate that 10% of the total glucose pool carries two ^{13}C-labeled carbons. Based on the MDV it is not possible to assess where the incorporation of label occurred.

When using stable isotope labeling it is important to correct for natural occurrence of stable isotopes of all atoms within a metabolite. This correction is particularly important when derivatization agents are used during sample preparation (e.g., GC-MS requires derivatization using TBDMS), highly abundant metabolites (e.g., glucose), or single labeled tracers ($n = 1$) are being used. For instance, carbon appears in the form for two stable isotopes, ^{12}C and ^{13}C, with a natural occurrence of ∼98.9 and 1.1%, respectively. When using ^{13}C-tracers, measurements need to be corrected for this natural occurrence. Several tools have been developed (see **Table 2**) (53–56) that allow automatic correction of labeled isotopologues of a given metabolite by solving a linear equation as follows:

$$\vec{X}_m = \overrightarrow{M}_a \cdot \overline{\overline{L}} \quad (5)$$

where $\vec{X}_m$ and $\overrightarrow{M}_a$ depict the measured MDV and actual MDVs for a metabolite, respectively. The jth row of the matrix $\overline{\overline{L}}$ contains the theoretically predicted MDV for the jth labeled isotopolog. Determining the actual MDVs for each metabolite is a critical step prior to further data analysis and flux interpretation (**Figure 3B**). To achieve quantitative information about metabolic conversion rates or flux rates different mathematical approaches need to be applied depending on the scope of the study and data type. Techniques in mathematical modeling can be broadly divided into ordinary differential equation and constrained based modeling. For a comprehensive compilation of different modeling techniques and applications, the reader is further referred to Klipp et al. (93).

Flux balance analysis (FBA) is a constrained-based modeling technique that relies on balancing fluxes around metabolites within a network stoichiometry (**Figure 3C**). Flux distributions in FBA are estimated based on (1) the steady-state assumption, (2) constraints derived from the metabolic environment (e.g., nutrient supply, oxygen consumption), and (3) an objective function such as biomass synthesis, energy provision or another cellular function that is critical for the organ system. Several groups have successfully applied this algorithm and integrated metabolomics data to study cardiac metabolism (35, 36, 40, 94). One limitation of FBA is the requirement for stationary flux patterns without any integration of thermodynamic feasibility. Several methods have been developed to allow inclusion of thermodynamic constraints and even dynamic optimization (95, 96).

^{13}C-Metabolic flux analysis (^{13}C-MFA) is most widely used in assessing flux in stable-isotope tracer experiments (92). In ^{13}C-MFA, isotopomer distributions from labeled substrates (e.g., ^{13}C-glucose) are incorporated into a mathematical model of atom transfers and combined with measurements of nutrient uptakes and secretions, and biomass function. The distribution

of fluxes throughout a cellular metabolism is mathematically estimated by iteratively solving a least-square regression problem of isotope labeling measurements and extracellular exchanges rates. The models applied to data regression comprise mass balances and isotopomer balances on all network components, thus often encompasses hundreds of equations. The sum of squared residuals (*SSR*) is defined as follows:

$$Minimize\ SSR = \sum \frac{(x - x_m)^2}{\sigma_x^2} + \sum \frac{(r - r_m)^2}{\sigma_r^2} \quad (6)$$

$$N \times v = 0 \quad (7)$$

$$R \times v = r \quad (8)$$

$$f_{isotopomer}(v) = 0 \quad (9)$$

Stationary fluxes (v) are estimated by the assumption of a steady state (equation 7) and minimizing SSRs between simulated (x) and experimentally derived (r) MDVs for a given metabolite *S*. The stoichiometry matrix of a given metabolic network is represented by *N*. Uncertainties, σ, can be estimated based on the root-mean square error of unenriched control samples and the standard error of measurement of technical MS replicates. For a metabolite *S*, steady state implies that the total rate at which it is supplied is equal to the total rate at which it is removed (see **Figure 3**). If the whole system is in a steady state these reaction rates are identical to the corresponding fluxes. Therefore, reaction rates and flux are often used interchangeably (97). In studies using direct infusion or *ex vivo* perfusion techniques, relative fluxes can be converted to absolute fluxes using known infusion rates or flow rates for specific tracers. A prerequisite for applying the above given mathematical concept is that measurements were conducted after reaching isotopic steady state.

A given metabolite comprising n atoms may exist in either labeled or unlabeled states with 2^n isotopomers. For example, glucose ($C_6H_{12}O_6$) consists of 64 carbon atom isotopomers ($n = 6$, 2^6), 4,096 hydrogen atom isotopomers ($n = 12$, 2^{12}), and combined 2.6×10^5 ($2^6 \times 2^{12}$) carbon and hydrogen isotopomers. Therefore, additional methods have been developed to allow the integration of multiple isotopic tracer systems (98). Without these methods, mathematical analysis of tracer studies is often limited to single isotopic tracers to allow efficient simulation of flux distributions. In the elementary metabolite units (EMU) framework labeling information is broken down into multiple individual sub-problems consisting of many coupled non-linear equations (98). The method uses a decomposition algorithm that identifies the minimum amount of information needed to simulate isotopic labeling within a given metabolic network. This approach is different from isotopomer methods, where the model includes all possible isotopomers resulting in an exponentially larger number of variables. The EMU framework requires fewer variables, thus allows the analysis of labeling by multiple isotopic tracers (**Figure 3D**). For a metabolite comprising n atoms, $(2^n - 1)$ EMUs are possible. The algorithm allows to identify a minimal set of EMUs to be considered in the simulation model, which reduces the overall number of variables and makes the computational analysis feasible even for multiple-tracer experiments and larger scale models (98). A given metabolic network is decomposed into different blocks of EMUs (98–100), which are expressed as follows:

$$A_i \cdot X_i = B_i \cdot Y_i \quad (10)$$

where matrices A_i and B_i are strictly linear functions of fluxes. In case ^{13}C labeling has not reached a steady state, isotopically non-stationary MFA (INST-MFA) methods can be used (62). INST-MFA describes the isotopomer balances using ordinary differential equations (ODEs) rather than linear regression models (92). The advantage of ^{13}C-MFA is a higher flux precision and enhanced confidence in the accuracy of estimated fluxes. A typical tracer experiment using [U-^{13}C]-glucose can result in 50 to 100 isotopic labeling measurements which are used to estimate just 20 to 30 independent metabolic flux parameters. This leads to redundancy in flux information and ultimately increases confidence.

Several publicly and commercially available software packages have been developed in recent years to facilitate network reconstructions and computational analysis of metabolic network using ^{13}C-MFA and INST-MFA methods (62). **Table 2** provides an overview of selected resources and repositories, which can be used to analyze stable-isotope tracer studies and may serve as a starting point for readers who are less familiar with including mathematical modeling into their data interpretation. Each of the listed resources serve a different purpose during the metabolomics workflow and in some instances can help with experimental design and selection of tracer probes or analytical platforms (**Figure 1**). For example, genome-scale reconstructions of cardiac metabolism allow to assess during the study design which metabolic reactions may be involved in the phenotype generation (35, 36, 39). *In silico* simulations can also determine which tracers are required or which metabolites need to be measured for the correct assessment of cardiac metabolic changes. MFA platforms like INCA and SumoFlux allow simulating tracer kinetics, which can be useful to determine when a given tracer may reach steady state under the experimental conditions (59, 63). Here, mathematical modeling can help narrowing done tracer options and provide unbiased analysis prior to experiments. EMU approaches can be used to select tracers for a given network and metabolic pathway by providing one optimal tracer or a reduced list of feasible tracers depending on the probe sensitivity, labeling pattern, and complexity of the metabolic network. Careful consideration of tracer type and labeling pattern prior to an experiment can help reducing potential computational burden of data analysis and improve overall data interpretation by providing clear isotope patterns.

PLATFORMS FOR METABOLOMICS AND SINGLE-CELL ANALYSIS

The goal of metabolomics is to comprehensively measure the metabolic composition of a sample in a single analysis. Different analytical platforms combine unbiased, rapid, reproducible, and stable analysis of complex samples in a single run. Each

technology has its advantages and disadvantages in terms of sensitivity, throughput, reproducibility, robustness, quantitation, and suitability for specific chemical classes of metabolites. These analytical chemistry techniques range from high-performance liquid chromatography (HPLC), gas chromatography-mass spectrometry (GC-MS), liquid chromatography-mass spectrometry (LC-MS), gas chromatography combustion isotope ratio mass spectrometry (GC-C-IRMS), capillary electrophoresis-mass spectrometry (CE-MS), Fourier transform-ion cyclotron-mass spectrometry (FT-ICR-MS), and nuclear magnetic resonance (NMR). Broadly, analytical chemistry techniques can be divided into (i) separation, (ii) identification, and (iii) quantification of metabolites from a complex sample (e.g., tissue, blood). The separation of metabolites is accomplished using chromatography (GC, HPLC) or CE. Sample detection is then achieved using fluorescence, ion conductivity, or spectrometry (MS, NMR, light absorption). MS and NMR are different types of spectrometers that measure physical characteristics over a given spectrum. MS measures masses within a chemical sample through their mass-to-charge ratio (m/z), while NMR measures the variation of nuclear resonant frequencies. Both detection techniques can be combined with a different separation method allowing customized application methods for a specific type of sample and compound. MS and NMR are widely used in metabolomics to detect and analyze stable isotope tracer studies, such as ^{1}H, ^{13}C, ^{14}N, and ^{31}P. A MS instrument consists of three main components: an ion source, a mass analyzer, and a detector. The ion source ionizes the sample, producing ions and fragment ions, then accelerated through the mass analyzer. Perpendicular magnetic fields deflect ions traveling through the mass analyzer according to their mass allowing to sort and detect ions based on their mass-to-charge ratio (m/z). The output is presented as a mass spectrum where each peak represents a different ion with a specific m/z, and the peak length corresponds with a relative abundance. Combining MS with separation techniques like GC or LC enables analysis of complex samples based on separation times (or retention times) and m/z ratios. The variable ionization of compounds, ion suppression, and instrument cycling times inherently limit the number and type of metabolites that can be distinguished in a single run. Different ionization techniques have been developed including electron ionization (EI) and chemical ionization (CI) for compounds in gas-phase, as well as electrospray ionization (ESI) and matrix-assisted laser desorption/ionization (MALDI) which are suitable for thermally labile and non-volatile analytes (101). After ionization, the mass analyzer sorts the ions by their m/z ratio using magnetic or electrical fields. Common analyzers use time of flight (TOF), quadrupole mass filter, quadrupole ion trap, Fourier transform-ion cyclotron or orbitrap. Each separated ion induces a specific charge which is finally measured in the detector. The advantage of MS over NMR is higher throughput, sensitivity, analysis speed, and a broader range of applications. Continuous improvements in instrumentation design and reduced running costs have led to increased accessibility and implementation of MS in research studies. The sensitivity and resolution of NMR instruments depend on the magnetic field strength, which has been improved in the past decade. ^{1}H NMR spectra have a small chemical shift range, which leads to overlapping peaks in complex samples, limiting detection, and lowering sensitivity. Combination of one-dimensional with two-dimensional NMR spectrometry has improved signal dispersion and compound identifications (102). Implementation of cryo-or microprobes further reduced scanning times needed to record a spectrum and greatly improved the sensitivity. Another advantage of NMR spectrometry is the quantitation and more uniform detection system, which can be directly used to identify and quantify metabolites both *ex vivo* and *in vivo*. In addition, the non-destructive nature of NMR methods leads to simplified sample preparation or even enables direct measurement of samples from body fluids (e.g., urine). Another advantage over MS is quantifying multiple compounds without the need for calibration curves for each compound. MS and NMR spectrometry have evolved as the most common techniques in stable isotope tracer and metabolomics studies. However, there is no single analytical platform that can achieve a complete quantification and identification of all molecules within a sample. Therefore, more than one method must be employed for comprehensive metabolic profiling. When deciding on an analytical avenue, the choice primarily depends on the focus of the research study and the nature of the samples, and instrument and know-how accessibility.

Single-cell analysis is a powerful tool to interrogate cellular heterogeneity within the same tissue, allowing for refined assessment of phenotypes and biomarker discovery. Metabolomics at the single-cell level holds the promise to obtain precise spatial and temporal information allowing to assess cell differentiation and division, cell-cell interactions, metabolic cooperation between cell populations and a detailed stress response analysis. In comparison to other omics technology, single-cell metabolomics faces several challenges because of the chemical diversity of metabolites, wide range of concentrations, sample stability, and lack of amplification (103). Recent studies have tried to circumvent challenges in single-cell metabolomics by using co-immunoprecipitation of proteins followed by MS to capture metabolic features (104). These strategies raise the question how much of metabolic regulation is dependent on protein abundance changes. The relationship between enzyme function and metabolites is multifactorial and dynamic, which explains poor correlation between individual proteins and metabolites (105, 106). Integration of proteomics and transcriptomics data with mathematical modeling and machine learning algorithms may improve the predictive value of these methods (107). Metabolomics at the single-cell level includes several pre-processing and sample conditioning steps, including desalting, to decomplexify the sample. These additional steps increase robustness but can also lead to sample loss. The limiting factor in stable-isotope labeling for single-cell analysis is sensitivity and isotopic resolution of a given analytical platform. Detection of metabolites in small sample volumes has been achieved with both NMR and MS (108). However, the sample volume for NMR application is larger than the single-cell level, thus NMR is commonly used with tissue samples or body fluids (e.g., plasma, urine). In recent years, progress has been made to facilitate mass spectrometry-based single-cell metabolomics

through increased instrument sensitivities and enhanced technologies. Mass spectrometry Imaging (MSI)-based methods are currently the most sensitive, thus preferred analytical platforms for single-cell metabolomics (103). MSI is a logic progression of laser microdissection technology and combines high-resolution microscopy with MS, which can be applied to thin tissue section or dispersed cell population attached to a grid. MALDI-MSI and ESI-MSI are the two conventional platforms applied for single-cell metabolomics. Both techniques allow spatial resolution of very small sample amounts (μl to pL range), analysis in the attomole ranges, and integration with automation. Recent studies demonstrate that these MS technologies can be applied to identify metabolic alterations in endothelial cell migration (109), tumor cell metastasis (110), and even to the single organelle level (111). The complementary nature of single-cell approaches enables spatial characterization of different cell types, reproducible measurement of metabolic states and organelle analysis when combined with other electrophysiological (e.g., patch clamping) techniques. However, single organelle analysis remains challenging due to limitations in reproducibility, low analyte abundances, limited sample volumes, and interference from sample impurities (103). Single-cell metabolomics is feasible across different platforms due to recent advance in MS technology, which enables enough resolution for monoisotopic detection. For studies that do not require a spatial resolution but molecular characterization at the single-cell level, separation-based methods like capillary electrophoresis (CE), LC, or GC combined with MS or fluorescent tagging approaches can provide sufficient sensitivity for certain applications (112). Analytical platforms like CE-ESI-MS allow qualitative and quantitative analyses of single cells and subcellular compartments with high resolving power and low sample input (<1 μl). CE is a powerful platform and can be coupled with optical, electrochemical, or MS-based detection expanding its applications (112). Compared to other application, one limitation of CE is its low throughput (113). Separations using CE can last up to 1 h, which limits the number of cells that can be assayed from one population (114). Therefore, recent methods have been introduced that directly inject cells into the capillary for lysis and separation reducing the time between cell rupture and analysis. Further advances in MSI and separation-based MS for single-cell metabolomics will offer unique approaches to classify cell types and identify subpopulation thus enhance our understanding of metabolic remodeling during cardiovascular diseases.

CONCLUDING REMARKS AND FUTURE CHALLENGES

Understanding how reprogrammed metabolism supports cardiac adaptation during stress and diseases requires a systems-wide approach. Translational models that recapitulate cardiac pathophysiology are critical to advance our understanding of CVDs and to utilize metabolic vulnerabilities through the development of novel therapeutics or biomarker identification. Stable-isotope labeling and mathematical modeling require multidisciplinary collaborations to bridging animal models into patients. Likewise, clinical studies should inform animal models for mechanistic hypothesis-driven testing. Challenges persist in accurate estimations of fluxes from stable-isotope tracers and integration into clinical trials. Evidence indicates that metabolic phenotypes are a key determinate of disease development and progression. Advancements in analytical methods to quantify metabolic phenotypes *in vivo* will be critical to identify metabolic vulnerabilities. Ultimately, these efforts may help clinicians to tailor therapeutic interventions based on the metabolic profile of the intact heart.

AUTHOR CONTRIBUTIONS

AK designed and wrote the manuscript.

FUNDING

This research was supported by R00-HL-141702 and institutional funds from Cedars-Sinai Medical Center to AK.

ACKNOWLEDGMENTS

The author acknowledges many fruitful discussions with Arpana Vaniya, Heidi Vitrac, and Aleksandr Stotland at UC Davis, Tosoh Biosciences, and Cedars-Sinai Medical Center. Figures were created with BioRender.com.

REFERENCES

1. Jaswal JS, Keung W, Wang W, Ussher JR, Lopaschuk GD. Targeting fatty acid and carbohydrate oxidation–a novel therapeutic intervention in the ischemic and failing heart. *Biochim Biophys Acta.* (2011) 1813:1333–50. doi: 10.1016/j.bbamcr.2011.01.015
2. Nederlof R, Denis S, Lauzier B, Rosiers CD, Laakso M, Hagen J, et al. Acute detachment of hexokinase II from mitochondria modestly increases oxygen consumption of the intact mouse heart. *Metabolism.* (2017) 72:66–74. doi: 10.1016/j.metabol.2017.04.008
3. Ritterhoff J, Young S, Villet O, Shao D, Neto FC, Bettcher LF, et al. Metabolic remodeling promotes cardiac hypertrophy by directing glucose to aspartate biosynthesis. *Circ Res.* (2020) 126:182–96. doi: 10.1161/CIRCRESAHA.119.315483
4. Heinrich R, Rapoport SM, Rapoport TA. Metabolic regulation and mathematical models. *Prog Biophys Mol Biol.* (1977) 32:1–82. doi: 10.1016/0079-6107(78)90017-2
5. Ruiz M, Gelinas R, Vaillant F, Lauzier B, Des Rosiers C. Metabolic tracing using stable isotope-labeled substrates and mass spectrometry in the perfused mouse heart. *Methods Enzymol.* (2015) 561:107–47. doi: 10.1016/bs.mie.2015.06.026
6. Hage FG, Aljaroudi WA. Review of cardiovascular imaging in the journal of nuclear cardiology in 2016: part 2 of 2-myocardial perfusion imaging. *J Nucl Cardiol.* (2017) 24:1190–9. doi: 10.1007/s12350-017-0875-2
7. Pirro M, Simental-Mendia LE, Bianconi V, Watts GF, Banach M, Sahebkar A. Effect of statin therapy on arterial wall inflammation based on 18F-FDG PET/CT: a systematic review and meta-analysis of interventional studies. *J Clin Med.* (2019) 8:118. doi: 10.3390/jcm8010118

8. Kim IY, Williams RH, Schutzler SE, Lasley CJ, Bodenner DL, Wolfe RR, et al. Acute lysine supplementation does not improve hepatic or peripheral insulin sensitivity in older, overweight individuals. *Nutr Metab.* (2014) 11:49. doi: 10.1186/1743-7075-11-49
9. Kim IY, Schutzler S, Schrader A, Spencer H, Kortebein P, Deutz NE, et al. Quantity of dietary protein intake, but not pattern of intake, affects net protein balance primarily through differences in protein synthesis in older adults. *Am J Physiol Endocrinol Metab.* (2015) 308:E21–8. doi: 10.1152/ajpendo.00382.2014
10. Neinast MD, Jang C, Hui S, Murashige DS, Chu Q, Morscher RJ, et al. Quantitative analysis of the whole-body metabolic fate of branched-chain amino acids. *Cell Metab.* (2019) 29:417–29 e414. doi: 10.1016/j.cmet.2018.10.013
11. Bleehen NM, Fisher, R.B. The action of insulin on the isolated rat heart. *J Physiol.* (1954) 123:260. doi: 10.1113/jphysiol.1954.sp005049
12. Morgan HE, Henderson MJ, Regen DM, Park CR. Regulation of glucose uptake in muscle. I. The effects of insulin and anoxia on glucose transport and phosphorylation in the isolated, perfused heart of normal rats. *J Biol Chem.* (1961) 236:253–61. doi: 10.1016/S0021-9258(18)64348-0
13. Williamson JR, Krebs HA. Acetoacetate as fuel of respiration in the perfused rat heart. *Biochem J.* (1961) 80:540–7. doi: 10.1042/bj0800540
14. Opie LH. Coronary flow rate and perfusion pressure as determinants of mechanical function and oxidative metabolism of isolated perfused rat heart. *J Physiol.* (1965) 180:529–41. doi: 10.1113/jphysiol.1965.sp007715
15. Taegtmeyer H, Hems R, Krebs HA. Utilization of energy-providing substrates in the isolated working rat heart. *Biochem J.* (1980) 186:701–11. doi: 10.1042/bj1860701
16. Salabei JK, Lorkiewicz PK, Mehra P, Gibb AA, Haberzettl P, Hong KU, et al. Type 2 diabetes dysregulates glucose metabolism in cardiac progenitor cells. *J Biol Chem.* (2016) 291:13634–48. doi: 10.1074/jbc.M116.722496
17. Lee MH, Malloy CR, Corbin IR, Li J, Jin ES. Assessing the pentose phosphate pathway using [2, 3-(13) C2]glucose. *NMR Biomed.* (2019) 32:e4096. doi: 10.1002/nbm.4096
18. Jin ES, Lee MH, Malloy CR. 13C NMR of glutamate for monitoring the pentose phosphate pathway in myocardium. *NMR Biomed.* (2021) 34:e4533. doi: 10.1002/nbm.4533
19. Olson AK, Bouchard B, Zhu WZ, Chatham JC, Des Rosiers C. First characterization of glucose flux through the hexosamine biosynthesis pathway (HBP) in *ex vivo* mouse heart. *J Biol Chem.* (2020) 295:2018–33. doi: 10.1074/jbc.RA119.010565
20. Zhang Y, Taufalele PV, Cochran JD, Robillard-Frayne I, Marx JM, Soto J, et al. Mitochondrial pyruvate carriers are required for myocardial stress adaptation. *Nat Metab.* (2020) 2:1248–64. doi: 10.1038/s42255-020-00288-1
21. Zhang H, Uthman L, Bakker D, Sari S, Chen S, Hollmann MW, et al. Empagliflozin decreases lactate generation in an NHE-1 dependent fashion and increases alpha-ketoglutarate synthesis from palmitate in Type II diabetic mouse hearts. *Front Cardiovasc Med.* (2020) 7:592233. doi: 10.3389/fcvm.2020.592233
22. Ronda O, Van De Heijning BJM, Martini IA, Koehorst M, Havinga R, Jurdzinski A, et al. An early-life diet containing large phospholipid-coated lipid globules programmes later-life postabsorptive lipid trafficking in high-fat diet- but not in low-fat diet-fed mice. *Br J Nutr.* (2021) 125:961–71. doi: 10.1017/S0007114520002421
23. Wust RCI, Coolen BF, Held NM, Daal MRR, Alizadeh Tazehkandi V, Baks-Te Bulte L, et al. The antibiotic doxycycline impairs cardiac mitochondrial and contractile function. *Int J Mol Sci.* (2021) 22:4100. doi: 10.3390/ijms22084100
24. Ragavan M, Li M, Giacalone AG, Wood CE, Keller-Wood M, Merritt ME. Application of carbon-13 isotopomer analysis to assess perinatal myocardial glucose metabolism in sheep. *Metabolites.* (2021) 11:33. doi: 10.3390/metabo11010033
25. Gibb AA, Lorkiewicz PK, Zheng YT, Zhang X, Bhatnagar A, Jones SP, et al. Integration of flux measurements to resolve changes in anabolic and catabolic metabolism in cardiac myocytes. *Biochem J.* (2017) 474:2785–801. doi: 10.1042/BCJ20170474
26. Madsen KL, Preisler N, Rasmussen J, Hedermann G, Olesen JH, Lund AM, et al. L-carnitine improves skeletal muscle fat oxidation in primary carnitine deficiency. *J Clin Endocrinol Metab.* (2018) 103:4580–8. doi: 10.1210/jc.2018-00953
27. Parry SA, Rosqvist F, Mozes FE, Cornfield T, Hutchinson M, Piche ME, et al. Intrahepatic fat and postprandial glycemia increase after consumption of a diet enriched in saturated fat compared with free sugars. *Diabetes Care.* (2020) 43:1134–41. doi: 10.2337/dc19-2331
28. Wang Y, Christopher BA, Wilson KA, Muoio D, Mcgarrah RW, Brunengraber H, et al. Propionate-induced changes in cardiac metabolism, notably CoA trapping, are not altered by l-carnitine. *Am J Physiol Endocrinol Metab.* (2018) 315:E622–33. doi: 10.1152/ajpendo.00081.2018
29. Renguet E, Ginion A, Gelinas R, Bultot L, Auquier J, Robillard Frayne I, et al. Metabolism and acetylation contribute to leucine-mediated inhibition of cardiac glucose uptake. *Am J Physiol Heart Circ Physiol.* (2017) 313:H432–45. doi: 10.1152/ajpheart.00738.2016
30. Zhang J, Wang YT, Miller JH, Day MM, Munger JC, Brookes PS. Accumulation of succinate in cardiac ischemia primarily occurs *via* canonical krebs cycle activity. *Cell Rep.* (2018) 23:2617–28. doi: 10.1016/j.celrep.2018.04.104
31. Watanabe K, Nagao M, Toh R, Irino Y, Shinohara M, Iino T, et al. Critical role of glutamine metabolism in cardiomyocytes under oxidative stress. *Biochem Biophys Res Commun.* (2021) 534:687–93. doi: 10.1016/j.bbrc.2020.11.018
32. Lindsay RT, Demetriou D, Manetta-Jones D, West JA, Murray AJ, Griffin JL. A model for determining cardiac mitochondrial substrate utilisation using stable (13)C-labelled metabolites. *Metabolomics.* (2019) 15:154. doi: 10.1007/s11306-019-1618-y
33. Khairallah M, Labarthe F, Bouchard B, Danialou G, Petrof BJ, Des Rosiers C. Profiling substrate fluxes in the isolated working mouse heart using 13C-labeled substrates: focusing on the origin and fate of pyruvate and citrate carbons. *Am J Physiol Heart Circ Physiol.* (2004) 286:H1461–70. doi: 10.1152/ajpheart.00942.2003
34. Crown SB, Kelleher JK, Rouf R, Muoio DM, Antoniewicz MR. Comprehensive metabolic modeling of multiple 13C-isotopomer data sets to study metabolism in perfused working hearts. *Am J Physiol Heart Circ Physiol.* (2016) 311:H881–91. doi: 10.1152/ajpheart.00428.2016
35. Karlstadt A, Fliegner D, Kararigas G, Ruderisch HS, Regitz-Zagrosek V, Holzhutter HG. CardioNet: a human metabolic network suited for the study of cardiomyocyte metabolism. *BMC Syst Biol.* (2012) 6:114. doi: 10.1186/1752-0509-6-114
36. Aksentijevic D, Karlstaedt A, Basalay MV, O'brien BA, Sanchez-Tatay D, Eminaga S, et al. Intracellular sodium elevation reprograms cardiac metabolism. *Nat Commun.* (2020) 11:4337. doi: 10.1038/s41467-020-18160-x
37. Wolfe RR, Park S, Kim IY, Moughan PJ, Ferrando AA. Advances in stable isotope tracer methodology part 2: new thoughts about an "old" method-measurement of whole body protein synthesis and breakdown in the fed state. *J Investig Med.* (2020) 68:11–5. doi: 10.1136/jim-2019-001108
38. Heise R, Fernie AR, Stitt M, Nikoloski Z. Pool size measurements facilitate the determination of fluxes at branching points in non-stationary metabolic flux analysis: the case of Arabidopsis thaliana. *Front Plant Sci.* (2015) 6:386. doi: 10.3389/fpls.2015.00386
39. Karlstaedt A, Khanna R, Thangam M, Taegtmeyer H. Glucose 6-phosphate accumulates *via* phosphoglucose isomerase inhibition in heart muscle. *Circ Res.* (2020) 126:60–74. doi: 10.1161/CIRCRESAHA.119.315180
40. Dougherty BV, Rawls KD, Kolling GL, Vinnakota KC, Wallqvist A, Papin JA. Identifying functional metabolic shifts in heart failure with the integration of omics data and a heart-specific, genome-scale model. *Cell Rep.* (2021) 34:108836. doi: 10.1016/j.celrep.2021.108836
41. Jassal B, Matthews L, Viteri G, Gong C, Lorente P, Fabregat A, et al. The reactome pathway knowledgebase. *Nucleic Acids Res.* (2020) 48:D498–503. doi: 10.1093/nar/gkz1031
42. Brunk E, Sahoo S, Zielinski DC, Altunkaya A, Drager A, Mih N, et al. Recon3D enables a three-dimensional view of gene variation in human metabolism. *Nat Biotechnol.* (2018) 36:272–81. doi: 10.1038/nbt.4072
43. Wang Y, Eddy JA, Price ND. Reconstruction of genome-scale metabolic models for 126 human tissues using mCADRE. *BMC Syst Biol.* (2012) 6:153. doi: 10.1186/1752-0509-6-153
44. Uniprot C. UniProt: the universal protein knowledgebase in 2021. *Nucleic Acids Res.* (2021) 49:D480–9. doi: 10.1093/nar/gkaa1100
45. Wishart DS, Feunang YD, Marcu A, Guo AC, Liang K, Vazquez-Fresno R, et al. HMDB 4.0: the human metabolome database for 2018. *Nucleic Acids Res.* (2018) 46:D608–17. doi: 10.1093/nar/gkx1089

46. Schomburg I, Chang A, Schomburg D. BRENDA, enzyme data and metabolic information. *Nucleic Acids Res.* (2002) 30:47–9. doi: 10.1093/nar/30.1.47
47. Scheer M, Grote A, Chang A, Schomburg I, Munaretto C, Rother M, et al. BRENDA, the enzyme information system in 2011. *Nucleic Acids Res.* (2011) 39:D670–6. doi: 10.1093/nar/gkq1089
48. Chang A, Jeske L, Ulbrich S, Hofmann J, Koblitz J, Schomburg I, et al. BRENDA, the ELIXIR core data resource in 2021: new developments and updates. *Nucleic Acids Res.* (2021) 49:D498–508. doi: 10.1093/nar/gkaa1025
49. Kanehisa M. The KEGG database. *Novartis Found Symp.* (2002) 247:91–101; discussion 101–103 119–128, 244–152. doi: 10.1002/0470857897.ch8
50. Kanehisa M. Molecular network analysis of diseases and drugs in KEGG. *Methods Mol Biol.* (2013) 939:263–75. doi: 10.1007/978-1-62703-107-3_17
51. Kanehisa M. KEGG bioinformatics resource for plant genomics and metabolomics. *Methods Mol Biol.* (2016) 1374:55–70. doi: 10.1007/978-1-4939-3167-5_3
52. Kanehisa M. Enzyme annotation and metabolic reconstruction using KEGG. *Methods Mol Biol.* (2017) 1611:135–45. doi: 10.1007/978-1-4939-7015-5_11
53. Selivanov VA, Benito A, Miranda A, Aguilar E, Polat IH, Centelles JJ, et al. MIDcor, an R-program for deciphering mass interferences in mass spectra of metabolites enriched in stable isotopes. *BMC Bioinformatics.* (2017) 18:88. doi: 10.1186/s12859-017-1513-3
54. Heinrich P, Kohler C, Ellmann L, Kuerner P, Spang R, Oefner PJ, et al. Correcting for natural isotope abundance and tracer impurity in MS-, MS/MS- and high-resolution-multiple-tracer-data from stable isotope labeling experiments with IsoCorrectoR. *Sci Rep.* (2018) 8:17910. doi: 10.1038/s41598-018-36293-4
55. Millard P, Letisse F, Sokol S, Portais JC. IsoCor: correcting MS data in isotope labeling experiments. *Bioinformatics.* (2012) 28:1294–6. doi: 10.1093/bioinformatics/bts127
56. Millard P, Delepine B, Guionnet M, Heuillet M, Bellvert F, Letisse F. IsoCor: isotope correction for high-resolution MS labeling experiments. *Bioinformatics.* (2019) 35:4484–7. doi: 10.1093/bioinformatics/btz209
57. Wiechert W, Mollney M, Petersen S, De Graaf AA. A universal framework for 13C metabolic flux analysis. *Metab Eng.* (2001) 3:265–83. doi: 10.1006/mben.2001.0188
58. Weitzel M, Noh K, Dalman T, Niedenfuhr S, Stute B, Wiechert W. 13CFLUX2–high-performance software suite for (13)C-metabolic flux analysis. *Bioinformatics.* (2013) 29:143–5. doi: 10.1093/bioinformatics/bts646
59. Kogadeeva M, Zamboni N. SUMOFLUX: a generalized method for targeted 13C metabolic flux ratio analysis. *PLoS Comput Biol.* (2016) 12:e1005109. doi: 10.1371/journal.pcbi.1005109
60. Quek LE, Wittmann C, Nielsen LK, Kromer JO. OpenFLUX: efficient modelling software for 13C-based metabolic flux analysis. *Microb Cell Fact.* (2009) 8:25. doi: 10.1186/1475-2859-8-25
61. Sokol S, Millard P, Portais JC. influx_s: increasing numerical stability and precision for metabolic flux analysis in isotope labelling experiments. *Bioinformatics.* (2012) 28:687–93. doi: 10.1093/bioinformatics/btr716
62. Young JD, Walther JL, Antoniewicz MR, Yoo H, Stephanopoulos G. An elementary metabolite unit (EMU) based method of isotopically nonstationary flux analysis. *Biotechnol Bioeng.* (2008) 99:686–99. doi: 10.1002/bit.21632
63. Young JD. INCA: a computational platform for isotopically non-stationary metabolic flux analysis. *Bioinformatics.* (2014) 30:1333–5. doi: 10.1093/bioinformatics/btu015
64. Rappez L, Stadler M, Triana S, Gathungu RM, Ovchinnikova K, Phapale P, et al. SpaceM reveals metabolic states of single cells. *Nat Methods.* (2021) 18:799–805. doi: 10.1038/s41592-021-01198-0
65. Heirendt L, Arreckx S, Pfau T, Mendoza SN, Richelle A, Heinken A, et al. Creation and analysis of biochemical constraint-based models using the COBRA Toolbox v.3.0. *Nat Protoc.* (2019) 14:639–702. doi: 10.1038/s41596-018-0098-2
66. Matlab. *version 9.10.0 (R2021a).* Natick, MA: The MathWorks, Inc. (2021)
67. Gurobi Optimization Llc. *Gurobi Optimizer Reference Manual, Version 9.1* (2021). Available online at: https://www.gurobi.com/documentation/9.1/refman/index.html
68. Cplex II. V12. 1: User's Manual for CPLEX. *Int Bus Mach Corp.* (2009) 46:157. Available online at: https://www.ibm.com/docs/en/icos/12.10.0?topic=cplex-users-manual
69. R Core Team. *R: A Language and Environment for Statistical Computing.* Vienna: R Foundation for Statistical Computing (2017).
70. Wall L.a.C, Tom, Orwant J. *Programming Perl.* Sebastopol, CA: O'Reilly Media, Inc. (2000).
71. Van Rossum G, Drake FL. *Python Reference Manual.* Amsterdam: Centrum voor Wiskunde en Informatica (1995).
72. Otasek D, Morris JH, Boucas J, Pico AR, Demchak B. Cytoscape automation: empowering workflow-based network analysis. *Genome Biol.* (2019) 20:185. doi: 10.1186/s13059-019-1758-4
73. Barupal DK, Fiehn O. Chemical similarity enrichment analysis (ChemRICH) as alternative to biochemical pathway mapping for metabolomic datasets. *Sci Rep.* (2017) 7:14567. doi: 10.1038/s41598-017-15231-w
74. Wohlgemuth G, Haldiya PK, Willighagen E, Kind T, Fiehn O. The chemical translation service–a web-based tool to improve standardization of metabolomic reports. *Bioinformatics.* (2010) 26:2647–8. doi: 10.1093/bioinformatics/btq476
75. Kim S, Chen J, Cheng T, Gindulyte A, He J, He S, et al. PubChem in 2021: new data content and improved web interfaces. *Nucleic Acids Res.* (2021) 49:D1388–95. doi: 10.1093/nar/gkaa971
76. Sud M, Fahy E, Cotter D, Azam K, Vadivelu I, Burant C, et al. Metabolomics Workbench: An international repository for metabolomics data and metadata, metabolite standards, protocols, tutorials and training, analysis tools. *Nucleic Acids Res.* (2016) 44:D463–70. doi: 10.1093/nar/gkv1042
77. Salek RM, Haug K, Conesa P, Hastings J, Williams M, Mahendraker T, et al. The metabolights repository: curation challenges in metabolomics. *Database.* (2013) 2013: bat029. doi: 10.1093/database/bat029
78. Jang C, Chen L, Rabinowitz JD. Metabolomics and isotope tracing. *Cell.* (2018) 173:822–37. doi: 10.1016/j.cell.2018.03.055
79. Liu H, Huang D, Mcarthur DL, Boros LG, Nissen N, Heaney AP. Fructose induces transketolase flux to promote pancreatic cancer growth. *Cancer Res.* (2010) 70:6368–76. doi: 10.1158/0008-5472.CAN-09-4615
80. Ying H, Kimmelman AC, Lyssiotis CA, Hua S, Chu GC, Fletcher-Sananikone E, et al. Oncogenic Kras maintains pancreatic tumors through regulation of anabolic glucose metabolism. *Cell.* (2012) 149:656–70. doi: 10.1016/j.cell.2012.01.058
81. Moon SJ, Dong W, Stephanopoulos GN, Sikes HD. Oxidative pentose phosphate pathway and glucose anaplerosis support maintenance of mitochondrial NADPH pool under mitochondrial oxidative stress. *Bioeng Transl Med.* (2020) 5:e10184. doi: 10.1002/btm2.10184
82. Lewis CA, Parker SJ, Fiske BP, Mccloskey D, Gui DY, Green CR, et al. Tracing compartmentalized NADPH metabolism in the cytosol and mitochondria of mammalian cells. *Mol Cell.* (2014) 55:253–63. doi: 10.1016/j.molcel.2014.05.008
83. Simithy J, Sidoli S, Yuan ZF, Coradin M, Bhanu NV, Marchione DM, et al. Characterization of histone acylations links chromatin modifications with metabolism. *Nat Commun.* (2017) 8:1141. doi: 10.1038/s41467-017-01384-9
84. Lund PJ, Kori Y, Zhao X, Sidoli S, Yuan ZF, Garcia BA. Isotopic labeling and quantitative proteomics of acetylation on histones and beyond. *Methods Mol Biol.* (2019) 1977:43–70. doi: 10.1007/978-1-4939-9232-4_5
85. Mcclatchy DB, Ma Y, Liu C, Stein BD, Martinez-Bartolome S, Vasquez D, et al. Pulsed azidohomoalanine labeling in mammals (PALM) detects changes in liver-specific LKB1 knockout mice. *J Proteome Res.* (2015) 14:4815–22. doi: 10.1021/acs.jproteome.5b00653
86. Lu W, Wang L, Chen L, Hui S, Rabinowitz JD. Extraction and quantitation of nicotinamide adenine dinucleotide redox cofactors. *Antioxid Redox Signal.* (2018) 28:167–79. doi: 10.1089/ars.2017.7014
87. Trefely S, Liu J, Huber K, Doan MT, Jiang H, Singh J, et al. Subcellular metabolic pathway kinetics are revealed by correcting for artifactual post harvest metabolism. *Mol Metab.* (2019) 30:61–71. doi: 10.1016/j.molmet.2019.09.004
88. Wollenberger A, Ristau O, Schoffa G. [A simple technic for extremely rapid freezing of large pieces of tissue]. *Pflugers Arch Gesamte Physiol Menschen Tiere.* (1960) 270:399–412. doi: 10.1007/BF00362995
89. Wollenberger A, Halle W, Kallabis E, Kleitke B, Hinterberger U, Schulze W. Cultivation of beating heart cells from frozen heart cell

suspensions. *Naturwissenschaften.* (1967) 54:174. doi: 10.1007/BF00590855
90. Janiszewski E, Wollenberger A. [Freezing preservation of heart cells and heart fragments]. *Acta Biol Med Ger.* (1972) 29:135–47.
91. Davogustto GE, Salazar RL, Vasquez HG, Karlstaedt A, Dillon WP, Guthrie PH, et al. Metabolic remodeling precedes mTORC1-mediated cardiac hypertrophy. *J Mol Cell Cardiol.* (2021) 158:115–27. doi: 10.1016/j.yjmcc.2021.05.016
92. Wiechert W. 13C metabolic flux analysis. *Metab Eng.* (2001) 3:195–206. doi: 10.1006/mben.2001.0187
93. Klipp E,LW, Wierling C, Kowald A. *Systems Biology.* Weinheim: Wiley-VCH (2016).
94. Karlstaedt A, Zhang X, Vitrac H, Harmancey R, Vasquez H, Wang JH, et al. Oncometabolite d-2-hydroxyglutarate impairs alpha-ketoglutarate dehydrogenase and contractile function in rodent heart. *Proc Natl Acad Sci USA.* (2016) 113:10436-41. doi: 10.1073/pnas.1601650113
95. Henry CS, Broadbelt LJ, Hatzimanikatis V. Thermodynamics-based metabolic flux analysis. *Biophys J.* (2007) 92:1792–805. doi: 10.1529/biophysj.106.093138
96. Hoppe A, Hoffmann S, Holzhutter HG. Including metabolite concentrations into flux balance analysis: thermodynamic realizability as a constraint on flux distributions in metabolic networks. *BMC Syst Biol.* (2007) 1:23. doi: 10.1186/1752-0509-1-23
97. Cornish-Bowden A. Metabolic control analysis in theory and practice. *Adv Mol Cell Biol.* (1995) 11:21–64. doi: 10.1016/S1569-2558(08)60247-7
98. Antoniewicz MR, Kelleher JK, Stephanopoulos G. Elementary metabolite units (EMU): a novel framework for modeling isotopic distributions. *Metab Eng.* (2007) 9:68–86. doi: 10.1016/j.ymben.2006.09.001
99. Antoniewicz MR, Kelleher JK, Stephanopoulos G. Determination of confidence intervals of metabolic fluxes estimated from stable isotope measurements. *Metab Eng.* (2006) 8:324–37. doi: 10.1016/j.ymben.2006.01.004
100. Antoniewicz MR, Stephanopoulos G, Kelleher JK. Evaluation of regression models in metabolic physiology: predicting fluxes from isotopic data without knowledge of the pathway. *Metabolomics.* (2006) 2:41–52. doi: 10.1007/s11306-006-0018-2
101. Cramer R. Maldi Ms. *Methods Mol Biol.* (2009) 564:85–103. doi: 10.1007/978-1-60761-157-8_5
102. Bingol K, Zhang F, Bruschweiler-Li L, Bruschweiler R. Quantitative analysis of metabolic mixtures by two-dimensional 13C constant-time TOCSY NMR spectroscopy. *Anal Chem.* (2013) 85:6414–20. doi: 10.1021/ac400913m
103. Taylor MJ, Lukowski JK, Anderton CR. Spatially resolved mass spectrometry at the single cell: recent innovations in proteomics and metabolomics. *J Am Soc Mass Spectrom.* (2021) 32:872–94. doi: 10.1021/jasms.0c00439
104. Hartmann FJ, Mrdjen D, Mccaffrey E, Glass DR, Greenwald NF, Bharadwaj A, et al. Single-cell metabolic profiling of human cytotoxic T cells. *Nat Biotechnol.* (2021) 39:186–97. doi: 10.1038/s41587-020-0651-8
105. Fendt SM, Buescher JM, Rudroff F, Picotti P, Zamboni N, Sauer U. Tradeoff between enzyme and metabolite efficiency maintains metabolic homeostasis upon perturbations in enzyme capacity. *Mol Syst Biol.* (2010) 6:356. doi: 10.1038/msb.2010.11
106. Zelezniak A, Sheridan S, Patil KR. Contribution of network connectivity in determining the relationship between gene expression and metabolite concentration changes. *PLoS Comput Biol.* (2014) 10:e1003572. doi: 10.1371/journal.pcbi.1003572
107. Zeleniak AE, Huang W, Fishel ML, Hill R. PTEN-dependent stabilization of MTSS1 inhibits metastatic phenotype in pancreatic ductal adenocarcinoma. *Neoplasia.* (2018) 20:12–24. doi: 10.1016/j.neo.2017.10.004
108. Comi TJ, Do TD, Rubakhin SS, Sweedler JV. Categorizing cells on the basis of their chemical profiles: progress in single-cell mass spectrometry. *J Am Chem Soc.* (2017) 139:3920–9. doi: 10.1021/jacs.6b12822
109. Wu D, Harrison DL, Szasz T, Yeh CF, Shentu TP, Meliton A, et al. Single-cell metabolic imaging reveals a SLC2A3-dependent glycolytic burst in motile endothelial cells. *Nat Metab.* (2021) 3:714–27. doi: 10.1038/s42255-021-00390-y
110. Ferraro GB, Ali A, Luengo A, Kodack DP, Deik A, Abbott KL, et al. Fatty acid synthesis is required for breast cancer brain metastasis. *Nat Cancer.* (2021) 2:414–28. doi: 10.1038/s43018-021-00283-9
111. Zhu H, Li Q, Liao T, Yin X, Chen Q, Wang Z, et al. Metabolomic profiling of single enlarged lysosomes. *Nat Methods.* (2021) 18:788–98. doi: 10.1038/s41592-021-01182-8
112. Kleparnik K. Recent advances in the combination of capillary electrophoresis with mass spectrometry: from element to single-cell analysis. *Electrophoresis.* (2013) 34:70–85. doi: 10.1002/elps.201200488
113. Marc PJ, Sims CE, Allbritton NL. Coaxial flow system for chemical cytometry. *Anal Chem.* (2007) 79:9054–9. doi: 10.1021/ac7017519
114. Chen S, Lillard SJ. Continuous cell introduction for the analysis of individual cells by capillary electrophoresis. *Anal Chem.* (2001) 73:111–8. doi: 10.1021/ac0009088

Conflict of Interest: The author declares that the research was conducted in the absence of any commercial or financial relationships that could be construed as a potential conflict of interest.

Publisher's Note: All claims expressed in this article are solely those of the authors and do not necessarily represent those of their affiliated organizations, or those of the publisher, the editors and the reviewers. Any product that may be evaluated in this article, or claim that may be made by its manufacturer, is not guaranteed or endorsed by the publisher.

frontiers in Cardiovascular Medicine

REVIEW
published: 23 December 2021
doi: 10.3389/fcvm.2021.778674

Longevity Factor FOXO3: A Key Regulator in Aging-Related Vascular Diseases

Yan Zhao [1,2] *and You-Shuo Liu* [1,2*]

[1] Department of Geriatrics, The Second Xiangya Hospital, Central South University, Changsha, China, [2] Institute of Aging and Age-Related Disease Research, Central South University, Changsha, China

Forkhead box O3 (FOXO3) has been proposed as a homeostasis regulator, capable of integrating multiple upstream signaling pathways that are sensitive to environmental changes and counteracting their adverse effects due to external changes, such as oxidative stress, metabolic stress and growth factor deprivation. FOXO3 polymorphisms are associated with extreme human longevity. Intriguingly, longevity-associated single nucleotide polymorphisms (SNPs) in human *FOXO3* correlate with lower-than-average morbidity from cardiovascular diseases in long-lived people. Emerging evidence indicates that FOXO3 plays a critical role in vascular aging. FOXO3 inactivation is implicated in several aging-related vascular diseases. In experimental studies, FOXO3-engineered human ESC-derived vascular cells improve vascular homeostasis and delay vascular aging. The purpose of this review is to explore how FOXO3 regulates vascular aging and its crucial role in aging-related vascular diseases.

Keywords: FOXO3, aging, vascular aging, vascular homeostasis, cardiovascular disease

OPEN ACCESS

Edited by:
Zhong Wang,
University of Michigan, United States

Reviewed by:
Richard Allsopp,
University of Hawaii, United States
Bradley Willcox,
University of Hawaii, United States

***Correspondence:**
You-Shuo Liu
liuyoushuo@csu.edu.cn

Specialty section:
This article was submitted to Cardiovascular Metabolism, a section of the journal Frontiers in Cardiovascular Medicine

Received: *17 September 2021*
Accepted: *06 December 2021*
Published: *23 December 2021*

Citation:
Zhao Y and Liu Y-S (2021) Longevity Factor FOXO3: A Key Regulator in Aging-Related Vascular Diseases. Front. Cardiovasc. Med. 8:778674. doi: 10.3389/fcvm.2021.778674

BACKGROUND

Cardiovascular disease (CVD) is the leading cause of morbidity and mortality in individuals aged 65 years and above (1). Vascular aging has been implicated as a driver of a number of aging-related vascular disorders (2). A large clinical study identified two specific age-related arterial phenotypes, endothelial dysfunction, and increased arterial stiffness as independent predictors for future diagnosis of CVD (3). At the macro level, aging vessels exhibit luminal expansion, diffused stiffness, wall thickening, and blunted angiogenesis (4, 5). Microscopically, aging vessels undergo vascular cell senescence and loss of vascular homeostasis, resulting in inflammation, oxidative stress, and calcification of blood vessels (4). The pace of vascular aging differs in individuals due to differences in their genetics and environment background.

The insulin/IFG-1 signaling (IIS) pathway is one of the major pathways involved in the regulation of aging rate, which negatively influences the activity of forkhead box O3 (FOXO3) (6). The first identified FOXO member, DAF-16/FOXO3, has been shown to prolong lifespan in *C. elegans* by regulating insulin-like metabolic signaling (7, 8). Additionally, studies have demonstrated that the IIS pathway is associated with an extended lifespan in a variety of species including worms, yeasts, flies, and mice (9). To assess the genetic contributions of genes associated with IIS signaling to human longevity, researchers performed a nested case-control study on 5 prospective longevity genes and found that *FOXO3* variation was strongly correlated with human longevity (10). Subsequently, this finding was quickly duplicated in a variety of populations around the world (11–13). Five *FOXO3* single nucleotide polymorphisms (SNPs) were shown to have

a significant correlation with longevity in a meta-analysis of 11 independent studies (14). *FOXO3* has been identified as the second most replicated gene associated with extreme human longevity (15). While *FOXO3* is a convincing longevity gene, the mechanism by which FOXO3 determines longevity remains unknown. Interestingly, long-lived individuals demonstrated some phenotypes associated with healthy aging, including a lower prevalence of CVD and cancer (10). Additionally, the longevity-associated *FOXO3* SNPs correlate with lower-than-average CVD morbidity in long-lived individuals (10, 16). Another study found that longevity-associated *FOXO3* genetic variants prolong lifespan only in individuals with cardiometabolic disease (CMD), but not in all individuals (17). These findings show that FOXO3 may maintain cardiovascular homeostasis, hence promoting longevity. A single-cell transcriptomic analysis of coronary arteries and aortas of young and elderly cynomolgus monkeys found that FOXO3 expression was downregulated in six subtypes of vascular cells in older monkeys compared to young monkeys (18). Although the underlying mechanisms are unknown, FOXO3 is require for maintaining vascular homeostasis under stressful conditions and preventing vascular aging. In this review, we will summarize the most recent findings on FOXO3 functions and mainly focus on its role in aging-related vascular diseases.

OVERVIEW OF FOXO3

FOXO proteins are ubiquitously expressed transcription factors that activate gene transcription when they recognize promoters containing the sequence 5′-TTGTTTAC-3′ (19). By integrating multiple upstream signaling pathways, FOXOs help maintain tissue homeostasis and counteract adverse effects of environmental changes such as oxidative stress, metabolic stress, and growth factor deprivation (20). The transcriptional targets of FOXOs include genes involved in cell cycle arrest (21), oxidative resistance (22), apoptosis (23), autophagy (24), DNA damage repair (25), and energy metabolism (26). The biological role of FOXOs is primarily to respond to stress conditions, rather than as an essential agent of normal physiology. In humans, the FOXO family comprises FOXO1, FOXO3, FOXO4, and FOXO6. FOXO3 has been associated with a number of age-related diseases, including cancer (27), CVD (28), intervertebral disc (IVD) degeneration (29), and neurodegenerative diseases (30). Particularly, the role of FOXO3 in CVD appears attractive.

REGULATION OF FOXO3

Numerous upstream factors regulate FOXO3 via post-transcriptional or post-translational modifications. The exquisite regulatory network formed by diverse upstream regulators and downstream effectors of FOXO3 contributes to its responsiveness to environmental changes and plays an important role in maintaining homeostasis (20).

MicroRNAs Contribute to Post-transcriptional Regulation of FOXO3

MicroRNAs (miRNAs) act as post-transcriptional regulators of gene expression (31). Numerous miRNAs, including miR-155, miR-132, miR-212, miR-223, miR-27a, miR-96, miR-30d, miR-182, miR-592, miR-1307 and miR-29a, bind to FOXO3 3′-UTR and inhibit its expression (27). Other miRNAs have an indirect effect on FOXO3, for example, by targeting upstream factors of FOXO3 to modulate its activity (32). Long non-coding RNAs (lncRNAs) and circular RNAs (circRNAs) are also known to regulate FOXO3 (33, 34). A comprehensive exploration of the relationship between non-coding RNAs and FOXO3 will help in the development of more effective chemotherapy.

Post-translational Modifications of FOXO3

FOXO3 activity is mainly regulated by post-translational modifications (PTMs), including phosphorylation, acetylation, methylation, ubiquitination, glycosylation, prenylation, and sulphation. Most of these PTMs change the subcellular localization of FOXO3 and its DNA binding affinity (27). The subcellular localization of FOXO3 is essential for its activity and function (35).

Phosphorylation and Dephosphorylation

The primary regulator of FOXO3 activity is its translocation between the nucleus and cytoplasm. Phosphorylation is a critical PTM that regulates FOXO3 activity. Numerous kinases recognize specific sites on FOXO3 and may exert opposing effects on its activity (36). FOXO3 is inactive under normal conditions, due to negative regulation by IIS-PI3K-Akt signaling. Akt phosphorylates FOXO3 at three highly conserved residues, T32, S253, and S315, establishing docking sites for the chaperone 14-3-3, preventing FOXO3 from re-entering the nucleus (37). PTEN antagonizes the effect of PI3K and induces FOXO3 activation. When cells are stressed, such as when reactive oxygen species (ROS) levels are elevated, FOXO3 translocates into the nucleus and exhibits increased transcriptional activity (20).

The majority of phosphorylases, including extracellular signal-regulated kinase (ERK), IκB kinase isoform β (IKKβ), serum-and glucocorticoid-inducible kinases (SGK), and inhibitor of nuclear factor kappa-B kinase subunit epsilon (IKBKE) suppress FOXO3 activity (38). In comparison, FOXO3 is activated upon phosphorylation by c-Jun N-terminal kinase (JNK), mammalian sterile 20-like kinase 1 (MST1), and AMP-activated protein kinase (AMPK) (39–41). AMPK-mediated phosphorylation impacts FOXO3's interaction with cofactors but does not affect does not affect its subcellular localization (42). JNK inhibits insulin signal transduction on multiple levels by reducing the activity of insulin receptor substrate (IRS) and inducing the release of FOXO3 from 14-3-3, hence surpassing growth factor-induced FOXO3 inhibition (19).

Acetylation and Deacetylation

Nuclear FOXO3 is acetylated by p300 and CBP and deacetylated by deacetylases such as SIRT1 and SIRT2. The effect on acetylation and deacetylation on FOXO3's affinity for DNA is controversial (43, 44). Notably, the effects of SIRT1 on FOXO3 activity are not fixed rigidly, for instance, SIRT1 promotes the expression of target genes associated with antioxidant stress but suppresses the expression of proapoptotic genes (45).

Ubiquitination and methylation also act as regulators of FOXO3, with multiubiquitination resulting in FOXO3

degradation. Different PTMs may occur on the same lysine residues on FOXO3, for example, lysine residues deacetylated by SIRT1 might be ubiquitinated, thereby degrading FOXO3 (46). Alterations in PTMs associated with aging may contribute to the onset of some age-associated diseases.

ROLE OF FOXO3 IN VASCULAR AGING

Aging-associated mechanisms, including deregulated nutrient sensing, oxidative stress, and epigenetic changes in the vascular system may contribute to the pathogenesis of vascular aging. FOXO3 acts as an integrator of multiple signaling pathways involved in the maintenance of vascular homeostasis, and its dysregulation is implicated in a variety of vascular disorders (**Figure 1**).

FOXO3 and Oxidative Stress

Oxidative stress is a major driving force for vascular aging. Age-related increases in reactive oxygen species (ROS) result in endothelial dysfunction and arterial stiffness (47, 48). Endothelium-derived nitric oxide (NO) possesses anti-inflammatory, anti-thrombotic, and anti-leukocyte adhesion properties. Under pathological condition, ROS inactivates NO, which may contribute to the development of atherosclerosis (49). Exercise can restore endothelium-dependent dilation in aged mice by increasing NO bioavailability and reducing oxidative stress (50).

FOXO3 deletion results in an increase in ROS in mouse hematopoietic stem cells (51). FOXO3 is indispensable for the antioxidant-mediated protection in cardiovascular system. FOXO3 protects vascular endothelial cells (ECs) and vascular smooth muscle cells (VSMCs) against oxidative stress injury by up-regulating the expression of antioxidant enzymes such as catalase and manganese-superoxide dismutase (MnSOD) (52, 53).

FOXO3 and Dysregulated Nutrient-Sensing Pathways

AMPK and mTOR

AMPK and mTOR are key regulators of energy homeostasis. AMPK promotes ATP synthesis in response to an energy deficit caused by glucose deprivation or exercise (54). Activated AMPK regulates cell growth and metabolism at low energy levels by phosphorylating a range of substrates (55). In VECs, AMPK activates endothelial nitric oxide synthase (eNOS), phosphorylating it directly and so promoting NO production (56). Second, AMPK activation inhibits the generation of inflammatory chemokines in VECs by attenuating nuclear factor-kappaB (NF-κB) signal transduction (54). Two more studies demonstrate that AMPK signaling in ECs is required for angiogenesis in response to hypoxic stress and differentiation of endothelial progenitor cells (57, 58). However, AMPK activity is reduced in the aorta and cerebral arteries of old rodents (50, 59).

mTOR is a key regulator of anabolic processes and its activity decreases in response to nutrient deprivation. Decreased mTOR activity influences aging and longevity in invertebrates and mice (60). Numerous studies have demonstrated that inhibiting mTOR delays EC senescence (61, 62). Additionally, mTOR inhibition mediates the phenotypic transition of VSMCs by

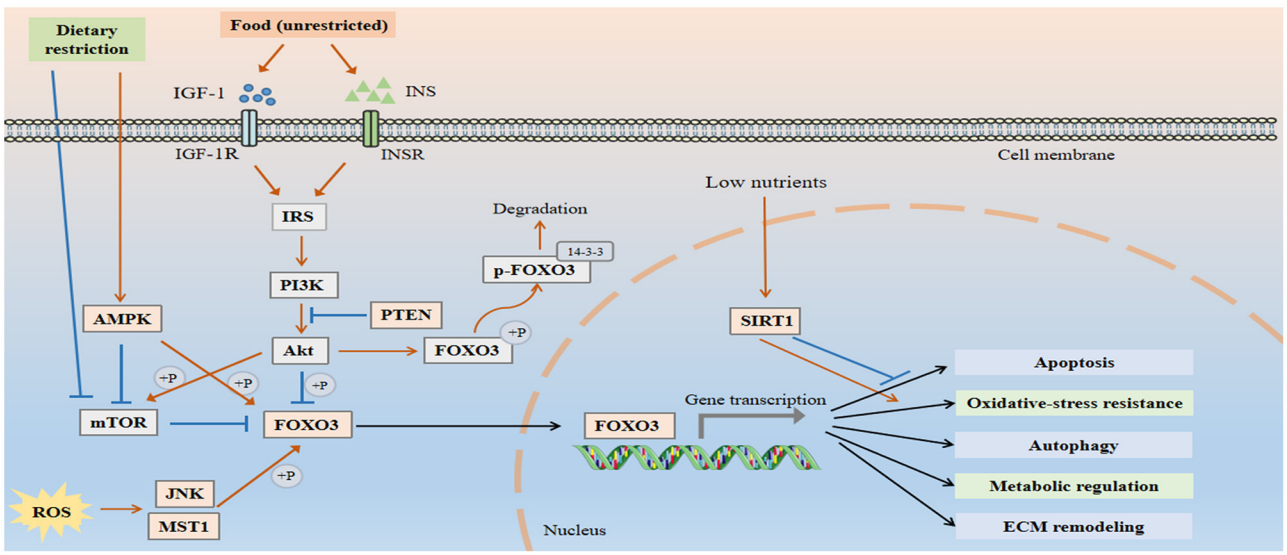

FIGURE 1 | FOXO3 is an integrator of multiple signaling pathways to maintain vascular homeostasis. Under normal conditions, FOXO3 is inactive due to the negative regulation by IIS-PI3K-Akt pathway. Akt phosphorylates FOXO3 at three highly conserved residues T32, S253, and S315, thereby establishing docking sites for the chaperone protein 14-3-3 and preventing it from re-entering the nucleus. PTEN antagonizes the effect of PI3K and induces FOXO3 activation. When cells are exposed to stress, including growth factor deprivation, metabolic stress, and oxidative stress, FOXO3 translocates into the nucleus and exhibits increased transcriptional activity. FOXO3 regulates a number of cellular processes, including apoptosis, autophagy, oxidative resistance, and metabolism, all of which are involved in the pathological process of vascular aging.

blocking the PDGF-induced contractile VSMC reduction (63). Rapamycin, an mTOR inhibitor, suppresses oxidative stress and vascular stiffness, revering the effects of age-related arterial dysfunction (64).

Between AMPK and mTOR, there are intricate and precise regulatory mechanisms that efficiently regulate energy metabolism. Akt, a positive regulator of energy metabolism, inhibits AMPK and promotes mTOR complex 1 (mTORC1) activation (65). AMPK is activated in response to energy stress, whereas mTORC1 is inactivated (66). Activated AMPK phosphorylates FOXO3 (42), which is an effector of AMPK-mediated apoptosis (67) and hypoxia-induced autophagy (68). Additionally, FOXO3 may suppress mTORC1 activity by inhibiting the regulatory associated protein of mTOR (Raptor) (69). AMPK promotes FOXO3 activation and inhibits mTOR, which seems to be protective in response to hypoxia, ROS, and starvation (70).

SIRTs

SIRTs are also activated in cells with inadequate nutritional status to increase their resistance to stress. The activated SIRT family members have anti-inflammatory, anti-oxidative stress and anti-senescence effects in the vasculature (71–74). SIRT1 acts as an anti-atherosclerotic factor in mice by preventing DNA damage (75). However, endogenous SIRT1 expression decreases with age (76). Decreased SIRT1 levels also contribute to vascular endothelial dysfunction associated with aging through its modulation of eNOS acetylation (77). Similarly, SIRT6 protects against DNA damage, telomere dysfunction, senescence, and atherosclerosis in vascular cells (78, 79).

Chronic hyperglycemia induces accelerated vascular aging. SIRT1-mediated deacetylation of FOXO3 is important for VECs survival under high-glucose conditions (80, 81). High glucose levels suppress the expression of SIRT1 and FOXO3 in VECs. SIRT1 overexpression protects VECs from high glucose-induced apoptosis (81). Additionally, the AMPK/SIRT1/FOXO3 signaling pathway affects the phenotypic switching of VSMCs (82). Moreover, the role of SIRT1 in ameliorating oxidative stress is associated with FOXO3 activation (22). SIRT1 enhances catalase activity and induces MnSOD expression by deacetylating FOXO3 to control intracellular ROS levels (83).

Although caloric restriction (CR) slows the aging process and decreases diabetes and CVD mortality, the underlying mechanisms are unknown (84). Numerous studies have highlighted the importance of nutrient-sensitive protein pathways such as AMPK, mTOR, SIRTs, and the insulin pathway (41). FOXO3 mediates cellular response to CR. By serving as a downstream effector for the insulin, AMPK and SIRTs pathways, FOXO3 stimulates the expression of stress genes in response to nutritional deficiency (85).

FOXO3 and Apoptosis

Apoptosis is evident in ECs and VSMCs in atherosclerotic plaques (86–88). FOXO3 up-regulates the expression of numerous apoptosis-related genes, including FasL, Bim, Puma, TRAIL, and Noxa (89). Bim is a proapoptotic member of the Bcl-2 family, and its expression is suppressed by Akt activation in VSMCs expressing wild-type FOXO3, but not in FOXO3 mutant cells (90). Apoptosis is an essential process by which unwanted or abnormal cells are removed during development. Apoptosis, however, may result in microvascular rarefaction and aneurysm in the vasculature. VSMCs apoptosis may even cause atherosclerotic plaque instability and rupture (91).

FOXO3 and Autophagy

Autophagy maintains homeostasis by removing damaged organelles and misfolded proteins (92). Autophagy has been shown to decrease with aging in animal models (93). Overexpression of autophagy-related gene 5 (*ATG5*) induces autophagy and prolongs life span in mice (94). In the vascular system, autophagy is associated with diverse physiological and pathophysiological processes, including angiogenesis, vascular calcification, and atherosclerosis (95). Reduced autophagy markers in senescent ECs may impair arterial endothelium-dependent dilatation (96). Autophagy is also reported to preserve arterial endothelial function by increasing NO bioavailability and reducing inflammation and oxidative stress (96). Additionally, spermidine-induced autophagy improves NO bioavailability and reduces arterial stiffness in aged mice (97).

Numerous autophagy-related genes, including *ATG12*, *BNIP3*, *ATG8*, and *GABARAPL1* are targets of FOXO3 (24, 98). FOXO3 is an important pro-autophagic factor in cardiomyocytes (99). In cardiac microvascular endothelial cells (CMECs), hypoxia suppresses phosphorylation of FOXO3 which induces autophagy formation (100). FOXO3 accumulation and nuclear translocation also elevate ATG protein levels in renal tubular epithelial cells, thus complementing the core component of autophagy (101).

FOXO3 and Epigenetics

Aging is a complex process driven by genetic and environmental factors. Epigenetics, an important interface between genetic and environmental factors influences aging as well as the occurrence and progression of aging-related disorders (102). Epigenetics, including DNA methylation patterns, histone modifications, and non-coding RNA regulation, play a crucial role in vascular aging (103).

MiRNA expression in VECs and VSMCs may correlate with vascular aging (104). Various miRNAs that directly influence FOXO3 expression, including miR-27a, miR-155, miR-233, and miR-29a affect vascular pathological processes. MiR-155 inhibits EC proliferation and migration, which eventually disrupts endothelial barriers (105). MiR-148a-3p upregulation in atherosclerotic patients suppresses FOXO3 expression and impairs EC proliferation and migration, ultimately aggravating atherosclerosis (106). Upregulation of a disintegrin and metalloproteinase with thrombospondin motifs-7 (ADAMTS-7) by miR-29a repression attenuates VSMC calcification (107). MiR-34a, upregulated in atherosclerotic plaques (108), targets SIRT1 3′ UTR to suppress SIRT1 expression (109). The role of SIRT1 in reducing oxidative stress depends on FOXO3 activation. Notably, the reversibility of epigenetic changes is a promising approach for developing epigenome-influencing interventions against cardiovascular disorders.

FOXO3 and ECM Remodeling

Aging alters extracellular matrix (ECM) synthesis and cell-ECM interactions (110). Decreased elastin synthesis with age reduces the elasticity and resilience of the vascular wall, impairing its ability to cope with mechanical damage and sudden changes in pulsatile pressure waves (111). Increased collagen synthesis in arterial walls linked with aging contributes to vascular fibrosis and arteriosclerosis (111). Aging also affects the secretion phenotype of VECs and VSMCs and affects matrix metalloproteinase (MMP) secretion (112). Elevated MMP activation by high ROS levels impairs the structural integrity of the vascular system and promotes pathological remodeling, contributing to the possibility of aneurysm formation and vascular rupture (112). Aging-related ECM remodeling also obstructs microvascular barrier function (113).

Studies on the effect of FOXO3 on MMPs have yielded inconsistent results. MMP13, MMP2 and MMP3 are considered FOXO3 targets. Activated FOXO3 induced ECM breakdown via MMP13 activation (28). Apelin, an adipocytokine, induces VSMC migration which is a critical event in atherosclerosis progression. Apelin promotes Akt-mediated phosphorylation of FOXO3, which enhances FOXO3 translocation from the nucleus to the cytoplasm and increases MMP2 levels (114). Additionally, FOXO3 phosphorylation has been shown to inhibit MMP3 promoter activity (115). ECMs are important in EC survival. Constitutively active FOXO3 enhances MMP3 expression and leads to EC apoptosis, which can be reversed by an MMP inhibitor, suggesting a novel mechanism of FOXO3-mediated EC apoptosis (116).

FOXO3 IN AGING-RELATED VASCULAR DISEASES

FOXO3 influences the progression of aging-related vascular diseases by regulating the expression of genes involved in oxidative stress, apoptosis, autophagy, and metabolic stress (**Figure 2**). In the following section, we will discuss the role of FOXO3 in diseases such as atherosclerosis, vascular calcification, hypertension, and vascular aging-related heart diseases, kidney diseases, and cerebrovascular diseases (**Table 1**).

The Role of FOXO3 in Atherosclerosis

FOXO3 genotypes are associated with the risk of death from coronary artery disease (CAD) in the elderly. The longevity-associated G allele of *FOXO3* SNP rs2802292 is protective against CAD mortality (117). The plasma TNF-α levels of G allele carriers were lower than that of non-carriers, implying that FOXO3-mediated inflammation inhibition is a protective mediator of CAD death risk (117). LDL-cholesterol is an important risk factor for CVD. FOXO3 and SIRT6 regulate LDL cholesterol homeostasis by regulating the *PCSK9* gene expression, which lowers LDL levels by inhibiting LDL receptor degradation (118).

Under normal growth conditions, FOXO3 is negatively regulated by IGF-1/PI3K/Akt signaling (20). Age-related decline of IGF-1R suppresses Akt/FOXO3 in VSMCs (119). Low levels of VSMC apoptosis occur in atherosclerotic plates. Compared with normal VSMCs, VSMCs in the atherosclerotic plate express lower IGF-1R levels and exhibit higher apoptosis. IGF-1R overexpression is reported to protect VSMCs from oxidative

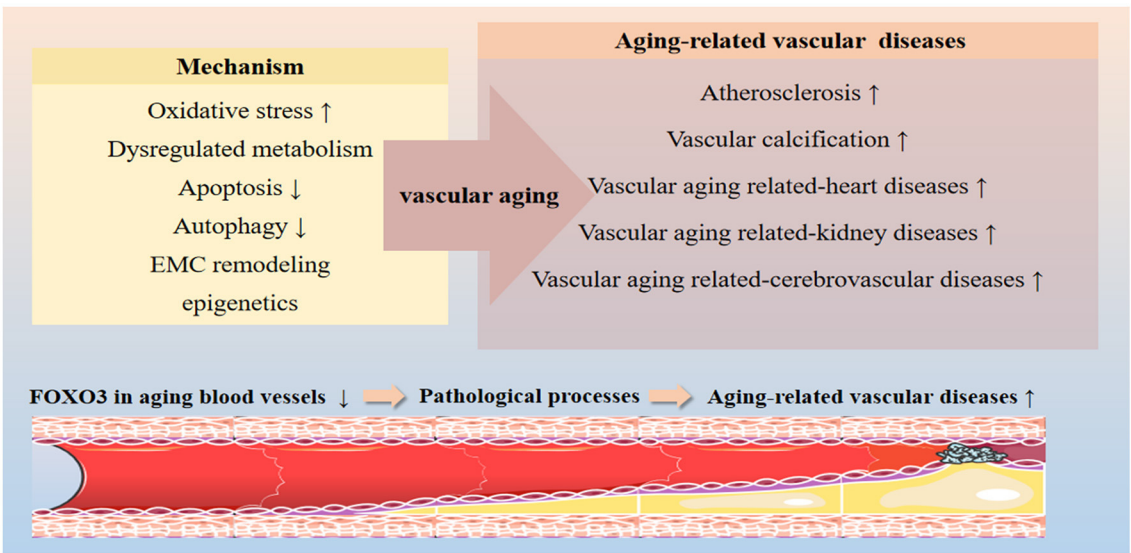

FIGURE 2 | Effects of FOXO3 on vascular aging-related diseases. FOXO3 participates in various cellular processes implicated in the progression of vascular aging, including oxidative resistance, apoptosis, autophagy, energy metabolism, and ECM remodeling processes by targeting the expression of effector genes. FOXO3 is a key protective factor in maintaining vascular homeostasis. Dysregulation of FOXO3 has been shown to contribute to a variety of vascular aging-related diseases, including atherosclerosis, vascular calcification, hypertension, and vascular aging-related heart diseases, kidney diseases, and cerebrovascular diseases.

TABLE 1 | FOXO3 cellular signaling in vascular aging-related diseases.

Diseases	Biological effects of FOXO3	References
Atherosclerosis	The longevity-associated G allele of *FOXO3* SNP rs2802292 is protective against CAD mortality	(117)
	Phosphorylated FOXO3 is increased in human carotid atherosclerotic plaques	(114)
	FOXO3 phosphorylated by Akt protects VSMCs from oxidative stress-induced apoptosis	(90)
	FOXO3 phosphorylation promotes VSMC migration	(114)
	Up-regulated AMPK/SIRT1/FOXO3 signaling increases the protein levels of the VSMC contractile markers	(84)
	FOXO3 suppresses VSMC proliferation and neointimal hyperplasia by downregulating CYR6	(122)
	Decreased FOXO3 inhibits NLRP3-mediated EC pyroptosis	(123)
	Melatonin ameliorates atherosclerosis by regulating SIRT3/FOXO3/Parkin signaling	(124)
Vascular calcification	FOXO3 phosphorylated by Akt promotes VSMC calcification	(125)
Vascular aging related-heart diseases	FOXO3-null mice developed dilated cardiomyopathy within 12 weeks of age	(129)
	Reduced FOXO3 in senescent cardiac microvascular ECs leads to inhibition of proliferation and tube formation	(130)
	FOXO3 overexpression suppressed the aging of cardiac microvascular ECs by regulating the antioxidant/ROS/p27 (kip1) pathway	(130)
	Downstream proapoptotic genes mediated by FOXO3 are activated in aging cardiomyocytes	(133)
	FOXO3 deficiency in the heart enhances paraquat-induced aging phenotypes	(134)
	FOXO3 activation and expression are reduced in cardiac fibroblasts. Overexpression of FOXO3 inhibited while knockdown of FOXO3 enhanced TFGβ1-induced cardiac myofibroblasts transformation	(135)
Vascular aging related-kidney diseases	FOXO3 promotes the expression of Atg proteins to sustain autophagy in the chronically hypoxic kidney	(101)
	FOXO3 deacetylated by SIRT1 induces the expression of BNIP3, and ultimately promotes mitochondrial autophagy, and protect aging kidneys	(137)
	Tubular deletion of FOXO3 aggravates renal structural and functional damage	(138)
	Activated FOXO3 in mice with unilateral ureteral obstruction contributes to high levels of autophagy	(139)
	FOXO3 ameliorates oxidative stress, suppressing renal fibrosis induced by diabetes and hypertension	(141–143)
Vascular aging related-cerebrovascular diseases	Increased risks of stroke are observed for *FOXO3* block-A haplotype 2 "GAGC" and haplotype 4 "AAAT" carriers	(144)
	Overexpressed FOXO3 in the cerebral cortex of MCAO mice promotes neuronal death	(145, 146)
	AMPK/FOXO3 and PTEN-Akt-FOXO3 pathways regulate neuronal apoptosis after hypoxia-ischemia in the developing rat brain	(67, 147)
	Increased FOXO3 activation has a protective effect on cerebral ischemia-reperfusion injury by promoting autophagy	(148)
Primary hypertension	Longevity related *FOXO3* variants may contribute to low risk for essential hypertension in Japanese women	(150)

stress-induced apoptosis by up-regulating Akt-mediated phosphorylation of FOXO3 (90).

VSMC migration is a key event in the development of atherosclerosis. In human carotid atherosclerotic plaques, apelin induces FOXO3 phosphorylation in a dose-dependent manner, and mediates VSMC migration (114). Glucagon-like peptide-1 receptor (GLP-1R) is widely expressed in various cell types, such as VSMCs and cardiomyocytes (120). GLP-1R agonist exendin-4 not only inhibits angiotensin II-induced cell senescence but also inhibits PDGF-induced VSMC proliferation and migration (121). Exendin-4 has been shown to elevate the expression of VSMC contractile markers, Calponin and SM22α, by upregulating AMPK/SIRT1/FOXO3 signaling (82). Cysteine-rich angiogenic protein 61 (CYR61) has been implicated in restenosis after angioplasty. FOXO3, a CYR61 antagonist, inhibits VSMC proliferation and neointimal hyperplasia (122).

The inflammatory response mediated by the NOD-like receptor family pyrin domain-containing 3 (NLRP3) inflammasome is associated with atherosclerosis progression. MiR-30c-5p downregulates FOXO3 expression, inhibiting NLRP3-mediated EC pyroptosis in atherosclerosis (123). Melatonin has been demonstrated to ameliorate atherosclerosis by inhibiting NLRP3 inflammasome, which is regulated by SIRT3/FOXO3/Parkin signaling (124).

The Role of FOXO3 in Vascular Calcification

Vascular calcification refers to the ectopic deposition of calcium salts in blood vessels. It is associated with vascular aging, atherosclerosis, advanced nephropathy, and diabetes (125). Runt-related transcription factor 2 (Runx2), a key osteogenic regulator, regulates VSMC osteogenic differentiation and vascular calcification in atherosclerosis (126). Akt activation is reported to contribute to oxidative stress-induced VSMC calcification by upregulating Runx2 expression (127). Deficiency in PTEN, an Akt inhibitor, results in sustained Akt activity, which results in FOXO3 phosphorylation, Runx2 ubiquitination, and VSMC calcification (125). Other members of the FOXO family have also been implicated in the regulation of vascular calcification. For example, FOXO1 dysregulation contributes to peripheral arterial calcification (128).

The Role of FOXO3 in Vascular Aging Related-Heart Diseases

Left ventricular hypertrophy is a crucial feature of cardiac aging, leading to diastolic dysfunction, atrial fibrillation, and heart failure. Moreover, atherosclerotic diseases (e.g., coronary heart disease) might result in chronic myocardial insufficiency, ischemic heart disease, or even heart failure. FOXO3 plays important role in the maintenance of cardiac homeostasis. For example, FOXO3-null mice developed dilated cardiomyopathy within 12 weeks of age (129). Low expression of FOXO3 in senescent cardiac microvascular ECs suppressed the ability of cell proliferation and tube formation. Additionally, it has also been observed that FOXO3 overexpression slowed the senescence of cardiac microvascular ECs via modulating the antioxidant/ROS/p27 (kip1) pathway (130).

A previous study reported that compared with young people, persons above the age of 70 years had 30% fewer myocardial cells (131), which may be ascribed to apoptosis (132). The aged heart is more susceptible to ischemia-reperfusion injury. SIRT1 expression was significantly reduced in aged cardiomyocytes, while FOXO3-mediated antioxidant kinase decreased and apoptosis increased, aggravating myocardial ischemia-reperfusion injury (133).

Paraquat inhibits FOXO3 activation and induces cardiomyocyte senescence phenotype. FOXO3 silencing in the heart greatly accelerated the aging phenotypes induced by paraquat, including proliferation inhibition, apoptosis, and galactosidase activity. FOXO3 has also been shown to protect the heart against paraquat-induced aging phenotypes by upregulating the expression of antioxidant enzymes and inhibiting oxidative stress (134).

Cardiac fibroblasts (CFs) contribute to the maintenance of the ECM balance in the normal heart. Under normal conditions, CFs exist in a quiescent state and secrete only a small amount of ECM components. However, CFs differentiate into more active cardiac myofibroblasts (CMFs) under pathological conditions. This CMF conversion is a hallmark of cardiac fibrotic diseases such as heart failure and diabetic cardiomyopathy. TGF-β1 is a key protein that regulates CMF transformation. Previously, it was reported that TGF-β1 decreased FOXO3 expression in a concentration-dependent manner in CFs. Overexpression of FOXO3 inhibited whereas knockdown of FOXO3 enhanced TFGβ1-induced CMF transformation (135). Therefore, FOXO3 may act as a negative regulator of CMF conversion triggered by TGF-β1.

The Role of FOXO3 in Vascular Aging Related-Kidney Diseases

Vascular aging increases the risk of chronic kidney disease (CKD). A previous investigation established that arterial stiffness contributed to the decline in kidney function (136). Hypoxia inhibits the hydroxylation of FOXO3 prolyl, thereby reducing the degradation of FOXO3. FOXO3 upregulates the expression of Atg proteins, which promote autophagy in chronically hypoxic kidneys (101). Calorie restriction maintains renal SIRT1 expression, and elevates BNIP3 expression by deacetylating FOXO3, which promotes mitochondrial autophagy and delays the effects of aging on kidneys (137). Previously, it was demonstrated that tubular deletion of FOXO3 aggravated renal structural and functional damage, leading to a more severe CKD phenotype (138). FOXO3 was discovered to be activated in mice with unilateral ureteral obstruction. Moreover, hypoxic proximal tubules activates autophagy in response to urinary tract obstruction (139).

Tissue fibrosis is a common manifestation of aging-related diseases. Currently, there are limited therapeutic targets to prevent fibrogenesis. As previously indicated, FOXO3 inhibits fibroblast activation and ameliorates fibrosis levels in many organs, including the kidney, liver, heart, and lung (140). Renal fibrosis, including glomerulosclerosis and tubulointerstitial fibrosis, is the pathological hallmark of CKD. FOXO3 ameliorates oxidative stress, thereby suppressing renal fibrosis associated with diabetes and hypertension (141, 142). FOXO3 was found to be directly regulated by miR-132 in a mouse model experiment. Indeed, silencing miR-132 delayed the progression of renal fibrosis, implying that miR-132 could be a potential therapeutic target for fibrosis treatment (143).

The Role of FOXO3 in Vascular Aging Related-Cerebrovascular Diseases

During vascular aging, entry of high pulsating blood flow into small cerebral vessels may damage the cerebral microvessels, resulting in cerebrovascular diseases or cognitive impairment. Haplotype analyses of *FOXO3* revealed that *FOXO3* block-A haplotype 2 "GAGC" and haplotype 4 "AAAT" carriers had a higher risk of stroke (144). Mice subjected to transient middle cerebral artery occlusion (MCAO) developed severe cerebral infarction and long-term neurological deficit. FOXO3 overexpression was previously described in the cerebral cortical neurons of MCAO mice. Downregulation of miR-9 and miR-122 promoted neuronal death by up-regulating FOXO3 expression in the brain of MCAO mice (145, 146). Moreover, AMPK/FOXO3 and PTEN-Akt-FOXO3 pathways have been implicated in the regulation of neuronal apoptosis in response to hypoxia-ischemia during the developmental stages of rat brain (67, 147). In addition, the ischemia-reperfusion injury resulted in

activation of FOXO3. Activated FOXO3 promotes autophagy, thereby reducing the injury caused by cerebral ischemia-reperfusion (148).

The Role of FOXO3 in Primary Hypertension

Clinical studies have shown that vascular aging is a predictor and risk factor for hypertension. Patients with hypertension, regardless of whether their blood pressure is normal or not, are at an increased risk of developing cardiovascular events. Researchers have found that patients receiving antihypertensive drugs still have a 50% residual risk of cardiovascular death (149). The longevity-related *FOXO3* polymorphisms may be associated with lower blood pressure (BP) in Japanese women with hypertension (150).

FOXO3 as a Promising Therapeutic Target in Aging-Related Vascular Diseases

FOXO3 is an ideal target for a variety of aging-related diseases, including cancer, degenerative diseases, and vascular aging. As previously described, FOXO3 is a good biomarker for cancer initiation, progression, and drug efficacy, and resistance. FOXO3 reactivation may be an efficient antitumor strategy. Furthermore, conditional deletion of *FOXO1/3/4* in mice triggered IVD degeneration, and therapeutic activation of FOXO could resist IVD degeneration by promoting stress resistance and autophagy (29). FOXO3 has a well-established function in the occurrence and pathogenesis of vascular aging-related diseases. The AMPK-FOXO3-Trx axis, which has been demonstrated to be a critical defensive mechanism against excessive generation of ROS induced by metabolic stress, may be a promising target in treating CVDs in metabolic syndrome (151). Akt inhibition activates FOXO3, which is also a good way to delay vascular aging (152). UCN-01, a drug currently used in clinical trials against cancer, inhibits Akt phosphorylation resulting in FOXO3 reactivation (153). UCN-01 was shown to be capable of reversing bleomycin- induced lung fibrosis *in vivo* by activating FOXO3 (153). Curcumin, a polyphenol, enhances FOXO3 function by inhibiting its phosphorylation, resulting in a two-fold increase in target gene expression (154). Further evidence confirmed that curcumin protects inflammatory cells in the vascular system against lipid and oxidant-induced damage by increasing FOXO3 activity, so lowering the risk for aging-related CVD (154). Additionally, human VECs, VSMCs, and MSCs expressing a constitutively active version of FOXO3 exhibited enhanced self-renewal capacity, greater regenerative capacity under ischemia conditions, and increased resistance to oxidative injury (155). The evidence presented above suggests that pharmacological reconstitution of FOXO3 may be a novel treatment option for aging-related vascular diseases.

Pharmaceutical regulation of the FOXO3 signaling pathway is a promising strategy to promote healthy longevity. It was found that FOXO3 longevity genotype mitigated the increased mortality risk in men with a cardiometabolic disease (CMD). Moreover, there was no association of *FOXO3* longevity genotype with lifespan in men without a CMD (17). Therefore, CMD patients without the *FOXO3* longevity genotype may benefit most from intervention targeting FOXO3. However, FOXO3 may not be a easily druggable target, because its activity is mediated by a complex network of interactions with other DNA, RNA, and proteins. Direct regulation of gene expression in a simple manner may not achieve the expected effect and cause redundant functions. FOXO3 activity is finely regulated by PTM modulators, which is a more feasible and acceptable therapy. Researchers have explored a number of agents identified as modulators of FOXO3 activity, including those that target nuclear export and import, drugs that target upstream regulatory targets, drugs that target FOXO3 protein interactions, and those that target DNA binding (156). FOXO3 exhibits variable affinity for target genes under different conditions (157). Consequently, the development of FOXO3-specific therapy based on multiple statuses is expected to improve efficacy and reduce the off-target effects. To improve the development of FOXO3-based treatment options, it is necessary to conduct additional studies on the regulatory networks, including upstream regulatory molecules and downstream pathways of FOXO3.

CONCLUSION

Healthy aging is critical for addressing the increasing severity of global population aging. The unique role of FOXO3 in the vasculature provides promising avenues for therapeutics against aging-related vascular diseases. PTMs that regulate FOXO3 activity may be potential therapeutic targets. It is expected that research into strategies for delaying the occurrence and development of vascular aging by targeting the FOXO3 will uncover novel perspectives for the development of new drugs. Despite advances in our understanding of FOXO3's function in retarding vascular senescence, the particular processes remain poorly known, and other issues remain unresolved. For instance, FOXO3 activation promotes VSMCs apoptosis, which may result in atherosclerotic plaque instability and rupture, causing myocardial infarction, and cerebral infarction. In some cases, FOXO3 promotes ECM degradation which may accelerate the progression of atherosclerosis. While therapies targeting FOXO3 seem appealing, we need to understand all the details to maximize its effectiveness. Despite these challenges, in-depth research into FOXO3 functions may pave the way for future therapeutic approaches.

AUTHOR CONTRIBUTIONS

YZ collected the literature and wrote the manuscript. Y-SL conceived the idea and had been involved in manuscript conception and drafting. YZ and Y-SL read and approved the final manuscript. All authors contributed to the article and approved the submitted version.

FUNDING

This work was supported by the National Natural Science Foundation of China (No. 82071593); the Fundamental Research Funds for the Central Universities of Central South University (No. 2021zzts0359); and Hunan Provincial Innovation Foundation for Postgraduate (No. CX20210128).

REFERENCES

1. Lozano R, Naghavi M, Foreman K, Lim S, Shibuya K, Aboyans V, et al. Global and regional mortality from 235 causes of death for 20 age groups in 1990 and 2010: a systematic analysis for the Global Burden of Disease Study 2010. *Lancet.* (2012) 380:2095–128. doi: 10.1016/S0140-6736(12)61728-0
2. Kennedy BK, Berger SL, Brunet A, Campisi J, Cuervo AM, Epel ES, et al. Geroscience: linking aging to chronic disease. *Cell.* (2014) 159:709–13. doi: 10.1016/j.cell.2014.10.039
3. van Bussel BC, Schouten F, Henry RM, Schalkwijk CG, de Boer MR, Ferreira I, et al. Endothelial dysfunction and low-grade inflammation are associated with greater arterial stiffness over a 6-year period. *Hypertension.* (2011) 58:588–95. doi: 10.1161/HYPERTENSIONAHA.111.174557
4. Ding Y-N, Tang X, Chen H-Z, Liu D-P. Epigenetic regulation of vascular aging and age-related vascular diseases. *Adv Exp Med Biol.* (2018) 1086:55–75. doi: 10.1007/978-981-13-1117-8_4
5. Regina C, Panatta E, Candi E, Melino G, Amelio I, Balistreri CR, et al. Vascular ageing and endothelial cell senescence:Molecular mechanisms of physiology and diseases. *Mech Ageing Dev.* (2016) 159:14–21. doi: 10.1016/j.mad.2016.05.003
6. Brunet A, Bonni A, Zigmond MJ, Lin MZ, Juo P, Hu LS, et al. Akt promotes cell survival by phosphorylating and inhibiting a forkhead transcription factor. *Cell.* (1999) 96:857–68. doi: 10.1016/S0092-8674(00)80595-4
7. Kenyon C, Chang J, Gensch E, Rudner A, Tabtiang R. A *C. elegans* mutant that lives twice as long as wild type. *Nature.* (1993) 366:461–4. doi: 10.1038/366461a0
8. Ogg S, Paradis S, Gottlieb S, Patterson GI, Lee L, Tissenbaum HA, et al. The forkhead transcription factor DAF-16 transduces insulin-like metabolic and longevity signals in *C. elegans*. *Nature.* (1997) 389:994–9. doi: 10.1038/40194
9. Katic M, Kahn CR. The role of insulin and IGF-1 signaling in longevity. *Cell Mol Life Sci.* (2005) 62:320–43. doi: 10.1007/s00018-004-4297-y
10. Willcox BJ, Donlon TA, He Q, Chen R, Grove JS, Yano K, et al. FOXO3A genotype is strongly associated with human longevity. *Proc Natl Acad Sci USA.* (2008) 105:13987–92. doi: 10.1073/pnas.0801030105
11. Anselmi CV, Malovini A, Roncarati R, Novelli V, Villa F, Condorelli G, et al. Association of the FOXO3A locus with extreme longevity in a southern Italian centenarian study. *Rejuvenation Res.* (2009) 12:95–104. doi: 10.1089/rej.2008.0827
12. Flachsbart F, Caliebe A, Kleindorp R, Blanché H, von Eller-Eberstein H, Nikolaus S, et al. Association of FOXO3A variation with human longevity confirmed in German centenarians. *Proc Natl Acad Sci USA.* (2009) 106:2700–5. doi: 10.1073/pnas.0809594106
13. Li Y, Wang W-J, Cao H, Lu J, Wu C, Hu F-Y, et al. Genetic association of FOXO1A and FOXO3A with longevity trait in Han Chinese populations. *Hum Mol Genet.* (2009) 18:4897–904. doi: 10.1093/hmg/ddp459
14. Bao J-M, Song X-L, Hong Y-Q, Zhu H-L, Li C, Zhang T, et al. Association between FOXO3A gene polymorphisms and human longevity: a meta-analysis. *Asian J Androl.* (2014) 16:446–52. doi: 10.4103/1008-682X.123673
15. Martins R, Lithgow GJ, Link W. Long live FOXO: unraveling the role of FOXO proteins in aging and longevity. *Aging Cell.* (2016) 15:196–207. doi: 10.1111/acel.12427
16. Willcox BJ, Tranah GJ, Chen R, Morris BJ, Masaki KH, He Q, et al. The FoxO3 gene and cause-specific mortality. *Aging Cell.* (2016) 15:617–24. doi: 10.1111/acel.12452
17. Chen R, Morris BJ, Donlon TA, Masaki KH, Willcox DC, Davy PMC, et al. FOXO3 longevity genotype mitigates the increased mortality risk in men with a cardiometabolic disease. *Aging.* (2020) 12:23509–24. doi: 10.18632/aging.202175
18. Zhang W, Zhang S, Yan P, Ren J, Song M, Li J, et al. A single-cell transcriptomic landscape of primate arterial aging. *Nat Commun.* (2020) 11:2202. doi: 10.1038/s41467-020-15997-0
19. van den Berg MCW, Burgering BMT. Integrating opposing signals toward forkhead box O. *Antioxid Redox Signal.* (2011) 14:607–21. doi: 10.1089/ars.2010.3415
20. Eijkelenboom A, Burgering BMT. FOXOs: signalling integrators for homeostasis maintenance. *Nat Rev Mol Cell Biol.* (2013) 14:83–97. doi: 10.1038/nrm3507
21. McGowan SE, McCoy DM. Platelet-derived growth factor-a regulates lung fibroblast S-phase entry through p27(kip1) and FoxO3a. *Respir Res.* (2013) 14:68. doi: 10.1186/1465-9921-14-68
22. Wang X, Meng L, Zhao L, Wang Z, Liu H, Liu G, et al. Resveratrol ameliorates hyperglycemia-induced renal tubular oxidative stress damage via modulating the SIRT1/FOXO3a pathway. *Diabetes Res Clin Pract.* (2017) 126:172–81. doi: 10.1016/j.diabres.2016.12.005
23. Chen Y-F, Pandey S, Day CH, Chen Y-F, Jiang A-Z, Ho T-J, et al. Synergistic effect of HIF-1α and FoxO3a trigger cardiomyocyte apoptosis under hyperglycemic ischemia condition. *J Cell Physiol.* (2018) 233:3660–71. doi: 10.1002/jcp.26235
24. Zhao J, Brault JJ, Schild A, Cao P, Sandri M, Schiaffino S, et al. FoxO3 coordinately activates protein degradation by the autophagic/lysosomal and proteasomal pathways in atrophying muscle cells. *Cell Metab.* (2007) 6:472–83. doi: 10.1016/j.cmet.2007.11.004
25. Fluteau A, Ince PG, Minett T, Matthews FE, Brayne C, Garwood CJ, et al. The nuclear retention of transcription factor FOXO3a correlates with a DNA damage response and increased glutamine synthetase expression by astrocytes suggesting a neuroprotective role in the ageing brain. *Neurosci Lett.* (2015) 609:11–7. doi: 10.1016/j.neulet.2015.10.001
26. Hu C, Ni Z, Li B-S, Yong X, Yang X, Zhang J-W, et al. hTERT promotes the invasion of gastric cancer cells by enhancing FOXO3a ubiquitination and subsequent ITGB1 upregulation. *Gut.* (2017) 66:31–42. doi: 10.1136/gutjnl-2015-309322
27. Liu Y, Ao X, Ding W, Ponnusamy M, Wu W, Hao X, et al. Critical role of FOXO3a in carcinogenesis. *Mol Cancer.* (2018) 17:104. doi: 10.1186/s12943-018-0856-3
28. Yu H, Fellows A, Foote K, Yang Z, Figg N, Littlewood T, et al. FOXO3a (forkhead transcription factor O subfamily member 3a) links vascular smooth muscle cell apoptosis, matrix breakdown, atherosclerosis, and vascular remodeling through a novel pathway involving MMP13 (matrix metalloproteinase 13). *Arterioscler Thromb Vasc Biol.* (2018) 38:555–65. doi: 10.1161/ATVBAHA.117.310502
29. Alvarez-Garcia O, Matsuzaki T, Olmer M, Miyata K, Mokuda S, Sakai D, et al. FOXO are required for intervertebral disk homeostasis during aging and their deficiency promotes disk degeneration. *Aging Cell.* (2018) 17:e12800. doi: 10.1111/acel.12800
30. Hu W, Yang Z, Yang W, Han M, Xu B, Yu Z, et al. Roles of forkhead box O (FoxO) transcription factors in neurodegenerative diseases: a panoramic view. *Prog Neurobiol.* (2019) 181:101645. doi: 10.1016/j.pneurobio.2019.101645
31. Ambros V. The functions of animal microRNAs. *Nature.* (2004) 431:350–5. doi: 10.1038/nature02871
32. Cai J, Fang L, Huang Y, Li R, Yuan J, Yang Y, et al. miR-205 targets PTEN and PHLPP2 to augment AKT signaling and drive malignant phenotypes in non-small cell lung cancer. *Cancer Res.* (2013) 73:5402–15. doi: 10.1158/0008-5472.CAN-13-0297
33. Yang W, Du WW, Li X, Yee AJ, Yang BB. Foxo3 activity promoted by non-coding effects of circular RNA and Foxo3 pseudogene in the inhibition of tumor growth and angiogenesis. *Oncogene.* (2016) 35:3919–31. doi: 10.1038/onc.2015.460
34. Du WW, Yang W, Chen Y, Wu Z-K, Foster FS, Yang Z, et al. Foxo3 circular RNA promotes cardiac senescence by modulating multiple factors associated with stress and senescence responses. *Eur Heart J.* (2017) 38:1402–12. doi: 10.1093/eurheartj/ehw001
35. Zanella F, Rosado A, García B, Carnero A, Link W. Chemical genetic analysis of FOXO nuclear-cytoplasmic shuttling by using image-based cell screening. *Chembiochem.* (2008) 9:2229–37. doi: 10.1002/cbic.200800255
36. van der Horst A, Burgering BMT. Stressing the role of FoxO proteins in lifespan and disease. *Nat Rev Mol Cell Biol.* (2007) 8:440–50. doi: 10.1038/nrm2190
37. Rinner O, Mueller LN, Hubálek M, Müller M, Gstaiger M, Aebersold R. An integrated mass spectrometric and computational framework for the analysis of protein interaction networks. *Nat Biotechnol.* (2007) 25:345–52. doi: 10.1038/nbt1289

38. Guo J-P, Tian W, Shu S, Xin Y, Shou C, Cheng JQ. IKBKE phosphorylation and inhibition of FOXO3a: a mechanism of IKBKE oncogenic function. *PLoS ONE.* (2013) 8:e63636. doi: 10.1371/journal.pone.0063636
39. Salih DAM, Brunet A. FOXO transcription factors in the maintenance of cellular homeostasis during aging. *Curr Opin Cell Biol.* (2008) 20:126–36. doi: 10.1016/j.ceb.2008.02.005
40. Calnan DR, Brunet A. The FOXO code. *Oncogene.* (2008) 27:2276–88. doi: 10.1038/onc.2008.21
41. Oellerich MF, Potente M. FOXOs and sirtuins in vascular growth, maintenance, and aging. *Circ Res.* (2012) 110:1238–51. doi: 10.1161/CIRCRESAHA.111.246488
42. Greer EL, Oskoui PR, Banko MR, Maniar JM, Gygi MP, Gygi SP, et al. The energy sensor AMP-activated protein kinase directly regulates the mammalian FOXO3 transcription factor. *J Biol Chem.* (2007) 282:30107–19. doi: 10.1074/jbc.M705325200
43. Giannakou ME, Partridge L. The interaction between FOXO and SIRT1: tipping the balance towards survival. *Trends Cell Biol.* (2004) 14:408–12. doi: 10.1016/j.tcb.2004.07.006
44. Wang F, Nguyen M, Qin FX-F, Tong Q. SIRT2 deacetylates FOXO3a in response to oxidative stress and caloric restriction. *Aging Cell.* (2007) 6:505–14. doi: 10.1111/j.1474-9726.2007.00304.x
45. Greer EL, Brunet A. FOXO transcription factors at the interface between longevity and tumor suppression. *Oncogene.* (2005) 24:7410–25. doi: 10.1038/sj.onc.1209086
46. Wang F, Chan CH, Chen K, Guan X, Lin HK, Tong Q. Deacetylation of FOXO3 by SIRT1 or SIRT2 leads to Skp2-mediated FOXO3 ubiquitination and degradation. *Oncogene.* (2012) 31:1546–57. doi: 10.1038/onc.2011.347
47. Donato AJ, Eskurza I, Silver AE, Levy AS, Pierce GL, Gates PE, et al. Direct evidence of endothelial oxidative stress with aging in humans: relation to impaired endothelium-dependent dilation and upregulation of nuclear factor-kappaB. *Circ Res.* (2007) 100:1659–666. doi: 10.1161/01.RES.0000269183.13937.e8
48. Jablonski KL, Seals DR, Eskurza I, Monahan KD, Donato AJ. High-dose ascorbic acid infusion abolishes chronic v asoconstriction and restores resting leg blood flow in healthy older men. *J Appl Physiol.* (2007) 103:1715–21. doi: 10.1152/japplphysiol.00533.2007
49. Ganz P, Vita JA. Testing endothelial vasomotor function: nitric oxide, a multipotent molecule. *Circulation.* (2003) 108:2049–53. doi: 10.1161/01.CIR.0000089507.19675.F9
50. Lesniewski LA, Zigler MC, Durrant JR, Donato AJ, Seals DR. Sustained activation of ampk ameliorates age-associated vascular endothelial dysfunction via a nitric oxide-independent mechanism. *Mech Ageing Dev.* (2012) 133:368–71. doi: 10.1016/j.mad.2012.03.011
51. Tothova Z, Kollipara R, Huntly BJ, Lee BH, Castrillon DH, Cullen DE, et al. FoxOs are critical mediators of hematopoietic stem cell resistance to physiologic oxidative stress. *Cell.* (2007) 128:325–39. doi: 10.1016/j.cell.2007.01.003
52. Li M, Chiu J-F, Mossman BT, Fukagawa NK. Down-regulation of manganese-superoxide dismutase through phosphorylation of FOXO3a by Akt in explanted vascular smooth muscle cells from old rats. *J Biol Chem.* (2006) 281:40429–39. doi: 10.1074/jbc.M606596200
53. Olmos Y, Valle I, Borniquel S, Tierrez A, Soria E, Lamas S, et al. Mutual dependence of Foxo3a and PGC-1alpha in the induction of oxidative stress genes. *J Biol Chem.* (2009) 284:14476–84. doi: 10.1074/jbc.M807397200
54. Cacicedo JM, Yagihashi N, Keaney JF, Ruderman NB, Ido Y. Ampk inhibits fatty acid-induced increases in nf-kappab transactivation in cultured human umbilical vein endothelial cells. *Biochem Biophys Res Commun.* (2004) 324:1204–9. doi: 10.1016/j.bbrc.2004.09.177
55. Hardie DG, Ross FA, Hawley SA. AMPK: a nutrient and energy sensor that maintains energy homeostasis. *Nat Rev Mol Cell Biol.* (2012) 13:251–62. doi: 10.1038/nrm3311
56. Morrow VA, Foufelle F, Connell JMC, Petrie JR, Gould GW, Salt IP. Direct activation of AMP-activated protein kinase stimulates nitric-oxide synthesis in human aortic endothelial cells. *J Biol Chem.* (2003) 278:31629–39. doi: 10.1074/jbc.M212831200
57. Nagata D, Mogi M, Walsh K. AMP-activated protein kinase (AMPK) signaling in endothelial cells is essential for angiogenesis in response to hypoxic stress. *J Biol Chem.* (2003) 278:31000–6. doi: 10.1074/jbc.M300643200
58. Li X, Han Y, Pang W, Li C, Xie X, Shyy JYJ, et al. AMP-activated protein kinase promotes the differentiation of endothelial progenitor cells. *Arterioscler Thromb Vasc Biol.* (2008) 28:1789–95. doi: 10.1161/ATVBAHA.108.172452
59. Pu Y, Zhang H, Wang P, Zhao Y, Li Q, Wei X, et al. Dietary curcumin ameliorates aging-related cerebrovascular dysfunction through the ampk/uncoupling protein 2 pathway. *Cell Physiol Biochem.* (2013) 32:1167–77. doi: 10.1159/000354516
60. Johnson SC, Sangesland M, Kaeberlein M, Rabinovitch PS. Modulating mTOR in aging and health. *Interdiscip Top Gerontol.* (2015) 40:107–27. doi: 10.1159/000364974
61. Wang C-Y, Kim H-H, Hiroi Y, Sawada N, Salomone S, Benjamin LE, et al. Obesity increases vascular senescence and susceptibility to ischemic injury through chronic activation of Akt and mTOR. *Sci Signal.* (2009) 2:ra11. doi: 10.1126/scisignal.2000143
62. Yepuri G, Velagapudi S, Xiong Y, Rajapakse AG, Montani J-P, Ming X-F, et al. Positive crosstalk between arginase-II and S6K1 in vascular endothelial inflammation and aging. *Aging Cell.* (2012) 11:1005–16. doi: 10.1111/acel.12001
63. Ha JM, Yun SJ, Kim YW, Jin SY, Lee HS, Song SH, et al. Platelet-derived growth factor regulates vascular smooth muscle phenotype via mammalian target of rapamycin complex 1. *Biochem Biophys Res Commun.* (2015) 464:57–62. doi: 10.1016/j.bbrc.2015.05.097
64. Lesniewski LA, Seals DR, Walker AE, Henson GD, Blimline MW, Trott DW, et al. Dietary rapamycin supplementation reverses age-related vascular dysfunction and oxidative stress, while modulating nutrient-sensing, cell cycle, and senescence pathways. *Aging Cell.* (2017) 16:17–26. doi: 10.1111/acel.12524
65. Hahn-Windgassen A, Nogueira V, Chen C-C, Skeen JE, Sonenberg N, Hay N. Akt activates the mammalian target of rapamycin by regulating cellular ATP level and AMPK activity. *J Biol Chem.* (2005) 280:32081–9. doi: 10.1074/jbc.M502876200
66. Inoki K, Zhu T, Guan K-L. TSC2 mediates cellular energy response to control cell growth and survival. *Cell.* (2003) 115:577–90. doi: 10.1016/S0092-8674(03)00929-2
67. Li D, Luo L, Xu M, Wu J, Chen L, Li J, et al. AMPK activates FOXO3a and promotes neuronal apoptosis in the developing rat brain during the early phase after hypoxia-ischemia. *Brain Res Bull.* (2017) 132:1–9. doi: 10.1016/j.brainresbull.2017.05.001
68. Chi Y, Shi C, Zhao Y, Guo C. Forkhead box O (FOXO) 3 modulates hypoxia-induced autophagy through AMPK signalling pathway in cardiomyocytes. *Biosci Rep.* (2016) 36:e00345. doi: 10.1042/BSR20160091
69. Chen C-C, Jeon S-M, Bhaskar PT, Nogueira V, Sundararajan D, Tonic I, et al. FoxOs inhibit mTORC1 and activate Akt by inducing the expression of Sestrin3 and Rictor. *Dev Cell.* (2010) 18:592–604. doi: 10.1016/j.devcel.2010.03.008
70. Zhou S, Lu W, Chen L, Ge Q, Chen D, Xu Z, et al. AMPK deficiency in chondrocytes accelerated the progression of instability-induced and ageing-associated osteoarthritis in adult mice. *Sci Rep.* (2017) 7:43245. doi: 10.1038/srep43245
71. Csiszar A, Labinskyy N, Jimenez R, Pinto JT, Ballabh P, Losonczy G, et al. Anti-oxidative and anti-inflammatory vasoprotective effects of caloric restriction in aging: role of circulating factors and SIRT1. *Mech Ageing Dev.* (2009) 130:518–27. doi: 10.1016/j.mad.2009.06.004
72. Ungvari Z, Labinskyy N, Mukhopadhyay P, Pinto JT, Bagi Z, Ballabh P, et al. Resveratrol attenuates mitochondrial oxidative stress in coronary arterial endothelial cells. *Am J Physiol Heart Circ Physiol.* (2009) 297:H1876–81. doi: 10.1152/ajpheart.00375.2009
73. Fry JL, Al Sayah L, Weisbrod RM, Van Roy I, Weng X, Cohen RA, et al. Vascular smooth muscle sirtuin-1 protects against diet-induced aortic stiffness. *Hypertension.* (2016) 68:775–84. doi: 10.1161/HYPERTENSIONAHA.116.07622
74. Baur JA, Ungvari Z, Minor RK, Le Couteur DG, de Cabo R. Are sirtuins viable targets for improving healthspan and lifespan? *Nat Rev Drug Discov.* (2012) 11:443–61. doi: 10.1038/nrd3738

75. Thompson AM, Wagner R, Rzucidlo EM. Age-related loss of SirT1 expression results in dysregulated human vascular smooth muscle cell function. *Am J Physiol Heart Circ Physiol.* (2014) 307:H533–41. doi: 10.1152/ajpheart.00871.2013
76. Gorenne I, Kumar S, Gray K, Figg N, Yu H, Mercer J, et al. Vascular smooth muscle cell sirtuin 1 protects against DNA damage and inhibits atherosclerosis. *Circulation.* (2013) 127:386–96. doi: 10.1161/CIRCULATIONAHA.112.124404
77. Donato AJ, Magerko KA, Lawson BR, Durrant JR, Lesniewski LA, Seals DR. SIRT-1 and vascular endothelial dysfunction with ageing in mice and humans. *J Physiol.* (2011) 589(Pt 18):4545–54. doi: 10.1113/jphysiol.2011.211219
78. Cardus A, Uryga AK, Walters G, Erusalimsky JD. SIRT6 protects hECs from DNA damage, telomere dysfunction, and senescence. *Cardiovasc Res.* (2013) 97:571–9. doi: 10.1093/cvr/cvs352
79. Xu S, Yin M, Koroleva M, Mastrangelo MA, Zhang W, Bai P, et al. SIRT6 protects against endothelial dysfunction and atherosclerosis in mice. *Aging.* (2016) 8:1064–82. doi: 10.18632/aging.100975
80. Brunet A, Sweeney LB, Sturgill JF, Chua KF, Greer PL, Lin Y, et al. Stress-dependent regulation of FOXO transcription factors by the SIRT1 deacetylase. *Science.* (2004) 303:2011–5. doi: 10.1126/science.1094637
81. Chen Y, Wang Y, Jiang Y, Zhang X, Sheng M. High-glucose treatment regulates biological functions of human umbilical vein endothelial cells via Sirt1/FOXO3 pathway. *Ann Transl Med.* (2019) 7:199. doi: 10.21037/atm.2019.04.29
82. Liu Z, Zhang M, Zhou T, Shen Q, Qin X. Exendin-4 promotes the vascular smooth muscle cell re-differentiation through AMPK/SIRT1/FOXO3a signaling pathways. *Atherosclerosis.* (2018) 276:58–66. doi: 10.1016/j.atherosclerosis.2018.07.016
83. Cheng Y, Takeuchi H, Sonobe Y, Jin S, Wang Y, Horiuchi H, et al. Sirtuin 1 attenuates oxidative stress via upregulation of superoxide dismutase 2 and catalase in astrocytes. *J Neuroimmunol.* (2014) 269:38–43. doi: 10.1016/j.jneuroim.2014.02.001
84. Colman RJ, Anderson RM, Johnson SC, Kastman EK, Kosmatka KJ, Beasley TM, et al. Caloric restriction delays disease onset and mortality in rhesus monkeys. *Science.* (2009) 325:201–4. doi: 10.1126/science.1173635
85. Harrison DE, Strong R, Sharp ZD, Nelson JF, Astle CM, Flurkey K, et al. Rapamycin fed late in life extends lifespan in genetically heterogeneous mice. *Nature.* (2009) 460:392–5. doi: 10.1038/nature08221
86. Pearson KJ, Baur JA, Lewis KN, Peshkin L, Price NL, Labinskyy N, et al. Resveratrol delays age-related deterioration and mimics transcriptional aspects of dietary restriction without extending life span. *Cell Metab.* (2008) 8:157–68. doi: 10.1016/j.cmet.2008.06.011
87. Csiszar A, Ungvari Z, Koller A, Edwards JG, Kaley G. Proinflammatory phenotype of coronary arteries promotes endothelial apoptosis in aging. *Physiol Genomics.* (2004) 17:21–30. doi: 10.1152/physiolgenomics.00136.2003
88. Lutgens E, de Muinck ED, Kitslaar PJ, Tordoir JH, Wellens HJ, Daemen MJ. Biphasic pattern of cell turnover characterizes the progression from fatty streaks to ruptured human atherosclerotic plaques. *Cardiovasc Res.* (1999) 41:473–9. doi: 10.1016/S0008-6363(98)00311-3
89. van Grevenynghe J, Cubas RA, DaFonseca S, Metcalf T, Tremblay CL, Trautmann L, et al. Foxo3a: an integrator of immune dysfunction during HIV infection. *Cytokine Growth Factor Rev.* (2012) 23:215–21. doi: 10.1016/j.cytogfr.2012.05.008
90. Allard D, Figg N, Bennett MR, Littlewood TD. Akt regulates the survival of vascular smooth muscle cells via inhibition of FoxO3a and GSK3. *J Biol Chem.* (2008) 283:19739–47. doi: 10.1074/jbc.M710098200
91. Ungvari Z, Kaley G, de Cabo R, Sonntag WE, Csiszar A. Mechanisms of vascular aging: new perspectives. *J Gerontol A Biol Sci Med Sci.* (2010) 65:1028–41. doi: 10.1093/gerona/glq113
92. Mizushima N, Levine B, Cuervo AM, Klionsky DJ. Autophagy fights disease through cellular self-digestion. *Nature.* (2008) 451:1069–75. doi: 10.1038/nature06639
93. Rubinsztein DC, Mariño G, Kroemer G. Autophagy and aging. *Cell.* (2011) 146:682–95. doi: 10.1016/j.cell.2011.07.030
94. Pyo K-H, Kim M-K, Shin K-S, Chun HS, Shin E-H. Involvement of trypsin-digested silk peptides in the induction of raw264.7 macrophage activation. *Nat Prod Commun.* (2013) 8:1755–8. doi: 10.1177/1934578X1300801226
95. Nussenzweig SC, Verma S, Finkel T. The role of autophagy in vascular biology. *Circ Res.* (2015) 116:480–8. doi: 10.1161/CIRCRESAHA.116.303805
96. LaRocca TJ, Henson GD, Thorburn A, Sindler AL, Pierce GL, Seals DR. Translational evidence that impaired autophagy contributes to arterial ageing. *J Physiol.* (2012) 590:3305–16. doi: 10.1113/jphysiol.2012.229690
97. LaRocca TJ, Gioscia-Ryan RA, Hearon CM, Seals DR. The autophagy enhancer spermidine reverses arterial aging. *Mech Ageing Dev.* (2013) 134:314–20. doi: 10.1016/j.mad.2013.04.004
98. Mammucari C, Milan G, Romanello V, Masiero E, Rudolf R, Del Piccolo P, et al. FoxO3 controls autophagy in skeletal muscle *in vivo*. *Cell Metab.* (2007) 6:458–71. doi: 10.1016/j.cmet.2007.11.001
99. Sengupta A, Molkentin JD, Yutzey KE. FoxO transcription factors promote autophagy in cardiomyocytes. *J Biol Chem.* (2009) 284:28319–31. doi: 10.1074/jbc.M109.024406
100. Wang R, Yang Q, Wang X, Wang W, Li J, Zhu J, et al. FoxO3α-mediated autophagy contributes to apoptosis in cardiac microvascular endothelial cells under hypoxia. *Microvasc Res.* (2016) 104:23–31. doi: 10.1016/j.mvr.2015.11.001
101. Lin F. Molecular regulation and function of FoxO3 in chronic kidney disease. *Curr Opin Nephrol Hypertens.* (2020) 29:439–45. doi: 10.1097/MNH.0000000000000616
102. Feinberg AP. The key role of epigenetics in human disease prevention and mitigation. *N Engl J Med.* (2018) 378:1323–34. doi: 10.1056/NEJMra1402513
103. Costantino S, Camici GG, Mohammed SA, Volpe M, Lüscher TF, Paneni F. Epigenetics and cardiovascular regenerative medicine in the elderly. *Int J Cardiol.* (2018) 250:207–14. doi: 10.1016/j.ijcard.2017.09.188
104. Ungvari Z, Tucsek Z, Sosnowska D, Toth P, Gautam T, Podlutsky A, et al. Aging-induced dysregulation of Dicer1-Dependent MicroRNA expression impairs angiogenic capacity of rat cerebromicrovascular endothelial cells. *J Gerontol A Biol Sci Med Sci.* (2013) 68:877–91. doi: 10.1093/gerona/gls242
105. Zheng B, Yin W-N, Suzuki T, Zhang X-H, Zhang Y, Song L-L, et al. Exosome-mediated miR-155 transfer from smooth muscle cells to endothelial cells induces endothelial injury and promotes atherosclerosis. *Mol Ther.* (2017) 25:1279–94. doi: 10.1016/j.ymthe.2017.03.031
106. Shang L, Quan A, Sun H, Xu Y, Sun G, Cao P. MicroRNA-148a-3p promotes survival and migration of endothelial cells isolated from Apoe deficient mice through restricting circular RNA 0003575. *Gene.* (2019) 711:143948. doi: 10.1016/j.gene.2019.143948
107. Du Y, Gao C, Liu Z, Wang L, Liu B, He F, et al. Upregulation of a disintegrin and metalloproteinase with thrombospondin motifs-7 by miR-29 repression mediates vascular smooth muscle calcification. *Arterioscler Thromb Vasc Biol.* (2012) 32:2580–8. doi: 10.1161/ATVBAHA.112.300206
108. Wang G, Yao J, Li Z, Zu G, Feng D, Shan W, et al. miR-34a-5p inhibition alleviates intestinal ischemia/reperfusion-induced reactive oxygen species accumulation and apoptosis via activation of SIRT1 signaling. *Antioxid Redox Signal.* (2016) 24:961–73. doi: 10.1089/ars.2015.6492
109. Yamakuchi M. MicroRNA regulation of SIRT1. *Front Physiol.* (2012) 3:68. doi: 10.3389/fphys.2012.00068
110. Phillip JM, Aifuwa I, Walston J, Wirtz D. The mechanobiology of aging. *Annu Rev Biomed Eng.* (2015) 17:113–41. doi: 10.1146/annurev-bioeng-071114-040829
111. Jacob MP. Extracellular matrix remodeling and matrix metalloproteinases in the vascular wall during aging and in pathological conditions. *Biomed Pharmacother.* (2003) 57:195–202. doi: 10.1016/S0753-3322(03)00065-9
112. Toth P, Tarantini S, Springo Z, Tucsek Z, Gautam T, Giles CB, et al. Aging exacerbates hypertension-induced cerebral microhemorrhages in mice: role of resveratrol treatment in vasoprotection. *Aging Cell.* (2015) 14:400–8. doi: 10.1111/acel.12315
113. Pascual G, Mendieta C, García-Honduvilla N, Corrales C, Bellón JM, Buján J. TGF-beta1 upregulation in the aging varicose vein. *J Vasc Res.* (2007) 44:192–201. doi: 10.1159/000100375
114. Wang C, Wen J, Zhou Y, Li L, Cui X, Wang J, et al. Apelin induces vascular smooth muscle cells migration via a PI3K/Akt/FoxO3a/MMP-2 pathway. *Int J Biochem Cell Biol.* (2015) 69:173–82. doi: 10.1016/j.biocel.2015.10.015

115. Gao X-W, Su X-T, Lu Z-H, Ou J. 17β-estradiol prevents extracellular matrix degradation by downregulating MMP3 expression via PI3K/Akt/FOXO3 pathway. *Spine*. (2020) 45:292–9. doi: 10.1097/BRS.0000000000003263
116. Lee H-Y, You H-J, Won J-Y, Youn S-W, Cho H-J, Park K-W, et al. Forkhead factor, FOXO3a, induces apoptosis of endothelial cells through activation of matrix metalloproteinases. *Arterioscler Thromb Vasc Biol.* (2008) 28:302–8. doi: 10.1161/atvbaha.107.150668
117. Willcox BJ, Morris BJ, Tranah GJ, Chen R, Masaki KH, He Q, et al. Longevity-associated FOXO3 genotype and its impact on coronary artery disease mortality in japanese, whites, and blacks: a prospective study of three american populations. *J Gerontol A Biol Sci Med Sci.* (2017) 72:724–8. doi: 10.1093/gerona/glw196
118. Tao R, Xiong X, DePinho RA, Deng C-X, Dong XC. FoxO3 transcription factor and Sirt6 deacetylase regulate low density lipoprotein (LDL)-cholesterol homeostasis via control of the proprotein convertase subtilisin/kexin type 9 (Pcsk9) gene expression. *J Biol Chem*. (2013) 288:29252–9. doi: 10.1074/jbc.M113.481473
119. Li M, Chiu J-F, Gagne J, Fukagawa NK. Age-related differences in insulin-like growth factor-1 receptor signaling regulates Akt/FOXO3a and ERK/Fos pathways in vascular smooth muscle cells. *J Cell Physiol.* (2008) 217:377–87. doi: 10.1002/jcp.21507
120. Ussher JR, Drucker DJ. Cardiovascular actions of incretin-based therapies. *Circ Res.* (2014) 114:1788–803. doi: 10.1161/CIRCRESAHA.114.301958
121. Zhou T, Zhang M, Zhao L, Li A, Qin X. Activation of Nrf2 contributes to the protective effect of exendin-4 against angiotensin II-induced vascular smooth muscle cell senescence. *Am J Physiol Cell Physiol.* (2016) 311:C572–82. doi: 10.1152/ajpcell.00093.2016
122. Lee H-Y, Chung J-W, Youn S-W, Kim J-Y, Park K-W, Koo B-K, et al. Forkhead transcription factor FOXO3a is a negative regulator of angiogenic immediate early gene CYR61, leading to inhibition of vascular smooth muscle cell proliferation and neointimal hyperplasia. *Circ Res.* (2007) 100:372–80. doi: 10.1161/01.RES.0000257945.97958.77
123. Li P, Zhong X, Li J, Liu H, Ma X, He R, et al. MicroRNA-30c-5p inhibits NLRP3 inflammasome-mediated endothelial cell pyroptosis through FOXO3 down-regulation in atherosclerosis. *Biochem Biophys Res Commun.* (2018) 503:2833–40. doi: 10.1016/j.bbrc.2018.08.049
124. Ma S, Chen J, Feng J, Zhang R, Fan M, Han D, et al. Melatonin ameliorates the progression of atherosclerosis via mitophagy activation and NLRP3 inflammasome inhibition. *Oxid Med Cell Longev.* (2018) 2018:9286458. doi: 10.1155/2018/9286458
125. Deng L, Huang L, Sun Y, Heath JM, Wu H, Chen Y. Inhibition of FOXO1/3 promotes vascular calcification. *Arterioscler Thromb Vasc Biol.* (2015) 35:175–83. doi: 10.1161/ATVBAHA.114.304786
126. Sun Y, Byon CH, Yuan K, Chen J, Mao X, Heath JM, et al. Smooth muscle cell-specific runx2 deficiency inhibits vascular calcification. *Circ Res.* (2012) 111:543–52. doi: 10.1161/CIRCRESAHA.112.267237
127. Byon CH, Javed A, Dai Q, Kappes JC, Clemens TL, Darley-Usmar VM, et al. Oxidative stress induces vascular calcification through modulation of the osteogenic transcription factor Runx2 by AKT signaling. *J Biol Chem.* (2008) 283:15319–27. doi: 10.1074/jbc.M800021200
128. Moorhead WJ, Chu CC, Cuevas RA, Callahan J, Wong R, Regan C, et al. Dysregulation of FOXO1 (forkhead box O1 protein) drives calcification in arterial calcification due to deficiency of CD73 and is present in peripheral artery disease. *Arterioscler Thromb Vasc Biol*. (2020) 40:1680–94. doi: 10.1161/ATVBAHA.119.313765
129. Ni YG, Berenji K, Wang N, Oh M, Sachan N, Dey A, et al. Foxo transcription factors blunt cardiac hypertrophy by inhibiting calcineurin signaling. *Circulation.* (2006) 114:1159–68. doi: 10.1161/CIRCULATIONAHA.106.637124
130. Qi X-F, Chen Z-Y, Xia J-B, Zheng L, Zhao H, Pi L-Q, et al. FoxO3a suppresses the senescence of cardiac microvascular endothelial cells by regulating the ROS-mediated cell cycle. *J Mol Cell Cardiol.* (2015) 81:114–26. doi: 10.1016/j.yjmcc.2015.01.022
131. Higami Y, Shimokawa I. Apoptosis in the aging process. *Cell Tissue Res.* (2000) 301:125–32. doi: 10.1007/s004419900156
132. Konstantinidis K, Whelan RS, Kitsis RN. Mechanisms of cell death in heart disease. *Arterioscler Thromb Vasc Biol.* (2012) 32:1552–62. doi: 10.1161/ATVBAHA.111.224915
133. Poulose N, Raju R. Aging and injury: alterations in cellular energetics and organ function. *Aging Dis.* (2014) 5:101–8. doi: 10.14336/ad.2014.0500101
134. Chang Z-S, Xia J-B, Wu H-Y, Peng W-T, Jiang F-Q, Li J, et al. Forkhead box O3 protects the heart against paraquat-induced aging-associated phenotypes by upregulating the expression of antioxidant enzymes. *Aging Cell.* (2019) 18:e12990. doi: 10.1111/acel.12990
135. Vivar R, Humeres C, Anfossi R, Bolivar S, Catalán M, Hill J, et al. Role of FoxO3a as a negative regulator of the cardiac myofibroblast conversion induced by TGF-β1. *Biochim Biophys Acta Mol Cell Res.* (2020) 1867:118695. doi: 10.1016/j.bbamcr.2020.118695
136. Sedaghat S, Mattace-Raso FUS, Hoorn EJ, Uitterlinden AG, Hofman A, Ikram MA, et al. Arterial stiffness and decline in kidney function. *Clin J Am Soc Nephrol.* (2015) 10:2190–7. doi: 10.2215/CJN.03000315
137. Nath KA. The role of Sirt1 in renal rejuvenation and resistance to stress. *J Clin Invest.* (2010) 120:1026–8. doi: 10.1172/JCI42184
138. Li L, Kang H, Zhang Q, D'Agati VD, Al-Awqati Q, Lin F. FoxO3 activation in hypoxic tubules prevents chronic kidney disease. *J Clin Invest.* (2019) 129:2374–89. doi: 10.1172/JCI122256
139. Li L, Zviti R, Ha C, Wang ZV, Hill JA, Lin F. Forkhead box O3 (FoxO3) regulates kidney tubular autophagy following urinary tract obstruction. *J Biol Chem*. (2017) 292:13774–83. doi: 10.1074/jbc.M117.791483
140. Xin Z, Ma Z, Hu W, Jiang S, Yang Z, Li T, et al. FOXO1/3: potential suppressors of fibrosis. *Ageing Res Rev.* (2018) 41:42–52. doi: 10.1016/j.arr.2017.11.002
141. Das F, Ghosh-Choudhury N, Dey N, Bera A, Mariappan MM, Kasinath BS, et al. High glucose forces a positive feedback loop connecting Akt kinase and FoxO1 transcription factor to activate mTORC1 kinase for mesangial cell hypertrophy and matrix protein expression. *J Biol Chem.* (2014) 289:32703–16. doi: 10.1074/jbc.M114.605196
142. Luo W-M, Kong J, Gong Y, Liu X-Q, Yang R-X, Zhao Y-X. Tongxinluo protects against hypertensive kidney injury in spontaneously-hypertensive rats by inhibiting oxidative stress and activating forkhead box O1 signaling. *PLoS ONE.* (2015) 10:e0145130. doi: 10.1371/journal.pone.0145130
143. Bijkerk R, de Bruin RG, van Solingen C, van Gils JM, Duijs JMGJ, van der Veer EP, et al. Silencing of microRNA-132 reduces renal fibrosis by selectively inhibiting myofibroblast proliferation. *Kidney Int.* (2016) 89:1268–80. doi: 10.1016/j.kint.2016.01.029
144. Kuningas M, Mägi R, Westendorp RGJ, Slagboom PE, Remm M, van Heemst D. Haplotypes in the human Foxo1a and Foxo3a genes; impact on disease and mortality at old age. *Eur J Hum Genet.* (2007) 15:294–301. doi: 10.1038/sj.ejhg.5201766
145. Xiong ZJ, Zhang Q, Wang DX, Hu L. Overexpression of TUG1 promotes neuronal death after cerebral infarction by regulating microRNA-9. *Eur Rev Med Pharmacol Sci.* (2018) 22:7393–400. doi: 10.26355/eurrev_201811_16278
146. Guo D, Ma J, Li T, Yan L. Up-regulation of miR-122 protects against neuronal cell death in ischemic stroke through the heat shock protein 70-dependent NF-κB pathway by targeting FOXO3. *Exp Cell Res.* (2018) 369:34–42. doi: 10.1016/j.yexcr.2018.04.027
147. Li D, Qu Y, Mao M, Zhang X, Li J, Ferriero D, et al. Involvement of the PTEN-AKT-FOXO3a pathway in neuronal apoptosis in developing rat brain after hypoxia-ischemia. *J Cereb Blood Flow Metab.* (2009) 29:1903–13. doi: 10.1038/jcbfm.2009.102
148. Zhou H, Wang X, Ma L, Deng A, Wang S, Chen X. FoxO3 transcription factor promotes autophagy after transient cerebral ischemia/reperfusion. *Int J Neurosci.* (2019) 129:738–45. doi: 10.1080/00207454.2018.1564290
149. Niiranen TJ, Kalesan B, Hamburg NM, Benjamin EJ, Mitchell GF, Vasan RS. Relative contributions of arterial stiffness and hypertension to cardiovascular disease: the framingham heart study. *J Am Heart Assoc.* (2016) 5:e004271. doi: 10.1161/JAHA.116.004271
150. Morris BJ, Chen R, Donlon TA, Evans DS, Tranah GJ, Parimi N, et al. Association analysis of FOXO3 longevity variants with blood pressure and essential hypertension. *Am J Hypertens.* (2016) 29:1292–300. doi: 10.1093/ajh/hpv171

151. Li X-N, Song J, Zhang L, LeMaire SA, Hou X, Zhang C, et al. Activation of the AMPK-FOXO3 pathway reduces fatty acid-induced increase in intracellular reactive oxygen species by upregulating thioredoxin. *Diabetes.* (2009) 58:2246–57. doi: 10.2337/db08-1512
152. Miyauchi H, Minamino T, Tateno K, Kunieda T, Toko H, Komuro I. Akt negatively regulates the *in vitro* lifespan of human endothelial cells via a p53/p21-dependent pathway. *EMBO J.* (2004) 23:212–20. doi: 10.1038/sj.emboj.7600045
153. Al-Tamari HM, Dabral S, Schmall A, Sarvari P, Ruppert C, Paik J, et al. FoxO3 an important player in fibrogenesis and therapeutic target for idiopathic pulmonary fibrosis. *EMBO Mol Med.* (2018) 10:276–93. doi: 10.15252/emmm.201606261
154. Zingg J-M, Hasan ST, Cowan D, Ricciarelli R, Azzi A, Meydani M. Regulatory effects of curcumin on lipid accumulation in monocytes/macrophages. *J Cell Biochem.* (2012) 113:833–40. doi: 10.1002/jcb.23411
155. Yan P, Li Q, Wang L, Lu P, Suzuki K, Liu Z, et al. FOXO3-engineered human ESC-derived vascular cells promote vascular protection and regeneration. *Cell Stem Cell.* (2019) 24:447–61. doi: 10.1016/j.stem.2018.12.002
156. Calissi G, Lam EWF, Link W. Therapeutic strategies targeting FOXO transcription factors. *Nat Rev Drug Discov.* (2021) 20:21–38. doi: 10.1038/s41573-020-0088-2
157. Schmitt-Ney M. The FOXO's advantages of being a family: considerations on function and evolution. *Cells.* (2020) 9:787. doi: 10.3390/cells9030787

Conflict of Interest: The authors declare that the research was conducted in the absence of any commercial or financial relationships that could be construed as a potential conflict of interest.

Publisher's Note: All claims expressed in this article are solely those of the authors and do not necessarily represent those of their affiliated organizations, or those of the publisher, the editors and the reviewers. Any product that may be evaluated in this article, or claim that may be made by its manufacturer, is not guaranteed or endorsed by the publisher.

frontiers in Cardiovascular Medicine

ORIGINAL RESEARCH
published: 07 February 2022
doi: 10.3389/fcvm.2021.813280

Association of Metabolic Syndrome With Long-Term Cardiovascular Risks and All-Cause Mortality in Elderly Patients With Obstructive Sleep Apnea

Lin Liu[1†], Xiaofeng Su[2†], Zhe Zhao[1†], Jiming Han[2], Jianhua Li[3], Weihao Xu[3], Zijun He[2], Yinghui Gao[4], Kaibing Chen[5], Libo Zhao[1], Yan Gao[6], Huanhuan Wang[2], JingJing Guo[7], Junling Lin[8], Tianzhi Li[9*] and Xiangqun Fang[1*]*

[1] Department of Pulmonary and Critical Care Medicine of the Second Medical Center and National Clinical Research Center for Geriatric Diseases, Chinese PLA General Hospital, Beijing, China, [2] Medical College, Yan'an University, Yan'an, China, [3] Cardiology Department of the Second Medical Center and National Clinical Research Center for Geriatric Diseases, Chinese PLA General Hospital, Beijing, China, [4] PKU-UPenn Sleep Center, Peking University International Hospital, Beijing, China, [5] Sleep Center, The Affiliated Hospital of Gansu University of Chinese Medicine, Lanzhou City, China, [6] Department of General Practice, 960th Hospital of PLA, Jinan, China, [7] Department of Pulmonary and Critical Care Medicine, Sleep Medicine Center, Peking University People's Hospital, Beijing, China, [8] Department of Pulmonary and Critical Care Medicine, Beijing Chaoyang Hospital Affiliated to Capital Medical University, Beijing, China, [9] The Second Medical Center and National Clinical Research Center for Geriatric Diseases, Chinese PLA General Hospital, Beijing, China

OPEN ACCESS

Edited by:
Zhong Wang,
University of Michigan, United States

Reviewed by:
Hongliang Yi,
Shanghai Jiao Tong University Affiliated Sixth People's Hospital, China
Bertram Pitt,
University of Michigan, United States

***Correspondence:**
Xiangqun Fang
fangxiangqun@hotmail.com
Tianzhi Li
litianzhi301@sina.com
Junling Lin
2949722786@qq.com

[†]These authors have contributed equally to this work

Specialty section:
This article was submitted to Cardiovascular Metabolism, a section of the journal Frontiers in Cardiovascular Medicine

Received: *11 November 2021*
Accepted: *30 December 2021*
Published: *07 February 2022*

Citation:
Liu L, Su X, Zhao Z, Han J, Li J, Xu W, He Z, Gao Y, Chen K, Zhao L, Gao Y, Wang H, Guo J, Lin J, Li T and Fang X (2022) Association of Metabolic Syndrome With Long-Term Cardiovascular Risks and All-Cause Mortality in Elderly Patients With Obstructive Sleep Apnea. Front. Cardiovasc. Med. 8:813280. doi: 10.3389/fcvm.2021.813280

Background: Evidence suggests that an increased risk of major adverse cardiac events (MACE) and all-cause mortality is associated with obstructive sleep apnea (OSA), particularly in the elderly. Metabolic syndrome (MetS) increases cardiovascular risk in the general population; however, less is known about its influence in patients with OSA. We aimed to assess whether MetS affected the risk of MACE and all-cause mortality in elderly patients with OSA.

Methods: From January 2015 to October 2017, 1,157 patients with OSA, aged ≥60 years, no myocardial infarction (MI), and hospitalization for unstable angina or heart failure were enrolled at baseline and were followed up prospectively. OSA is defined as an apnea-hypopnea index of ≥5 events per hour, as recorded by polysomnography. Patients were classified on the basis of the presence of MetS, according to the definition of the National Cholesterol Education Program (NCEP). Incidence rates were expressed as cumulative incidence. Cox proportional hazards analysis was used to estimate the risk of all events. The primary outcomes were MACE, which included cardiovascular death, MI, and hospitalization for unstable angina or heart failure. Secondary outcomes were all-cause mortality, components of MACE, and a composite of all events.

Results: MetS was present in 703 out of 1,157 (60.8%) elderly patients with OSA. During the median follow-up of 42 months, 119 (10.3%) patients experienced MACE. MetS conferred a cumulative incidence of MACE in elderly patients with OSA (log-rank, $P < 0.001$). In addition, there was a trend for MACE incidence risk to gradually increase in individuals with ≥3 MetS components ($P = 0.045$). Multivariate analysis showed that MetS was associated with an incidence risk for MACE [adjusted hazard ratio (aHR), 1.86; 95% confidence interval (CI), 1.17–2.96; $P = 0.009$], a composite of all events (aHR, 1.54;

95% CI, 1.03–2.32; $P = 0.036$), and hospitalization for unstable angina (aHR, 2.01; 95% CI, 1.04–3.90; $P = 0.039$). No significant differences in the risk of all-cause mortality and other components of MACE between patients with and without MetS ($P > 0.05$). Subgroup analysis demonstrated that males (aHR, 2.23; 95% CI, 1.28–3.91, $P = 0.05$), individuals aged <70 years (aHR, 2.36; 95% CI, 1.27–4.39, $P = 0.006$), overweight and obese individuals (aHR, 2.32; 95% CI, 1.34–4.01, $P = 0.003$), and those with moderate-severe OSA (aHR, 1.81;95% CI: 1.05–3.12, $P = 0.032$) and concomitant MetS were at a higher risk for MACE.

Conclusion: MetS is common in elderly patients with OSA in the absence of MI, hospitalization for unstable angina or heart failure. Further, it confers an independent, increased risk of MACE, a composite of all events, and hospitalization for unstable angina. Overweight and obese males, aged <70 years with moderate-severe OSA combined with MetS presented a significantly higher MACE risk.

Keywords: obstructive sleep apnea, metabolic syndrome, elderly, major adverse cardiovascular events, mortality, cardiovascular disease

INTRODUCTION

Obstructive sleep apnea (OSA) is the most common form of sleep-related breathing disorders (1). It has become a leading health concern owing to its growing prevalence and strong association with all-cause mortality (2–4). In addition to a higher risk of acute coronary syndrome (5), recent data demonstrate that OSA confers an increased risk of composite cardiovascular endpoints, including myocardial infarction (MI), hospitalization for heart failure, and cardiovascular death. These risks have not been sufficiently addressed with current OSA treatment strategies (6).

Understanding the link between OSA, long-term cardiovascular risks, and all-cause mortality are imperative for devising effective preventive strategies. OSA is often associated with cardiovascular disease risk factors, such as MetS, diabetes, hypertension, and obesity (7–9); therefore, it is possible that a convergence of multiple risk factors could potentiate cardiovascular risks and all-cause mortality. This is exemplified by MetS, which is a highly prevalent, multifaceted disease. It is characterized by a series of abnormalities that include abdominal adiposity, hypertension, dyslipidemia, and elevated fasting plasma glucose (10).

The growing burden of obesity, sedentary lifestyles, and dietary patterns has led to an increase in the prevalence of MetS. Further, it has been associated with a higher risk of MACE when compared with general population (11). Our group has previously shown a longitudinal association between type 2 diabetes and MACE, hospitalization for unstable angina, and a composite of all events in elderly patients with OSA (12). A recent study reported that prediabetes, the precursor stage of diabetes, is often accompanied with a manifestation of much broader underlying disorders, including MetS (13). However, the incidence and long-term risk of cardiovascular disease and all-cause mortality related to MetS in elderly patients with OSA have not been established. Furthermore, questions remain as to whether MetS confers an incremental risk of MACE or all-cause mortality, beyond the cumulative incidence tendency that is contributed by OSA itself. Resolving these issues is important before considering MetS as part of the preventive strategies in patients with OSA, especially in the elderly population.

We hypothesized that MetS confers a higher risk of long-term cardiovascular disease (CVD) and all-cause mortality in elderly patients with OSA. Hence, the primary aim of the present study was to assess the prognostic implication of MetS for incident MACE (cardiovascular death, MI, and hospitalization for unstable angina or heart failure) in a cohort of patients with OSA in the absence of MI, hospitalization for unstable angina, or heart failure at baseline. Secondary outcomes included the individual components of MACE, a composite of all events, and all-cause mortality.

Abbreviations: CVD, Cardiovascular disease; MetS, Metabolic syndrome; OSA, Obstructive sleep apnoea; MACE, Major adverse cardiovascular events; PSG, Polysomnography; AHI, The apnoea-hypopnoea index; BMI, Body mass index; NC, Neck circumference; WC, Waist circumference; WHR, Waist/hip ratio; SBP, Systolic blood pressure; DBP, Diastolic blood pressure; TG, Triglyceride; HDL, High-density lipoprotein; FPG, Fasting plasma glucose; LAT, The longest apnea time; MAT, The mean apnea time; TOT, Total monitoring time; T90, Percentage of the times for SaO_2<90% in TOT during overnight sleep; TSA90, The duration of time with SaO_2 <90%; ODI, The oxygen desaturation index; $MSpO_2$, The mean pulse oxygen saturation; $LSpO_2$, The lowest pulse oxygen saturation; CHD, Coronary heart disease; COPD, Chronic obstructive pulmonary disease; MI, Myocardial infarction; AF, Atrial fibrillation; CPAP, Continuous positive airway pressure; aHR, Adjusted hazard ratios; CI, Confidence intervals; NCEP, National cholesterol education program; ATP, Adult treatment panel.

METHODS

Study Design and Participants

This study was designed as an multi-center, prospective, observational cohort study that recruited elderly (age ≥ 60 years) patients with OSA free of MI, hospitalization for unstable angina, or heart failure at baseline. This was diagnosed at the departments

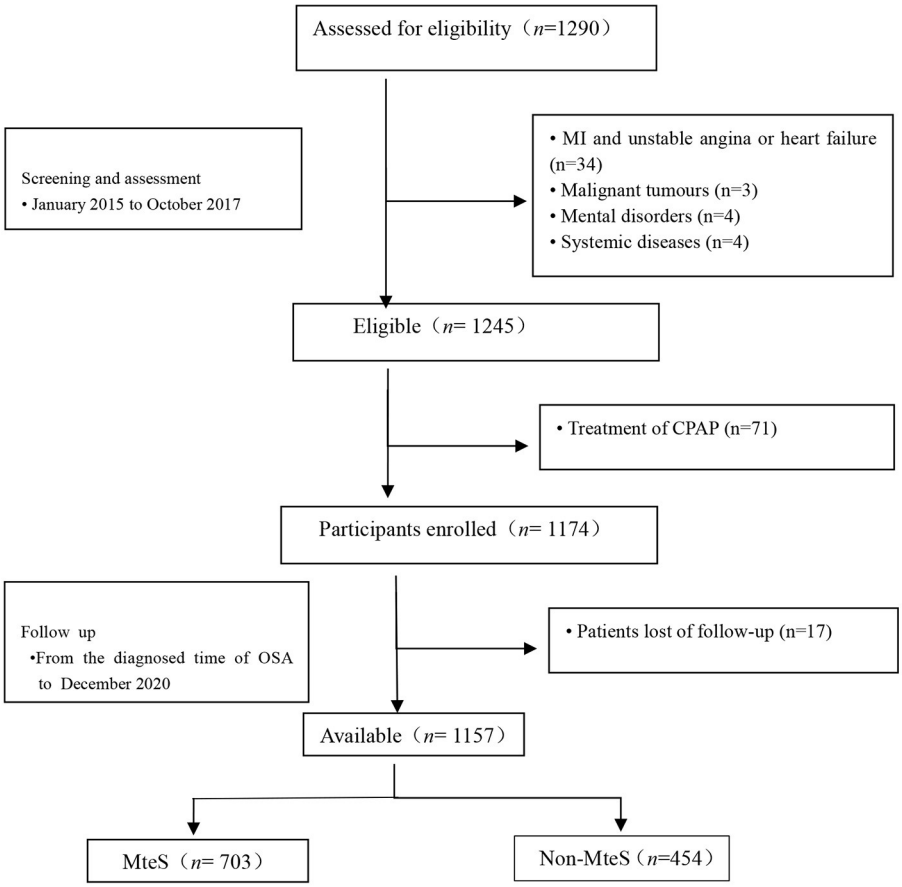

FIGURE 1 | Study flowchart. MteS, metabolic sydrome; CPAP indicates continuous positive airway pressure; MI, myocardial infarction.

or sleep medicine centers of six hospitals, including Chinese PLA General Hospital, Peking University International Hospital, Peking University People's Hospital, Beijing Chaoyang Hospital, 960th Hospital of PLA, and the affiliated Hospital of Gansu University of Chinese Medicine between January 2015 to October 2017. OSA was defined as an apnea-hypopnea index (AHI) of ≥5 events per hour. The AHI was calculated as the number of apnea and hypopnea events per hour of sleep. Taken together, we consecutively enrolled 1,290 patients with a first diagnosis of OSA who underwent an overnight sleep study after clinical stabilization during hospitalization at the sleep center (within 1 week after admission) of six hospitals. The study flowchart is presented in **Figure 1**. Inclusion criteria were (1) aged ≥60 years and (2) a diagnosis of OSA. Exclusion criteria were (1) a diagnosis of MI, hospitalization for unstable angina, or heart failure; (2) history of malignant tumors; (3) mental disorders; (4) systemic diseases; and (5) previous OSA diagnosis or continuous positive air pressure (CPAP) treatment. Furthermore, we excluded those lost during follow-up. The final study population was 1,157 elderly patients with OSA.

This study conformed to the Strengthening the Reporting of Observational studies in Epidemiology (STROBE) guidelines. It was performed in accordance with the Declaration of Helsinki. The study was approved by the Ethics Committee of Chinese PLA General Hospital (S2019-352-01) and all participants provided a written informed consent.

Overnight Sleep Study

All patients underwent an overnight sleep study within 1 week after admission at a sleep center (from 21:00 to 07:00 the next day). The sleep study was performed using a portable laboratory-based polysomnography (PSG) instrument (Compumedics, Melbourne, Australia), as described previously (12). Patients abstained from caffeine, hypnotic drugs, or sedatives for 1 day before their sleep study. OSA diagnosis and sleep tests were first scored according to the Guideline of the American Academy of Sleep Medicine (2012) (14). Standard PSG parameters were measured, including continuous polygraphic recordings from surface leads for electroencephalography, electrooculography, electrocardiography, nasal and oral airflow, thoracic and abdominal impedance belts for respiratory effort, pulse oximetry for oxyhemoglobin concentration, tracheal microphone for snoring, and a sensor for sleep position. Data were subjected to automatic computer analysis followed by manual correction by two sleep technologists and a senior physician. OSA was defined as AHI ≥5 events/hour. AHI was calculated as the total number

of apnea and hypopnea events divided by the sleep duration (in hours). OSA was classified as mild (AHI = 5–14.9), moderate (AHI = 15–30), or severe (AHI >30) (14, 15).

Covariates

Participant baseline characteristics were designated as regular laboratory test data from the 2nd day after the overnight study. These included demographic data [age, sex, body mass index (BMI), systolic blood pressure (SBP), diastolic blood pressure (DBP), waist-hip ratio, neck circumference, waist circumference, and self-reported smoking and alcohol use]; laboratory data [fasting plasma glucose (FPG), triglyceride (TG), high-density lipoprotein (HDL)]; comorbidities [diabetes, hypertension, hyperlipidemia, atrial fibrillation (AF), chronic obstructive pulmonary disease (COPD), carotid atherosclerosis, hyperlipidemia, coronary heart disease (CHD)]; and sleep parameters [oxygen desaturation index (ODI), mean pulse oxygen saturation ($MSpO_2$), lowest pulse oxygen saturation ($LSpO_2$), duration of time with SaO_2 <90% (TSA90), percentage of times SaO_2 <90% during the total monitoring time of overnight sleep (T90), and apnea time]. These data were collected by two experienced physicians who were blinded to the clinical outcomes and sleep patterns of the patients using pre-established case report forms. Disagreements were resolved by consensus. The categories of covariates were listed in **Supplementary Table S1**.

BMI was expressed in kg/m^2. Smoking was defined as at least one cigarette per day currently or within the past 2 years. Drinking was defined as drinking once per week for at least half a year. SBP and DBP were measured three times. Hypertension was recorded if the mean of at least two consecutive measurements of SBP/DBP was ≥140/90 mmHg or the use of antihypertension medication (16). Dyslipidemia was defined using the Chinese Guidelines for the management of hyperlipidemia in adults. This was defined as 1) serum cholesterol concentration ≥4.7 mmol/L; 2) TG concentration ≥2.3 mmol/L; or 3) low-density lipoprotein concentration ≥4.1 mmol/L. Patients who met one of these three criteria were defined as having hyperlipidemia (17). AF was defined based on the ESC 2016 guidelines (18). Type 2 diabetes was defined as existing diabetes treatment or fasting blood glucose ≥7.0 mmol/L and 1) 2-h oral glucose tolerance test ≥11.1 mmol/L or 2) hemoglobin A_{1C} ≥6.5% (19). Carotid atherosclerosis, CHD, and COPD were determined using the records of relevant diagnostic clinical (Read) codes indicating the presence of the condition (20).

MetS Assessment

MetS was defined according to the National Cholesterol Education Program Adult Treatment Panel III (NCEP ATP III) criteria (with the modified waist circumference criteria for Asians) as the presence of at least three of the following five clinical features: (1) waist circumference ≥80 cm in women, and ≥90 cm in men; (2) elevated plasma TG (≥1.7 mmol/L), or treatment for high TG; (3) low-plasma HDL (<1.3 mmol/L for women and <1.03 mmol/L for men); (4) high FPG (≥5.6 mmol/L) or currently taking anti-diabetic medication; and (5) SBP ≥130 or DBP ≥85 mmHg or current treatment for hypertension (21, 22).

Procedures, Follow-Up, and Outcomes

Each patient was closely managed in the sleep centers of the six study hospitals according to the American Academy of Sleep Medicine guidelines on OSA (2012) (14). All patients underwent PSG within 7 days of admission and regular laboratory tests on the 2nd day after the overnight study. Patients with OSA (AHI ≥15 events/hour), particularly those with excessive daytime sleepiness, were referred to the sleep center for further evaluation.

Patients were prospectively followed-up for approximately 4 years after their diagnosis and PSG assessment. All follow-ups were completed by December 2020. Follow-ups ended at the first MACE or all-cause mortality. Patients or their proxies were contacted by telephone by two investigators who were blinded to patients' PSG results at 1 month, 3 months, 6 months, 1 year, and then every 6 months thereafter (at least 3 months and up to 1 years). Participant follow-up outcomes were further verified by a clinic visit and medical chart review, which lasted until end of the study. The cause of death was ascertained from hospital discharge letters or death certificates provided by patients' family members. In difficult cases, three senior investigators, blinded to MetS, status adjudicated study outcomes by a consensus of opinion. All clinical events were confirmed by source documentation and were adjudicated by the clinical event committee.

The primary endpoint of our study was MACE, defined as MI, cardiovascular death, and hospitalization for unstable angina or heart failure. Secondary outcomes were all-cause mortality, a composite of all events, and individual components of MACE.

Statistical Analysis

Continuous variables are shown as mean ± SD or median (interquartile range). Categorical variables are shown as counts and proportions (%). The quantitative variables were not normally distributed; therefore, the Mann-Whitney U test was used for further analyses. The relationship between MetS and time-to-event End Points were summarized using Kaplan-Meier curves and compared using the log-rank test. Crude and adjusted hazard ratios (aHR), and their corresponding 95% confidence intervals (CI), were calculated for the association between MetS and incidence risk of all events using Cox proportional hazards regression models. Two Cox proportional hazards regression models were conducted to examine the association between OSA with MetS and long-term MACE risks, and all-cause mortality in elderly patients. Model 1 was unadjusted; Model 2 was adjusted for potential risk factors, including age, sex, BMI, alcohol use, SBP, DBP, waist circumference, WHR, neck circumference, FPG, TG, HDL, comorbidities of CHD, hyperlipidemia, hypertension, carotid atherosclerosis, diabetes, and sleep parameters of AHI, ODI, T90, TSA90, and $LSpO_2$. A 2-sided P <0.05 was considered statistically significant. All analyses were conducted using the SPSS (version 25.0, SPSS Inc., Chicago, Illinois, USA).

TABLE 1 | General characteristics of study subjects according to MetS.

	Total (n = 1,157)	Non-MteS (n = 454)	MteS (n = 703)	P-value
Demographics				
Age, y	66.0 (62.0, 71.0)	65.0 (62.0, 69.0)	66.0 (63.0, 72.0)	<0.001
Male, *n* (%)	704 (60.8)	263 (57.9)	441 (62.7)	0.102
BMI, kg/m^2	26.4 (24.0, 29.0)	25.1 (22.8, 27.3)	27.2 (24.7, 29.7)	<0.001
NC, mm	38.0 (35.0, 40.0)	37.5 (35.0, 40.0)	38.0 (35.5, 41.0)	0.043
waist-hip ratio, %	90 (79, 102)	85 (75, 96)	93 (83, 105)	<0.001
Drinking, *n* (%)	116 (10.0)	36 (7.9)	80 (11.4)	0.055
Smoking, *n* (%)	256 (22.1)	97 (21.4)	159 (22.6)	0.608
SBP, mmHg	133.0 (124.0, 144.0)	124.0 (120.0, 128.0)	140.0 (133.0, 150.0)	<0.001
DBP, mmHg	76.0 (70.0, 81.0)	73.0 (70.0, 80.0)	78.0 (70.0, 85.0)	<0.001
WC, mm	91.0 (80.0, 100.0)	87.5 (78.0, 96.0)	94.0 (86.0, 102.0)	<0.001
FPG, mmol/L	5.7 (5.1, 6.6)	5.4 (5.0, 6.1)	5.9 (5.3, 6.8)	<0.001
TG, mmol/L	1.5 (1.0, 1.9)	1.3 (1.0, 1.7)	1.6 (1.1, 2.0)	<0.001
HDL, mmol/L	1.1 (0.9, 1.4)	1.2 (1.0, 1.5)	1.0 (0.9, 1.3)	<0.001
Sleep parameters				
AHI, events/h	27.2 (14.95, 45.40)	25.6 (13.9, 39.3)	28.6 (15.6, 48.4)	0.004
TST, h	7.05 (6.14, 7.47)	7.05 (6.10, 7.45)	7.04 (6.17, 7.47)	0.632
ODI, events/h	22.1 (10.3,40.5)	19.5 (10.1, 34.7)	23.5 (11.0, 43.2)	0.002
TSA90, min	14.00 (2.28, 60.52)	10.44 (1.82, 46.45)	16.45 (2.90, 69.25)	0.003
T90, %	3 (0, 15)	3 (0, 12)	4 (1, 17)	0.003
$MSpO_2$, %	93.0 (91.7,95.0)	93.7 (92.0, 95.0)	93.0 (91.0, 95.0)	0.099
$LSpO_2$, %	80.0 (72.0, 85.0)	81.0 (74.0, 85.0)	80.0 (71.0, 85.0)	0.033
Average heart Rate, events/min	63.0 (57.6, 68.4)	63.0 (58.0, 68.6)	63.5 (57.4, 68.3)	0.833
Average apnea time, s	22.4 (19.5, 25.4)	22.3 (19.1, 25.7)	22.4 (19.6, 25.3)	0.999
Maximum apnea time, s	51.0 (32.9, 75.0)	49.0 (32.0, 74.2)	51.7 (33.0, 75.0)	0.966
Medical history, *n* (%)				
Severity of OSA				0.035
Mild OSA	289 (25.0)	123 (27.1)	166 (23.6)	
Moderate OSA	347 (30.0)	148 (32.6)	199 (28.3)	
Severe OSA	521 (45.0)	183 (40.3)	338 (48.1)	
Hypertension	739 (63.9)	47 (10.4)	692 (98.4)	<0.001
CHD	265 (22.9)	62 (13.7)	203 (28.9)	<0.001
Hyperlipidemia	325 (28.1)	90 (19.8)	235 (33.4)	<0.001
AF	97 (8.4)	40 (8.8)	57 (8.1)	0.664
Carotid atherosclerosis	296 (25.6)	90 (19.8)	206 (29.3)	<0.001
Diabetes	286 (24.7)	54 (11.9)	232 (33.0)	<0.001
COPD	80 (6.9)	34 (7.5)	46 (6.5)	0.536

BMI, body mass index; NC, neck circumference; WC, waist circumference; WHR, waist/hip ratio; SBP, systolic blood pressure; DBP, diastolic blood pressure; AHI, the apnea-hypopnea index; FPG, fasting plasmaglucose; TG, triglyceride; HDL, high-density lipoprotein; ODI, the oxygen desaturation index; $MSpO_2$, the mean pulse oxygen saturation; $LSpO_2$, the lowest pulse oxygen saturation; TSA90, the duration of time with $SaO_2 < 90\%$; T90, percentage of the times for $SaO_2 < 90\%$ in total monitoring time during overnight sleep; LAT, the longest apnea time; MAT, the mean apnea time; OSA, obstructive sleep apnea; CHD, coronary heart disease; AF, atrial fibrillation; COPD, chronic obstructive pulmonary disease.

RESULTS

Baseline Characteristics

After excluding patients with MI, hospitalization for unstable angina, or heart failure at screening, 1,245 eligible patients were identified. Of these, 71 had previously received CPAP treatment. Therefore, 1,174 patients were enrolled. Follow-up status was unavailable for 17 (1.4%) patients. Finally, 1,157 patients with OSA were included in the analyses (**Figure 1**). Patient baseline characteristics (median age, 66.0 years, 60.8% male) are presented in **Table 1**. Among the 1,157 patients, 454 (39.2%) had no MetS (median age, 65 years, male/female = 263/191) and 703 (60.8%) had MetS (median age, 66 years, male/female = 441/262), with AHI values of 28.6 and 25.6, respectively ($P = 0.004$).

Patients with MetS had a significantly higher proportion of comorbidities, such as hypertension (98.4 vs. 10.4%), CHD (28.9 vs. 13.7%), hyperlipidemia (33.4 vs. 19.8%), carotid atherosclerosis (29.3 vs. 19.8%), diabetes (33.0 vs. 11.9%) (all $P < 0.001$). Additionally, their median age (66 vs. 65 years), BMI (27.2 vs. 25.1 kg/m^2), waist-hip ratio (93 vs. 85%), SBP (140 vs.

124 mmHg), DBP (78 vs. 73 mmHg), neck circumference (38.0 vs. 37.5 mm) waist circumference (94.0 vs. 87.5 mm), FPG (5.9 vs. 5.4 mmol/L), TG (1.6 vs. 1.3 mmol/L), ODI (23.5 vs. 19.5 times/h), TSA90 (16.45 vs. 10.44 min), T90 (4 vs. 3%) were significantly higher (all $P < 0.001$). By contrast, patients without MetS were more likely to have a higher median HDL (1.2 vs. 1.0 mmol/L) and $LSpO_2$ (81 vs. 80%) (all $P < 0.001$). Conversely, there were no differences with respect to sex, drinking status, smoking status, AF, COPD, and other sleep parameters (all $P > 0.05$) between patients with and without MetS.

Primary Outcomes: MACE

Patients were prospectively followed for 42 months or until MACE, providing 1,157 patient observations. MACE occurred in 119 (10.3%) patients at a median follow-up period of 42 months (range, 1–72 months); 90 (12.8%) of those patients had MetS and 29 (6.4%) had no MetS. To further elucidate the relationship between MetS and MACE in elderly OSA patients, we analyzed the incidence risk of MACE (HR 95% CI) according to the number of MetS components in individual patients. There was a trend for MACE incidence risk to gradually increase in individuals with ≥3 MetS components ($P = 0.045$) (**Figure 2**). Additionally, the Kaplan-Meier curve that associated MetS status with the cumulative incidence of MACE demonstrated a significantly higher cumulative event-rate of MACE in patients with MetS when compared with patients without MetS (Log-rank test, $P = 0.000$; **Figure 3**).

The unadjusted Cox proportional hazard model showed that MetS was associated with a HR of 2.13 (95% CI, 1.36–3.34; $P = 0.001$) for MACE. After adjustment for age, sex, BMI, alcohol use, WHR, comorbidities of CHD, hyperlipidemia, hypertension, carotid atherosclerosis and diabetes, sleep parameters of AHI, ODI, T90, TSA90 and $LSpO_2$, and MetS components, the HR for MACE was moderately attenuated; however, it remained statistically significant (aHR, 1.86; 95% CI, 1.17–2.96; $P = 0.009$; **Table 2**). In the subgroup analysis, the aHR for MACE by MetS were higher in overweight and obese individuals (aHR, 2.32; 95% CI, 1.34–4.01, $P = 0.003$), males (aHR, 2.23; 95% CI, 1.28–3.91, $P = 0.005$), those aged <70 years (aHR, 2.36; 95% CI, 1.27–4.39, $P = 0.006$), and patients with moderate-severe OSA (aHR, 1.81; 95% CI, 1.05–3.02, $P = 0.032$; **Table 3**).

Secondary Outcomes: All-Cause Mortality, Components of MACE, and a Composite of All Events

The crude values for the secondary end points events are shown in **Table 4**. Fifty-four patients died during the follow-up period. The proportions of MetS vs. non-MetS patients was 5.5 vs. 3.3%. Kaplan-Meier analysis revealed significant differences in the incidence of all-cause mortality (Log-rank test, $P = 0.038$; **Supplementary Figure S1**). Similarly, univariate analysis showed that MetS was associated with a higher (approximately 4-year) risk of all-cause mortality in elderly OSA patients (HR, 1.86; 95% CI, 1.02–3.04, $P = 0.042$). However, the aHR for all-cause mortality fell short of statistical significance (aHR, 1.56; 95% CI, 0.84–2.83, $P = 0.162$; **Table 2**).

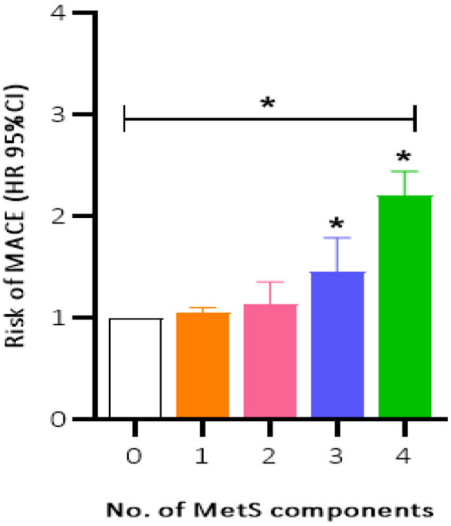

FIGURE 2 | Incidence risk of MACE (HR 95% CI) by the number of the MetS components present in patients, *P* for trend = 0.045. MACE, major adverse cardiovascular event; MetS, metabolic syndrome. *$P < 0.05$.

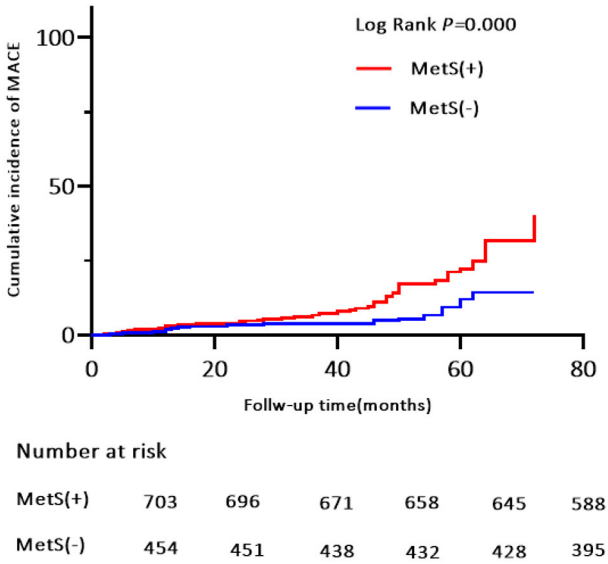

FIGURE 3 | Kaplan-Meier estimates of cumulative incidence (%) for MACE (Primary end points). Log-rank test, $P = 0.000$. MACE, major adverse cardiovascular event.

Of the 119 MACE events, 38 (3.3%) patients had MI and 75 (6.5%) patients were hospitalized for heart disease (64 and 11 cases of hospitalization for unstable angina and heart failure, respectively). In addition, 25 (2.2%) patients died of a cardiovascular event during the follow-up period (**Table 4**). Kaplan-Meier analysis showed no significant differences in the incidence of cardiovascular death and hospitalization for heart failure, except for a higher rate of hospitalization for unstable angina, composite of all events, and MI in the MetS group than

TABLE 2 | Association between MetS and incidence of all events.

	Unadjusted analysis		Adjusted analysis	
	***HR* (95% *CI*)**	***P*-Value**	***HR* (95% *CI*)**	***P*-Value**
MACE	2.13 (1.36, 3.34)	0.001	1.86 (1.17, 2.96)	0.009
Cardiovascular death	2.32 (0.92,5.82)	0.074	2.01 (0.74, 5.39)	0.173
MI	2.22 (1.07, 4.57)	0.031	1.66 (0.73, 3.79)	0.227
Hospitalization for unstable angina	2.58 (1.43, 4.67)	0.002	2.01 (1.04, 3.90)	0.039
Hospitalization for heart failure	3.11 (0.67, 14.34)	0.147	5.087 (0.59, 4.25)	0.141
All-cause mortality	1.86 (1.02 3.40)	0.042	1.56 (0.84, 2.83)	0.162
Composite of all events	2.04 (1.41, 2.95)	0.000	1.54 (1.03, 2.32)	0.036

MACE, major adverse cardiovascular event; MI, myocardial infarction.

TABLE 3 | Subgroup analysis of the associations between MetS and MACE.

	Unadjusted analysis		Adjusted analysis	
	***HR* (95%*CI*)**	***P*-Value**	***HR* (95%*CI*)**	***P*-Value**
Age				
<70	2.66 (1.53,4.62)	0.001	2.36 (1.27, 4.39)	0.006
≥70	1.62 (0.85, 3.10)	0.143	1.48 (0.71, 3.08)	0.291
Severity of OSA				
Mild	2.66 (1.13,6.24)	0.025	1.92 (0.73, 5.04)	0.188
Moderate-severe	2.23 (1.37,3.61)	0.001	1.81 (1.05, 3.12)	0.032
Gender				
Male	2.40 (1.40,4.13)	0.002	2.23 (1.28, 3.91)	0.005
Female	2.14 (1.10,4.18)	0.026	1.7 3(0.86, 3.49)	0.125
BMI				
Normal (18.5–22.9)	1.14 (0.43,3.01)	0.785	0.68 (0.22, 2.12)	0.501
Overweight and obese (≥23)	2.84 (1.72,4.68)	0.000	2.32 (1.34, 4.01)	0.003

BMI, body mass index; OSA, obstructive sleep apnea.

in the non-MetS group (log-rank test, $P = 0.001$, $P = 0.000$, $P = 0.024$, respectively, **Figures 4**, **5**, **Supplementary Figure S2**). Multivariate analysis showed a higher risk of hospitalization for unstable angina in patients with MetS when compared with those without MetS (aHR, 2.01; 95% CI, 1.04–3.90; $P = 0.039$; **Table 2**). Moreover, the incidence of a composite of all events was significantly higher in the MetS group than in the non-MetS group in the adjusted Cox regression analysis (aHR, 1.54; 95% CI, 1.03–2.32; $P = 0.036$; **Table 2**).

DISCUSSION

This was a multi-center, prospective, observational study of 1,157 elderly patients with OSA in the absence of MI, hospitalization for unstable angina, or heart failure at baseline. First, we found that MetS, as defined by the NCEP ATP III criteria, was highly prevalent in our study population; it affected more than two thirds of the elderly patients with OSA. Second, patients with MetS had a higher incidence risk of MACE during the median 42-month follow-up when compared with patients without MetS. Moreover, the trend of MACE risk gradually increased in patients with ≥3 MetS components. Third, MetS conferred an approximately 2.0-fold higher risk for MACE, 1.54-fold risk for a composite of all events, and independently increased the risk of hospitalization for unstable angina. Finally, the risk of MACE was more strongly correlated with MetS in obese and overweight males aged <70 years and in patients with moderate-severe OSA.

TABLE 4 | Crude number of adverse events during follow-up.

Follow-up outcomes	Total (*n* = 1,157)	MteS (*n* = 703)	Non-MteS (*n* = 454)
MACE, *n* (%)	119 (10.3)	90 (12.8)	29 (6.4)
Cardiovascular death, *n* (%)	25 (2.2)	19 (2.7)	6 (1.3)
MI, *n* (%)	38 (3.3)	28 (4.0)	10 (2.2)
Hospitalization for unstable angina, *n* (%)	64 (5.5)	50 (7.1)	14 (3.1)
Hospitalization for heart failure, *n* (%)	11 (1.0)	9 (1.3)	2 (0.4)
All-cause mortality, *n* (%)	54 (4.7)	39 (5.5)	15 (3.3)
Composite of all events, *n* (%)	145 (12.5)	106 (15.1)	39 (8.6)

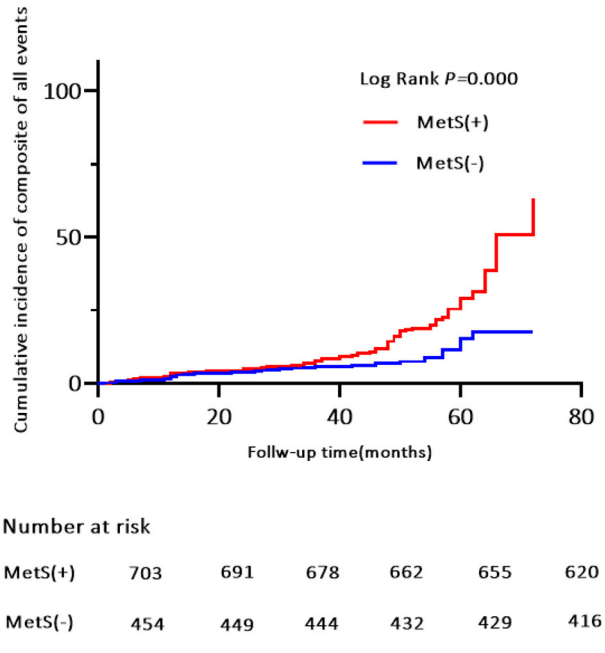

FIGURE 4 | Kaplan-Meier estimates of cumulative incidence (%) for composite of all events. Log-rank test, $P = 0.000$.

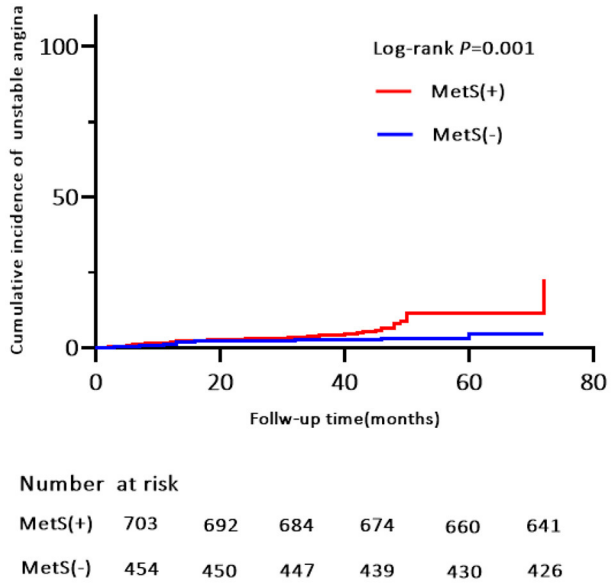

FIGURE 5 | Kaplan-Meier estimates of cumulative incidence (%) for hospitalization for unstable anginal. Log-rank test, $P = 0.001$.

Approximately 17% of the total population is affected by OSA; however, its prevalence varies widely according to age, ethnicity, and sex of the population studied (23). MetS is strongly associated with long-term cardiovascular risks, such as MI, hospitalization for heart failure or unstable angina, and cardiovascular death (24); therefore, this study is important to address the public health care burden of OSA-related complications. A cross-sectional study investigated the association between MetS and the attenuation of heart rate recovery after maximal exercise (ΔHRR) by grouping all participants into two categories (AHI ≥ 15 events/h or AHI <15 events/h) in the Brazilian population. They findings indicated that ΔHRR is impaired to a greater degree where OSA patients with MetS (25). Roche et al. used data from a population-based sample of older adult participants in South Africa and founded that the components of MetS (such as waist circumference, HDL, and TG, et al.) was associated with a increased risk of cardiometabolic risk (CMR) in elderly OSA patients (26). Moreover, another study demonstrated that OSA increases sympathetic peripheral and central chemoreflex response in young to middle-aged patients with MetS from the Unit of Cardiac Rehabilitation and Exercise Physiology of the Heart Institute (InCor), which seems to explain the increase in sympathetic nerve activity and consequent may cause a increased risk of CVD (27). Also, previous one epidemiological study among 1,727 Asian OSA patients (aged 30–54) in Shanghai showed that cardiometabolic disorders (including the biomarkers of MetS) in OSA may potentiate their unfavorable effects on CVD, which is in concordance with our results, but the study was a cross-sectional study and excluded a geriatric population (10). Our study population had a median age at mid-sixties, which emphasizes the awareness of the elderly at risk of MACE and early initiation of prevention strategies. Moreover, we found that individuals who exhibited three or more components of MetS had a gradual increase in the risk of MACE, indicating that more complex MetS phenotypes may lead to worsened prognoses. Therefore, it is crucial to minimize the Mets-related cardiovascular risk in patients with OSA.

Most MACE in our study presented as hospitalization for unstable angina (5.5%), which confirms observations that there was a higher risk for unstable angina than other individual components of MACE in patients with MetS during the median 42-month follow-up. OSA involves complex mechanisms, including mechanical, chemical, neural, hemodynamic, and inflammatory processes, that may interact to increase the risk of MACE (28, 29). OSA patients have a higher risk of MACE and all-cause mortality (4). A recent population-based cohort study has shown that OSA and OSA-induced hypoxia may correlate with the severity of MI, increase the incidence of heart rhythm disorders in elderly patients with subacute MI, and worsen their short-term poor outcomes (30). A growing amount of evidence has reported the risk factors for MetS, including obesity, poor diet, sedentary behavior, and genetics. These share considerable overlap with OSA risk factors; therefore, the severity of OSA may be related to MetS. The co-existence of MetS and OSA may aggravate the severity of carotid intima-media thickness and atherosclerosis. Additionally, it potentiates other underlying mechanisms of CVD, which may explain the increased incidence risk for MACE (30–32). Thus, our study further investigated the impact of concomitant MetS on the long-term risk of MACE in elderly patients with OSA. Notably, our findings as a multicenter OSA population-based study that adjusted for potential confounders confirmed the significance for MACE between patients with OSA with and without MetS.

MetS predisposes individuals to OSA development; epidemiological studies have reported that MetS is 6–9 times more likely to be present in individuals with OSA when compared with the general population (7). In our study, patients with MetS demonstrated risk factor clustering and a higher burden of comorbidities (e.g., carotid atherosclerosis, hypertension, and hyperlipidemia) pertinent to long-term prognosis. Of note, patients with MetS experienced MACE approximately 2-times more often when compared with patients without MetS. As a result, the median 42-month crude number of cardiovascular deaths, MI, hospitalization for unstable angina, and hospitalization for heart failure in patients with MetS (2.7, 4.0, 7.1, and 1.3%, respectively) was considerably higher than in patients free of MetS (1.3, 2.2, 3.1, and 0.4%, respectively). Several potential mechanisms the association between MetS and risks of MACE in elderly OSA patients. Firstly, this association may be related to metabolic changes that transpire during sleep in OSA. OSA recurrence increases plasma free fatty acids (FFAs) and glucose during sleep, associated with sympathetic and adrenocortical activation. Recurring exposure to these metabolic changes may foster CVD risks (33). Secondly, the increased expression of mineralocorticoid receptor (MR) in the elderly, which may provided a further

explanation for enhanced cardiovascular risk in the elderly. MR activation contributes to increase blood pressure with aging by vascular oxidative stress that are important mechanisms of CVD risk in OSA and MetS. In the elderly, dysregulation of MR signaling is associated with increased cardiovascular risk in OSA patients combined MetS (34, 35). Thirdly, preclinical and clinical trials have demonstrated that GLP-1 receptors are abundantly present in the heart (36). GLP-1 receptor agonists (GLP-1RAs), a group of widely used anti-hyperglycaemic agents, which work on the incretin axis and improve insulin secretion, has resulted in improved cardiovascular outcomes along with improved metabolic control and significant weight reduction (37).

To the best of our knowledge, this is the first study to report MetS as a multivariable predictor of MACE in elderly patients with OSA. A previous study has shown that the prevalence of MetS declines in older age and that the cardiometabolic comorbidities associated with OSA diminish in parallel (38). Additional studies have demonstrated that the incidence of stroke, but not coronary heart disease, is increased in elderly patients with severe OSA (39). Our data further demonstrated that MetS diagnosed in patients aged <70 years with moderate-severe OSA have a higher risk (approximately 4-year) of MACE. This may be explained by the fact that the prevalence of OSA peaks at <70 years of age. Furthermore, moderate intermittent hypoxia can protect the myocardium from ischemic injury in elderly patients with mild OSA (40).

There are higher risk-adjusted odds of survival in obese and overweight patients with heart failure (41), which is consistent with the "obesity paradox". However, recent evidence has shown a shift in the obesity paradox with aging; there are diminished cardiac benefits with overweight and obesity in elderly patients (42). Obesity is a common pathogenic factor of OSA and MetS. Our datas revealed that MetS was associated with a higher incidence risk of MACE in overweight and obese elderly patients with OSA. Nonetheless, further research is needed to clarify the underlying mechanisms and to define the optimal incidence risk for MACE to reduce CVD complications in obese and overweight OSApatients combined MetS.

OSA and MetS lead to CVD (4). The prevalence of MetS and OSA are different in males and females. A cross sectional study has shown that women with OSA have higher chances of having MetS than men (43). Our findings revealed that male elderly patients with OSA and MetS had a higher risk of MACE. This may be due to metabolic differences, which are more prevalent in women following hormonal changes like menopause. This may explain the delay in OSA or MetS peak prevalence when compared with men. In addition, our study showed that patients with MetS were associated an increased incidence of all-cause mortality; however, this was not significant. This may be because the patients with OSA and Mets in our study were under guideline-based therapy and in a stable condition with no target organ damage. Nonetheless, the complex pathophysiology of MetS in elderly patients with OSA and the potential impact on all-cause mortality and MACE cannot be ignored in clinical risk assessment, diagnosis, and treatment.

STUDY LIMITATIONS

First, a major limitation to the present study is the homogenous Asian study population. This means that the study's findings are not representative of the global population and should be evaluated in other ethnicities. Second, MetS status and its components are variable; they can change dynamically over time. This could have biased the results. Third, the incidence of MACE and all-cause mortality are complex processes and correlated with multiple factors. We adjusted for as many CVD-related risk factors as possible; however, there may be other unmeasured confounders. Nevertheless, these limitations do not fundamentally affect the value of our study.

CONCLUSION

In our Asian population-based multicenter cohort study, MetS was a complex risk factor that independently increased the risk for MACE, hospitalization for unstable angina, and a composite of all events in elderly patients with OSA in the absence of MI, hospitalization for unstable angina, or heart failure. In the subgroup analysis, overweight and obese males, aged <70 years, with moderate-severe OSA concomitant MetS presented a higher risk for MACE. Our findings reinforce the clinical utility of MetS for CVD risk assessment in elderly patients with OSA. Furthermore, we suggest that MetS is considered as a modifiable risk factor in cardiovascular prevention in patients with OSA. This possibility requires further confirmation in future large-scale, multi-racial, multicenter, prospective cohort studies.

DATA AVAILABILITY STATEMENT

The original contributions presented in the study are included in the article/**Supplementary Material**, further inquiries can be directed to the corresponding authors.

ETHICS STATEMENT

The studies involving human participants were reviewed and approved by the Ethics Committee of Chinese PLA General Hospital (S2019-352-01). The patients/participants provided their written informed consent to participate in this study.

AUTHOR CONTRIBUTIONS

LL, XS, ZZ, JH, JLi, WX, ZH, YiG, YaG, KC, JG, LZ, and HW collected the data. LL, XS, and ZZ analyzed the data and wrote the manuscript draft. JH revised the manuscript. JLin, TL, and XF designed this study. All authors have read and approved the manuscript.

SUPPLEMENTARY MATERIAL

The Supplementary Material for this article can be found online at: https://www.frontiersin.org/articles/10.3389/fcvm.2021.813280/full#supplementary-material

REFERENCES

1. Chan MTV, Wang CY, Seet E, Tam S, Lai HY, Chew EFF, et al. Association of unrecognized obstructive sleep apnea with postoperative cardiovascular events in patients undergoing major noncardiac surgery. *JAMA*. (2019) 321:1788–98. doi: 10.1001/jama.2019.4783
2. Dodds S, Williams LJ, Roguski A, Vennelle M, Douglas NJ, Kotoulas SC, et al. Mortality and morbidity in obstructive sleep apnoea-hypopnoea syndrome: results from a 30-year prospective cohort study. *ERJ Open Res.* (2020) 6:00057–2020. doi: 10.1183/23120541.00057-2020
3. Loo GH, Rajan R, Mohd Tamil A, Ritza Kosai N. Prevalence of obstructive sleep apnea in an Asian bariatric population: an underdiagnosed dilemma. *Surg Obes Relat Dis.* (2020) 16:778–83. doi: 10.1016/j.soard.2020.02.003
4. Trzepizur W, Blanchard M, Ganem T, Balusson F, Feuilloy M, Girault JM, et al. Sleep apnea specific hypoxic burden, symptom subtypes and risk of cardiovascular events and all-cause mortality. *Am J Respir Crit Care Med.* (2021) 205:108–17. doi: 10.1164/rccm.202105-1274OC
5. Jia S, Zhou YJ Yu Y, Wu SJ, Sun Y, Wang ZJ, et al. Obstructive sleep apnea is associated with severity and long-term prognosis of acute coronary syndrome. *J Geriatr Cardiol.* (2018) 15:146–52. doi: 10.11909/j.issn.1671-5411.2018.02.005
6. Aurora RN, Crainiceanu C, Gottlieb DJ, Kim JS, Punjabi NM. Obstructive sleep apnea during REM sleep and cardiovascular disease. *Am J Respir Crit Care Med.* (2018) 197:653–60. doi: 10.1164/rccm.201706-1112OC
7. Gaines J, Vgontzas AN, Fernandez-Mendoza J, Bixler EO. Obstructive sleep apnea and the metabolic syndrome: the road to clinically-meaningful phenotyping, improved prognosis, and personalized treatment. *Sleep Med Rev.* (2018) 42:211–9. doi: 10.1016/j.smrv.2018.08.009
8. Gottlieb DJ, Punjabi NM. Diagnosis and management of obstructive sleep apnea: a review. *JAMA*. (2020) 323:1389–400. doi: 10.1001/jama.2020.3514
9. Song SO, He K, Narla RR, Kang HG Ryu HU, Boyko EJ. Metabolic consequences of obstructive sleep apnea especially pertaining to diabetes mellitus and insulin sensitivity. *Diabetes Metab J.* (2019) 43:144–55. doi: 10.4093/dmj.2018.0256
10. Zhao X, Li X, Xu H, Qian Y, Fang F, Yi H, et al. Relationships between cardiometabolic disorders and obstructive sleep apnea: implications for cardiovascular disease risk. *J Clin Hypertens.* (2019) 21:280–90. doi: 10.1111/jch.13473
11. Fanta K, Daba FB, Asefa ET, Chelkeba L, Melaku T. Prevalence and impact of metabolic syndrome on short-term prognosis in patients with acute coronary syndrome: prospective cohort study. *Diabetes Metab Syndr Obes.* (2021) 14:3253–62. doi: 10.2147/DMSO.S320203
12. Su X, Li JH, Gao Y, Chen K, Gao Y, Guo JJ, et al. Impact of obstructive sleep apnea complicated with type 2 diabetes on long-term cardiovascular risks and all-cause mortality in elderly patients. *BMC Geriatr.* (2021) 21:508. doi: 10.1186/s12877-021-02461-x
13. Chen Z, Wu S, Huang J, Yuan J, Chen H, Chen Y. Metabolic syndrome increases cardiovascular risk in a population with prediabetes: a prospective study in a cohort of Chinese adults. *J Diabetes Investig.* (2019) 10:673–9. doi: 10.1111/jdi.12958
14. Berry RB, Budhiraja R, Gottlieb DJ, Gozal D, Iber C, Kapur VK, et al. Rules for scoring respiratory events in sleep: update of the 2007 AASM Manual for the Scoring of Sleep and Associated Events. Deliberations of the sleep apnea definitions task force of the american academy of sleep medicine. *J Clin Sleep Med.* (2012) 8:597–619. doi: 10.5664/jcsm.2172
15. Patil SP, Ayappa IA, Caples SM, Kimoff RJ, Patel SR, Harrod CG. Treatment of adult obstructive sleep apnea with positive airway pressure: an American academy of sleep medicine clinical practice guideline. *J Clin Sleep Med.* (2019) 15:335–43. doi: 10.5664/jcsm.7640
16. Ma YN, Xie WX, Hou ZH, An YQ, Ren XS, Ma YJ, et al. Association between coronary artery calcification and cognitive function in a Chinese community-based population. *J Geriatr Cardiol.* (2021) 18:514–22. doi: 10.11909/j.issn.1671-5411.2021.07.002
17. Joint committee issued Chinese guideline for the management of dyslipidemia in adults. *Zhonghua Xin Xue Guan Bing Za Zhi.* (2016) 44:833–53. doi: 10.3760/cma.j.issn.0253-3758.2016.10.005
18. Kirchhof P, Benussi S, Kotecha D, Ahlsson A, Atar D, Casadei B, et al. 2016 ESC guidelines for the management of atrial fibrillation developed in collaboration with EACTS. *Eur Heart J.* (2016) 37:2893–962. doi: 10.1093/eurheartj/ehw210
19. Anno T, Mune T, Takai M, Kimura T, Hirukawa H, Kawasaki F, et al. Decreased plasma aldosterone levels in patients with type 2diabetes mellitus: a possible pitfall in diagnosis of primary aldosteronism. *Diabetes Metab.* (2019) 45:399–400. doi: 10.1016/j.diabet.2018.06.003
20. Charlson ME, Pompei P, Ales KL, MacKenzie CR, A. new method of classifying prognostic comorbidity in longitudinal studies: development and validation. *J Chronic Dis.* (1987) 40:373–83. doi: 10.1016/0021-9681(87)90171-8
21. Fu Y, Xu H, Xia Y, Qian Y, Li X, Zou J, et al. Excessive daytime sleepiness and metabolic syndrome in men with obstructive sleep apnea: a large cross-sectional study. *Oncotarget.* (2017) 8:79693–702. doi: 10.18632/oncotarget.19113
22. Grundy SM, Cleeman JI, Daniels SR, Donato KA, Eckel RH, Franklin BA, et al. Diagnosis and management of the metabolic syndrome: an American heart association/national heart, lung, and blood institute scientific statement. *Circulation.* (2005) 112:e297. doi: 10.1161/CIRCULATIONAHA.105.169405
23. Framnes SN, Arble DM. The bidirectional relationship between obstructive sleep apnea and metabolic disease. *Front Endocrinol.* (2018) 9:440. doi: 10.3389/fendo.2018.00440
24. Park S, Han K, Lee S, Kim Y, Lee Y, Kang MW, et al. Association between moderate-to-vigorous physical activity and the risk of major adverse cardiovascular events or mortality in people with various metabolic syndrome status: a nationwide population-based cohort study including 6 million people. *J Am Heart Assoc.* (2020) 9:e016806. doi: 10.1161/JAHA.120.016806
25. Cepeda FX, Toschi-Dias E, Maki-Nunes C, Rondon MU, Alves MJ, Braga AM, et al. Obstructive sleep apnea impairs postexercise sympathovagal balance in patients with metabolic syndrome. *Sleep.* (2015) 38:1059–66. doi: 10.5665/sleep.4812
26. Roche J, Rae DE, Redman KN, Knutson KL, von Schantz M, Gómez-Olivé FX, et al. Impact of obstructive sleep apnea on cardiometabolic health in a random sample of older adults in rural South Africa: building the case for the treatment of sleep disorders in underresourced settings. *J Clin Sleep Med.* (2021) 17:1423–34. doi: 10.5664/jcsm.9214
27. Trombetta IC, Maki-Nunes C, Toschi-Dias E, Alves MJ, Rondon MU, Cepeda FX, et al. Obstructive sleep apnea is associated with increased chemoreflex sensitivity in patients with metabolic syndrome. *Sleep.* (2013) 36:41–9. doi: 10.5665/sleep.2298
28. Javaheri S, Barbe F, Campos-Rodriguez F, Dempsey JA, Khayat R, Javaheri S, et al. Sleep apnea: types, mechanisms, and clinical cardiovascular consequences. *J Am Coll Cardiol.* (2017) 69:841–58. doi: 10.1016/j.jacc.2016.11.069
29. Xie JY, Liu WX Ji L, Chen Z, Gao JM, Chen W, et al. Relationship between inflammatory factors and arrhythmia and heart rate variability in OSAS patients. *Eur Rev Med Pharmacol Sci.* (2020) 24:2037–53. doi: 10.26355/eurrev_202002_20382
30. Wang LJ, Pan LN, Yan RY, Quan WW, Xu ZH. Obstructive sleep apnea increases heart rhythm disorders and worsens subsequent outcomes in elderly patients with subacute myocardial infarction. *J Geriatr Cardiol.* (2021) 18:30–8. doi: 10.11909/j.issn.1671-5411.2021.01.002
31. Chuang HH, Liu CH, Wang CY, Lo YL, Lee GS, Chao YP, et al. Snoring sound characteristics are associated with common carotid artery profiles in patients with obstructive sleep apnea. *Nat Sci Sleep*. (2021) 13:1429–30. doi: 10.2147/NSS.S311125
32. Potočnjak I, Trbušić M, Terešak SD, Radulović B, Pregartner G, Berghold A, et al. Metabolic syndrome modulates association between endothelial lipase and lipid/lipoprotein plasma levels in acute heart failure patients. *Sci Rep*. (2017) 7:1165. doi: 10.1038/s41598-017-01367-2
33. Chopra S, Rathore A, Younas H, Pham LV, Gu C, Beselman A, et al. Obstructive sleep apnea dynamically increases nocturnal plasma free fatty acids, glucose, and cortisol during sleep. *J Clin Endocrinol Metab.* (2017) 102:3172–81. doi: 10.1210/jc.2017-00619
34. DuPont JJ, McCurley A, Davel AP, McCarthy J, Bender SB, Hong K, et al. Vascular mineralocorticoid receptor regulates microRNA-155 to promote vasoconstriction and rising blood pressure with aging. *JCI Insight.* (2016) 1:e88942. doi: 10.1172/jci.insight.88942

35. Nanba K, Vaidya A, Williams GH, Zheng I, Else T, Rainey WE. Age-related autonomous aldosteronism. *Circulation.* (2017) 136:347–55. doi: 10.1161/CIRCULATIONAHA.117.028201
36. Heuvelman VD, Van Raalte DH, Smits MM. Cardiovascular effects of glucagon-like peptide 1 receptor agonists: from mechanistic studies in humans to clinical outcomes. *Cardiovasc Res.* (2020) 116:916–30. doi: 10.1093/cvr/cvz323
37. Nauck MA, Quast DR, Wefers J, Meier J. GLP-1 receptor agonists in the treatment of type 2 diabetes e state-of-the-art. *Mol Metab.* (2021) 46:101102. doi: 10.1016/j.molmet.2020.101102
38. Ford ES, Giles WH, Dietz WH. Prevalence of the metabolic syndrome among US adults: findings from the third National Health and Nutrition Examination Survey. *JAMA.* (2002) 287:356–9. doi: 10.1001/jama.287.3.356
39. Catalan-Serra P, Campos-Rodriguez F, Reyes-Nuñez N, Selma-Ferrer MJ, Navarro-Soriano C, Ballester-Canelles M, et al. Increased incidence of stroke, but not coronary heart disease, in elderly patients with sleep apnea. *Stroke.* (2019) 50:491–4. doi: 10.1161/STROKEAHA.118.023353
40. Mohananey D, Villablanca PA, Gupta T, Agrawal S, Faulx M, Menon V, et al. Recognized obstructive sleep apnea is associated with improved in-hospital outcomes after ST elevation myocardial infarction. *J Am Heart Assoc.* (2017) 6:e006133. doi: 10.1161/JAHA.117.006133
41. Horwich TB, Fonarow GC, Clark AL. Obesity and the obesity paradox in heart failure. *Prog Cardiovasc Dis.* (2018) 61:151–6. doi: 10.1016/j.pcad.2018.05.005
42. Wang S, Ren J. Obesity paradox in aging: from prevalence to pathophysiology. *Prog Cardiovasc Dis.* (2018) 61:182–9. doi: 10.1016/j.pcad.2018.07.011
43. Chaudhary P, Goyal A, Goel SK, Kumar A, Chaudhary S, Kirti Keshri S, et al. Women with OSA have higher chances of having metabolic syndrome than men: effect of gender on syndrome Z in cross sectional study. *Sleep Med.* (2021) 79:83–7. doi: 10.1016/j.sleep.2020.12.042

Conflict of Interest: The authors declare that the research was conducted in the absence of any commercial or financial relationships that could be construed as a potential conflict of interest.

Publisher's Note: All claims expressed in this article are solely those of the authors and do not necessarily represent those of their affiliated organizations, or those of the publisher, the editors and the reviewers. Any product that may be evaluated in this article, or claim that may be made by its manufacturer, is not guaranteed or endorsed by the publisher.

frontiers | Frontiers in Cardiovascular Medicine

ORIGINAL RESEARCH
published: 12 May 2022
doi: 10.3389/fcvm.2022.727474

MCC950, a Selective NLRP3 Inhibitor, Attenuates Adverse Cardiac Remodeling Following Heart Failure Through Improving the Cardiometabolic Dysfunction in Obese Mice

*Menglong Wang[1,2,3†], Mengmeng Zhao[1,2,3†], Junping Yu[1,2,3†], Yao Xu[1,2,3], Jishou Zhang[1,2,3], Jianfang Liu[1,2,3], Zihui Zheng[1,2,3], Jing Ye[1,2,3], Zhen Wang[1,2,3], Di Ye[1,2,3], Yongqi Feng[1,2,3], Shuwan Xu[1,2,3], Wei Pan[1,2,3], Cheng Wei[1,2,3] and Jun Wan[1,2,3]**

[1] Department of Cardiology, Renmin Hospital of Wuhan University, Wuhan, China, [2] Cardiovascular Research Institute, Wuhan University, Wuhan, China, [3] Hubei Key Laboratory of Cardiology, Wuhan, China

OPEN ACCESS

Edited by:
Zhong Wang,
University of Michigan, United States

Reviewed by:
John Reyes Ussher,
University of Alberta, Canada
Goro Katsuumi,
Juntendo University, Japan

***Correspondence:**
Jun Wan
wanjun@whu.edu.cn

† These authors have contributed equally to this work

Specialty section:
This article was submitted to Cardiovascular Metabolism, a section of the journal Frontiers in Cardiovascular Medicine

Received: *18 June 2021*
Accepted: *28 March 2022*
Published: *12 May 2022*

Citation:
Wang M, Zhao M, Yu J, Xu Y, Zhang J, Liu J, Zheng Z, Ye J, Wang Z, Ye D, Feng Y, Xu S, Pan W, Wei C and Wan J (2022) MCC950, a Selective NLRP3 Inhibitor, Attenuates Adverse Cardiac Remodeling Following Heart Failure Through Improving the Cardiometabolic Dysfunction in Obese Mice. Front. Cardiovasc. Med. 9:727474. doi: 10.3389/fcvm.2022.727474

Obesity is often accompanied by hypertension. Although a large number of studies have confirmed that NLRP3 inhibitors can improve cardiac remodeling in mice with a normal diet, it is still unclear whether NLRP3 inhibitors can improve heart failure (HF) induced by pressure overload in obese mice. The purpose of this study was to explore the role of MCC950, a selective NLRP3 inhibitor, on HF in obese mice and its metabolic mechanism. Obese mice induced with a 10-week high-fat diet (HFD) were used in this study. After 4 weeks of HFD, transverse aortic constriction (TAC) surgery was performed to induce a HF model. MCC950 (10 mg/kg, once/day) was injected intraperitoneally from 2 weeks after TAC and continued for 4 weeks. After echocardiography examination, we harvested left ventricle tissues and performed molecular experiments. The results suggest that in obese mice, MCC950 can significantly improve cardiac hypertrophy and fibrosis caused by pressure overload. MCC950 ameliorated cardiac inflammation after TAC surgery and promoted M2 macrophage infiltration in the cardiac tissue. MCC950 not only restored fatty acid uptake and utilization by regulating the expression of CD36 and CPT1β but also reduced glucose uptake and oxidation *via* regulating the expression of GLUT4 and p-PDH. In addition, MCC950 affected the phosphorylation of AKT and AMPK in obese mice with HF. In summary, MCC950 can alleviate HF induced by pressure overload in obese mice *via* improving cardiac metabolism, providing a basis for the clinical application of NLRP3 inhibitors in obese patients with HF.

Keywords: metabolic remodeling, MCC950, inflammasome, pressure overload, cardiac hypertrophy, heart failure

INTRODUCTION

Heart failure (HF) is a very common progressive disease today, with high morbidity and mortality. Most patients require hospitalization, which puts continuous pressure on the clinical and public health systems. The main risk factors for HF include coronary heart disease, hypertension, diabetes, and obesity (1). Studies have shown that obese patients with a higher body mass index (BMI) have

a higher risk of HF (2, 3). A higher BMI is associated with a higher risk of hospitalization and death with HF (4). In addition, visceral fat accumulation is significantly associated with poor cardiac remodeling (5). The metabolic derangements caused by obesity are believed to be closely related to the development of HF. As shown in animal experiments, obesity induced by a high-fat diet (HFD) can aggravate cardiac remodeling (6, 7). And attenuating the metabolic disorder induced by obesity can effectively reduce cardiac remodeling (8). These studies suggest that reducing obesity-induced metabolic disorders may be one of the effective strategies for the treatment of HF. At present, many drugs have been reported to play the role of attenuating cardiac remodeling and HF in mice with a normal diet. However, it is still unclear whether the same cardioprotective effect is available in obese mice.

It has been reported that changes in cardiac metabolism precede the occurrence of HF (9). Damage to cardiac metabolism increases cardiomyocyte death and exacerbates pathological cardiac remodeling. Insufficient ATP production directly changes contractile function and leads to HF. The fatty acid (FA) sources of ATP decrease, while glycolysis and other forms of metabolism source of ATP increase in a failed heart (10). This process is called metabolic reprogramming and is accompanied by changes in genes encoding proteins related to mitochondrial function (11). Moreover, cardiometabolic reprogramming is considered to be the direct cause of pathological hypertrophy (12). Relieving mitochondrial dysfunction and metabolic remodeling have been reported to attenuate the development of pathological hypertrophy and cardiac systolic dysfunction (13, 14). These findings provide new ideas for the treatment of cardiac remodeling and HF.

Nod-like receptor family pyrin domain-containing 3 (NLRP3) inflammasome is a multi-protein complex composed of NLRP3, speck-like protein (ASC), and pro-caspase-1. NLRP3 inflammasome is mainly activated by pathogen-related molecular patterns and danger-related molecular patterns, and further activates caspase-1, thereby promoting the maturation of proinflammatory cytokines IL-1β and IL-18 (15). NLRP3 inflammasome plays an important role in the occurrence and prognosis of HF. A clinical trial involving 54 HF patients reported that compared with the control group, the ASC methylation in the exercise group increased, and the plasma IL-1β and ASC mRNA levels decreased, suggesting that exercise can improve the prognosis of HF through epigenetic regulation of ASC (16). In addition, NLRP3 inflammasome is involved in pathological processes leading to HF, such as cardiac hypertrophy and fibrosis. In the pressure overload model, NLRP3 inflammasome is activated, and inhibiting the expression or activation of NLRP3 can effectively alleviate cardiac remodeling caused by pressure overload (17, 18). In addition, many previous studies have shown that there is a close interaction between NLRP3 and metabolism (19, 20). β-Hydroxybutyrate (BHB), a kind of ketone body, inhibits the activation of NLRP3 inflammasome by preventing K^+ efflux and reducing ASC oligomerization and speck formation (21). *In vivo*, BHB or ketogenic diet attenuated caspase-1 activation and IL-1β secretion in the mouse models of NLRP3-mediated disease. Increasing the BHB levels attenuates NLRP3 inflammasome formation and antagonizes proinflammatory cytokine-induced mitochondrial dysfunction and fibrosis, thereby improving HF (22). This suggests that NLRP3 may be involved in cardiometabolic reprogramming. However, there is currently a lack of relevant evidence to prove the role of NLRP3 in cardiac metabolic reprogramming in obese mice. Therefore, we used MCC950, a selective inhibitor of NLRP3, to explore the effect of NLRP3 on cardiometabolic reprogramming during HF in obese mice.

MATERIALS AND METHODS

Reagents

MCC950 and wheat germ agglutinin (WGA, 1:200 dilution) was purchased from Sigma-Aldrich (St. Louis, MO, United States). GAPDH (1:2,500 dilution), α-smooth muscle actin (α-SMA, 1:500 dilution), CD68 (1:200 dilution), CD206 (1:200 dilution), CD36 (1:500 dilution), glucose transporter 4 (GLUT4, 1:500 dilution) were purchased from Abcam (Cambridge, MA, United States). Collagen 1 (COL1, 1:1,000 dilution), COL3 (1:1,000 dilution), carnitine palmitoyl transferase 1β (CPT1β, 1:1,000 dilution), total acetyl-CoA carboxylase (t-ACC, 1:1,000 dilution), phosphorylated-ACC (Ser79) (p-ACC, 1:1,000 dilution), malonyl-CoA decarboxylase (MCD, 1:1,000 dilution), GLUT1 (1:1,000 dilution), total pyruvate dehydrogenase (t-PDH, 1:1,000 dilution), phosphorylated-PDH (Ser232) (p-PDH, 1:1,000 dilution), pyruvate dehydrogenase kinase 4 (PDK4, 1:1,000 dilution) were purchased from Proteintech (Wuhan, China). Caspase-1 (1:500 dilution) and interleukin 1β (IL1β; 1:500 dilution) were purchased from Santa Cruz (United States). Total protein kinase B (t-AKT, 1:1,000 dilution), phosphorylated-AKT (Ser473) (p-AKT, 1:1,000 dilution), total AMP-activated protein kinase α (t-AMPKα, 1:1,000 dilution), and phosphorylated-AMPKα (Thr172) (p-AMPKα,1:1,000 dilution) were purchased from Cell Signaling Technology (United States). Secondary antibodies were obtained from LI-COR Biosciences (Lincoln, NE, United States). All other chemicals were of analytical grade. The catalog numbers are provided in **Supplementary Table 1**.

Animal Models

C57BL/6J mice (6 weeks, males, Gempharmatech Co., Ltd.) in this study were raised in a specific pathogen-free mouse room in the Renmin Hospital of Wuhan University. The room provided the mice with stable temperature (20–22°C), humidity (50 ± 5%), plenty of water, and food for free drinking and eating. We performed mouse experiments and took care following the Guidelines for the Care and Use of Laboratory Animals published by the National Institutes of Health. The Animal Care and Use Committee of Renmin Hospital of Wuhan University (Wuhan, China) has reviewed and approved this research.

At 8 weeks of age, the mice were initiated with a HFD, containing 60% fat by kcal content (product D12492, Research

Diets, New Brunswick, NJ, United States) to produce obese models (23). We divided these mice into four groups based on the treatment given: sham + vehicle, sham + MCC950, TAC + vehicle, TAC + MCC950 (n = 10, per group). The mice had *ad libitum* access to food and water during the whole experiments. And 4 weeks after HFD, the transverse aortic constriction (TAC) or sham surgery was performed. Briefly, the mice were anesthetized with 2% isoflurane inhalation. The mice were then placed in the supine position and orally intubated with a 20-gauge tube and ventilated (Harvard Apparatus Rodent Ventilator, Model 845) at 120 breaths per minute (0.1 ml tidal volume). The thoracic cavity was exposed by incising the proximal portion of the sternum. After isolating the aortic arch between the innominate and left common carotid arteries, the transverse aortic arch was ligated with a covered 26-gauge needle. Then the needle was removed, leaving a discrete area of stenosis. The sham-operated mice underwent the same surgical procedure, including isolation of the aorta, but no sutures were placed. Normal saline was intraperitoneally injected as a vehicle. MCC950 or vehicle (10 mg/kg of body weight, once/day) was intraperitoneally injected into the mice 2 weeks after the TAC or sham surgery (24, 25). HFD was maintained after surgery for 6 weeks for heart mass, cardiac function, and other analyses. And the left ventricle (LV) tissue was harvested for further experiments. The design of this study is shown in **Supplementary Figure 1**.

Echocardiography

Mylab 30CV ultrasound (Biosound Esaote) equipped with a 10-MHz linear array ultrasound transducer was used to perform echocardiography in the anesthetized (1.5–2% isoflurane) mice. The LV dimensions were assessed at the parasternal short axis at the level of the papillary muscles. The LV end-systolic diameter (LVEDs), LV end-diastolic diameter (LVEDd), interventricular septal thickness at end-diastole (IVSd), interventricular septal thickness at end-systole (IVSs), LV posterior wall thickness at end-diastole (LVPWd), LV posterior wall thickness at end-systole (LVPWs), LV ejection fraction (EF), and fractional shortening (FS) were measured.

Histological Analysis

There were five samples per group for histological analysis. We took four images of each sample for quantification. Hematoxylin-eosin (H&E) and WGA staining were performed to examine the size of cardiomyocytes. Masson staining was used to observe collagen deposition in the perivascular space and interstitium of the four groups of mice. We determined the cross-sectional area of cardiomyocytes with WGA staining and the fibrotic areas with Masson staining by using a digital image analysis system (Image-Pro Plus 6.0, Media Cybernetics, Bethesda, MD, United States). In WGA staining, we selected seven cardiomyocytes in each image to measure the cardiomyocyte size. In Masson staining, we examined the ratio of collagen fibers to the cross-sectional area of the ventricle. Immunohistochemistry and immunofluorescence staining were performed to examine the macrophage infiltration as per the protocols mentioned in a previous study (26). We examined the percentage of positive cells in immunohistochemical staining for aSMA, CD68, and immunofluorescence staining for CD206 using Image J 2.1.0.

Quantitative Polymerase Chain Reaction

The RNA was extracted from the LV tissue using TRIzol (Invitrogen Life Technologies, Carlsbad, CA, United States), and cDNA was synthesized using 2 μg RNA of each treatment group with oligo (dT) primers and a Transcriptor First Strand cDNA Synthesis Kit (Roche, Basel, Switzerland). Quantitative analysis was performed using a Light Cycler 480 and SYBR Green Master Mix (Roche). Details of the primer sequences are shown in **Supplementary Table 2**.

Measurement of Blood Parameters

After a 12-h fast, blood was collected from the retro-orbital plexus to measure the serum levels of blood glucose, triglyceride (TG), non-esterified fatty acids (NEFAs), and BHB following the instructions. All the detection kits were purchased from Nanjing Jiancheng Bioengineering Institute, China.

Measurement of Triglyceride, Glycogen, and Pyruvate Dehydrogenase Activity in Hearts

The ventricles were immediately snap-frozen in liquid nitrogen and pulverized with a mortar and pestle in liquid nitrogen. TG and glycogen concentrations in the heart, as well as PDH activity, were then determined according to the manufacturer's instructions. All the detection kits were purchased from Nanjing Jiancheng Bioengineering Institute, China.

Western Blotting

We extracted proteins from the cardiac tissue using radioimmunoprecipitation assay (RIPA) buffer and measured protein concentration using the BCA protein assay kit. The proteins (50 μg) were separated by sodium dodecyl sulfate-polyacrylamide gel electrophoresis (SDS-PAGE) and subsequently transferred to Immobilon-P membranes (Millipore, Beijing, China) by a gel transfer apparatus (Invitrogen). The membranes were incubate with different primary antibodies over night at 4°C. After washing, the membranes were incubated with secondary antibodies for 1h at room temperature. The blots were scanned by a two-color infrared imaging system (Odyssey; LI-COR) to quantify the protein expression. The protein expression levels were normalized to the corresponding GAPDH levels.

Statistical Analysis

The results were presented as mean ± standard deviation (SD). Statistical differences between two groups were compared using Student's t-tests, and the differences between multiple groups were compared by two-way analysis of variance (ANOVA), followed by Tukey's multiple

comparisons test. All the data were analyzed using SPSS 26.0 software, and a p-value < 0.05 was considered statistically significant and was the threshold used to reject the null hypothesis.

RESULTS

MCC950 Alleviated Cardiac Dysfunction Induced by Transverse Aortic Constriction Surgery in Obese Mice

The ratio of heart weight (HW)/body weight (BW) increased after the TAC surgery, which revealed the compensatory cardiac weight gain (**Figure 1A**). MCC950 reversed these increases significantly. Six weeks after the TAC surgery, the cardiac function of the obese mice was significantly impaired, as shown by the decreased LVEF and LVFS and increased LVEDd and LVEDs (**Figures 1B–F** and **Supplementary Table 3**). MCC950 treatment increased LVEF and FS and reduced LVEDd and LVEDs after TAC. There was no difference in the heart rate (HR) between the four groups (**Figure 1G**). Taken together, MCC950 alleviated cardiac dysfunction induced by TAC surgery.

MCC950 Attenuated the Cardiac Hypertrophy Induced by Transverse Aortic Constriction Surgery in Obese Mice

Cardiac hypertrophy was induced by TAC surgery as shown by the gross morphology and coronal sections of the heart (**Figure 2A**). The size of cardiomyocytes increased significantly after TAC surgery as shown by the H&E and WGA staining (**Figures 2A,B**). The MCC950 treatment reversed the increased size of heart and cardiomyocytes induced by pressure overload (**Figures 2A,B**). In addition, MCC950 reduced the TAC-induced increased mRNA expression level of the genes related to cardiac hypertrophy, including atrial natriuretic peptide (ANP), brain natriuretic peptide (BNP), and β-myosin heavy chain (β-MHC) (**Figures 2C–E**). These results revealed that MCC950 attenuated the pressure-overload-induced cardiac hypertrophy in obese mice.

MCC950 Ameliorated the Cardiac Fibrosis Induced by Pressure Overload in Obese Mice

To validate the cardiac fibrosis induced by pressure overload, masson staining was conducted. Cardiac fibrosis was found around the peripheral blood vessels and in the myocardial interstitium, which was attenuated by the MCC950 treatment (**Figures 3A,B**). MCC950 also reduced the expression of α-SMA after TAC surgery (**Figures 3A,C**). Besides, the mRNA expression of COL1 and COL3 increased significantly after TAC surgery. MCC950 reversed this increase (**Figures 3D,E**). In addition, MCC950 attenuated the increased expression level of matrix metalloproteinase 2 (MMP-2) and MMP-9 induced by pressure overload (**Figures 3F,G**). MCC950 also reduced the protein levels of COL1 and COL3 after TAC surgery (**Figures 3H–J**). Together, these data indicated that MCC950 ameliorated the cardiac fibrosis induced by pressure overload in obese mice.

MCC950 Attenuated the Cardiac Inflammation Induced by Transverse Aortic Constriction Surgery in Obese Mice

The mRNA expression level of proinflammatory cytokines including IL1β and IL18 increased significantly after TAC surgery (**Figures 4A,B**). MCC950 reversed these increases. Interestingly, MCC950 also reduced the increased expression of anti-inflammatory cytokine IL10 induced by pressure overload (**Figure 4C**). In addition, MCC950 reduced the infiltration of macrophages induced by TAC surgery as shown by CD86 immunohistochemical staining (**Figures 4D,E**). We next examined the polarization of macrophages in the cardiac tissues. The immunofluorescence results showed that MCC950 treatment can significantly increase the expression of CD206, a marker of M2 macrophage (**Figures 4F,G**). And we also tested the mRNA expression levels of other markers of macrophage polarization. After TAC surgery, the expression of arginase 1 (ARG1, a marker of M2 macrophage) was significantly reduced, and the expressions of CD80 and CD86 (M1 macrophage markers) were significantly increased (**Figures 4H–J**). MCC950 treatment increased the expression of ARG1 and inhibited the expressions of CD80 and CD86. These results indicate that MCC950 treatment can induce M2 polarization of macrophages. Taken together, MCC950 attenuated the cardiac inflammation induced by pressure overload in obese mice.

MCC950 Reduced the Metabolic Reliance on Glucose in Failed Hearts

We next examined the levels of metabolism related biochemical parameters in the serum and heart after TAC surgery. MCC950 did not affect TG and NEFA in the serum of mice after TAC surgery (**Figures 5A,B**). After TAC surgery, the accumulation of TG, a storage form of FA, in the heart is significantly reduced, suggesting that the uptake of FA by myocardial tissue is reduced (**Figure 5C**). However, the MCC950 treatment can significantly increase the level of accumulated TG in the heart. The circulating levels of BHB decreased significantly after TAC surgery (**Figure 5D**). However, the MCC950 treatment did not affect the circulating levels of BHB. We also tested the circulating level of glucose and found that there was no significant change in the serum glucose levels either in TAC surgery or the MCC950 treatment group (**Figure 5E**). Glycogen, a storage form of glucose, increased significantly in the heart after TAC surgery, indicating that the cardiac tissue heavily relies on glucose after TAC. MCC950 can significantly reduce the accumulation of glycogen in the heart (**Figure 5F**). These results indicate that MCC950 treatment can reduce the dependence

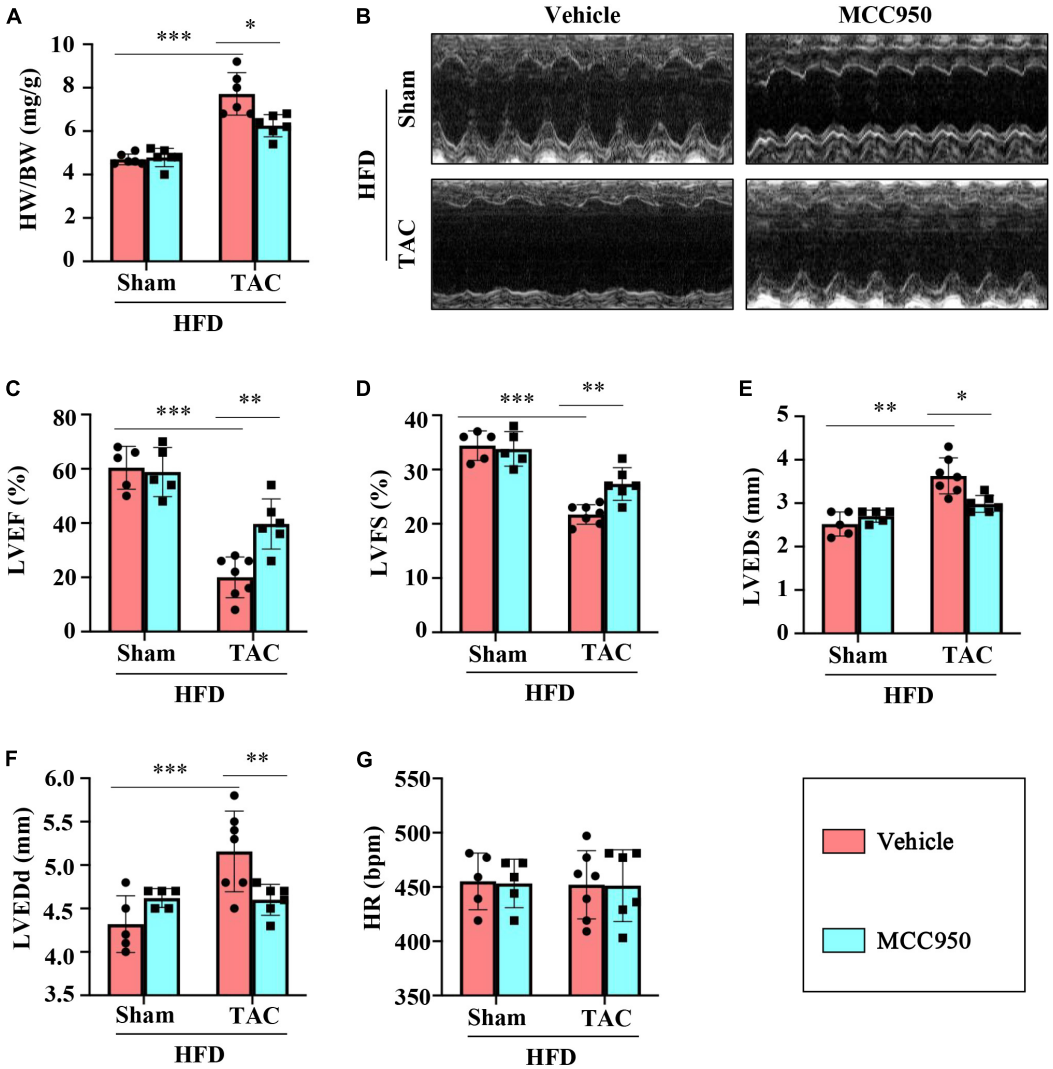

FIGURE 1 | MCC950 reversed the cardiac dysfunction post-TAC. **(A)** The ratio of heart weight (HW)/body weight (BW) in different groups, $n = 6$. **(B)** Representative images of echocardiography. **(C–G)** Echocardiography measurements of LVEDd, LVEDs, LVEF, LVFS, and HR, respectively, $n = 6$. LVEF, left ventricle ejection fraction; LVFS, left ventricle fractional shortening; LVEDs, LV end-systolic diameter; LVEDd, LV end-diastolic diameter; HR, heart rate. $^{*}p < 0.05$, $^{**}p < 0.01$, $^{***}p < 0.001$.

of cardiac tissue on glucose after HF, and at the same time restore the use of FA.

MCC950 Increased the Gene Expression for Fatty Acid Use in Obese Mice After Transverse Aortic Constriction Surgery

We first examined the mRNA expression of the genes relevant to FA uptake and oxidation, including peroxisome proliferator-activated receptor α (PPARα) and its co-activators PPARγ-coactivator-1(PGC1) α and β. MCC950 did not change the expression of these three genes in the mice after TAC surgery (**Figures 6A–C**). Consistent with these findings, MCC950 did not change the expression of the genes regulated by the PPARα/PGC1 complex, including carnitine palmitoyltransferase (CPT) 2, medium-chain acyl-CoA dehydrogenase (MCAD), short-chain acyl-CoA dehydrogenase (SCAD), and uncoupling protein 2 (UCP2) (**Figures 6D–G**). However, the MCC950 treatment significantly increased the mRNA expression of CPT1β, which plays an important role in the oxidation of FA, after TAC surgery (**Figure 6H**). We also tested the expression of genes involved in FA uptake, including fatty acid transport protein 1(FATP1) and thrombospondin receptor (CD36) (**Figures 6I,J**). Compared with the sham group, the mRNA expression of CD36 in the heart of the TAC group was significantly reduced. The MCC950 treatment can alleviate this reduction. This suggests that MCC950 can promote the intake of FA in the heart. In addition, we also tested the expression level of FA binding proteins (FABP) involved in the intracellular transport of FA (**Figures 6K,L**). MCC950 increased the expression of FABP4 and FABP5 in the hearts of mice in the TAC group,

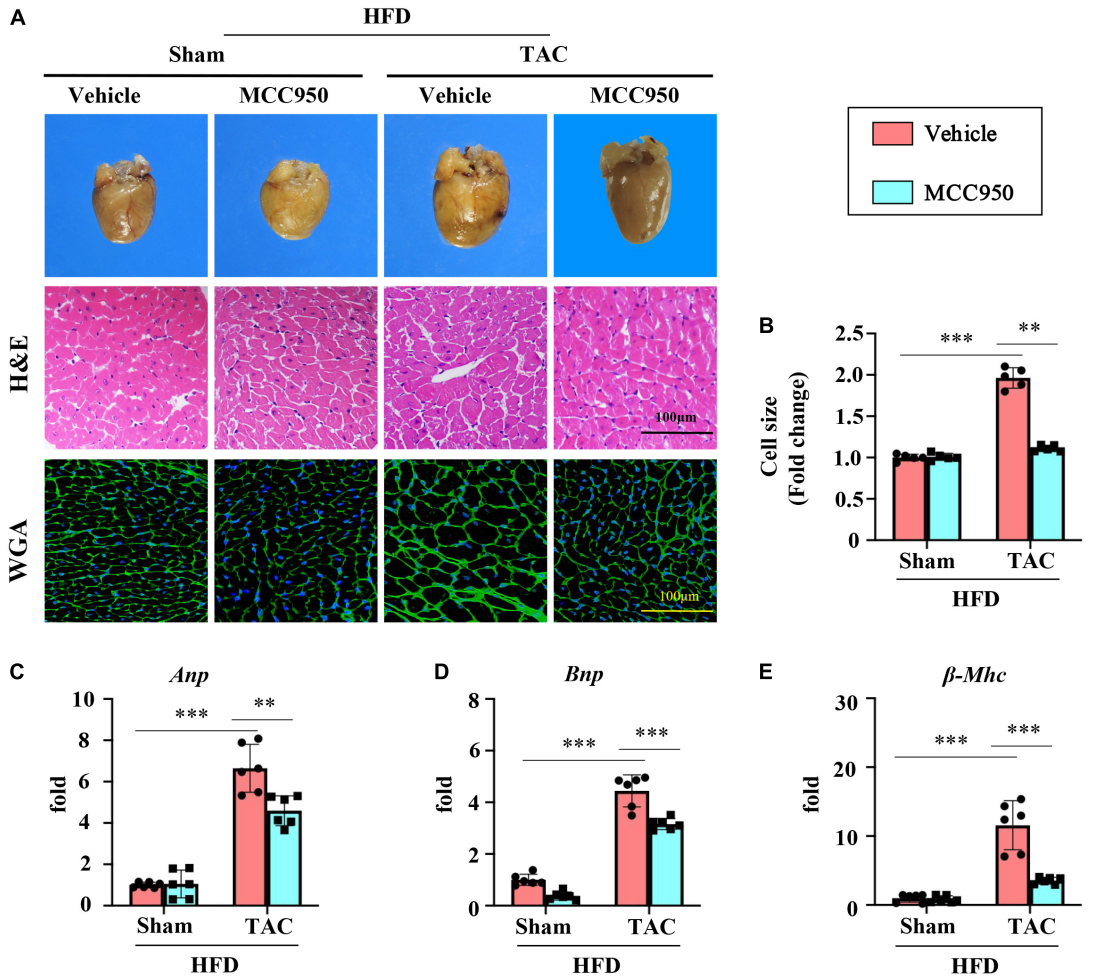

FIGURE 2 | MCC950 alleviated pressure overload-induced cardiac hypertrophy. **(A)** Representative photographs presenting morphology of the hearts, representative images of hematoxylin-eosin (H&E), and WGA staining for the determination of cardiomyocyte cell size, $n = 5$. **(B)** Cardiac hypertrophy was quantified by measuring the cross-sectional cell-surface area of cardiomyocyte from WGA staining, $n = 5$. **(C–E)** Q-PCR to measure mRNA expression of ANP, BNP, and β-MHC, respectively; $n = 6$. H&E, hematoxylin-eosin; WGA, wheat germ agglutinin; ANP, atrial natriuretic peptide; BNP, brain natriuretic peptide; β-MHC, β-myosin heavy chain. $^{*}p < 0.05$, $^{**}p < 0.01$, $^{***}p < 0.001$.

suggesting that it promoted the transport and oxidation of intracellular FA.

We further tested the protein expression levels of CPT1β and CD36 (**Figures 6M–O**). Compared with the sham group, the expression levels of CPT1β and CD36 in the heart of the TAC group were significantly reduced, and MCC950 significantly reversed this reduction. The key site regulating FA oxidation is the inhibition of CPT1β by malonyl-COA. The synthesis of malonyl-COA is regulated by ACC and the degradation is controlled by MCD. We tested the protein levels of ACC and MCD (**Figures 6P,Q**). After TAC surgery, p-ACC in the mouse heart was significantly reduced, suggesting an increase in ACC activity. Compared with mice in the sham group, the expression of MCD in the heart of the TAC group was reduced. The MCC950 treatment can significantly increase the phosphorylation level of ACC and increase the protein level of MCD. These results indicate that MCC950 can restore the uptake and oxidation of FA in the cardiac tissue after HF in obese mice.

MCC950 Regulated the Gene Expression Relevant to Glucose Metabolism in Obese Mice After Transverse Aortic Constriction Surgery

We then examined the mRNA expression of the gene relevant to glucose metabolism. In the heart, the most abundant GLUTs are GLUT1 and GLUT4, which are of great significance for the uptake and transport of glucose. The mRNA expression of GLUT1 increased, while the expression of GLUT4 decreased after TAC surgery (**Figures 7A,B**). Interestingly, MCC950 reversed the increase of GLUT1 induced by pressure overload. Consistently, the total protein expression levels of GLUT1 increased, while GLUT4 decreased after TAC surgery (**Figures 7E–G**). MCC950

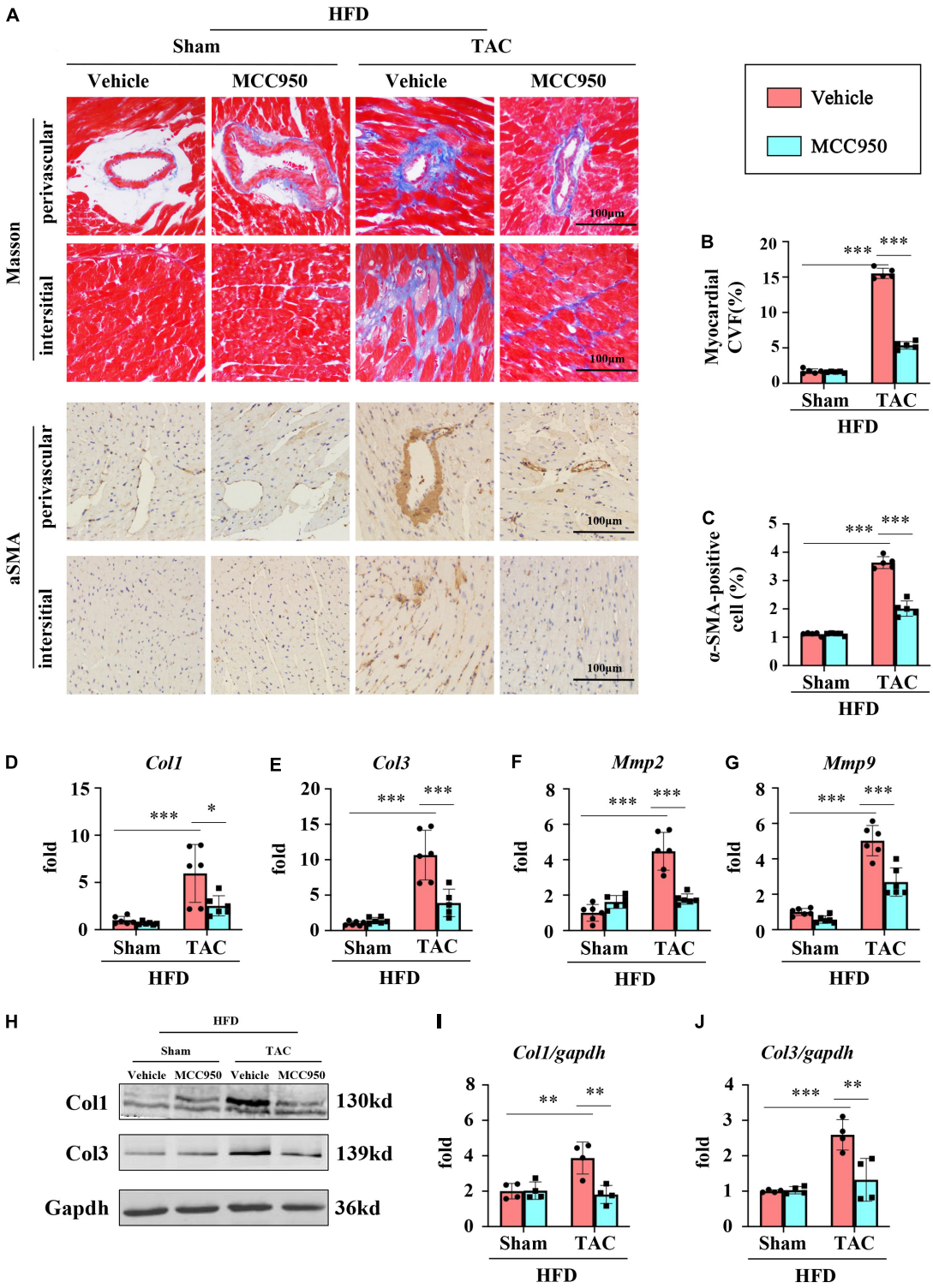

FIGURE 3 | MCC950 ameliorates pressure overload-induced cardiac fibrosis. **(A)** Representative images of Masson's trichrome and αSMA immunohistochemistry staining, $n = 5$. **(B)** Statistical results for the fibrotic areas in the indicated groups, $n = 5$. **(C)** Statistical results for the αSMA positive cells in the indicated groups, $n = 5$. **(D)** Relative mRNA expression of COL1, **(E)** COL3, **(F)** MMP-2, **(G)** MMP-9, $n = 6$. **(H–J)** Representative Western blot and quantitative analysis showing the expression levels of COL1 and COL3. αSMA, α-smooth muscle actin; COL, collagen; MMP, matrix metalloproteinase. $^{*}p < 0.05$, $^{**}p < 0.01$, $^{***}p < 0.001$.

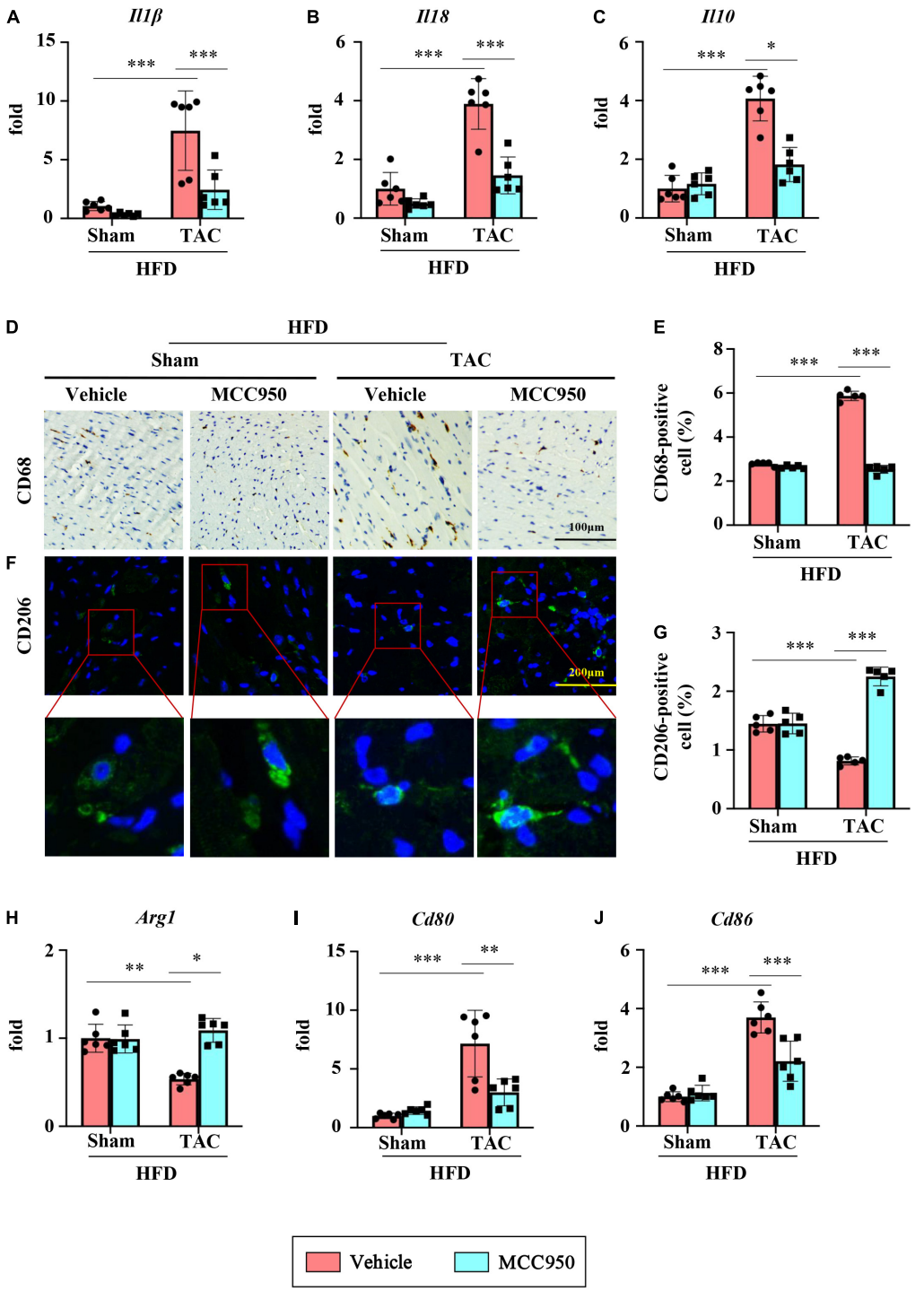

FIGURE 4 | MCC950 attenuates pressure overload-induced cardiac inflammation. Relative mRNA expression of **(A)** IL1β, **(B)** IL18, and **(C)** IL10, $n = 6$. **(D,E)** Immunohistochemical analysis of CD68, $n = 3$. **(F,G)** immunofluorescence analysis of CD206, $n = 3$. **(H–J)** Relative mRNA expression of Arg1, CD80, and CD86, $n = 6$. IL, interleukin; Arg1, arginase 1. $^{*}p < 0.05$, $^{**}p < 0.01$, $^{***}p < 0.001$.

reduced the level of GLUT1 and increased the level of GLUT4. Glycolysis increases the supply of pyruvate for mitochondrial glucose oxidation through the PDH complex, the rate-limiting enzyme for glucose oxidation. The activity of PDH in the cardiac tissue increased significantly after TAC surgery and recovered after the MCC950 treatment (**Figure 7C**). The activity of PDH is mainly regulated by its phosphorylation state and is active when it is dephosphorylated. Consistently, the ratio

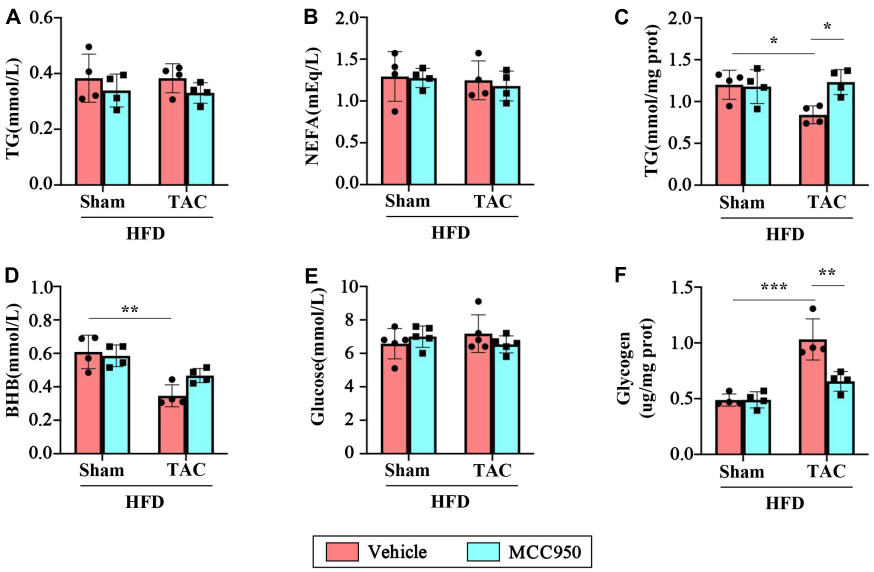

FIGURE 5 | MCC950 reduced the metabolic reliance on glucose in TAC hearts. Serum levels of TG **(A)** and NEFA **(B)**, $n = 4$. **(C)** Level of TG in the cardiac, $n = 4$. Serum levels of BHB **(D)** and glucose **(E)**, $n = 4$. **(F)** glycogen levels in the cardiac, $n = 4$. TG, triglyceride; NEFA, non-esterified fatty acids; BHB, β-hydroxybutyrate. $^{*}p < 0.05$, $^{**}p < 0.01$, $^{***}p < 0.001$.

of p-PDH to t-PDH is significantly reduced after TAC surgery, and the MCC950 treatment can promote PDH phosphorylation (**Figure 7H**). The PDH complex can be phosphorylated and inhibited by pyruvate dehydrogenase kinase (PDK). Our results suggest that the mRNA expression level and protein expression level of PDK4 are significantly reduced after TAC surgery, and MCC950 can effectively promote the expression of PDK4 (**Figures 7D,I**). These results suggest that MCC950 can regulate the expression of genes related to glucose metabolism after HF in obese mice.

MCC950 Attenuated Cardiometabolic Disorder *via* the Protein Kinase B/AMP-Activated Protein Kinase α Pathway

We first examined the inhibitory effect on the activation of NLRP3 of MCC950. The expression level of c-caspase-1 and IL-1β increased after pressure overload, suggesting that the NLRP3 inflammasome was activated. The selective inhibitor of NLRP3, MCC950, significantly reversed these increases (**Figures 8A–E**). AMPK acts as an energy sensor to regulate multiple physiological processes in the cardiovascular system. Previous studies have shown that AMPK can improve HF by restoring energy supply and mitochondrial function (27). We detected the level of t-AMPKα and p-AMPKα. The level of p-AMPKα decreased after TAC surgery and increased with MCC950 treatment (**Figure 8F**). In addition, we also examined the phosphorylation level of AKT, an upstream regulator of AMPKα. The ratio of p-AKT to t-AKT increased after TAC surgery while it decreased with the MCC950 treatment (**Figure 8G**). Taken together, these results suggested that MCC950 attenuated cardiac metabolic disorder *via* AKT/AMPKα pathway (**Figure 9**).

DISCUSSION

In the present study, MCC950 significantly ameliorated the cardiac dysfunction, hypertrophy, and fibrosis induced by pressure overload in obese mice. The increased inflammation after TAC surgery was attenuated by the MCC950 treatment. Besides, MCC950 reversed the cardiac metabolic disorder *via* AKT/AMPK pathway as shown by the regulation of glucose and FA uptake and oxidation. Taken together, these results suggested the treatment effect of MCC950 in obese mice with HF.

MCC950 Protected Left Ventricle Function and Structure in Obese Mice With Pressure Overload

Many reports indicated that NLRP3 inflammasome may be a new promising effective therapeutic target to slow down the disease progression of HF (28). Our previous study found that MCC950 can reverse HF induced by pressure overload in mice (29). This study further indicated that MCC950 can also effectively improve LV function in obese mice, as shown by improved LVEF and FS. The improvement of cardiac function may be related to the alleviated cardiac remodeling by the MCC950 treatment. MCC950 can significantly inhibit heart enlargement and cardiac hypertrophy. In addition, the MCC950 treatment ameliorated cardiac fibrosis induced by pressure overload, as shown by the alleviated expression of COL1, COL3, and a-SMA. In short, MCC950 protected LV function and structure in obese mice with pressure overload.

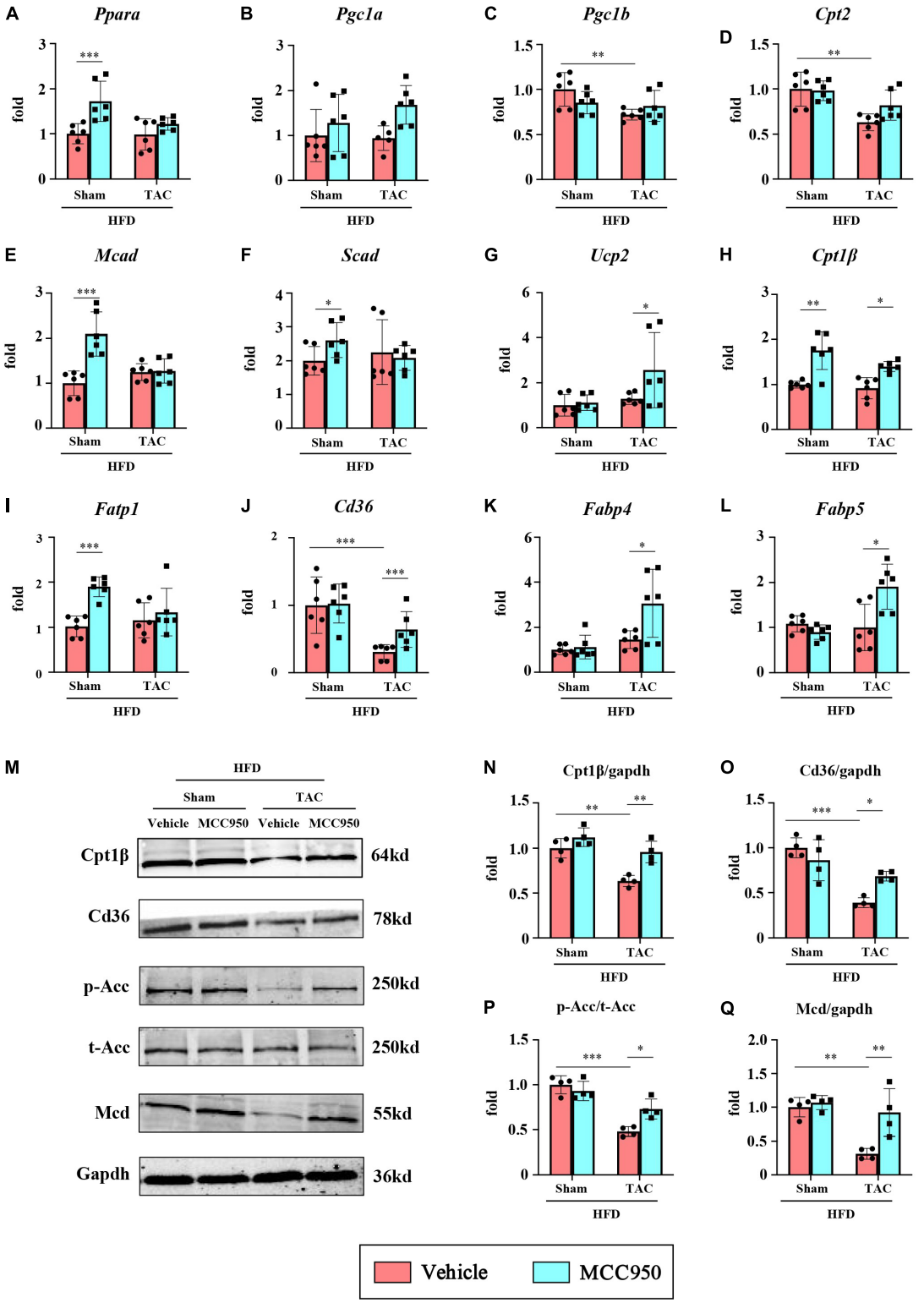

FIGURE 6 | MCC950 increased the gene expression for FA use in obese mice after TAC surgery. Relative mRNA expression of **(A)** PPARα, **(B)** PGC1α, **(C)** PGC1β, **(D)** CPT2, **(E)** MCAD, **(F)** SCAD, **(G)** UCP2, **(H)** CPT1β, **(I)** FATP1, **(J)** CD36, **(K)** FABP4, **(L)** FABP5, $n = 6$. **(M–Q)** Representative blots and quantitative analysis showing the expression levels of CPT1β, CD36, p-ACC, t-ACC, and MCD, $n = 4$. PPAR, peroxisome proliferator-activated receptor; PGC1, PPARγ-coactivator-1; CPT, carnitine palmitoyl transferase; MCAD, medium-chain acyl-CoA dehydrogenase; SCAD, short-chain acyl-CoA dehydrogenase; UCP2, uncoupling protein 2; FATP, FA transport protein; FABP, FA binding protein. ACC, acetyl-CoA carboxylase; MCD, malonyl-CoA decarboxylase. $^{*}p < 0.05$, $^{**}p < 0.01$, $^{***}p < 0.001$.

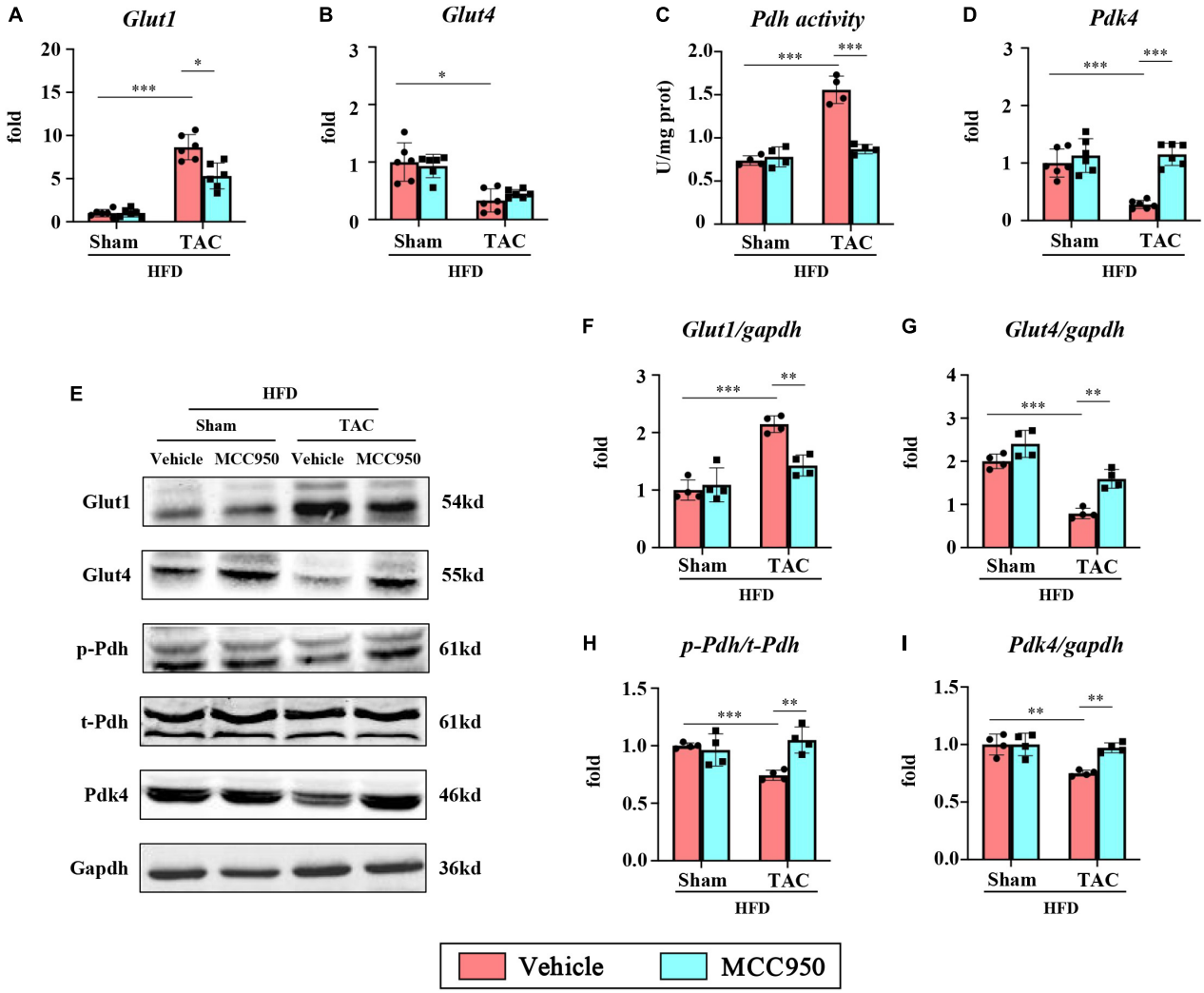

FIGURE 7 | MCC950 regulated the gene expression relevant to glucose metabolism in obese mice after TAC surgery. Relative mRNA expression of **(A)** GLUT1 and **(B)** GLUT4, $n = 6$. **(C)** PDH activity in the cardiac tissue, $n = 4$. **(D)** Relative mRNA expression of PDK4, $n = 6$. **(E–I)** Representative blots and quantitative analysis showing the expression levels of GLUT1, GLUT4, p-PDH, t-PDH, and PDK4, $n = 4$. GLUT, glucose transporter; PDH, pyruvate dehydrogenase; PDK, pyruvate dehydrogenase kinase. $^{*}p < 0.05$, $^{**}p < 0.01$, $^{***}p < 0.001$.

MCC950 Ameliorated Cardiac Inflammation After Transverse Aortic Constriction Surgery in Obese Mice

Inflammatory responses play an important role in the development of HF. IL1β is one of the most important proinflammatory cytokines involved in HF. The link between IL1β and HF is supported by the elevated level of IL1β in patients with worsening HF symptoms and outcomes (30). Direct reduction of IL1β levels or blocking of the downstream signal of IL1β contribute to helpful cardiac remodeling and improvements of HF phenotype induced by ischemia/infarction, pressure overload, or anthracycline toxicity (31). As the maturation of IL1β is regulated *via* the activation of the NLRP3 inflammasome, NLRP3 is considered a potential therapeutics target for HF. The cardiac beneficial effects of some molecules are reported to be relevant to the inhibition of the NLRP3 inflammasome (32, 33). Treatments inhibiting the activation of NLRP3 contributed to improved cardiac function and remodeling in the mice with myocardial infarction and cardiac hypertrophy (18, 34). Corresponding with these reports, MCC950 significantly inhibited the activation of NLRP3, preserved cardiac function, and alleviated the inflammation post pressure overload in obese mice. The expression levels of IL1β and other cytokines were significantly reduced, which may contribute to the improvement of HF phenotype and cardiac remodeling. In addition, the MCC950 treatment induced M2 polarization as shown by the increased expression of CD206 and ARG1. The NLRP3 inflammasome was reported to induce M1 polarization in the previous studies (19). In our study, we did not discuss the mechanism by which MCC950 induced M2 polarization. Studies

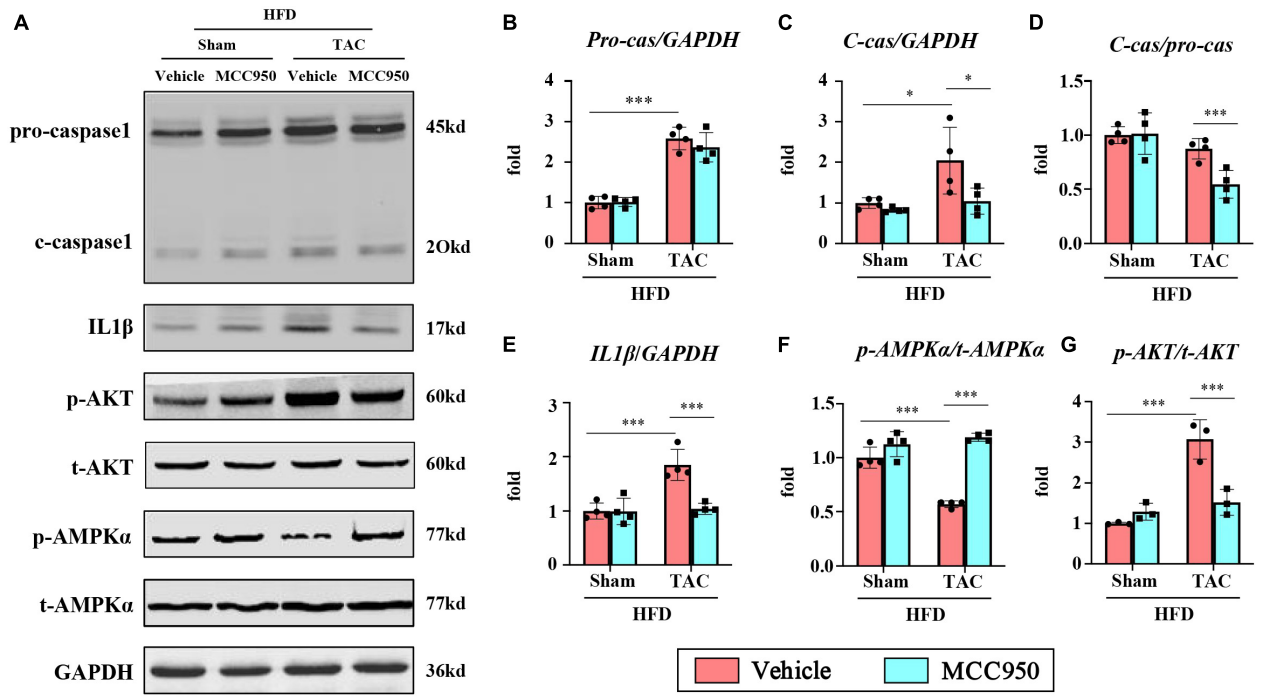

FIGURE 8 | MCC950 attenuated cardiometabolic disorder *via* AKT/AMPK pathway. **(A)** Representative Western blot and quantitative analysis showing the expression levels of **(B)** pro-caspase-1, **(C)** c-caspase-1, **(D)** the ratio of c-caspase-1/pro-caspase-1, **(E)** IL-1β, **(F)** p-AMPKα, and **(G)** p-AKT in different groups, $n = 4$. IL, interleukin; AKT, phospho-protein kinase B; AMPKα, AMP-activated protein kinase α. $^{*}p < 0.05$, $^{**}p < 0.01$, $^{***}p < 0.001$.

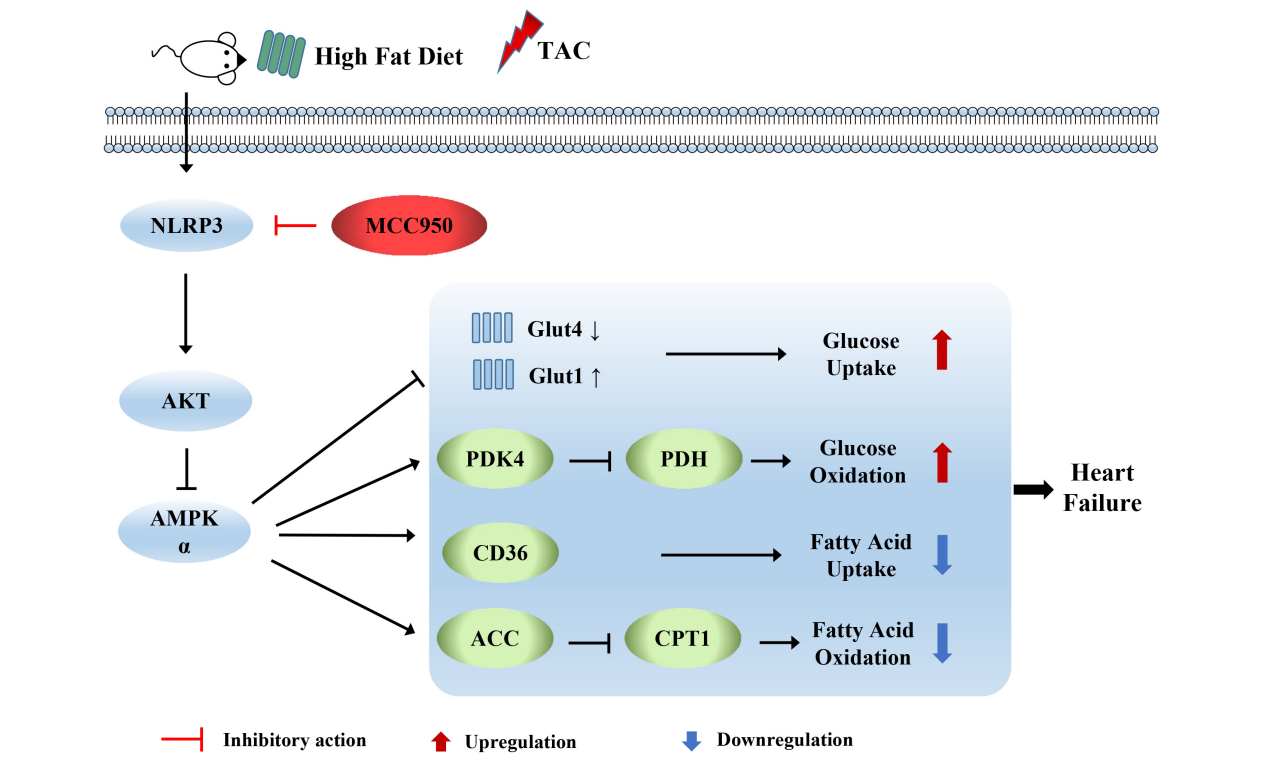

FIGURE 9 | Diagram depicting the mechanism by which MCC950 regulates cardiometabolism in obese mice with heart failure.

have shown that macrophage polarization is closely related to cell metabolism (35). Therefore, we speculate that in addition to inhibiting the IL1β expression, MCC950 may also induce M2 polarization by affecting the cell metabolism, which needs further exploration.

MCC950 Treatment Alleviated the Glucose Dependence of Cardiometabolism in Obese Mice With Heart Failure

Fatty acid is the primary fuel for cardiomyocytes to produce energy in normal adults. But in the development of pathological hypertrophy and HF, cardiomyocytes reduce FA-derived energy and increase glycolysis, anaplerosis, and other forms of metabolism, such as the use of lactate, branched-chain amino acids, and ketone bodies, remodeling ATP production mechanism. This shift in the energy production machinery is known as metabolic reprogramming and is accompanied by the downregulation of genes involved in mitochondrial energy transduction and respiratory pathways (12). In our study, we did not observe the changes in TG, glucose, and NEFA in the serum of obese mice after HF. Only the serum levels of BHB were significantly decreased after HF, suggesting that cardiac utilization of BHB was increased after HF. MCC950 treatment had no apparent effect on the levels of these markers in the serum of obese mice, which may be related to the HFD diet during the experiment. However, we observed decreased TG accumulation and increased glycogen levels in the LV of obese mice after HF, suggesting that mouse cardiometabolism relies more on glucose after HF. Furthermore, the MCC950 treatment increased TG accumulation and decreased glycogen levels in the heart. In a word, MCC950 treatment alleviated the glucose dependence of cardiometabolism and restored FA uptake and utilization.

MCC950 May Promote Cardiac Fatty Acid Metabolism in Obese Mice With Pressure Overload

In our study, MCC950 did not significantly alter the expression of some genes related to FA metabolism, such as PPARα, PGC1α, and β, CPT2, MCAD, SCAD, and UCP2, which may be related to the HFD in the experiment. HFD has been reported to affect the progression of HF and may also affect the expression of metabolism-related genes (36). However, we observed a marked decrease in the expression of CD36 and CPT1β after HF. CD36 plays an important role in FA uptake in the cardiac. The CD36 knockout mice showed reduced rates of FA transport and oxidation, and significantly increased glucose use in the heart, ultimately exacerbating stress overload-induced HF (37). CPT1β is the rate-limiting step in mitochondrial β-oxidation by controlling mitochondrial uptake of long-chain acyl-CoA. It has been reported that the CPT1β deficiency exacerbates pressure overload-induced cardiac hypertrophy (38). The current findings suggest that MCC950 promoted the expression of CD36 and CPT1β after TAC surgery, implying that MCC950 can promote FA transport and oxidation in the hearts of obese mice with HF. Furthermore, CPT1β is inhibited by malonyl-CoA, the carboxylation product of acetyl-CoA, which is produced by the action of ACC and decarboxylated by MCD (39). In this study, MCC950 increased the phosphorylation level of ACC and increased the expression of MCD, thereby reducing the production of malonyl-CoA and promoting its degradation, ultimately increasing the level of CPT1β.

Modulation of cardiometabolic substrates is one of the strategies for the treatment of HF. However, FA is often discarded due to its high oxygen consumption and potential lipotoxicity (40). Considering that FA produces approximately three times as much ATP per molecule as glucose, it is impossible to rely on glucose alone to provide energy for cardiometabolism. Enhancing FA metabolic preference may be another strategy to restore cardiac energy and function. In our study, MCC950 not only increased the expression of CD36 but also promoted the expression of CPT1β. This means that MCC950 promotes the uptake and oxidation of FA in the heart, which may alleviate the lipotoxicity caused by the accumulation of FA. Taken together, the effect of MCC950 on CD36 and CPT-1β suggests that it may have a benign regulatory effect on cardiac FA metabolism, although it requires further exploration.

MCC950 Reduced Cardiac Glucose Uptake and Utilization in Obese Mice With Heart Failure

The first step in carbohydrate metabolism involves the uptake of glucose by cardiomyocytes through the action of GLUTs. Glucose transport by these proteins is one of the rate-limiting steps in substrate utilization in the myocardium (41). GLUT4 is insulin-sensitive and is the major isoform in adult myocardium. GLUT1 is insulin-independent and mainly expressed in the fetal heart (39). The GLUT4/GLUT1 ratio has been reported to be reduced in patients with LV hypertrophy (42). Similar observations were made in animal models of pathological cardiac hypertrophy. The pressure overload increased GLUT1 expression but decreased GLUT4 expression, and these changes were associated with increased distribution of both transporters to the plasma membrane (43). Changes from GLUT4 to GLUT1 have been found in failed myocardium, but the mechanism remains unknown (44). Insulin resistance may be one of the reasons why GLUT4 expression is suppressed during HF (45). Therefore, GLUT1 expression may be increased to compensate. In this study, MCC950 significantly downregulated the expression of GLUT1 and restored the content of GLUT4, which may be related to the improvement of insulin resistance after HF by MCC950. The activation of NLRP3 is closely related to insulin resistance in many metabolic diseases (19). In a word, MCC950 promotes glucose uptake in failed hearts in a GLUT4-dependent manner.

Glucose is metabolized by oxidative metabolism under aerobic conditions, or by anaerobic glycolysis in the presence of hypoxia. The pyruvate derived from glucose is converted by PDH to acetyl-CoA for aerobic respiration and is inhibited when phosphorylated by PDH kinase (46). In the mice with HF, the source of cardiac energy changed from FA-dominated to glucose-oxidized-dominant. Consistent with the previous studies, the activity of PDH was significantly increased

after TAC surgery. The p-PDH expression and p-PDH/t-PDH ratio were significantly decreased after TAC surgery. The PDK4 expression was significantly reduced in failed hearts. The MCC950 treatment reversed PDH activity and increased PDK4 expression, promoting PDH phosphorylation. These results suggest that the MCC950 treatment reduces glucose oxidation, which may be associated with the restoration of FA metabolism.

MCC950 Attenuated Cardiometabolic Disorder *via* Protein Kinase B/AMP-Activated Protein Kinase α Pathway in Obese Mice

The changes in AKT activity are an alteration in pathological cardiac hypertrophy. AKT activation not only stimulates protein synthesis and growth but also integrates intracellular signaling into nutrient metabolism by promoting cell membrane translocation of GLUT4 and gene expression of glucokinase and FA synthase. In the absence of AKT, the expression levels of the genes responsible for glucose utilization and lipid synthesis were significantly reduced (47). AMPK, one of the downstream signals of AKT, acts as an energy sensor that regulates multiple physiological processes in the cardiovascular system and maybe a potential therapeutic target for HF. AMPK can similarly mediate the translocation of GLUT4, thereby increasing glucose uptake as a cardioprotective and adaptive response of the failed heart (48). AMPK also inhibits glycogen synthesis and promotes glucose oxidation (49). In addition, AMPK promotes the absorption and oxidation of FA. It increases the translocation of CD36 to the membrane and promotes FA uptake by cardiomyocytes. The Activated AMPK increases the CPT-1β activity by reducing malonyl-CoA production by inhibiting the ACC activity. Therefore, AMPK can increase FA oxidation (50). All of these effects ultimately increase ATP production to improve the imbalance between energy supply and energy demand in the failed heart. Moreover, previous studies reported that MCC950 exerts a protective effect by inducing autophagy through an AMPK-dependent mechanism (51). Consistent with previous reports, AKT activation was increased while AMPKα activation was inhibited after TAC surgery. The MCC950 treatment inhibited AKT activation and increased the phosphorylation levels of AMPKα. The effect of MCC950 on the AKT/AMPKα pathway may explain the changes in cardiometabolism, which needs further research.

This study has several limitations. We only explored the effect of MCC950 on metabolism after HF *in vivo*. Studies *in vitro* may help to explore the mechanism of the protective role of MCC950. In addition, the effects of MCC950 on HFD-induced metabolism dysfunction need further exploration.

CONCLUSION

In conclusion, the most important finding is the protective role of MCC950 in alleviating HF induced by pressure overload in obese mice, and its mechanism is related to the improvement of cardiac metabolism. Our study provides a basis for the clinical application of NLRP3 inhibitors in obese patients with HF.

DATA AVAILABILITY STATEMENT

The original contributions presented in the study are included in the article/**Supplementary Material**, further inquiries can be directed to the corresponding author.

ETHICS STATEMENT

The animal study was reviewed and approved by the Animal Care and Use Committee of Renmin Hospital of Wuhan University.

AUTHOR CONTRIBUTIONS

MW, MZ, and JYu contributed to the experimental design and wrote the manuscript. JL, JYe, ZW, and YX contributed to the acquisition and analysis of the data. ZZ, DY, YF, SX, WP, JZ, and JW reviewed the manuscript. All authors contributed to the article and approved the submitted version.

FUNDING

This work was supported by grants from the National Natural Science Foundation of China (82070436) and the Natural Science Foundation of Hubei Province (2020CFB234).

SUPPLEMENTARY MATERIAL

The Supplementary Material for this article can be found online at: https://www.frontiersin.org/articles/10.3389/fcvm.2022.727474/full#supplementary-material

REFERENCES

1. Mosterd A, Hoes AW. Clinical epidemiology of heart failure. *Heart.* (2007) 93:1137–46. doi: 10.1136/hrt.2003.025270
2. Kenchaiah S, Evans JC, Levy D, Wilson PW, Benjamin EJ, Larson MG, et al. Obesity and the risk of heart failure. *N Engl J Med.* (2002) 347:305–13.
3. Kenchaiah S, Sesso HD, Gaziano JM. Body mass index and vigorous physical activity and the risk of heart failure among men. *Circulation.* (2009) 119:44–52. doi: 10.1161/circulationaha.108.807289
4. Levitan EB, Yang AZ, Wolk A, Mittleman MA. Adiposity and incidence of heart failure hospitalization and mortality: a population-based prospective study. *Circ Heart Fail.* (2009) 2:202–8.
5. Neeland IJ, Gupta S, Ayers CR, Turer AT, Rame JE, Das SR, et al. Relation of regional fat distribution to left ventricular structure and function. *Circ Cardiovasc Imaging.* (2013) 6:800–7. doi: 10.1161/CIRCIMAGING.113.000532
6. Shiou YL, Huang IC, Lin HT, Lee HC. High fat diet aggravates atrial and ventricular remodeling of hypertensive heart disease in aging rats. *J Formos Med Assoc.* (2018) 117:621–31. doi: 10.1016/j.jfma.2017.08.008

7. Holzem KM, Marmerstein JT, Madden EJ, Efimov IR. Diet-induced obesity promotes altered remodeling and exacerbated cardiac hypertrophy following pressure overload. *Physiol Rep.* (2015) 3:e12489. doi: 10.14814/phy2.12489
8. Reddy SS, Agarwal H, Barthwal MK. Cilostazol ameliorates heart failure with preserved ejection fraction and diastolic dysfunction in obese and non-obese hypertensive mice. *J Mol Cell Cardiol.* (2018) 123:46–57. doi: 10.1016/j.yjmcc.2018.08.017
9. Zhang L, Jaswal JS, Ussher JR, Sankaralingam S, Wagg C, Zaugg M, et al. Cardiac insulin-resistance and decreased mitochondrial energy production precede the development of systolic heart failure after pressure-overload hypertrophy. *Circ Heart Fail.* (2013) 6:1039–48. doi: 10.1161/CIRCHEARTFAILURE.112.000228
10. Neubauer S. The failing heart–an engine out of fuel. *N Engl J Med.* (2007) 356:1140–51. doi: 10.1056/NEJMra063052
11. Aubert G, Vega RB, Kelly DP. Perturbations in the gene regulatory pathways controlling mitochondrial energy production in the failing heart. *Biochim Biophys Acta.* (2013) 1833:840–7. doi: 10.1016/j.bbamcr.2012.08.015
12. Nakamura M, Sadoshima J. Mechanisms of physiological and pathological cardiac hypertrophy. *Nat Rev Cardiol.* (2018) 15:387–407. doi: 10.1038/s41569-018-0007-y
13. Kolwicz SC Jr., Olson DP, Marney LC, Garcia-Menendez L, Synovec RE, Tian R. Cardiac-specific deletion of acetyl CoA carboxylase 2 prevents metabolic remodeling during pressure-overload hypertrophy. *Circ Res.* (2012) 111:728–38. doi: 10.1161/CIRCRESAHA.112.268128
14. Cai J, Shi G, Zhang Y, Zheng Y, Yang J, Liu Q, et al. Taxifolin ameliorates DEHP-induced cardiomyocyte hypertrophy via attenuating mitochondrial dysfunction and glycometabolism disorder in chicken. *Environ Pollut.* (2019) 255:113155. doi: 10.1016/j.envpol.2019.113155
15. Latz E, Xiao TS, Stutz A. Activation and regulation of the inflammasomes. *Nat Rev Immunol.* (2013) 13:397–411. doi: 10.1038/nri3452
16. Butts B, Butler J, Dunbar SB, Corwin E, Gary RA. Effects of exercise on ASC methylation and IL-1 cytokines in heart failure. *Med Sci Sports Exerc.* (2018) 50:1757–66. doi: 10.1249/MSS.0000000000001641
17. Tang X, Pan L, Zhao S, Dai F, Chao M, Jiang H, et al. SNO-MLP (S-nitrosylation of muscle LIM Protein) facilitates myocardial hypertrophy through TLR3 (toll-like receptor 3)-mediated RIP3 (receptor-interacting protein kinase 3) and NLRP3 (NOD-like receptor pyrin domain containing 3) inflammasome activation. *Circulation.* (2020) 141:984–1000. doi: 10.1161/CIRCULATIONAHA.119.042336
18. Li X, Zhu Q, Wang Q, Zhang Q, Zheng Y, Wang L, et al. Protection of sacubitril/valsartan against pathological cardiac remodeling by inhibiting the NLRP3 inflammasome after relief of pressure overload in mice. *Cardiovasc Drugs Ther.* (2020) 34:629–40. doi: 10.1007/s10557-020-06995-x
19. Haneklaus M, O'Neill LA. NLRP3 at the interface of metabolism and inflammation. *Immunol Rev.* (2015) 265:53–62. doi: 10.1111/imr.12285
20. Zhao Q, Bi Y, Guo J, Liu YX, Zhong J, Pan LR, et al. Pristimerin protects against inflammation and metabolic disorder in mice through inhibition of NLRP3 inflammasome activation. *Acta Pharmacol Sin.* (2020) 42:975–86. doi: 10.1038/s41401-020-00527-x
21. Youm YH, Nguyen KY, Grant RW, Goldberg EL, Bodogai M, Kim D, et al. The ketone metabolite β-hydroxybutyrate blocks NLRP3 inflammasome-mediated inflammatory disease. *Nat Med.* (2015) 21:263–9. doi: 10.1038/nm.3804
22. Deng Y, Xie M, Li Q, Xu X, Ou W, Zhang Y, et al. Targeting mitochondria-inflammation circuit by β-hydroxybutyrate mitigates HFpEF. *Circ Res.* (2021) 128:232–45. doi: 10.1161/CIRCRESAHA.120.317933
23. Xu L, Kim JK, Bai Q, Zhang X, Kakiyama G, Min HK, et al. 5-cholesten-3β,25-diol 3-sulfate decreases lipid accumulation in diet-induced nonalcoholic fatty liver disease mouse model. *Mol Pharmacol.* (2013) 83:648–58. doi: 10.1124/mol.112.081505
24. Gao R, Shi H, Chang S, Gao Y, Li X, Lv C, et al. The selective NLRP3-inflammasome inhibitor MCC950 reduces myocardial fibrosis and improves cardiac remodeling in a mouse model of myocardial infarction. *Int Immunopharmacol.* (2019) 74:105575. doi: 10.1016/j.intimp.2019.04.022
25. Li X, Yang W, Ma W, Zhou X, Quan Z, Li G, et al. 18F-FDG PET imaging-monitored anti-inflammatory therapy for acute myocardial infarction: exploring the role of MCC950 in murine model. *Journal of Nuclear Cardiology.* (2021) 28:2346–57. doi: 10.1007/s12350-020-02044-0
26. Wang Z, Xu Y, Wang M, Ye J, Liu J, Jiang H, et al. TRPA1 inhibition ameliorates pressure overload-induced cardiac hypertrophy and fibrosis in mice. *EBioMedicine.* (2018) 36:54–62. doi: 10.1016/j.ebiom.2018.08.022
27. Li X, Liu J, Lu Q, Ren D, Sun X, Rousselle T, et al. AMPK: a therapeutic target of heart failure-not only metabolism regulation. *Biosci Rep.* (2019) 39:BSR20181767. doi: 10.1042/BSR20181767
28. Del Buono MG, Crea F, Versaci F, Biondi-Zoccai G. NLRP3 inflammasome: a new promising therapeutic target to treat heart failure. *J Cardiovasc Pharmacol.* (2021) 77:159–61. doi: 10.1097/FJC.0000000000000946
29. Zhao M, Zhang J, Xu Y, Liu J, Ye J, Wang Z, et al. Selective inhibition of NLRP3 inflammasome reverses pressure overload-induced pathological cardiac remodeling by attenuating hypertrophy, fibrosis, and inflammation. *Int Immunopharmacol.* (2021) 99:108046. doi: 10.1016/j.intimp.2021.108046
30. Testa M, Yeh M, Lee P, Fanelli R, Loperfido F, Berman JW, et al. Circulating levels of cytokines and their endogenous modulators in patients with mild to severe congestive heart failure due to coronary artery disease or hypertension. *J Am Coll Cardiol.* (1996) 28:964–71. doi: 10.1016/s0735-1097(96)00268-9
31. Abbate A, Toldo S, Marchetti C, Kron J, Van Tassell BW, Dinarello CA. Interleukin-1 and the inflammasome as therapeutic targets in cardiovascular disease. *Circ Res.* (2020) 126:1260–80. doi: 10.1161/CIRCRESAHA.120.315937
32. Byrne NJ, Matsumura N, Maayah ZH, Ferdaoussi M, Takahara S, Darwesh AM, et al. Empagliflozin blunts worsening cardiac dysfunction associated with reduced NLRP3 (Nucleotide-binding domain-like receptor protein 3) inflammasome activation in heart failure. *Circ Heart Fail.* (2020) 13:e006277. doi: 10.1161/CIRCHEARTFAILURE.119.006277
33. Byrne NJ, Soni S, Takahara S, Ferdaoussi M, Al Batran R, Darwesh AM, et al. Chronically elevating circulating ketones can reduce cardiac inflammation and blunt the development of heart failure. *Circ Heart Fail.* (2020) 13:e006573. doi: 10.1161/CIRCHEARTFAILURE.119.006573
34. van Hout GP, Bosch L, Ellenbroek GH, de Haan JJ, van Solinge WW, Cooper MA, et al. The selective NLRP3-inflammasome inhibitor MCC950 reduces infarct size and preserves cardiac function in a pig model of myocardial infarction. *Eur Heart J.* (2017) 38:828–36. doi: 10.1093/eurheartj/ehw247
35. Zhu L, Zhao Q, Yang T, Ding W, Zhao Y. Cellular metabolism and macrophage functional polarization. *Int Rev Immunol.* (2015) 34:82–100. doi: 10.3109/08830185.2014.969421
36. Heyne E, Schrepper A, Doenst T, Schenkl C, Kreuzer K, Schwarzer M. High-fat diet affects skeletal muscle mitochondria comparable to pressure overload-induced heart failure. *J Cell Mol Med.* (2020) 24:6741–9. doi: 10.1111/jcmm.15325
37. Umbarawan Y, Syamsunarno MRAA, Koitabashi N, Obinata H, Yamaguchi A, Hanaoka H, et al. Myocardial fatty acid uptake through CD36 is indispensable for sufficient bioenergetic metabolism to prevent progression of pressure overload-induced heart failure. *Sci Rep.* (2018) 8:12035. doi: 10.1038/s41598-018-30616-1
38. He L, Kim T, Long Q, Liu J, Wang P, Zhou Y, et al. Carnitine palmitoyltransferase-1b deficiency aggravates pressure overload-induced cardiac hypertrophy caused by lipotoxicity. *Circulation.* (2012) 126:1705–16. doi: 10.1161/CIRCULATIONAHA.111.075978
39. Pasqua T, Rocca C, Giglio A, Angelone T. Cardiometabolism as an interlocking puzzle between the healthy and diseased heart: new frontiers in therapeutic applications. *J Clin Med.* (2021) 10:721. doi: 10.3390/jcm10040721
40. Heggermont WA, Papageorgiou AP, Heymans S, van Bilsen M. Metabolic support for the heart: complementary therapy for heart failure? *Eur J Heart Fail.* (2016) 18:1420–9. doi: 10.1002/ejhf.678
41. Manchester J, Kong X, Nerbonne J, Lowry OH, Lawrence JC Jr. Glucose transport and phosphorylation in single cardiac myocytes: rate-limiting steps in glucose metabolism. *Am J Physiol.* (1994) 266:E326–33. doi: 10.1152/ajpendo.1994.266.3.E326
42. Paternostro G, Pagano D, Gnecchi-Ruscone T, Bonser RS, Camici PG. Insulin resistance in patients with cardiac hypertrophy. *Cardiovasc Res.* (1999) 42:246–53. doi: 10.1016/s0008-6363(98)00233-8

43. Tian R, Musi N, D'Agostino J, Hirshman MF, Goodyear LJ. Increased adenosine monophosphate-activated protein kinase activity in rat hearts with pressure-overload hypertrophy. *Circulation.* (2001) 104:1664–9. doi: 10.1161/hc4001.097183
44. Rosenblatt-Velin N, Montessuit C I. Papageorgiou. J. Terrand, and R. Lerch, Postinfarction heart failure in rats is associated with upregulation of GLUT-1 and downregulation of genes of fatty acid metabolism. *Cardiovasc Res.* (2001) 52:407–16. doi: 10.1016/s0008-6363(01)00393-5
45. Karwi QG, Zhang L, Wagg CS, Wang W, Ghandi M, Thai D, et al. Targeting the glucagon receptor improves cardiac function and enhances insulin sensitivity following a myocardial infarction. *Cardiovasc Diabetol.* (2019) 18:1. doi: 10.1186/s12933-019-0806-4
46. Gupta A, Houston B. A comprehensive review of the bioenergetics of fatty acid and glucose metabolism in the healthy and failing heart in nondiabetic condition. *Heart Fail Rev.* (2017) 22:825–42. doi: 10.1007/s10741-017-9623-6
47. Qi Y, Xu Z, Zhu Q, Thomas C, Kumar R, Feng H, et al. Myocardial loss of IRS1 and IRS2 causes heart failure and is controlled by p38α MAPK during insulin resistance. *Diabetes.* (2013) 62:3887–900. doi: 10.2337/db13-0095
48. Eberli FR, Weinberg EO, Grice WN, Horowitz GL, Apstein CS. Protective effect of increased glycolytic substrate against systolic and diastolic dysfunction and increased coronary resistance from prolonged global underperfusion and reperfusion in isolated rabbit hearts perfused with erythrocyte suspensions. *Circ Res.* (1991) 68:466–81. doi: 10.1161/01.res.68.2.466
49. Klein DK, Pilegaard H, Treebak JT, Jensen TE, Viollet B, Schjerling P, et al. Lack of AMPKalpha2 enhances pyruvate dehydrogenase activity during exercise. *Am J Physiol Endocrinol Metab.* (2007) 293:E1242–9. doi: 10.1152/ajpendo.00382.2007
50. Dyck JR, Lopaschuk GD. AMPK alterations in cardiac physiology and pathology: enemy or ally? *J Physiol.* (2006) 574:95–112. doi: 10.1113/jphysiol.2006.109389
51. Saber S, El-Kader EMA. Novel complementary coloprotective effects of metformin and MCC950 by modulating HSP90/NLRP3 interaction and inducing autophagy in rats. *Inflammopharmacology.* (2021) 29:237–51. doi: 10.1007/s10787-020-00730-6

Conflict of Interest: The authors declare that the research was conducted in the absence of any commercial or financial relationships that could be construed as a potential conflict of interest.

Publisher's Note: All claims expressed in this article are solely those of the authors and do not necessarily represent those of their affiliated organizations, or those of the publisher, the editors and the reviewers. Any product that may be evaluated in this article, or claim that may be made by its manufacturer, is not guaranteed or endorsed by the publisher.

Advantages of publishing in Frontiers

OPEN ACCESS
Articles are free to read for greatest visibility and readership

FAST PUBLICATION
Around 90 days from submission to decision

HIGH QUALITY PEER-REVIEW
Rigorous, collaborative, and constructive peer-review

TRANSPARENT PEER-REVIEW
Editors and reviewers acknowledged by name on published articles

Frontiers
Avenue du Tribunal-Fédéral 34
1005 Lausanne | Switzerland

Visit us: www.frontiersin.org
Contact us: frontiersin.org/about/contact

REPRODUCIBILITY OF RESEARCH
Support open data and methods to enhance research reproducibility

DIGITAL PUBLISHING
Articles designed for optimal readership across devices

FOLLOW US
@frontiersin

IMPACT METRICS
Advanced article metrics track visibility across digital media

EXTENSIVE PROMOTION
Marketing and promotion of impactful research

LOOP RESEARCH NETWORK
Our network increases your article's readership